Seismic Design of Asymmetric Ductile Systems

A thesis submitted in partial fulfilment
of the requirements for the Degree
of
Doctor of Philosophy
in
Civil Engineering

by

Rolando Castillo

University of Canterbury
Christchurch, New Zealand
2004

To my wife ***Eliana***

Abstract

The research promotes a better understanding of the response of torsionally unrestrained and restrained ductile systems by examining the mechanism developed during the torsional response of systems as they are affected by the dynamic actions of the translational and rotational mass.

A simple but effective design strategy for the seismic design of torsionally asymmetric systems is suggested based on the estimate of the system displacement ductility capacity and the distribution of the estimated system strength to its elements. The strength eccentricity is considered the main parameter to influence the ductile response of asymmetric systems.

The possible success of the design strategy to limit displacement demands of the elements to less than their displacement ductility capacity, for zero and increasing strength eccentricities, was examined against the effects of key parameters expected to influence response. These parameters are: strength eccentricity and the associated increase of system strength, mass eccentricity, ratio of radii of gyration of strength and mass, reduced system displacement ductility capacity, transverse elements and their degree of torsional restraint, the ratio of element nominal yield displacement, i.e., $\alpha=\Delta_{ye2}/\Delta_{ye1}$, and associated stiffness eccentricity, uncoupled translational period, consideration of different earthquake records and their direction of application.

Elements are modelled with a realistic relationship between element strength, stiffness and nominal yield displacement. The stiffness is strength dependant and the nominal yield displacement is a geometric and material property independent of strength. The centre of strength and stiffness are, therefore, not independent parameters.

This research focuses on analytical studies of torsionally unrestrained and restrained single-mass asymmetric systems. Single, two and multi-element systems were examined. An experimental programme was also undertaken on single-mass models to verify some of the analytical findings.

The findings suggest that the suggested design strategy is successful in limiting the displacement demands on elements to less than their displacement capacity for zero and increasing strength eccentricities. No differentiation is required between systems having or not having mass eccentricity. The proposed design strategy is slightly different for torsionally unrestrained and restrained systems. It promises to be straightforward, rational and in terms of design efforts most user friendly.

Acknowledgments

The research work reported in this thesis was carried out in the Department of Civil Engineering of the University of Canterbury under the overall guidance of its Head, Professor Andrew Buchanan. The assistance of the academic staff of the department is gratefully acknowledged.

I wish to express my deepest gratitude to Dr. Athol J. Carr, under whose supervision this project was undertaken, for his guidance and constructive criticism throughout all stages of this research.

I also want to acknowledge Professor Tom Paulay for his invaluable help, guidance and encouragement during the past years. I will always treasure those long and enlightening informal discussions we had on many engineering issues and other topics of interest from which I learned so much. He show me how determination and passion in what you are doing can make a big difference in someone's life.

The guidance of Dr. Jose Restrepo on the set up of the experimental programme, before his departure from the department, is gratefully acknowledged. I would also like to thank Dr. Nigel Cooke for his comments and suggestions on the experimental programme and other parts of the thesis.

My thanks are extended to all people of the Engineering Library, especially to former and current librarian Heather McCarrigan and Ann Ready, respectively, for giving me the opportunity of being a 'library insider' while completing my degree.

I would like to acknowledge my officemates Jeff Mathews and Ping Dong for their unconditional friendship.

I also like to thank the technical staff of the Civil Engineering laboratory in particular John Maley, Stuart Toase, and Kevin Wines for their valuable contribution to the experimental work.

Financial support from the following organisations in New Zealand is gratefully acknowledged: The Doctoral Scholarship from University of Canterbury, the New Zealand Society for Earthquake Engineering, the New Zealand Concrete Society, the Royal Society of New Zealand-Canterbury Branch and the Department of Civil Engineering of the University of Canterbury.

Finally, I wish to express my deepest gratitude to my wife Eliana, to whom this thesis is dedicated, for her understanding, encouragement and long-lasting support during the past years.

TABLE OF CONTENTS

NOTATION

A	=Floor dimension parallel to the *X*-axis
A_g	=Gross cross section area of a wall component
A_i	=Fraction of the total floor area
A_{rw}	=Aspect ratio of a wall
A_{rb}	=Aspect ratio of a beam
A_T	=Total floor area
B	=Floor dimension parallel to the *Y*-axis
b_f	=Width of a fuse or width of a reinforced concrete flanged structural wall
c	=Neutral axis depth
C	=Coefficient associated with the lateral force pattern
C_1, C_2	=Coefficients associated with elements *(1)* and *(2)* to estimate the displacement capacity of the system
[*C*]	=Damping matrix
CM	=Centre of mass
CR	=Centre of stiffness or rigidity
CV	=Centre of strength or resistance
D	=Distance of outermost resisting elements parallel to the *Y*-axis
E	=Distance of outermost resisting elements parallel to the *X*-axis
$\bar{e}_r, \bar{e}_{rx}, \bar{e}_{ry}$	=Ratio of stiffness eccentricity and radius of gyration of mass
e_1	=Artificial eccentricity for use in the Eurocode torsional provisions only
E_c, E_s	=Modulus of elasticity of concrete and steel, respectively
e_d	=Design eccentricity
ESDOF	= Equivalent single degree of freedom system
e_m, e_{mx}, e_{my}	=Mass eccentricity
e_r, e_{rx}, e_{ry}	=Stiffness eccentricity
e_r/D, e_{rx}/D, e_{ry}/D	=Stiffness eccentricity ratio

e_v, e_{vx}, e_{vy}	=Strength eccentricity
e_v/D, e_{vx}/D, e_{vy}/D	=Strength eccentricity ratio
$f_c^{'}$	=Compressive strength of concrete
F_s	=Force measured with a load cell
f_{sh}	=Steel stress attained within the strain hardening region
f_{su}	=Ultimate steel stress attained in the strain hardening region
f_y	=Yield strength of reinforcement
g	=Acceleration of gravity
GC	=Geometric centre
h	=Total height of a building
h_b	=Depth of a beam
h_c	=Depth of a column
h_f	=Thickness of a fuse
h_i	=Level of the accelerated mass of wall components, substitute wall-elements, frame elements and systems where the total seismic force is assumed to act
I_e	=Effective second moment of area (Cracked sections)
I_g	=Gross second moment of area (Uncracked sections)
I_m	=Rotational inertia of distributed mass
I_{me}	=Effective rotational inertia of distributed mass
I_o	=Mass rotational inertia of a square plan floor
$k_{\theta f}$	=Rotational stiffness of a fuse
$(k_{\theta f})_e$	=Effective rotational stiffness of a fuse
$(k_e)_e$, $(k_{ei})_e$	=Effective translational stiffness of an element
$(K_s)_e$, $(K_{xs})_e$, $(K_{ys})_e$	=Effective translational stiffness of an elastic system
[K]	=Stiffness matrix
$K_\theta^{'}$	=Torsional stiffness of the system with respect to the centre of stiffness including all elements of the system

k_e, k_{ei}	= Translational stiffness of an element
k_x, k_y, k_{yei}, k_{xei}	= Translational stiffness of elements along the *X* and *Y*-axis
k_i	=Translational stiffness of a component
K_s, K_{xs}, K_{ys}	=Translational stiffness of an elastic system
k_u	=Post-elastic stiffness of a component
K_θ	=Torsional stiffness of the system with respect to the centre of stiffness including all elements within the system
$K_{\theta y}$, $K_{\theta x}$	=Torsional stiffness of the system with respect to the centre of stiffness not including those perpendicular elements to the direction being analysed
M	=Total translational mass of the system
[M]	=Mass matrix
MDOF	=Multi-degree of freedom system
M_e	=Effective translational mass of the system
m_i	=Fraction of the total mass
M_i	=Flexural moment of a component
M_n	= Flexural nominal moment
M_p	= Flexural plastic moment
M_r	= Flexural normalized moment, $M_n(N\geq 0)/M_n(N=0)$
M_{sh}	= Flexural moment after strain hardening
M_y	=Flexural moment at first yield
N, N_i	=Axial load in a column or wall component
P_n	=Lateral force applied at level *n* of a multi-storey system
R	=Force reduction factor
r	=Post-yield stiffness coefficient
r_k, r_{kx}, r_{ky}	=Radius of gyration of stiffness
r_m	=Radius of gyration of mass
r_o	=Radius of gyration of distributed mass of a square floor diaphragm
r_v ,r_{vx}, r_{vy}	=Radius of gyration of strength

r_v/r_m, r_{vx}/r_m, r_{vy}/r_m	=Ratio of the radii of gyration of strength and mass
S	=Plastic section modulus of a steel member
SDOF	=Single degree of freedom system
SHS	=Square hollow section
T	=System torque
t_f	=Thickness of the flange of a reinforced concrete structural wall
T_m	=Dynamic torque introduced by the mass rotational inertia
T_s	=Uncoupled translational period of the elastic system
t_w	=Thickness of the web of a reinforced concrete structural wall
T_x, T_y	=Uncoupled translational period along the *X* and *Y*-axis of the elastic system
T_θ	=Uncoupled rotational period about the *Z*-axis of the elastic system
$\dot{u}$	= Translational velocity of the system
$\ddot{u}_\theta$	=Rotational acceleration of the system
u_θ	=System rotation
$\ddot{u}_{xo}, \ddot{u}_{yo}$	= Translational acceleration of the ground motion
$\ddot{u}$, $\ddot{u}_x, \ddot{u}_y$	= Translational acceleration of the system
u, u_x, u_y	= Translational displacement of the system
u_i	=Location of an element from the centre of stiffness
u_n, u_{n+1}	=Amplitude of two successive displacements of the free vibration test
V_E	=Static force applied at the centre of mass of the system
V_i, V_{ei}	=Base shear assigned to an element
V_{ne}, V_{nei}	=Nominal strength assigned to an element
V_{yns}^x	=Excess nominal strength assigned to a system
K_{ys}^x	=Excess translational stiffness of an elastic system
$K_{\theta y}^x$	=Excess rotational stiffness of an elastic system

V_{she} =Strength of the elements of the test model after strain hardening

V_{re} =Residual strength of an element

V_{re} =Residual strength of an element`

V_{ni} =Nominal strength assigned to a component

V_{ns}, V_{xns}, V_{yns} =Nominal strength assigned to a system

V_{shs}, V_{xshs}, V_{yshs} =Nominal strength of the test model after strength hardening

V_t =Redistributed base shear due to an external torque $T=e_v V_{ns}$ to selected couple of elements

V_x, V_y =unit strength assigned to the system along the X or Y-axis

V_{xne}, V_{yne} =Nominal strength assigned all elements parallel to the X or Y-axis, respectively

V_{ye} =Force at first yield of an element

$V_{\theta y}$, $V_{\theta x}$ =Rotational strength contributed by those element parallel to the Y or X-axis

w_θ =Rotational frequency

w, w_x, w_y =Translational frequency

$\bar{x}_i, \bar{y}_i$ =Location coordinates of a fraction of the total floor area A_i from an arbitrary reference axis

x_i, y_i =Location coordinates of an element from the centre of mass

$\bar{x}, \bar{y}$ =Location coordinates of the geometric centre from an arbitrary reference axis.

X, Y, Z =Principal axes of the system

Z =Elastic section modulus of steel member

$(\Delta_{ys})_e$ =Effective nominal yield displacement of a system

$\Delta'_{ye}, \Delta'_{yei}$ =Displacement at first yield of an element

$(\Delta_{ye})_e$ =Effective nominal yield displacement of an element

$(\Delta_{ye})_{min}$ =Smallest nominal yield displacement of parallel elements within a system

Δ_d =Design displacement of the system

Δ_{max} =Maximum displacement at level x

Δ_{avg} =Average displacement at the extreme point of the structure at level x

Δ_i =Lateral displacement of the elastic component, element or system

Δ_s =Displacement introduced to the shake table

Δ_t =Time step used in the numerical integration of the equations of motion

Δ_{ue},Δ_{uei} =Displacement demand or capacity of an element

$(\Delta_{ue})_d$, $(\Delta_{uei})_d$ =Displacement demand of an element

$(\Delta_{ue})_c$, $(\Delta_{uei})_c$ =Displacement capacity of an element

Δ_{us}, Δ_{xus}, Δ_{yus} =Displacement demand or capacity of a system

$(\Delta_{us})_d$ =Displacement demand of a system

$(\Delta_{us})_c$ =Displacement capacity of a system

Δ_u, Δ_{ui} =Displacement demand or capacity of a component

Δ_{ye}, Δ_{yei} =Nominal yield displacement of an element

Δ_{yi} =Nominal yield displacement of a component

Δ'_{ys} =Yield displacement of the system at first yield

Δ_{ys}, Δ_{xs} =Nominal yield displacement of the system along the *X* and *Y*-axes

Δ, Δ_e, Δ_s =Lateral displacement of the elastic component, element or system, respectively

α =Ratio of nominal yield displacement of parallel elements in a two-element system

β =Coefficient quantifying the distance between centre of mass and an element as a function of *D*; Coefficient for the accidental eccentricity

δ_u, δ_{ui} =Drift capacity

δ_y, δ_{yi} =Nominal yield drift

ε_{sh} =Strain of steel at the beginning of strain hardening

ε_{su} =Strain of steel associated with ultimate tensile strength

ε_s =Strain of steel within the elastic range

ε_y =Tensile yield strain of steel material or reinforcement

ϕ =Curvature of the elastic component

$(\phi_{yf})_e$ =Effective nominal yield curvature of a fuse section

$\phi_y^{'}, \phi_{yi}^{'}$ =Curvature at the onset of yielding

ϕ_{uf} =Curvature capacity of a fuse section

ϕ_{ui} =Ultimate curvature of a section

ϕ_{yf} =Nominal yield curvature of a fuse section

ϕ'_{yf} =Yield curvature of a fuse section at first yield

ϕ_{yi} =Nominal yield curvature of a section

γ = Coefficient for the dynamic eccentricity

η =Curvature coefficient of a section

$(\ell_f)_e$ =Effective length of the fuse

$\ell_b^{'}$ =Length of beams between fuses in the frames of the test model

ℓ_b =Length of beams in the frames of the test model

ℓ_c =Length of columns in the frames of the test model

ℓ_f =Length of a fuse

ℓ_i =Length of a substitute wall-element

λ_i =Excess strength factor quantifying the excess strength assigned to element i.

ℓ_s =Length of the beam in the beam–column fuse test

ℓ_w, ℓ_{wi} =Length of a wall component

λ_{ys} =Excess strength factor quantifying the excess strength assigned to the system

$\mu_{\Delta i}$ =Displacement ductility of a component or element

$\mu_{\Delta s}$ =Displacement ductility of a system

$\mu_{\Delta e}$ =Displacement ductility of an element

$\mu_{\phi i}$ =Curvature ductility of a section

θ =System rotation

θ_f =Fuse rotation

θ_{yc} =Column rotation associated with the rotation at first yield of the beam fuses in the test model

FC =Fuse connection

SB =Spherical bearing

UH =Unidirectional hinge

ES =Encased shaft

OP =Opening

LI =Lead ingot

TU =Torsionally unrestrained

TR =Torsionally restrained

θ'_{yf} =Fuse rotation at first yield

θ_s =System rotation

θ_y, θ_{yi} =Nominal yield drift angle

θ_{yf} =Nominal yield rotation of a fuse

$(\theta_{yf})_e$ =Effective nominal yield rotation of a fuse

ρ_b, ρ_{b1}, ρ_{b2} =Reinforcement ratio of concentrated steel at the ends of a structural wall

ρ_{max} =Maximum reinforcement ratio

ρ_{min} =Minimum reinforcement ratio

ρ_ℓ =Ratio of distributed reinforcement in a structural wall

ξ =Neutral axis coefficient to estimate the depth of the neutral axis from the extreme fibre in tension

ζ =Damping ratio expressed as a percentage of the critical damping

ζ_x, ζ_y, ζ_θ =Damping ratio as a percentage associated with the *X*, *Y* and *Z* modes of free vibration of single-mass systems

Chapter 1. Introduction

1.1 Background

There is enough evidence to suggest that during past earthquakes, one of the causes of severe damage and even collapse of buildings has been excessive diaphragm rotations. A review of the technical literature indicates that the damage to buildings caused by torsional effects has occurred frequently. For instance, ground accelerations of *0.14g* to *0.18g* in the Great Alaska Earthquake of 1964 [C10] generated extensive building damage including the J.C Penney Building that collapsed due to excessive twisting. During the Miyagi-Ken earthquake of 1978 [Y1] ground accelerations of *0.25g* to *0.40g* were reported, generating damage to several buildings including the Obisan Building that failed due to torsional effects. Of the total buildings that collapsed or suffered excessive damage during the Mexico Earthquake of 1985 [R5], *42%* were corner buildings which are known to be susceptible to excessive diaphragm rotations; the maximum ground acceleration reported at the lake bed was *0.20g*. The Northridge Earthquake of 1994 [G3] resulted in ground accelerations between *0.20g* and *1.0g*. The Barrington Medical Building in Santa Monica, a six-storey non-symmetric framed structure, exhibited damage due to torsional effects. The Kobe Earthquake [C11] of 1995, with a reported maximum acceleration of *0.80g*, caused the partial collapse of a number of corner buildings.

Are current seismic torsional design provisions really enabling structural engineers to design buildings to exhibit satisfactory ductile behaviour? It seems that after four decades of research, no general conclusions have been reached concerning the torsional response of ductile structures subjected to earthquakes. Chandler, et al [C8] comments on the research progress and controversies concerning seismic torsional response. "*Progress in understanding the seismic response behaviour of asymmetric building systems has been rather slow, considering the research efforts devoted to this subject during the last four decades. This is manifested in the relative scarcity of conclusions of general validity*". Besides the question posed above, others that also require an answer are: Do we really have a thorough understanding of the torsional behaviour of ductile systems? Are our modelling assumptions for elements, and hence that of systems, close enough to reality?

A variety of research findings on torsional behaviour are familiar to the structural engineering profession. In the 1930's, experimental studies were initiated on the elastic behaviour of simple one-storey systems [A5]. With the arrival of the computer in the 1960's, more sophisticated research of elastic systems were conducted and subsequently extended to cover also ductile systems [S4]. By the 1980's, the parameters governing the response of elastic systems were clearly identified and their effects on the response were understood [K1]. Research efforts since then have dominantly focused on ductile behaviour. However, as previously stated, no convincing conclusions have been reached yet when dealing with ductile systems.

Current seismic design provisions for torsion of most building codes [I1] are intended for both elastic and ductile systems. They originated from the studies by Rosenblueth and Elorduy [R3] of elastic systems. Their approach was based on a design eccentricity that includes both dynamic and accidental eccentricities as to be explained in detail in Section 1.2.3. The dynamic eccentricity is a modification of the stiffness eccentricity to account for the role of the mass rotational inertia on the system response. The accidental eccentricity accounts for unforeseen differences between the calculated and the actual properties of the structure and the probable presence of rotational ground motions. This first seismic torsional provision was introduced

some 40 years ago in several codes. It was intended to address elastic response. However, it has also been extensively used in the estimation of strength demands on ductile systems.

The scenario presented above was perceived to justify further studies on the torsional seismic response of ductile systems. It is hoped that this may contribute to improvement of design procedure.

1.2 Literature Review

1.2.1 Review of relevant previous studies

To aid an appreciation of research advancements in this field, a brief review of a few selected projects is undertaken here to outline specific key issues and developments, as they emerged over the last decades.

An early study on the torsional response of structures published by Ayre [A5,1938] is considered to be a pioneering. It examined, for the first time, the response of single and two-storey elastic test models to free vibration. The models had one and two-fold symmetry, i.e., unidirectional or bidirectional stiffness eccentricity. The theory, used to identify features of free vibration of single-storey buildings, was merely the application of the principles of vibration of systems of several degrees of freedom [T1,1928]. Parameters such as centres of rigidity and mass were already of common knowledge. The concepts of symmetry and asymmetry were used to describe the relationship between mass and stiffness distribution in the system and without reference to its plan geometry. The main objective was to provide a better understanding of the vibration of buildings where horizontal translation and rotations about a vertical axis are interconnected due to different mass and rigidity distributions. It was advocated that engineers should strive for symmetry since such types of systems are easier to analyse.

Another investigation conducted by Ayre [A6,1943] studied the response of the single-mass system described above when subjected to an idealized ground motion. The experimental tests were conducted with a shake table built at the University of Stanford [J1, 1929], believed to be the first of its class in the United States. The structure was subjected to a short, unidirectional and damped sinusoidal motion. The idealised ground motion was varied for a wide range of frequencies to include the natural frequencies of the models. The direction of application was also varied. It was found that a change in the ground motion frequency was accompanied by the usual pronounced difference in response at resonance and non-resonance frequencies. Changes in ground motion direction were, in general, of less importance than changes in frequency; however, at near-resonance frequencies, the direction was important in determining the response.

In another pioneering paper, Housner and Outinen [H2,1958] identified for the first time differences in response between static and dynamic analyses of elastic systems. These were found to originate from the engagement of the mass rotational inertia and influencing system responses. They compared maximum dynamic-induced stresses by the earthquake in unsymmetrical elastic structures with those induced by equivalent static lateral forces. It was concluded that the static method of analysis underestimates significantly the magnitude of the maximum stresses during dynamic analyses. It was evident that the greater the eccentricity, measured between centres of mass and rigidity, the greater the differences between predictions of dynamic and static analyses.

The first attempt at addressing seismic design provisions for asymmetric elastic structures was that of Bustamante and Rosenblueth [B2, 1960]. They stated that actual eccentricities of horizontal storey shear might be much in excess of what can be accounted for by static computations. This implies that this may be one of the reasons why damage from torsional oscillations was observed. Other identified reasons for discrepancies relevant to analytical solutions are: uncertainties in the calculations of the relative rigidities and hence in the location of the centre of rotation, differences between dynamic and static behaviour, uncertainties in the force distribution and nonlinear behaviour. They also observed that building codes [S1, 1958 and B1,R4,1960] adopted, for the first time, a minimum stiffness eccentricity of 5% of the plan dimensions to account for uncertainties during torsional response. They concluded, from studies on multi-storey elastic systems, that the dynamic eccentricity exceeded statically computed values and that a rough estimate of dynamic effects on asymmetric multi-storey buildings can be obtained from the response of an asymmetric single-storey structure with similar characteristics.

Rosenblueth and Elorduy[R3,1969] proposed a design eccentricity for the Mexican Building Code. They suggested that to overcome the deficiencies of the static method, a design eccentricity of $e_d=1.0e_r$ or $1.5e_r$, whichever provides more severe actions, should be considered. This is the first torsional provision that took into account the dynamic effects of the mass rotational inertia on the response of elastic systems.

Shibata, Onose and Shiga [S4,1969] examined the nonlinear response of eccentric single-storey structures when subjected to one and two-directional idealized input ground motions. They found that the nonlinear response is dependant on the horizontal distribution of strength and that the ground motion in the *X* and *Y*-direction should be considered in the analysis. This was because, as they pointed out, yielding in one direction will affect the response in the other direction.

Rutenberg [R6,1992] and Rutenberg et al [R7,1995] provided comprehensive state of the art reviews of the nonlinear response of asymmetric building structures and building code provisions covering the research advancements until 1994.

Chandler, Duan and Rutenberg [C8,1996] prepared, as part of the Task Group 8 of the European Association of Earthquake Engineering, a most critical review of the research efforts dedicated to this field. They expressed concern that few valid conclusions have been reached during the last four decades. They pointed out that the main reasons for this was the lack of consistent definitions of governing system parameters, the choice of structural models particularly, for the evaluation of non-linear behaviour and the arbitrary selection of earthquake records. They identified several key areas where a lack of agreement with respect to results was apparent. They are briefly summarised as follows:

1. *The choice of models for inelastic analysis.* The choice of structural models for inelastic analysis appears to be the main source of variation among findings. Some researchers had reached conclusions based on systems displaying transverse elements providing additional torsional resistance whereas other investigators have reached different conclusions with systems not including such types of elements. Two models are commonly examined: stiffness and/or mass-eccentric models. They had, in most cases, two, three or four parallel elements along the direction of application of the earthquake record.

2. *Accidental eccentricity.* The inclusion of an accidental eccentricity, into the design eccentricity provisions for seismic design, has been a controversial issue. This provision, stipulated in most building codes, intends to account for uncertainties in calculated and

actual properties of the structure and the probable presence of a rotational component of the ground motion. In inelastic analyses, the fact of including or not the accidental eccentricity results in different strength distributions and total strength. Some researchers believe that the accidental eccentricity should not be included in the analyses because it is intended to account for unpredictable variations of assumed system properties and characteristics. Other investigators argue that findings obtained from systems not accounting for the accidental eccentricity are not correct because the model analyzed is not representative of the one actually designed.

3. *The choice of the reference system for comparing the response of asymmetric systems.* It has been common practice to refer to asymmetric structures as "Torsionally unbalanced systems". These systems are characterised by non-coincident centres of mass and stiffness. Two reference models have been used to compare its response: a single degree of freedom (SDOF) system having the same translational period and strength as the asymmetric system or alternatively, a "Torsionally balanced system". The latter is the same as the original model; however, its centre of mass is shifted to coincide with the centre of stiffness. This has been a popular choice, primarily because, based on traditional modelling of force-displacement relationships, the variation of element strength changes the nominal yield displacement of the elements.

4. *Excess strength of systems.* Excess strength arises when the nominal lateral strength of a code-designed "torsionally unbalanced system" exceeds that of the corresponding "torsionally balanced system". It is the result of assigning strength to the elements due to different values of design eccentricity. Some investigators normalize the strength by considering the ratio of the total strength of the torsionally unbalanced system and that of its torsionally balanced reference model. This is done to separate the effect of the increased total strength from the effect of the strength distributions among elements. It was mentioned as a better approach for optimising strength distributions. The analyses of systems considering just their computed strength were mentioned as just suitable for comparing the response of the asymmetric system with their reference model.

5. *Transverse elements.* The response of systems where the transverse elements introduce or do not introduce torsional resistance seems to be one of the reasons why researchers have disagreed in their findings. It was pointed out that if transverse elements provide torsional resistance then it is essential that the system is also subjected to the transverse component of the earthquake record excitation. This has been a source of controversy. It was mentioned that transverse elements contributing with torsional resistance may affect response. However, it was also pointed out that there was no justification to extend analyses on these type of systems because findings from models where transverse elements do not introduce torsional resistance and subjected to unidirectional input only are considered to provide a critical torsional response.

6. *Rotational strength and radius of gyration of strength.* They also commented that it is necessary to identify those parameters affecting the response of inelastic systems. Besides the total translational strength and the centre of strength, the rotational strength and the radius of gyration of strength were proposed to quantify the response of ductile systems. It is believed that the radius of gyration of element nominal strength is better for this purpose.

7. *Uncoupled torsional to lateral frequency ratio.* This ratio, which is equivalent to the ratio of radius of gyration of element stiffness and that of distributed mass, has also been a

controversial parameter. This is because different locations have been used as reference by researchers for the derivation of the torsional stiffness and the radius of gyration of mass. The torsional stiffness and radius of gyration of mass has been measured relative from either the centre of stiffness or from the centre of mass. In a third definition, the torsional stiffness is taken about the centre of stiffness whereas the radius of gyration of mass is taken about the centre of mass. Differences between these definitions increase with increasing eccentricities. It is evident that results obtained form identical values of uncoupled torsional to lateral frequency ratio, but differently defined, will not be in complete agreement.

8. *Damping ratio.* Differences in the magnitude of this characteristic were mentioned as a relevant parameter. However, they indicated that it is not considered a source leading to significant variations in the results.

9. *Secondary slope ratio.* The modification of the post-elastic stiffness of elements was mentioned as a possible source for differences in findings. It was indicated, however, that they appear not to be significant.

10. *Earthquake record characteristics.* It was also mentioned that the frequency content of the earthquake, pattern of pulses in the record, number of records considered in the parametric studies and the relative levels of ground motion to which those records are normalized affects torsional response. Hence, conclusions obtained from an arbitrary selection of earthquake records are difficult to assess.

From 1995 until today, studies on the torsional response of ductile systems have focussed on that of multi-storey asymmetric models [D7,D8] and systems comprising transverse elements introducing torsional resistance and subjected to bidirectional earthquake input [A4,C12,D1,D4,D6,H3,R2,L1] and pushover analysis of buildings [T2]. The Task Group 8 of the European Association of Earthquake Engineering has also been very active organizing three Workshops dealing exclusively with Asymmetric and Irregular Structures [R1,K4,D5].

Based on the research over the past 15 years on the ductile response of asymmetric systems, several common key features were recognized in these studies:

- All studies have based the research on assumed force-displacement modelling of elements where strength has been made traditionally proportional to assumed stiffness.

- In most studies, the stiffness eccentricity is considered as the main parameter influencing the response of both elastic and ductile structures.

- Although the centre of strength has been recognized as a relevant parameter influencing torsional response, no study appears to have offered thorough explanations of its role in the system response.

- Extensive research effort addressed optimal strength distributions to elements, which would lead to ductility demands on elements less or equal to their ductility capacity.

- A large number of studies are related to examinations of current code provisions.

- Many studies concentrated on identifying trends rather than attempting to provide explanations why some seismic design provisions for torsional behaviour do not satisfactorily predict ductility demands on flexible and stiff side elements in the structure.

- The traditional force-displacement modelling applicable to elements assumes their stiffness as a geometric property independent of strength. System strength is assigned to the elements in proportion to the element stiffness taking elastic translational or rotational-imposed system displacement into account. Assumptions for element stiffness are generally cursory and often bear little relationship to real conditions such as will arise in reinforced concrete members, subjected within the elastic domain, to intense shaking. Cursory stiffness values may lead generally to gross underestimation of displacements to be expected. Stiffness of the elements was not considered to be affected by assignment of strength.

- The increase of system strength has been associated with the stiffness eccentricity and the radius of gyration of the element stiffness.

Recently, Paulay [P2~P12] has shown particular interest in the torsional seismic response of ductile buildings after enquiries relevant to how the displacement ductility capacity of existing asymmetric buildings can be assessed. His view on this issue is summarized below.

- He indicates that current provisions are based on properties of elastic systems and therefore have limited relevance to ductile systems. The element stiffness and, hence, stiffness eccentricity is the main parameter influencing response of elastic systems. In contrast, element strength and, thus, strength eccentricity is believed to be the main parameter to influence the response of ductile systems.

- The concept of stiffness being strength-dependant is introduced. This realistic relationship demonstrates that centres of strength and stiffness are not independent parameters. It is shown that the nominal yield displacement of an element is a geometric and materials property which is independent of strength.

- Paulay introduced the idea that the displacement ductility capacity of a system is based on the displacement capacity of its critical elements.

- Another contribution of Paulay was his review, using statics, of mechanisms developed during torsional behaviour of two-element asymmetric ductile systems. It was shown how the dynamic actions of the mass translational and rotational inertia interact with the strength of the elements.

- A conceptual study on systems was also presented for cases when an earthquake record is applied from different directions. It was recalled that once the translational strengths of the system, along the principal axes, was established, the system strength, at any other oblique direction, is larger.

- Paulay also proposed a mechanism based design approach. Its drawback was that it mistakenly did not account for the role of the mass rotational inertia on the response.

- With respect to the issue of system strength distribution, it was stated that the assignment of element strength is under the control of the designer and therefore a particular strength eccentricity, believed to generate an optimal system response, can be selected. It was

proposed, for the required translatory system strengths, to reduce or eliminate strength eccentricity.

- It was expressed that an elimination or reduction of system rotations, due to torsional behaviour, should not need to be the primary design aim. Instead system rotations should be accepted and perhaps even encouraged, if it is shown that displacement ductility criteria for different translatory elements are not violated. Thereby, greater energy dissipation and consequent effective damping is achievable.

Tso and Myslimaj [T3,M3] recently recognized, like Paulay, that strength and stiffness of reinforced concrete elements are related. They stated that the stiffness distribution was not known prior to the assignment of strength to the elements. Consequently, current strength distribution guidelines, based on element stiffness, need to be changed. They also considered that the designer is in control of the location of the centre of strength and associated stiffness. They concluded, based on the response of single-storey systems, that system rotations should be minimized to prevent large torques and maintain small rotational responses. They established that this is achieved if the centre of strength and stiffness are located at opposite sides with respect to the centre of mass; a strength distribution which they referred to as the "balanced CV-CR" location. They suggested guidelines for a strength distribution based on the yield displacement of the elements.

1.2.2 Review of relevant previous experimental studies

A review of the technical literature, focussing on the research of ductile systems using experimental models, was carried out with the aim of assessing whether they provided experimental verification of the analytical research.

Shibata [S4, 1969] carried out tests using reinforced concrete single-storey structures comprising two frames along the *X* and *Y*-directions. Two models were tested: one symmetric and another asymmetric. The symmetric model had uniform distribution of mass, stiffness and nominal strength. The asymmetric structure had an uneven distribution of stiffness and strength. This was achieved by reducing the cross section dimensions and reinforcement of two columns. Both specimens were subjected to a simple sinusoidal excitation. It was found that the response is affected during the dynamic excitation by distributions of strength and stiffness. The ratios of rotational and translational displacement increased as the amplitude of the sinusoid motion was increased. Collapse occurred due to excessive rotations.

Dusicka [D9, 2000] completed experimental studies of a single-storey ductile structure. It comprised a single mass connected to vertical rectangular flat bars to resist the dynamic lateral forces. The models had different stiffness, strength and mass distributions. The change in stiffness was achieved by reducing the height of the flat bars. Bidirectional ground motions were also introduced to the structure. Comparisons between experimental and idealised models were undertaken, and a consistent level of correlation was found in the results. They suggested that this research provided confidence in the numerical and experimental models used to study inelastic response of torsionally susceptible ductile structures. Torsional response was observed for all models including those that had no stiffness eccentricity. The strength eccentric models had significantly higher demands on the stronger and stiffer element.

De Stefano et al [S2, 2001] conducted several shake table tests of a three-storey steel model structure. The model was a *1/5* scale of its prototype. The structure consisted of welded

rectangular hollow sections. The mass of the first test was symmetrically located along the structure. Centres of strength and mass were coincident and also coincided with the geometric centre of the system. In a second test, the elements of the model remained unchanged; however, structural asymmetry was achieved by shifting the centre of mass by *200* mm from its geometric centre. Hence, centres of mass and strength did not coincide. Comparisons between experimental and idealised models were undertaken and it was found that the response of the asymmetric building models was characterised by similar and significant torsional motions along the height of the building. It was also found that the edge displacements induced by maximum rotations were on average *29%* of the maximum displacement demand attained at the centre of stiffness at all floors.

The above mentioned studies suggests that there is a scarcity of experimental verification of the analytical research conducted on single and multi-storey asymmetric ductile structures. This is a regrettable limitation on the advancements in this field of study not only for a better understanding of the torsional behaviour and verification of modelling assumptions but also for the development of better seismic design provisions.

1.2.3 Review of building code provisions for seismic design of asymmetric systems

Systems with a base shear capacity, V_E, reduced below that required for an elastic response, are expected to deform beyond the elastic range during strong ground motions. These systems should be able to sustain seismic-induced forces by limiting displacement demands on inelastic elements to less than their displacement capacity. This, in fact, may be achieved through hysteretic energy dissipation at plastic hinges expected to develop at specific locations of the elements.

Seismic-induced forces, expected during ground motions, are modelled as external forces applied at the centre of mass. The application of a static lateral force to the centre of mass of a symmetric system will lead only to translations because centres of mass, strength and stiffness are coincident.

In the case of asymmetric systems, the application of a static force to its centre of mass is expected to also generate rotations because the centre of mass does not coincide with the centres of strength and/or stiffness. It is widely accepted that the distribution of the design base shear has a relevant effect on their response. This should be distributed on the elements of symmetric and asymmetric with or without mass eccentricity to satisfy static equilibrium, i.e., e_v=*0.0*.

Static equilibrium is traditionally achieved in practice by distributing the design base shear on elements according to the following expression.

$$V_i = \left(\frac{k_{ei}}{\sum k_{ei}} \right) V_E + \left(\frac{e_r}{K_\theta} u_i k_{ei} \right) V_E \qquad \textbf{(1-1)}$$

where k_{ei} is the stiffness of an element, e_r is the stiffness eccentricity, u_i is the distance of the corresponding element from the centre of stiffness and $K_\theta = \sum k_{ei} u_i^2$ is the torsional stiffness of the system taken with respect to the centre of stiffness.

The first term of Eq 1-1 corresponds to the design base shear being distributed on the elements in proportion to their translational stiffness. The resulting centre of strength coincides with the centre of stiffness; but not necessarily matching the centre of mass. The centre of strength is then shifted to the centre of mass with the second term. Here, the design base shear is redistributed among the elements in proportion to their distance from the centre of stiffness.

Seismic design provisions for torsion in most building codes recommend that the stiffness eccentricity, shown in Eq 1-1, should be replaced by the design eccentricity. This eccentricity is expressed as,

$$e_d = \gamma e_r + \beta A \qquad \textbf{(1-2(a))}$$

$$e_d = e_r + \beta A + e_1 \text{ (Eurocode provision only)} \qquad \textbf{(1-2(b))}$$

It consists of a dynamic eccentricity, γe_r, which takes into account the dynamic effect of the mass rotational inertia on the system response. The factor, γ, increases or reduces the stiffness eccentricity by a codified quantity, as shown in Table 1-1. The accidental eccentricity, βA, accounts for unforeseen differences between the calculated and actual properties of the structure and probable presence of a rotational component of ground motions. This is commonly a fraction of the diaphragm plan dimension.

The eccentricity e_1 is only applicable to the Eurocode torsional provisions. This provision considers the likely effect of the mass rotational inertia on the system response through this artificial eccentricity, as shown in Table 1-1. This provision is also based on the response of elastic systems [M2]. It depends on the configuration of the floor plan, the stiffness eccentricity and radii of gyration of stiffness and mass.

Table 1-1. Design eccentricity coefficients

Country	*Design eccentricity Coefficients*		e_1
	γ	β	
New Zealand [I1]	*1.00*	*± 0.10*	*Not applicable*
Costa Rica [I1]	*2.00*	*0.00*	
	0.00	*0.00*	
Japan [I1]	*1.00*	*0.00*	
USA (UBC) [I1]	*1.00*	*± 0.05 A_x*	
Eurocode [I1]	*1.00*	*+0.05*	*The smallest value of the next two expressions.* $e_1 = 0.1(A+B)\sqrt{10(e_r/A)} \le 0.10(A+B)$ $e_1 = 1/2e_r(r_m^2 - e_r^2 - r_k^2 + \sqrt{(r_m^2+e_r^2-r_k^2)^2 + 4e_r^2 r_k^2})$ *or* *if* $r_k^2 = 5(r_m^2 + e_r^2)$ *then* $e_1 = 0.0$
	1.00	*-0.05*	*0.00*

Note: When torsional irregularity exists, as defined in the UBC, they may be accounted for by increasing the accidental eccentricity in each level by an amplification factor, $A_x=(\Delta_{max}/1.2\Delta_{avg})^2 \le 3.0$, where Δ_{avg} is the average of the displacements at the extreme points of the structure at level x and Δ_{max} is the maximum displacement at level x.

The dynamic and accidental eccentricity coefficients γ and β and the eccentricity e_1 (applicable to the Eurocode provision only) are summarized in Table 1-1. Some of these coefficients are explicitly stipulated whereas others were implicitly deduced.

The design eccentricity, taken relative from the computed stiffness eccentricity, establishes the location on the floor diaphragm where the external static forces should be applied. Although, the resultant of the seismic-induced forces should be applied at the centre of mass, in some cases, the magnitude of the design eccentricity will indicate that they should be applied at a different location. Although this is not physically correct, it turns to be a mere manipulation of the static analysis to achieve an optimal distribution of system strength among elements which is expected to generate a satisfactory inelastic and elastic torsional response.

The substitution of the design eccentricity, as expressed by Eq.1-2, into equation Eq.1-1 has been shown to introduce a strength eccentricity and an increase of system strength. The increase of system strength is a function of the stiffness eccentricity and the radius of gyration of element stiffness [Z2].

The Earthquake resistant design method for buildings in Japan [I1] is the only provision examined in this study, which does not explicitly stipulate a design eccentricity. It recommends a direct increase of the ultimate lateral shear strength of the system which depends on the ratio of stiffness eccentricity and radius of gyration of element stiffness along the principal axes, i.e., e_r/r_k ratio. For instance, a building is considered regular in plan if $e_r/r_k \leq 0.15$ and hence no increase of system strength is required. In case of $e_r/r_k > 0.15$, the ultimate lateral shear strength of each storey shall be increased by a factor F_e, as shown in Table 1-2.

Table 1-2. Relationship between the e_r/r_k ratio and the excess strength factor F_e

e_r/r_k	F_e
$e_r/r_k \leq 0.15$	1.00
$0.15 \leq e_r/r_k \leq 0.30$	Linear interpolation
$e_r/r_k \geq 0.30$	1.50

Building code provisions, in general, provides additional criteria to establish plan regularity besides minimum values of stiffness eccentricity [I1]. For instance, there are restrictions on the plan configuration of the building, such as minimum dimensions for re-entrant corners, diaphragm openings and even limitations on the torsional stiffness of the building.

If the system is irregular in plan, additional limitations should also be satisfied for use of the static method in seismic design along with the corresponding torsional provisions described above [I1]. The most significant limitation is that the centre of mass and centre of stiffness should be located along two vertical lines along the height of the structure.

The seismic design provisions for torsion of ductile systems described above have three disadvantages:

- They consider the stiffness eccentricity as the main parameter to influence the response of ductile systems. No mention is given to the strength eccentricity.

- No differentiation is made for asymmetric systems expected to respond elastically or inelastically.

- It does not consider the fact (to be demonstrated in Chapter 2) that the stiffness of an element is not known until its strength is established.

This situation justifies further studies into the seismic response of asymmetric systems, aiming at improving current design provisions for ductile asymmetric systems.

1.3 Statement of the problem

It is perceived that there is a lack of understanding of the torsional response of ductile structures. There are many studies identifying trends in behaviour from inelastic time history analyses rather than analysing in depth structural behaviour when certain parameters are varied. Studies are conducted considering stiffness as the primary parameter influencing response rather than strength and displacements resulting in conclusions, reached by authors, that are often contradictory. Efforts are required to explain the role of the different strength-related parameters and the means by which adverse effects of torsional behaviour can be rationally reduced by the structural engineer.

Seismic design provisions for torsional behaviour of ductile systems are still predominantly based on the elastic properties of the structure, i.e., stiffness eccentricity, without taking into account parameters that dominate ductile response, i.e., strength eccentricity [P11]. These provisions do not differentiate between serviceability and ultimate limit states. At a serviceability limit state (SLS) the structure is expected to respond essentially in the elastic domain. The parameters that govern at this stage are: translational periods, the ratio of translational to torsional periods, stiffness eccentricity, damping, and ground motion input. In contrast, at the ultimate limit state (ULS), ductile behaviour is expected and other parameters become dominant. They are: strength eccentricity and associated system strength, distribution of mass and nominal strength of the elements, nominal yield displacements and the plan-wise location of elements.

Current design aims are inclined towards an optimal distribution of strengths on the lateral force resisting elements leading to element displacement ductility demands equal or smaller than their displacement ductility capacity. These aims significantly differ from those of a displacement-focused design, where it is advocated that displacements are the main causes of structural damage and therefore they should be limited to satisfy performance criteria.

Structural designers do not have access to a simple, rational and versatile design procedure for use in the design of ductile buildings. There is a need for a design strategy that is flexible enough to be used as part of a force or a displacement-focused seismic design strategy. It should be applicable to systems where the design criteria are to develop the displacement ductility capacity of elements or to develop element maximum displacements associated with specific performance criteria, whichever is critical. This design strategy should also address the vulnerability assessment and retrofit of existing structures[P17, P19]. The latter, however, was not contemplated in this study.

Another dilemma resulting from current research is with respect to the bilinear force-displacement modelling of elements relevant to ductile systems. According to traditional modelling, the nominal yield displacement of an element increases by increasing its strength. Recent studies [P11,P18,P20,P21] have demonstrated, however, that the nominal yield displacement of a component is essentially a function of its dimensions and the yield strain, ε_y.

It is insensitive to strength and realistic values of axial load. Thus, if the nominal yield displacement is essentially constant, once the component's geometry is defined, an increase of strength will only increase its stiffness. Consequently, stiffness becomes proportional to strength. The effect of this approach, which is claimed to be more realistic than current modelling, is that centres of strength and stiffness are not independent. This realistic relationship is a major consideration in this study.

A review of the technical literature, as presented in Section 1.2.2, indicates that experimental studies on the torsional response of asymmetric systems are scarce. It seems there is a need to conduct more research on this field to verify findings derived from analytical models and to improve current seismic design provisions dealing with ductile systems.

In the endeavour to improve understanding of structural behaviour and to trace the reasons for torsional features, details of this study are restricted to single-mass ductile systems. It is felt that improved understanding of the relevant behaviour would also effectively influence the designer's approach to the behaviour that may arise in multi-storey systems.

1.4 Objectives

In summary the objectives of this study are:

1. Develop a simple and rational design strategy, independent of current building code provisions, which is likely to lead to the avoidance of excessive displacement demands on particular elements resulting from system rotations.
2. Contribute to the understanding of the torsional response of ductile systems from strength rather than a stiffness-based perspective.
3. Explain how the dynamic actions of the mass rotational and translational inertia during a dynamic response influence the torsional behaviour of the systems.
4. Generalise the findings relevant to ductile systems having any plan configuration with or without mass eccentricity.
5. Establish rational relationships between stiffness and displacement capacity of a system and its constituent's elements.
6. Conduct limited experimental studies on simple structural models and predict their response with analytical models.
7. Conduct, for specific cases, a study gauging seismic excitations in directions different from the principal axes of the model system.

1.5 Scope and limitations

Chapter 2 examines factors affecting the modelling of components and their effects on the force-displacement relationship of common structural elements. It also summarizes the fundamental theory concerning single-mass asymmetric systems. Chapter 3 considers in depth the response of two and multi-element systems when no torsional strength and stiffness is provided by transverse elements. Chapter 4 extends the study on two and multi-element systems having transverse elements providing torsional and lateral resistance to the system. Chapter 5 presents experimental behaviour of torsionally unrestrained and restrained single-storey structures subjected to lateral seismic excitation. Chapter 6 summarizes a suggested design procedure

based on the understanding of the torsional issues. Chapter 7 restates the main conclusions reached in this research and identify problems considered unsolved and research needs for the future.

Chapter 2. Fundamental Relationships

2.1 Introduction

This study deals with two and multi-element ductile asymmetric systems comprising substitute wall-elements representing any lateral force-resisting element. These elements will be modelled with a realistic bilinear force-displacement relationship. Parameters are suggested to relate the plan configuration of systems to its rotational mass and to measure the effect of the mass rotational inertia on system rotations. A simple and rational design strategy is proposed which aims at quantifying the displacement ductility capacity of the system and suggests a distribution of strength among its elements to limit their displacement demands to less than their displacement capacity for zero and increasing strength eccentricities.

2.2 Design criteria

The design criteria for systems in general, including those prone to torsional behaviour to be adopted in this study, is claimed to be rational, deterministic, and simple. It is necessary to limit directly acceptable displacement demands of systems to less than their displacement capacities rather than their strengths. The displacement capacities of systems are controlled by the displacement capacities of their critical elements.

In the case of reinforced concrete structures, the displacement capacity of the elements is limited as follows:

(a) It is restricted by the verified displacement ductility capacity of components, as detailed and constructed or,

(b) The displacement capacity of the elements may be restricted by limiting storey drifts to minimize the P-Δ effect. The storey drifts should not exceed those acceptable for buildings. These storey drift limits usually vary between 0.015 and 0.025[S6] or,

(c) Storey drift limits may also restrict the displacement capacity of the elements to satisfy specific performance criteria. This is intended to limit the amount of structural or non-structural damage and provide protection to the contents of buildings [S5]. This is sometimes referred to as a serviceability limit state.

2.3 Definition of a structural system and its three dimensional characteristics

A structural system consists of a set of lateral force resisting elements providing resistance to dynamic forces and gravity loads. It also comprises a rigid diaphragm component intended to carry gravity loads and lateral force-induced actions. Elements may exhibit different lateral displacements due to torsional effects. Each element comprises one or more components to be subjected to identical lateral displacements.

For instance, consider a four-storey system displaying two lateral force-resisting elements along the *X* and *Y*-axes, as shown in Figure 2-1 and Figure 2-2. Element *(1)*, shown in Figure 2-1(a), is

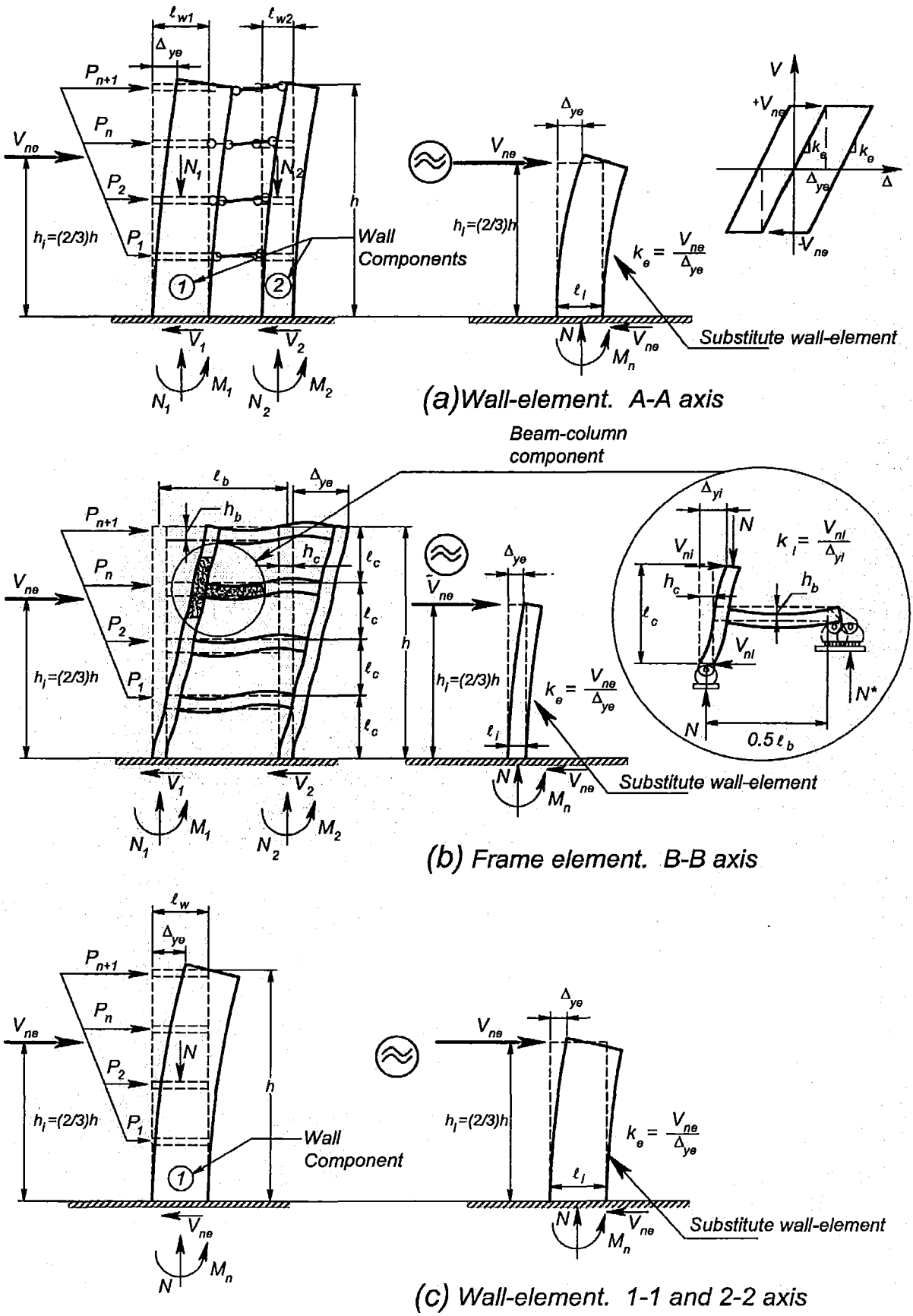

Figure 2-1. Examples of elements and their corresponding substitute wall element

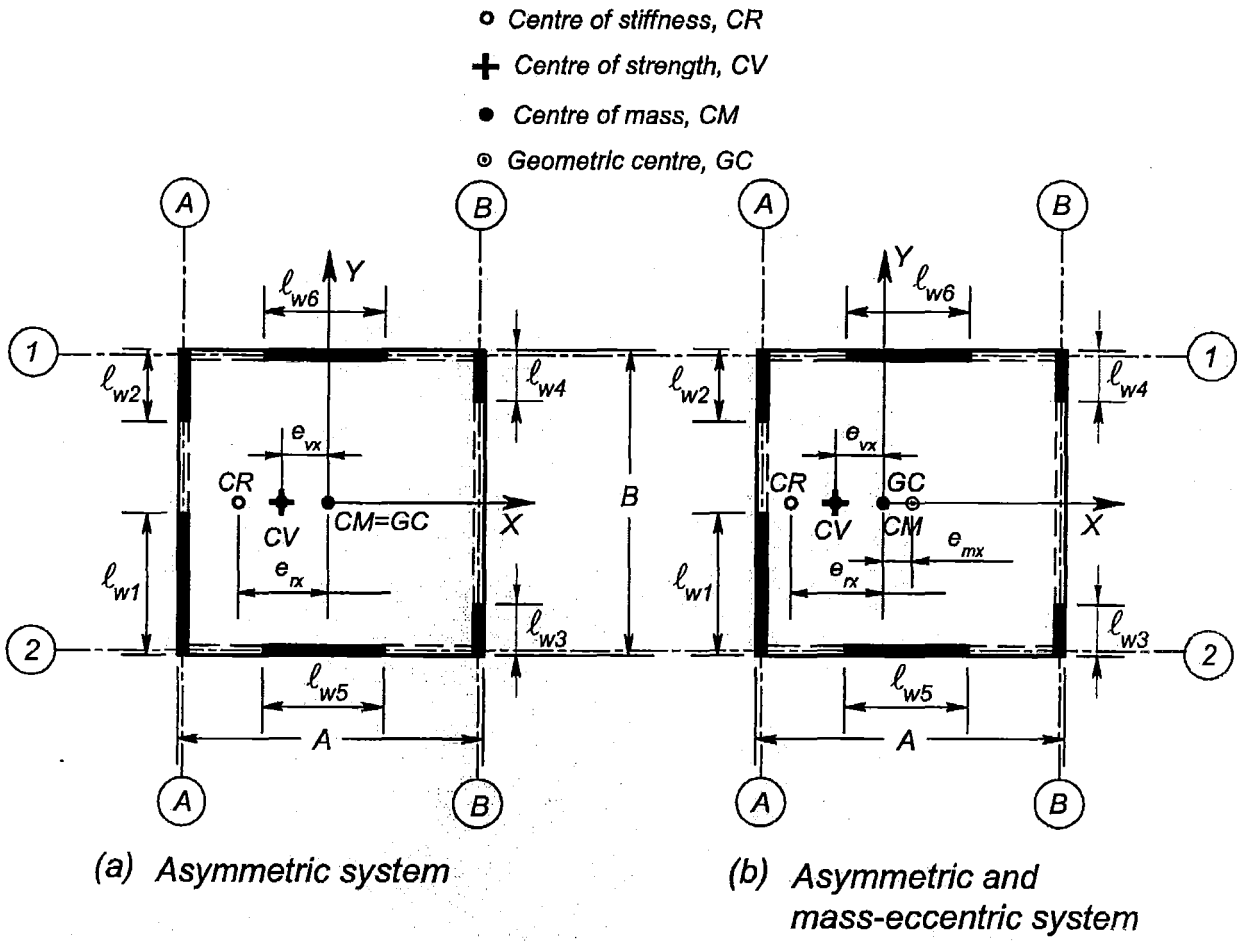

Figure 2-2. Examples of plan configurations and element distribution of a building

a wall element placed along gridline *A-A* comprising two interconnected wall components of different lengths whereas element *(2)* is a frame element; see Figure 2-1(b), comprising several beam-columns components. Elements *(3)* and *(4)*, as illustrated in Figure 2-1(c), are wall elements along gridlines *1-1* and *2-2* comprising just one wall component. For the sake of simplicity, the system is reduced to a single-mass system where the effective mass of the system associated with a triangular inverted displacement pattern [L3], M_e, is assumed concentrated at the level of the accelerated mass of the system (h_i=*2/3h*) where the centre of seismic force is assumed to act. Each element is then reduced to a substitute wall-element comprising a single wall component of height h_i and length ℓ_i; see Figure 2-1. They will have the same properties of strength, V_{ne}, nominal yield displacement, Δ_{ye}, and stiffness, k_e, of the original elements.

The geometric centre, *GC*, or centre of area of the single-mass system floor diaphragm is referred to the point that satisfies the following relationships,

$$\bar{x} = \frac{\sum A_i \bar{x}_i}{\sum A_i} \qquad \bar{y} = \frac{\sum A_i \bar{y}_i}{\sum A_i} \tag{2-1}$$

where, A_i is a fraction of the total floor area, $A_T = \sum A_i$ is the total area of the floor and $(\bar{x}_i, \bar{y}_i)$ are the location coordinates of a fraction of the floor area A_i with respect to an arbitrary reference axis.

The centre of mass, *CM*, also referred to as the centre of inertia, is the point where the mass of the single-mass system is considered concentrated. All external lateral forces are applied at that point. For the system shown in Figure 2-2(a), the centre of mass coincides with the geometric centre of the diaphragm. The system displays a mass eccentricity, e_m, if these two points do not coincide; see Figure 2-2(b). This eccentricity corresponds to the distance between the centre of mass and geometric centre.

The effective mass of the system, M_e, is assumed uniformly distributed over a rectangular plan, *(AxB)*. The rotational mass, I_m, is therefore

$$I_m = \frac{1}{12} M_e (A^2 + B^2) \tag{2-2}$$

The radius of gyration of the uniformly distributed mass, r_m, is expressed by

$$r_m = \sqrt{\frac{I_m}{M_e}} \tag{2-3}$$

The centre of strength, *CV*, which is also referred to as the centre of resistance, is the location of the resultant nominal strength of all elements in the system. The strength eccentricity, e_v, is the distance between centre of mass and centre of strength. The coordinates of the centre of strength (e_{vx}, e_{vy}) with respect to the centre of mass are

$$e_{vx} = \frac{\sum V_{ynei}\, x_i}{\sum V_{ynei}} \tag{2-4(a))}$$

$$e_{vy} = \frac{\sum V_{xnei}\, y_i}{\sum V_{xnei}} \tag{2-4(b))}$$

where (x_i, y_i) are the location coordinates of element *i*. V_{xnei} and V_{ynei} are the nominal strengths of the elements located parallel to the *X* and *Y*-axes, respectively.

The radius of gyration of strength, r_v, is defined as the square root of the ratio of torsional strength, $V_{\theta y}$ and $V_{\theta x}$, to system translational strength, V_{ns}, as shown below.

$$r_{vy} = \sqrt{\frac{V_{\theta y}}{V_{yns}}} \qquad r_{vx} = \sqrt{\frac{V_{\theta x}}{V_{xns}}} \tag{2-5}$$

where, $V_{\theta y} = \sum V_{ynei}(x_i - e_{vx})^2$ and $V_{\theta x} = \sum V_{xnei}(y_i - e_{vy})^2$ are the torsional strengths contributed only by parallel elements along the Y and X-axes, respectively. These quantities are taken with respect to the centre of strength. The strength of elements normal to their plane is considered to be zero. $V_{xns} = \sum V_{xnei}$ and $V_{yns} = \sum V_{ynei}$ are the translational strengths of the system along the X and Y-axes, respectively.

In case of single-mass elastic systems, the centre of stiffness, *CR*, is the point at which the application of a static lateral horizontal force will impose lateral displacements without generating system rotations. It is also the point that remains motionless when it is subjected to a torque. Other terms commonly encountered in the technical literature defining this point are: centre of rigidity, centre of twist, shear centre, and centre of decoupling [H1,T4]. The coordinates of this point are

$$e_{rx} = \frac{\sum k_{yei}\, x_i}{\sum k_{yei}} \qquad e_{ry} = \frac{\sum k_{xei}\, y_i}{\sum k_{xei}} \tag{2-6}$$

where k_{xei} and k_{yei} are the translational stiffness of element i along the X and Y-axes, respectively.

The radius of gyration of stiffness, r_k, is defined as the square root of the ratio of torsional stiffness, $K_{\theta y}$ and $K_{\theta x}$, to system translational stiffness, K_s.

$$r_{ky} = \sqrt{\frac{K_{\theta y}}{K_{ys}}} \qquad r_{kx} = \sqrt{\frac{K_{\theta x}}{K_{xs}}} \tag{2-7}$$

where, $K_{\theta y} = \sum k_{yei}(x_i - e_{rx})^2$ and $K_{\theta x} = \sum k_{xei}(y_i - e_{ry})^2$ are the torsional stiffness, taken with respect to the centre of stiffness, contributed only by parallel elements along the Y and X-axes, respectively. $K_{xs} = \sum k_{xei}$ and $K_{ys} = \sum k_{yei}$ are the system's translational stiffness along the X and Y-axes, respectively.

2.4 Equations of motion of structural systems

The study will focus on the inelastic seismic response of idealized single-mass models. For instance, consider the idealized system shown in Figure 2-3. It comprises two substitute wall elements along the X and Y-axis. The elements are modelled as axially inextensible spring members attached to the ground with in-plane stiffness, neglecting its out of plane and torsional stiffness. The system consists of a rigid floor diaphragm with three degree of freedom: two translational (X and Y-direction) and one rotational degree of freedom about the Z-axis. The analysis is simplified by relating the degrees of freedom of all the nodes at a floor level to the degrees of freedom of the floor diaphragm. Systems will be analytically modelled with the three-dimensional inelastic analysis program 3D-Ruaumoko [C1].

The motions of an undamped single-mass system subjected to a ground motion input, $\ddot{u}_o$, are governed by three equations of motions [S3].

$$M\,\ddot{u}_x + \sum k_{xi}\left(u_x - y_i u_\theta\right) = -M\,\ddot{u}_{xo} \qquad \textbf{(2-8(a))}$$

$$M\,\ddot{u}_y + \sum k_{yi}\left(u_y + x_i u_\theta\right) = -M\,\ddot{u}_{yo} \qquad \textbf{(2-8(b))}$$

$$I_m\,\ddot{u}_\theta - \sum k_{xi}\left(u_x - y_i u_\theta\right) y_i + \sum k_{yi}\left(u_y + x_i u_\theta\right) x_i = 0 \qquad \textbf{(2-8(c))}$$

These are obtained through equilibrium of dynamic forces along the X and Y-axes and moments about the centre of mass. In this expression, u_x and u_y, are the displacements imposed at the centre of mass along the principal axes and u_θ is the rotation of the system. The sign convention used for these equations is shown in Figure 2-3. Because the floor diaphragm is assumed infinitely rigid in-plane, the displacement at any location within the system is obtained as a combination of u_x, u_y and u_θ.

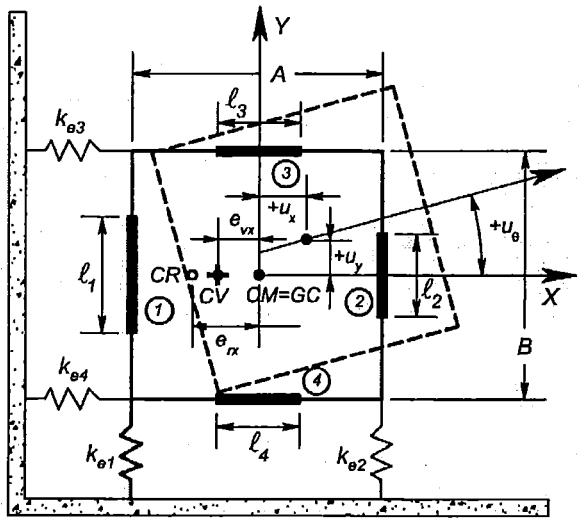

Figure 2-3. Modelling of a single-mass system for analysis purposes and sign convention

This expression can be simplified in matrix format, for elastic undamped systems, as shown below.

$$\begin{pmatrix} \ddot{u}_x \\ \ddot{u}_y \\ r_m\ddot{u}_\theta \end{pmatrix} + \begin{bmatrix} w_x^2 & 0 & -w_x^2\bar{e}_{ry} \\ 0 & w_y^2 & w_y^2\bar{e}_{rx} \\ -w_x^2\bar{e}_{ry} & w_y^2\bar{e}_{rx} & w_\theta^2 \end{bmatrix} \begin{pmatrix} u_x \\ u_y \\ r_m u_\theta \end{pmatrix} = - \begin{pmatrix} \ddot{u}_{xo} \\ \ddot{u}_{yo} \\ 0 \end{pmatrix} \qquad \textbf{(2-9)}$$

where

$$w_x^2 = \frac{K_{xs}}{M}\ ;\ w_y^2 = \frac{K_{ys}}{M}\ ;\ w_\theta^2 = \frac{K_\theta}{I_m}\ ;\ \bar{e}_{rx} = \frac{e_{rx}}{r_m}\ ;\ \bar{e}_{ry} = \frac{e_{ry}}{r_m} \qquad \textbf{(2-10)}$$

w_x, w_y and w_θ are the translational frequencies of the undamped system along the degrees of freedom of the floor diaphragm.

Equation 2-9 can be reduced even further for elastic systems exhibiting stiffness eccentricity along the *X*-axis only as shown below,

$$\ddot{u}_x + w_x^2 u_x = -\ddot{u}_{xo} \qquad \text{(2-11(a))}$$

$$\begin{pmatrix} \ddot{u}_y \\ r_m \ddot{u}_\theta \end{pmatrix} + w_y^2 \begin{bmatrix} 1 & \bar{e}_{rx} \\ \bar{e}_{rx} & \left(\frac{r_k}{r_m}\right)^2 + \bar{e}_{rx}^2 \end{bmatrix} \begin{pmatrix} u_y \\ r_m u_\theta \end{pmatrix} = -\begin{pmatrix} 1 \\ 0 \end{pmatrix} \ddot{u}_{yo} \qquad \text{(2-11(b))}$$

These expressions indicate that the vibration of the undamped system is independent along the *X*-axis whereas oscillations along the *Y*-axis and about the *Z*-axis are coupled. The parameters affecting the torsional response of elastic systems having unidirectional stiffness eccentricity are: the translational frequency along the *Y*-axis, stiffness eccentricity, and the ratio of radii of gyration of stiffness and mass.

The Newmark constant average acceleration (β=*0.25*) method [S3] is used to determine the inelastic response of the system. For this purpose, a general expression, in matrix format, comprising Eq. 2-8 and including the system's damping characteristics is solved. This expression is,

$$[M]\{\ddot{u}\} + [C]\{\dot{u}\} + [K]\{u\} = -[M]\{\ddot{u}_o\} \qquad \text{(2-12)}$$

where the mass matrix, [*M*], is diagonal because all nodes at a floor level are related to the degrees of freedom of the floor diaphragm. The damping matrix, [*C*], is assumed, for convenience, to be diagonal. The damping ratio, ζ, measuring the system's damping as a percentage of the critical damping, is assumed as *5%* for each mode of vibration unless stated otherwise. The stiffness matrix, [*K*], of ductile systems is time dependant.

A small time step, Δ_t, is required to represent accurately the input ground motion. The time step to be used is Δ_t=*0.01 sec*. This is less than the recommended value of $\Delta_t = 0.10T_s$ where T_s is the translational period with the highest mode of vibration significantly contributing to the response of the system.

2.5 Earthquake records for dynamic analyses

It is well known that due to differences in frequency content of earthquake records, diverse system responses are expected even when the earthquake records possess a similar maximum acceleration. Therefore, to examine the effect of different ground motions on the torsional response, three earthquake records were selected.

An Artificial earthquake record is considered; see Figure 2-4(a). The El Centro record is massaged to match the design acceleration spectrum for intermediate soil specified in the New Zealand loading standard[S6]. It has a duration of *20.0* seconds and exhibits a maximum acceleration and velocity of *0.36g* and *0.66 m/sec*, respectively.

The Bucharest earthquake record, shown in Figure 2-5(a), occurred *170 km* away from the epicentre at a depth of *110 km* and had a Richter magnitude of *7.1*. It has two large acceleration

amplitude pulses of *0.18g* and *0.20g*. The duration of the record is *15.0 sec.* It has a maximum ground acceleration and velocity of *0.20g* and *0.74 m/sec.*

The Kobe earthquake record, illustrated in Figure 2-6(a), took place near the city of Kobe, Japan at a depth of *16.0 km* and had a Richter magnitude of *7.1.* It exhibits large cycles of ground accelerations between *4.0* and *9.0* seconds. The duration of the record is *20.0 sec.* The maximum acceleration and velocity of the record is *0.84g* and *0.92m/sec*, respectively.

2.6 Response spectra of the chosen earthquake records and scaling procedure

The elastic and inelastic response spectra are used to identify distinctive characteristics of each earthquake record on the response of single degree of freedom systems.

The response spectra of elastic single-degree-of-freedom systems subjected to the earthquake records described in Section 2.5 are shown in Figure 2-4(b) and (c), Figure 2-5(b) and (c), and Figure 2-6(b) and (c). These spectra are derived using the SPECTRA program [C4] for damping ratios of ζ=*5%, 10%, 20%, and 40%.* In general, all three-ground motions exhibit, as expected, a reduction in spectral accelerations and displacements as the damping ratio increases. The Artificial earthquake response spectra show, as expected, spectral accelerations matching the design spectrum for intermediate soil of the New Zealand loading standard [S6]. Displacements increase linearly as the system translational period increases. The Bucharest earthquake response spectra present a quite different response. Two peak spectral accelerations are observed at *0.5* and near *1.5* seconds. The spectral displacements increase linearly as the translational period increases. However, for the first *0.8* seconds the displacements are essentially the same and independent of the damping ratio. The Kobe earthquake response spectra exhibit two big spectral accelerations for translational periods of *0.4* and *0.8* seconds. The spectral displacements increase linearly up to a period of *1.0* seconds and thereafter they remain essentially constant.

Figure 2-4(d) and (e), Figure 2-5(d) and (e) and Figure 2-6(d) and (e) show the response spectra of inelastic single-degree-of-freedom systems subjected to the three earthquake records mentioned before. The system's hysteretic behaviour is modelled using a simple elasto-plastic force-displacement relationship, as shown in Figure 2-7(a). These spectra are derived using the INSPECT program [C3] for a *5%* damping ratio and assuming displacement ductility demands of $\mu_{\Delta s}$=*1.0,* $\mu_{\Delta s}$=*3.0, and* $\mu_{\Delta s}$=*5.0.* All three accelerograms exhibit a reduction in the spectral acceleration as the displacement ductility demand increases. The Artificial earthquake record shows similar displacements for the elastic and inelastic system up to a period of T_s=*0.5*, thereafter the spectral displacements increase as the displacement ductility factor increases. The Bucharest record has the peculiarity that after the first *1.5* seconds the displacements with the elastic system are larger than that of inelastic systems. The Kobe record also generates a similar displacement behaviour beyond the translational period of *0.8* seconds.

The earthquake records described before will be scaled to impose on asymmetric systems, to be described in subsequent sections, specific values of displacement ductility demands. This scaling procedure will help identify differences in response between earthquakes, in particular, those concerning with torsional motions. The procedure contrasts with the commonly used approach where the maximum elastic response acceleration is reduced by a reduction factor,*R*,[G2,H3,R2].

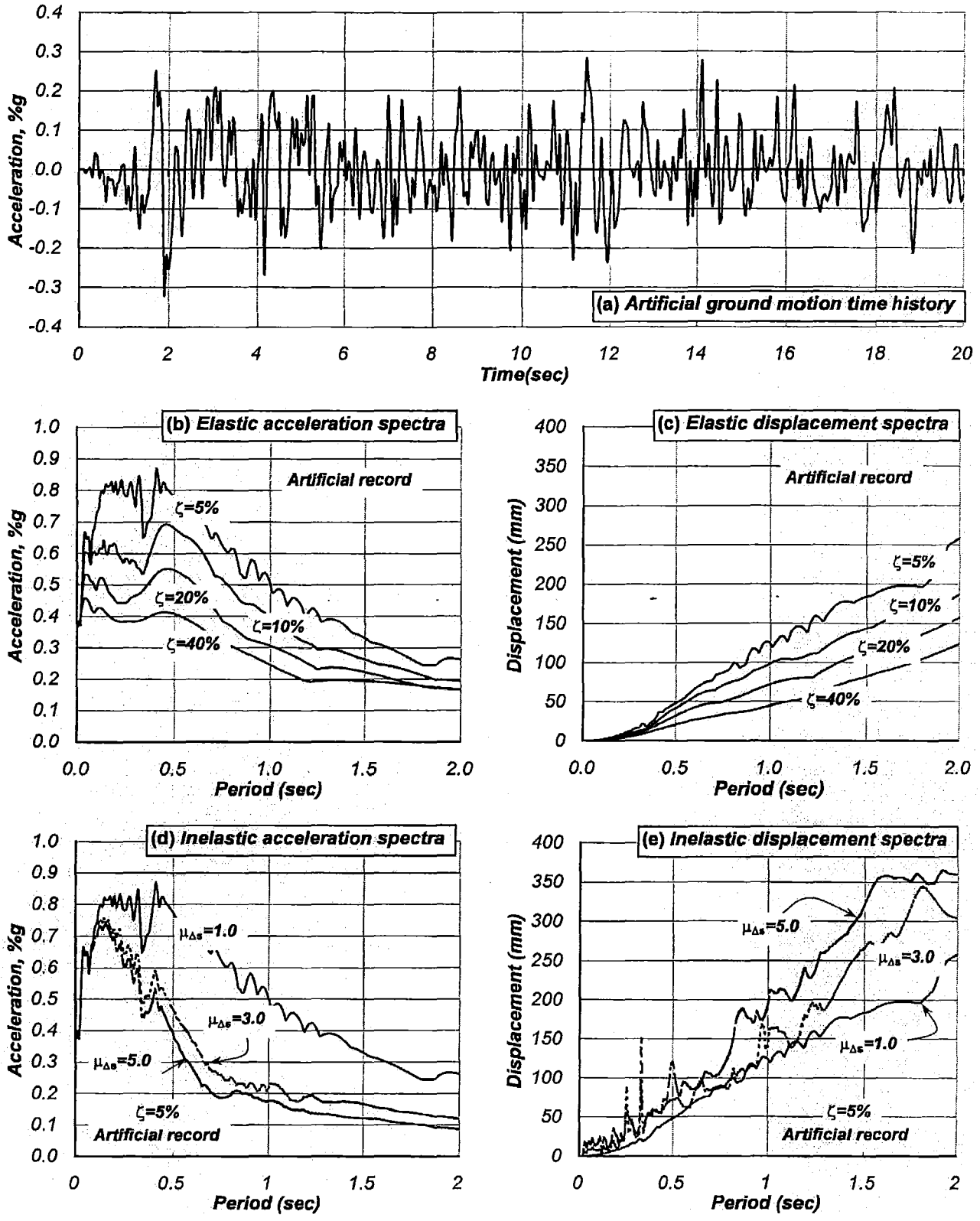

Figure 2-4. Elastic and inelastic response spectra of SDOF systems subjected to the Artificial earthquake record

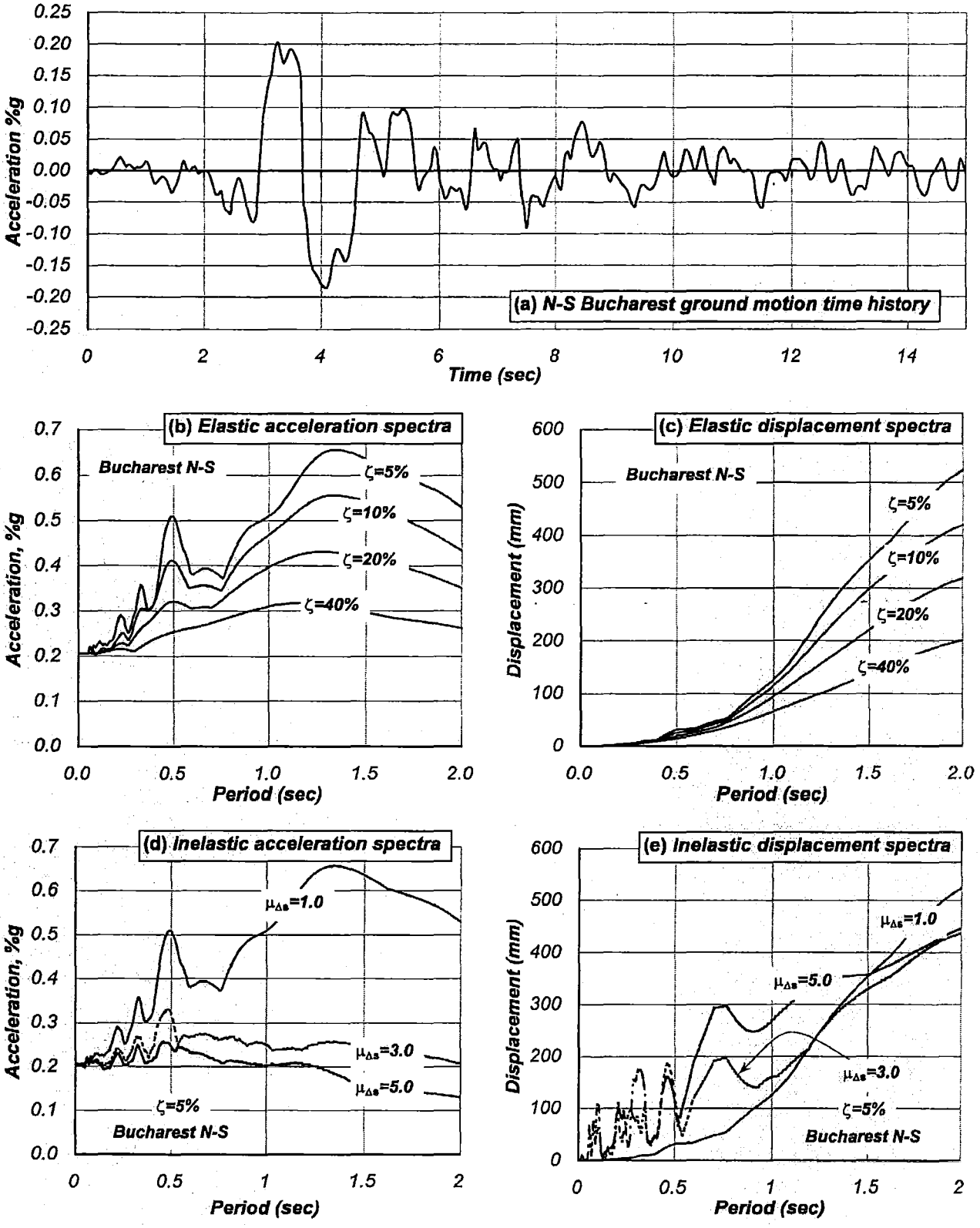

Figure 2-5. Elastic and inelastic response spectra of SDOF systems subjected to the N-S component of Bucharest earthquake record

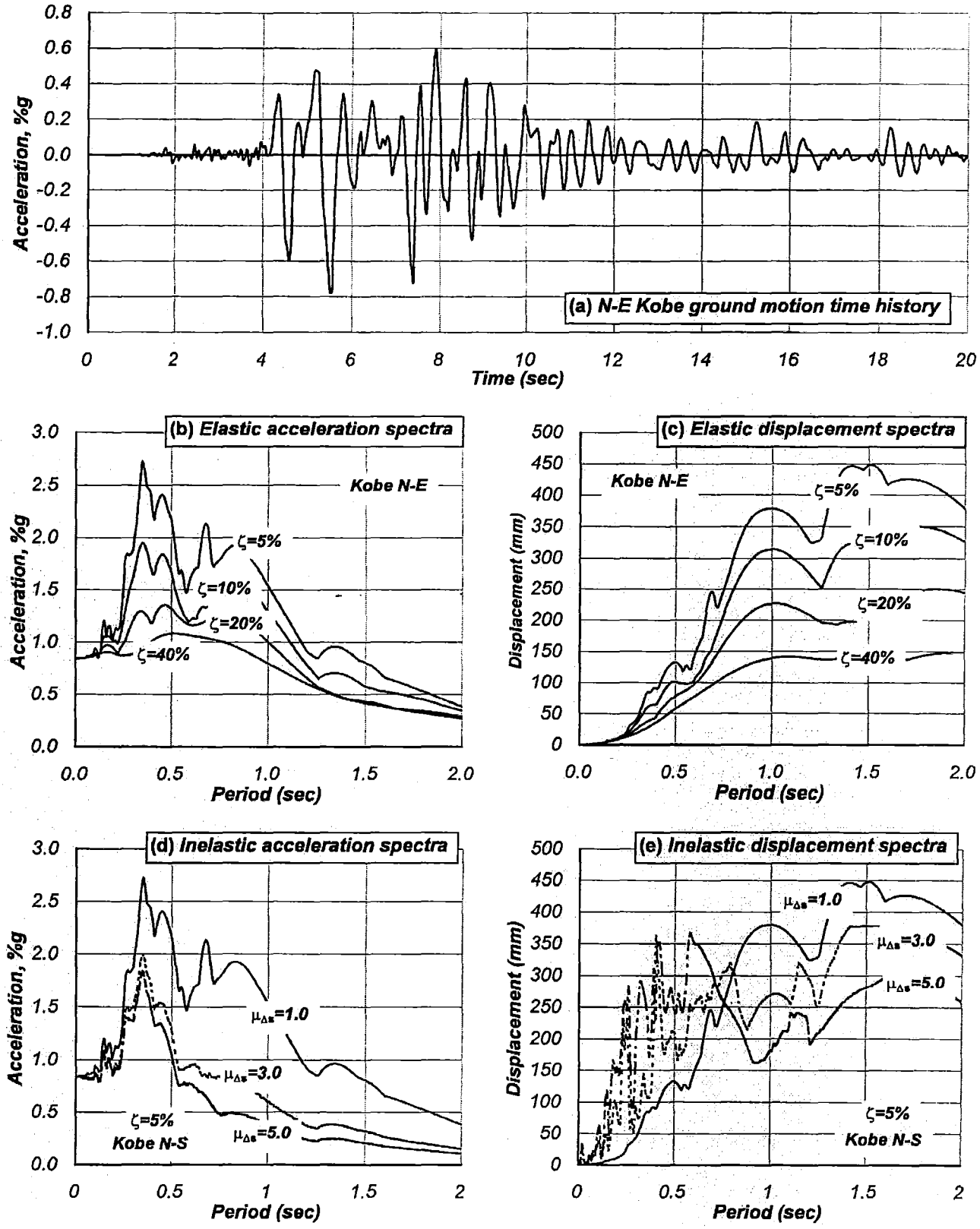

Figure 2-6. Elastic and inelastic response spectra of SDOF systems subjected to the N-E component of Kobe earthquake record

The drawback of the reduction factor is that it does not guarantee a displacement ductility demand of the same order on systems having different translational periods when subjected to different ground motions having a similar maximum acceleration.

2.7 Modelling the inelastic behaviour of structural components

In the research concerning the inelastic response and behaviour of structural asymmetric systems, it has been a common practice to model the non-linear behaviour of structural components and elements with simple bilinear force-displacement relationships. The shape of this bilinear relationship will depend on the component's material (composite or homogenous), its strain hardening characteristics and the means of energy dissipation (bending, shear, and/or axial inelastic deformations and axial buckling). The study will consider four common force-displacement simulation representing inelastic flexural deformations of reinforced concrete and structural steel components.

(a) The elastic-perfectly plastic simulation shown in Figure 2-7(a), represents the simplest model for the hysteretic bilinear behaviour of reinforced concrete and steel components and elements. It assumes the same loading and unloading stiffness. The model does not include strain hardening or stiffness degradation.

(b) The bilinear model illustrated in Figure 2-7(b) has the characteristics of the elastic perfectly plastic model. However, it also includes strain-hardening characteristics of the component by specifying its post-yielding stiffness.

(c) The modified Takeda model [O1] shown in Figure 2-7(c) has specific characteristics suitable for the modelling of reinforced concrete components by approximating the effects of stiffness degradation and strain hardening.

(d) The Al-Bermani model [Z1] exhibited in Figure 2-7(d) reflects a smooth transition between the elastic and post-yielding stiffness. It is particularly useful to represent the hysteretic behaviour of steel components. However, it does not consider stiffness degradation.

2.8 Properties of structural components

2.8.1 Nominal yield curvature

In seismic design, it is considered satisfactory to represent the non-linear moment-curvature relationship of a section with a bilinear relationship. Two particular points are of interest: the yield curvature, ϕ'_{yi}, and the nominal yield curvature, ϕ_{yi} as shown in Figure 2-8.

The yield curvature, ϕ'_{yi}, associated with the onset of yielding, is expressed as,

$$\phi'_{yi} = \frac{\varepsilon_y}{\xi \ell_i} \tag{2-13}$$

where ε_y is the tensile yield strain of the material, i.e. the reinforcing steel, and $\xi \ell_i$ is the depth of the neutral axis from the extreme fibre in tension of the section, as shown in Figure 2-8(b).

The other point of practical interest is the nominal yield curvature, ϕ_{yi}. This is a linear extension of the yield curvature. It is expressed as,

$$\phi_{yi} = \left(\frac{M_n}{M_y}\right)\phi'_{yi} \tag{2-14}$$

where M_n is the nominal flexural strength of the section associated with a nominal yield curvature of $\phi_{yi} = 7\phi'_{yi}$ and M_y is the flexural yield strength associated with the curvature at the onset of yielding, ϕ'_{yi}.

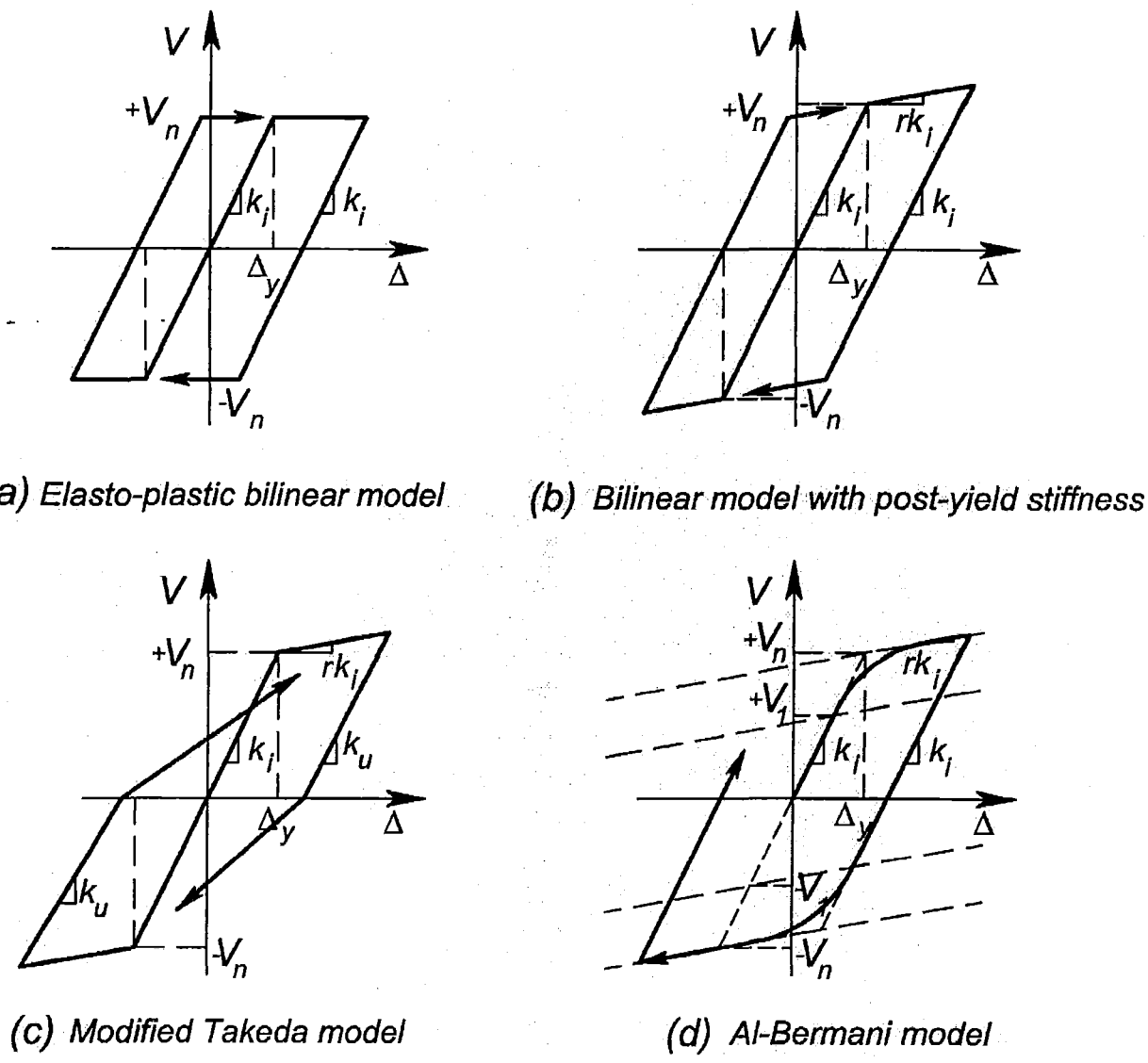

Figure 2-7. Examples of force-displacement relationships used in this study

By substituting Eq. 2-13 into Eq. 2-14, the nominal yield curvature results to be

$$\phi_{yi} = \left(\frac{M_n}{\xi M_y}\right)\frac{\varepsilon_y}{\ell_i} = \eta\frac{\varepsilon_y}{\ell_i} \tag{2-15}$$

where η is the curvature coefficient suggested by Paulay [P11] that depends on the shape of the cross section and the distribution of the reinforcement.

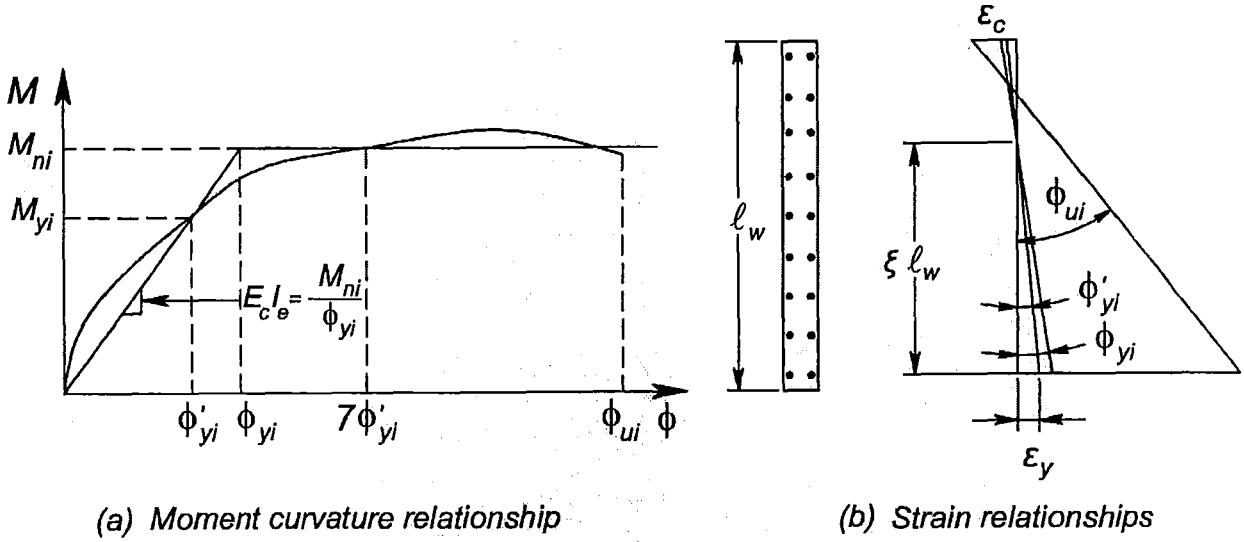

Figure 2-8. Realistic force-displacement relationship

The curvature coefficient, η, enables a realistic definition of the bilinear force-displacement relationship of ductile components. Paulay [P11] has suggested approximate values of curvature coefficient for structural steel and reinforced concrete components with different cross section. The results are summarized in Table 2-1. Some of these results are based on moment-curvature analyses carried out within this project; see Appendix *A*. These results were obtained using practical values of the ratios of distributed, ρ_ℓ, and boundary reinforcement, ρ_b, and axial load ratios, $N/(f'_c A_g)$, encountered in actual buildings.

Table 2-1. Curvature coefficients, η, for structural steel and reinforced concrete components [P11]

1	2	3	4	5	6	7	8	9
Section Geometry		Steel D	Steel D	D	D RC	RC	RC	RC
Strain Pattern	εy	εy	0.66D	≈0.75D	≈0.80D	≈0.90D	≈0.94D	≈0.70D
Stress pattern at Ultimate	fy	fy	fy	fy f'c	fy f'c	fy f'c	fy f'c	fy f'c
ξ	0.50	0.50	≈0.66	≈0.75	≈0.80	≈0.90	≈0.94	≈0.70
M_n/M_y	1.5	≈1.15	≈1.77	≈1.50	≈1.40	≈1.25	≈1.32	≈1.27
η	3.0	≈2.3	≈2.7	≈2.0	≈1.8	≈1.4	≈1.4	≈1.8

Note: Further details are presented in Appendix A.

Priestley [P16] has also suggested a similar coefficient, κ, for reinforced concrete sections, as shown in Table 2-2.

Table 2-2. Curvature coefficients, κ, for some reinforced concrete components[P16]

Reinforced concrete components	$\kappa = \phi_y \frac{\ell}{\varepsilon_y}$
Circular Column	*2.45±15%*
Rectangular Column	*2.14±10%*
Rectangular Wall	*2.0±15%*
Flanged, Rectangular Beams	*1.7±10%*

In the case of reinforced concrete sections, the yield curvature can be readily determined using the properties of a transformed concrete section with given geometry and with known quantity and arrangement of reinforcement. This procedure, however, is not suitable for design purpose particularly when reinforcement details are not yet known. The significance of Eq. 2-15 is that with the aid of the approximate value of curvature coefficient and nominal yield curvature, subsequent nominal elastic displacements, Δ_e, can be readily estimated. An accurate curvature evaluation can be made after the design and the detailing of the structure has been completed. This, however, will seldom be necessary because, as Appendix *A* will show, the nominal yield curvature is insensitive to the nominal flexural strength assigned to a section.

The nominal yield curvature of a section is a characteristic independent of the nominal flexural strength. It can be readily used in current design practice. For the analysis of the full detailed structure, with known strength properties, the traditional expression of curvature $\phi=M/EI$, can be rearranged to obtain an effective second moment of area, I_e, as a fraction of the gross second moment of area, I_g, i.e.,

$$I_e = \left[\frac{M_n}{\phi_{yi} E_c I_g}\right] I_g \qquad \text{(2-16)}$$

This expression indicates that the effective moment of inertia can be estimated only after the nominal flexural strength has been assigned to the section. It also depends on the nominal yield curvature associated with the corresponding curvature coefficient. The effective moment of inertia will enable realistic predictions of component displacements. Displacements obtained using the gross section moment of inertia or reduced values, as recommended elsewhere for cracked reinforced concrete sections [S7], will significantly underestimate the actual displacements relevant to limit states in seismic design.

2.8.2 Traditional and realistic relationship of component properties

Section 2.8.1 has questioned the traditional relationship between nominal flexural strength, M_n, flexural rigidity, E_cI_e, and nominal yield curvature, ϕ_{yi}. The common assumption that the flexural rigidity of a reinforced concrete section is independent of its flexural strength turns out to be unrealistic. In contrast, it was shown that the flexural rigidity of a section is proportional to

its nominal flexural strength while its nominal yield curvature is a material and geometric property insensitive to the nominal flexural strength.

In both research and structural design, it is common practice to consider the flexural rigidity of a section as independent of its flexural strength. Figure 2-9(a) shows the effective height of a cantilever reinforced concrete wall component subjected to a concentrated force at the top. Once the dimension of the component cross section is known, its flexural rigidity is readily obtained. The second moment of area is calculated based on the gross section, in the case of uncracked reinforced concrete sections, or as a fraction of it in the case of cracked sections. With this traditional approach, the flexural rigidity of the section is considered a constant and independent of its flexural strength. According to Figure 2-9(b), the nominal yield curvature of the section is dependant on the flexural strength. An increase in flexural strength from M_{n1} to M_{n2}, due to an increase in reinforcement content, is believed to increase the nominal yield curvature from ϕ_{y1} to ϕ_{y2}. The flexural rigidity remains unchanged.

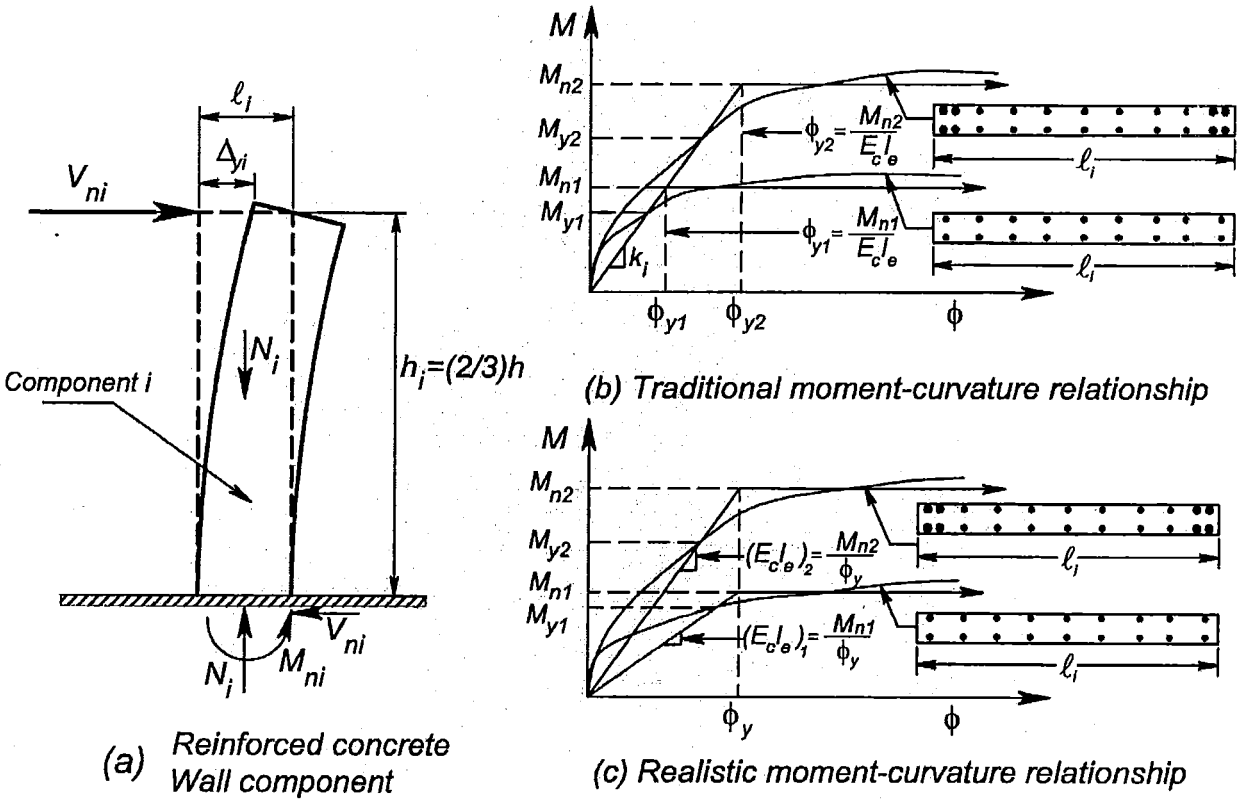

Figure 2-9. Moment-curvature relationships for cantilever wall components

In contrast, Section 2.8.1 has demonstrated that for reinforced concrete (composite material) sections the flexural rigidity and the flexural strength are not independent parameters. In addition, the nominal yield curvature depends solely on the geometry of the components cross-section and the reinforcement tensile yield strain. Figure 2-9(c) shows the bilinear modelling of the section based on this realistic relationship. An increase in flexural strength form M_{n1} to M_{n2} generates a direct increase in flexural rigidity while the nominal yield curvature remains essentially unchanged. This study will consider this realistic relationship to model the elements of the asymmetric systems to be examined.

2.8.3 Nominal yield displacement

The nominal yield displacement, Δ_{yi}, of a component is associated with the attainment of the nominal yield curvature in the plastic hinge region. The nominal yield displacement of a cantilever reinforced concrete wall component is,

$$\Delta_{yi} = C\phi_{yi}h_i^2 \tag{2-17}$$

where ϕ_{yi} is the nominal yield curvature as established by Eq. 2-15, h_i is the effective height of the component and C is the lateral force coefficient quantifying the distribution pattern of the lateral forces. For example, for cantilever components, $C=11/40$ for an inverted triangular force pattern and $C=1/3$ for a concentrated force at the top of the component.

By substituting the corresponding nominal yield curvature into Eq. 2-17, the nominal yield displacement is

$$\Delta_{yi} = C\eta\varepsilon_y h_i A_{rw} \tag{2-18}$$

where η is the curvature coefficient, ε_y is the yield strain of the material and $A_{rw}=h_i/\ell_i$ is the effective aspect ratio of the wall component. In accordance with assumptions made with respect to Eq. 2-15, the nominal yield displacement of a component is also insensitive of strength.

In most buildings, it is likely that all components will have the same effective height, h_i. The cross section of the cantilever component, the lateral force pattern coefficient and the yield strain of the material or reinforcement are assumed to be constant. Therefore, the relative nominal yield displacement can be simplified to

$$\Delta_{yi} = \left[C\eta\varepsilon_y h_i^2\right]\frac{1}{\ell_i} \propto \frac{1}{\ell_i} \tag{2-19}$$

This simple expression can be used to evaluate the relative displacements and hence displacement ductility demands on the components. This considers flexural deformations only. Additional deformations due to slip at anchorages, elastic elongation of reinforcement and shear deformations of the wall may also need to be considered in a similar way as suggested for the beam-column components [P20].

2.8.4 Limiting drift and displacement ductility capacity of cantilever wall components

The displacement ductility capacity, $\mu_{\Delta i}$, of a cantilever wall component is the ratio of its displacement capacity and nominal yield displacement, as shown below.

$$\mu_{\Delta i} = \frac{\Delta_{ui}}{\Delta_{yi}} \tag{2-20}$$

The displacement capacity of the wall component may be limited by material strain limits or it may be further restricted by codified drifts limits, associated with specific performance criteria, as described in Section 2.2. At this stage, the knowledge of its seismic strength is not required [P11].

Figure 2-10 shows two wall components subjected to concentrated lateral force at the top and an inverted triangular force pattern, respectively. The nominal yield displacement of walls, better expressed as a nominal yield drift, depends on the lateral force pattern and is expressed as,

$$\delta_{yi} = \frac{\Delta_{yi}}{h_i} = C\phi_{yi}h_i \qquad \textbf{(2-21)}$$

where *C=1/3* is for a concentrated force at the top and *C=11/40* is for an inverted triangular force pattern.

Another convenient expression is the nominal yield drift angle, θ_{yi}, which is the angle of the slope tangent to the elastic displacement curve at top of the wall, as shown in Figure 2-10, and expressed as,

$$\theta_{yi} = 1/2\phi_{yi}h_i \textbf{ (Concentrated top force)} \qquad \textbf{(2-22(a))}$$

$$\theta_{yi} = 3/8\phi_{yi}h_i \textbf{ (Triangular force pattern)} \qquad \textbf{(2-22(b))}$$

The nominal yield drift and its associated nominal yield drift angle are related. This relationship is,

$$\theta_{yi} = (3/2)\delta_{yi} \textbf{ (Concentrated top force)} \qquad \textbf{(2-23(a))}$$

$$\theta_{yi} = (15/11)\ \delta_{yi} \textbf{ (Triangular force pattern)} \qquad \textbf{(2-23(b))}$$

The ductility capacity of the wall component, in terms of drifts, is

$$\mu_{\Delta i} = \frac{\delta_{ui}}{\delta_{yi}} \qquad \textbf{(2-24)}$$

It might happen that, for an expected displacement ductility capacity associated with material strain limits, components with a large nominal yield drift may end up with an excessive drift exceeding codified limits. For instance, it may exceed the drift limits of *0.015* to *0.025* as recommended for buildings [S6] unless performance based criteria require a smaller displacement [S5]. This issue can be evaluated with an expression relating the displacement ductility capacity of the cantilever component as a function of codified drift limits. This may be derived with Eqs 2-22, 2-21 and 2-15 leading to an expression function of the lateral force coefficient pattern.

$$\mu_{\Delta i} = \frac{\delta_{ui}}{C\eta\varepsilon_y A_{rw}} \qquad \textbf{(2-25)}$$

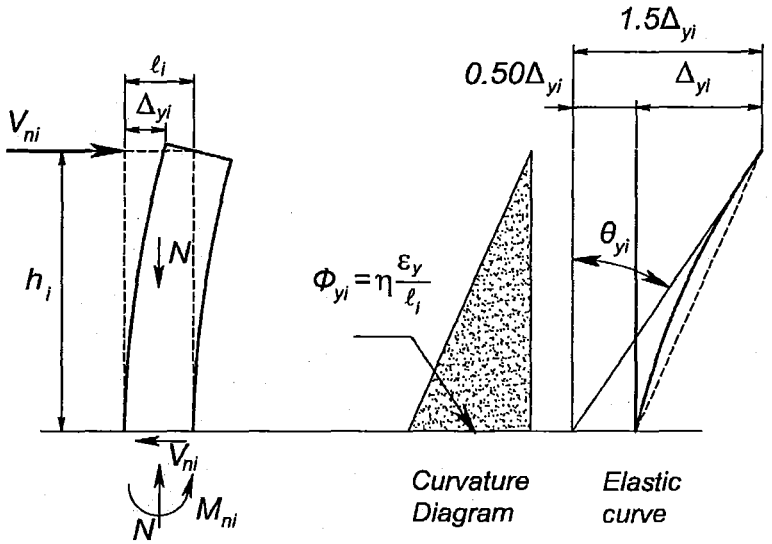

(a) Cantilever component subjected to a top lateral force

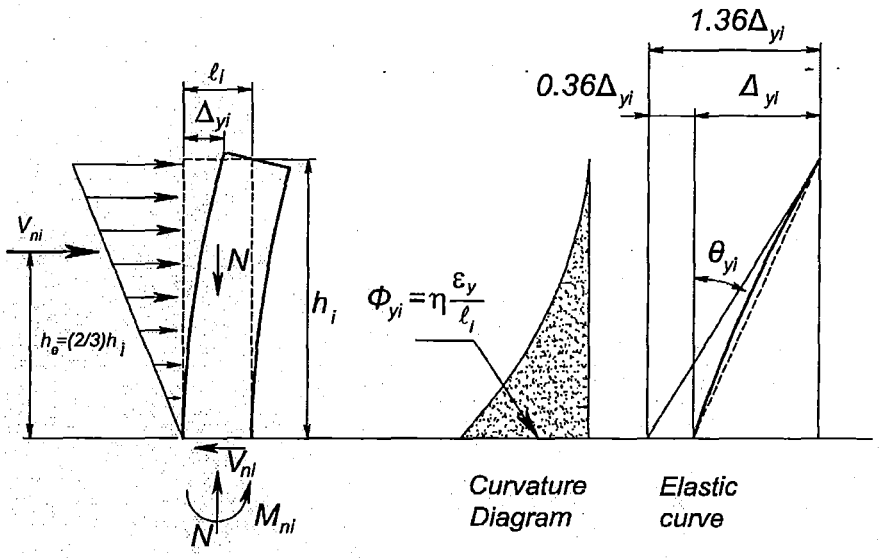

(b) Cantilever component subjected to an inverted triangular lateral force

Figure 2-10. Nominal yield drift of a cantilever wall component

For instance, by substituting, into Eq. 2-23, the curvature coefficient of a rectangular reinforced concrete wall section, $\eta=1.8$, and the lateral force pattern coefficient for the walls, as shown in Figure 2-10, the displacement ductility capacity results in

$$\mu_{\Delta i} = \frac{1.67\delta_{ui}}{\varepsilon_y A_{rw}} \text{ (Concentrated top force)} \qquad \text{(2-26(a))}$$

$$\mu_{\Delta i} = \frac{2.02\delta_{ui}}{\varepsilon_y A_{rw}} \text{ (Triangular force pattern)} \qquad \text{(2-26(b))}$$

Based on this expression, Figure 2-11 shows the usable displacement ductility capacity of both wall components for a drift limit of $\delta_{ui}=0.025$ and increasing yield strain e_y, i.e., increase in yield strength of reinforcement. It is evident that the displacement ductility capacity reduces as the aspect ratio is increased.

In terms of structural design practice, a reduction of the displacement ductility capacity implies an increase in base shear and hence the need for additional strength. The economic benefit of using higher-grade reinforcement is thus largely cancelled [P11].

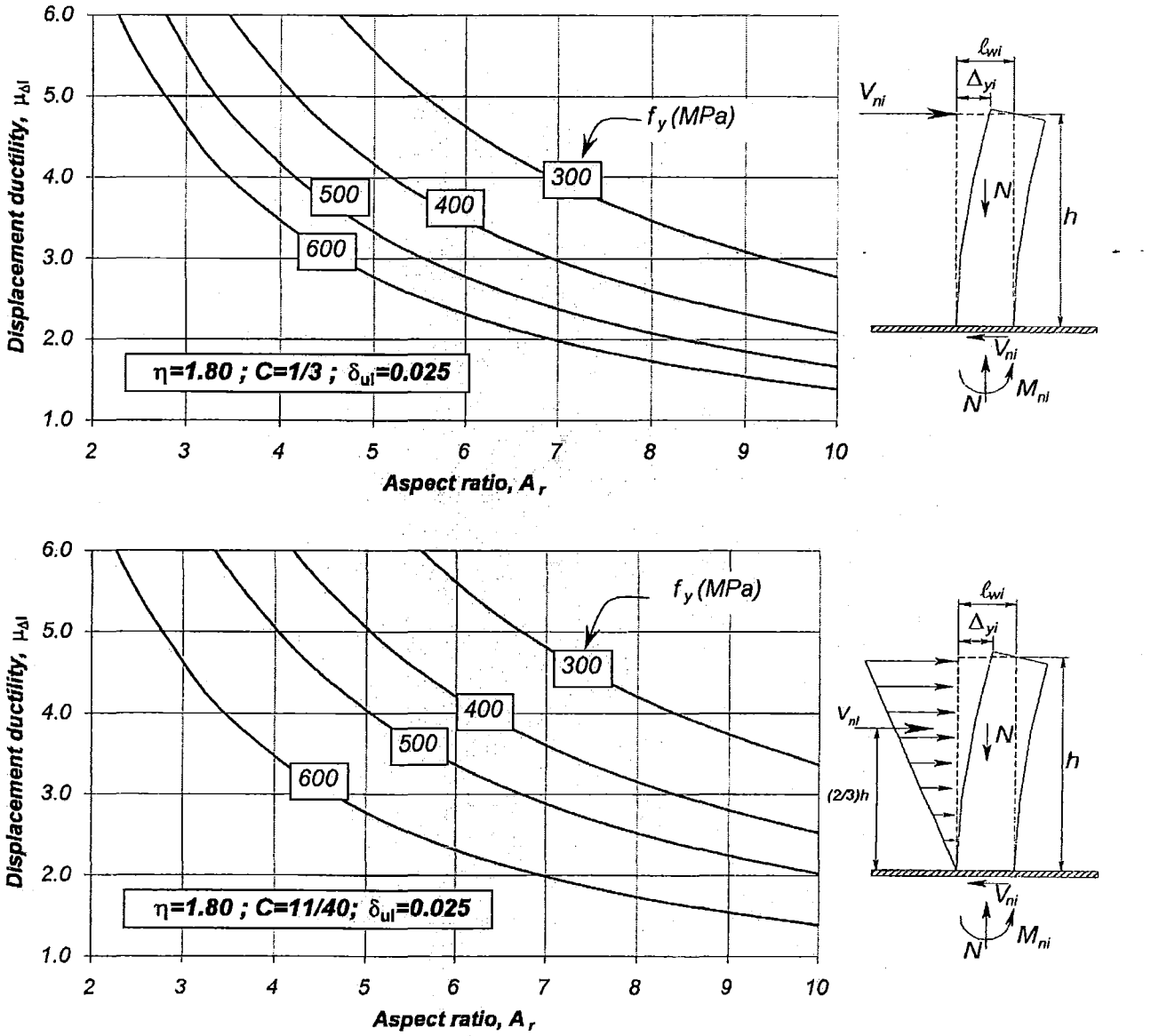

Figure 2-11. Limitations on the displacement ductility capacity of cantilever wall components

2.8.5 Component stiffness

The component stiffness, k_i, is taken as the ratio of its nominal strength, V_{ni}, to nominal yield displacement, Δ_{yi}. It indicates that stiffness is not a constant property, as traditionally assumed, and is dependent of the component's nominal strength.

$$k_i = \frac{V_{ni}}{\Delta_{yi}} \tag{2-27}$$

2.9 Properties of structural elements

2.9.1 Assignment of strength to components of an element

The usual distribution of element strength in proportion to the stiffness of the components is no longer necessary because the nominal yield displacement of a component is independent of strength. Element strength can be assigned in any way to benefit the structural response of the system. As an example, Paulay [P11] has suggested a strength distribution in proportion to the wall components length squared, $V_{ne} \propto \ell_w^2$ because it will assign a similar reinforcement ratio to each component.

2.9.2 Structural element

A structural element is a set of interconnected components subjected to the same lateral displacement, as shown in Figure 2-2.

The element nominal strength, V_{ne}, is simply the sum of the nominal strengths of the components, i.e.,

$$V_{ne} = \sum V_{ni} \tag{2-28}$$

The element stiffness, k_e, may then be defined as the sum of stiffness of all the components

$$k_e = \sum k_i \tag{2-29}$$

The nominal yield displacement of the element, Δ_{ye}, may be approximated as,

$$\Delta_{ye} = \frac{V_{ne}}{k_e} \tag{2-30}$$

The nominal yield displacement of an element is a reference displacement that enables a bilinear force-displacements modelling to be used, as shown in Figure 2-12. It is hardly affected by the distribution of strength to components of the element, as the example provided in Section 2.9.3

will show. It does not contradict the fundamental property established in Section 2.8.3 where the nominal yield displacement of a component was shown to be insensitive to strength.

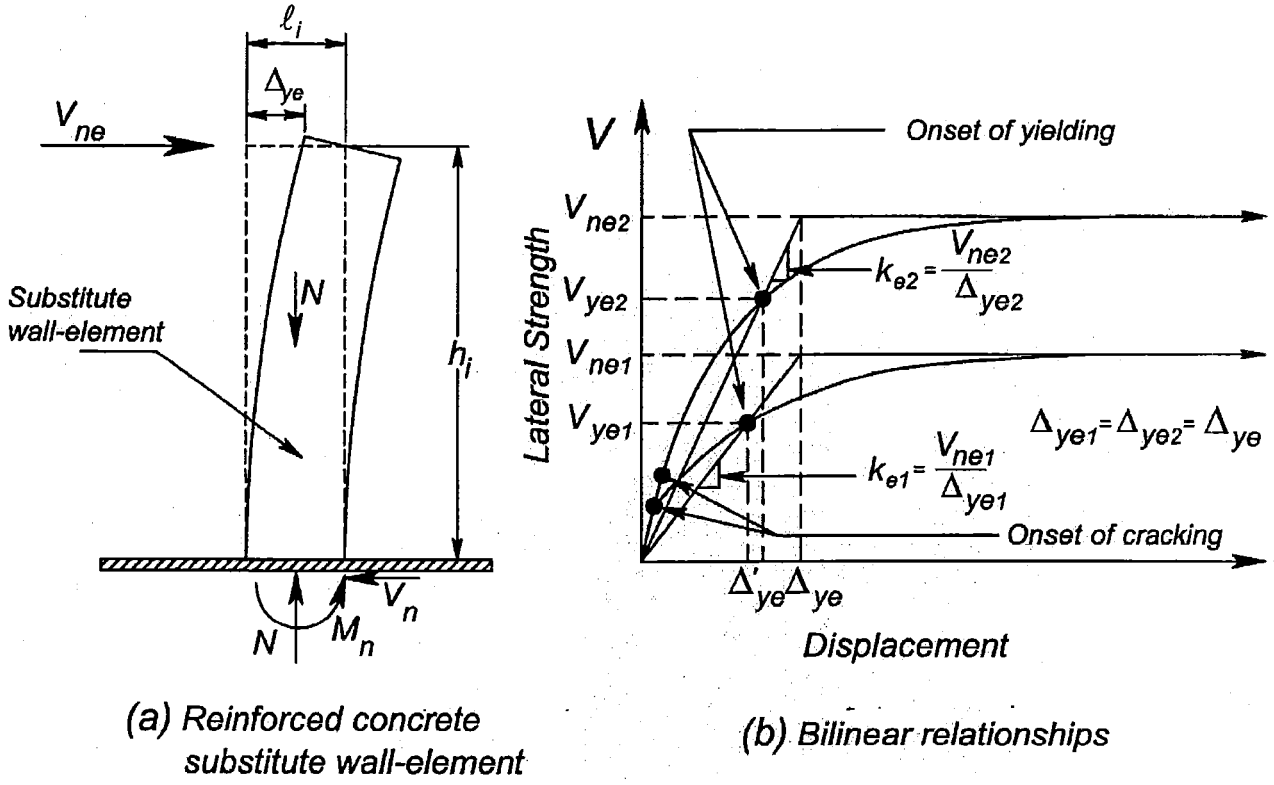

Figure 2-12. Bilinear force-displacement modelling of substitute elements

2.9.3 Example of a wall element

Paulay [11] has extensively used an example of an element comprising several interconnected cantilever wall components to show the applicability of Eqs 2-26 to 2-28 to estimate elements' stiffness and nominal yield displacements and to derive its displacement and ductility capacity. This example is repeated here to clarify the interpretation of element properties.

The wall element shown in Figure 2-13 consists of four interconnected reinforced concrete wall components. The rectangular walls have identical thickness and height. The relative lengths units of the wall components are $\ell_{w1}=1.0$, $\ell_{w2}=1.26\ell_{w1}$, $\ell_{w3}=1.59\ell_{w1}$ and $\ell_{w4}=2.0\ell_{w1}$. The element is subjected to an inverted triangular lateral force with a unit resultant base shear acting at the level of the accelerated mass. Interconnections will ensure identical lateral displacements of wall components at all levels.

The nominal yield displacement of the wall components is readily derived with Eq 2-19. It is a property independent of strength, as already explained in Section 2.8. For ease in the derivation of the component's nominal yield displacement lets assume that the product of the variables into the brackets of Eq 2-19 is a constant equal to unity, i.e., $[C\eta\varepsilon_y h^2]=1.0$. Also, consider the relative values of wall component's length previously provided as the actual length of the wall components. According to Eq 2-19, the nominal yield displacement of the components is equal to the inverse of the wall length. Hence, the nominal yield displacement of the wall components is $\Delta_{y1}=1/1.0=1.0$, $\Delta_{y2}=1/1.26=0.79$, $\Delta_{y3}=1/1.59=0.63$ and $\Delta_{y4}=1/2.0=0.50$.

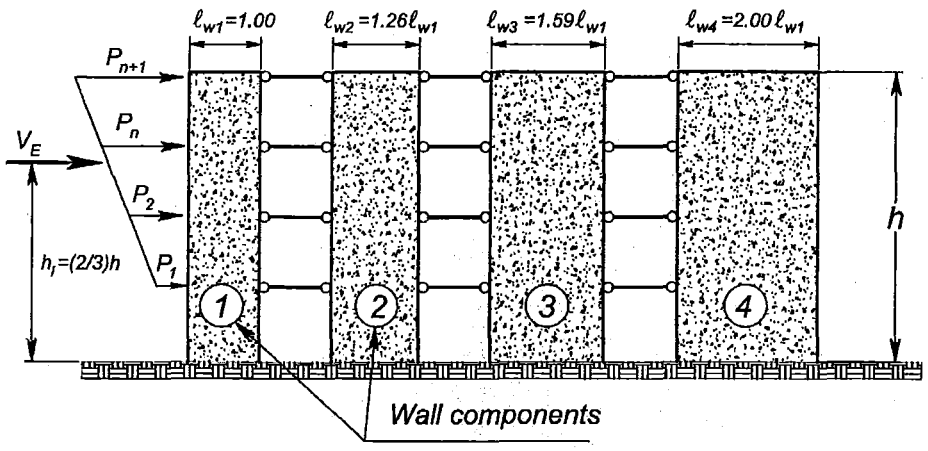

Figure 2-13. Example of interconnected reinforced concrete wall components

This example also examines the effect of the strength distribution on the element's stiffness and its nominal yield displacement. For this purpose, two arbitrary distributions of strength are considered:

(a) element strength is distributed in proportion to the component's flexural rigidity or stiffness, as it is traditionally undertaken and

(b) element strength is distributed in proportion to the component's length squared $V_{ne} \propto \ell_{wi}^2$ as suggested elsewhere [P11].

In the first alternative, element strength is distributed in proportion to the component's flexural rigidity or stiffness, i.e., in proportional to the element length cube, as shown below

$$V_{ne} \propto k_i = \frac{3EI}{h^3} \propto \ell_{wi}^3 \tag{2-31}$$

It is widely accepted that if element strength is assigned in this manner, all components will yield simultaneously. This situation is because stiffness is assumed a constant once the dimensions of the walls are known. The element strength is subsequently assigned to the components in proportion to their stiffness. The nominal yield displacement of each component is simply the ratio of its strength and stiffness.

However, it has been shown in Section 2.8 (see Eq 2-19) that the above is true only if the lengths of the wall components are identical.

Figure 2-14(a) shows the force-displacement relationship of the element and its components when a unit base shear is distributed according to $V_{ne} \propto \ell_{wi}^3$. The nominal yield displacement and stiffness of the wall element is $\Delta_{ye}=V_{ne}/k_e=0.58$ and $k_e=\sum k_i=\sum V_{ni}/\Delta_{yi}=1.725$, respectively.

It has been recently suggested that distributing the element strength to its wall components in proportion to $V_{ne} \propto \ell_{wi}^2$ has the advantage of providing approximately the same reinforcement ratios. Figure 2-14(b) shows the case when a unit base shear is distributed in this fashion. It

leads to an element nominal yield displacement and stiffness of $\Delta_{ye}=0.61$ and $k_e=\sum k_i=\sum V_{ni}/\Delta_{yi}=1.65$.

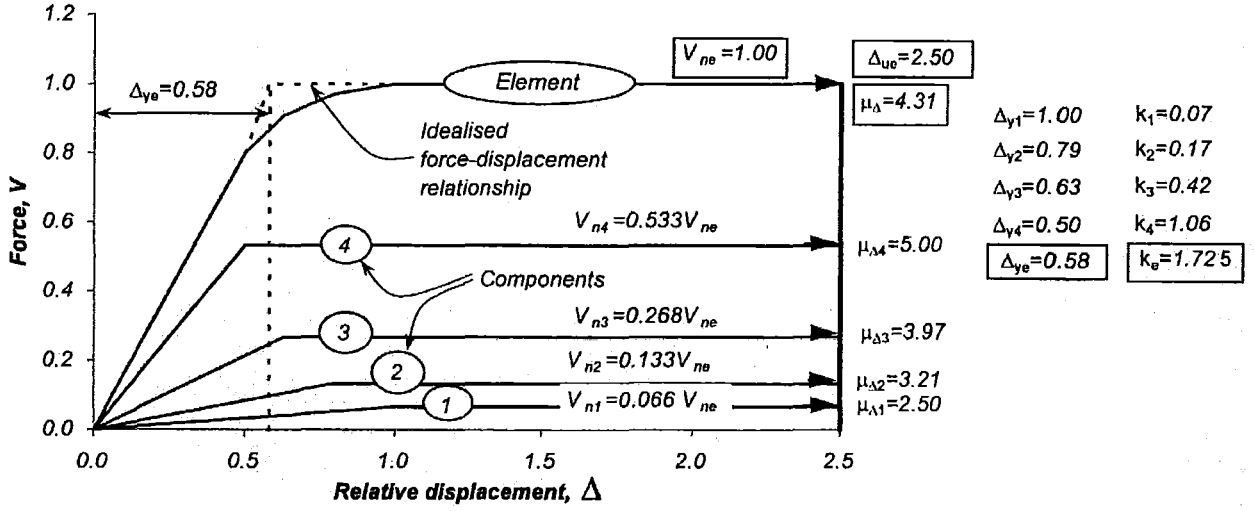

(a) Traditional distribution of strength, $V_{ne} \propto \ell_{wi}^3$

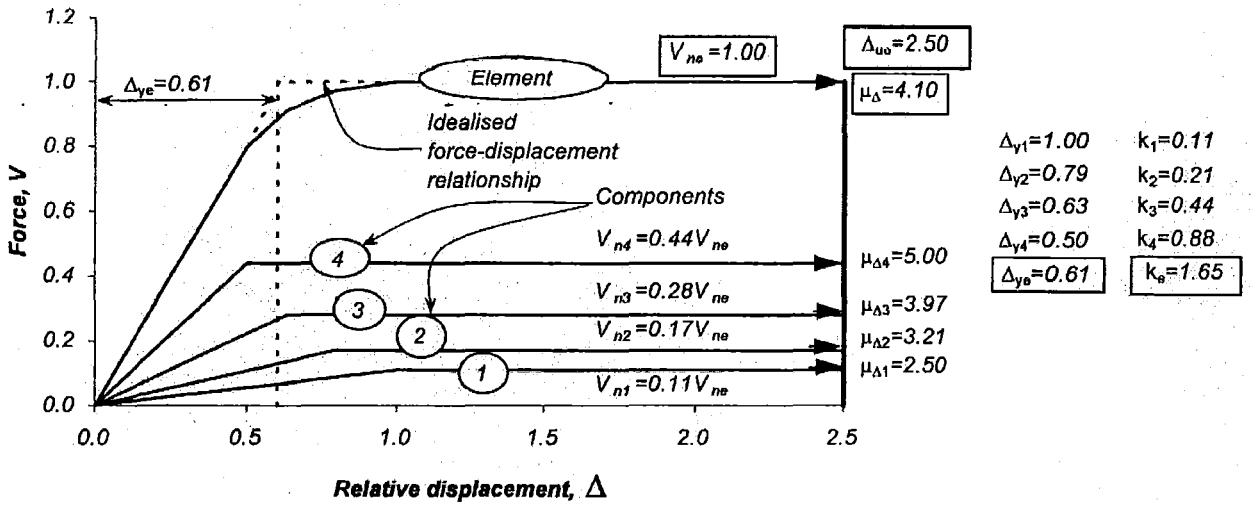

(b) Alternative distribution of strength, $V_{ne} \propto \ell_{wi}^2$

Figure 2-14. Idealized force-displacement relationship of an element comprising wall components

A comparison of both strength distributions, (Figure 2-14(a) and (b)) shows that, in terms of seismic design, the element nominal yield displacement of an element can be considered essentially unaffected by the strength distribution.

The displacement and ductility capacity of the wall element is limited by the critical wall component. This component is that having the smallest displacement capacity. The displacement capacity is defined based on a specific limit state of those described in Section 2.2. In this example, it is assumed that all components have the same displacement ductility capacity of $\mu_{\Delta i}=5.0$ and that a specific drift limit will not be exceeded. Element *(4)*, having the smallest nominal yield displacement, is the critical element with a displacement capacity of $\Delta_{u4}=\mu_{e4}\Delta_{y4}=5.0x0.5=2.5$. All other element will have a larger displacement capacity when their displacement ductility capacity is reached. Hence, the displacement and ductility capacity of the

element, as restricted by the displacement capacity of element *(4)*, is $\Delta_{ue}=\Delta_{u4}=2.5$ and $\mu_{\Delta e}=\Delta_{us}/\Delta_{ye}=2.5/0.61=4.10$, as shown in Figure 2-14(b).

2.9.4 Frames, coupled walls and other elements

Frame elements, as that shown in Figure 2-2(b), consist of one subframe per storey comprising two or more interconnected beam-column components. The nominal yield displacement of each beam-column component may be estimated with a simplified expression suggested by Priestley [P20]. Its applicability is illustrated in the design example of Appendix D.

Paulay [P13,P14,P15] has recently shown a simple procedure to estimate the nominal yield displacement and displacement capacity of coupled walls and dual elements systems. The corresponding displacement and ductility capacities, satisfying specific performance criteria, may be established before the required strength of the system is known. No sophisticated computer analysis is needed. It was shown that the nominal yield displacement of the element can be estimated based on the effective aspect ratio of the walls and the relative strength to be assigned to the walls, frames and coupling beams. The design example provided in Appendix D gives an insight of this proposed method and its applicability to asymmetric systems.

2.10 Properties of a structural system

By similarity with Section 2.9.1, the distribution of system strength to its elements in proportion to the stiffness of the elements is no longer necessary. Strength can be assigned in any way to benefit the system structural response. Section 2.11 will provide some basic guidelines for its distribution among elements.

The system strength, V_{ns}, is defined as the sum of the nominal strength of the elements.

$$V_{ns} = \sum V_{nei} \tag{2-32}$$

By similarity to equation 2-27, the system stiffness, K_s, is the sum of the stiffness of the elements. It is associated with systems subjected to translation only.

$$K_s = \sum k_{ei} \tag{2-33}$$

The above two expressions enable the nominal yield displacement of the system, Δ_{ys}, to be determined as,

$$\Delta_{ys} = \frac{V_{ns}}{K_s} \tag{2-34}$$

By similarity with the element nominal yield displacement, as defined in Section 2.9.2, the system nominal yield displacement depends on the system strength and stiffness. It is also used as reference to model the bilinear force-displacement relationship of a system. It does not

contradict the fundamental property established in Section 2.8.3 where the nominal yield displacement of a component was shown to be independent of its strength.

2.11 A proposed design strategy

A design strategy is proposed considering the design criteria already described in Section 2.2.

1. It aims at quantifying the displacement ductility capacity of the system, $\mu_{\Delta s}=\Delta_{us}/\Delta_{ys}$. The displacement capacity of the system, Δ_{us}, is limited by the displacement capacity of the elements based on the design criteria adopted in Section 2.2. It is expected that the structural designer is able to estimate the nominal yield displacement of the lateral force-resisting elements, Δ_{ye}, and hence that of the system, Δ_{ys}. The nominal strength to be eventually assigned to the system should ensure that displacement demands to be imposed to the elements does not exceed their established displacement capacities.

2. It is suggested that the nominal strength is assigned to the elements of a typical system without gross irregularities so that the centre of nominal strengths of elements, with respect to the principal direction, X or Y, of earthquake-induced displacements, coincides with the centre of mass [P11]. The design aim is thus, to avoid strength eccentricity, which is considered to be the main feature enhancing system rotations. Zero strength eccentricity reduces but, as a general rule, does not eliminate stiffness eccentricity in asymmetric systems as will be shown in Section 2.18. The allocation of fractions of the required total system strength to three or more parallel elements, satisfying static equilibrium criteria, i.e., $e_v=0.0$, as defined above, may be freely chosen by the designer, preferably to serve desirable features of behaviour or economy. To achieve this goal, there are an infinite number of solutions. Therefore, no set method is suggested for distributing the system strength to the elements of the system.

   As a basic guideline, the initial attempt to distribute system strength should consider the axial load, location and dimensional characteristics of elements. It is preferable to assign more strength to the inner rather than to the edge elements of the system. This is because edge elements with low axial loads and high seismic strength may require excessively large foundations. It is also preferable to distribute a higher base shear to the longer elements with a small nominal yield displacement and to check that the shear demand, due to the flexural strength, is below the code limits.

   A strength eccentricity may arise after an arbitrary distribution of system strength. To eliminate this likely strength eccentricity, it is suggested that it should be eliminated by redistributing the strength of one or more couples of selected elements to resist an external torque of $T=e_{vx}V_{ns}$. The system strength should remain constant. An example is provided in Section 2.11.3.

3. In recognition of the fact that, due to variable tolerances in detailing and construction and codified constraints on minimum and maximum reinforcement ratios, the intended location of the centre of nominal strength cannot be achieved, the existence of some inevitable strength eccentricity should be acknowledged. Such quantified eccentricity may be accepted provided that they result from the nominal strength of any element being in excess of that satisfying zero strength eccentricity. The translatory strength of such a system will thus be in excess of its originally intended strength. Simultaneous excess strength in more than one

element may also occur. This may well result in reduced strength eccentricity or greater enhancements of the system strength.

4. Accidental eccentricities, although not examined in the study, can be considered following current recommendations where the centre of mass is shifted by a specific distance from its assessed location. This shift introduces strength eccentricities and increased system strength.

2.11.1 Rationale of the proposed design strategy

The rationale of the strategy is that if, due to inevitable system rotations, displacements, additional to those resulting from system translations, are introduced to one of the elements, the total displacement demand on it should not exceed its displacement capacity.

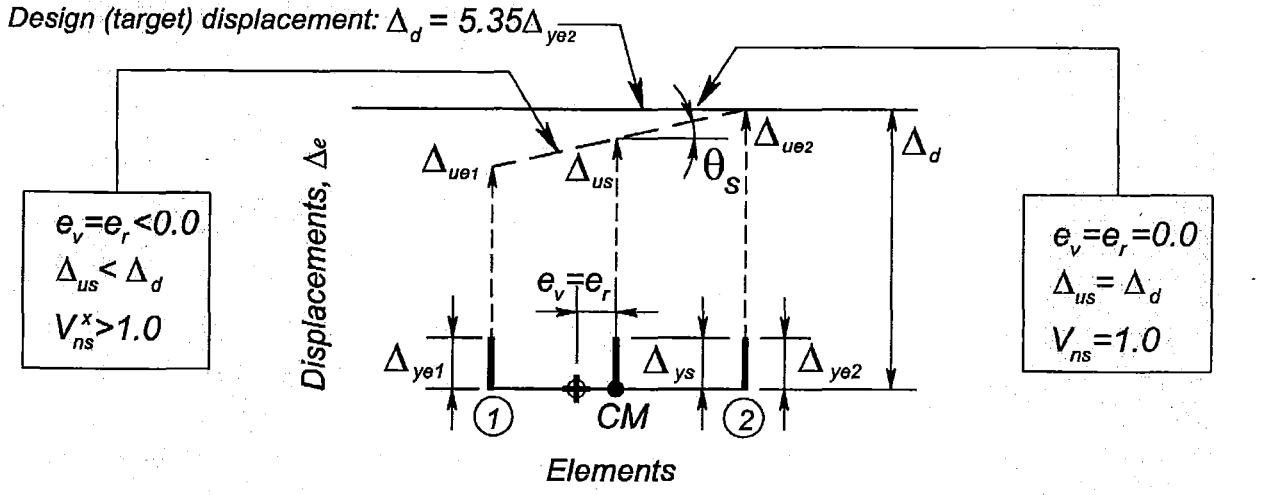

Figure 2-15. The rationale of the proposed design strategy

This situation is shown in Figure 2-15 for element *(2)*. As the primary cause of rotations, i.e., strength eccentricity, is associated with a corresponding increase of system strength, a reduction of the translatory displacement demand at the centre of mass can be expected to compensate for the torsion-induced displacements of critical element *(2)*. The displacement ductility capacity of the system is expected to reduce with increasing rotations if the displacement of the critical element controls the maximum displacement.

2.11.2 Distribution of system strength on two-element systems

The primary aim in the distribution of the system strength to the two-element system is to satisfy static equilibrium, i.e. $e_v=0.0$. Thereafter, it is necessary to comply, in the case of reinforced concrete components, with codified minimum and maximum requirements of reinforcement ratios or, in case of structural steel, availability of commercial sections.

Figure 2-16 shows examples of structurally symmetric and asymmetric single-mass systems. In symmetric *System A*, the centre of mass coincides with the geometric centre of the floor plan. Two identical reinforced concrete substitute wall elements, i.e., $\ell_1=\ell_2$, with unit nominal yield displacement provide the seismic strength of the system along the *Y*-axis. These elements emulate, as stated before, any kind of lateral force resisting element in these planes. Asymmetric *System B* is similar to Symmetric *System A*. The only difference is that elements *(1)* and *(2)* have

nominal yield displacements of $\Delta_{ye1}=0.714$ and $\Delta_{ye2}=1.0$ associated with relative lengths of $\ell_1=1.4\ell_2$ and $\ell_2=1.0$.

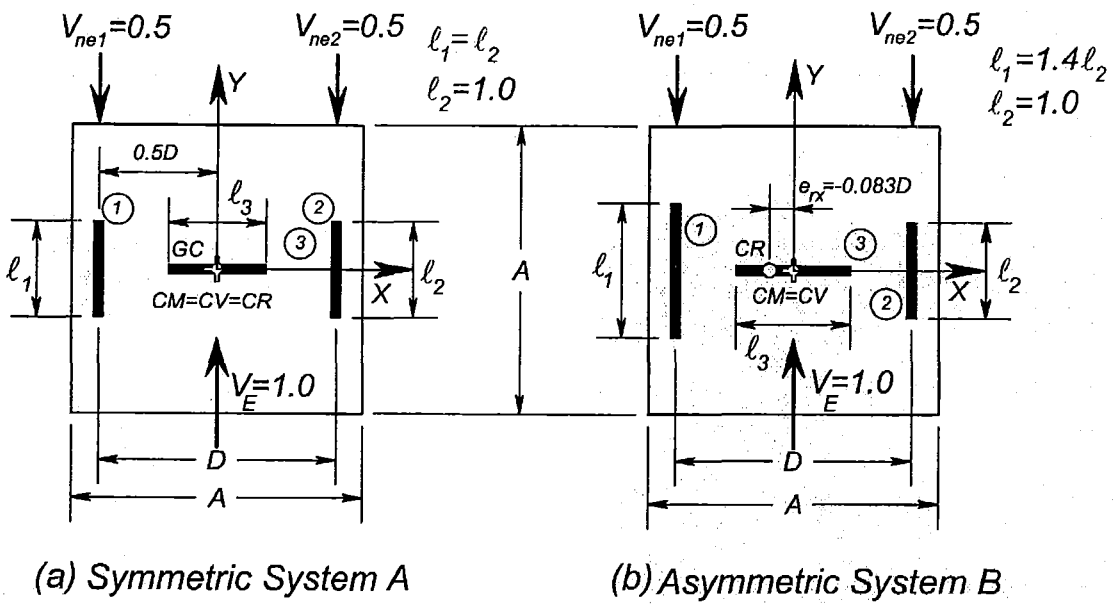

Figure 2-16. Examples of two-element single-mass systems

In case of symmetric *System A*, it is obvious that to satisfy static equilibrium, each substitute wall will have *50%* of the total base shear. In theory, neither strength nor stiffness eccentricity will exist. However, once the building is built, an evaluation of the element's nominal and over-strengths may indicate that one of them has a relative excess strength. This will introduce a strength and stiffness eccentricity and will increase the system strength. The ductile dynamic response of such a system will be examined in Chapter 3.

While strength assigned to elements *(1)* and *(2)* of asymmetric *System B* may result in no strength eccentricity, stiffness eccentricity will exist because of differences in nominal yield displacements of the elements, i.e., element length, as will be described in Section 2.18. Hence, it is necessary to consider changes in the distribution of strengths to elements affecting eccentricities in both the elastic and inelastic range of response.

2.11.3 Distribution of nominal strength in multi-element systems

As stated before, a structural engineer should aim to satisfy static equilibrium when distributing strength to the elements of the system. In case of multi-element systems, there are innumerable alternatives in achieving this purpose. However, by considering guidelines based on the understanding of structural behaviour, the number of viable solutions reduces. As an example, it has been suggested, in case of elements comprising interconnected wall components; see Section 2.9.3, to distribute the elements strength in proportion to it length squared ($V_{ne} \propto \ell_i^2$), i.e., inversely proportional to the nominal yield displacement of the elements squared, $V_{ne} \propto 1/\Delta_{ye}^2$. By similarity, the design base shear of the structural system can also be initially distributed to the substitute wall elements in the same manner. However, it is unlikely that this distribution will satisfy static equilibrium. Subsequent adjustment of strength of all or certain elements will lead to a satisfactory distribution.

For instance, Figure 2-17 shows a multi-element system to which the system strength should be distributed to satisfy zero strength eccentricity. It has three reinforced concrete substitute wall elements along its *Y*-axis with relative lengths of $\ell_1=\ell_3=1.0$ and $\ell_2=2.0\ell_1$ and associated nominal yield displacements of $\Delta_{ye1}=\Delta_{ye3}=1.0$ and $\Delta_{ye2}=0.5$.

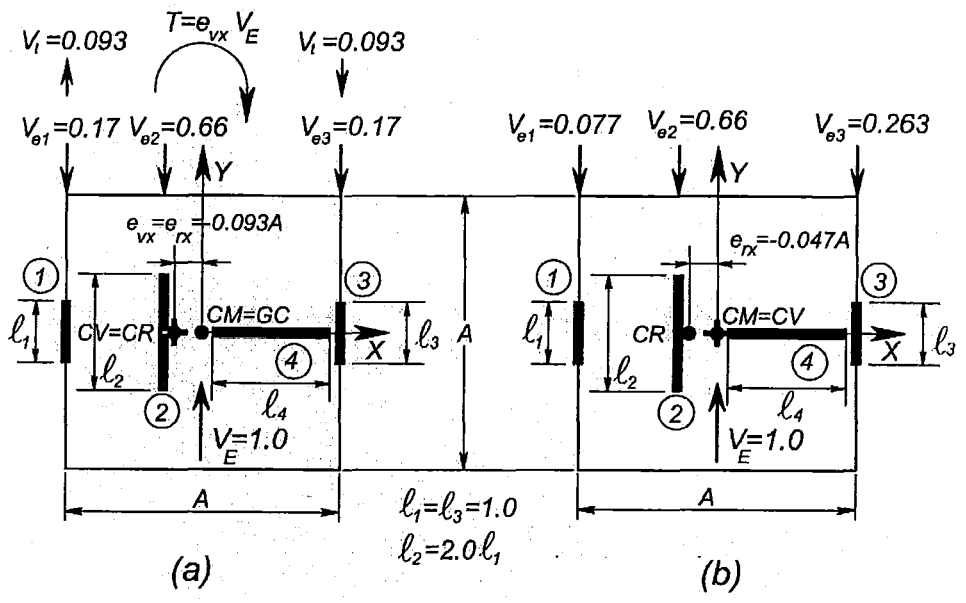

Figure 2-17. Distribution of strength to multi-elements system

As a first step, it is decided to distribute the base shear inversely proportional to the substitute wall-elements nominal yield displacement. Figure 2-17(a) shows a unit base shear distributed on elements according to this criterion. This initial distribution generates, a strength and stiffness eccentricity of $e_{vx}\approx e_{rx}=-0.093A$. The stiffness of each element is obtained with Eq 2-27. The strength eccentricity is eliminated by redistributing the torque $T=e_{vx}V_E=0.07D$ to the couple of elements *(1)* and *(3)*, as shown on top of Figure 2-17(a). This leads to a reduction and increase of the design base shear of elements *(1)* and *(3)* of $V_t=T/A=0.093$, respectively. Figure 2-17(b) shows the final design base shear distribution satisfying static equilibrium, i.e. $e_{vx}=0.0$, but generating a stiffness eccentricity of $e_{rx}=-0.047D$ due to the differences in element nominal yield displacement, i.e., differences in substitute wall-element lengths.

A system may finish with a strength eccentricity and excess strength if any of the elements as built has excess strength in relation to that satisfying zero strength eccentricity. As in the previous example, the strength of elements, as built, is likely to be different from that resulting in no strength eccentricity. It is assumed that the strength of any element will not be less than that dictated by the design base shear and static equilibrium. The effect of eccentricities on the ductile seismic behaviour of systems based on excess strength of some elements is a major issue of this study.

2.12 A relative measure of system's plan configuration

The total mass of the system and its distribution along the floor plan plays an important role in the seismic torsional response of ductile structures. Whereas, the mass is a measure of the body's resistance to accelerate while subjected to lateral dynamic motions, the rotational mass,

which quantifies the distribution of the mass along the floor plan, is a measure of the body's resistance to angular acceleration. In the case of systems exhibiting torsional response, it is certain that the mass rotational inertia will influence system rotations as affected by strength and stiffness eccentricities.

After years of research, it seems that there is no clear understanding of how the inertia of the rotational mass affects the response of ductile systems. In an attempt to clarify this issue, the influence of the plan configuration on the rotational mass is quantified by means of a reference radius of gyration of the mass.

Consider as reference, the radius of gyration of uniformly distributed mass over a square area, (*AxA*). The corresponding rotational mass, denoted as I_o, and its corresponding radius of gyration of the mass, r_o, are expressed as

$$I_o = \frac{1}{6} MA^2 \qquad r_o = \frac{1}{\sqrt{6}} A \tag{2-35}$$

The radius of gyration of mass, r_m, for several plan configurations in buildings as those shown in Figure 2-18, are normalized by using the reference value, r_o. All examples used here, have the same total mass and it is assumed to be uniformly distributed, hence, the plan area and total mass are proportional.

The mass eccentricity of the systems shown in Figure 2-18(c) and (d) may exist if the storey in display is part of a system comprising upper storeys with different centres of mass. An example of such systems is a setback building. The location of the centre of mass in one or more stories of such type of buildings is not the same in every storey which affects the location of the centre of mass of the system. Therefore, the centre of mass of the system in a given storey may not coincide with the centre of mass of that same single storey even when its mass is uniformly distributed.

Among other information, Figure 2-18 presents several plan configurations and its corresponding r_m/r_o ratio to show how the plan configuration affects the rotational mass. It is seen from Figure 2-18(d) that a rectangular configuration with mass eccentricity provides the largest r_m/r_o ratio whereas the circular configuration provides the smallest r_m/r_o ratio; see Figure 2-18(g). Plans with openings; see Figure 2-18(b) to (f), show the largest increase of the r_m/r_o ratio. The **T**, **+** and **L** plan shape diaphragms, see Figure 2-18(h) to (j), do not lead to a significant increase of the r_m/r_o ratio. It is evident that the r_m/r_o ratio increases as the uniformly distributed mass is placed further away from the centre of mass and increases on systems having mass eccentricity.

The r_m/r_o ratio is a useful dimensionless parameter to quantify the effect of the plan configuration on the magnitude of the rotational mass. This parameter, however, does not provide an insight on how the mass rotational inertia may affect the torsional response. Section 2.13 provides an alternative parameter to overcome this differently.

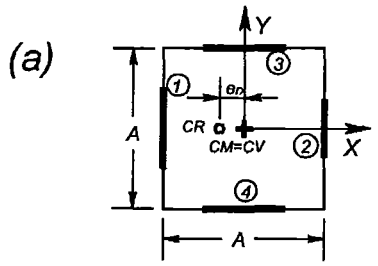

r_m/r_o	r_m	$r_{vy}=r_{vx}$	$r_{vy}/r_m=r_{vx}/r_m$
1.00	0.41A	0.5A	1.22

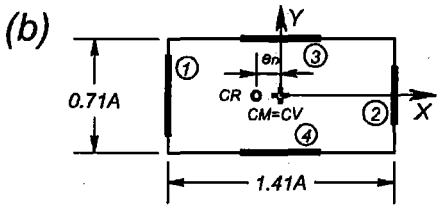

r_m/r_o	r_m	r_{vy}	r_{vx}	r_{vy}/r_m	r_{vx}/r_m
1.12	0.46A	0.71A	0.36A	1.54	0.76

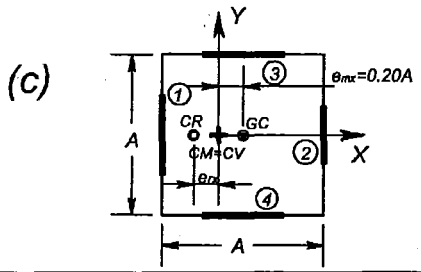

r_m/r_o	r_m	r_{vy}	r_{vx}	r_{vy}/r_m	r_{vx}/r_m
1.10	0.45A	0.46A	0.50A	1.02	1.10

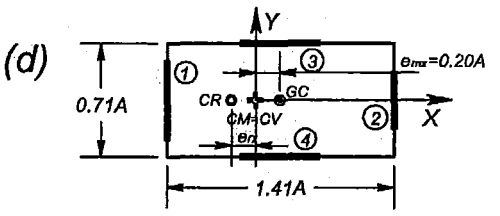

r_m/r_o	r_m	r_{vy}	r_{vx}	r_{vy}/r_m	r_{vx}/r_m
1.32	0.54A	0.65A	0.36A	1.20	0.65

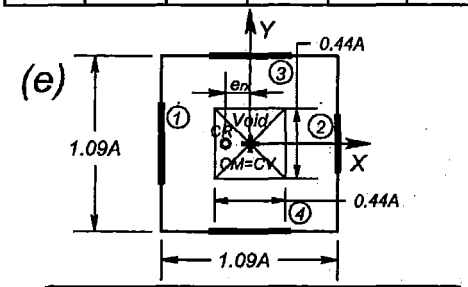

r_m/r_o	r_m	$r_{vy}=r_{vx}$	$r_{vy}/r_m=r_{vx}/r_m$
1.17	0.48A	0.54A	1.13

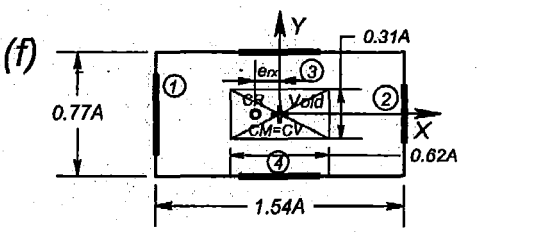

r_m/r_o	r_m	r_{vy}	r_{vx}	r_{vy}/r_m	r_{vx}/r_m
1.29	0.53A	0.77A	0.39A	1.45	0.73

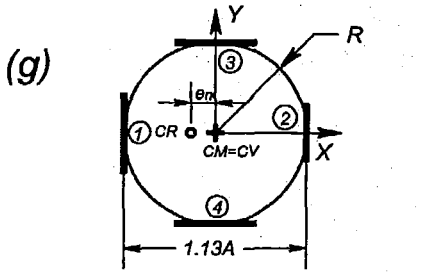

r_m/r_o	r_m	$r_{vy}=r_{vx}$	$r_{vy}/r_m=r_{vx}/r_m$
0.98	0.40A	0.56A	1.41

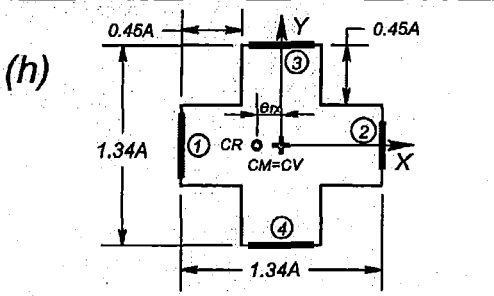

r_m/r_o	r_m	$r_{vy}=r_{vx}$	$r_{vy}/r_m=r_{vx}/r_m$
1.07	0.44A	0.67A	1.52

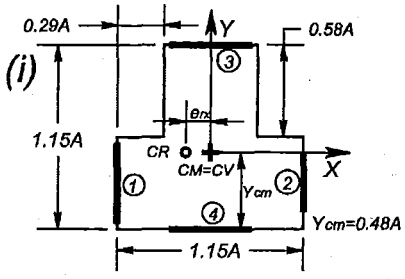

r_m/r_o	r_m	r_{vy}	r_{vx}	r_{vy}/r_m	r_{vx}/r_m
1.05	0.43A	0.58A	0.57A	1.34	1.32

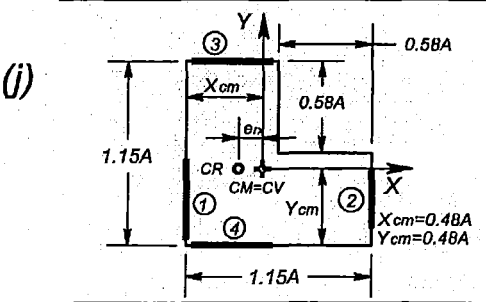

r_m/r_o	r_m	$r_{vy}=r_{vx}$	$r_{vy}/r_m=r_{vx}/r_m$
1.11	0.45A	0.57A	1.27

Figure 2-18 The effects of plan configurations on mass rotational inertia of uniformly distributed mass

2.13 The relevance of the ratio of radii of gyration of strength to mass

The distribution of the nominal strength among elements of systems and the corresponding distribution of mass are considered, in this study, two important parameters, which influence the torsional behaviour of asymmetric systems. The ratio of radii of gyration of strength to mass, r_v/r_m, is a dimensionless parameter suggested to measure the effect of the mass rotational inertia on system rotations. The radius of gyration of the element nominal strength is selected to gauge the importance of the radius of gyration of mass. It has the advantage of remaining essentially constant during ductile behaviour and is easily established once strengths are assigned to elements of the system. For convenience, its effect will be measured in terms of a reference value of $r_{vy}/r_m=1.0$.

The radius of gyration of strength will only consider the nominal strengths of those elements parallel to the direction being considered for the earthquake excitation. The nominal strength of the transverse elements is not to be taken into account because it is assumed that the transverse component of the ground motion may have caused them to yield. This simplification may not be valid for torsionally restrained systems subjected to unidirectional earthquake record input because transverse elements are likely to remain elastic. However, when these systems are to be subjected to an earthquake record along different directions, transverse elements are expected to yield and hence torsionally restrained systems become, for short instances, torsionally unrestrained. Another reason for neglecting the ratio of the nominal strength of the transverse elements to the radius of gyration of strength is because the degree of torsional restraint, as measured by the r_{vx}/r_{vy} ratio will not have a major effect in the response, as it will be shown in Chapter 4. System rotations are expected to be relatively small; hence, no difference will be made if their contribution to the torsional resistance is included in this parameter.

The r_v/r_m ratio may be varied by changing the radius of gyration of the mass only or by varying both radii of gyration of strength and mass. A change of the radius of gyration of mass, while that of strength remains unaffected, is considered in this study to check the sensitivity of the system response due to differences between the computed and the actual distribution of mass. For this purpose, the radius of gyration of mass is varied by $\pm 20\%$ to account for this likely scenario.

On the other hand, the r_v/r_m ratio may be also affected by a change in both the plan configuration of the diaphragm and the distribution of strength. Figure 2-18 shows the r_v/r_m ratio of several plan configurations comprising two elements along both principal axes. The total mass is uniformly distributed over the plan area and is constant for all systems. The r_v/r_m ratio is obtained for each principal axis without including the strength of the transverse elements due to the reasons explained above. The elements are placed at the edges of the floor diaphragm. This will provide an upper bound of the r_v/r_m ratio. The inclusion of parallel inner elements to the systems will reduce this ratio.

The reference square-plan system has $r_v/r_m=1.22$ along both axis, as shown in Figure 2-18(a). This ratio is reduced on a square plan with mass eccentricity, see Figure 2-18(c), and a square plan with an opening; see Figure 2-18(d). The rectangular system shown in Figure 2-18(b) has $r_{vy}/r_m=1.54$ along the Y-direction and $r_{vx}/r_m=0.76$ along the X-axis. This ratio is also reduced in the rectangular mass-eccentric system and that with an opening; see Figure 2-18(d) and (f) because the increase of radius of gyration of mass is larger than that of strength. For the rest of the floor diaphragms; see Figure 2-18(g) to (j), the r_v/r_m ratio also increased relative to that of a

square diaphragm due to a larger increase of radius of gyration of element strength. It is evident that the different systems may have a similar r_v/r_m ratio.

2.14 Torsional restraint

The seismic torsional behaviour of multi-storey buildings is complex. A large number of parameters is known to influence ductile response, in particular: strength and stiffness eccentricity, system uncoupled translational and rotational periods, radius of gyration of strength, stiffness and mass, number and location of lateral force resisting elements and ground motion input. To minimize the number of parameters affecting the response, researchers have been using structural models with two main simplifications:

(a) Multi-storey systems are reduced to equivalent single-storey systems. This study considers it more appropriate to refer to single-mass systems, as already described in Section 2.3. This simplified system will have similar properties of mass, strength and stiffness to the multi-storey system. It is expected to generate a similar response even though it does not take into account the effect of higher modes on the system response [B2].

(b) An additional simplification is the elimination of the transverse elements providing torsional restraint. It is argued that the transverse component of the ground motion input will cause these elements to yield. However, to what extent this is realistic has led to recent studies being directed toward the inclusion of transverse elements [H3,R2,F1,D4,D3,G1,D1,C5].

Based on the simplifications enumerated above, for the purpose of this study, single-mass systems are classified as [P11]:

(i) Torsionally un-restrained systems (*TU*). A single-mass system is torsionally unrestrained if the elements acting in a direction transverse to the application of the unidirectional ground motion input do not provide any torsional resistance. This is achieved when these transverse components act through the centre of mass.

(ii) Torsionally restrained systems (*TR*). A single-mass system is torsionally restrained if at least one transverse plane of resistance, eccentric with respect to the centre of mass, exists providing translational and torsional resistance. The degree of torsional restraint provided by the transverse elements is quantified by the r_{vx}/r_{vy} ratio.

For the sake of simplicity, the study considers two-element systems to reduce the number of parameters influencing the response. Thereafter, single-mass multi-element systems are also considered to examine the effects that the number and location of the elements may also have on the torsional response.

2.15 Classification of structural systems

Systems are also classified based on the distribution of strength and stiffness relative to the location of the centre of mass [P11].

(i) Structurally symmetric systems (*CV=CR=CM=GC*). A system is structurally symmetric when centres of strength, stiffness, mass, and geometry are coincident. The application of static or dynamic forces at the centre of mass will generate only translation in both the elastic and inelastic range of response. In case of two and multi-element systems, this is achieved if the nominal yield displacement of all elements is the same. Structural symmetry is also attained with multi-elements systems having elements with different nominal yield displacements. This is possible if elements are symmetrically arranged with respect to the centre of mass in accordance to their nominal yield displacement, as shown in Figure 2-19.

(ii) Structurally symmetric systems with mass eccentricity (*CV=CR=CM≠GC*). A structurally symmetric system is mass eccentric when the centre of mass does not coincide with the geometric centre of the floor diaphragm. Independent of the location of the centre of mass, a system is structurally symmetric when the centres of mass, strength and stiffness are coincident. The coincidence of centre of strength and stiffness is only possible when elements of two or multi-element systems have the same nominal yield displacement. It also happens when elements with different nominal yield displacement are symmetrically located with respect to the centre of mass.

(iii) Structurally asymmetric systems (*CV≠CR; CM=GC*). A system is structurally asymmetric when the centres of strength and stiffness are non-coincident. This is a feature of systems with elements having different nominal yield displacements and arranged arbitrarily with respect to the centre of mass.

(iv) Structurally asymmetric systems with mass eccentricity (*CV≠CR; CM≠GC*). A structurally asymmetric system is mass eccentric, as previously explained in point (ii), when the centre of mass does not coincide with the geometric centre. The centres of strength and stiffness will never coincide because the elements have different nominal yield displacement and are not arranged symmetrically with respect to the centre of mass.

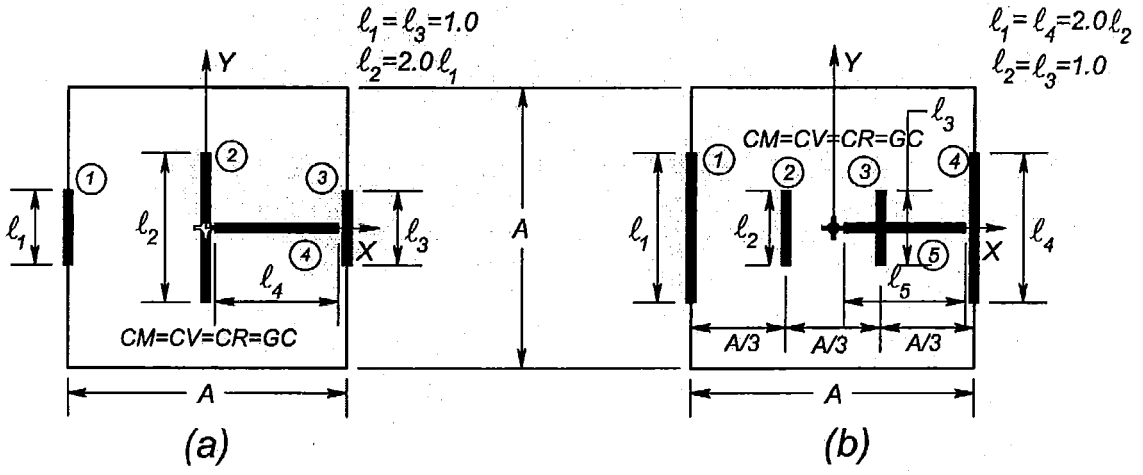

Figure 2-19. Example of structurally symmetric systems comprising elements with different nominal yield displacement

2.16 Two-element structurally symmetric *System 1* (*CV=CR=CM=GC*)

2.16.1 Description and properties of *System 1*

Systems 1A and 1B are torsionally unrestrained and restrained, respectively, as shown by the specific layout in Figure 2-20(a) and (b). They consist of an infinitely rigid in-plane square diaphragm of (*AxA*) with uniformly distributed mass. The centres of mass and geometry are coincident. The lateral force resisting elements consist of substitute wall-elements *(1)* and *(2)* having equal nominal yield displacement, i.e., identical lengths, $\ell_1=\ell_2=1.0$, parallel to the *Y*-axis providing translational and, if required, torsional strength to the system. *System 1A* has a third substitute wall-element placed parallel to the *X*-axis coinciding with a line passing through the centre of mass. This element will provide transverse strength and stability without contributing to the torsional resistance of the system. In contrast, *System 1B* has two *X*-direction elements *(3)* and *(4)* eccentric with respect to the centre of mass. They will introduce translational strength along the *X*-axis and torsional resistance. The strength and nominal yield displacement of *Systems 1A* and *1B* are the same along the *X* and *Y*-axis, hence their stiffness is the same. To achieve this characteristic, the length of elements *(3)* and *(4)* must be equal to $\ell_3=\ell_4=1.0\ell_2$.

All elements are modelled as substitute cantilever wall elements with fully restrained bases representing any lateral force resisting element. They have the same height, h_i and are assumed to exhibit elasto-plastic force-deformation behaviour. For simplicity, this study does not consider wall-rocking, loss of bond between concrete and reinforcement, elastic elongation of reinforcement at anchorages and shear deformations. However, these features are expected to influence to some degree the nominal yield displacement of the elements.

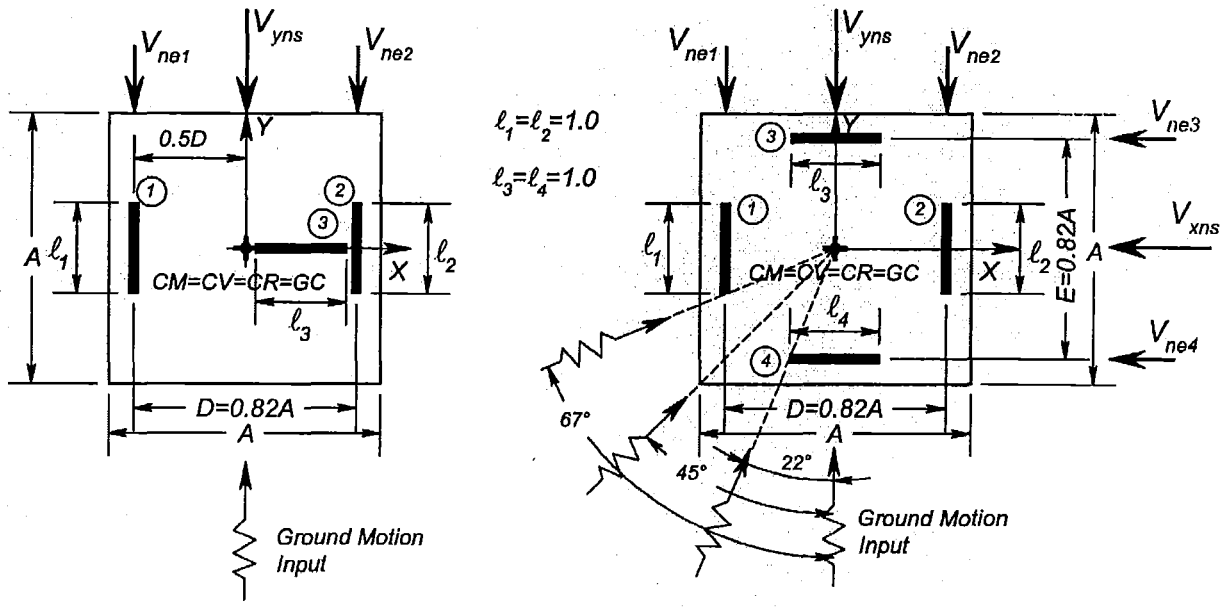

(a) System 1A, torsionally unrestrained (b) System 1B, torsionally restrained

Figure 2-20. Two-element structurally symmetric *System 1*

The properties of *System 1* can be defined after selecting and distributing the design base shear. This is assigned to the elements to satisfy static equilibrium and hence, resulting in identical element strengths. The location of the elements parallel to the *X* and *Y*-direction is such that the

ratio of radii of gyration of strength to radius of gyration of mass of a square diaphragm, r_o, are the same, as shown in Table 2-3. In the calculation of the r_v/r_o, the radii of gyration of strength does not include the nominal strength of the transverse elements due to the reasons provided in Section 2.13. *D* and *E* are the distances between elements *(1)-(2)* and *(3)-(4)*, respectively. In these particular systems, these dimensions have the same value of *D=E=0.82A*. Appendix *B* summarizes the properties of *System 1* when system strength is distributed to elements to satisfy zero strength eccentricity.

Table 2-3 Radii of gyration of mass, strength and stiffness and relevant ratios of *System 1*

	e_{vx}=0.0		e_{rx}=0.0	e_{mx}=0.0	D=E=0.82A		
System	r_m/r_o	r_m	$r_{vy}=r_{ky}$	$r_{vx}=r_{kx}$	$r_{vy}/r_o=r_{ky}/r_o$	$r_{vx}/r_o=r_{kx}/r_o$	r_{vx}/r_{vy}
1A	1.00	0.41A	0.41A	0.00	1.00	0.00	0.00
1B	"	"	"	0.41A	"	1.00	1.00

The effects of the direction of application of the earthquake record on the system torsional response are a concern in this study. For this purpose, the systems will be subjected to earthquake records at different direction relative to the reference *Y*-axis, as shown in Figure 2-20. The ductile behaviour of the systems will be presented in Chapters 3 and 4.

These systems and all those to be described in subsequent sections will have the same strength along the *Y* and *X*-axes. They can sustain a larger static lateral force at any horizontal directions other than the *X* and *Y*-axes [P3]. For instance, the system can resist at 45^o angle, a force *41%* larger than that to be resisted along the principal axes. The system may also sustain at 67^o and 22^o angles a *16%* larger force. It is evident that the static lateral force to be sustained by a system with given strength along the *X* and *Y*-direction increases as the direction of application of the lateral force increases and reaches a maximum at a 45^o angle. This may be an advantage in seismic design of systems subjected to ground motions at diagonal directions because the observed increase of system nominal strength may limit the displacement ductility demand on the elements to less than their ductility capacity.

The nominal yield displacement of the systems to be examined will also be the same along the principal axes. By similarity to the system strength, the nominal yield displacement at the centre of mass will be larger at any diagonal direction and proportional to the increase of system strength. Thus, the translational stiffness of the system at diagonal directions will remain unchanged.

2.16.2 Excess strength of elements of *System 1*

Systems 1A and 1B, shown in Figure 2-20(a) and (b), will exhibit translation without rotation in both the elastic and inelastic responses, if both elements have the same strength, hence static equilibrium is satisfied. It is obvious that this strength distribution should be the aim of the structural engineer. At this stage, no strength or stiffness eccentricities arise. However, it is possible that for a particular reason one of the elements has a strength in excess of that dictated by static equilibrium while the strength of the other element remains unchanged. The excess strength of either element *(1)* or *(2)* will introduce a strength and stiffness eccentricity and a system excess strength. The presence of a strength eccentricity will make the symmetric system structurally non-symmetric. Excess strength factors λ_1 and λ_2 are used to quantify the excess strength of either element *(1)* or *(2)*, respectively relative to that required to satisfy static equilibrium.

Figure 2-21(a) shows the relationship between the excess strength of element *(1)* ($\lambda_1>1.0$), the strength and stiffness eccentricities and the resulting system excess strength. The strength of element *(2)* remains unchanged and equal to that dictated by static equilibrium. It is evident that identical strength and stiffness eccentricities arise. The increase in element strength will lead to the same increase of element stiffness because the nominal yield displacement of elements *(1)* and *(2)* are the same. The system will have an excess strength of *50%* when the strength of element *(1)* is doubled ($\lambda_1=2.0$). Under these conditions, a strength eccentricity is associated with a system excess strength. The same effect will occur if element *(2)* is the one with excess strength while that of element *(1)* remains unchanged.

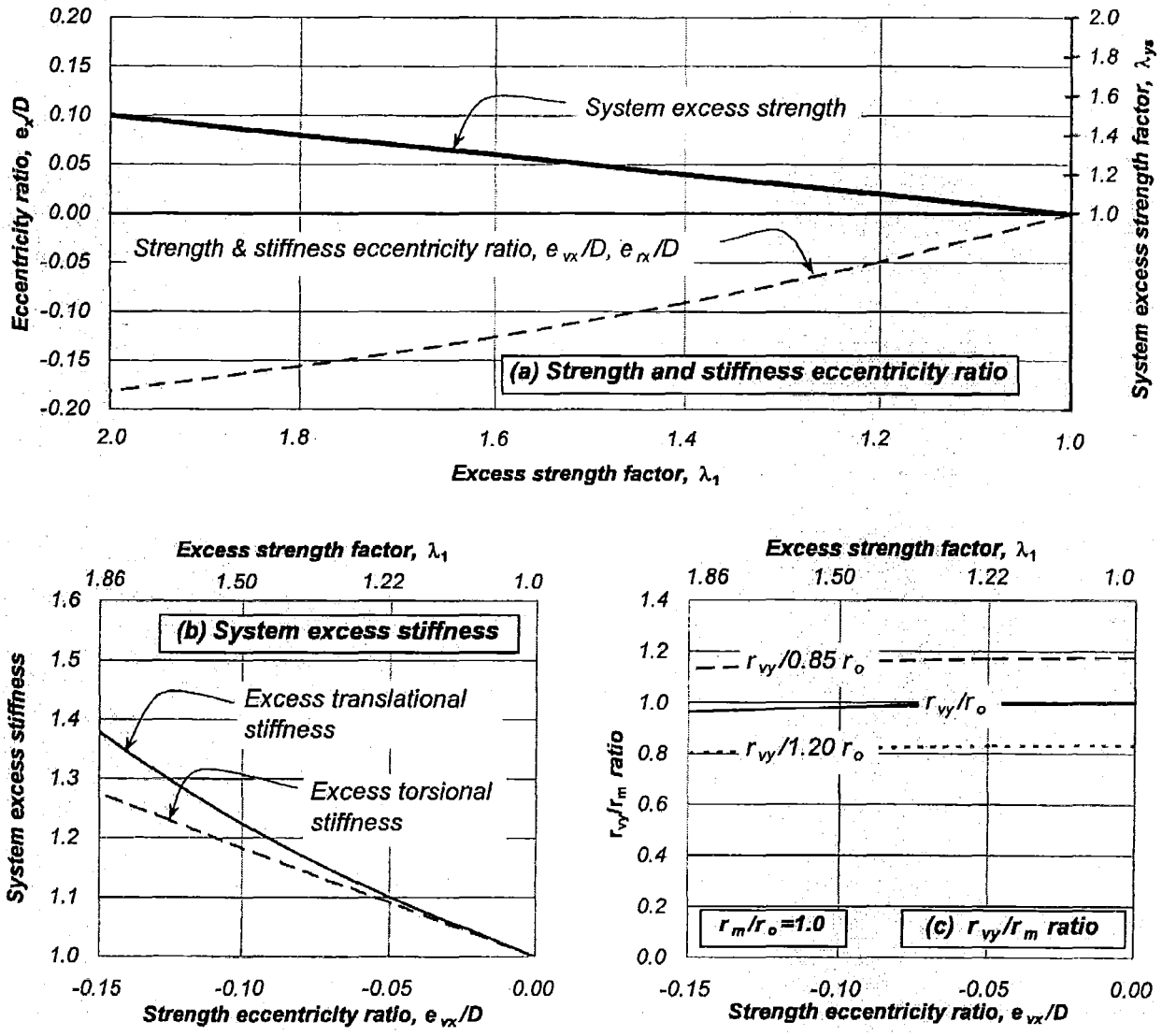

Figure 2-21. Parameters affecting strength and stiffness eccentricity ratios and properties of *System 1*

The variation of strength and stiffness eccentricities of structurally symmetric *Systems 1A* and *1B*, as a function of the excess strength factors (λ_1 and λ_2) are expressed as,

$$\frac{e_{vx}}{D}=\frac{e_{rx}}{D}=0.5\frac{(1-\lambda_1)}{(1+\lambda_1)} \qquad \frac{e_{vx}}{D}\le 0 \qquad \text{(2-36(a))}$$

$$\frac{e_{vx}}{D}=\frac{e_{rx}}{D}=0.5\frac{(\lambda_2-1)}{(\lambda_2+1)} \qquad \frac{e_{vx}}{D}\geq 0 \qquad \textbf{(2-36(b))}$$

where λ_1 and λ_2 are excess strength factors quantifying the excess strength of element *(1)* and *(2)*, respectively, and D is the distance between them. Figure 2-20(a) shows the sign convention used.

The system excess strength and stiffness relative to that associated with static equilibrium and function of the strength eccentricity ratio, e_{vx}/D, are expressed as,

$$\frac{V_{yns}^{x}}{V_{yns}}=\frac{K_{ys}^{x}}{K_{ys}}=\left(\frac{1}{2\frac{e_{vx}}{D}+1}\right) \qquad \frac{e_{vx}}{D}\leq 0 \qquad \textbf{(2-37(a))}$$

$$\frac{V_{yns}^{x}}{V_{yns}}=\frac{K_{ys}^{x}}{K_{ys}}=\left(\frac{1}{1-2\frac{e_{vx}}{D}}\right) \qquad \frac{e_{vx}}{D}\geq 0 \qquad \textbf{(2.37(b))}$$

where V_{yns} and K_{ys} are the system strength and stiffness, respectively, when strength is distributed according to static equilibrium. V_{yns}^{x} and K_{ys}^{x} are the system excess strength and stiffness associated with excess strength of either element *(1)* or *(2)*.

Figure 2-21(b) shows the effect of excess strength of element *(1)* ($\lambda_1>1.0$) on the increase of translational and torsional stiffness of *Systems 1A* and *1B*. The system torsional stiffness does not include, as explained before, the torsional stiffness contribution of the transverse elements. The system excess translational stiffness increases by the same amount as the system strength; see Eq 2-35. In contrast, the excess torsional stiffness increases at a smaller rate, for example by 33% when doubling the strength of element *(1)* ($\lambda_1=2.0$). The excess torsional stiffness, as a function of the strength eccentricity ratio is expressed as,

$$\frac{K_{\theta y}^{x}}{K_{\theta y}}=1-2\frac{e_{vx}}{D} \qquad \frac{e_{vx}}{D}\leq 0 \qquad \textbf{(2-38)}$$

where $K_{\theta y}$ is the system torsional stiffness when system strength is distributed according to static equilibrium and $K_{\theta y}^{x}$ is the system torsional stiffness when element *(1)* has excess strength. As explained before, the torsional stiffness contributed by the *X*-direction elements is not taken into account in this expression.

Figure 2-21(c) shows the variation of selected r_{vy}/r_m ratios as a function of the strength eccentricity. It is evident that the strength eccentricity hardly affects the r_{vy}/r_m ratio. Thus, the strength eccentricity does not influence the radius of gyration of strength.

2.16.3 Base shear-torque relationships of *System 1*

The base shear-torque relationship provides a panorama of all possible combinations of base shear and torque to be developed in the system when both or just one element is still elastic. Kan and Chopra [K2] developed this concept to study the inelastic torsional response of single element systems whereas De la Llera and Chopra [D2] extended it to systems comprising more than one lateral force-resisting element. It is a useful relationship providing better understanding of the strength development in ductile mechanisms due to torsional behaviour. However, it is of limited interest in structural design because it does not address the main cause of structural damage in buildings: displacements.

Figure 2-22(a) shows the familiar base shear-torque relationship of the torsionally unrestrained *System 1A*. A unit base shear along the *X* and *Y*-axis ($V_x=V_y=1.0$) is assumed to have been distributed to the elements to satisfy static equilibrium. Thus, all elements have identical strength of $V_{ne1}=V_{ne2}=0.5V_y$ and no strength eccentricity arises ($e_{vx}=0$). The strength of elements *(1)* and *(2)* develop simultaneously when a unit lateral force is applied at the centre of mass; see point *(A)* in Figure 2-22(a). At this point, the system cannot resist a torque. The system is able to a sustain static or a dynamic-induced torque only if the base shear reduces. It will sustain a maximum torque of $T=0.41A$ with zero base shear; see point *(B)* in Figure 2-22(a). This would occur when elements *(1)* and *(2)* develop their maximum base shear in opposite directions. In reality, the system will never develop such a large torque because the rotational component of the seismic excitation is rather small. It is seen from Figure 2-22(a), as De la Llera and Chopra [D2] pointed out, that there will be an element associated with each branch of the base shear-torque relationship. The length of each branch is proportional to its nominal strength. The middle point of each branch corresponds to the base shear and torque combination generated when the associated element exhibits no base shear.

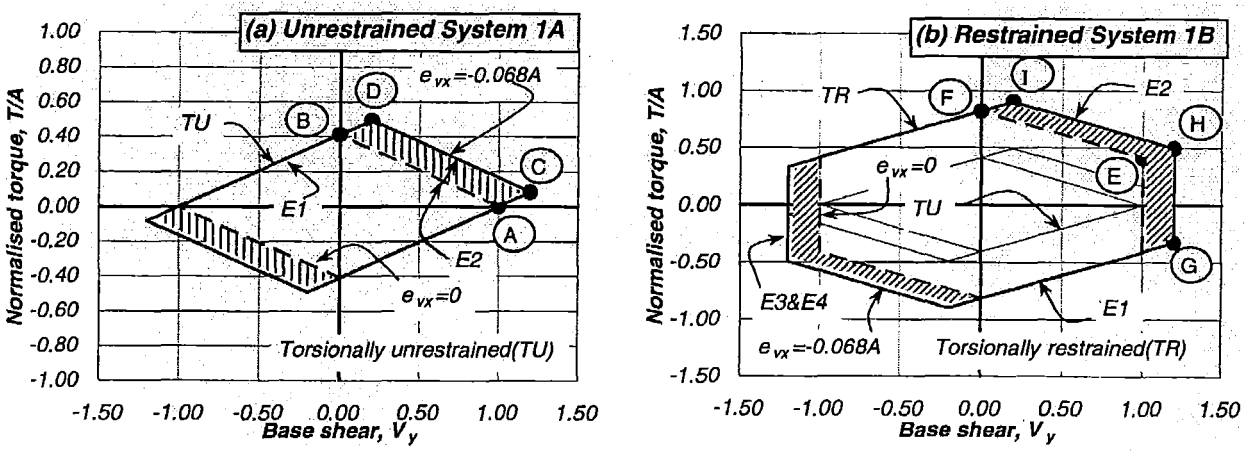

Figure 2-22. Base shear-torque relationships of *System 1*

Figure 2-22(a) also shows the base shear-torque relationship of the unrestrained *System 1* when element *(1)* has say *40%* excess strength ($\lambda_1=1.4$). The strength of element *(1)* increases to $V_{ne1}=1.4*0.5V_y=0.7=0.58V_y$ while the strength of element *(2)* is assumed to remain unchanged. This excess strength introduces a strength and stiffness eccentricity of $e_{vx}=e_{rx}=-0.068A$. Moreover, the system base shear increases *20%* to $V_y=1.2$. Under static conditions, this strength development is not possible. To develop the additional system base shear, the mass rotational inertia must introduce a dynamic-induced torque equal to $T_m=e_{vx}V_y=0.068A*1.20=0.082A$; see point *(C)* in Figure 2-22(a). Theoretically, the system could resist a maximum torque of

$T=(0.7+0.5)*0.41A=0.49A$ associated with a system base shear of only $V_y=(0.7-0.5)=0.2$; see point *(D)* in Figure 2-22(a).

Figure 2-22(a) also shows two shaded areas. They correspond to the dynamic-induced base shear and torque combinations of unrestrained *System 1A*. No static-induced force and torque combinations can develop the full nominal strength of the elements associated with these areas.

To illustrate this relationship, generally not appreciated in routine structural design, Figure 2-23(a) shows the properties of unrestrained *System 1A* when element *(1)* has a *40%* excess strength. It is evident that elements *(1)* and *(2)* will develop a base shear of $V_{e1}=V_{e2}=0.5$ each if a unit lateral force is applied at the centre of mass; see Figure 2-23(b). At this stage, however, element *(1)* still has a residual strength of $V_{re1}=0.2$. Only a dynamic-induced torque can develop this remaining strength through the engagement of the mass translational and the rotational inertia of the system.

Figure 2-23(c) shows the resistance provided by the mass translational inertia of $V_m=0.2$, which enables the mass rotational inertia to introduce a dynamic-induced torque of $T_m=(0.2*0.41A)=0.082A$. This torque is simply equal to the product $T=e_{vx}V_y$.

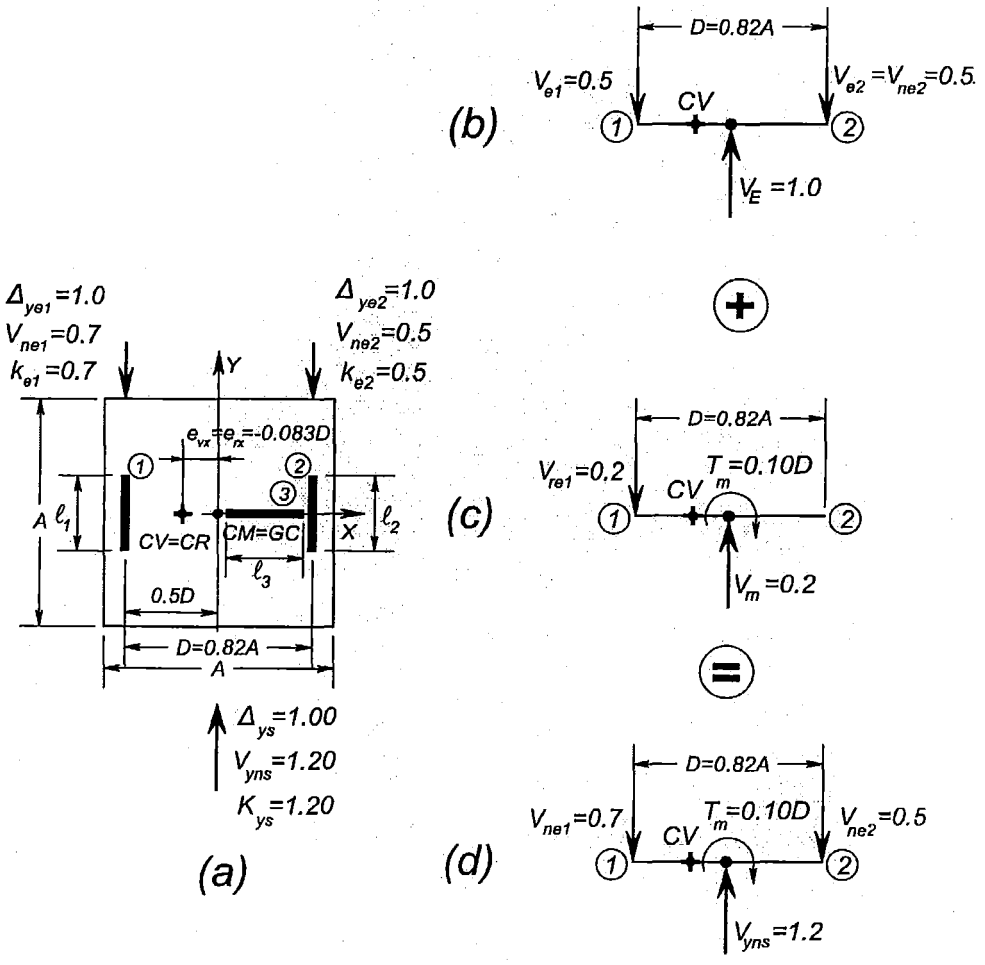

Figure 2-23 Torsional mechanisms of unrestrained *System 1A*

The superposition of both static and dynamic actions indicates that equilibrium associated with full strength development of the system is satisfied, as shown in Figure 2-23(d). The same will

occur with point *(D)*, see Figure 2-22(a), representing the extreme situation when both elements of unrestrained *System 2A* reach their maximum strength in opposite directions. However, a demand like this is never likely to occur since earthquake ground motions introduce primarily translational motions.

Figure 2-22(b) shows the effect on the base shear-torque relationship of the unrestrained *System 1A* (denoted *TU)* when two *X*-direction elements *(3)* and *(4)* are introduced. This new system is referred to as the restrained *System 1B* (denoted *TR*). The *X*-direction elements introduce two vertical branches to the base shear-torque relationship indicating an increase in the system torsional resistance. The system can resist a maximum base shear of $V_y=1.0$ when elements *(1)* and *(2)* yield simultaneously. At the same time, it can also resist a torque of $T=0.41A$ which is contributed solely by the *X*-direction elements *(3)* and *(4)*; see point *(E)* in Figure 2-22(b). As the base shear reduces, the system torque increases and reaches a maximum of $T=0.82A$ with zero base shear; see point *(F)* in Figure 2-22(b). At this point, all elements contribute to the system torsional resistance. However, a demand like this is unlikely to arise in practice.

Figure 2-22(b) also shows that a *40%* excess strength of element *(1)* also modifies the base shear-torque relationship of the restrained *System 1B*. This excess strength increases both the base shear and maximum torque capacities. Figure 2-22(b) shows, as with the unrestrained *System 1A*; see Figure 2-22(a), an increase of *20%* of system base shear to $V_y=1.2$. At this stage, the system can also resist, for a positive base shear, two torques of $T=-0.33A$ and $T=+0.49A$ depending on the sense of system rotation; see points *(G)* and *(H)* in Figure 2-22(b). To develop the maximum system torque of $T=0.90A$, a reduced system base shear of $V_y=0.2$ is required; see point *(I)* in Figure 2-22(b). The shaded areas correspond, as already explained, to the base shear and torque combinations that can only be developed by dynamic-induced actions.

2.17 Two-element structurally symmetric and mass-eccentric *System 2* (*CV=CR=CM≠GC*)

2.17.1 Description and properties of *System 2*

System 2A and *2B* are structurally symmetric and mass eccentric, as illustrated in Figure 2-24. They have a mass eccentricity of $e_{mx}=-0.20A$ corresponding to the distance between the mass and geometric centres of the system. The nominal yield displacement of elements *(1)* and *(2)* are the same, hence, their length is identical, $\ell_1=\ell_2=1.0$. The centres of strength and stiffness will always coincide. The elements will provide lateral strength along the *Y*-axis and torsional strength to the system. *System 2A* is torsionally unrestrained because transverse element *(3)* does not provide torsional resistance. In contrast, *System 2B* is torsionally restrained due to the torsional resistance contributed by the *X*-direction elements *(3)* and *(4)*. These elements also have the same nominal yield displacement, hence their length is identical $\ell_3=\ell_4=1.0\ell_2$. The system will be subjected to earthquake records at different directions as Figure 2-24 shows.

The location of the elements is such that the radii of gyration of strength and mass are equal thus generating relevant ratios, as those shown in Table 2-4. To achieve this characteristic, the distance between centres of elements *(1)* and *(2)* is $D=0.99A$ and the distance between elements *(3)* and *(4)* is $E=0.90A$. The strength and stiffness of the transverse elements are not included in the ratios of radii of gyration. The strength and translatory stiffness of the system is equal along both principal axes. This is possible as all elements have the same unit length. Appendix B lists the properties of *System 2* when strength is distributed to satisfy static equilibrium.

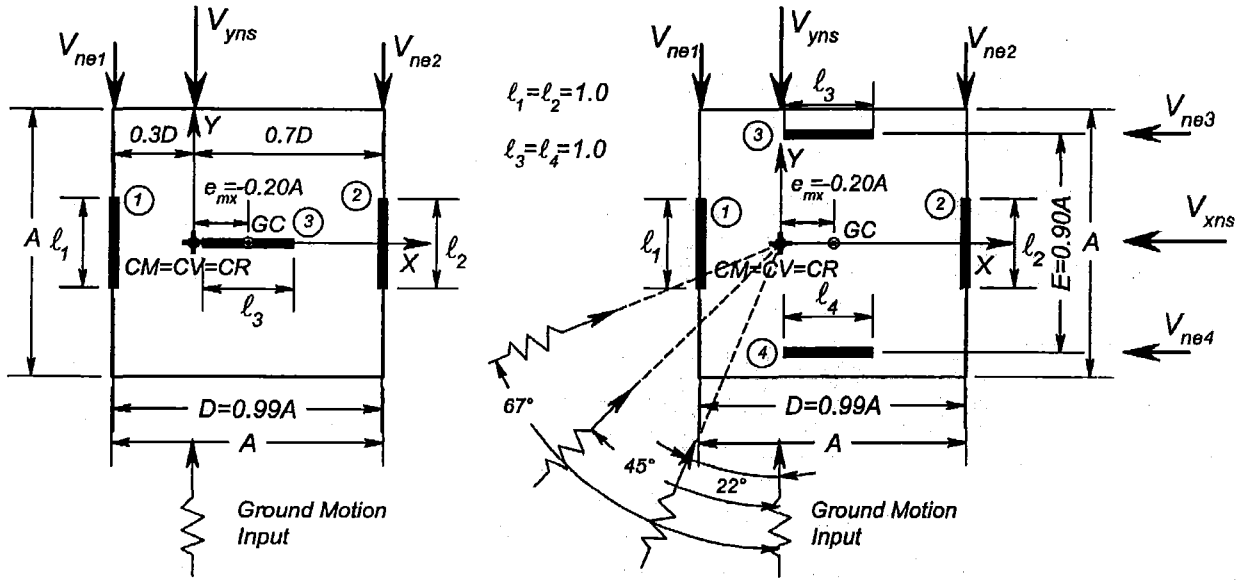

(a) System 2A, torsionally unrestrained (b) System 2B, torsionally restrained

Figure 2-24. Two-element structurally symmetric and mass-eccentric *System 2*

The nominal strength assigned to *System 2* will be the same along the principal axes. This strength is larger along directions other than those of the principal axes, as already explained for *System 1*; see Section 2.16.1. The fact that the system is mass eccentric does not influence this feature.

Table 2-4 Radii of gyration of mass, strength and stiffness relevant ratios of *System 2*

	e_{vx}=0.0	e_{rx}=0.0	e_{mx}=-0.20A		D=0.99A	E=0.90A	
System	r_m/r_o	r_m	$r_{vy}=r_{ky}$	$r_{vx}=r_{kx}$	$r_{vy}/r_m=r_{ky}/r_m$	$r_{vx}/r_m=r_{kx}/r_m$	r_{vx}/r_{vy}
2A	1.10	0.45A	0.50A	0.00	1.00	0.00	0.00
2B	"	"	"	0.45A	"	1.00	1.00

2.17.2 Excess strength of elements on *System 2*

Figure 2-25(a) shows the effect of excess strength of either element *(1)* or *(2)* on strength and stiffness eccentricities and system excess strength. Excess strength factors λ_1 and λ_2 quantify the excess strength of either element relative to that required to satisfy static equilibrium. The excess strength of element *(1)*(λ_1>*1.0*) introduces negative strength and stiffness eccentricities between *0.0* and *-0.12D*. The system strength increases by *70%* when doubling the strength of elements *(1)*. In contrast, an excess strength of element *(2)* (λ_2>*1.0*) leads to positive strength and stiffness eccentricities varying between *0.0* and *+0.16D* and the system strength increases only by *30%* when the strength of element *(2)* is doubled. These results simply indicate that the system excess strength depends on the position of the elements relative to the centre of mass.

The relationship between excess strength factors and strength and stiffness eccentricity ratios of the example *System 2* is expressed as,

$$\frac{e_{vx}}{D}=\frac{e_{rx}}{D}=\frac{1}{2.33\lambda_1+1}-0.3 \qquad \frac{e_{vx}}{D}\le 0 \qquad \text{(2-39(a))}$$

$$\frac{e_{vx}}{D} = \frac{e_{rx}}{D} = \frac{\lambda_2}{2.33+\lambda_2} - 0.3 \qquad \frac{e_{vx}}{D} \geq 0 \qquad \textbf{(2-39(b))}$$

The relationship between the strength and stiffness of the system and the strength eccentricity is

$$\frac{V_{yns}^x}{V_{yns}} = \frac{K_{ys}^x}{K_{ys}} = \left(\frac{1}{3.33\frac{e_{vx}}{D}+1} \right) \qquad \frac{e_{vx}}{D} \leq 0 \qquad \textbf{(2-40(a))}$$

$$\frac{V_{yns}^x}{V_{yns}} = \frac{K_{ys}^x}{K_{ys}} = \left(\frac{1}{1-1.43\frac{e_{vx}}{D}} \right) \qquad \frac{e_{vx}}{D} \geq 0 \qquad \textbf{(2-40(b))}$$

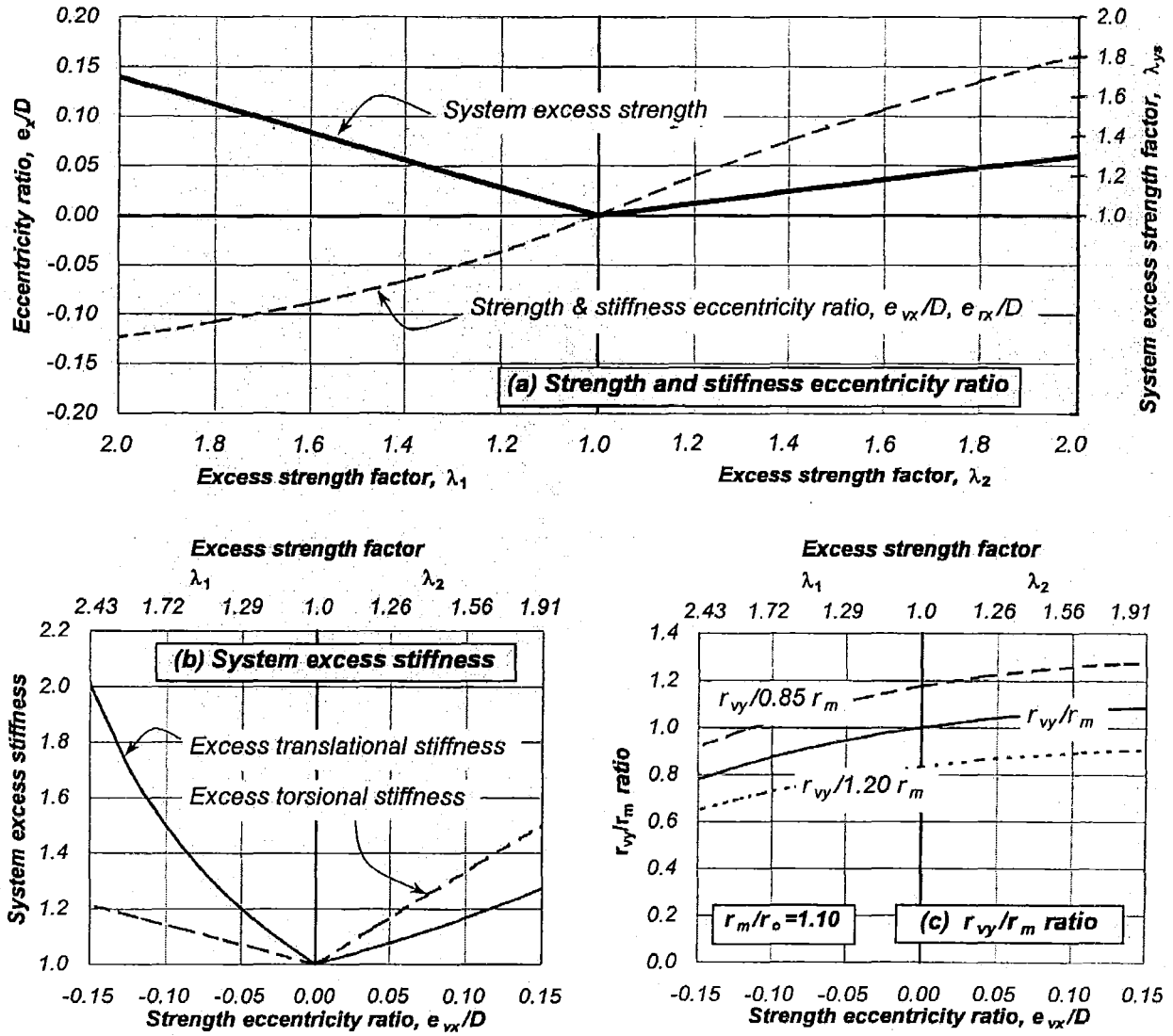

Figure 2-25. Parameters affecting strength and stiffness eccentricity ratios and properties of *System 2*

Figure 2-25(b) shows the effect of the strength eccentricity on the excess translational and torsional stiffness of the system. The system excess of stiffness is also equal to the increase of system strength. Excess strength of element *(1)* ($\lambda_1>1.0$) results in a larger excess translational stiffness than excess torsional stiffness. This is because element *(1)* has initially a greater strength and is the closest element to the centre of stiffness. In contrast, excess strength of element *(2)* ($\lambda_2>1.0$) leads to a larger excess torsional stiffness because the element is further from the centre of stiffness. The large distance between this element and the centre of stiffness means that the torsional stiffness of the system increases at a faster rate.

An expression that quantifies the excess torsional stiffness as a function of the strength eccentricity, not including the torsional stiffness contribution of the *X*-direction elements, is expressed as,

$$\frac{K^x_{\theta y}}{K_{\theta y}} = 1 - \frac{1}{0.7}\frac{e_{vx}}{D} \qquad \frac{e_{vx}}{D} \le 0 \qquad \textbf{(2-41(a))}$$

$$\frac{K^x_{\theta y}}{K_{\theta y}} = 1 + \frac{1}{0.3}\frac{e_{vx}}{D} \qquad \frac{e_{vx}}{D} \ge 0 \qquad \textbf{(2-39(b))}$$

Figure 2-25(c) shows the effect of the strength eccentricity ratio on the r_{vy}/r_m ratio. It is evident that the position of the centre of mass affects the radius of gyration of strength. The radius of gyration of strength reduces and increases with negative and positive strength eccentricities, respectively. This is because the system excess strength differs if a negative or a positive strength eccentricity is introduced to the system. For *System 2*, excess strength of element *(1)* introduces the largest system excess strength. This reduces the radius of gyration of strength and therefore reduces the r_{vy}/r_m ratio.

2.17.3 Base shear-torque relationships of *System 2*

Figure 2-26(a) shows the base shear-torque relationships of unrestrained *System 2A*. The system, as in the previous case, is subjected to a unit static base shear, $V_y=1.0$. According to static equilibrium, elements *(1)* and *(2)* will have strengths of $0.70V_y$ and $0.30V_y$, respectively. The centres of mass, strength and stiffness coincide. Therefore, no strength or stiffness eccentricities are generated. The application of a unit lateral force, as in the previous case, develops simultaneously the base shear of both elements. At this stage, no torque can be sustained; see point *(A)* in Figure 2-26(a). The system can also resist a maximum torque of $T=0.7*0.3D*2=0.42A$ that develops for a reduced positive system base shear of $V_y=0.4$; see point *(B)* in Figure 2-26(a). This contrasts with unrestrained *System 1A*, shown in Figure 2-22(a), where the maximum torque develops for zero base shear force.

Consider the case, when for a particular reason, element *(1)* has an excess base shear of say *40%*, i.e. $V_{nel}=1.4*0.7V_y=0.98=0.77V_y$, while that of element *(2)* remains unchanged, thus, the system base shear increases to $V_y=1.28$. This base shear is associated with a torque of $T_v=e_{vx}V_y=0.065A*1.28=0.083A$; see point *(C)* in Figure 2-26. The system can resist a maximum torque of $T=(0.98*0.3A+0.3*0.7A)=0.50A$ for a reduced system base shear of $V_y=(0.98-0.3)=0.68$; see point *(D)* in Figure 2-26. The shaded areas correspond, as explained before, to base shear and torque combinations that can only be developed by dynamic-induced actions.

In case of restrained *System 2B*, the addition of the *X*-direction elements *(3)* and *(4)*, as shown in Figure 2-26(b), has a similar effect on the base shear-torque relationship as already observed for *System 1B*. The transverse elements provide additional torque resistance of $T=0.45A$. Therefore, when elements *(1)* and *(2)* of the restrained *System 2B* develop their maximum base shear of $V_y=1.0$, the system can also sustain a torque of $T=0.45A$; see point *(E)* in Figure 2-26(b). The torque increases as the base shear reduces and reaches a maximum of $T=0.87A$ for a reduced base shear of $V_y=0.40$; see point *(F)* in Figure 2-26(b). If element *(1)* has an excess strength of *40%*, the system base shear increases to $V_y=1.20$ and simultaneously the system can also resist, for a positive base shear, a torque of $T=-0.37A$ and $T=+0.53A$ depending on the sense of system rotation; see points *(G)* and *(H)* in Figure 2-26(b). The system could reach a maximum torque of $T=0.95A$ for a system base shear of $V_y=0.68$; see point *(I)* in Figure 2-26(b). The shaded areas correspond, as indicated before, to those base shear and torque combinations that can only be developed by dynamic-induced actions. High torques are not likely to approach the strength boundary. They can only occur when at least one element is elastic. This situation is, therefore, not critical in terms of element displacements.

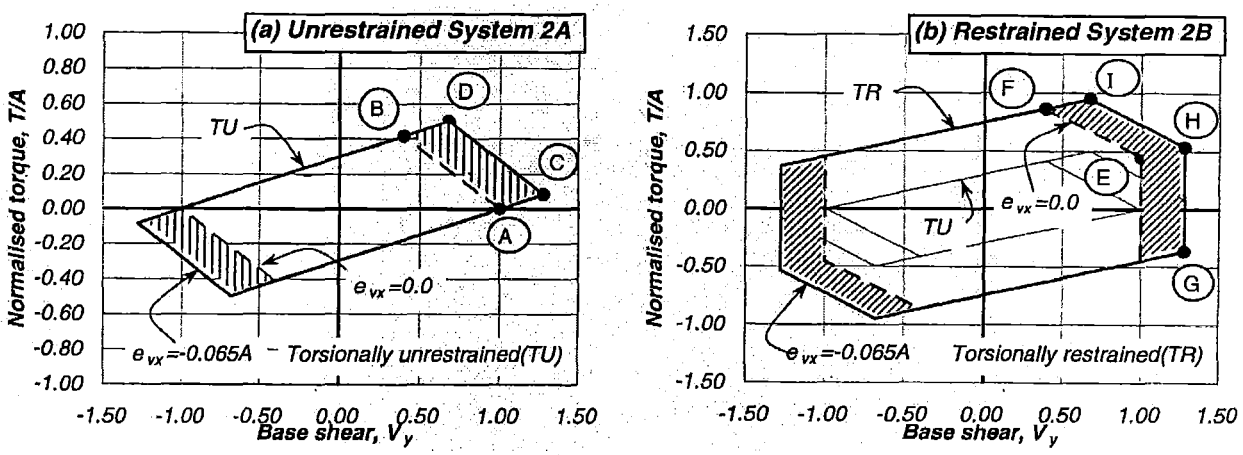

Figure 2-26 Base shear-torque relationships of *System 2*

2.18 Two-element structurally asymmetric *Systems 3, 4 and 5* (*CV=CM≠CR; CM=GC*)

2.18.1 Description and properties of *Systems 3, 4 and 5*

Systems 3, 4 and 5 consist of two wall-elements *(1)* and *(2)* parallel to the *Y*-axis with relative lengths of $\ell_1=1.40\ell_2$ and $\ell_2=1.0$, as shown in Figure 2-27. Hence, their nominal yield displacements are different. The geometric and mass centres of all systems are coincident. The configuration of the floor diaphragm and hence the element locations are different in each system.

The ratio of element nominal yield displacement, α,

$$\alpha = \frac{\Delta_{ye2}}{\Delta_{ye1}} \propto \frac{\ell_1}{\ell_2} \qquad \Delta_{ye2} \geq \Delta_{ye1} \qquad \ell_1 \geq \ell_2 \tag{2-42}$$

is a measure, in case of the two-element systems, of the relative nominal yield displacement of elements. It has a direct effect on the stiffness eccentricity associated with a given strength distribution. As a rule, centres of strength and stiffness will never coincide due to differences in the element's nominal yield displacement.

Systems 3, 4 and 5 have the same strength and nominal yield displacement along the *X* and *Y*-axis. Hence, their translational stiffness is also the same. To achieve this feature, the length and hence associated nominal yield displacement of the substitute elements along the *X*-direction, for any particular ratio of nominal yield displacement, can be obtained with the following expression.

$$\ell_3 = \ell_4 = 0.5(1+\alpha)\ell_2 \qquad \textbf{(2-43)}$$

The length of the *X*-direction elements *(3)* and *(4)* must be $\ell_3=\ell_4=1.20\ell_2$ length units for both unrestrained and restrained systems when the ratio of nominal yield displacement of elements *(1)* and *(2)*, is equal to $\alpha=1.40$ and the relative length of substitute element *(2)* is $\ell_2=1.0$.

The unrestrained *System 3A*, shown in Figure 2-27(a), has a single element along the *X*-axis providing translational stability and resistance but no torsional resistance. In contrast, restrained *System 3B* has two *X*-direction elements *(3)* and *(4)*, equidistant from the centre of mass, providing torsional resistance. The system strength is distributed to the elements to satisfy static equilibrium criteria. The distance between elements *(1)* and *(2)* of $D=0.83A$ was selected to achieve a ratio of radii of gyration of strength and mass of $r_{vy}/r_m=1.01$. The chosen distance between those elements generates an uncoupled translational period along the *Y*-axis equal to the uncoupled rotational period of the system when the stiffnesses of *X*-direction elements *(3)* and *(4)* are neglected due to the reasons provided in Section 2.13. Hence, the ratio of radii of gyration of stiffness and mass is $r_{ky}/r_m=1.0$. The distance between the *X*-direction elements *(3)* and *(4)* is also equal to $E=0.83A$. Hence, the system ratios along the *X*-axis are the same; $r_{vx}/r_m=r_{kx}/r_m=1.01$. The nominal yield displacement of the *X*-direction elements are identical.

System 4A and *4B* are torsionally unrestrained and restrained, respectively, having a rectangular diaphragm of *(1.41A* 0.71A)*, as shown in Figure 2-27(c) and (d). The total mass of the system is equal to that of *System 3* but its distribution is different. This is reflected by the different radius of gyration of mass of the rectangular and the square diaphragm, as described in Section 2.12. Elements *(1), (2), (3)* and *(4)* are placed at the edges of the floor diaphragm. The ratio of nominal yield displacement of elements *(1)* and *(2)* is again $\alpha=1.40$. The nominal yield displacement of the system is the same along the principal axes if the length of the *X*-direction elements is also $\ell_3=\ell_4=1.20\ell_2$.

System 5 has the same floor diaphragm configuration of *System 4*, as shown in Figure 2-26(e) and (f). However, elements *(1)* and *(2)* are positioned at the edges of the long side of the diaphragm. The ratio of nominal yield displacement of elements *(1)* and *(2)* is also $\alpha=1.40$ and the the length of the *X*-direction elements is also $\ell_3=\ell_4=1.20\ell_2$.

All three systems will be subjected to earthquake records along different directions relative to the reference Y-axis, as Figure 2-27 shows.

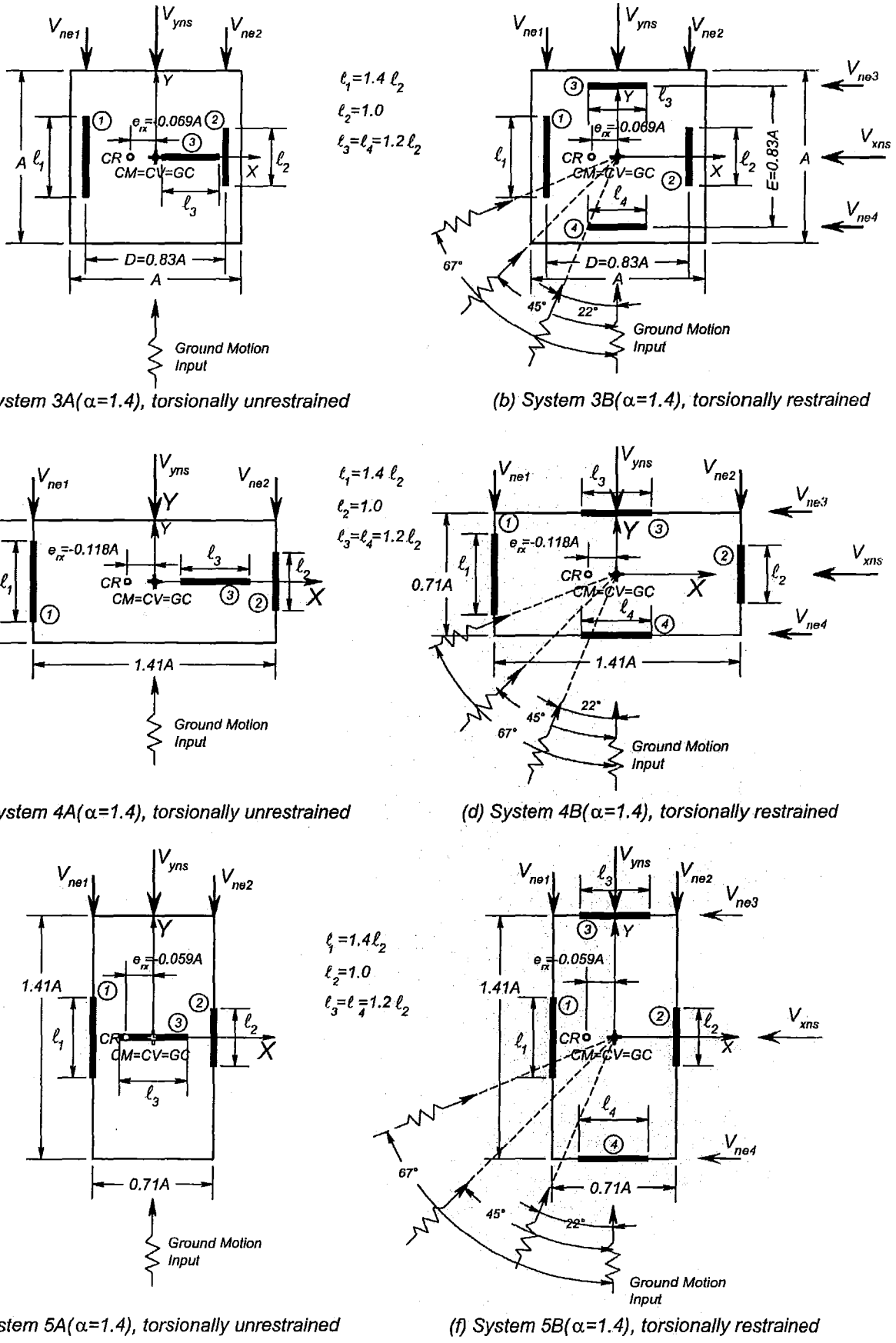

(a) System 3A(α=1.4), torsionally unrestrained

(b) System 3B(α=1.4), torsionally restrained

(c) System 4A(α=1.4), torsionally unrestrained

(d) System 4B(α=1.4), torsionally restrained

(e) System 5A(α=1.4), torsionally unrestrained

(f) System 5B(α=1.4), torsionally restrained

Figure 2-27. Two-element structurally asymmetric *Systems 3, 4,* and *5*

(a) Variation of the ratio of nominal yield displacement on the elements

It was stated before that the ratio of element nominal yield displacement of the elements has an effect on the stiffness eccentricity. For instance, consider *System 3* having a ratio of the nominal yield displacements of elements *(1)* and *(2)* of α=*1.2, 1.6, 2.0* and *2.5*. These systems are denoted herein as *Systems 3(α=1.2), 3(α=1.6), 3(α=2.0)* and *3(α=2.5)*. These ratios, associated with zero strength eccentricity, i.e., (λ_1 =*1.0*), results in stiffness eccentricities of e_{rx}=*-0.0455D, -0.0833D, -0.1154D, -0.1667D and -0.2143D*, respectively.

Table 2-5 summarizes radii of gyration and ratios of *Systems 3, 4,* and *5* when the system strength is distributed to satisfy static equilibrium and the ratio of element nominal yield displacement is varied between α=*1.0* and *2.5* for *System 3*.
Appendix B summarizes the properties of the systems for a fixed nominal yield displacement ratio of α=*1.4*.

Table 2-5 Radii of gyration of strength, stiffness and mass and relevant ratios for *Systems 3, 4* and *5*

		e_{vx}=0.0	e_{mx}=0.0		D=E=0.83A			
System	$\alpha=\Delta_{ye2}/\Delta_{ye1}$	e_{rx}	r_m	r_{vy}	r_{vx}	r_{vy}/r_m	r_{vx}/r_m	r_{vx}/r_{vy}
3A(α=1.0)	1.00	0.00	0.41A	0.42A	0.0	1.01	0.000	0.00
3B(α=1.0)	"	"	"	"	0.42A	"	1.014	1.00
3A(α=1.2)	1.20	-0.038A	"	"	0.0	"	0.000	0.00
3B(α=1.2)	"	"	"	"	0.42A	"	1.014	1.00
3A(α=1.4)	1.40	-0.069A	"	"	0.0	"	0.000	0.00
3B(α=1.4)	"	"	"	"	0.42A	"	1.014	1.00
3A(α=1.6)	1.60	-0.096A	"	"	0.0	"	0.000	0.00
3B(α=1.6)	"	"	"	"	0.42A	"	1.014	1.00
3A(α=2.0)	2.00	-0.139A	"	"	0.0	"	0.000	0.00
3B(α=2.0)	"	"	"	"	0.42A	"	1.014	1.00
3A(α=2.5)	2.50	-0.178A	"	"	0.0	"	0.000	0.00
3B(α=2.5)	"	"	"	"	0.42A	"	1.014	1.00
	e_{vx}=0.0		e_{mx}=0.0	D=1.41A		E= 0.71A		
4A(α=1.4)	1.40	-0.118A	0.46A	0.71A	0	1.54	0	0.00
4B(α=1.4)	"	"	"	"	0.36A	"	0.76	1.00
	e_{vx}=0.0		e_{mx}=0.0	D=0.71A		E=1.41A		
5A(α=1.4)	1.40	-0.059A	0.46A	0.36A	0	0.76	0	0.00
5B(α=1.4)	"	"	"	"	0.71A	"	1.54	1.00

(b) The nominal yield displacement of the systems

The nominal yield displacement of the systems, having different ratios of element nominal yield displacement, may remain constant if they satisfy the following expressions.

$$\Delta_{ye1} = \frac{(\alpha+1)}{2\alpha}\Delta_{ys} \qquad \textbf{(2-44(a))}$$

$$\Delta_{ye2} = \alpha\Delta_{ye1} \qquad \textbf{(2-42(b))}$$

For example, *System 3* has *Y*-direction elements *(1)* and *(2)* with nominal yield displacement of Δ_{ye1}=*36.0mm* and Δ_{ye2}=*50.0mm*, i.e., α=*1.40*, respectively and a system nominal yield displacement at the centre of mass, associated with zero strength eccentricity, of Δ_{ys}=*42mm*. The same system nominal yield displacement can be achieved with another system having a ratio of element nominal yield displacement of α=*2.0*. According to Eq 2-42, elements *(1)* and *(2)* should have nominal yield displacements of Δ_{ye1}=*31.5mm* and Δ_{ye2}=*63.0mm*, respectively to retain the same system nominal yield displacement of Δ_{ys}=*42mm*.

2.18.2 Excess strength of elements of *Systems 3, 4 and 5*

Figure 2-28(a) shows the effect of excess strength of either element *(1)* or *(2)* on the system excess strength and on eccentricities of *Systems 3, 4* and *5*. This is also presented in Table 2-6 for some specific strength eccentricities. An excess strength of element *(1)* (λ_1>*1.0*) introduces negative strength and stiffness eccentricities and a system excess strength as discussed before. The difference between strength and stiffness eccentricities is almost constant for the range of values considered (*1.0*<λ_1<*2.0*). A similar feature occurs with excess strength of element *(2)*(λ_2>*1.0*). At this stage, it is also evident that stiffness eccentricity can be eliminated. This will depend on the excess strength assigned to element *(2)* and the system nominal yield displacement ratio. This feature is useful for systems expected to respond in the elastic range. It indicates that the structural designer has the ability to influence system response by distributing strength in a particular manner to achieve a more desirable structural behaviour.

Equation 2-34 also quantifies for *Systems 3, 4, and 5* the system excess strength as a function of the strength eccentricity ratio.

The variation of the stiffness eccentricity ratio, as a function of excess strength factors λ_1 and λ_2 and the ratio of element nominal yield displacement of *Y*-direction elements is expressed as,

$$\frac{e_{rx}}{D} = 0.5\frac{(1-\alpha\lambda_1)}{(1+\alpha\lambda_1)} \qquad \lambda_1 \geq 1.0 \qquad \frac{e_{vx}}{D} \leq 0 \qquad \textbf{(2-45(a))}$$

$$\frac{e_{rx}}{D} = 0.5\frac{(\lambda_2-\alpha)}{(\lambda_2+\alpha)} \qquad \lambda_2 \geq 1.0 \qquad \frac{e_{vx}}{D} \geq 0 \qquad \textbf{(2-45(b))}$$

Figure 2-28(b) shows the effect of excess strength of either element *(1)* or *(2)* on the system's translational and torsional stiffness for α=*1.40*. The contribution of the stiffness of the *X*-direction elements is neglected. The excess strength of element *(1)* (λ_1>*1.0*) introduces an increase of translational stiffness at a faster rate than the increase of the torsional stiffness. This happens because element *(1)* has a smaller nominal yield displacement and is closer to the centre of stiffness. On the other hand, the excess strength of element *(2)* (λ_2>*1.0*) introduces a larger increase of torsional stiffness. This happens because element *(2)* has a larger nominal yield displacement which offsets the large distance between element *(1)* and the centre of stiffness, thus producing a similar increase of translational and torsional stiffness.

Table 2-6. Summary on strength and stiffness eccentricities of *Systems 3A-1.3(α=variable)*.

α	λ_1	Strength and stiffness eccentricities						
		λ_1=1.86	λ_1=1.50	λ_1=1.22	λ_1=1.0	λ_2=1.22	λ_2=1.50	λ_2=1.86
$\Delta_{ye2}/\Delta_{ye1}$	e_{vx}/D	-0.15	-0.1	-0.05	0	0.05	0.1	0.15
α=1.0		-0.150	-0.100	-0.050	0.000	0.050	0.100	0.150
α=1.2		-0.191	-0.143	-0.094	-0.045	0.004	0.056	0.108
α=1.4		-0.223	-0.177	-0.131	-0.083	-0.034	0.017	0.071
α=1.6	e_{rx}/D	-0.248	-0.206	-0.161	-0.115	-0.067	-0.016	0.038
α=2.0		-0.288	-0.250	-0.209	-0.167	-0.121	-0.071	-0.018
α=2.5		-0.323	-0.289	-0.253	-0.214	-0.172	-0.125	-0.073
α=4.0		-0.382	-0.357	-0.330	-0.300	-0.266	-0.227	-0.183

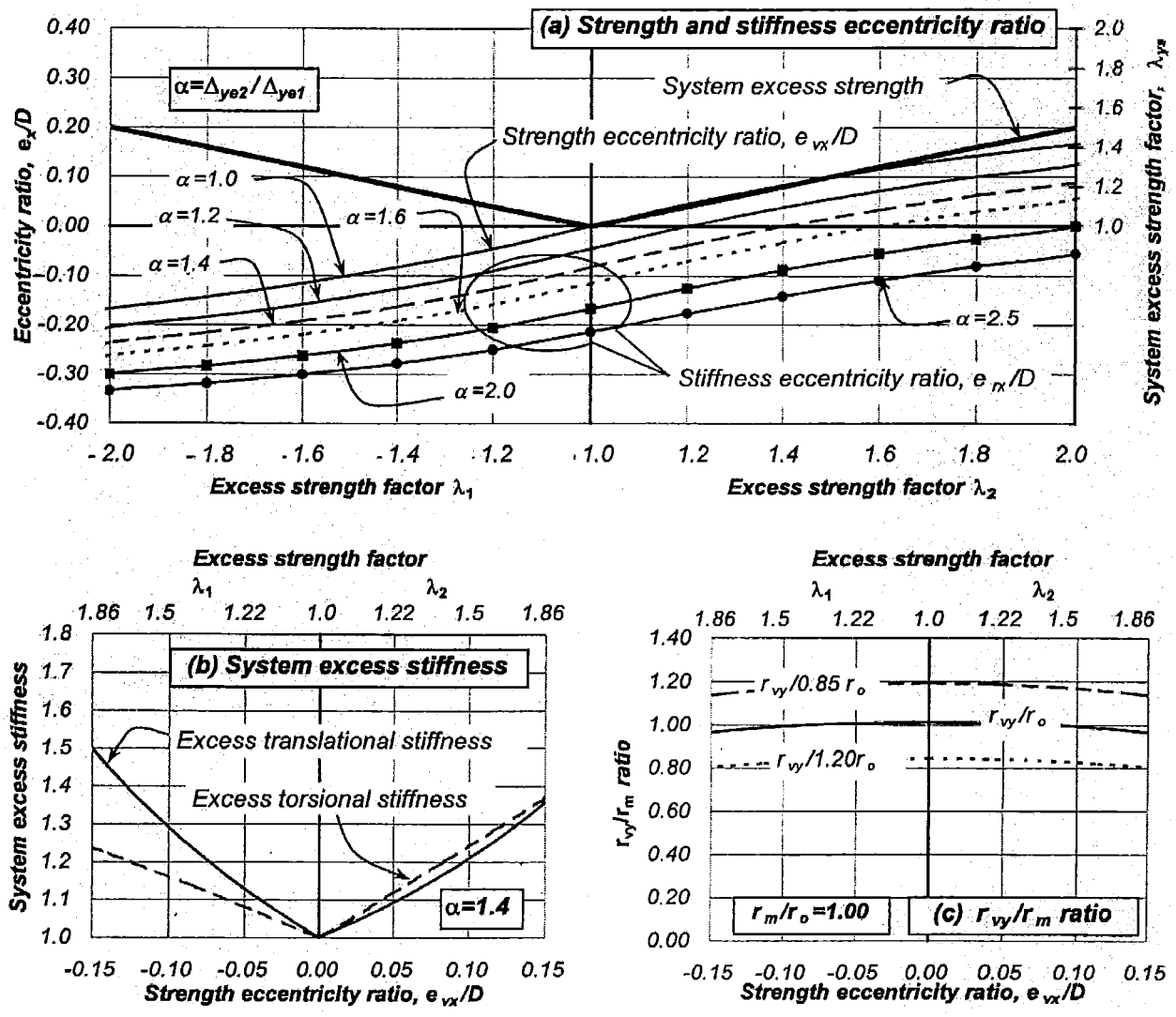

Figure 2-28. Parameters affecting the strength and stiffness eccentricity and properties of *Systems 3, 4 and 5*

The effect of the strength eccentricity and the ratio of element nominal yield displacement on the increase of translational stiffness is expressed as,

$$\frac{K_{ys}^{x}}{K_{ys}} = \left(\frac{2}{(1+\alpha)\left(2\frac{e_{vx}}{D}+1\right)} \right) \qquad \frac{e_{vx}}{D} \le 0 \qquad \textbf{(2-46(a))}$$

$$\frac{K_{ys}^{x}}{K_{ys}} = \left(\frac{2\alpha}{(1+\alpha)\left(1-2\frac{e_{vx}}{D}\right)} \right) \qquad \frac{e_{vx}}{D} \ge 0 \qquad \textbf{(2-46(b))}$$

The effect of the strength eccentricity and the ratio of the nominal yield displacement of the elements on the relative increase of torsional stiffness of the system is expressed as,

$$\frac{K_{\theta y}^{x}}{K_{\theta y}} = 0.5\left(\frac{1+\alpha}{\alpha}\right)\left(1-2\frac{e_{vx}}{D}\right) \qquad \frac{e_{vx}}{D} \le 0 \qquad \textbf{(2-47(a))}$$

$$\frac{K_{\theta y}^{x}}{K_{\theta y}} = 0.5(1+\alpha)\left(1-2\frac{e_{rx}}{D}\right) \qquad \frac{e_{vx}}{D} \ge 0 \qquad \textbf{(2-47(b))}$$

Figure 2-28(c) shows the same reduction of the r_{vy}/r_m ratio already observed for *System 1* as the strength eccentricity increases. It indicates that the strength eccentricity essentially does not affect the radius of gyration of strength if the system has no mass-eccentricity.

2.18.3 Base shear-torque relationships

The base shear-torque boundaries of *Systems 3, 4 and 5* exhibit characteristics similar to those already established for *System 1*, as shown in Figure 2-29(a) to (f). It is evident that the unrestrained *System 4A* can resist a larger torque because of the larger distance between elements *(1)* and *(2)*. This system also exhibits the largest strength eccentricity e_{vx}=*-0.118A* when element *(1)* has a *40%* excess strength. This results, as shown in Figure 2-29(c), in the largest shaded area of all the systems. It indicates that the mass rotational inertia introduces the largest dynamic torque to the unrestrained *System 4A* ($T=e_{vx}*V_y=0.14A$) when elements *(1)* and *(2)* are yielding. A similar feature occurs with the restrained *System 4B*; see Figure 2-29(d).

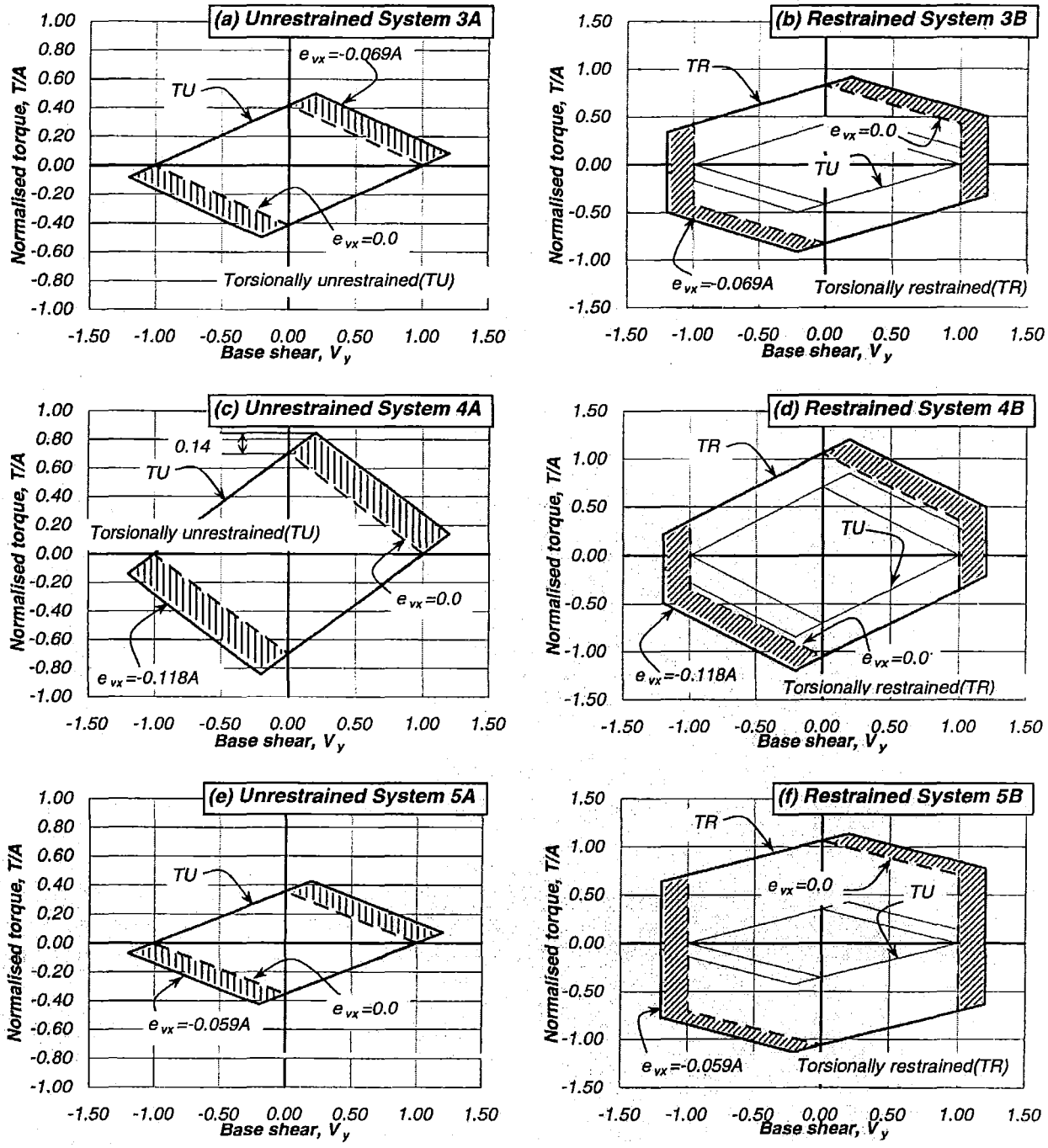

Figure 2-29. Base shear-torque relationships or *Systems 3, 4 and 5*

2.19 Two-element structurally asymmetric and mass eccentric *System 6* (*CV=CM≠CR; CM≠GC*)

2.19.1 Description and properties of *System 6*

System 6 is structurally asymmetric and mass eccentric, as shown in Figure 2-30. This system has similar characteristics as the previously described *System 2*. It has a square configuration of (*AxA*) and a mass eccentricity of e_{mx}=*-0.20A* indicating that the centres of mass and geometry are non-coincident. The ratio of the nominal yield displacement of elements *(1)* and *(2)* is α=*1.40*.

The associated relative length of the substitute wall-elements is $\ell_1=1.4\ell_2$ and $\ell_2=1.0$, respectively. The position of elements *(1)* and *(2)* is the same as that of *System 2*, thus the radius of gyration of strength and mass is $r_{vy}/r_m=1.0$. The ratio of radius of gyration of stiffness and mass is $r_{ky}/r_m=0.92$ due to differences in the nominal yield displacement of elements *(1)* and *(2)*. The nominal yield displacement of *System 6* will be the same along both axis if the relative lengths of the *X*-direction wall elements *(3)* and *(4)* is made equal to $\ell_3=\ell_4=1.20\ell_2$. The unrestrained *System 6A* will be subjected to earthquake records along the *Y*-axis whereas they are applied along different directions to the restrained *System 6B*.

Table 2-7 lists the radii of gyration of mass, strength and stiffness and relevant ratios of *System 6*. Appendix *B* provides more details of the systems properties.

Table 2-7 Radii of gyration of strength, stiffness and mass and relevant ratios of *Systems 6*

	e_{vx}=0.0	e_{rx}=-0.066D	e_{mx}=-0.20D	D=0.99A	E=0.90A			
System	r_m/r_o	r_m	r_{vy}	$r_{vx}=r_{kx}$	r_{vy}/r_m	$r_{vx}/r_m=r_{kx}/r_m$	r_{ky}	r_{ky}/r_m	r_{vx}/r_{vy}
6A	1.10	0.45	0.46D	0.00	1.00	0.00	0.42D	0.92	0.00
6B	"	"	"	0.50E	"	1.00	"	"	1.00

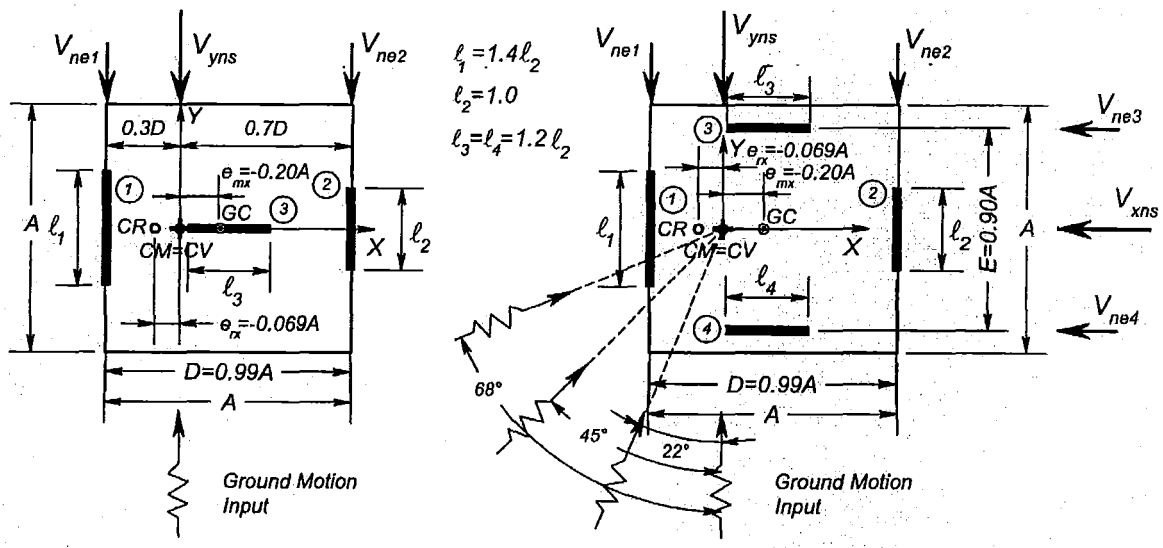

(a) System 6A(α=1.4), torsionally unrestrained *(b) System 6B(α=1.4), torsionally restrained*

Figure 2-30 Structurally asymmetric and mass eccentric *System 6*

2.19.2 Excess strength associated with *System 6*

Figure 2-31(a) shows the effect that excess strength of either element *(1)* or *(2)* has on strength and stiffness eccentricities and system excess strength. The layout is similar to that of *System 2*, shown in Figure 2-24. The distribution of strength according to static equilibrium, as already described for unrestrained *System 2A*, generates zero strength eccentricity. A stiffness eccentricity of $e_{rx}=-0.066A$ is, however, introduced due to differences in the nominal yield displacement of elements *(1)* and *(2)*, i.e., *(α=1.4)*. The distance between the strength and stiffness eccentricity is essentially a constant as negative or positive strength eccentricities are introduced to the system.

Equation 2-37, which also applies to structurally symmetric *System 2*, quantifies the variation of the strength eccentricity ratio of *System 6* as a function of excess strength factors λ_1 and λ_2.

The variation of the stiffness eccentricity ratio as a function of the excess strength factors is expressed as,

$$\frac{e_{rx}}{D} = \frac{0.21(1-1.4\lambda_1)}{0.98\lambda_1 + 0.3} \qquad \lambda_1 \geq 1.0 \qquad \frac{e_{vx}}{D} \leq 0 \qquad \textbf{(2-48(a))}$$

$$\frac{e_{rx}}{D} = \frac{0.21(\lambda_2 - 1.4)}{0.98 + 0.3\lambda_2} \qquad \lambda_2 \geq 1.0 \qquad \frac{e_{vx}}{D} \geq 0 \qquad \textbf{(2-48(b))}$$

The relationship between the system excess strength and the strength eccentricity ratio is also given by Eq 2-38.

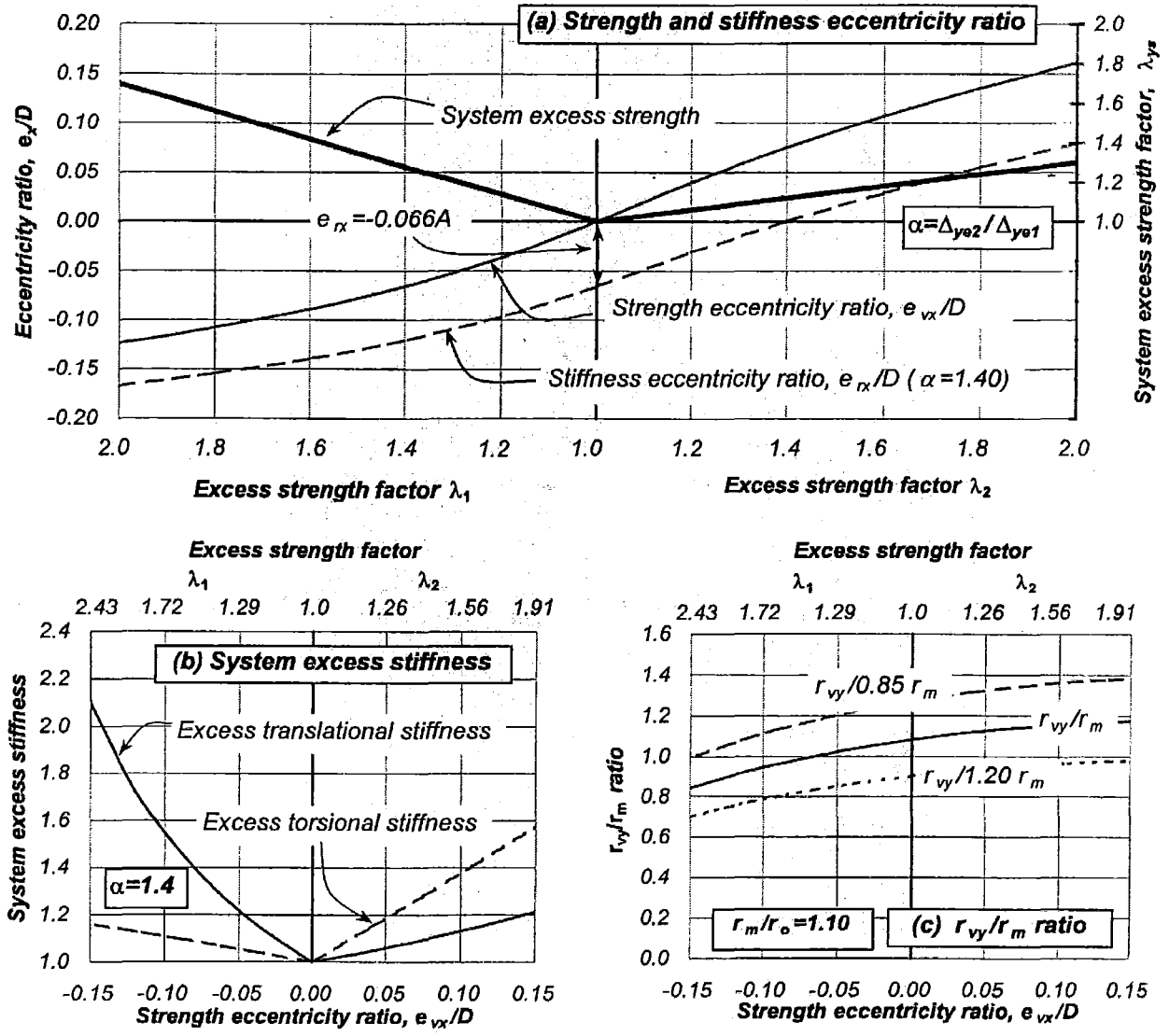

Figure 2-31. Properties affecting strength and stiffness eccentricity ratios and properties of *System 6*

Figure 2-31(b) shows the effect that excess strength of elements *(1)* and *(2)* has on the relative translational and torsional stiffness of *System 6*. It is evident that the excess strength of element *(1)*, which is the element with a relative larger nominal strength, generates a large increase of translational stiffness. In contrast, excess strength of element *(2)*, which was assigned a relatively smaller nominal strength, introduces a large excess torsional stiffness. This variation is due to the same reasons provided for *System 2*; see Section 2.17.2.

The variation of the r_{vy}/r_m ratio and the base shear-torque relationships is the same as that of *System 2*; see Figure 2-26. The fact that the stiffness of the elements are different does not have an effect on the base shear-torque relationship.

2.20 Single-element structurally asymmetric *Systems 7, 8* and *9* (*CV=CR≠CM; CM=GC*)

2.20.1 Description and properties of *Systems 7, 8* and *9*

Systems 7, 8 and 9, shown in Figure 2-32, are simple and extremely eccentric asymmetric systems. They may not be realistic but they can provide a good understanding of the response of asymmetric systems. Every system has a different plan configuration and element layout. Centres of mass and geometry are coincident in all systems.

Torsionally unrestrained *Systems 7A, 8A and 9A*, as shown in Figure 2-32(a),(c) and (e), do not have torsional resistance and are unstable when subjected to a static lateral force. The systems, although unstable when subjected to static lateral forces, are of particular interest because they become stable when subjected to dynamic-induced forces due to the mass rotational inertia of the floor about the vertical axis. These systems will be subjected to unidirectional earthquake records along the *Y*-axis.

These systems comprise only two elements. The *Y*-direction element *(1)* is placed at the left, a distance of *0.41A, 0.71A* and *0.35A*, respectively, from the centre of mass. This element will provide, during dynamic response, lateral strength and stability along the *Y*-axis and will contribute to torsional resistance of the system. Position *(2)* is the location in the floor diaphragm opposite to that of element *(1)* where displacements demands will be measured. The *X*-direction element *(3)*, coinciding with a line passing through the centre of mass, provides only lateral strength and stability along this axis.

Torsionally restrained *Systems 7B, 8B and 9B*, shown in Figure 2-32(b), (d) and (f), comprise two *X*-direction elements. The distance *E* between these elements is variable as shown. These elements provide lateral strength and stability and provide torsional resistance. The systems will be subjected to earthquake records at different angles as shown, i.e., 22°, 45°, 67° and 90°.

These systems have different properties, as illustrated in Table 2-8 and Appendix *B*. They have different plan configurations. However, the total mass of all systems is constant. The differences in mass distributions are quantified with the radius of gyration of mass. Strength and stiffness eccentricities are obviously different in each system. The radius of gyration of strength, r_{vy}, with respect to the *Y*-axis, is zero in these systems. Hence, it is not possible to differentiate the systems with the r_{vy}/r_m ratio established before. This issue is overcome by using the e_{vx}/r_m ratio.

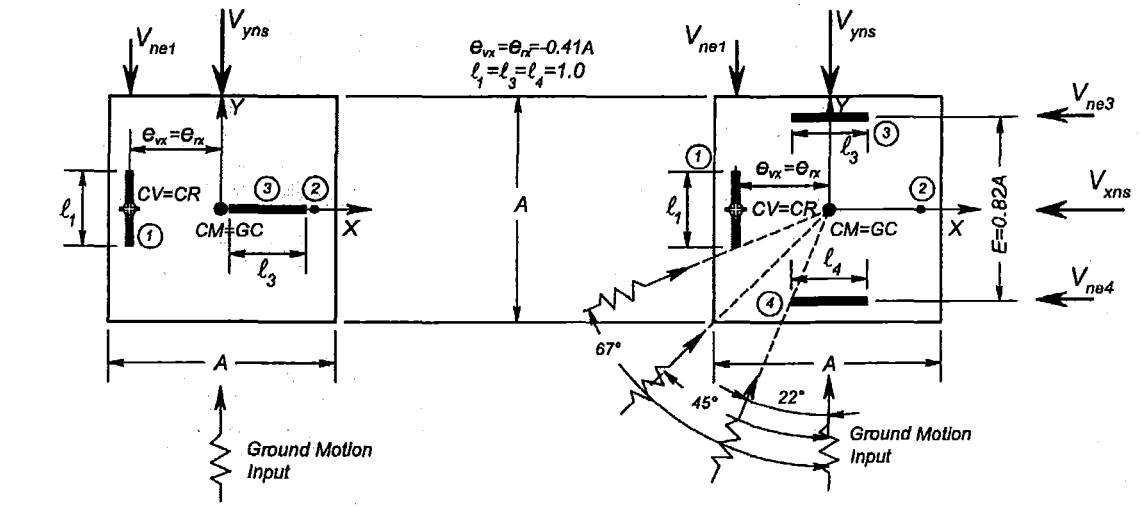

(a) System 7A, torsionally unrestrained (b) System 7B, torsionally restrained

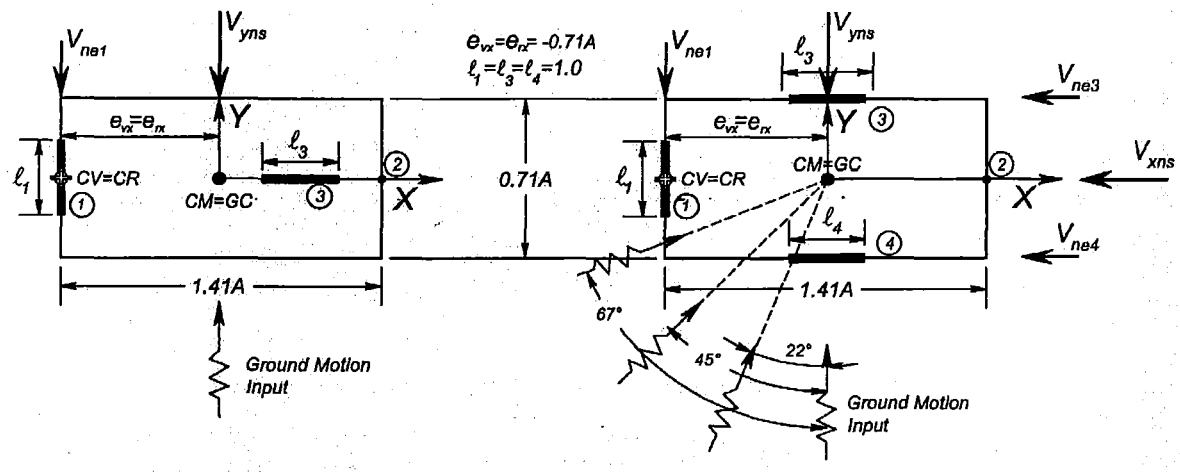

(c) System 8A, torsionally unrestrained (d) System 8B, torsionally restrained

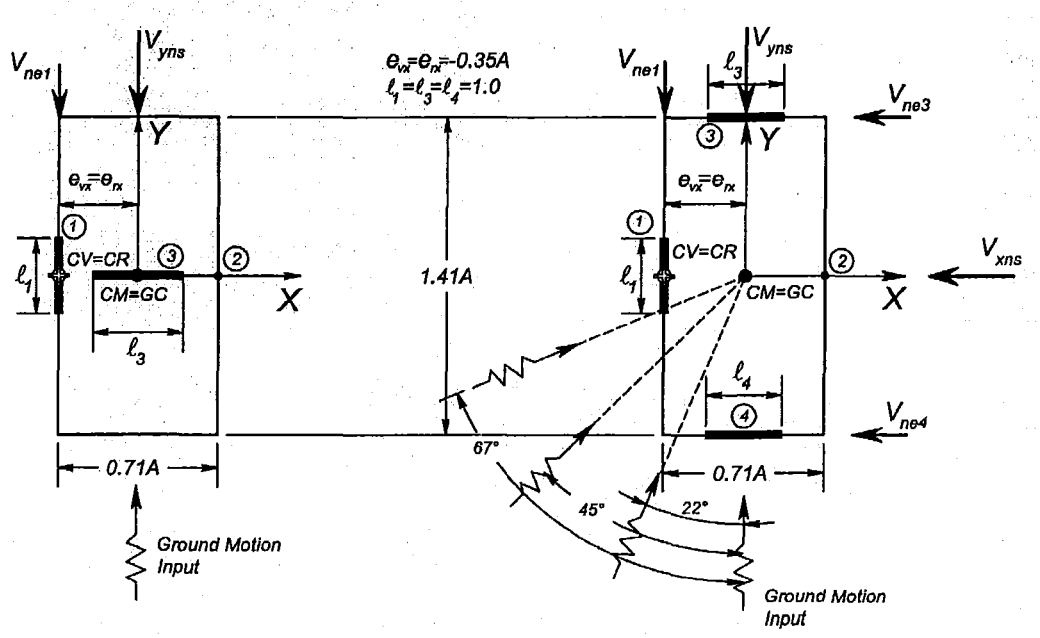

(e) System 9A, torsionally unrestrained (f) System 9B, torsionally restrained

Figure 2-32. Structurally asymmetric *Systems 7, 8 and 9*

Table 2-8. Radii of gyration of mass, strength and stiffness and relevant ratios of *Systems 7, 8 and 9*

System	$e_{vx}=e_{rx}$	r_m/r_o	r_m	e_{vx}/r_m	$r_{vy}=r_{ky}$	$r_{vx}=r_{kx}$
7A	*0.41A*	*1.00*	*0.41A*	*1.0*	*0.0*	*0.0*
7B	"	"	"	"	"	*0.41A*
8A	*0.71A*	*1.12*	*0.46A*	*1.54*	*0.0*	*0.00*
8B	"	"	"	"	"	*0.71A*
9A	*0.35A*	*1.12*	*0.46A*	*0.76*	*0.0*	*0.00*
9B	"	"	"	"	"	*0.35A*

The excess strength of element *(1)* increases the translatory strength of the system along the *Y*-direction and as expected does not have an effect on its strength eccentricity.

2.20.2 Base shear-torque relationships of asymmetric *Systems 7, 8 and 9*

The base shear-torque relationships of the unrestrained *Systems 7A, 8A and 9A* are illustrated in Figure 2-33(a),(c) and (e). It is evident that a linear variation between base shears and torques in both the elastic and inelastic range of response may be developed. This relationship, however, cannot be developed when the systems are subjected to static forces because, as explained above, they are statically unstable systems. Stability may be achieved if the system is subjected to dynamic-induced forces when the opposition of the mass rotational inertia to system rotation is triggered. This action allows element (1) to develop its strength.

In case of unrestrained *System 7A*, point *(A)* corresponds to the maximum torque associated with the full strength of the system, and hence that of element *(1)*, when it is subjected to dynamic induced forces along the *Y*-axis, i.e., $T=e_{vx}V_{yns}=0.41A$. This torque may be increased to $T=0.49A$ by increasing the strength of element *(1)*, and hence that of the system, by say 20%, as shown by point *(B)* in Figure 2-33(a).

Systems 8A and 9A, although having the same translational strength, can develop a different torque when subjected to dynamic induced forces because they have different strength eccentricities, as shown in Table 2-8. For instance, the unrestrained *System 8A* shows the largest torque, $T=0.71A$, due its larger strength eccentricity, see Figure 2-33(c).

The systems are not capable or resisting static lateral force along the *Y*-axis. The application of a positive lateral force at the centre of mass would introduce an anticlockwise system rotation about its centre of strength and stiffness and no resistance is expected from any element. No equilibrium can be maintained. The system is unstable, i.e., a mechanism develops. Therefore, considerations of static actions are unable to contribute to the prediction of system rotations. The torque to be eventually introduced to the system, as indicated by the base shear torque relationship, must be entirely due to dynamic actions of the inertia of the translational and rotational mass. This dynamic behaviour will be described in Section 3.7.2.

The base shear-torque relationships of the restrained *Systems 7B, 8B and 9B* are also presented in Figure 2-33(b), (d) and (f). It is evident that the inclusion of *X*-direction elements provides torsional strength to the system. In case of restrained *System 7B*, the magnitude of the torsional resistance depends on the base shear being positive or negative. For instance, for a positive base shear, the system cannot resist a positive or anticlockwise torque; see point *(D)* in Figure 2-33(b), but it can resist a negative or clockwise torque of $T=-0.82A$; see point *(C)*. The torsional strength of the different systems differs, as explained before, due to differences in the location of

the *X*-direction elements. As expected, restrained *System 9B*, shown in Figure 2-33(f), has the largest increase of torsional strength.

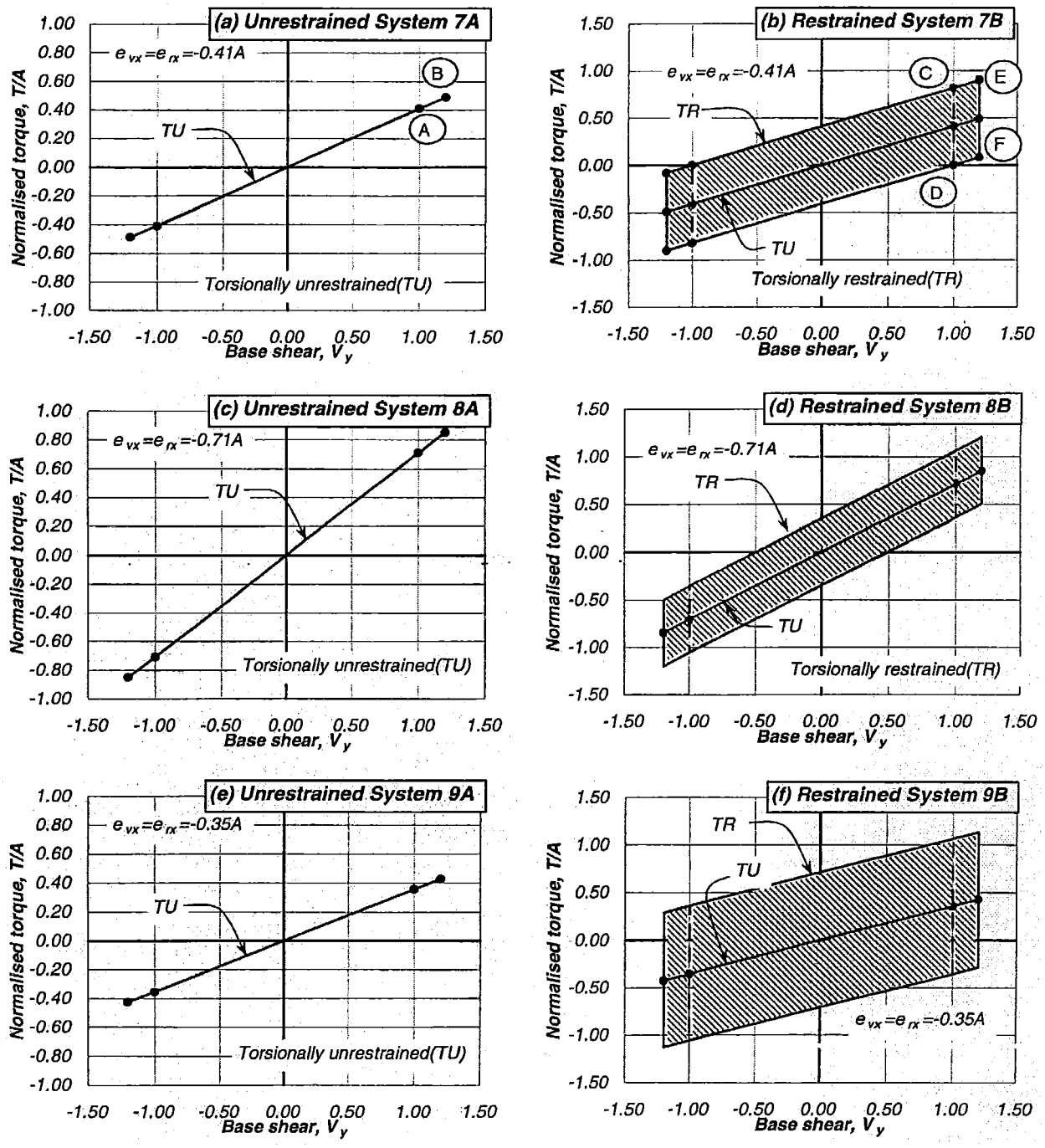

Figure 2-33. Base shear-torque relationships of *Systems 7, 8 and 9*

The effect of providing 20% excess strength to element *(1)*, and hence to the system, is also presented in Figure 2-33(b), (d) and (f). It is shown again that the increase in the system base shear capacity also increases its lateral and torsional resistance. In case of *System 7B*; see Figure 2-33(b), a positive base shear can sustain maximum and minimum negative torques of T=-*0.082A* and T=-*0.90A*, respectively. It is evident that all combinations of base shear and torque that can only be achieved by the dynamic action of both the mass rotational and translational inertia as the shaded area shows.

2.21 Three-element structurally asymmetric *System 10* (*CV≠CR; CM=GC*)

2.21.1 Description and properties of *System 10*

System 10, as shown in Figure 2-34, consists of a square rigid diaphragm of (*AxA*) and three parallel *Y*-direction elements *(1)*, *(2)* and *(3)*. They are substitute walls with relative lengths of $\ell_1=1.0$, $\ell_2=2.0\ell_1$ and $\ell_3=1.0\ell_1$. These elements will provide translational strength along the *Y*-axis and torsional resistance. Unrestrained *System 10A* has a fourth *X*-direction element providing translational strength and stability but no torsional resistance. On the other hand, restrained *System 10B* has two *X*-direction elements *(4)* and *(5)* providing translational strength and system torsional resistance. Elements *(1)* and *(3)* are at the edges of the square plan and element *(2)* is placed at a distance *0.14A* left of the centre of mass. The translational strength and stiffness of the system is the same along both principal axes. To achieve this characteristic, the length of wall-elements *(4)* and *(5)* is made equal to $\ell_4=\ell_5=1.63\ell_1$ length units. The systems will be subjected to earthquake records at different angles.

The distribution of system strength to the elements should preferably satisfy static equilibrium. There are unlimited solutions that may satisfy this criterion, as already stated in Section 2.11.3. For instance, the strength may initially be distributed inversely proportional to the nominal yield displacement of the wall squared, $V_{ne} \propto 1/\Delta_{ye}^2$, as shown in Figure 2-17, leading to a strength eccentricity of $e_{vx}=-0.093A$. To eliminate this strength eccentricity, a torque of $T=e_{vx}V_y=0.093A$ was redistributed to elements *(1)* and *(3)*, as explained in Section 2.11.3.

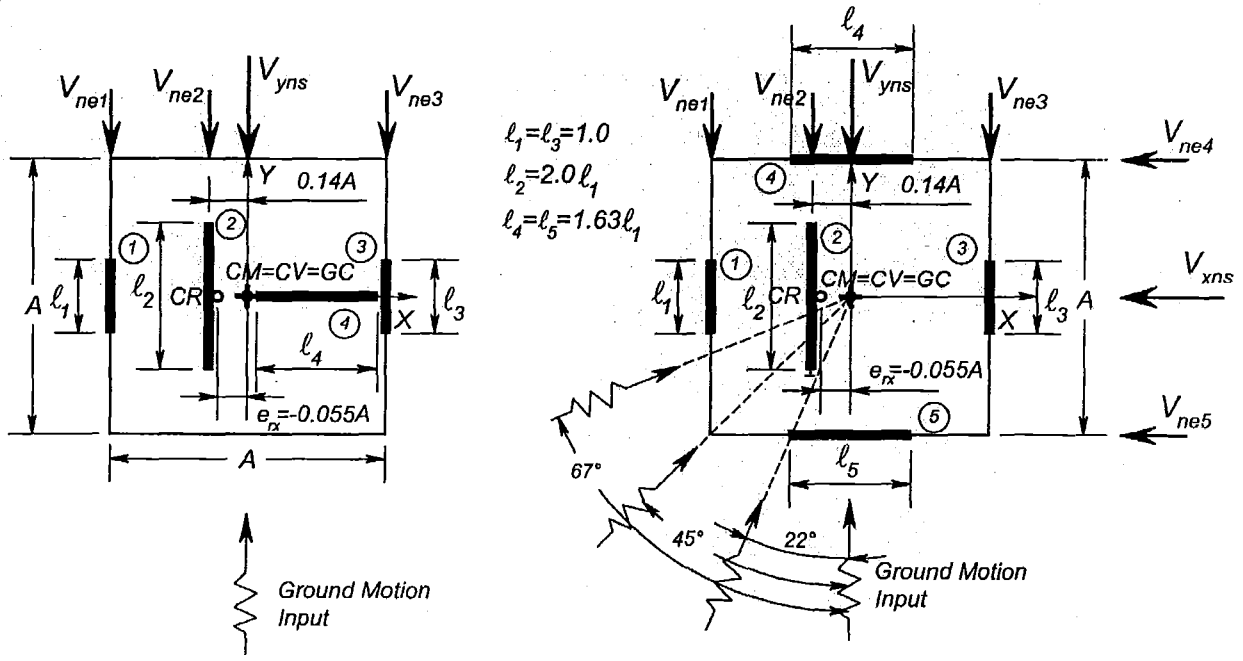

(a) System 10A, torsionally unrestrained *(b) System 10B, torsionally restrained*

Figure 2-34. Three-element structurally asymmetric *System 10*

Table 2-9 summarizes the radius of gyration of strength, stiffness and mass and the relevant ratios of *System 10* when strength is distributed to the elements to satisfy static equilibrium. Appendix *B* summarizes the properties of strength and stiffness of the system.

Table 2-9. Radii of gyration of strength, stiffness and mass and relevant ratios of *System 10*

				e_{vx}=0.0		e_{rx}=-0.055A					
System	r_m/r_o	r_m	r_{vy}	r_{vx}	r_{vy}/r_o	r_{vx}/r_o	r_{ky}	r_{kx}	r_{ky}/r_o	r_{kx}/r_o	r_{vx}/r_{vy}
10A	1.00	0.41A	0.32A	0.00	0.78	0.00	0.26A	0.00	0.63	0.00	0.00
10B	"	"	"	0.50A	"	1.22	"	0.50A	"	1.22	1.22

2.21.2 Excess strength associated with *System 10*

System 10 will have a strength eccentricity if one or more elements have strength in excess of that satisfying static equilibrium. In case of multi-element systems, a strength eccentricity is associated with several values of element excess strength. The critical scenario will occur when either edge elements *(1)* or *(3)* have excess strength. Their excess strength will introduce the largest possible strength eccentricity for the smallest increase of system strength. For instance, to reach a maximum negative and positive strength eccentricity of $e_{vx}=\pm 0.15D$ the excess strength factor of elements *(1)* or *(3)* will need to be of $\lambda_1=5.54$ and $\lambda_3=2.58$, respectively which are unrealistic values of element excess strength. The excess strength of element *(2)* will generate a less critical relationship between system excess strength and strength eccentricity.

Figure 2-35(a) shows the effect that excess strength of either element *(1)* or *(3)* has on strength and stiffness eccentricities. The excess strength of element *(1)*($\lambda_1>1.0$) introduces a negative strength eccentricity. It is evident that strength and stiffness eccentricities do not increase by the same order because element *(1)* has a small nominal yield displacement and therefore the increase of strength of element *(1)* does not generate a proportional increase in element stiffness. The distance between centres of strength and stiffness reduces reaching the same value when $\lambda_1=4.8$. In contrast, the excess strength of element *(3)* ($\lambda_3>1.0$) introduces a positive strength eccentricity. The distance between the centre of strength and stiffness increases due to the same reasons explained before. It is also evident, that it is possible to eliminate the stiffness eccentricity of the system if element *(3)* has excess strength of approximately *70%* ($\lambda_3=1.7$). This is associated with a strength eccentricity of approximately $e_{vx}=+0.075D$.

The relationship between strength eccentricity and system excess strength of *System 10* shown in Figure 2-35(a), is similar to that of two-element *Systems 1 and 3*; see Figure 2-21(a) and Figure 2-28(a). This indicates that the critical relationship of system excess strength and strength eccentricity of multi-element systems can be readily approximated with the simple expression relevant to a two-element system. The only difference between *Systems 1, 3 and 10* will be the non-proportional variation of the stiffness eccentricity. The likely effect of the stiffness eccentricity on the response of ductile systems will be examined in Sections 3.5.9 and 4.3.3.

Figure 2-35(b) shows the effect that excess strength of either element *(1)* or *(3)* has on excess translational and torsional stiffness of *System 10*. The increase of torsional stiffness is larger than the excess translational stiffness for negative and positive strength eccentricities. The reason for this is that element *(2)* represents most of the system strength while the nominal strength of edge elements *(1)* and *(3)* is relatively small. Due to the increase of stiffness of either

element *(1)* or *(3)*, the increase of system translational stiffness will be as large as the increase of system torsional stiffness.

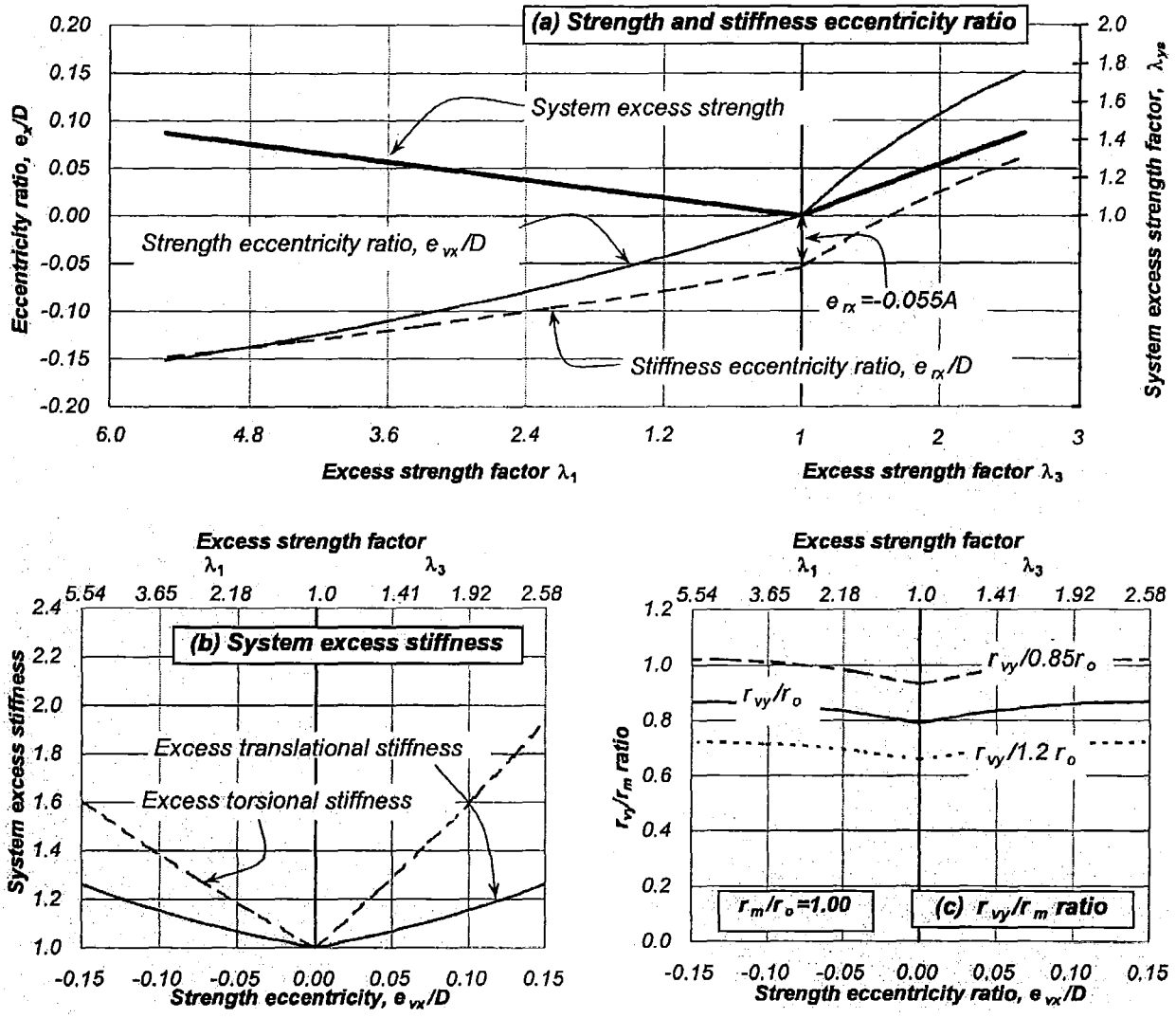

Figure 2-35. Parameters affecting strength and stiffness eccentricity ratios and properties of *System 10*

Figure 2-35(c) shows the variation of the r_{vy}/r_m ratio as function of the strength eccentricity ratio. It shows a reduced value of $r_{vy}/r_o=0.80$ when strength is distributed according to static equilibrium. This low value of r_{vy}/r_m ratio occurs because inner element *(2)* provides most of the system total strength *(63%)*. The excess strength of edge elements *(1)* or *(3)* slightly increases the r_{vy}/r_m ratio due to an increase of the radius of gyration of strength. The small increase in the radius of gyration of strength happens because the torsional strength increases at a larger rate than does the translational strength.

2.21.3 Base shear-torque relationships of *System 10*

Figure 2-36 shows the base shear-torque relationships of unrestrained *System 10A* and restrained *System 10B*. The addition of a third element to the system along the *Y*-axis introduces another branch to the base shear-torque relationship. The shaded area corresponds, as previously stated, to all those base shear-torque combinations introduced by dynamic-induced actions.

It was stated in Sections 2.16.3 and 2.17.3 that the elements of two–element unrestrained systems reach simultaneously their nominal strength when a static force is applied at the centre of mass if the system strength is distributed according to static equilibrium. At this stage, no torque is resisted. In case of unrestrained *System 10*, it is also possible to develop the full strength of the elements due to a static force applied at the centre of mass if system strength is also distributed in the same manner. However, not all elements will reach their nominal strength simultaneously. Element *(2)* will yield first. As the displacement increases, elements *(1)* and *(3)* would yield at the same time.

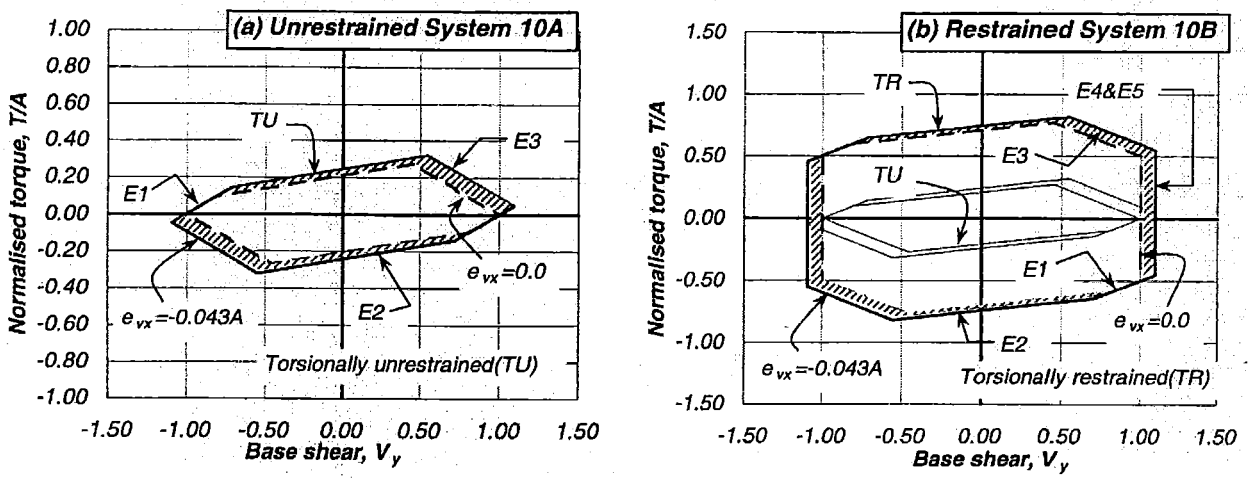

Figure 2-36. Base shear-torque relationships of *System 10*

Consider the situation when element *(1)* of unrestrained *System 10A* has twice the strength required to satisfy static equilibrium and the system is subjected to a static force at the centre of mass, as shown in Figure 2-37(a). The system has a strength eccentricity of e_{vx}=–*0.043A* and a stiffness eccentricity of e_{rx}=*-0.079A*, due to differences in nominal yield displacement of the elements. The application of a static force at the centre of mass of V_E=*0.924* develops the nominal strength of element *(2)* of V_{n2}=*0.634*; see Figure 2-37(b). Subsequently, its stiffness vanishes as the lateral force gradually increases. Elements *(1)* and *(3)* only provide additional translational resistance. Figure 2-37(c) shows that element *(3)* will also reach immediately its nominal strength, V_{n3}=*0.271*, as the static force is slightly increased by V_E=*0.076*. At this stage, element *(1)* has a remaining strength of V_m=*0.095*. This residual strength can only be developed if a force couple exists. One of the forces is, of course the residual strength of element *(1)* and the other is the dynamic action of the mass translational inertia, as explained in Section 2.16.3. The translational mass provides a resistance equal and opposite to the residual strength of element *(1)*, i.e. V_m= V_{r1}=*0.095*. This enables the mass rotational inertia to introduce a clockwise dynamic torque of *T=-0.048A*, as shown in Figure 2-37(d). The full strength of the system is achieved and equilibrium is satisfied, as shown in Figure 2-37(e).

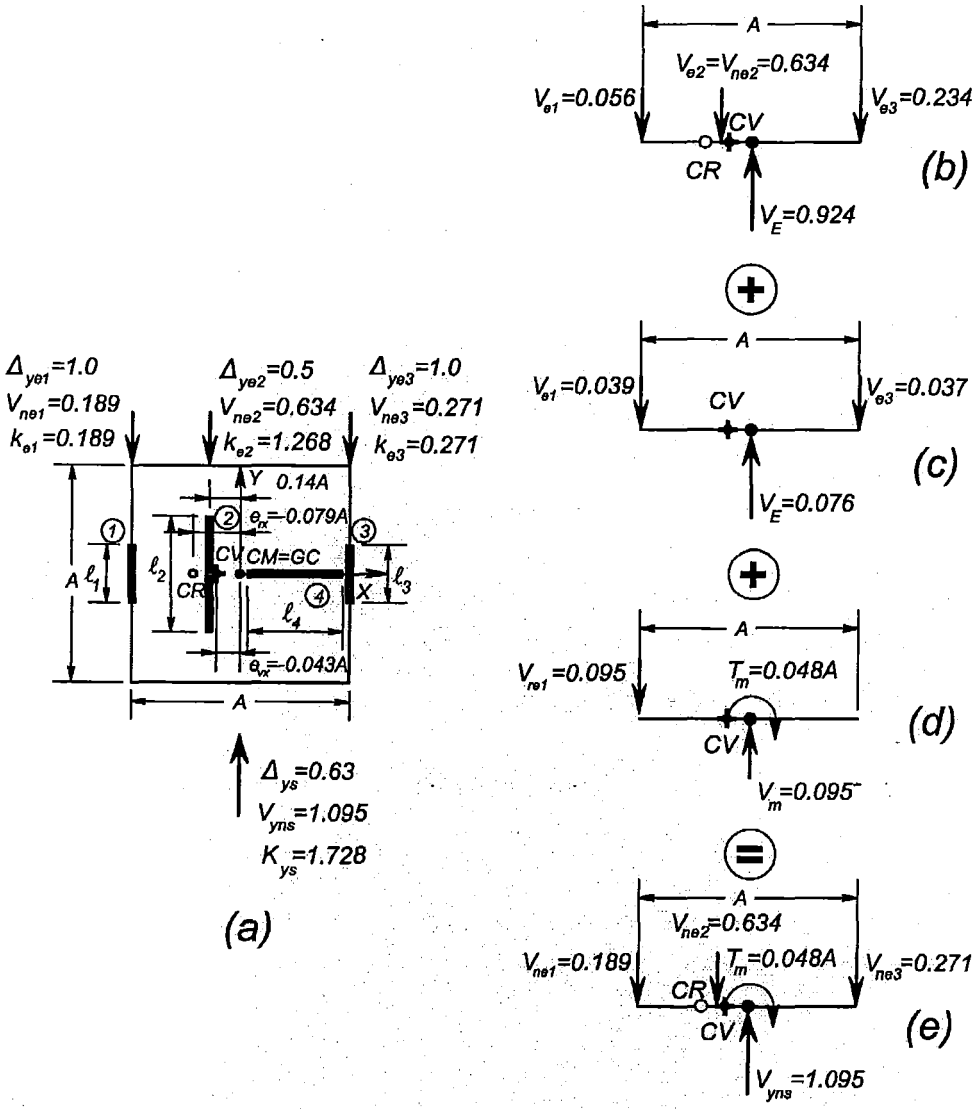

Figure 2-37. Torsional mechanisms of unrestrained *System 10A*

2.22 Four-element structurally asymmetric *System 11* (*CV≠CR; CM=GC*)

2.22.1 Description and properties of *System 11*

System 11 is a single-mass system, as shown in Figure 2-38, comprising again a square rigid diaphragm of *AxA* and four substitute wall-elements along the *Y*-axis with relative lengths of $\ell_1=2.0\ell_2$, $\ell_2=1.0$, $\ell_3=1.26\ell_2$ and $\ell_4=1.59\ell_2$. These elements are equally spaced a distance of *A/3*. Unrestrained *System 14A* has a fifth element placed parallel to the *X*-axis along a line passing through the centre of mass. It will provide translational strength and stability and no torsional resistance. In contrast, Restrained *System 14B* is torsionally restrained with two elements parallel to the *X*-axis. These are placed at the edges of the floor diaphragm.

Unrestrained *System 11A* and restrained *System 11B* will have the same system strength and stiffness along the *X* and *Y*-axes. This is achieved if the substitute wall-elements *(5)* and *(6)* have a length of $\ell_5=\ell_6=1.67\ell_2$. The system will be also subjected to earthquake records at different angles.

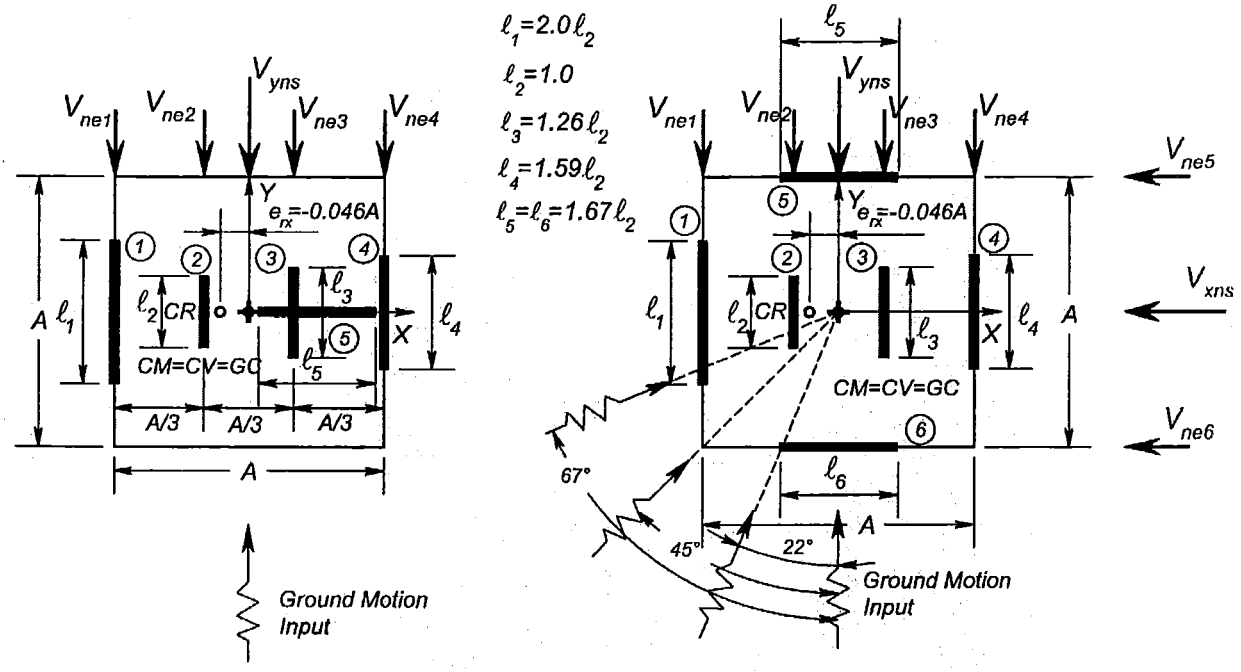

Figure 2-38. Four-element structurally asymmetric *System 11*

The system strength is distributed to satisfy static equilibrium. For this purpose, the strength is initially assigned in proportion to the length squared of the walls. Thereafter, the strength eccentricity resulting from this initial distribution of strength, is eliminated by redistributing the torque $T=e_{vx}V_{yns}$ between pairs of elements, i.e., elements *(1)* and *(4)*, in a similar way to the procedure explained in Section 2.11.3.

Table 2-10 summarizes the radii of gyration of mass, strength and stiffness and relevant ratios when strength is assigned to the elements according to static equilibrium, i.e. $e_{vx}=0.0$. Appendix *B* summarizes the properties of the systems.

Table 2-10. Radii of gyration of mass, strength and stiffness and relevant ratios of *System 11*

				e_{vx}=0.0		e_{rx}=-0.046A					
System	r_m/r_o	r_m	r_{vy}	r_{vx}	r_{vy}/r_o	r_{vx}/r_o	r_{ky}	r_{kx}	r_{ky}/r_o	r_{kx}/r_o	r_{vx}/r_{vy}
11A	1.00	0.41A	0.43A	0.00	1.05	0.00	0.45A	0.00	1.10	0.00	0.00
11B	"	"	"	0.50A	"	1.22	"	0.50A	"	1.22	1.22

2.22.2 Excess strength associated with *System 11*

Excess strength is assigned to either edge element *(1)* and *(4)* only because it will generate a critical relationship between strength eccentricity and system excess strength. It introduces the largest strength eccentricity for the smallest increase in system strength. Excess strength on any other element will generate less critical relationships. Excess strength of elements *(1)* or *(4)* are assumed leading to a strength eccentricity of $e_{vx}=\pm 0.15D$, respectively. Excess strength factors, λ_1 and λ_4, recorded in Figure 2-39(a), quantify the excess strength of either element *(1)* or *(4)*.

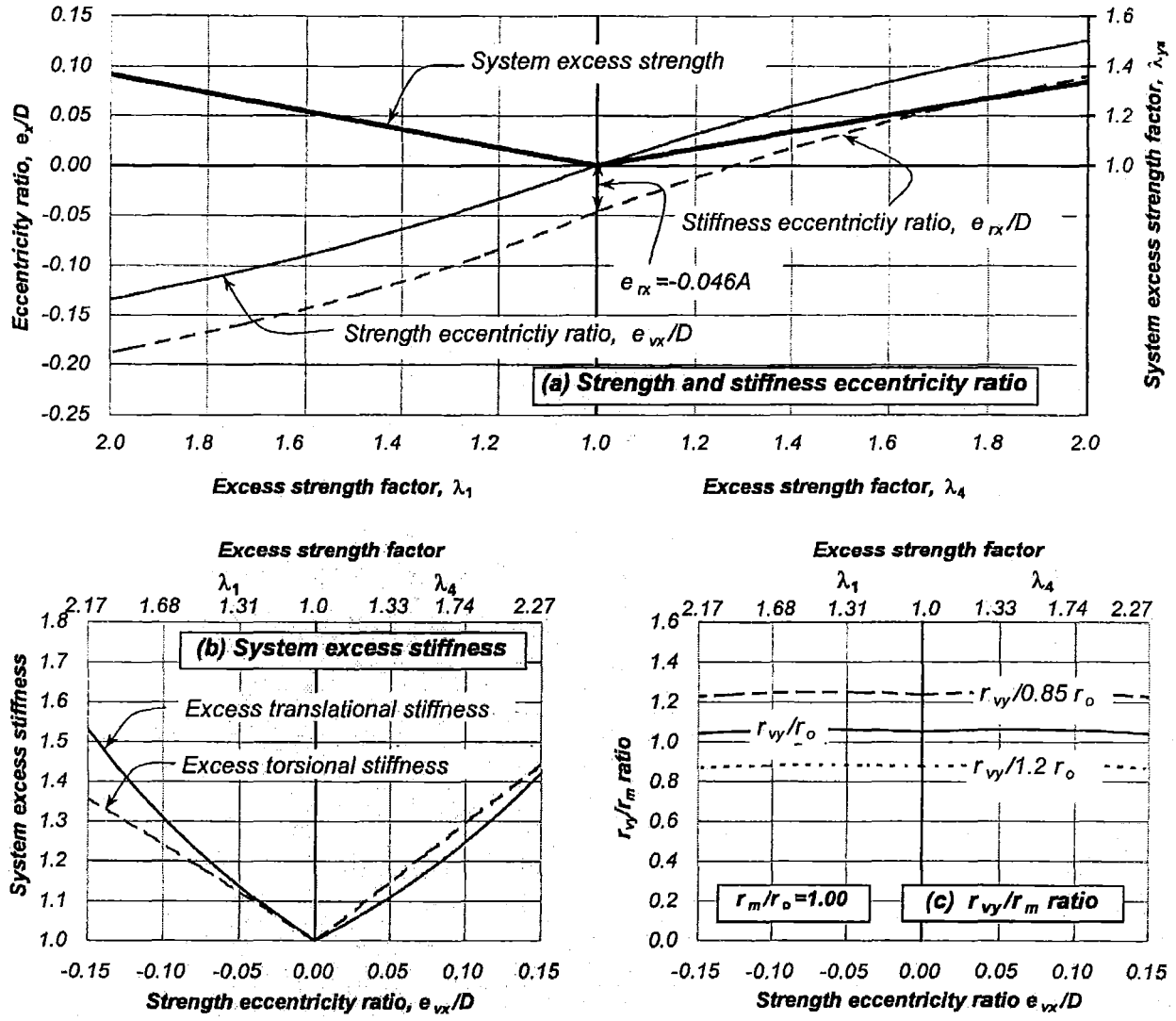

Figure 2-39. Parameters affecting strength and stiffness eccentricity ratios and properties of *System 11*

Figure 2-39(a) shows that *100%* excess strength of element *(1)*, i.e., λ_1=*2.0*, results in a maximum strength eccentricity of e_{vx}=*–0.14D*. The stiffness eccentricity also increases in proportion to the strength eccentricity thus the distance between the centre of strength and stiffness remains essentially the same. Excess strength of element *(4)* (λ_4>*1.0*) introduces a positive strength eccentricity. The distances between the centres of strength and stiffness reduce slightly because element *(4)* has a small nominal yield displacement.

The relationship between system excess strength and strength eccentricity, shown in Figure 2-39(a), indicates that a strength eccentricity of approximately e_{vx}=±*0.14D* is associated with a *35%* increase of system strength, i.e., λ_{ys}=*1.35*. These results are similar to those obtained for two-element *System 3* and three-element *System 11*; see Figure 2-28(a) and Figure 2-35(a). This validates the suggestion of simplifying the most critical relationship of system excess strength and strength eccentricity for multi-element systems with that of simple two-element systems.

Figure 2-39(b) also shows the effect that the excess strength of either element *(1)* or *(4)* has on the excess translational and torsional stiffness of the system. The excess strength of element *(1)* (λ_1≈*2.2*) results in *50%* and *35%* excess translational and torsional stiffness of the system,

respectively. Excess strength of element *(4)* ($\lambda_4 \approx 2.2$) leads to a similar excess translational and torsional stiffness of approximately *40%*.

Figure 2-39(c) shows the variation of the r_{vy}/r_m ratio as affected by the strength eccentricity ratio. It is evident that the r_{vy}/r_m ratio remains, as expected, essentially constant with increasing negative and positive strength eccentricities. This indicates that the radius of gyration of strength is essentially unaffected by the strength eccentricity.

2.22.3 Base shear-torque relationships of *System 11*

Figure 2-40 shows the base shear-torque relationship of *System 11*. It is seen that the unrestrained *System 11A* can sustain a torque larger than that resisted by the three-element unrestrained *System 10A*; for the same base shear. This happens because the system strength is mostly concentrated at the edge elements *(1)* and *(4)* whereas unrestrained *System 10A* has most of its strength supplied by element *(2)*. Figure 2-40 also shows the branches and corresponding elements. It is evident that the addition of a fourth element along the *Y*-axis introduces another branch to the base shear-torque relationship. The shaded areas correspond to the base shear and torque combinations that can only be attained by dynamic-induced actions.

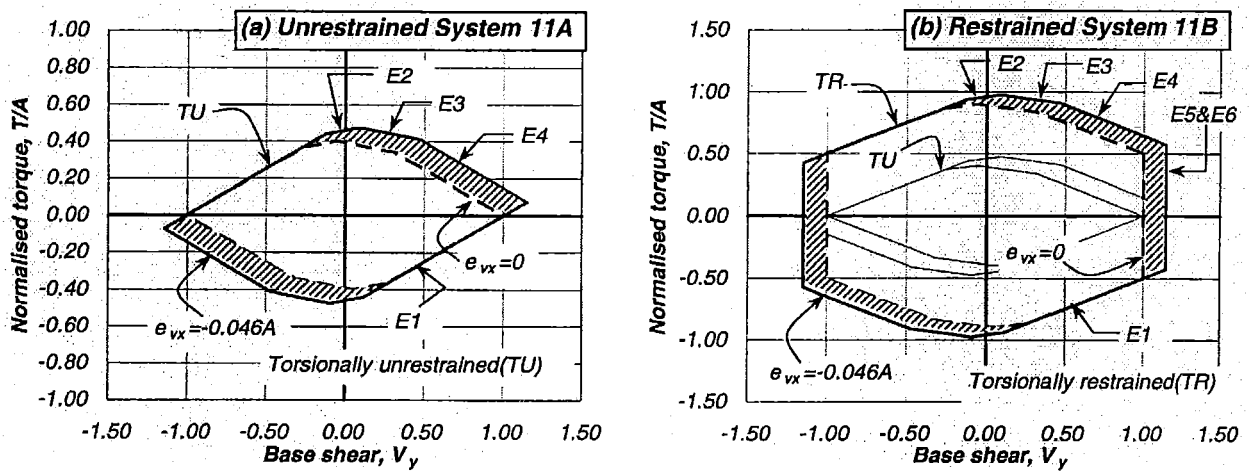

Figure 2-40. Base shear-torque relationships of *System 11*

Chapter 3. Torsionally Unrestrained Systems

3.1 Introduction

To be consistent with past studies on torsional response, this study focuses, at first, on torsionally unrestrained systems having one or more structural elements acting along the direction of the ground motion input [T5,C13]. Transverse elements do not provide torsional restraint. Systems are symmetric or asymmetric.

This study examined the response of those systems using a rational and simple design strategy suggested in Section 2.11. No consideration was given to the seismic design provisions for torsion of any particular building code or standard.

Based on the proposed design strategy, this chapter aims to:

- ✓ Estimate the displacement capacity of torsionally unrestrained systems,
- ✓ Assess displacement demands on elements due to increasing strength eccentricities,
- ✓ Examine effects of system uncoupled translational periods,
- ✓ Identify differences in response, if any, between systems with one or more parallel elements along the direction of earthquake input,
- ✓ Examine the effect of mass eccentricity,
- ✓ Investigate the effects of the mass rotational inertia on the torsional behaviour,
- ✓ Assess the role of the $\alpha=\Delta_{ye2}/\Delta_{ye1}$ ratio and its associated stiffness eccentricity,
- ✓ Examine the response of systems having different displacement ductility capacities and
- ✓ Study the effect of the frequency contents of different earthquake records.

The parameters of interest considered to influence ductile response were: strength eccentricity and associated increase of system strength, the ratio of element nominal yield displacements, $\alpha=\Delta_{ye2}/\Delta_{ye1}$, and their associated stiffness eccentricity, different earthquake record inputs, reduced system displacement ductility capacity and the ratio of radii of gyration of strength and mass.

3.2 General considerations for the analyses of unrestrained systems

Simple two and multi-element asymmetric systems were selected to examine their torsional response when subjected to the earthquake records described in Section 2.5. They were designed according to the suggested design strategy described in Section 2.11.

The displacement ductility capacity of the system should be a characteristic readily estimated before the system is designed. For the sake of consistency, this was assumed in all systems to be equal to the displacement ductility capacity of the elements, i.e., $\mu_{\Delta s}=5.35$. At this stage, it was uncertain if the displacement ductility capacity of the elements will be or not be exceeded. If the ductility capacities are exceeded, suggestions will be provided on how to estimate the system displacement ductility capacity preventing any element from exceeding its ductility capacity.

The Artificial earthquake record was applied along the *Y*-direction. It was scaled to impose, on systems with zero strength eccentricity and fixed value of r_{vy}/r_m ratio, a maximum displacement ductility demand equal to the systems ductility capacity. This record was then applied, without

further modifications, to identical systems having other r_{vy}/r_m ratios. The objective of this approach is to concentrate on torsional behaviour rather than on the question why different ground motions with similar response accelerations may generate different displacement demands at the centre of mass. The force reduction factor, R, a parameter supposedly influencing torsional response and widely considered in many studies [T5,G2,C6,C14], was neglected in this research.

3.3 Two-element structurally symmetric *System 1A* (CV=CR=CM=GC)

3.3.1 Response of the unrestrained *System 1A-1.3*

A two-element system is considered a simple but effective model to study torsional response due to the small number of parameters governing its behaviour. The elements were modelled as substitute walls with given relative length representing any type of lateral force resisting element, i.e., frame, coupled walls, braced frames, etc. The relevant properties of the elements are their nominal strength and nominal yield displacement.

The systems were designed according to a suggested design criteria described in Section 2.11. The aim was to assess if the proposed method was able to limit displacement demands on elements to be within their displacement ductility capacity.

The unrestrained *System 1A* had two substitute wall-elements along the *Y*-axis, as it was shown in Figure 2-20(a). The nominal yield displacement of the elements, and hence that of the system, is a readily derived property independent of strength. They were set in this example to a selected value of $\Delta_{ye1}=\Delta_{ye2}=\Delta_{ys}=42mm$. The system strength was then adjusted to achieve an uncoupled translational period of free vibration of $T_s=1.3$ seconds. It was denoted unrestrained *System 1A-1.3*. Section 2.16 described its characteristics and Appendix *B* summarizes its properties.

The displacement ductility capacity of the unrestrained *System 1A-1.3*, $\mu_{\Delta s}$, was assumed equal to the displacement ductility capacity of the two identical elements. In this example, this was $\mu_{\Delta s}=\mu_{\Delta 1}=\mu_{\Delta 2}=5.35$.

The system was subjected to the Artificial earthquake record along the *Y*-direction. The earthquake record was scaled to generate, on the reference unrestrained *System 1A-1.3* having $r_{vy}/r_o=1.0$, a system displacement ductility demand of $\mu_{\Delta s}=5.35$. This scaled record was also applied, without further modifications, to identical systems with other r_{vy}/r_m ratios, i.e., $r_{vy}/0.85r_o$ and $r_{vy}/1.20r_o$, to examine the effect of the mass rotational inertia on the response.

The design strategy summarised in Section 2.11 suggests that the system nominal strength, distributed among elements to satisfy static equilibrium, i.e., $e_{vx}=0.0$, should prevent the system, and hence the elements, from exceeding their displacement ductility capacity. The objective is to avoid strength eccentricities, which are the main cause of rotations on ductile systems. In the case of the unrestrained *System 1A-1.3*, this is achieved if the strength to be assigned to each element is the same.

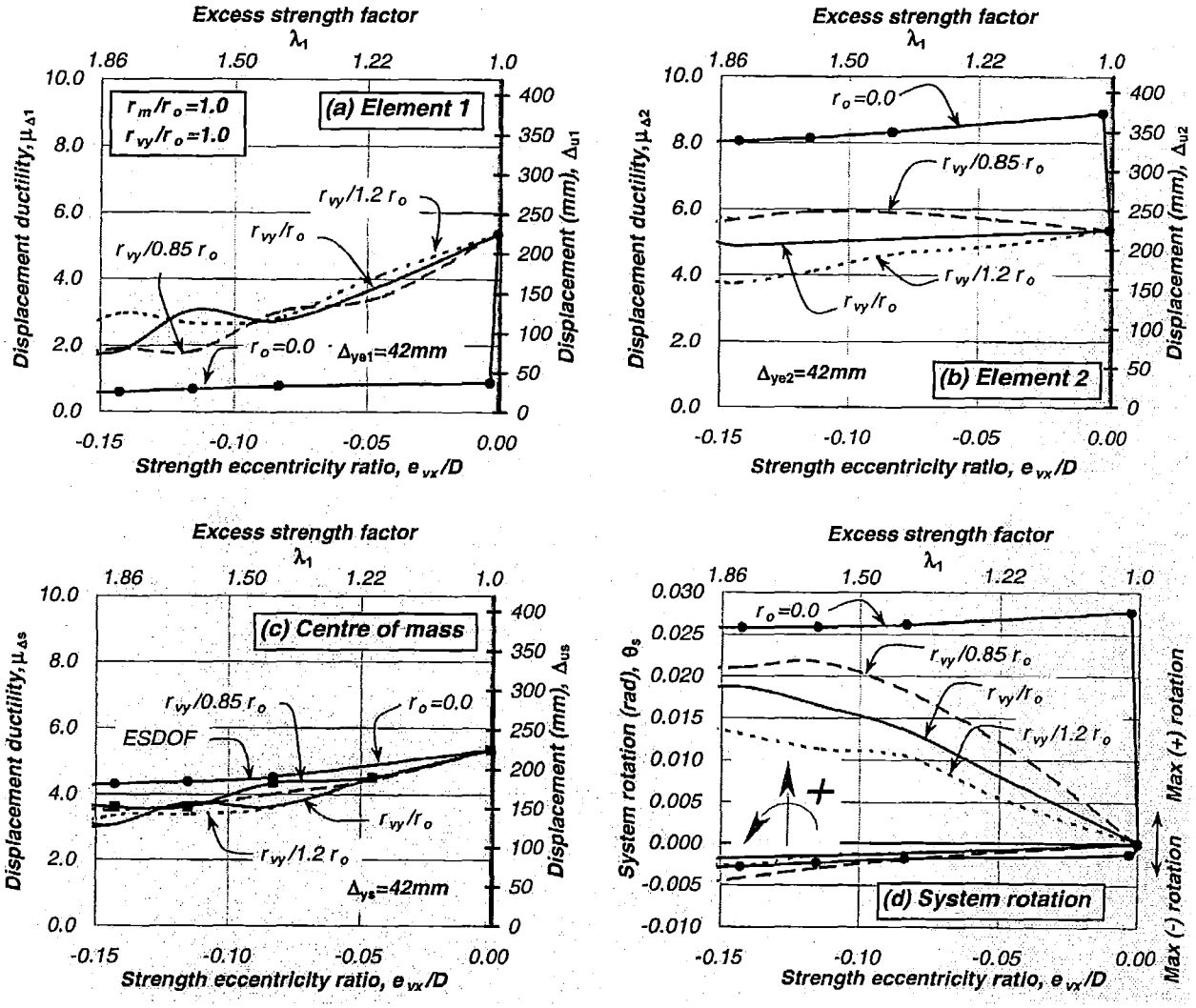

Figure 3-1. Response of the unrestrained *System 1A-1.3*, T_s=1.30 sec, e_{mx}=0.0, e_{vx}=e_{rx}=variable, $\mu_{\Delta s}$=*5.35*, r_m/r_o=1.0, r_{vy}/r_m=variable.

As expected, Figure 3-1 exhibits, for zero strength eccentricity, a maximum displacement ductility demand on elements *(1)*, *(2)* and at the centre of mass of $\mu_{\Delta s}=\mu_{\Delta 1}=\mu_{\Delta 2}=5.35$.

The design strategy also suggests that strength eccentricities may be accepted if by some reason a relative excess strength is assigned to one of the elements. This excess strength will increase the translational strength of the system, as already shown in Figure 2-21(a). The rationale behind the design strategy was explained in Section 2.11.1.

Figure 3-1 plots the system response when element *(1)* had by some reason an excess strength ($\lambda_1>1.0$) whereas the strength of element *(2)* remained unchanged. Consider the case when the unrestrained *System 1A-1.3* had $r_{vy}/r_o=1.0$. The excess strength of element *(1)* introduced negative strength and stiffness eccentricities of the same order and increased the system strength, as already shown in Figure 2-21(a). Element *(1)* having excess strength exhibited, as expected, a reduction in its displacement ductility demands, see Figure 3-1(a). An interesting feature was the fact that the response of element *(2)*, which is traditionally described as the flexible element, was not significantly affected by increasing eccentricities; see Figure 3-1(b). The displacement

demands on element *(2)* remained essentially constant and less than that attained for zero strength eccentricity, i.e., $\mu_{\Delta 2}=5.35$. Note that an excess strength of element *(1)* of $\lambda_1>1.25$ is unlikely in a rationally designed symmetric system.

The excess strength of either element *(1)* or *(2)* increased the system strength. Figure 3-1(c) reveals that the increase of strength reduced, as expected, the displacement ductility demand at the centre of mass.

Figure 3-1(d) shows, for clarity, maximum positive and negative system rotations. It is evident that increasing strength eccentricities increased rotations. Therefore, the reduction of the displacement demands at the centre of mass, as a result of an increase of system strength, did compensate for the torsion-induced displacements imposed on element *(2)*, additional to those resulting from system translations.

The effect of the mass rotational inertia on the response of the unrestrained *System 1A-1.3* is quantified with the ratio of radii of gyration of strength and mass, r_{vy}/r_m. This ratio was changed to r_{vy}/r_o, $r_{vy}/0.85r_o$ and $r_{vy}/1.20r_o$ to examine, as explained in Section 2.13, the sensitivity of the system response to likely differences between the computed and the actual distribution of mass. The r_{vy}/r_m ratio also considers the effect on the response of different diaphragm configurations provided the total mass remained constant and the radius of gyration of element nominal strength also remained unchanged.

Figure 3-1 shows that, for increasing strength eccentricities, the variation of the r_{vy}/r_m ratio did not have a significant influence on the response of element *(1)* and at the centre of mass. However, it did have an effect on element *(2)*. For instance, the unrestrained *System 1A-1.3*, having a reference value of $r_{vy}/r_o=1.0$, exhibited in element *(2)* an essentially constant displacement ductility demand with increasing strength eccentricities. The displacement ductility demands on element *(2)* slightly increased when the radius of gyration of mass was reduced to $r_m=0.85r_o$ or reduced as the mass radius was increased to $r_m=1.20r_o$. This is because the opposition of the mass rotational inertia on system rotations intensifies as the rotational mass was increased. It is also evident from Figure 3-1(c) and (d) that, although the mass rotational inertia significantly reduced system rotations, it did not have a significant effect on system translations.

To highlight the contribution of the mass rotational inertia on the torsional response, the hypothetical extreme case when the mass was concentrated at the centre of mass was also examined, i.e., $r_o=0.0$. Figure 3-1(a) and (b) show that element *(1)* remained elastic, even with a very small excess strength, while element *(2)* exceeded its displacement ductility capacity. This is the response expected from a system having an excess strength on one of its elements and subjected to a static lateral force.

The above findings suggest that the proposed design strategy limits the maximum displacement demands of elements to less than the maxima established if strength eccentricities are associated with an increase of system strength. This increase of strength reduced the displacement demand at the centre of mass which compensated for the rotation-induced displacements of the critical element, additional to those resulting from system translations; hence its displacement capacity was not exceeded. This torsional behaviour applied to systems having $r_{vy}/r_m\leq 1.0$ whereas the displacement ductility capacity of the critical element was slightly exceeded for $r_{vy}/r_m>1.0$. It was also observed that the effect of the mass rotational inertia is to restrain system rotations.

3.3.2 Time history response of the unrestrained *System 1A-1.3*

The time history response was examined to provide further understanding from a behavioural perspective rather than just that of observed trends of the torsional mechanism involved during the dynamic response of symmetric systems having by some reason an excess strength in one of its elements.

The unrestrained *System 1A-1.3*(T_s=*1.3sec)* was considered again. The system strength of V_{yns}=*176 kN* was initially assigned to satisfy static equilibrium, i.e., e_{vx}=*0.0*. Hence, elements *(1)* and *(2)* had the same nominal strength of $V_{ne1}=V_{ne2}=88kN$. The system would be non-symmetric for any values of $\lambda_{1,2}\neq 1.0$. In this example, element *(1)* had for some reason a *40%* excess strength (λ_1=*1.4*). The nominal strength of element *(1)* was increased to $V_{ne1}=88*1.4=123$ *kN* while that of element *(2)* remained at V_{ne2}=*88 kN*. The excess strength of element *(1)* introduced a strength and stiffness eccentricity of $e_{vx}=e_{rx}=-0.083D$ and increased the system strength by *20%* (λ_{ys}=*1.2*) to V_{yns}=*211kN*. The nominal yield displacement of the elements was not affected by the increase of element strength, as it is traditionally believed but is a function of geometry. The system was subjected to the Artificial earthquake record along the *Y*-direction

Consider the torsional mechanism when a positive static force is applied at the centre of mass. Element *(2)* will develop its nominal strength while that of element *(1)* can never be reached. The system will exhibit an anticlockwise rotation due to its negative stiffness eccentricity.

The time history response presented a different behaviour. Figure 3-2(a) shows that element *(1)* reached at instant *(A)* its nominal strength before element *(2)* did. Therefore, for a positive base shear, a clockwise dynamic torque was generated for element *(1)* to reach first its nominal strength. This torque was induced in the elastic system by the mass rotational inertia restraining the negative or clockwise system rotation. Figure 3-3 (a) shows the displacement profile associated with instant *(A)*. It is evident that the displacement of element *(1)* was slightly larger than that of element *(2)* corroborating that the mass rotational inertia, indeed, restrained rotations and, therefore, element *(1)* yielded first.

Element *(2)* also reached, at instant *(B)*, its nominal strength slightly after element *(1)* yielded, as shown in Figure 3-2(a). The question that arises at this stage is: How was it possible for element *(2)* to reach its nominal strength, as indeed took place, once element *(1)* yielded? For this to happen the clockwise torque was reduced after element *(1)* yielded due to a rotational deceleration of the rotational mass; see instant *(A)* in Figure 3-2(c). However, to reduce this torque a force couple was required at that instant. Element *(2)* provided one of these forces because, at this stage, it was still elastic and thus had some additional strength contributing to the development of the full base shear capacity of the system. The other line of resistance was dynamically induced by the mass translational inertia. A force at the centre of mass may represent this resistance. Thus, as Figure 3-2(c) shows this force couple enabled a reduction of the clockwise torque leading element *(2)* to reach its nominal strength at instant *(B)*. The associated displacement profile shown in Figure 3-3 (b) indicates that the displacement on element *(2)* increased at a faster rate than that on element *(1)*, the system rotation changed direction from negative to positive and, as expected, the torque reduced to *T=-220kNm* which is associated with yielding of both elements.

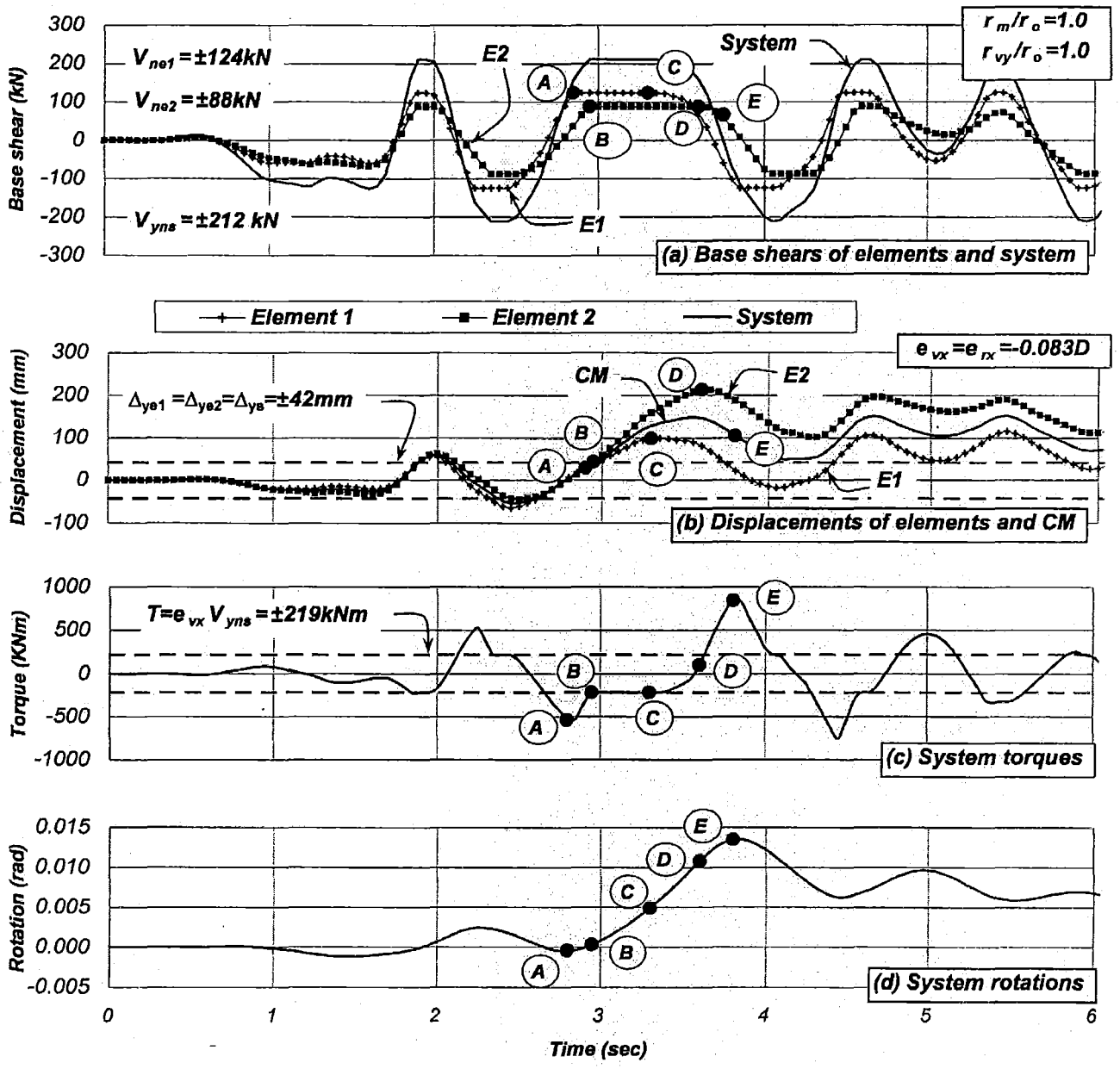

Figure 3-2. Time history response of the unrestrained *System 1A-1.3*, T_s=1.30 sec, e_{mx}=0.0, $e_{vx}=e_{rx}$=-0.083D (λ_1=1.4), $\mu_{\Delta s}$=*5.35*, r_m/r_o=1.0, r_{vy}/r_m=1.0

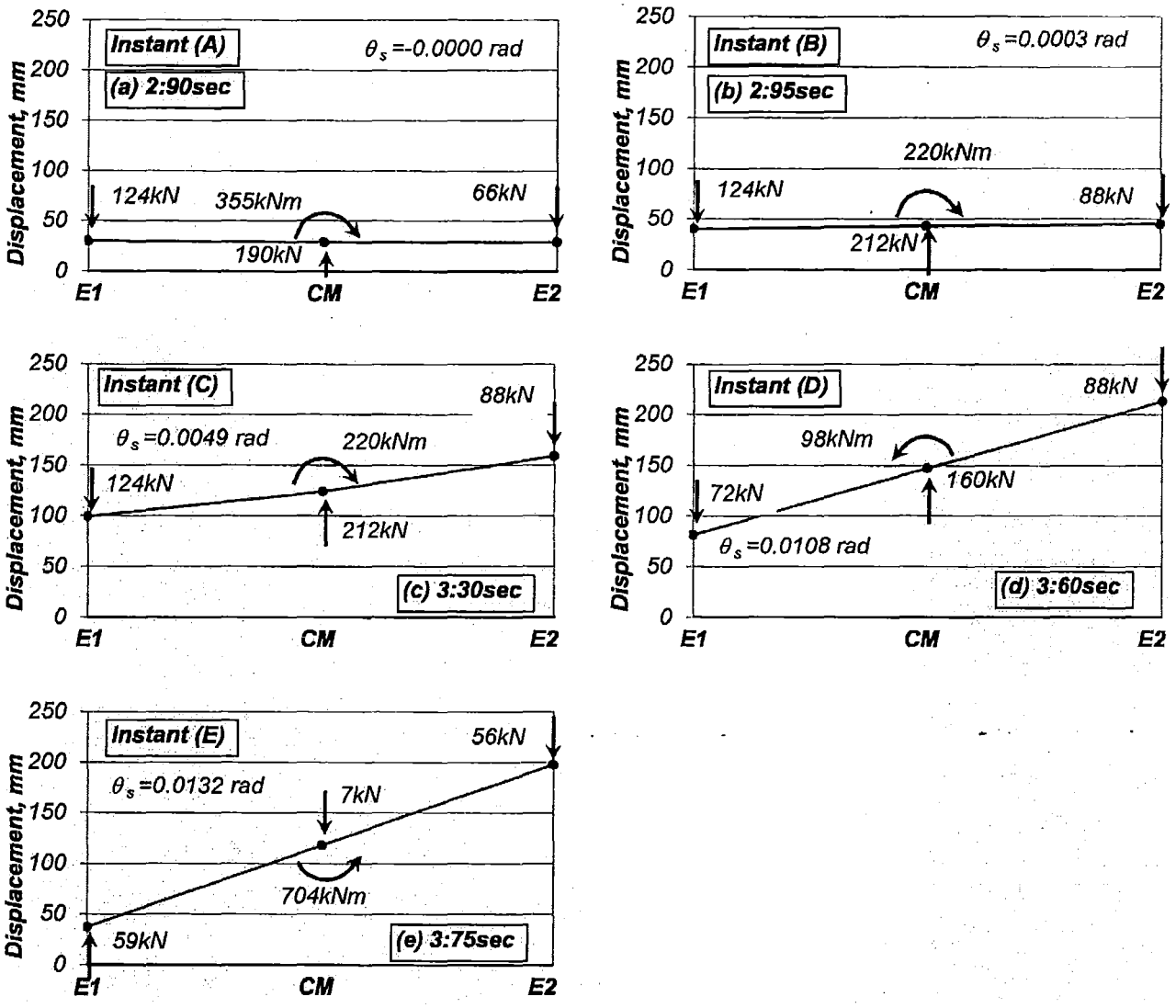

Figure 3-3. Displacement profiles and actions introduced to the unrestrained *System 1A-1.3*, T_s=1.30sec, e_{mx}=0.0, $e_{vx}=e_{rx}$=-0.083D (λ_1=1.4), $\mu_{\Delta s}$=*5.35*, r_m/r_o=1.0, r_{vy}/r_m=1.0

A change in the sense of system rotation, once element *(1)* reached its nominal strength at instant *(A)*; see Figure 3-2(d), shows that the deceleration of the mass rotational inertia restrained further rotations in the opposite direction. The system torque of $T=e_{vx}V_{yns}$=*-220kNm* remained constant as the system developed its full base shear capacity between instants *(B)* and *(C)*.

Instant *(C)* corresponds to the moment when element *(1)*, having developed its maximum displacement, became elastic again. The displacement profile associated with this instant, see Figure 3-3 (c), shows that the displacements in both elements increased. This increase was much larger on element *(2)*, hence system rotations increased while the torque remained constant. Thereafter, the torque diminished because the rotational mass continued to decelerate. The torque eventually changed sign from negative to positive after the centre of mass reached it peak displacement. Yet, the sense of the diaphragm rotation did not change.

At instant *(D)*, element *(2)* reached a maximum displacement and re-entered the elastic domain. With both elements operating in the elastic range, the total base shear reduced; see Figure 3-2(a). Its associated displacement profile; see Figure 3-3(d) shows, relative to instant *(C)*, a reduction of the displacement of element *(1)* while it increased on element *(2)*. The torque, although

increasing, is smaller and opposite to that attained at instant *(C)* whereas system rotations have substantially increased. This illustrates that there is no proportionality between rotations and torques.

In spite of a significant increase of torques and system rotations, as shown at instant *(E)* in Figure 3-2(c) and (d), no large displacement demands arose for the two elements; see Figure 3-2(b). The displacements of elements *(1)* and *(2)* were less than the maxima reached when the system strength was distributed to satisfy static equilibrium, i.e., $e_{vx}=0.0$; see also Figure 3-1. The corresponding displacement profile shown in Figure 3-3(e) indicates that the maximum system rotation occurred when both elements were elastic and hence was associated with a large torque. The results demonstrate that torque and system rotations are poor indicators of element maximum displacement demands.

The torsional mechanism described before illustrates that the action of the mass rotational inertia is to restrain system rotations. This caused element *(1)*, in spite of having excess strength, to yield first and subsequently enabled element *(2)* to yield instants later. The maximum displacement of the elements occurred for a system rotation smaller than the maximum rotation. This peak rotation occurred when both elements, while remaining elastic, developed a large relative displacement. Torsional mechanisms of asymmetric systems generated by static or dynamic-induced forces are obviously different due to the effects of the mass rotational inertia.

3.3.3 Profiles of instantaneous displacements of the unrestrained *System 1A-1.3*

The instantaneous displacement profiles associated with the maximum displacements of elements and at the centre of mass are assessed. The aim is to determine if the displacement demands of elements and at the centre of mass is reached independently or simultaneously. It will also show, in a global context, the torsional behaviour of the system as affected by assigning excess strength to one of its elements, as suggested in the design strategy.

The unrestrained *System 1A-1.3*($T_s=1.30$ sec) having $r_{vy}/r_m=1.0$ was considered again. It was subjected to the Artificial earthquake record along the *Y*-direction. The system nominal strength was initially distributed to achieve zero strength eccentricity. However, an excess strength was assigned to element *(1)* ($\lambda_1>1.0$) while that of element *(2)* remained unchanged. The excess strength of element *(1)* is quantified through excess strength factors of $\lambda_1=1.0, 1.2, 1.6$ and 2.0. These excess strengths introduced negative strength eccentricities and increased the system strength, as already shown in Figure 2.21.

The instantaneous displacement profiles, presented in Figure 3-4, as a function of the excess strength factor, λ_1, shows that the maximum response attained at elements *(1)* and *(2)* and at the centre of mass; see Figure 3-4(a), (b) and (c), did not occur simultaneously nor were they associated with the maximum system rotation. Element *(1)* and the centre of mass reached maximum displacements at similar instants even for different values of excess strength factors. Element *(2)* reached it maximum displacement for a large system rotation. This, however, was less than the maximum rotation imposed on the system of $\theta_s=+0.015$ *rad*; see Figure 3-4(d).

Figure 3-4(c) shows that increasing the strength of element *(1)* reduced its displacement demand and that at the centre of mass and increased the system maximum rotation, as Figure 3-4(d) shows. However, the maximum response of critical element *(2)* never exceeded the displacement demands attained for zero strength eccentricity ($\lambda_1=1.0$). Thus, the reduction of the displacements at the centre of mass due to an increase of system strength did compensate for

the torsion-induced displacements imposed on critical element *(2)*, additional to those resulting from system translations.

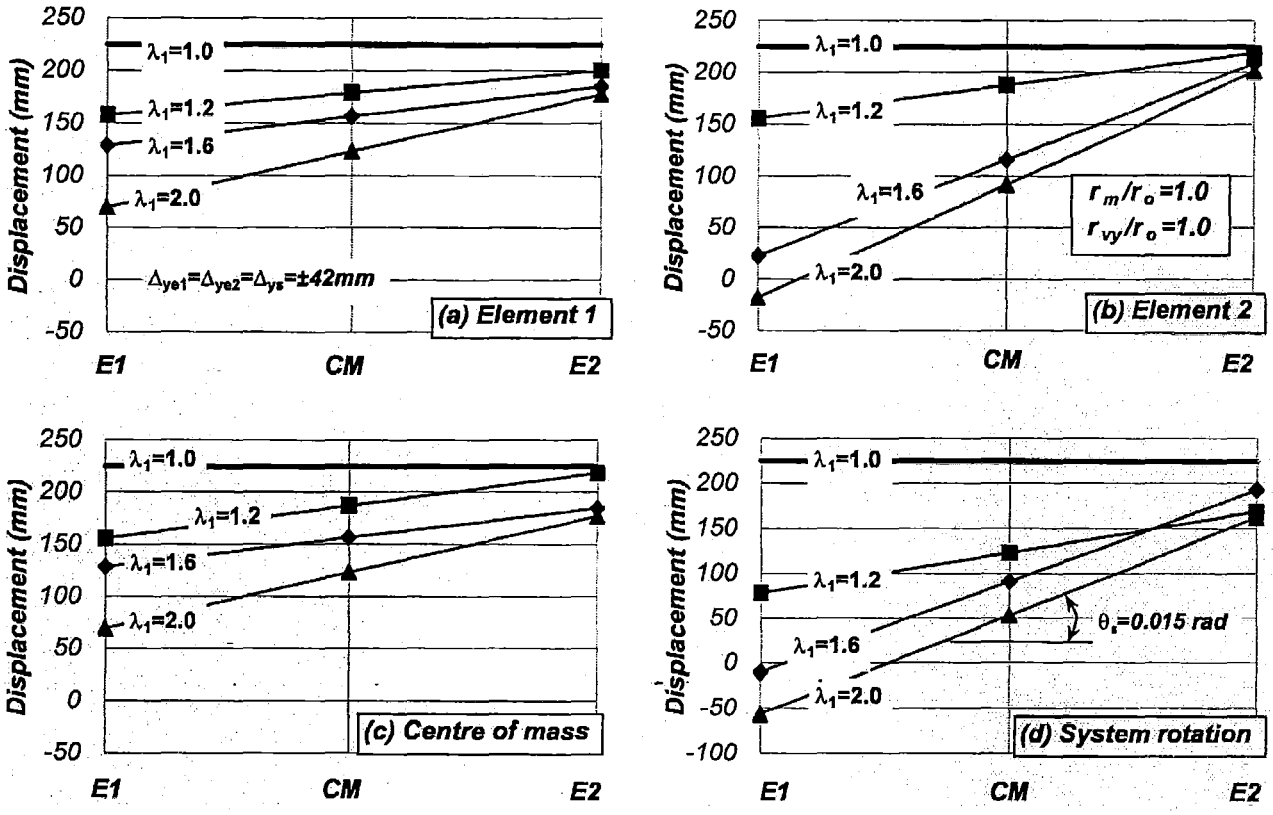

Figure 3-4. Displacement profiles of the unrestrained *System 1A-1.3*, T_s=1.30 sec, e_{mx}=0.0, λ_1=variable, $\mu_{\Delta s}$=5.35, r_m/r_o=1.0, r_{vy}/r_m=1.0

These results show that the maximum displacement demands on elements and at the centre of mass are not attained simultaneous nor are they associated with the system maximum rotation.

3.3.4 Response of the unrestrained *System 1A-1.3* when using different element modelling

This section aims to examine if conclusions already derived using a simple elasto-plastic relationship were also valid for other common structural systems having different hysteretic behaviour.

The unrestrained *System 1A-1.3(T_s=1.30* sec) was considered again. The substitute wall-elements were modelled with Bilinear, Takeda[O1], and Al-Bermani[Z1] simulations and the already assessed elasto–plastic force-displacement relationship. Section 2.7 provided a description of these hysteretic models. The system was subjected to the Artificial earthquake record along the *Y*-direction.

Figure 3-5 shows, as expected, little differences in the system response when using different element modelling. The system with stiffness degrading elements, i.e., the Takeda model, exhibited the largest displacement ductility demands of elements and at the centre of mass. This response was followed by the system having elasto-plastic hysteretic elements behaviour, which displayed the second largest element displacement ductility demands and the largest system

rotation. The maximum and minimum displacement ductility demands at the centre of mass were obtained with the Takeda and Bilinear models.

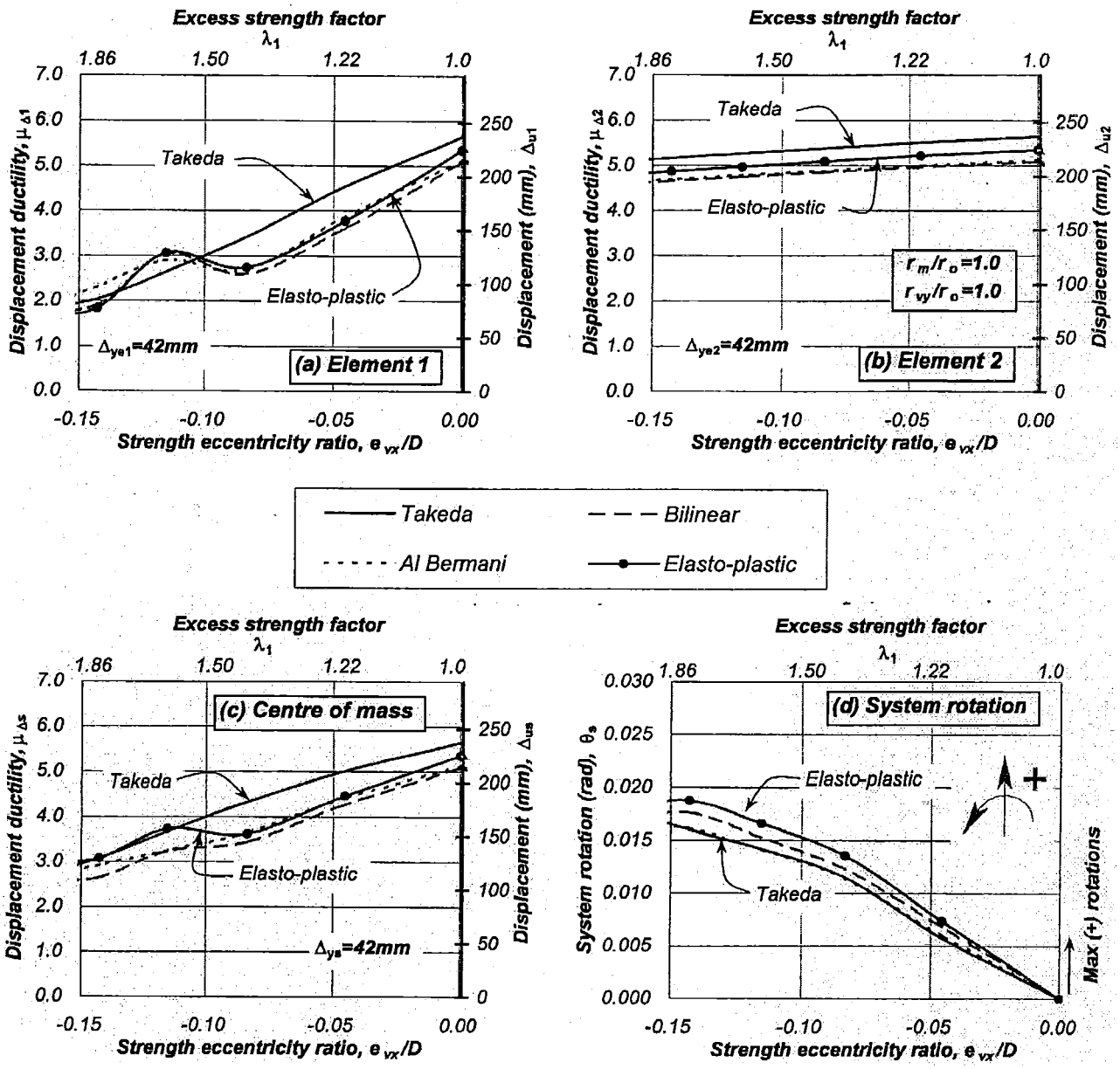

Figure 3-5. Response of the unrestrained *System 1A-1.3* when considering different element modelling, T_s=1.30 sec, e_{mx}=0.0, e_{vx}=e_{rx}=variable, $\mu_{\Delta s}$=*5.35*, r_m/r_o=1.0, r_{vy}/r_m=1.0

These results show that differences of predicted displacements for the elements modelled with selected hysteretic models were not significant. Conclusions derived from systems where the elements are modelled with a simple bilinear force-displacement relationship should also be valid for most common structural systems when gauging displacements demands due to torsional behaviour.

3.3.5 Response of the unrestrained *System 1A-0.5*

The response of a system having a short translational period and designed according to the suggested design strategy was examined. Past studies [C14] have reached different conclusions with regard to the dependence of response on the uncoupled translational period of free vibration

of the system. The aim is to clarify this issue and verify if the design method can limit displacement demands on elements to less than their displacement ductility capacity.

The unrestrained *System 1A* was considered again. The nominal yield displacement of elements and that of systems is a readily derived property independent of strength. In this example, they were set, as in previous systems, to $\Delta_{ye1}=\Delta_{ye2}=\Delta_{ys}=42mm$. The system strength was subsequently adjusted to achieve an uncoupled translational period of free vibration of $T_s=0.5$ sec. It was denoted as *System 1A-0.5*. The characteristics of the system were the same as those described in Section 2.16. Its properties are summarised in Appendix *B*. The general considerations described in Section 3.2 were used to analyse this system.

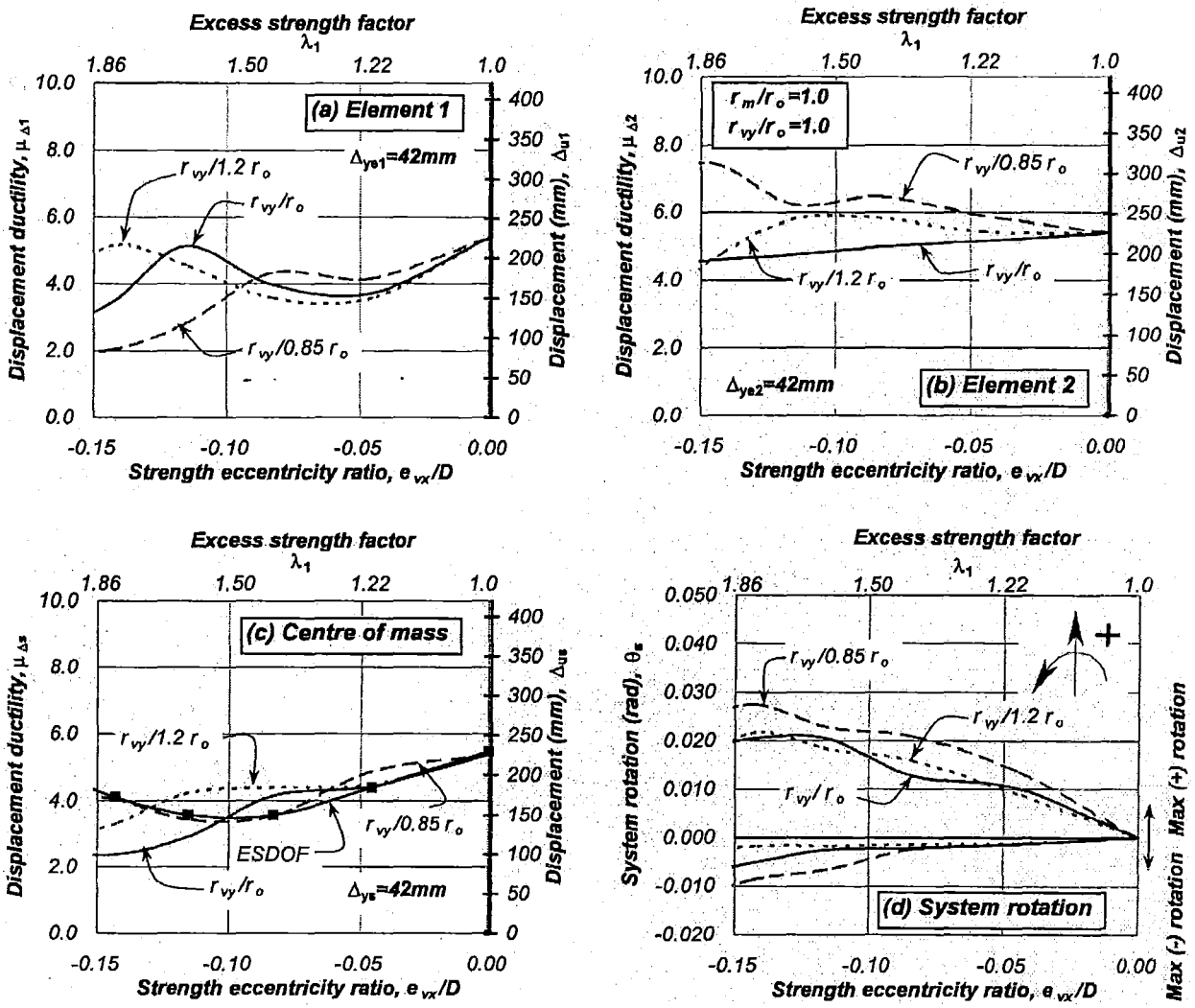

Figure 3-6. Response of the unrestrained *System 1A-0.5*, T_s=0.50 sec, e_{mx}=0.0, $e_{vx}=e_{rx}$=variable, $\mu_{\Delta s}$=5.35, r_m/r_o=1.0, r_{vy}/r_m=variable

As expected, Figure 3-6 records, for zero strength eccentricity, a maximum displacement ductility demand on the elements and at the centre of mass of $\mu_{\Delta s}=\mu_{\Delta 1}=\mu_{\Delta 2}=5.35$. This maximum displacement demand is equal to the system displacement ductility capacity and therefore should not be exceeded even when the system experiences rotations.

Excess strength of element *(1)* introduced increasing negative strength eccentricities that, as expected, reduced its displacement ductility demands; see Figure 3-6(a). Variations of the r_{vy}/r_m

ratios generated slightly different displacement ductility demands on element *(2)*. In the case of $r_{vy}/r_m \leq 1.0$, element *(2)* exhibited displacement ductility demands smaller than those attained for zero strength eccentricity; see Figure 3-6(b). However, for $r_{vy}/r_m > 1.0$, element *(2)* slightly exceeded its displacement ductility capacity. This response agreed with the response observed before for the unrestrained *System 1A-1.3*; see Figure 3-1(b).

The displacement ductility demands at the centre of mass; see Figure 3-6(c), reduced with increasing strength eccentricities due to the increase of system strength. It is also seen that the response was essentially unaffected by variations of the r_{vy}/r_m ratio.

Figure 3-6(d) shows, as expected, that system rotations increased with strength eccentricities and were also affected by the r_{vy}/r_m ratio. A comparison of Figure 3-1(d) and Figure 3-6(d) shows that the unrestrained *Systems 3A-05* and *3A-1.3* developed similar system rotations.

The findings described above suggest that the torsional response is sensitive to the uncoupled translational period of free vibration. In spite of this behaviour, the proposed design strategy is successful in limiting displacement demands of elements to less than their displacement capacities due to increasing strength eccentricities.

3.3.6 Response comparison of the unrestrained *Systems 1A-1.3* and *1A-0.5* with their corresponding equivalent single degree of freedom system

The objective of this section is to examine the way that elements and centre of mass reach their maximum response at different instants may affect the maximum displacement demand attained at the centre of mass. For this purpose, the displacement ductility demands at the centre of mass of the unrestrained *Systems 1A-1.3*(T_s=*1.30*) and *1A-0.5*(T_s=*0.50*) and that of an equivalent single degree of freedom (ESDOF) system were compared. This equivalent system is assumed to have the same translational properties, i.e., strength, stiffness, and nominal yield displacement of the torsionally unrestrained system; however, it is not affected by torsion.

It is evident from Figure 3-1(c) and Figure 3-6(c) that the corresponding equivalent single degree of freedom system predicted essentially the same maximum displacement demand at the centre of mass of the systems for zero and increasing strength eccentricities. This result was valid in spite of elements *(1)* and *(2)* reaching their maximum response at different instants. This indicates that the actions of the mass rotational inertia on system rotations did not have a significant effect on system translations.

The fact that an equivalent single degree of freedom system can predict, with adequate accuracy, the response at the centre of mass should appeal to structural engineers. The centre of mass may be considered, in case of ductile systems, as a convenient reference location where translational and rotational motions may be separated.

3.4 Two-element structurally symmetric and mass-eccentric *System 2A* (*CV=CR=CM≠GC*)

3.4.1 Response of the unrestrained *System 2A-1.3*

This section examines the response of a symmetric structural system having mass eccentricity and designed according to the suggested design strategy. The research on these types of

systems is necessary because structures, in general, will exhibit non-coincident centres of mass and geometry. It is required to assess if systems with or without mass eccentricity should be treated differently [C8, T5].

The unrestrained *System 2A*, shown in Figure 2-24(a), had a mass eccentricity of e_{mx}=*-0.10A*, hence, the centre of mass did not coincide with the geometric centre. The nominal yield displacement of substitute wall-elements *(1)* and *(2)* were the same because the centres of mass, strength and stiffness are coincident. This was achieved because the system strength was assigned to elements to satisfy static equilibrium, i.e., e_v=*0.0*. The nominal yield displacement of the elements, and hence that of the system, was the same and equal to $\Delta_{ye1}=\Delta_{ye2}=\Delta_{ys}$=*42mm*. The system strength was adjusted to achieve an uncoupled translational period of free vibration of *1.3* seconds. It was denoted unrestrained *System 2A-1.3*. Section 2-17 described in detail its characteristics and Appendix *B* summarizes its properties. The displacement ductility capacity of unrestrained *System 2A-1.3* was the same as the unrestrained *System 1A-1.3* previously examined. This was equal to the displacement ductility capacity of the two identical elements, i.e., $\mu_{\Delta s}=\mu_{\Delta 1}=\mu_{\Delta 2}$=*5.35*. The system was analysed based on the considerations already explained in Section 3.2.

The nominal strength to be assigned to each element, complying with static equilibrium, was obviously different. Element *(1)* and *(2)* had *70%* and *30%*, respectively, of the system nominal strength. Subsequently, the system became non-symmetric when excess strength was assigned to either element *(1)* or *(2)*, as already explained in Section 2.17.2. This excess strength introduced strength eccentricities and increased the translational strength of the system. This relationship will depend on which element the excess strength was assigned to, as already shown in Figure 2-25(a).

Figure 3-7 show the response of the system due to zero and increasing strength eccentricities. The torsional behaviour was similar to that attained with structurally symmetric *Systems 1A-1.3* and *1A-0.5*; as Figure 3-1 and Figure 3-6 shows. This behaviour is briefly summarised. As expected, the displacement demand on elements and at the centre of mass, for zero strength eccentricity, was $\mu_{\Delta s}=\mu_{\Delta 1}=\mu_{\Delta 2}$=*5.35*. Excess strength of element *(1)* (λ_1>*1.0*) introduced increasing negative strength eccentricities that reduced its displacement ductility demands and those at the centre of mass. The response of element *(2)* depends on the r_{vy}/r_m ratio. In case of $r_{vy}/r_m \leq 1.0$, the displacements demands of element *(2)* were equal or smaller than that attained for zero strength eccentricity. The demands slightly exceeded the displacement capacity of element *(2)* for r_{vy}/r_m>*1.0*, i.e., r_{vy}/*1.20*r_m. Rotations increased due to increasing strength eccentricities and r_{vy}/r_m ratios. Rotations were, however, not an issue because they were not associated with the maximum displacement demand on the elements. The corresponding equivalent single degree of freedom systems predicted, with adequate accuracy, the displacement demand at the centre of mass. The torsional behaviour of the system due to the excess strength of element *(2)* was essentially the same.

The results indicates that mass eccentric systems with $r_{vy}/r_m \leq 1.0$ and designed with the suggested design strategy exhibit a satisfactory seismic performance. The maximum displacement demand on the critical element may slightly exceed the maxima established for r_{vy}/r_m>*1.0*. This torsional behaviour is similar to that of the unrestrained *System 1A-1.3* previously examined; see Figure 3-1, indicating that there is no need to differentiate between systems with or without mass-eccentricity. Hence, mass eccentricity is not a parameter to influence the behaviour of asymmetric systems. This finding contradicts the common belief that systems with or without mass eccentricity should be considered separately.

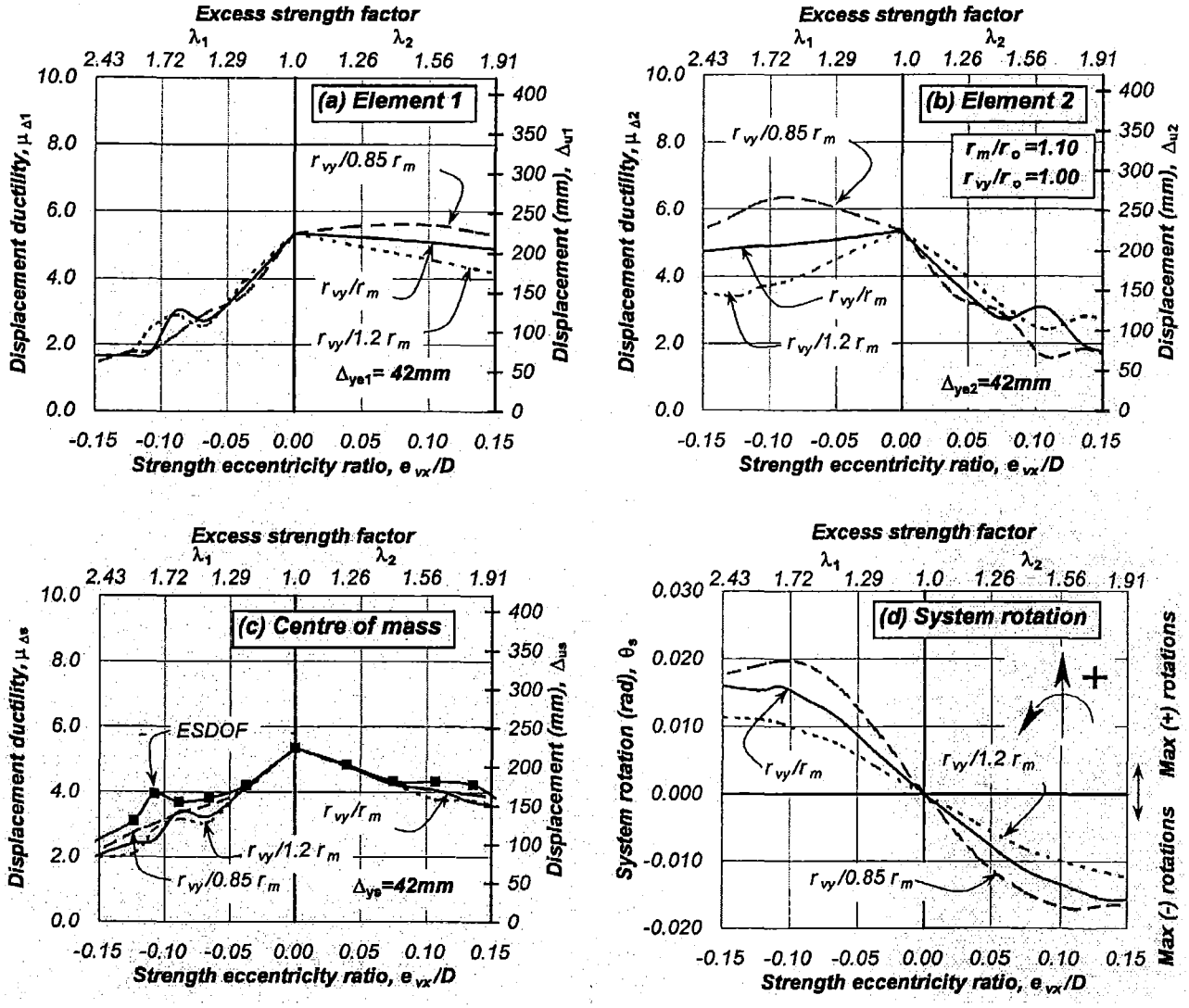

Figure 3-7. Response of the unrestrained *System 2A-1.3*, T_s=1.30 sec, e_{mx}=-0.10A, $e_{vx}=e_{rx}$=variable, $\mu_{\Delta s}$=5.35, r_m/r_o=1.10, r_{vy}/r_m=variable

3.4.2 Response of the unrestrained *System 2A-0.5*

The likely effects of the uncoupled translational period of free vibration on the torsional response of a symmetric and mass eccentric system are also examined. The unrestrained *System 2A–0.5* with a translational period of T_s=*0.5* seconds was considered. It had the same physical characteristics of the unrestrained *System 2A-1.3* but different properties, as shown in Appendix *B*. The considerations already explained in Section 3.2 were also used for the analysis of the system.

The torsional behaviour of the unrestrained *System 2A-0.5*, shown in Figure 3-8, was essentially the same as that of the unrestrained *System 2A-1.3*; see Figure 3-7. It did show, however, a more sensitive response. This was particularly evident for $r_{vy}/r_m>1.0$. For instance, in case of $r_{vy}/1.20r_o$, Figure 3-8(b) shows that increasing negative strength eccentricities generated large displacement ductility demands on element *(2)* in contrast to the response previously obtained for the unrestrained *System 2A-1.3*, see Section 3.4.1. Figure 3-8(c) shows that the equivalent single degree of freedom systems still predicted well the maximum displacement demand at the

centre of mass. The system rotations were also essentially the same on both unrestrained *Systems 2A-1.3* and *2A-0.5*; see Figure 3-7(d) and Figure 3-8(d).

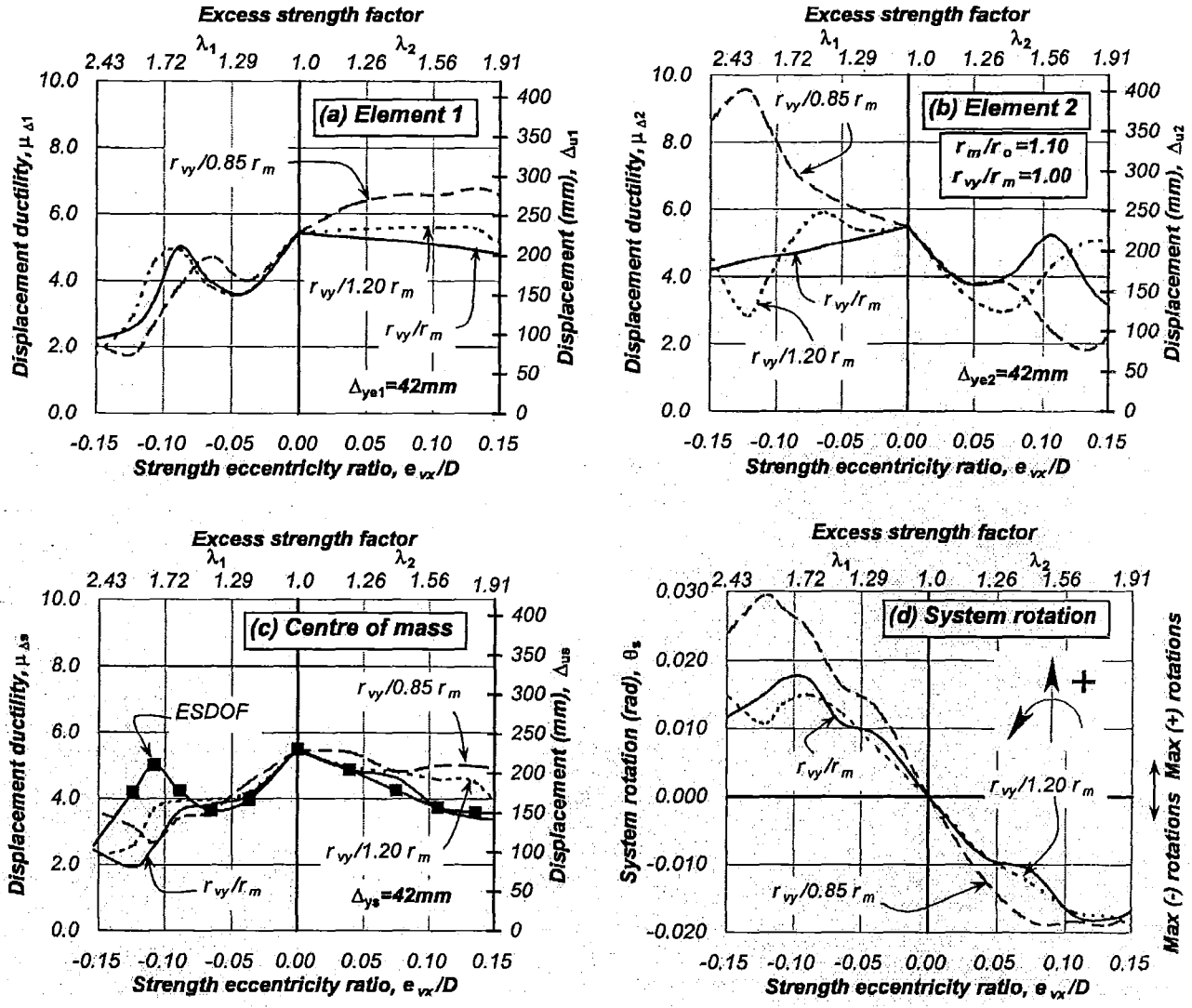

Figure 3-8. Response of the unrestrained *System 2A-0.5*, T_s=0.50 sec, e_{mx}=-0.10A, $e_{vx}=e_{rx}$=variable, $\mu_{\Delta s}$=5.35, r_m/r_o=1.10, r_{vy}/r_m=variable

It is evident from the above findings that mass eccentric systems with short translational periods and designed with the suggested design strategy will exhibit an acceptable seismic performance. Displacement demands of elements were limited to less than their ductility capacity due to increasing strength eccentricities. It also shows that the torsional response becomes sensitive as the translational period of free vibration of the system was reduced.

3.5 Two-element structurally asymmetric *System 3A* (*CV≠CR; CM=GC*)

3.5.1 Response of the unrestrained *System 3A-1.3(α=1.4)*

This section examines the seismic torsional response of a two-element asymmetric system designed with the strategy suggested in Section 2.12. The aim was to verify if the proposed design strategy was able to limit displacement demands on elements to be within their displacement capacity.

The unrestrained *System 3A* shown in Figure 2-27(a) was considered. It had two substitute wall-elements with unequal length. The nominal yield displacement of elements *(1)* and *(2)* was $\Delta_{ye1}=36mm$ and $\Delta_{ye2}=50mm$, hence $\alpha=\Delta_{ye2}/\Delta_{ye1}=1.40$. They were associated with a system nominal yield displacement of $\Delta_{ys}=42mm$. The system strength was adjusted to achieve an uncoupled translational period of free vibration of *1.3* seconds. It was denoted unrestrained *System 3A-1.3(α=1.4)*. Centres of strength and stiffness never coincide due to differences in the nominal yield displacement of the elements. For zero strength eccentricity, the system had a stiffness eccentricity of $e_{rx}=-0.083D$ and $r_{vy}/r_o=1.0$. Section 2.18 describes in detail its characteristics and Appendix *B* summarizes its properties. The considerations already explained in Section 3.2 were also used for the analysis of the system.

The suggested design strategy, described in Section 2.11, states that the system nominal strength, necessary to prevent that the displacement ductility capacity of any element being exceeded, should be distributed among the elements to satisfy static equilibrium requirements, i.e., $e_{vx}=0.0$. It may not be achieved in practice but it is considered to be a reference distribution of strength. The response of the system, for zero strength eccentricity, is of interest because, it is the case when the system maximum response is expected. Hence, the displacement capacity of the system should be related to this response. In the case of the unrestrained *System 3A-1.3*, zero strength eccentricity was achieved when the elements had the same nominal strength.

Table 3-1 summarizes the response for zero strength eccentricity. It is evident that the maximum displacement demand of the elements relative to that at the centre of mass was influenced by the r_{vy}/r_m ratio. As the r_{vy}/r_m ratio was reduced, the maximum displacement demand of the elements and at the centre of mass became essentially the same. It is seen that element *(1)* exceeded its displacement ductility capacity of $\mu_{\Delta 1}=5.35$ for r_{vy}/r_o and $r_{vy}/1.20r_o$ whereas element *(2)* showed a reduction in demand. Element *(1)* was obviously the critical element. Hence, the displacement ductility capacity of the system associated with zero strength eccentricity should be further restricted to prevent critical element *(1)* from exceeding its ductility capacity for all cases of r_{vy}/r_m ratio.

The displacement demands at the centre of mass were essentially the same for systems having different r_{vy}/r_m ratios, as Table 3-1 shows. It was also observed that the corresponding equivalent single degree of freedom system predicted, with adequate accuracy, the system maximum displacement demand. This shows that the centre of mass is a convenient reference location where translations and rotational motions may be separated and not influenced by variations of the r_{vy}/r_m ratio. The actions of the mass rotational inertia on system rotations did not have a significant effect on system translations.

Table 3-1. Response of the unrestrained *System 3A-1.3(α=1.4)*, T_s=1.30 sec, e_{mx}=0.0, e_{vx}=0.0, e_{rx}=-0.083D, $\mu_{\Delta s}$=5.35, r_m/r_o=1.0, r_{vy}/r_m=variable

	Displacements, mm, and displacement ductility demands (μ_s)				***Displacement demand ratios***	
r_{vy}/r_m	***E1***	***CM***	***E2***	***ESDOF***	$(\Delta_{ue1}/\Delta_{us})_d$	$(\Delta_{ue2}/\Delta_{us})_d$
$r_{vy}/0.85r_o$	*191(5.31)*	*221(5.26)*	*265(5.25)*	*225 (5.35)*	*0.86*	*1.20*
$r_{vy}/r_o=1.01$	*198(5.50)*	*224(5.33)*	*251(4.98)*	"	*0.88*	*1.12*
$r_{vy}/1.20r_o$	*216(6.00)*	*227(5.40)*	*238(4.72)*	"	*0.95*	*1.05*

The maximum displacements reached by elements *(1)* and *(2)* and at the centre of mass, as shown in Table 3-1, were not attained at the same time nor were they reached when the system developed its maximum rotation. Therefore, it is not possible to relate the system maximum displacement with its maximum rotation to derive the maximum displacement of the elements. Due to this behaviour, the problem was solved with the ratio of maximum displacement demands of the elements and that at the centre of mass. This is expressed as,

$$\left(\frac{\Delta_{ue1}}{\Delta_{us}}\right)_d \quad \text{and} \quad \left(\frac{\Delta_{ue2}}{\Delta_{us}}\right)_d \tag{3-1}$$

where Δ_{ue1} and Δ_{ue2} are the maximum displacement demands of elements *(1)* and *(2)*, respectively, and Δ_{us} is that at the centre of mass. The subscript "d" refers to demand quantities. A ratio less than unity indicate that the displacement demand on the associated element is less than that at the centre of mass. This relationship is particularly useful considering that the response at the centre of mass is easily predicted with an equivalent single degree of freedom system.

It is evident from Table 3-1 that the ratios of displacement demands are a function of the r_{vy}/r_m ratio. Its value reduced as the r_{vy}/r_m ratio was reduced. This indicates that the maximum displacements demands of the elements and that at the centre of mass became similar as the r_{vy}/r_m ratio was reduced.

Zero strength eccentricity may not be achieved in practice due to requirements of minimum reinforcement stipulated for reinforced concrete elements. It is likely that one element may finish with some excess strength but never less than that required to satisfy zero strength eccentricity. This scenario will introduce a strength eccentricity and an increase of system strength, as already shown in Figure 2-28(a).

Figure 3-9 shows the response of the unrestrained *System 3A-1.3* when excess strength was assigned to either element *(1)* or *(2)* due to the reasons given before. Consider, first, the case when the system had $r_{vy}/r_m \leq 1.0$, *i.e.*, r_{vy}/r_o and $r_{vy}/1.20r_o$. It is evident a similar behaviour to that of the unrestrained *System 1A-1.3* already described in Section 3.3. For example, excess strength of element *(1)*, which introduced increasing negative strength eccentricities, generated a reduction in its displacement ductility demands relative to the maximum attained for zero strength eccentricity whereas displacement ductility demands on element *(2)* remained equal or smaller.

In the case of the system having $r_{vy}/r_o > 1.0$, i.e., $r_{vy}/0.85r_o$, excess strength of element *(1)* ($\lambda_1 > 1.0$) still led to a reduction of its displacement ductility demands relative to that attained for zero strength eccentricity whereas those of element *(2)* slightly exceeded the maximum ductility demand attained for such strength distribution. This indicates that the reduction of the displacement at the centre of mass, originated by the increase in system strength, was not enough to compensate for the rotation-induced displacement imposed on element *(2)*, additional to those resulting from system translations.

A similar behaviour occurred when element *(2)* had excess strength ($\lambda_2 > 1.0$) and hence increasing positive strength eccentricities were introduced. However, positive strength eccentricities larger than $e_{vx} > 0.05D$ are considered an unlikely scenario in practical design and

hence, the response was just presented to clarify trends in behaviour. This is because, although an excess strength may be assigned to element *(2)*, the total strength to be assigned to this element may not be larger than that of element *(1)* if requirements of minimum or maximum reinforcement content are to be satisfied. For instance, element *(1)*, being longer than element *(2)*, will require a larger reinforcement content, and hence larger lateral strength, to comply with the recommended minimum reinforcement content, hence, it seems unlikely that a large positive strength eccentricity may be introduced to the system. Another scenario not allowing the introduction of a positive strength eccentricity is when an excess strength, relative to that satisfying zero strength eccentricity, cannot be assigned to element *(2)* because the strength assigned to this element already satisfies the recommended ratio of maximum reinforcement content.

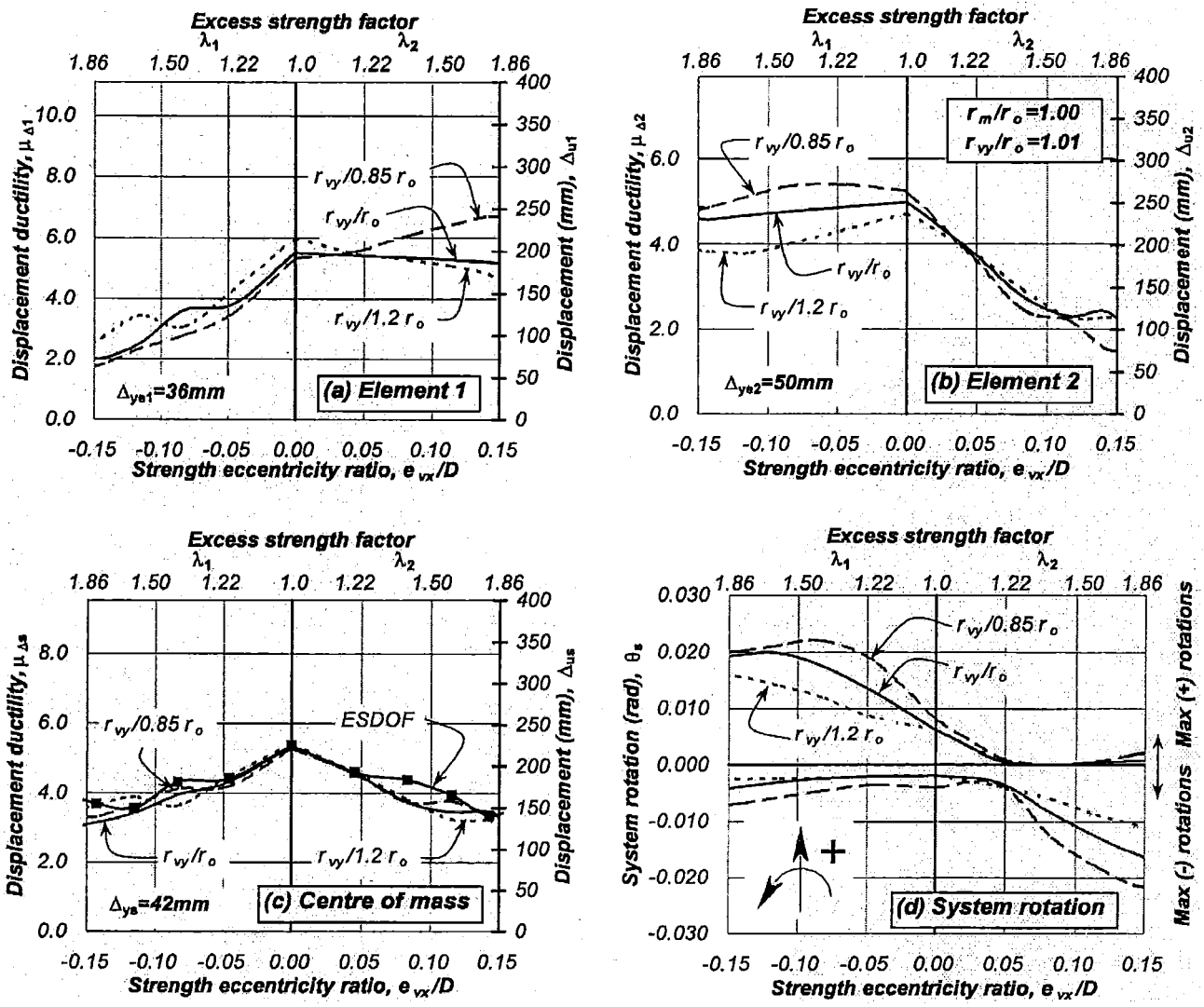

Figure 3-9. Response of the unrestrained *System 3A-1.3(α=1.4)*, T_s=1.30 sec, e_{mx}=0.0, e_{vx}≠e_{rx}=variable, $\mu_{\Delta s}$=5.35, r_m/r_o=1.0, r_{vy}/r_m=variable

The system nominal strength increased with the excess strength of either element *(1)* or *(2)*. Figure 3-9(c) reveals that the displacement demands at the centre of mass were reduced with increasing strength eccentricities. It also shows that the response was essentially the same irrespective of the r_{vy}/r_m ratio. The equivalent single degree of freedom still predicted, without

much difference, the maximum displacement ductility demands at the centre of mass for zero and increasing strength eccentricities. This was not affected by the fact that elements reached their maximum response at different instances.

System rotations were also influenced by the strength eccentricity and the r_{vy}/r_m ratio. Figure 3-9(d) shows, for clarity, maximum positive and negative rotations imposed on the system. As expected, the dominant positive system rotations increased with negative strength eccentricities. It is also evident that for any given negative strength eccentricity, the system exhibited a larger system rotation with $r_{vy}/0.85r_o$ than with $r_{vy}/1.2r_o$. In contrast, the introduction of positive strength eccentricities reduced even further the maximum positive and negative rotations until reaching a minimum for $e_{vx}\approx+0.04D$. Thereafter, the system rotation increased with primarily negative system rotations. It is evident that for a strength eccentricity between zero and $e_{vx}\approx+0.04D$, the r_{vy}/r_m ratio did not have a significant influence in the response due to the small rotations experienced by the system.

A strength eccentricity of $e_{vx}\approx+0.04D$ was associated with the centre of mass located half way between the centre of strength and centre of stiffness [C6, M3]. At this point, the whole system translated without exhibiting large rotations. Thus, the maximum displacements of the elements and at the centre of mass were essentially the same and attained at similar instants. Section 3.5.2 will explain the reason of this behaviour by analysing the time history response.

The ideal distribution of strength previously described is unlikely to be achieved in practice. This is because it is probable that a long wall (representing any element having a small nominal yield displacement) will have strength in excess to that satisfying zero strength eccentricity so that requirements of minimum reinforcement are satisfied. Another reason for not achieving zero strength eccentricity may occur when the strength of the short wall cannot be further increased because the maximum allowable strength that can be assigned to it was already provided.

It is seen from Table 3-1 that limiting the maximum displacement ductility demand of the system to the displacement ductility capacity of the elements, i.e., $\mu_{\Delta s}=\mu_{\Delta 1}=\mu_{\Delta 2}=5.35$, did not prevent element *(1)* from exceeding its displacement ductility capacity; particularly for r_{vy}/r_o and $r_{vy}/1.2r_o$. It was observed that the maximum displacement demands of the elements became similar as the r_{vy}/r_m ratio was reduced. The displacement ductility demand of critical element *(1)* increased above its capacity whereas that of element *(2)* further reduced as the r_{vy}/r_m ratio was reduced. To prevent critical element *(1)* from exceeding it displacement capacity, it is necessary to restrict even further the system displacement capacity. This reduction should apply to systems having any r_{vy}/r_m ratio. How this may be achieved in practice is subsequently explained.

For the suggested design strategy, the displacement capacity of the system should be associated with the system response for zero strength eccentricity. This is when the displacement demands of the system, and that of the elements, are expected to reach a maximum and rotations are rather small. It was shown, however, that rotations may be reduced even further when the centre of mass was located half way between the centre of strength and stiffness. However, instead of having to derive the location of the stiffness eccentricity to establish such particular location, it is enough to aim for zero strength eccentricity and assume, for any r_{vy}/r_m ratio, that the system does not rotate and hence the maximum displacement demand of the elements and that at the centre of mass will be the same.

Table 3-1 shows that the displacement demands of elements and at the centre of mass became very similar as the r_{vy}/r_m ratio was reduced. The consideration of equal displacement demands, for zero strength eccentricity, on elements may be conservative for some r_{vy}/r_m ratios. This assumption, however, accounts for all the responses of critical element *(1)* due to different r_{vy}/r_m ratios. In case of element *(2)*, the actual displacements were, in fact, slightly larger as the r_{vy}/r_m ratio was increased and not equal to that of element *(1)*. In spite of this behaviour, the displacement demands imposed on element *(2)* were less than its displacement capacity associated with the strain limits of the materials. In an attempt to establish the displacement and ductility capacity of the system, it is assumed that for zero strength eccentricity the maximum displacement demands of the elements and at the centre of mass is the same. Hence, the displacement demand of the system should be limited to that of the element having the smallest displacement capacity.

In this example, element *(1)* has the smallest displacement capacity. Hence, the displacement capacity of the system should be limited to $\Delta_{us}=\Delta_{ye1}\mu_{\Delta 1}$. This is expressed as,

$$\mu_{\Delta s} = \frac{(\Delta_{us})_{\min}}{\Delta_{ys}} = \frac{\Delta_{ye1}\mu_{\Delta 1}}{\Delta_{ys}} \qquad (3\text{-}2)$$

The displacement ductility capacity of the unrestrained *System 3A-1.3(α=1.4)* should be reduced from the assumed value of $\mu_{\Delta s}=5.35$ to $\mu_{\Delta s}=(\Delta_{ye1}\mu_{\Delta 1})/\Delta_{ys}=4.60$. With this approach, the displacement ductility demands of element *(1)* are expected to reach its ductility capacity of $\mu_{\Delta 1}=\Delta_{us}/\Delta_{ye1}=5.35$. Element *(2)*, is expected to reach and even exceed a maximum displacement ductility demand of $\mu_{\Delta 2}=\Delta_{us}/\Delta_{ye2}=3.83$, which is less than its capacity of $\mu_{\Delta 2}=5.35$. The inelastic element *(2)* can still develop additional displacements before reaching its available capacity associated with the strain limits of the materials.

It was mentioned before that the consideration of system translation only for unrestrained systems, where its strength is assigned to the elements to satisfy zero strength eccentricity, may conservatively predict the maximum displacement demand expected on element *(1)* whereas possibly underestimating that of element *(2)*. A better estimate of the system displacement and ductility capacity should take into the account the effect of system rotations on the displacement demands of the elements. For instance, the maximum displacement demands of element *(2)* may be much larger than that expected at the centre of mass and it is likely that element *(2)* rather than element *(1)* is the critical element of the system. This likely scenario will be explained in Section 3.10.1.

The findings presented in Table 3-1, for zero strength eccentricity, may be a point of discussion because they contrast with failures observed in many asymmetric buildings. For instance, the flexible element, which in this case is element *(2)*, was expected to show excessive structural damage as has been observed in many buildings during actual earthquake events. However, according to the analytical findings, structural damage for zero strength eccentricity appeared in critical element *(1)*, traditionally termed the stiff element, having the smallest displacement capacity and exhibiting the largest displacement ductility demand. On the other hand, flexible element *(2)*, having the largest nominal yield displacement and same displacement ductility capacity, will exhibit displacement demands less than the maxima established. This response is, however, unlikely to occur because a strength distribution satisfying zero strength eccentricity

will be difficult to achieve in practice. Then, why does the outermost flexible element of actual buildings exhibit most of the structural damage?

Three reasons are attributed to the excessive structural damage and/or failure observed in the flexible element of asymmetric structures.

(a) Although the estimated system strength necessary limiting displacement demands at the centre of mass to less than its capacity may have been correctly estimated, this may have not been suitably distributed among the elements. For instance, the strength assigned to certain elements may have been less than that required to satisfy zero strength eccentricity.

(b) The estimated system strength, for the particular seismic region, although correctly distributed on the elements, was not sufficient to limit the displacement demands at the centre of mass to less than its capacity. In such situation, it is expected that the displacement demand on the flexible element *(2)* due to additional displacement demands imposed on the element by increasing system rotations will increase and may even exceed its displacement capacity whereas element *(1),* having an excess strength, is not expected to become critical.

(c) A combination of the above.

The ideal response is expected to occur when the system strength, necessary to limit displacement demand at the centre of mass and that of the elements to less that its capacity, is assigned to elements *(1)* and *(2)* to satisfy zero strength eccentricity. Element *(1)*, however, may have some excess strength, relative to that satisfying zero strength eccentricity, to comply, for instance, with requirements of minimum reinforcement whereas the strength of element *(2)* remains unchanged. For this strength distribution, the excess strength of element *(1)* is expected to reduce its displacement demand and hence becomes less susceptible to failure. On the other hand, the displacement demands on element *(2)* are not expected to exceed its capacity even with increasing strength eccentricities.

The above findings suggest that the proposed distribution of system strength is effective in limiting the displacement demand of the elements to less than their displacement ductility capacities due to increasing strength eccentricities. As a first attempt, displacement capacity of the unrestrained systems should be limited to that of the element with the smallest displacement capacity. This is based on the simplification that, for zero strength eccentricity, the maximum displacement demand on the elements is assumed the same. This approach may be, however, overly conservative and hence a refined method is proposed for a better estimate of the displacement and ductility capacity of systems which accounts for the effect of system rotations on the maximum displacement demand of the elements. It was also found that the torsional behaviour of symmetric and asymmetric systems having increasing strength eccentricities is essentially the same. The only difference is that the rotations of asymmetric systems reach a minimum when the centre of mass is located half way between the centres of strength and stiffness.

3.5.2 Time history response of the unrestrained *System 3A-1.3(α=1.4)*

Time history responses were examined to provide further understanding of the torsional behaviour during dynamic response. This should assist in a better understanding of the torsional mechanism rather than just examining observed trends.

(a) *Unrestrained System 3A-1.3 [e_{vx}=0.0 (λ_1=1.0), e_{rx}=-0.083D (α=1.4)]*

The unrestrained *System 3A-1.3(α=1.4)*, as shown in Figure 2-27(a), was considered again. The system strength was assigned to the elements according to static equilibrium, i.e., e_{vx}=0.0. Hence, elements *(1)* and *(2)* had the same nominal strength of V_{ne1}=V_{ne2}=88 *kN*. For zero strength eccentricity, a stiffness eccentricity of e_{rx}=-0.083D (α=1.4) (*D*=12.42*m*) was introduced due to differences in nominal yield displacements of the elements. The structure had r_{vy}/r_m=1.0 and r_m/r_o=1.0 and was subjected to the Artificial earthquake record along the *Y*-direction.

Consider the torsional mechanism involved when a positive static force is applied at the centre of mass. Elements *(1)* and *(2)* should attain their nominal strength simultaneously. The system will also develop an anticlockwise rotation due to its negative stiffness eccentricity.

On the other hand, Figure 3-10 shows that during the dynamic response the above-mentioned mechanism did not apply. The response was studied in detail between *3.0* and *4.0* seconds when the elements and centre of mass reached their maximum displacement demands. Element *(1)* reached first its nominal strength at instant *(A)*, as shown in Figure 3-10(a). This was because the stiffness eccentricity triggered immediately a clockwise dynamic torque before any element reached its nominal strength, as shown in Figure 3-10(c). This dynamic torque restrained the anticlockwise rotations expected if a positive static force is applied at the centre of mass. This torque meant that element *(1)* was first to reach its nominal strength. The peak torque was *T=366kNm*, see Figure 3-10(c). The displacement profile and actions associated with instant *(A)*; see Figure 3-11(a), shows element *(1)* displaying a displacement demand slightly larger than that of element *(2)*. This shows that system rotations were restrained by the mass rotatational inertia.

Element *(2)* reached its nominal strength at instant *(B)*. This was because after element *(1)* reached its nominal strength at instant *(A)*, the system torque reached a peak and then a rotational deceleration happened due to the opposition of the rotational mass to a clockwise rotation. This rotational deceleration was generated, as previously explained in Section 3.3.2, because a couple of forces provided torsional resistance. Element *(2)* provided one of the forces since it still had some residual resistance. The other force was the dynamic resistance of the mass translational inertia. The displacement profile and actions associated with instant *(B)*; see Figure 3-11(b), indicates that as element *(2)* reached its nominal strength at instant *(B)*, the displacement of the elements and that at the centre of mass were, at this instant, essentially the same and yet well below their peak values.

At instant *(B)*, the system torque becomes zero. This scenario is expected from systems having zero strength eccentricity and elements yielding in the same direction. The system torque remained constant between instants *(B)* and *(C)* when both elements were yielding, as shown in Figure 3-10(c). No translational or rotational acceleration was observed during these instants. The displacements of the elements and at the centre of mass and the system rotations increased due to the translational and angular velocity of the system.

At instant *(C)*, element *(1)* reached its peak displacement. The associated displacement profile and actions, shown in Figure 3-11(c), shows that the system rotation increased due to the increase in the displacement of element *(2)*.

An instant later at *(D)*, element *(2)* also reached its peak displacement and subsequently become inelastic. The torque, generated due to a rotational acceleration, increased when the centre of mass reached its maximum displacement. Element *(1)* was again elastic and showed a displacement reduction. Figure 3-11(d) shows that the system rotation increased due to the displacement reduction exhibited by element *(1)*.

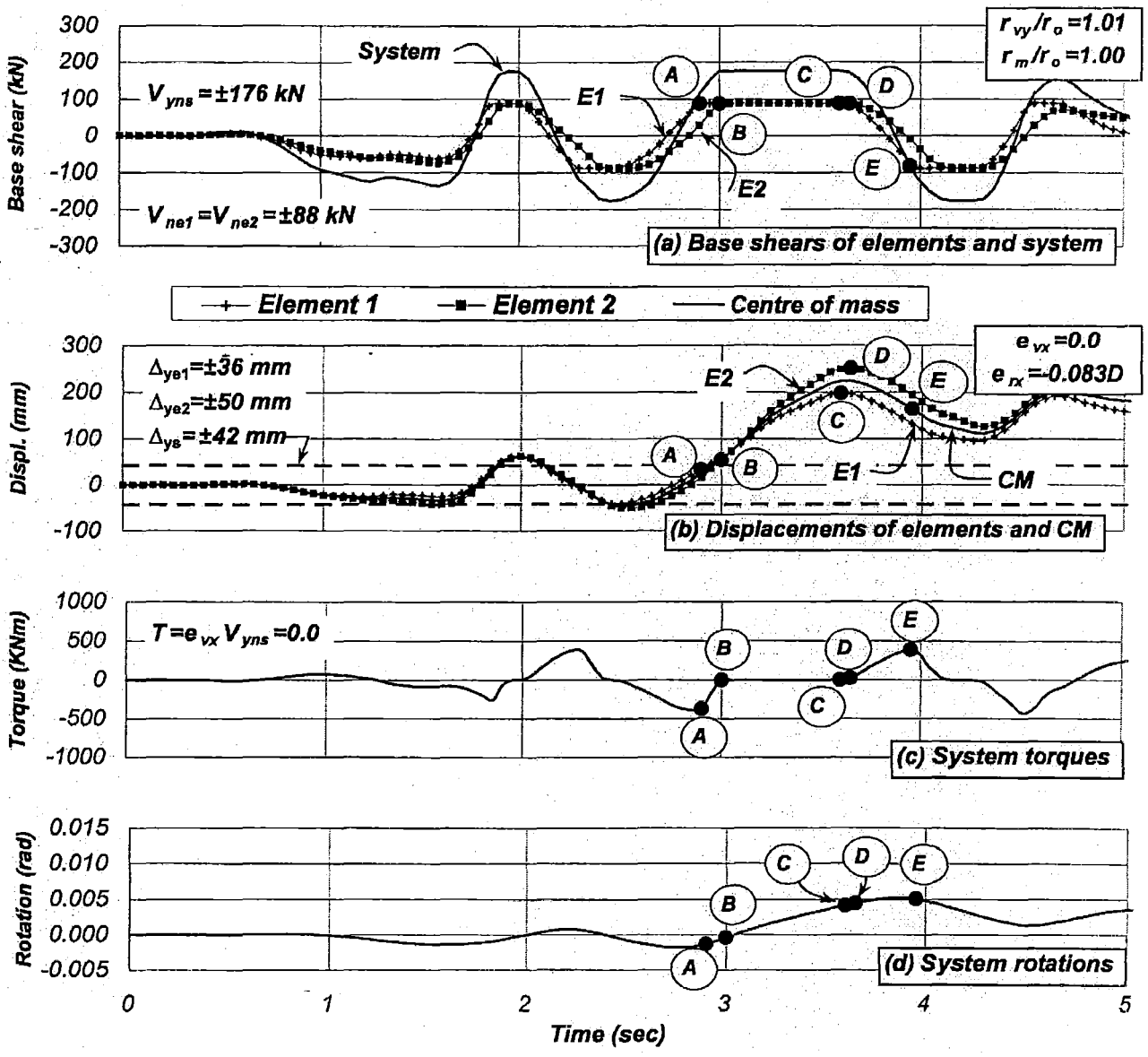

Figure 3-10. Time history response of the unrestrained *System 3A-1.3(α=1.4)*, T_s=1.30 sec, e_{mx}=0.0, e_{vx}=0.0, e_{rx}=-0.083D, $\mu_{\Delta s}$=5.35, r_m/r_o=1.0, r_{vy}/r_m=1.01

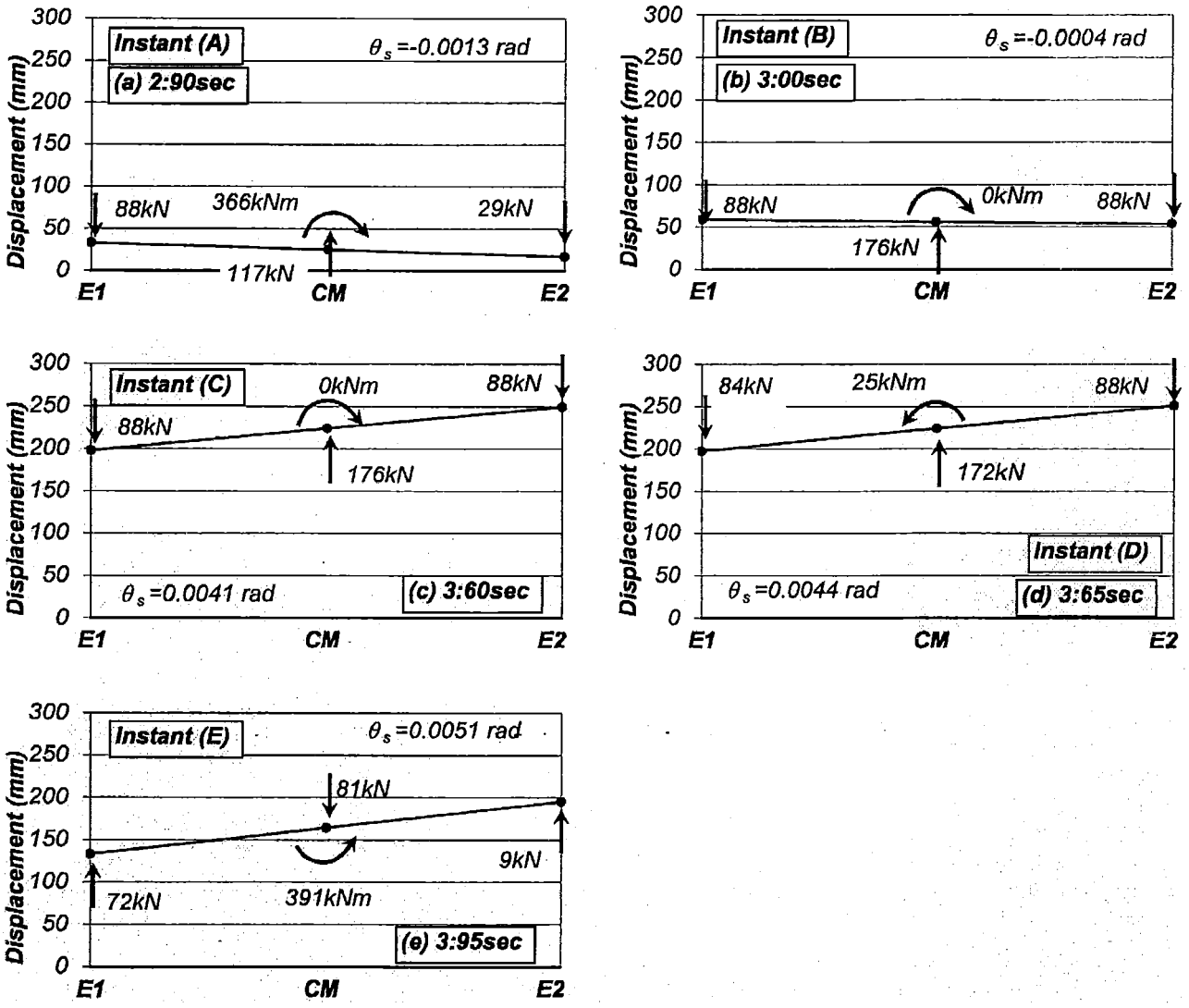

Figure 3-11. Displacement profiles and actions introduced to the unrestrained *System 3A-1.3*(α=1.4), T_s=1.30 sec, e_{mx}=0.0, e_{vx}=0.0, e_{rx}=-0.083D, $\mu_{\Delta s}$=5.35, r_m/r_o=1.0, r_{vy}/r_m=1.01

The system rotation reached a maximum when the system torque attained a peak at instant *(E)*. This instant was not associated with the maximum displacement demands of the elements or that at the centre of mass, as shown in Figure 3-10(e). The associated displacement profile shown in Figure 3-11(e) shows that both elements remained elastic and the torque increased.

(b) *Unrestrained System 3A-1.3* [e_{vx}=-0.045D (λ_1=1.2), e_{rx}=-0.13D (α=1.4)]

The unrestrained *System 3A-1.3*(α=1.4) was considered again. This time, element *(1)* had a *20%* excess strength. The nominal strength of element *(1)* increased to V_{ne1}=106kN while that of element *(2)* remained at V_{ne2}=88kN. The excess strength of element *(1)* introduced a strength eccentricity of e_{vx}=-0.045D and increased the stiffness eccentricity to e_{rx}=-0.13D (α=1.4). The system strength was, therefore, increased to V_{yns}=194 kN. It was subjected to the Artificial earthquake along the *Y*-direction.

The application of a positive static force at the centre of mass would indicate that element *(2)* should reach first its nominal strength whereas element *(1)* can never yield. The system will also exhibit an anticlockwise rotation due to its negative eccentricity.

On the other hand, the dynamic response again presented a different behaviour. Figure 3-12(a) shows that, in spite of its excess strength, element *(1)* reached its nominal strength at instant *(A)* before element *(2)* did. This was, as previously stated, due to the restraining action of the mass rotational inertia to system rotations which introduced a clockwise dynamic torque of $T=652kNm$. Figure 3-12(c) shows that this clockwise torque was larger than that attained when the system had zero strength eccentricity, as already shown in Figure 3-10(c). The associated displacement profile, shown in Figure 3-13(a), exhibits that the displacement of element *(1)* was much larger than that of element *(2)*.

After element *(1)* reached its nominal strength, the torque reduced because the rotational mass decelerated due to the opposition of the rotational mass to an opposite clockwise rotation. This made element *(2)* reach its nominal strength at instant *(B)*. However, the time required for this to happen slightly increased when compared to the case described before in (a). The instantaneous displacement profile at instant *(B)*, shown in Figure 3-13(b), shows similar displacement demands of the elements. The torque and system rotations reduced as the displacement of element *(2)* matched that of element *(1)*.

Between instants *(B)* and *(C)*, elements *(1)* and *(2)* were yielding in the same direction. At this stage, a constant torque of $T=e_{vx}V_{yns}=-110kNm$ was developed due to the strength eccentricity of the system; see Figure 3-12(d). The system rotation, shown in Figure 3-12(c), was larger than that of the system with zero strength eccentricity due to its larger angular velocity, see Figure 3-10(c).

Element *(1)* reached its maximum displacement at instant *(C)*; see Figure 3-12(b). The displacement profile shown in Figure 3-13(c) indicates that the maximum displacement attained by element *(1)* reduced due to its excess strength relative to that observed when the system had zero strength eccentricity; see Figure 3-11(c). In case of element *(2)* this remained essentially the same, hence system rotations increased; as Figure 3-13(c) shows. Thereafter, the torque reduced and eventually changed from negative to positive as the centre of mass reached its maximum displacement.

A comparison of Figure 3-10(b) and Figure 3-12(b) at instant *(C)* shows, as expected, that in spite of a larger strength eccentricity, the displacement demands of element *(1)* and at the centre of mass reduced whereas the maximum displacements of element *(2)* remained essentially the same. It is evident that the increase in torque and rotations bear little relevance to the important feature of behaviour; maximum displacement demands on the elements.

It took a little longer for element *(2)* to reach its maximum displacement at instant *(D)* for a reduced total base shear; see Figure 3-12(a). The displacement profile shows that the system rotation increased because the displacement of elastic element *(1)* reversed whereas element *(2)* reached a maximum; see Figure 3-13(d). The torque slightly increased.

Figure 3-12(c) and (d) shows that, at instant *(E)*, the torque and system rotation attained a maximum. This behaviour was reached when both elements were still elastic, see Figure 3-13(e). However, they were not associated with the maximum displacement demands of elements and centre of mass, as shown in Figure 3-12(e). This demonstrates their irrelevance during dynamic response. In spite of significant increase of torques and system rotations, the displacement demands on the elements were not a maximum.

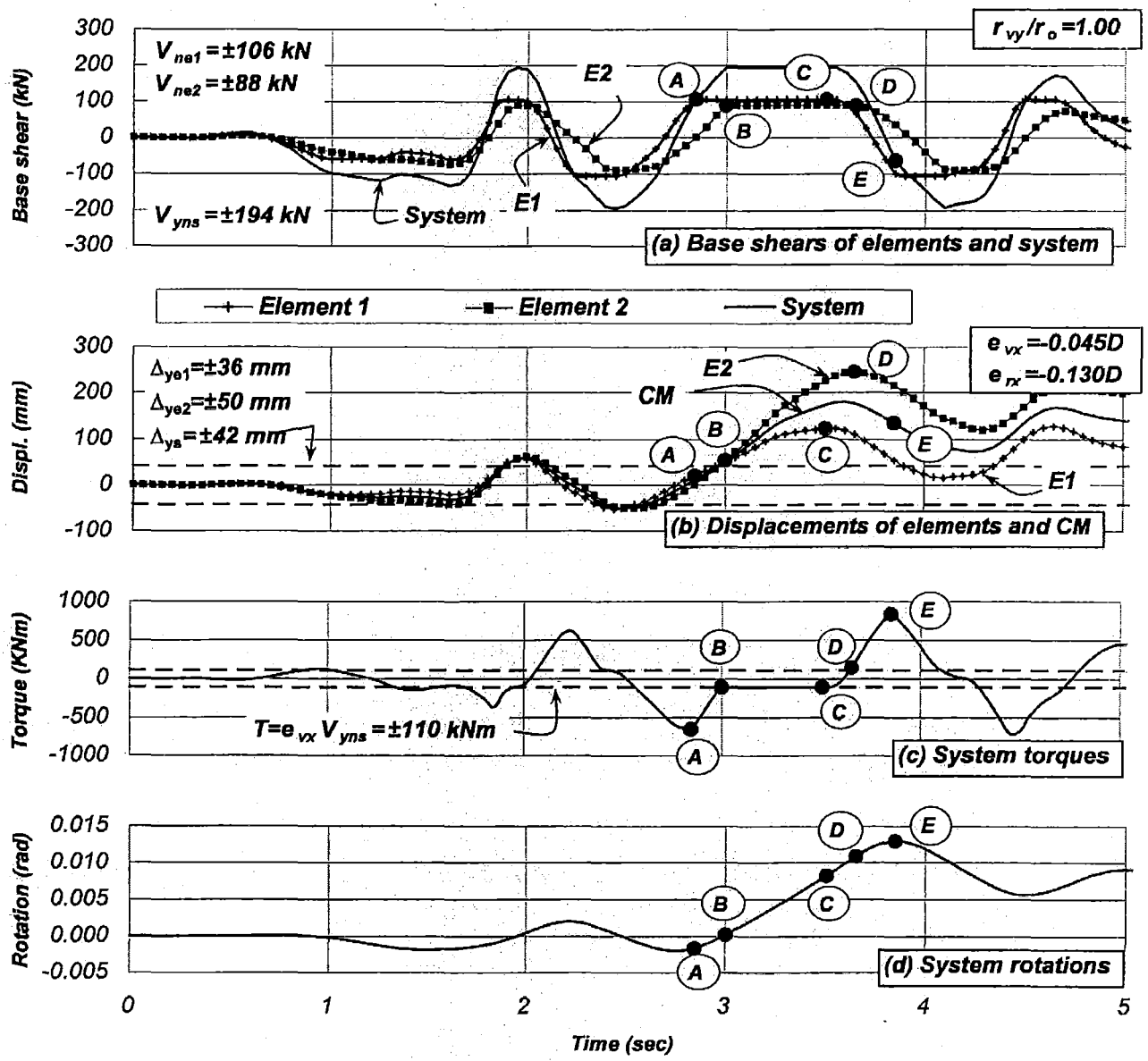

Figure 3-12. Time history response of the unrestrained *System 3A-1.3*(α=1.4), T_s=1.30 sec, e_{mx}=0.0, e_{vx}=-0.045D, e_{rx}=-0.083D, $\mu_{\Delta s}$=5.35, r_m/r_o=1.0, r_{vy}/r_m=1.01

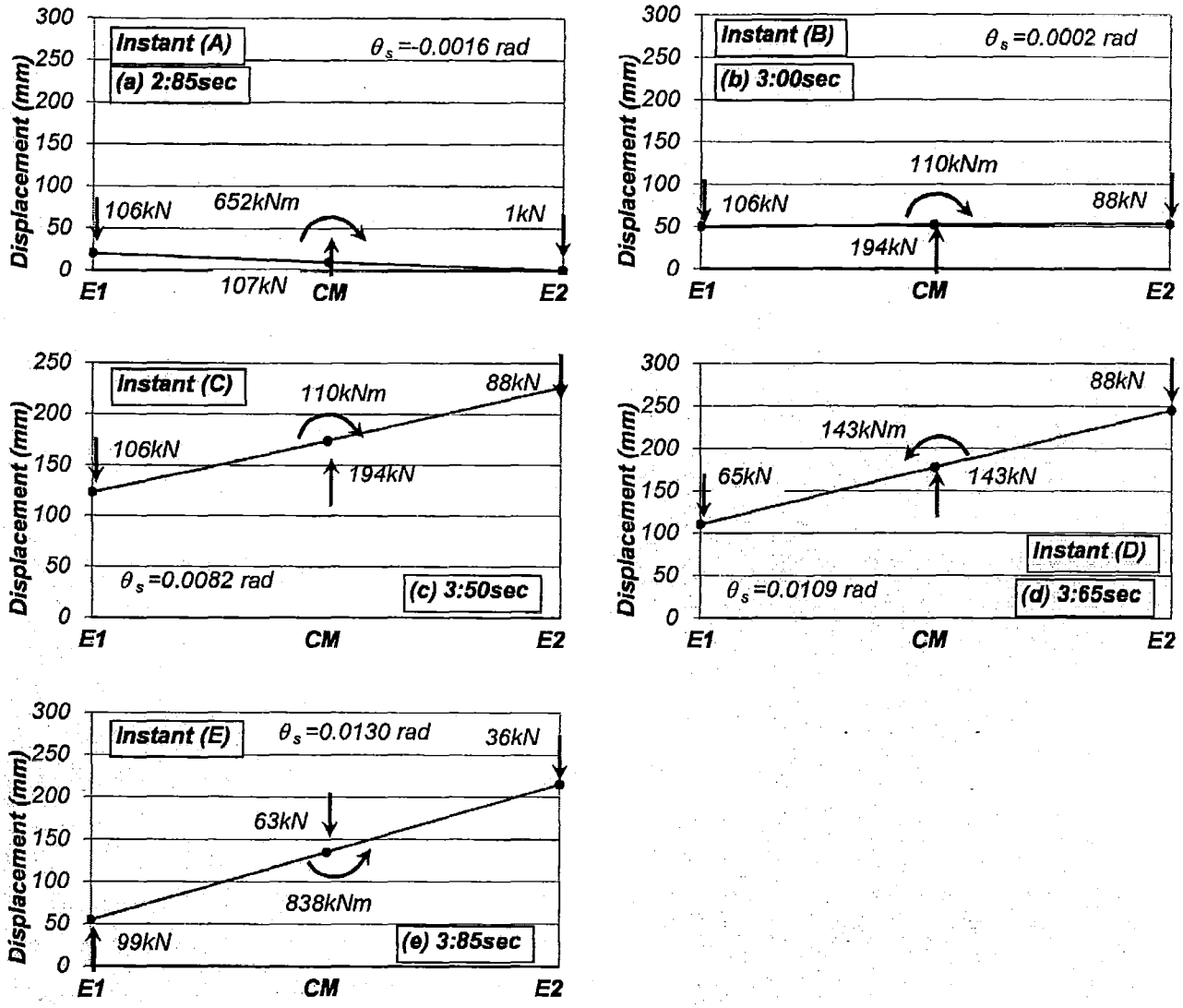

Figure 3-13. Displacement profiles and actions introduced to the unrestrained *System 3A-1.3*(α=1.4), T_s=1.30 sec, e_{mx}=0.0, e_{vx}=-0.045D, e_{rx}=-0.083D, $\mu_{\Delta s}$=5.35, r_m/r_o=1.0, r_{vy}/r_m=1.01

(c) *Unrestrained System 3A-1.3* [e_{vx}=+0.045D (λ_2=1.2), e_{rx}=-0.04D (α=1.4)]

The unrestrained *System 3A-1.3*(α=1.4) was considered again. Element *(1)* retained its initial nominal strength of V_{ne1}=88kN while element *(2)* had a *20%* excess strength (V_{ne2}=1.20*88=106kN). The excess strength of element *(2)* introduced a positive strength eccentricity of e_{vx}=+0.045D and reduced the stiffness eccentricity to e_{rx}=-0.04D (α=1.4). This strength eccentricity was associated with the centre of mass located half way between centres of strength and stiffness, as already pointed out in Section 3.5.1. The system strength increased to V_{yns}=194 kN. The nominal yield displacement of the elements remained unchanged. It was subjected to the Artificial earthquake record along the *Y*-direction.

Consider once more the torsional mechanism induced when a positive static force is applied at the centre of mass. Element *(1)* will reach first its nominal strength while element *(2)* will never yield. The system will still exhibit an anticlockwise rotation due to its small but still negative strength eccentricity.

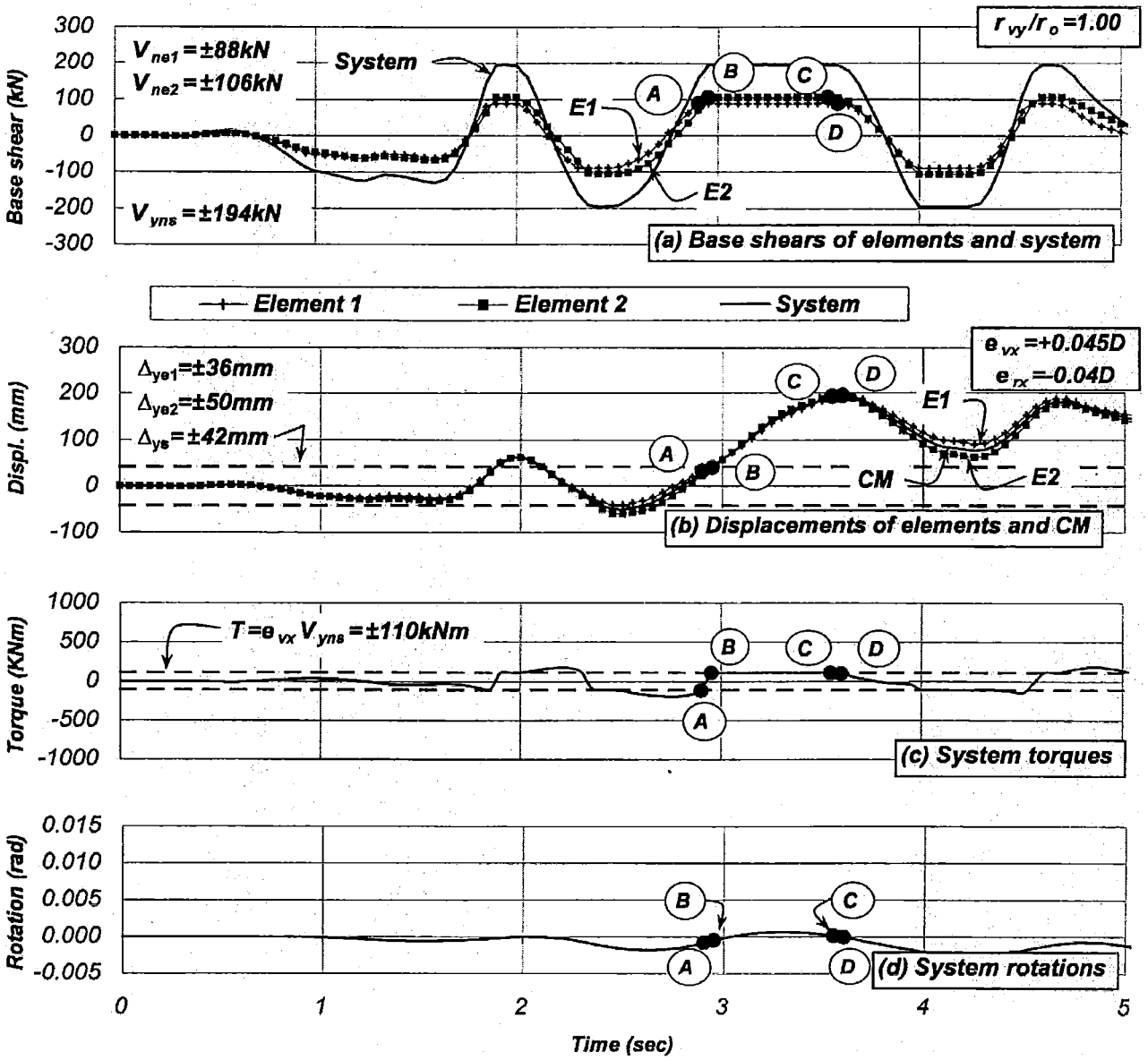

Figure 3-14. Time history response of the unrestrained *System 3A-1.3*(α=1.4), T_s=1.30 sec, e_{mx}=0.0, e_{vx}=+0.045D (λ_2=1.2), e_{rx}=-0.040D, $\mu_{\Delta s}$=5.35, r_m/r_o=1.0, r_{vy}/r_m=1.01

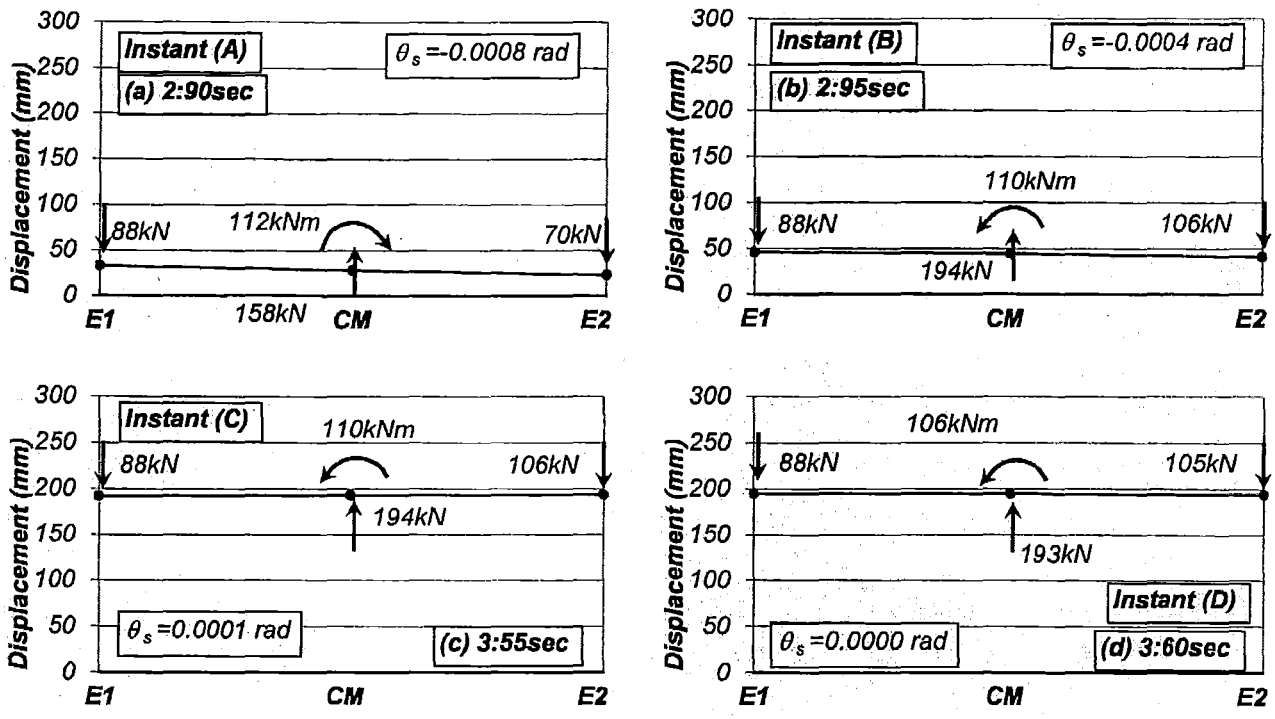

Figure 3-15. Displacement profiles and actions introduced to the unrestrained *System 3A-1.3*(α=1.4), T_s=1.30 sec, e_{mx}=0.0, e_{vx}=+0.045D(λ_2=1.2), e_{rx}=-0.040D, $\mu_{\Delta s}$=*5.35*, r_m/r_o=1.0, r_{vy}/r_m=1.01

In contrast, the dynamic response, shown in Figure 3-14(a), indicates, once again, that before yielding occurs in any element, the mass rotational inertia introduced a clockwise dynamic torque due to the negative stiffness eccentricity. Figure 3-14(a) and (c) show that element *(1)* still attained its nominal strength first at instant *(A)*. A small clockwise torque of *T=-110kNm* was introduced by the mass rotational inertia to restrain the anticlockwise rotations expected before yielding occurred. The associated displacement profile; see Figure 3-15(a), exhibit similar displacements for the elements but, as expected, slightly a larger displacement for element *(1)*.

Element *(2)* reached its nominal strength, a fraction of a second later, for the same but opposite dynamic torque of $T_v=e_{vx}V_{yns}=-110$ *kNm* at instant *(B)*. The displacement demand on both elements increased but remained very similar; see Figure 3-15(b). The combined effect of a clockwise torque in the elastic system and then an opposite torque once element *(1)* yielded led to a minimum system rotation. Thereafter, the inelastic displacements of the elements increased and the whole system translated without large rotations. Thus, the maximum displacements of the elements and at the centre of mass were essentially the same; see instant *(C)* in Figure 3-15(c). This was also evident from Figure 3-14(c), (d) and (e) when compared with their counterparts in Figure 3-10 and Figure 3-12.

It is evident from the time histories examined before that the role of the mass rotational inertia is its opposition to system rotations. Torques and rotations increased or reduced depending on the distribution of system strength, i.e., strength eccentricity, and hence influenced the relative displacements demand of the elements. However, as pointed out earlier, the increase in torque and rotations are not associated with the maximum displacement demands of elements and, therefore, had little relevance to the important feature of behaviour, the maximum displacement demand on elements.

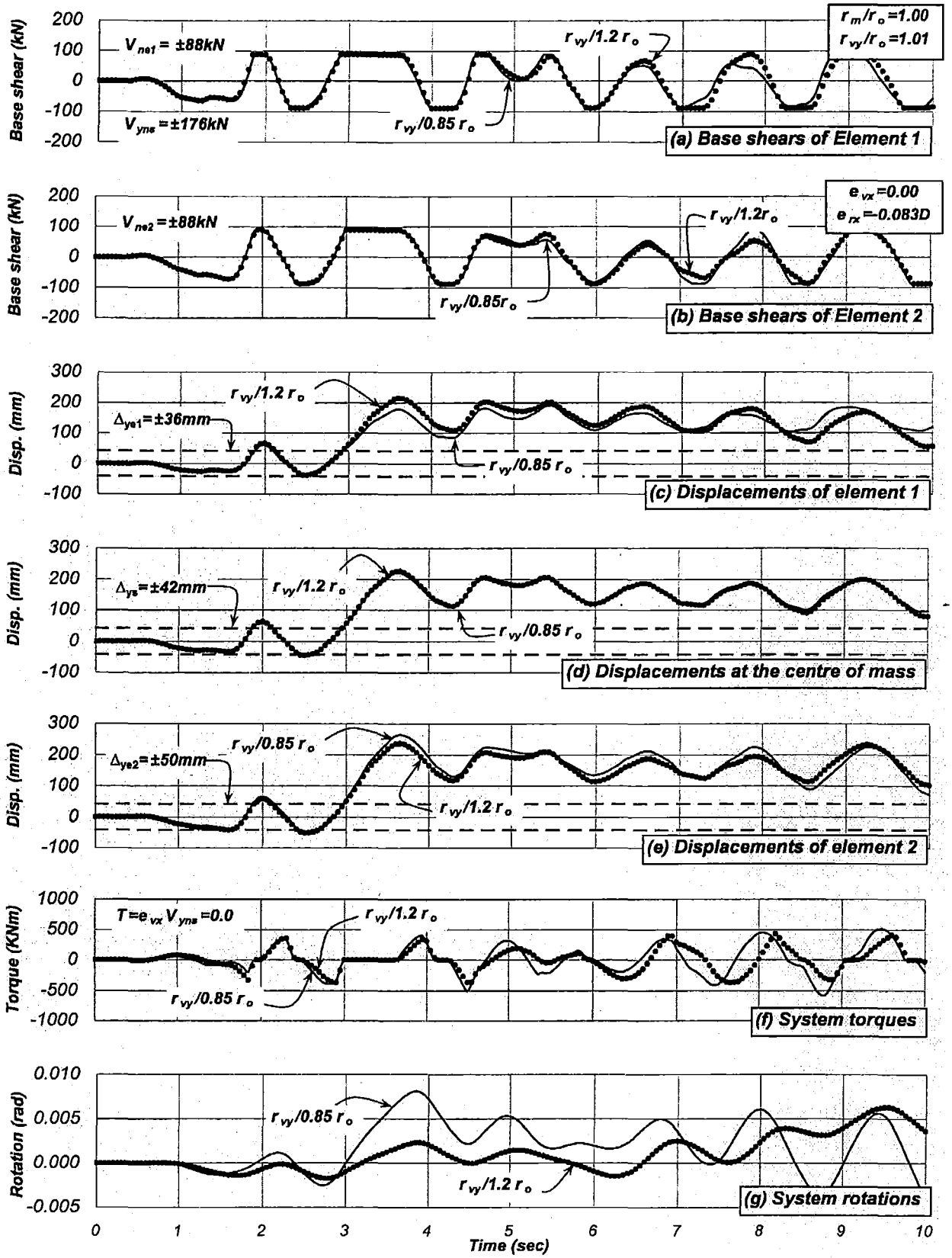

Figure 3-16. Time history response of the unrestrained *System 3A-1.3(α=1.4)*, T_s=1.30 sec, e_{mx}=0.0, e_{vx}=0.0, e_{rx}=-0.083D, $\mu_{\Delta s}$=5.35, r_m/r_0=1.0, r_{vy}/r_m=variable

3.5.3 Time history response of the unrestrained *Systems 3A-1.3(α=1.4)* having different r_{vy}/r_m ratios

It is already evident from Figure 3-9 that the r_{vy}/r_m ratio is a useful parameter quantifying the restraining effect of the mass rotational inertia on system rotations. To provide a better understanding of its effect on the system behaviour, the time history response of two identical unrestrained *Systems 3A-1.3(α=1.4)* with zero strength eccentricity and unchanged properties but having radii of gyration of mass of $r_m=0.85r_o$ and $1.20r_o$ were compared. The radius of gyration of strength remained constant. They were denoted unrestrained *Systems 3A-1.3(0.85r_o)* and *3A-1.3(1.20r_o)*.

It is evident from Figure 3-16(a) and (b) that elements *(1)* and *(2)* reached, in both systems, their nominal strength, at essentially the same instant. The variation of the system's torques along the time domain was quite similar, as shown in Figure 3-16(e). However, the variation of rotations, as shown in Figure 3-16(f), demonstrates that the rotational mass was not mobilised in the same manner because the angular velocity in each case was different. For instance, unrestrained *System 3A-1.3(1.20r_o)* exhibited reduced system rotations. This was expected since it had a large rotational mass. This generated similar displacement demands of elements *(1)* and *(2)*, as shown in Figure 3-16(c) and (e). As the system rotations reduced, the element with the smallest displacement capacity is likely to be critical.

It is seen from Figure 3-16(d) that the displacement demands at the centre of mass remained essentially the same in both systems. Hence, it demonstrates that the actions of the mass rotational inertia did not influence system translations.

The above results suggest that the r_{vy}/r_m ratio quantifies well the restraining effect of the mass rotational inertia on the system rotations. This ratio dictates which element is likely to become critical on identical systems but having a different radius of gyration of mass. This explains, in part, why some past studies [C15] reach contradictory conclusions with regard to which element is critical, the stiff or the flexible element.

3.5.4 Response comparison of the unrestrained *Systems 3A-1.3(α=1.4), 4A-1.3(α=1.4)* and *5A-1.3(α=1.4)*

Until now, this study had considered systems with a square diaphragm and a specific location of elements to achieve $r_{vy}/r_m = 1.0$. The radius of gyration of mass was then modified to $r_m=0.85r_o$ and $r_m=1.20r_o$ while the radius of gyration of element nominal strength remained constant, see Section 2.13.

The study, so far, has, however, not yet considered a change in both the arrangement of the elements and the plan configuration to modify the r_{vy}/r_m ratio. In fact, two systems can have the same r_{vy}/r_m ratio for different diaphragm configurations and element locations. The response comparison of these systems should help verify the generality of the findings obtained so far with regard to the r_{vy}/r_m ratio.

The unrestrained *Systems 3A, 4A* and *5A* described in Section 2.18.1; having different r_{vy}/r_m ratios, as shown in Table 2-5, are considered. The systems had an uncoupled translational period of $T_s=1.30$ seconds. The displacement ductility capacity of the systems was also assumed as $\mu_{\Delta s}=5.35$. They were subjected to the Artificial record along the *Y*-direction. They all have

$\alpha=\Delta_{ye2}/\Delta_{ye1}=1.4$. They were denoted as *Systems 3A-1.3(α=1.4), 4A-1.3(α=1.4)* and *5A-1.3(α=1.4).*

The design strategy suggests that the system nominal strength, necessary to ensure that the displacement ductility capacity of any element is not exceeded, should be distributed on the elements to satisfy static equilibrium requirements, i.e., $e_{vx}=0.0$. This strength distribution may not be achieved in practice but it is of interest because it is where the system reaches its maximum response and, therefore, provides the basis to estimate its displacement capacity.

Table 3-2 summarizes the response of the system for zero strength eccentricity. As expected, the maximum displacement demands of the elements and at the centre of mass was slightly different but became similar as the r_{vy}/r_m ratio was reduced. Displacement demand ratios associated with elements *(1)* and *(2)* also reduced as the r_{vy}/r_m ratio was reduced. This torsional behaviour was similar to that observed for the unrestrained *System 3A-1.3(α=1.4)* having different r_{vy}/r_m ratios; see Figure 3-9. The equivalent single degree of freedom system predicted, with adequate accuracy, the maximum response attained at the centre of mass for all systems which shows that it is not affected by the variation of the r_{vy}/r_m ratio.

It is seen again that limiting the displacement ductility capacity of the system to $\mu_{\Delta s}=5.35$ did not prevent critical element *(1)* from exceeding its displacement capacity. This may be avoided if the displacement capacity of the system is limited to that of element *(1)* exhibiting the smallest displacement capacity. This limitation is based on the assumption that maximum displacement demands of the elements and at the centre of mass are essentially the same and a maximum for zero strength eccentricity. The displacement ductility capacity for all three systems having different r_{vy}/r_m ratios should, therefore, be $\mu_s=4.60$, as already explained in Section 3.5.1.

Table 3-2. Response of the unrestrained *Systems 3A-1.3(α=1.4), 4A-1.3(α=1.4)* and *5A-1.3(α=1.4)*, T_s=1.30 sec, e_{mx}=0.0, e_{vx}=0.0, e_{rx}=-0.083D, $\mu_{\Delta s}$=5.35, r_m/r_o=1.0, r_{vy}/r_m=variable

		Displacements, mm, and displacement ductility demands (μ_s)				Displacement demand ratios	
System	r_{vy}/r_m	E1	CM	E2	ESDOF	$(\Delta_{ue1}/\Delta_{us})_d$	$(\Delta_{ue2}/\Delta_{us})_d$
4A	1.54	178(4.93)	217(5.16)	274(5.44)	225 (5.35)	0.82	1.26
3A	1.00	198(5.50)	224(5.34)	251(4.98)	"	0.88	1.12
5A	0.78	222(6.28)	227(5.41)	232(4.61)	"	0.98	1.02

Zero strength eccentricity may not be achieved because one element may require some excess strength relative to that satisfying zero strength eccentricity to comply with requirements of minimum reinforcement stipulated for reinforced concrete members. Figure 2-28(a) has already shown that the excess strength of either element *(1)* or *(2)* introduced a strength eccentricity and increased the system strength.

Figure 3-17 shows the response due to an excess strength of either element *(1)* or *(2)* and hence increasing negative and positive strength eccentricities, respectively. It is evident that the displacement ductility demands of element *(1)* reduced with increasing negative strength eccentricities. Interestingly, the displacement ductility demand of the critical element *(2)* barely increased for the unrestrained *System 4A-1.3* having $r_{vy}/r_m>1.0$, which was expected to be critical. This indicates that the realistic scenario of increasing negative strength eccentricities introduced a system excess strength that reduced the displacement demand at the centre of mass. This reduction did compensate for the torsion-induced displacement introduced to the critical

element *(2)*, additional to those resulting from system translations and irrespective of the r_{vy}/r_m ratio.

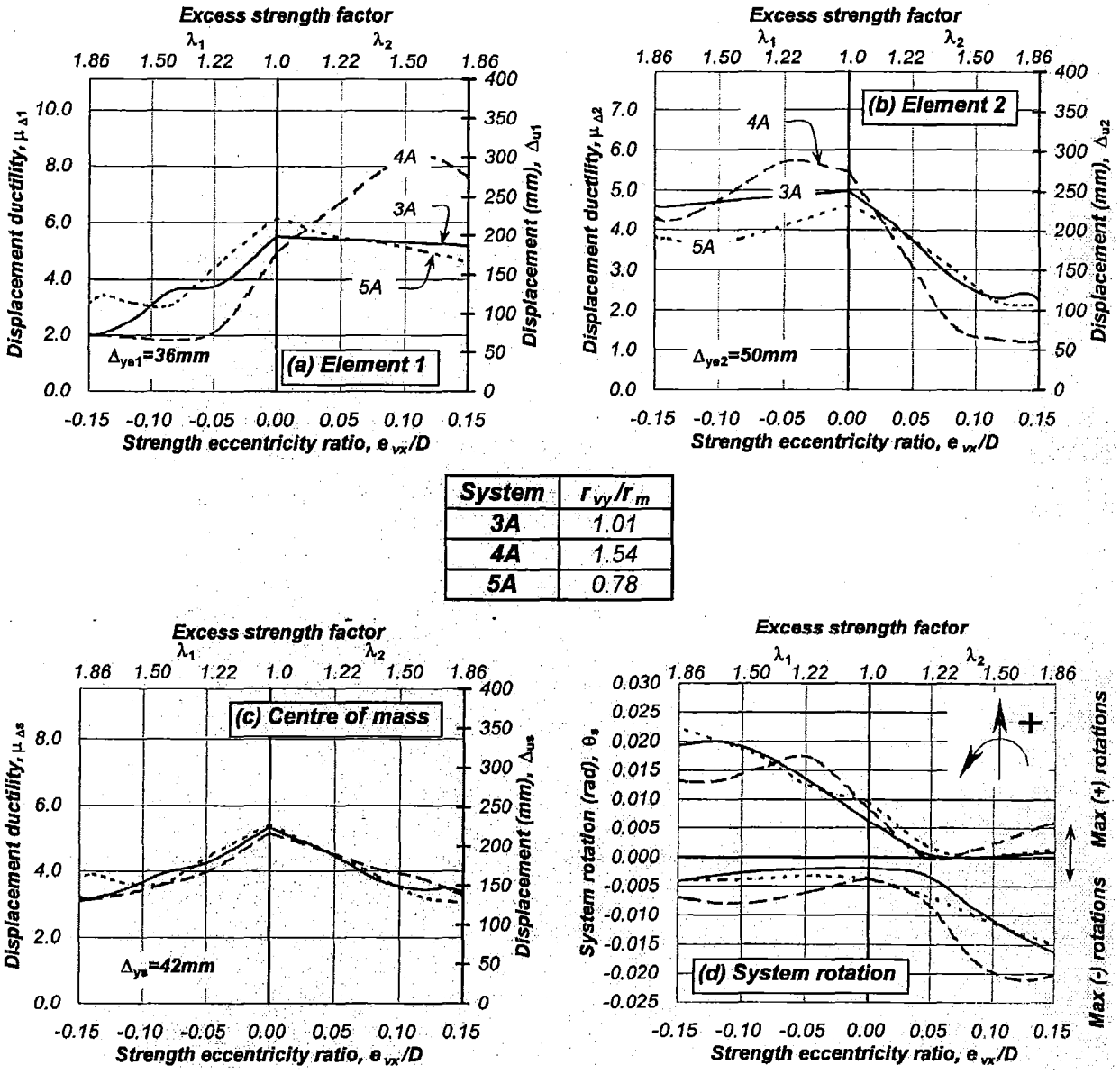

System	r_{vy}/r_m
3A	1.01
4A	1.54
5A	0.78

Figure 3-17 Response of the unrestrained *Systems 3A-1.3(α=1.4)*, *4A-1.3(α=1.4)* and *5A-1.3(α=1.4)*, T_s=1.30 sec, e_{mx}=0.0, e_{vx}≠e_{rx}=variable, $\mu_{\Delta s}$=5.35, r_m/r_o=1.0, r_{vy}/r_m=variable

Figure 3-17 also shows the response for increasing positive strength eccentricities. A strength eccentricity of $e_{vx}>+0.05D$ is, however, an unlikely scenario due to the reasons provided in Section 3.5.1, hence was just presented to clarify trends and no further comments were provided.

Figure 3-17(d) exhibits, however, the unexpected feature that system rotations slightly increased as the r_{vy}/r_m ratio was reduced. This behaviour was contrary to the findings observed before; see Section 3.5.1. This behaviour implies that the response of systems having different r_{vy}/r_m ratios due to variations in both radii of gyration of strength and mass cannot be compared. It did show, however, that the relative displacement demands of the elements and that at the centre of mass reduced as the r_{vy}/r_m ratio was reduced. This last observation agreed with those findings already

described in Section 3.5.1. Hence, the r_{vy}/r_m ratio may be used as a parameter quantifying how system rotations may influence the maximum displacement demands of elements.

It is evident from the above findings that the suggested distribution of the system strength to its elements is successful to limit the element displacement demands to less than their displacement capacity due to increasing strength eccentricities; a characteristic independent of the r_{vy}/r_m ratio. The r_{vy}/r_m ratio is then a parameter quantifying how system rotations may influence the maximum displacement demands of elements.

3.5.5 Time history response comparison of the unrestrained *Systems 3A-1.3(α=1.4), 4A-1.3(α=1.4)* and *5A-1.3(α=1.4)*

To provide a better understanding of the response previously described in Section 3.5.4, the time history response of the unrestrained *Systems 3A-1.3(α=1.4), 4A-1.3(α=1.4)* and *5A-1.3(α=1.4)* were also examined. The system strength was distributed to achieve zero strength eccentricity in the three systems. The stiffness eccentricities were e_{rx}=*0.069A, -0.118A* and *-0.059A* respectively. Elements *(1)* and *(2)* had nominal yield displacements of Δ_{ye1}=*36.0 mm* and Δ_{ye2}=*50.0 mm* in all systems.

The base shear variation of elements was essentially the same for all three systems, as Figure 3-18 shows. The displacements at the centre of mass were also similar. Figure 3-18(f) shows, as expected, differences in system rotations. The largest system rotation was experienced by unrestrained *System 5A-1.3*. This finding was, however, not expected in a system with a small r_{vy}/r_m ratio. This was because a system with a similar r_{vy}/r_m ratio, as that analysed in Section 3.3.2, showed that rotations reduced as the r_{vy}/r_m ratio reduced. This behaviour suggests that systems where the r_{vy}/r_m ratio varies due to changes on the ratio of gyration of mass only may not be comparable to systems where both the radii of gyration of strength and mass are varied. Figure 3-18(c), (d), (e) and (g) shows at *3.8* seconds that the r_{vy}/r_m ratio actually shows how well related are the maximum displacement demands of the elements and system rotations. The unrestrained *System 5A-1.3* developed the largest rotations at approximately *15.5* seconds (not shown in Figure 3-18(g)). It was found, however, that it was not associated with the maximum response of the elements.

The above findings suggest that, although changes in the r_{vy}/r_m ratio influence system rotations, the r_{vy}/r_m ratio is a parameter quantifying the effect of the system rotations on the maximum displacement demands of the elements. The effect of system rotations on the displacement demands of the elements reduces as the r_{vy}/r_m ratio also reduces even though rotations have increased.

3.5.6 Profiles of instantaneous displacements of the unrestrained *System 3A-1.3(α=1.4)*

This section examined the torsional behaviour of the unrestrained *System 3A-1.3(α=1.4)* through instantaneous displacement profiles to identify differences in behaviour, if any, with the symmetric *System 1A-1.3*, already examined in Section 3.3.3. Each profile is associated with the maximum displacement demands attained by the elements and at the centre of mass.

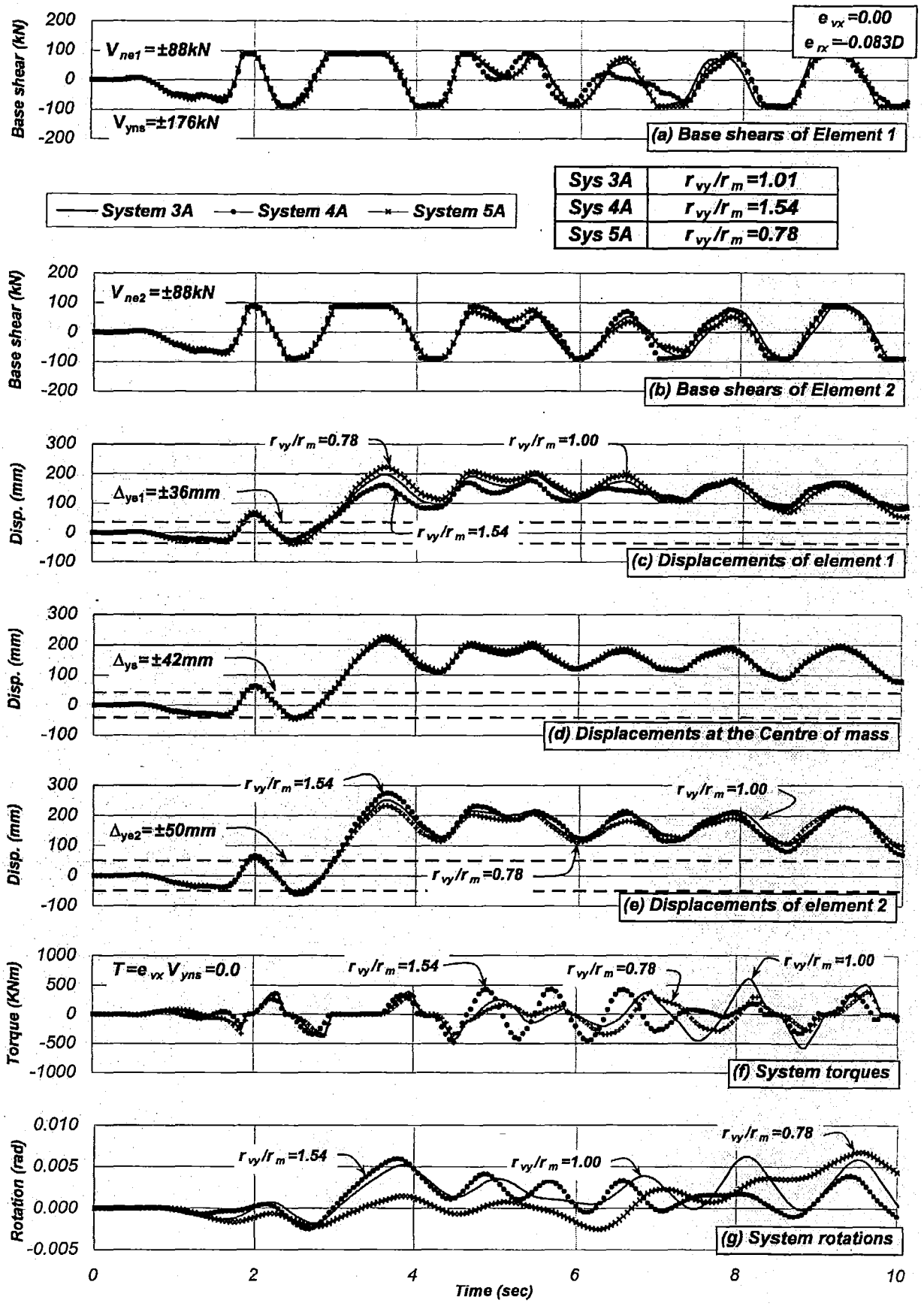

Figure 3-18. Time history response of the unrestrained *Systems 3A-1.3(α=1.4)*, *4A-1.3(α=1.4)* and *5A-1.3(α=1.4)*, T_s=1.30 sec, e_{mx}=0.0, e_{vx}=0.0, e_{rx}=-0.083D, $\mu_{\Delta s}$=5.35, r_m/r_o=1.0, r_{vy}/r_m=variable

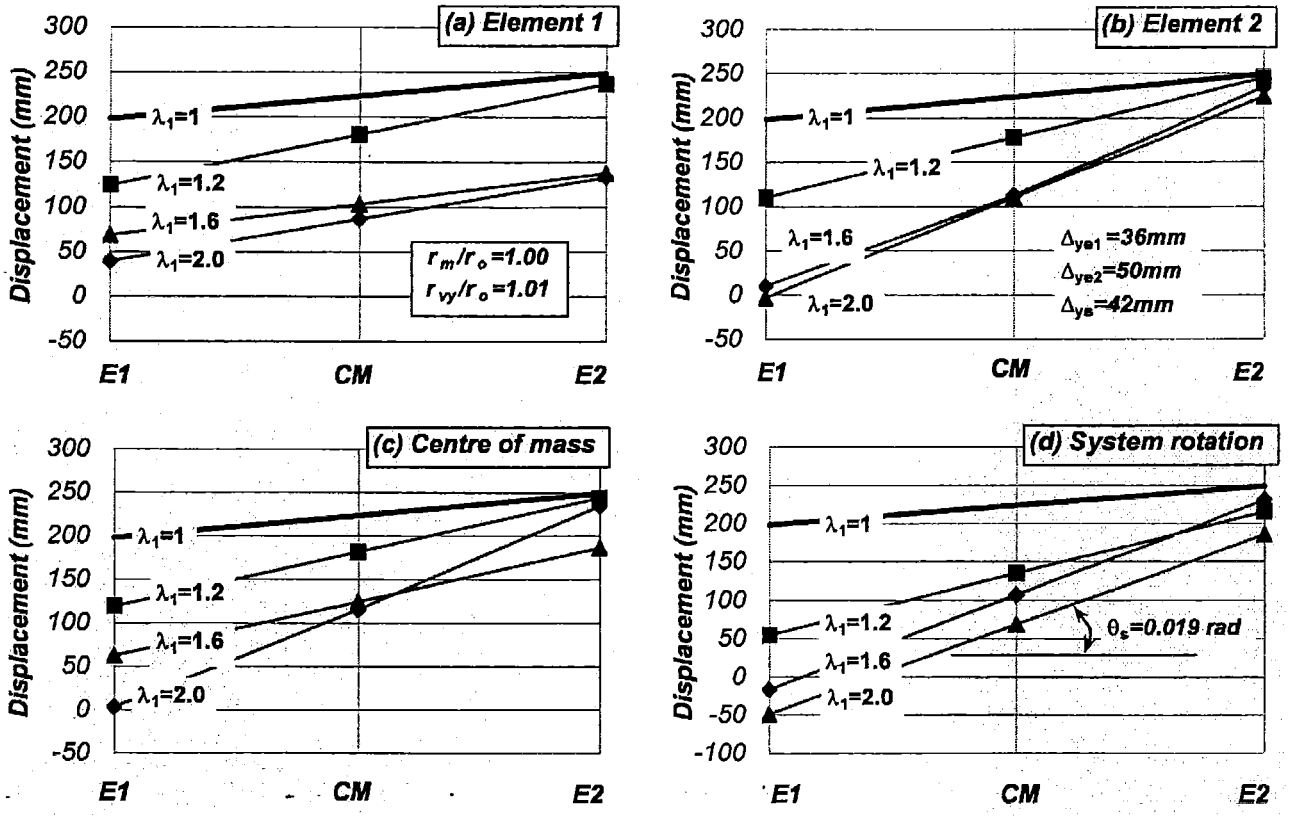

Figure 3-19 Instantaneous displacement profiles of the unrestrained *System 3A-1.3(α=1.4)*, T_s=1.30 sec, e_{mx}=0.0, λ_1=variable, $\mu_{\Delta s}$=5.35, r_m/r_o=1.0, r_{vy}/r_m=1.01

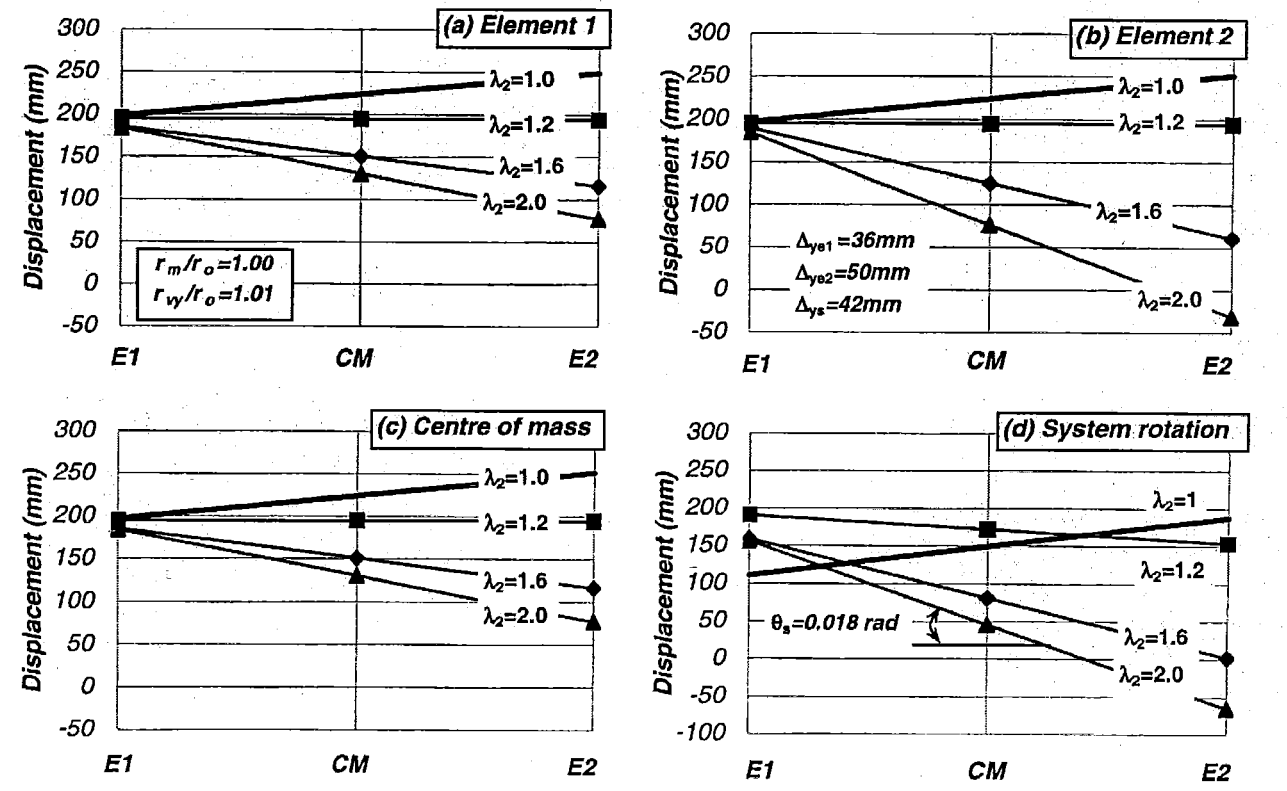

Figure 3-20 Instantaneous displacement profiles of the unrestrained *System 3A-1.3(α=1.4)*, T_s=1.30 sec, e_{mx}=0.0, λ_2=variable, $\mu_{\Delta s}$=5.35, r_m/r_o=1.0, r_{vy}/r_m=1.01

The unrestrained *System 3A-1.3(α=1.4)* having r_{vy}/r_o=*1.0* was considered again. The system strength was initially distributed to the elements to achieve zero strength eccentricity. Thereafter, excess strength was assigned to either element *(1)* or *(2)*. The displacement ductility capacity of the system was assumed equal to $\mu_{\Delta s}$=*5.35*, as in previous examples. It was subjected to the Artificial earthquake along the *Y*-direction.

Figure 3-19 shows the instantaneous displacement profiles of the system when element *(1)* had excess strength (λ_1>*1.0*). As expected, the excess strength of element *(1)* reduced its displacement demands as well as at the centre of mass and increased the system rotations. These combined effects did not lead to an increase of the displacements of the critical element *(2)* when r_{vy}/r_o=*1.0*. Figure 3-19(d) confirms that the maximum system rotation was not associated with the maximum displacement demands on the elements and at the centre of mass. Moreover, the maximum displacement demands on elements and at the centre of mass did not occur at the same instant.

Figure 3-20 shows the instantaneous displacement profiles when element *(2)* had excess strength (λ_2>*1.0*). This is, however, an unrealistic scenario only presented to clarify trends in behaviour. As in the previous case, with increasing values of excess strength factor, λ_2, i.e. increasing positive strength eccentricities, the displacement of element *(2)* reduced. For an excess strength factor of λ_2=*1.2* the elements and centre of mass exhibited similar displacement demands. They occurred at a similar instant and hence the system rotation was largely reduced. This scenario was related to a strength distribution where the centre of mass was halfway between the centre of strength and stiffness, as already described in Section 3.5.2(c). With further increase of λ_2, as expected, the system rotations reversed and increased in the opposite direction. The displacement demands of element *(2)* and centre of mass also reduced. These combined effects did not increase the displacement demands of critical element *(1)* above that attained for zero strength eccentricity (λ_2=*1.0*).

These findings show that the maximum displacement of the elements is not associated with maximum system rotations. Another feature observed and relevant to structural design is that the sense of system rotation could be controlled by changing the distribution of systems strength, i.e., modifying the strength eccentricity. This, however, may be achieved for a limited range of strength eccentricities due to physical limitations of the elements and/or codified requirements of minimum reinforcement.

3.5.7 Response of the unrestrained *System 3A-1.3(α=1.4)* having different displacement ductility capacities

It is likely that during the design process, the displacement capacity of elements of asymmetric systems needs to be drastically restricted. This is required when the element's displacement capacity is associated with a limit state requiring a rigorous displacement control. Therefore, the displacement ductility capacity of such systems will need to be substantially reduced to prevent the elements from exceeding their capacity. How a reduction on the system displacement capacity might influence torsional behaviour is subsequently examined.

Three unrestrained *Systems 3A-13(α=1.4)* with r_{vy}/r_m=*1.01* and having each a different system displacement ductility capacity were examined. For each system, the displacement capacity of the *Y*-direction elements was the same and equal to $\mu_{\Delta 1}=\mu_{\Delta 2}$=*5.35, 3.44* and *1.80*, respectively. The displacement ductility capacity of the system was assumed the same as that of the elements,

i.e., $\mu_{\Delta s}=\mu_{\Delta 1}=\mu_{\Delta 2}$. Hence, three systems having displacement ductility capacity of $\mu_{\Delta s}$ =*5.35, 3.44* and *1.80* were examined. They were analysed assuming the general considerations described in Section 3.2.

Table 3-3 summarizes the response for zero strength eccentricity. It is evident that the ratio of maximum displacement demands of the elements and that at centre of mass remains the same as the displacement ductility capacity of the system was reduced. It is observed, once again, that the displacement ductility capacity of the system could have been limited to that of the element with the smallest displacement capacity. This is, as explained before, because the maximum response of the system is attained for zero strength eccentricity and is assumed that the maximum displacement demand of the elements and at the centre of mass will be essentially the same.

Table 3-3. Response of the unrestrained *Systems 3A-1.3(α=1.4)*, T_s=1.30 sec, e_{mx}=0.0, e_{vx}=0.0, e_{rx}=-0.083D, μ_s=variable, r_m/r_o=1.0, r_{vy}/r_m=1.01

	Displacements, mm, and displacement ductility demands (μ_s)			***Displacement demand ratios***	
$\mu_{\Delta s}$	*E1*	*CM*	*E2*	$(\Delta_{ue1}/\Delta_{us})_d$	$(\Delta_{ue2}/\Delta_{us})_d$
5.35	*198(5.50)*	*224(5.34)*	*251(4.98)*	*0.88*	*1.12*
3.44	*128(3.56)*	*144(3.44)*	*164(3.26)*	*0.89*	*1.14*
1.80	*80(2.22)*	*75(1.78)*	*88(1.74)*	*1.06*	*1.17*

Figure 3-21 shows the response of the systems for increasing strength eccentricities. It is evident that irrespective of the system displacement ductility capacity, the maximum displacement demand of the elements occurred always for zero strength eccentricity ($\lambda_1=\lambda_2=1.0$) and these displacement demands were not exceeded with increasing strength eccentricities. It is also seen, as expected, that maximum rotations experienced by the systems reduced as the displacement ductility capacity of the system was reduced; see Figure 3-21(d).

The above findings confirm that the suggested distribution of strength among elements also ensures a satisfactory torsional performance on systems with reduced displacement ductility capacity. The torsional response of the system is less critical as its displacement capacity is reduced. It also demonstrates that the estimate of the displacement ductility capacity of the system should be associated with zero strength eccentricity when the system attains its maximum response.

3.5.8 Response of the unrestrained *System 3A-1.3(α=1.4)* under different earthquake records

This section provides an insight into the seismic response of asymmetric systems when subjected to different earthquake records. It aims to examine effects on system torsional behaviour due to the frequency contents characteristics of different earthquake records. It is stressed that this study concentrates on torsional behaviour rather than on the question why different ground motions with similar response accelerations may generate different displacement ductility demands at the centre of mass. Hence, to avoid this issue, the records were scaled to impose the same displacement ductility demand at the centre of mass.

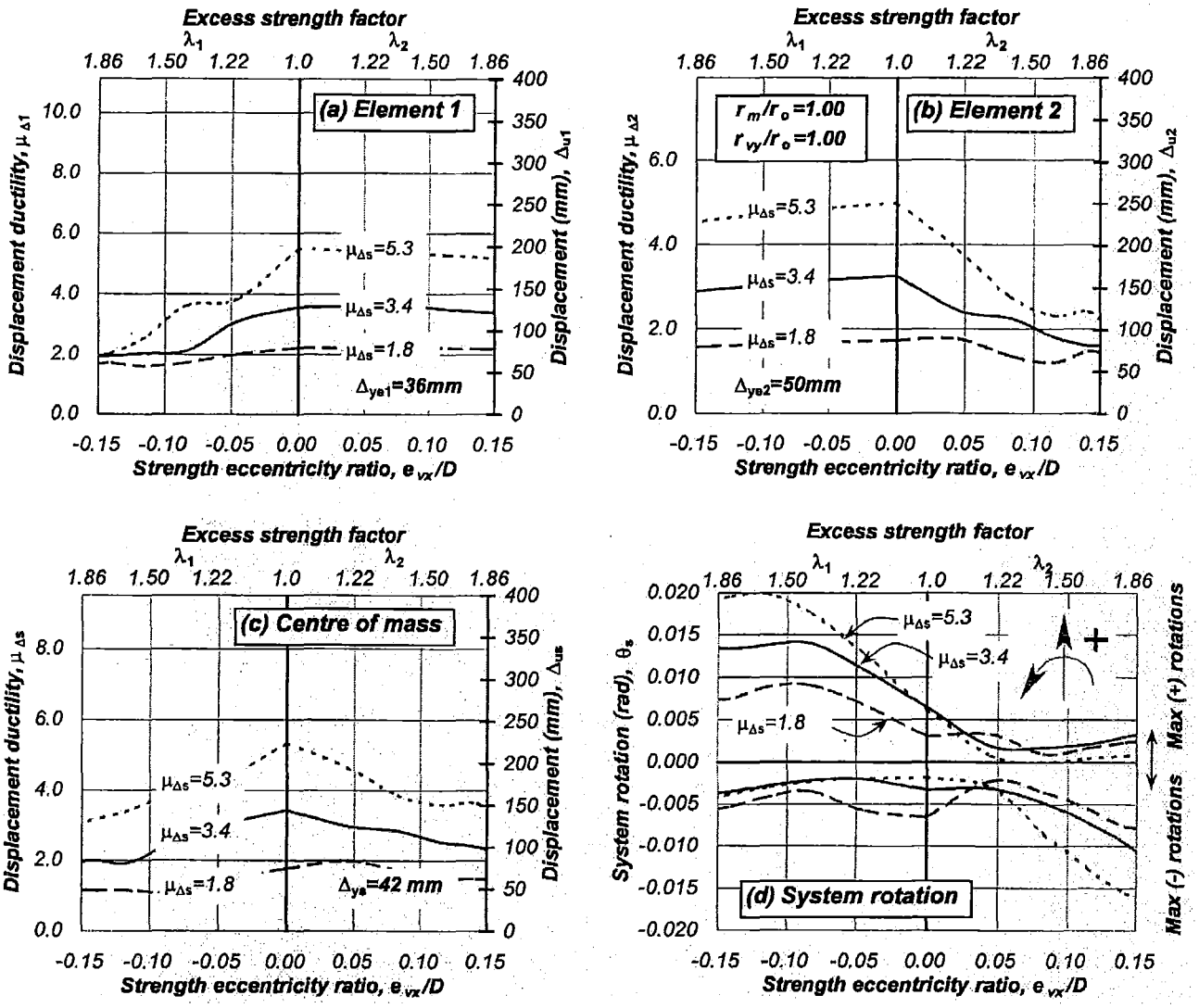

Figure 3-21. Response of the unrestrained *Systems 3A-1.3(α=1.4)* having different displacement ductility capacities, T_s=1.30 sec, e_{mx}=0.0, $e_{vx} \neq e_{rx}$=variable, μ_s=variable, r_m/r_o=1.0, r_{vy}/r_m=1.01

The unrestrained *System 3A-1.3(α=1.4)* having $r_{vy}/r_m=1.01$ was considered again. It was assumed to have a system displacement ductility capacity of $\mu_{\Delta s}=5.35$ to be consistent with those systems previously analysed. It was subjected to the Bucharest and Kobe earthquake records along the *Y*-direction. The records were scaled to impose a maximum system displacement ductility demand equal to the system capacity as already done for the Artificial earthquake record.

Figure 3-22 shows the response for zero strength eccentricity. It is evident from Figure 3-22(a) and (b) that the displacement ductility demands of elements *(1)* and *(2)* were quite similar. It shows, as expected, the same ductility demand at the centre of mass with the different earthquake records; see Figure 3-22(c). The system also exhibited similar negative and positive rotations, as shown in Figure 3-22(d). The torsional behaviour of systems subjected to different earthquake records and exhibiting the same displacement ductility demand at the centre of mass, appeared, at this stage, independent of the earthquake record frequency content.

Figure 3-22 also shows the response for increasing strength eccentricities. It is evident that increasing negative and positive strength eccentricities generated a similar response with all three

earthquakes. However, some differences in response were observed with the Kobe earthquake. For instance, element *(1)* exhibited a sudden increase in displacement ductility demand with increasing negative eccentricities above that attained for zero strength eccentricity. This was expected due to the particular frequency characteristics of the record. This is an indication that the torsional response is, in fact, sensitive to the characteristics of the earthquake record.

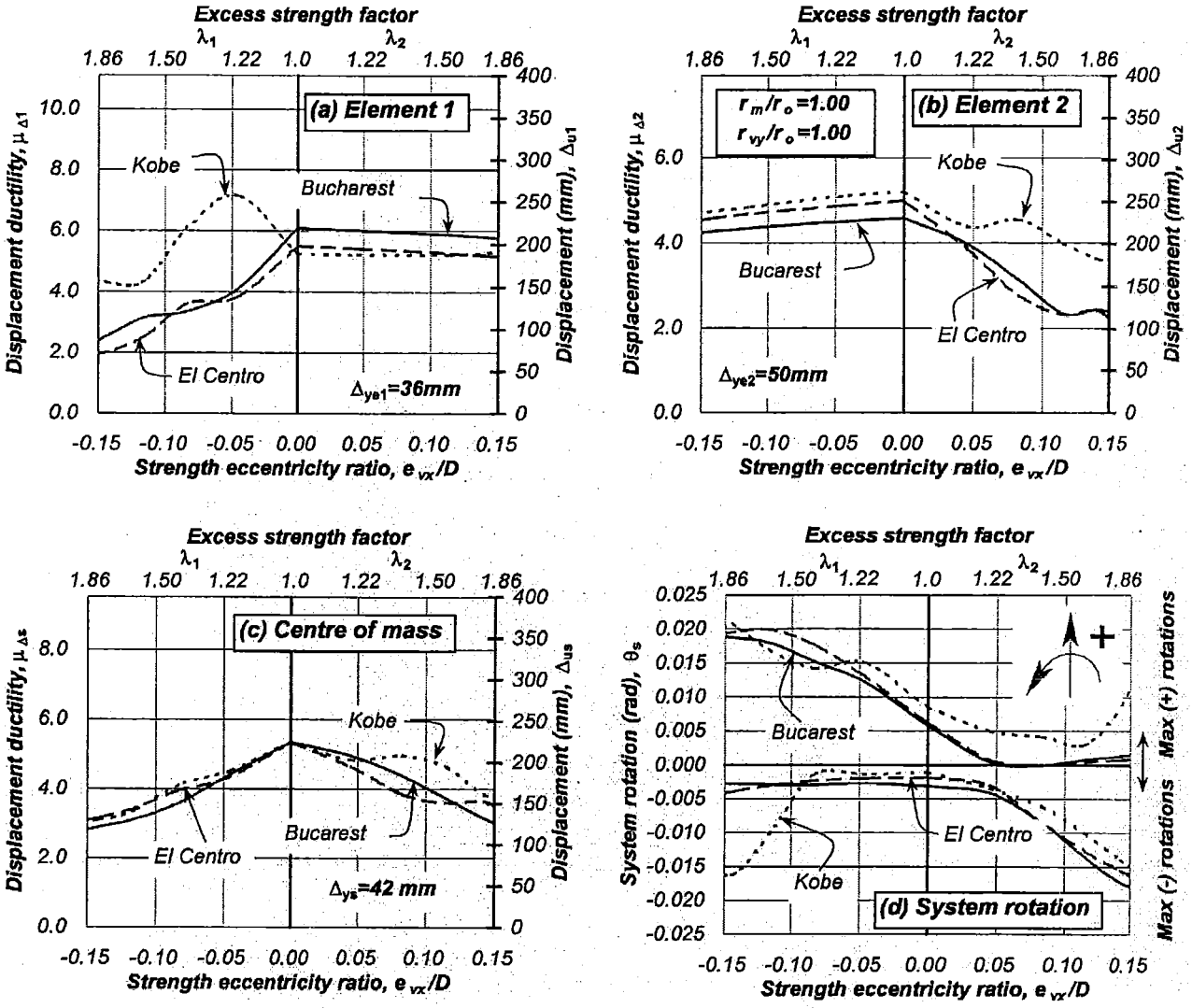

Figure 3-22. Response of the unrestrained *System 3A-1.3(α=1.4)* under different earthquake records, T_s=1.30 sec, e_{mx}=0.0, $e_{vx} \neq e_{rx}$=variable, $\mu_{\Delta s}$=5.35, r_m/r_o=1.0, r_{vy}/r_m=1.01

3.5.9 Response of the unrestrained *Systems 3A-1.3(α=variable)*

The role of the $\alpha=\Delta_{ye2}/\Delta_{ye1}$ ratio and its associated stiffness eccentricity on the torsional response of ductile systems is examined. This parameter is not expected to have a significant effect on the response of ductile systems. This, however, may be a point of discussion because it is certain that elements may remain elastic for short instants and, hence, it is during those instants that stiffness eccentricity might have a major effect on the system rotations and the maximum response of the elements. The aim of this section is, therefore, to find out to what extent the stiffness eccentricity may influence torsional response of ductile systems.

The torsionally unrestrained *System 3A*, as shown in Figure 2-25(a), was considered. In the case of a two-element system such as this one, the ratio of nominal yield displacement of the elements is a relevant parameter leading to different stiffness eccentricities. They are also influenced by the distribution of strength on the elements. To study this issue, several systems, having different ratios of element nominal yield displacement of $\alpha=\Delta_{ye2}/\Delta_{ye1}=1.2, 1.4, 1.6, 2.0$ and 2.5, were examined. Systems with such ratios and zero strength eccentricity are associated with stiffness eccentricities of $e_{rx}=-0.045D, -0.083D, -0.115D, -0.167D$ and $-0.214D$. In spite of differences in the $\alpha=\Delta_{ye2}/\Delta_{ye1}$ ratios(or stiffness eccentricities associated with zero strength eccentricity) their response could be compared because the nominal yield displacement of the systems was fixed. To be consistent with the systems previously examined, this was set in every system to $\Delta_{ys}=42mm$. This was achieved by appropriate changes of the relative nominal yield displacement of the elements, i.e., variations on the relative length of the substitute wall-elements, as explained in Section 2.18.2. A summary of these properties are presented in Appendix B. The nominal strength assigned to the systems was the same. This was adjusted to achieve an uncoupled translational period of free vibration of $T_s=1.30$ seconds. These systems were denoted unrestrained Systems *3A-1.3*($\alpha=1.2$), *3A-1.3*($\alpha=1.4$), *3A-1.3*($\alpha=1.6$), *3A-1.3*($\alpha=2.0$) and *3A-1.3*($\alpha=2.5$). They had the same ratios of $r_{vy}/r_m=1.01$ and $r_m/r_o=1.0$.

The displacement ductility capacity of the unrestrained *Systems 3A-1.3(α=variable)* was assumed as in previous examples equal to the displacement ductility capacity of the elements, i.e., $\mu_{\Delta s}=\mu_{\Delta 1}=\mu_{\Delta 2}=5.35$, even though the nominal yield displacement of the elements was different. At this stage, it was uncertain if the displacement ductility capacities of the elements were going to be or not to be exceeded.

The Artificial earthquake record was the benchmark record for the analyses and acted in the *Y*-direction. It was scaled to induce a displacement ductility demand of $\mu_{\Delta s}=5.35$ on the reference unrestrained *System 3A-1.3*($\alpha=1.4$). This scaled record was then applied, without further modifications, to systems having other $\alpha=\Delta_{ye2}/\Delta_{ye1}$ ratios. The use of such a record plus the fact that the uncoupled translational period of free vibration of all the systems was the same enabled a direct comparison to be made of their responses.

Based on Eq. 3-2, which assumes, for zero strength eccentricity, the same maximum displacement demands on elements and at the centre of mass, the displacement capacity of the system should be limited to that of element *(1)* because it has the smallest displacement capacity. The corresponding system displacement ductility capacities are summarized in Table 3-4 as a function of the $\alpha=\Delta_{ye2}/\Delta_{ye1}$ ratio for a fixed system nominal yield displacement. It is evident that the displacement ductility capacity of the system reduces as the $\alpha=\Delta_{ye2}/\Delta_{ye1}$ ratio was increased.

Table 3-4. Displacement ductility capacity of the unrestrained *Systems 3A-1.3 (α=variable)*, T_s=1.30 sec, e_{mx}=0.0, e_{vx}=0.0, e_{rx}=variable, $\mu_{\Delta s}=5.35$, r_m/r_o=1.0, r_{vy}/r_m=1.01

α	$e_{vx}=0.0$	Δ_{ye1}	Δ_{ye2}	Δ_{ys}	$\mu_{\Delta 1}=\mu_{\Delta 2}$	$\mu_{\Delta s}$
$=\Delta_{ye2}/\Delta_{ye1}$	e_{rx}	*(mm)*			$=\Delta_{ul}/\Delta_{ye1}$	$=(\Delta_{ye1}/\Delta_{ys})\mu_{\Delta 1}$
$\alpha=1.0$	0.00	42.0	42.0	42.0	5.35	5.35
$\alpha=1.2$	-0.045D	38.5	46.2	42.0	"	4.90
$\alpha=1.4$	-0.083D	36.0	50.4	42.0	"	4.59
$\alpha=1.6$	-0.115D	34.1	54.6	42.0	"	4.34
$\alpha=2.0$	-0.167D	31.5	63.0	42.0	"	4.01
$\alpha=2.5$	-0.214D	29.4	73.5	42.0	"	3.75

Table 3-5 illustrates, for zero strength eccentricity, the response of the systems having different $\alpha=\Delta_{ye2}/\Delta_{ye1}$ ratios and hence stiffness eccentricities associated with zero strength eccentricity. Relative displacement demands between the elements and the centre of mass were observed. This was reflected in the variation of the displacement ratios associated with each element. These variations were roughly the same for the different $\alpha=\Delta_{ye2}/\Delta_{ye1}$ ratios suggesting that this parameter does not have a significant effect on the displacement demands of the elements. This is, however not a applicable to all systems as will be shown in Section 3.10.

Table 3-5 shows, in terms of displacement ductility capacity associated with the strain limit of the materials, that displacement ductility demand of element *(1)* increased as the $\alpha=\Delta_{ye2}/\Delta_{ye1}$ ratio was increased. Element *(2)*, on the other hand, exhibits displacements larger than that attained at the centre of mass even though the displacement ductility demand reduced. Element *(2)* may have been the critical element of the system if its displacement capacity had been substantially reduced to comply with allowable drift limits associated with specific performance criteria.

The variation of the r_{vy}/r_m ratio is expected to have an effect on the torsional response of systems with different $\alpha=\Delta_{ye2}/\Delta_{ye1}$ ratios. Although, in these particular systems, this was fixed to $r_{vy}/r_m=1.01$, there is not doubt that its variation will change the relative displacement demand of the elements and that at the centre of mass for this particular earthquake record.

It is evident from Figure 3-24 and Table 3-5 that, for zero strength eccentricity, the displacement ductility capacity of critical element *(1)* increased as the $\alpha=\Delta_{ye2}/\Delta_{ye1}$ ratio was increased due to differences in the nominal yield displacement of the elements. Element *(2)*, on the other hand, displayed a reduction in displacement ductility demand. This behaviour indicates that the displacement ductility capacity of the system must be reduced, as the $\alpha=\Delta_{ye2}/\Delta_{ye1}$ ratio is increased, to prevent critical element *(1)* from exceeding its displacement ductility capacity whereas the displacement ductility capacity of element *(2)* was not fully used.

Table 3-5. Response of the unrestrained *Systems 3A-1.3(α=variable)*, T_s=1.30 sec, e_{mx}=0.0, e_{vx}=0.0, e_{rx}=variable, $\mu_{\Delta s}$=5.35, r_m/r_o=1.0, r_{vy}/r_m=1.01

α	e_{vx}=0.0	Displacements, mm, and displacement ductility demands, (μ)				Displacement demand ratios	
$=\Delta_{ye2}/\Delta_{ye1}$	e_{rx}	E1	CM	E2	ESDOF	$(\Delta_{ue1}/\Delta_{us})_d$	$(\Delta_{ue2}/\Delta_{us})_d$
1.0	0.00	225(5.35)	225(5.35)	225(5.35)	225(5.35)	1.00	1.00
1.2	-0.045D	210(5.45)	225(5.35)	239(5.17)	"	0.93	1.06
1.4	-0.083D	198(5.50)	224(5.33)	251(4.98)	"	0.88	1.12
1.6	-0.115D	193(6.21)	223(5.31)	259(4.74)	"	0.86	1.16
2.0	-0.167D	208(6.60)	217(5.17)	249(3.95)	"	0.96	1.15
2.5	-0.214D	220(7.48)	212(5.05)	235(3.19)	"	1.03	1.11

The response at the centre of mass, for zero strength eccentricity, was insensitive to the stiffness eccentricity as Table 3-5 shows. It shows that an equivalent single degree of freedom system predicted well the displacement demands at the centre of mass of systems having, for the same uncoupled translational period, different stiffness eccentricities. It is also evident from Figure 3-23(d) that, for zero strength eccentricity, system rotations increased with increasing $\alpha=\Delta_{ye2}/\Delta_{ye1}$ ratios and hence increasing stiffness eccentricities. System rotations were, however, not an issue because they did not significantly influence the maximum displacement demands of elements *(1)* and *(2)*.

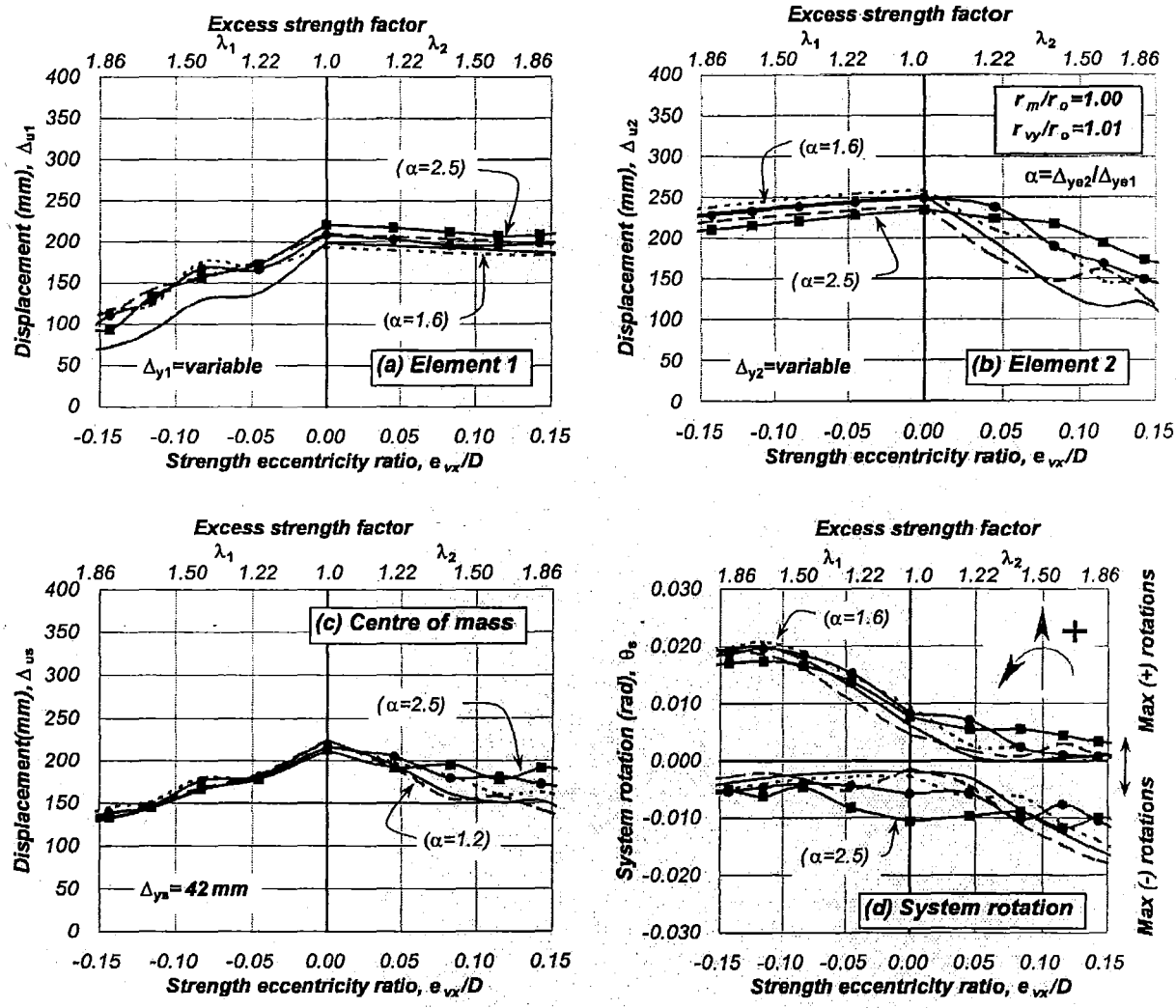

α	Δ_{ye1}	Δ_{ye2}	e_{vx}=0.0
$\Delta_{ye2}/\Delta_{ye1}$	(mm)		e_{rx}
1.2	38.5	46.2	-0.045D
1.4	36.0	50.4	-0.083D
1.6	34.1	54.6	-0.115D
2.0	31.5	63.0	-0.167D
2.5	29.4	73.5	-0.210D

Figure 3-23. Displacements of the unrestrained *System 3A-1.3(α=variable)*, T_s=1.30 sec, e_{mx}=0.0, $e_{vx} \neq e_{rx}$=variable, $\mu_{\Delta s}$=5.35, r_m/r_o=1.0, r_{vy}/r_m=1.01

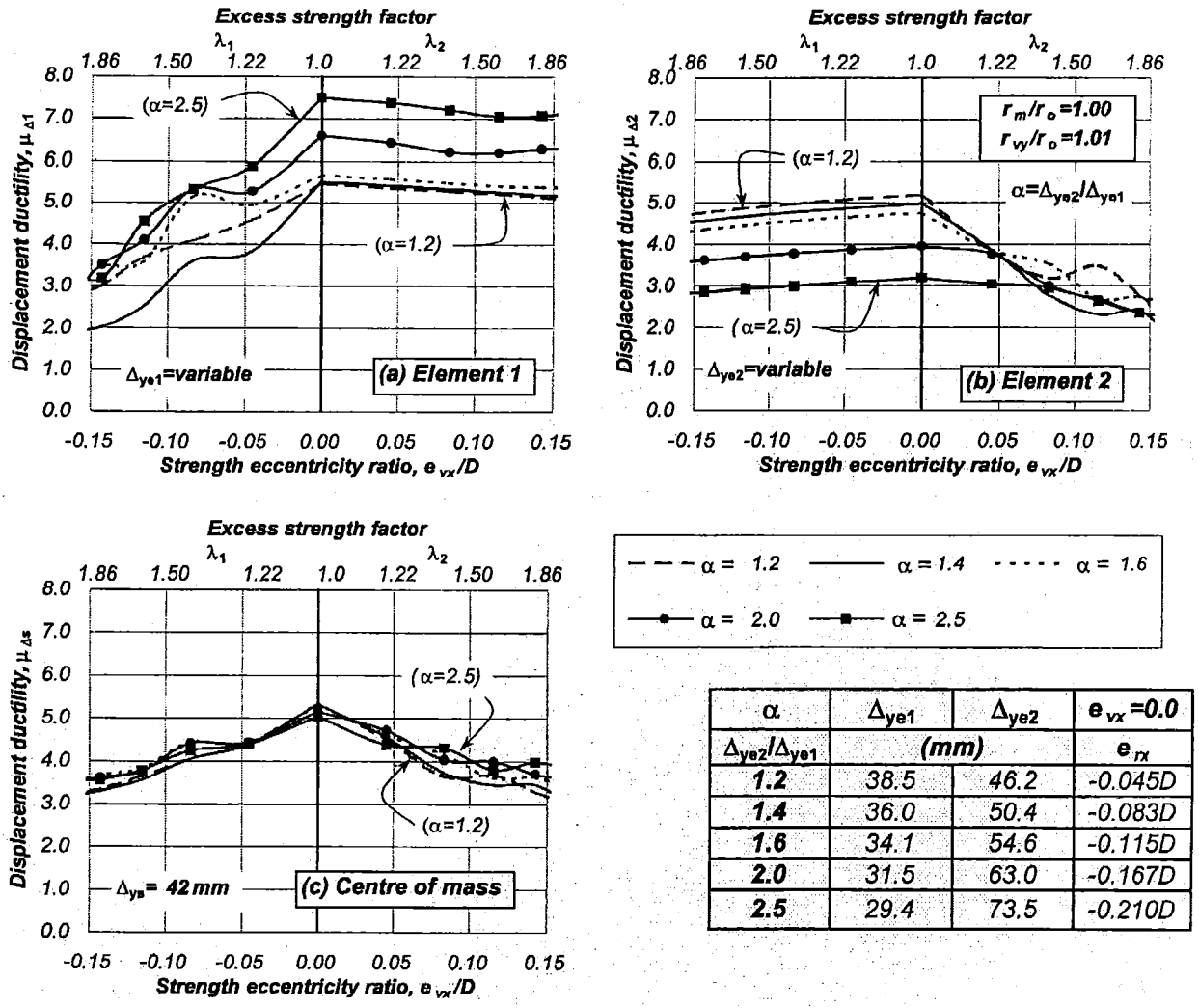

α	Δ_{ye1}	Δ_{ye2}	e_{vx}=0.0
$\Delta_{ye2}/\Delta_{ye1}$	(mm)		e_{rx}
1.2	38.5	46.2	-0.045D
1.4	36.0	50.4	-0.083D
1.6	34.1	54.6	-0.115D
2.0	31.5	63.0	-0.167D
2.5	29.4	73.5	-0.210D

Figure 3-24. Ductility demands of the unrestrained *System 3A-1.3(α=variable)*, T_s=1.30 sec, e_{mx}=0.0, $e_{vx} \neq e_{rx}$=variable, $\mu_{\Delta s}$=5.35, r_m/r_o=1.0, r_{vy}/r_m=1.01

Figure 3-23 and Figure 3-24 show the system response for increasing strength eccentricities. It was evident that the maximum response was attained for zero strength eccentricity. Thereafter, increasing negative strength eccentricities reduced the displacement demands on element *(1)* whereas those on element *(2)* remained equal or smaller. This response was essentially the same for all systems having different $\alpha=\Delta_{ye2}/\Delta_{ye1}$ ratios, a behaviour compatible with that observed in previous systems. It is seen that the torsional response of systems due to increasing strength eccentricities was not affected by variations of the $\alpha=\Delta_{ye2}/\Delta_{ye1}$ ratio up to $\alpha=2.5$ and hence an associated stiffness eccentricity of e_{rx}=-0.21D. Section 3.10 will examine if these findings are also valid for systems with other uncoupled translational periods and $\alpha=\Delta_{ye2}/\Delta_{ye1}$ ratios (or stiffness eccentricities associated with zero strength eccentricity).

A similar behaviour occurs in case of increasing positive strength eccentricities. This is, however, an unlikely scenario due to the reasons provided in Section 3.5.1 and was just presented to clarify trends and no further comments were given.

The time history response of the unrestrained *Systems 3A-1.3*(α=1.4) and *3A-1.3*(α=2.5) were also analysed to provide further understanding of the effects of the $\alpha=\Delta_{ye2}/\Delta_{ye1}$ ratios and its associated stiffness eccentricities on the torsional response. The figures, although not presented

here, showed that increasing the $\alpha=\Delta_{ye2}/\Delta_{ye1}$ ratio, for a given distribution of strength, increased system rotations. In spite of this behaviour, system rotations did not influence the maximum displacement demands of the translatory elements.

The suggested design strategy provides a satisfactory seismic performance of systems having different stiffness eccentricities. The $\alpha=\Delta_{ye2}/\Delta_{ye1}$ ratio, and associated stiffness eccentricities, did not have a significant effect on the torsional response of ductile systems. The displacement capacity of the system should be limited to that of the element with the smallest displacement capacity. Hence, the displacement capacity needs to be reduced as the $\alpha=\Delta_{ye2}/\Delta_{ye1}$ ratio is increased.

3.5.10 Response of the unrestrained *System 3A-0.5(α=1.4)*

In order to identify the likely effects of the uncoupled translational periods of free vibration on the response of torsionally unrestrained systems, a system with a short period of free vibration was also examined.

The unrestrained *System 3A-0.5* having an uncoupled translational period of free vibration of *0.50* seconds was considered. The ratio of element nominal yield displacement was $\alpha=\Delta_{ye2}/\Delta_{ye1}=1.4$. It was denoted *System 3A-0.5(α=1.4)*. The nominal yield displacement of the elements and that of the system was equal to $\Delta_{ye1}=36mm$, $\Delta_{ye2}=50mm$ and $\Delta_{ys}=42mm$. The system strength was then adjusted to achieve the desired uncoupled period. The system was also analysed considering the approach explained in Section 3.2.

Table 3-6 summarises the seismic response for zero strength eccentricity. It is evident that, for most r_{vy}/r_m ratios, the displacement demands of element *(1)* were slightly larger than those developed at the centre of mass. It also exceeded its displacement ductility capacity of $\mu_{\Delta 1}=5.35$. The maximum displacement demand ratios associated with elements *(1)* and *(2)* were, therefore, opposite to those previously obtained with *System 3A-1.3(α=1.4)*. This confirms earlier findings that systems with short translational periods have a sensitive response. It also exhibits some differences in the displacement demands at the centre of mass for the different r_{vy}/r_m ratios. The maximum response predicted by the equivalent single degree of freedom system was *87%* of that attained at the centre of mass. In spite of this result, the equivalent single degree of freedom system is still considered, for practical purposes, an appropriate model to predict the maximum displacement demand at the centre of mass. The centre of mass is assumed, for convenience, the location where translations and rotations of the ductile system may be decoupled but its accuracy reduces as the translational period is also reduced. This is because the actions of the mass rotational inertia influence the displacement demands at the centre of mass. The response of short period systems is quite sensitive but without showing any particular trend.

Table 3-6. Response of the unrestrained *System 3A-0.5(α=1.4)*, T_s=0.50 sec, e_{mx}=0.0, e_{vx}=0.0, e_{rx}=-0.083D, $\mu_{\Delta s}=5.35$, r_m/r_o=1.0, r_{vy}/r_m=variable

	Displacements, mm, and displacement ductility demands (μ_s)				*Displacement demand ratios*	
r_{vy}/r_m	*E1*	*CM*	*E2*	*ESDOF*	$(\Delta_{ue1}/\Delta_{us})_d$	$(\Delta_{ue2}/\Delta_{us})_d$
$r_{vy}/0.85r_o$	*183(5.07)*	*189(4.27)*	*191(3.78)*	*184 (4.38)*	*0.97*	*1.01*
$r_{vy}/r_o=1.00$	*251(6.98)*	*212(5.04)*	*210(4.16)*	"	*1.18*	*0.99*
$r_{vy}/1.20r_o$	*233(6.50)*	*213(5.08)*	*199(3.96)*	"	*1.09*	*0.93*

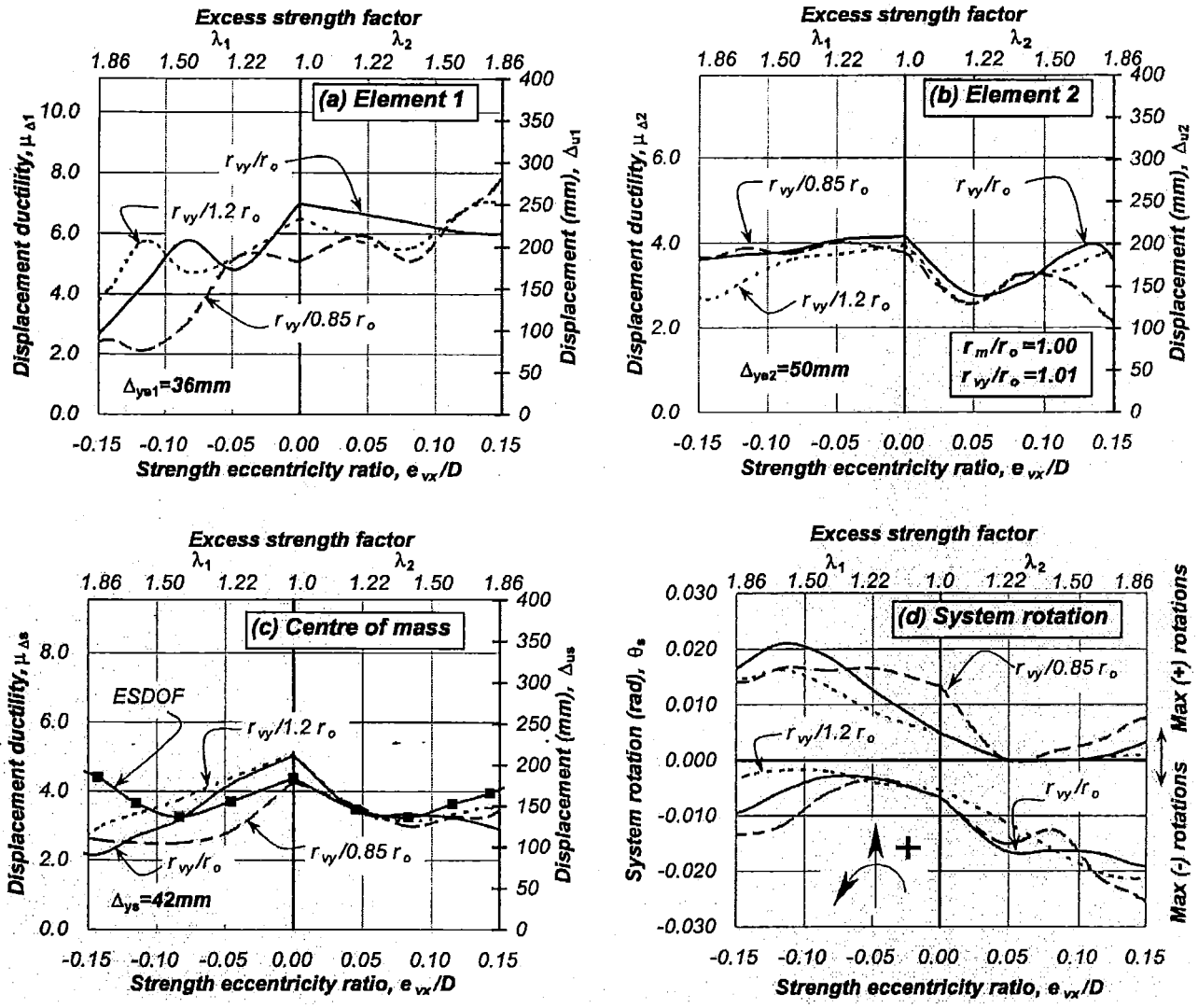

Figure 3-25. Response of the unrestrained *System 3A-0.5(α=1.4)*, T_s=0.50 sec, e_{mx}=0.0, $e_{vx} \neq e_{rx}$=variable, $\mu_{\Delta s}$=5.35, r_m/r_o=1.0, r_{vy}/r_m=variable

Figure 3-25 exhibits the effects of the excess strength of either element *(1)* or *(2)* on the response. Increasing negative and positive strength eccentricities reduced the displacement ductility demand of the elements to less than that demanded for zero strength eccentricity. The response of element *(1)* was, on the other hand, quite sensitive to the r_{vy}/r_m ratio. The response at the centre of mass varied slightly with the r_{vy}/r_m ratio. The corresponding equivalent single degree of freedom system predicted well the response at the centre of mass although some variations were observed. The system rotation did not show the evident reduction of system rotations for a strength eccentricity of e_{vx}=+*0.04D* as happened with its unrestrained counterpart *System 3A-1.3*. It did show, however, increasing positive rotations with increasing negative strength eccentricities and negative rotations with increasing positive strength eccentricities. In general, the overall torsional behaviour for zero and increasing strength eccentricities was similar to that of the unrestrained *System 3A-1.3*; see Figure 3-19.

The findings above shows that short period systems have a sensitive torsional response. It also confirms that the proposed distribution of system strength is successful in limiting, for zero and increasing strength eccentricities, the displacement demands of the elements to less than the maximum displacement demand attained for zero strength eccentricity. The displacement

capacity of the system should, therefore, be associated with the maximum response expected for zero strength eccentricity. In spite of differences in response between the asymmetric systems and their equivalent single degree of freedom system, the latter is still considered a valid model in predicting the maximum response at the centre of mass of systems having different uncoupled translational periods.

3.6 Two-element structurally asymmetric and mass-eccentric *System 6A(CV≠CR; CM≠GC)*

3.6.1 Response of the unrestrained *System 6A-1.3(α=1.4)*

This section considers the response of an asymmetric system having mass eccentricity. It aims to show if there is a need to differentiate between asymmetric systems with or without mass eccentricity.

The unrestrained *System 6A* having a mass eccentricity of e_{mx}=*-0.10A*; see Figure 2-30(a), was considered. The ratio of the element nominal yield displacement is also $\alpha=\Delta_{ye2}/\Delta_{ye1}=1.40$. The nominal yield displacement of the system was set equal to $\Delta_{ys}=42mm$, as in the previous examples. The system strength was then adjusted to achieve an uncoupled translational period of *1.30* seconds. It was denoted as *Systems 6A-1.3(α=1.4)*. For zero strength eccentricity, it had a stiffness eccentricity of e_{rx}=*-0.066D*. Section 2.19.1 provided detailed information of its characteristics and Appendix *B* summarizes its properties. The system was analyzed using the general considerations described in Section 3.2.

Table 3-7 summarizes the torsional response for zero strength eccentricity. Displacement demands of elements relative to that attained at the centre of mass reduced as the r_{vy}/r_m ratio was reduced. This behaviour is reflected in the variation of the ratio of displacement demands associated with the elements. Its corresponding equivalent single degree of freedom system still predicted, with adequate accuracy, the response at the centre of mass. This response is similar to that of the unrestrained *System 3A-1.3(α=1.4);* see Table 3-1.

Table 3-7. Response of the unrestrained *System 6A-1.3(α=1.4)*, T_s=1.30 sec, e_{mx}=-0.10, e_{vx}=0.0, e_{rx}=-0.066D, $\mu_{\Delta s}$=5.35, r_m/r_o=1.10, r_{vy}/r_m=variable

	Displacements, mm, and displacement ductility demands (μ_s)				Displacement demand ratios	
r_{vy}/r_m	E1	CM	E2	ESDOF	$(\Delta_{ue1}/\Delta_{us})_d$	$(\Delta_{ue2}/\Delta_{us})_d$
$r_{vy}/0.85r_m$	194 (5.0)	218 (5.2)	285 (5.3)	225 (5.35)	0.89	1.30
$r_{vy}/r_m=1.05$	204 (5.3)	222 (5.3)	267 (5.0)	"	0.92	1.20
$r_{vy}/1.20r_m$	217 (5.7)	226 (5.4)	247 (4.6)	"	0.96	1.09

Figure 3-26 show the torsional response for increasing stiffness eccentricities. It was evident, once again that elements and the centre of mass exhibited their maximum displacement ductility demand for zero strength eccentricity and $r_{vy}/r_m \leq 1.0$. Increasing negative strength eccentricities, associated with excess strength of element *(1)*, reduced its displacement ductility demands whereas those of critical element *(2)* remained essentially the same for $r_{vy}/r_m=1.05$ and reduced even further with $r_{vy}/1.20r_m$. In case of $r_{vy}/0.85r_m$, the demand of critical element *(2)* associated with zero strength eccentricity was slightly exceeded. The unlikely scenario of increasing

positive strength eccentricities, due to the reasons provided in Section 3.5.1, was only presented to clarify trends in the response and hence comments were not provided.

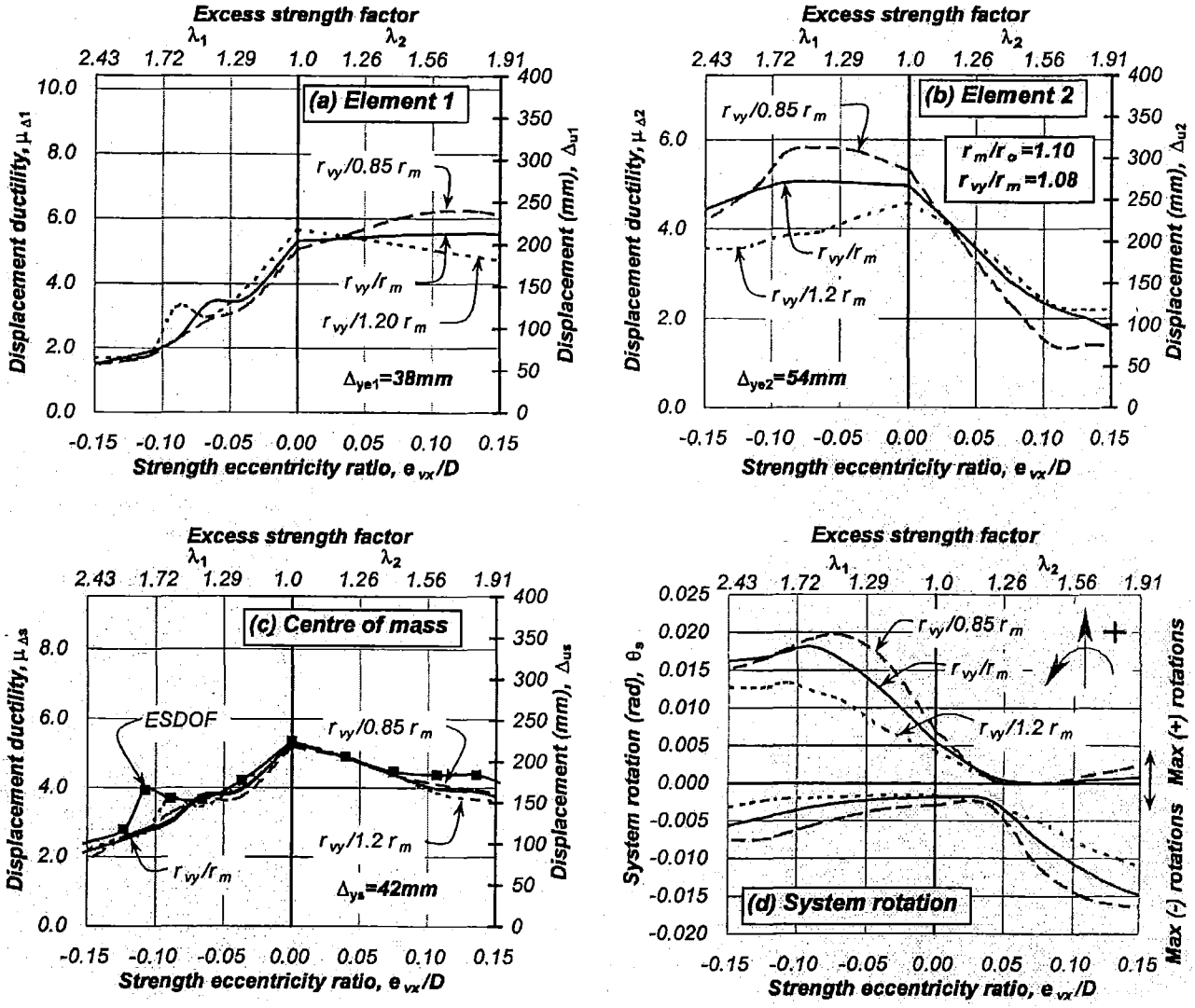

Figure 3-26. Response of the unrestrained *System 6A-1.3(α=1.4)*, T_s=1.30 sec, e_{mx}=-0.10A, $e_{vx} \neq e_{rx}$=variable, $\mu_{\Delta s}$=5.35, r_m/r_o=1.10, r_{vy}/r_m=variable

The above findings suggest that the proposed design strategy achieves a good seismic performance on systems with or without mass eccentricity and $r_{vy}/r_m \leq 1.0$. The maximum displacement demand on the critical element slightly exceeded the maximum established for $r_{vy}/r_m > 1.0$. the above findings suggest that there is no need to differentiate between the response of torsionally unrestrained asymmetric systems with or without mass-eccentricity.

3.6.2 Response of the unrestrained *System 6A-0.5(α=1.4)*

The uncoupled translational period of the unrestrained *System 6A* was reduced to T_s=0.5 seconds by adjusting the system strength. The ratio of element nominal yield displacement (α=1.4) and the nominal yield displacement of the system (Δ_{ys}=42mm) remained unchanged. Those general considerations described in Section 3.2 were also followed in its analysis.

Table 3-8 summarizes the response for zero strength eccentricity. As expected, it showed a sensitive torsional response without showing any particular trend. It was evident that the relative displacements between elements and that at the centre of mass were not significant. As in previously examined unrestrained *System 3A-0.5(α=1.4)*, the maximum displacement demand of element *(1)* was slightly larger than that of element *(2)* and at the centre of mass. The equivalent single degree of freedom system predicted the response at the centre of mass well.

Table 3-8. Response of the unrestrained *System 6A-0.5(α=1.4)*, T_s=0.50 sec, e_{mx}=-0.10A, e_{vx}=e_{rx}=0.0, e_{rx}=-0.066D, $\mu_{\Delta s}$=5.35, r_m/r_o=1.0, r_{vy}/r_m=variable

	Displacements, mm, and displacement ductility demands (μ_s)				Displacement demand ratios	
r_{vy}/r_m	E1	CM	E2	ESDOF	$(\Delta_{ue1}/\Delta_{us})_d$	$(\Delta_{ue2}/\Delta_{us})_d$
$r_{vy}/0.85r_m$	214 (5.94)	217 (5.17)	243 (4.82)	225 (5.35)	0.99	1.12
r_{vy}/r_m =1.05	247 (6.86)	225 (5.35)	224 (4.44)	"	1.10	0.99
$r_{vy}/1.20r_m$	229 (6.36)	222 (5.29)	218 (4.32)	"	1.03	0.98

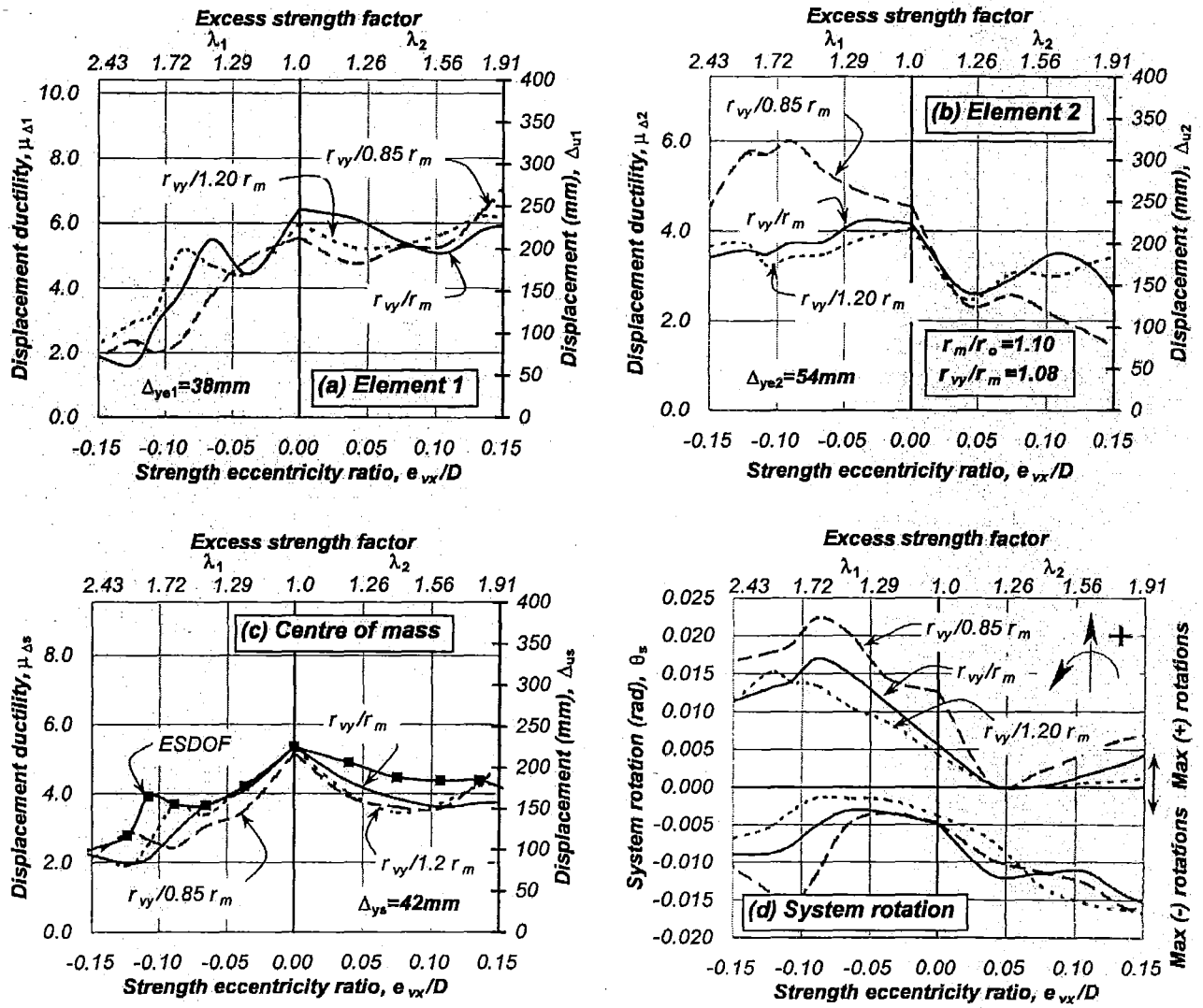

Figure 3-27. Response of the unrestrained *System 6A-0.5(α=1.4)*, T_s=0.50 sec, e_{mx}=-0.10A, e_{vx}≠e_{rx}=variable, $\mu_{\Delta s}$=5.35, r_m/r_o=1.10, r_{vy}/r_m=variable

Figure 3-27 shows the response for zero and increasing strength eccentricities. In the case of increasing negative strength eccentricities, the displacement demands of element *(1)* reduced whereas those of element *(2)* did not exceed the maximum attained for zero strength eccentricity. Again, the excess strength of element *(2)*, i.e., increasing positive strength eccentricities, is an unlikely situation just presented to clarify the system's idealized behaviour.

The findings suggest that the proposed design strategy also achieved an acceptable seismic performance for short period systems with mass eccentricity. It prevented the elements from exceeding their displacement ductility capacity for zero and increasing strength eccentricities. It also demonstrates that the torsional response becomes sensitive as the translational period of free vibration is reduced.

3.7 Single-element structurally asymmetric *Systems 7A, 8A* and *9A* (*CV=CR≠CM; CM=GC*)

3.7.1 Response of the unrestrained *Systems 7A-1.3, 8A-1.3 and 9A-1.3*

This section examines the torsional response of three extremely eccentric systems. The systems are unstable when subjected to static lateral forces; however, they become stable when subjected to dynamic-induced forces as will be shown next. The study of such systems may contribute to a better understanding of the effect of the mass rotational inertia on the response of asymmetric systems.

The extremely eccentric *Systems 7A, 8A and 9A* had a single substitute wall-element *(1)* along the *Y*-axis, as shown in Figure 2-32. The nominal yield displacement of the *Y*-direction element *(1)* and the *X*-direction element *(3)* were the same, $\Delta_{ye1}=\Delta_{y3}=42$ *mm*. The nominal yield displacement of the system was, therefore, the same along both principal axes, $\Delta_{ys}=42mm$. The systems' strength was adjusted to achieve an uncoupled translational period of free vibration of *1.30* seconds. These were denoted unrestrained *Systems 7A-1.3, 8A-1.3 and 9A-1.3*. The actions of the mass rotational inertia and the effect of the strength eccentricity in the response was quantified by the parameter e_{vx}/r_m rather that the r_{vy}/r_m ratio. This is because the radius of gyration of strength is zero for the three systems having different strength eccentricities. Section 2.20 described in detail its characteristics and Appendix *B* summarizes its properties.

The displacement ductility capacity of the systems was assumed equal to the displacement ductility capacity of element *(1)* ($\mu_{\Delta s}=\mu_{\Delta 1}=5.35$) to be consistent with those systems previously examined. The systems were subjected to the Artificial earthquake record along the *Y*-direction. The earthquake record was scaled to generate, on the reference unrestrained *System 7A-1.3* having $e_{vx}/r_m=1.0$, a system displacement ductility demand of $\mu_{\Delta s}=5.35$. This scaled record was also applied, without further modifications, to unrestrained *Systems 8A-1.3 and 9A-1.3* having other e_{vx}/r_m ratios.

Table 3-9 summarizes the response of the systems subjected to dynamic induced forces when element *(1)*, and hence the system, had no excess strength, i.e., $\lambda_1=\lambda_{ys}=1.0$. It is evident that the displacement demands on element *(1)* and at position *(2)* varied depending on the distribution of mass, as quantified by the ratio of radii of gyration of mass and strength eccentricity, e_{vx}/r_m. For instance, the relative displacement demand between element *(1)* and position *(2)* were, in fact, quite large for the unrestrained *System 8A-1.3* having $e_{vx}/r_m=1.54$. This is because the displacement demands of element *(1)* and position *(2)* were significantly affected by system

rotation as the e_{vx}/r_m ratio was increased due to the reduction of the radius of gyration of mass. It is also evident that in case of systems having the same radius of gyration of mass, as it was the case for the unrestrained *Systems 8A-1.3* and *9A-1.3*, a reduction of strength eccentricity reduced system rotations and hence its influence on the displacement demands of element *(1)* and position *(2)*.

It was possible for element *(1)* to yield due to the opposition of the mass rotational inertia to system rotations. This opposition was triggered when the systems were subjected to dynamic excitations. The mass rotational inertia interacts with the mass translational inertia allowing *Y*-direction element *(1)* to yield as to be explained in Section 3.7.2.

It is evident that the displacement ductility capacity of element *(1)* was not exceeded in any of the systems. The response of element *(1)* is, however, expected to become critical if the e_{vx}/r_m ratio would have been further reduced because the response of element *(1)* is expected to be less affected by system rotations. An issue of concern is the large displacement demands recorded at position *(2)*, which could be exceeding the drift limits specified in many design standards.

It was also observed from Table 3-9 that the equivalent single degree of freedom system did not predict well the response at the centre of mass of the systems; particularly that of the unrestrained *System 8A-1.3*. Its accuracy, however, improved as the e_{vx}/r_m ratio was reduced. It is evident that the torsional responses of these extremely eccentric unrestrained systems were quite sensitive because the actions of the mass rotational inertia significantly affected the displacement at the centre of mass.

Table 3-9. Response of the unrestrained *Systems 7A-1.3, 8A-1.3 and 9A-1.3*, T_s=1.30 sec, e_{mx}=0.0, $e_{vx}=e_{rx}$=variable, $\mu_{\Delta s}$=5.35, r_m/r_o=variable, e_{vx}/r_m=variable

			Displacements, mm, and displacement ductility demands (μ_i)				Displacement demand ratios	
System	e_{vx}	e_{vx}/r_m	E1	CM	Position 2	ESDOF	$(\Delta_{ue1}/\Delta_{us})_d$	$(\Delta_{ue2}/\Delta_{us})_d$
7A	0.41A	1.00	129(3.07)	225(5.35)	453	225(5.35)	0.57	2.01
8A	0.71A	1.54	84(2.00)	320(7.62)	609	"	0.26	1.90
9A	0.35A	0.76	225(5.37)	195(4.63)	356	"	1.15	1.82

Figure 3-28 illustrates the response of the systems when the strength of element *(1)*, and hence that of the system, was gradually increased to twice its original strength, i.e., $1.0<\lambda_1=\lambda_{ys}\leq 2.0$. As its strength was increased by only *20%* ($\lambda_{ys}=1.20$), a significant reduction in the displacement demands of element *(1)* is evident, particularly for the unrestrained *System 9A-1.3*; see Figure 3-28(a). Thereafter, in spite of an additional increase of element strength, its displacement demands remained essentially unchanged. On the other hand, Figure 3-28(b) shows that the displacement demands at position *(2)* slightly reduced with increasing strength of element *(1)*. Figure 3-28(c) shows a similar response at the centre of mass. Systems rotations, although large, remained essentially constant in the three systems; see Figure 3-28(d). As was the case of two-element torsionally unrestrained systems, increasing the strength of element *(1)* did not reduce the displacement demands at position *(2)*. This is a concern because it seems impossible to reduce, for such extremely eccentric systems, the large displacement demands at position *(2)*, which may exceed drift limits specified in design standards associated with a given performance criterion. It is confirmed that the equivalent single degree of freedom system did not predict the maximum displacement demand well at the centre of mass of such extremely eccentric systems.

The concept of maximum displacement demand ratios suggested before is not valid for these extreme systems.

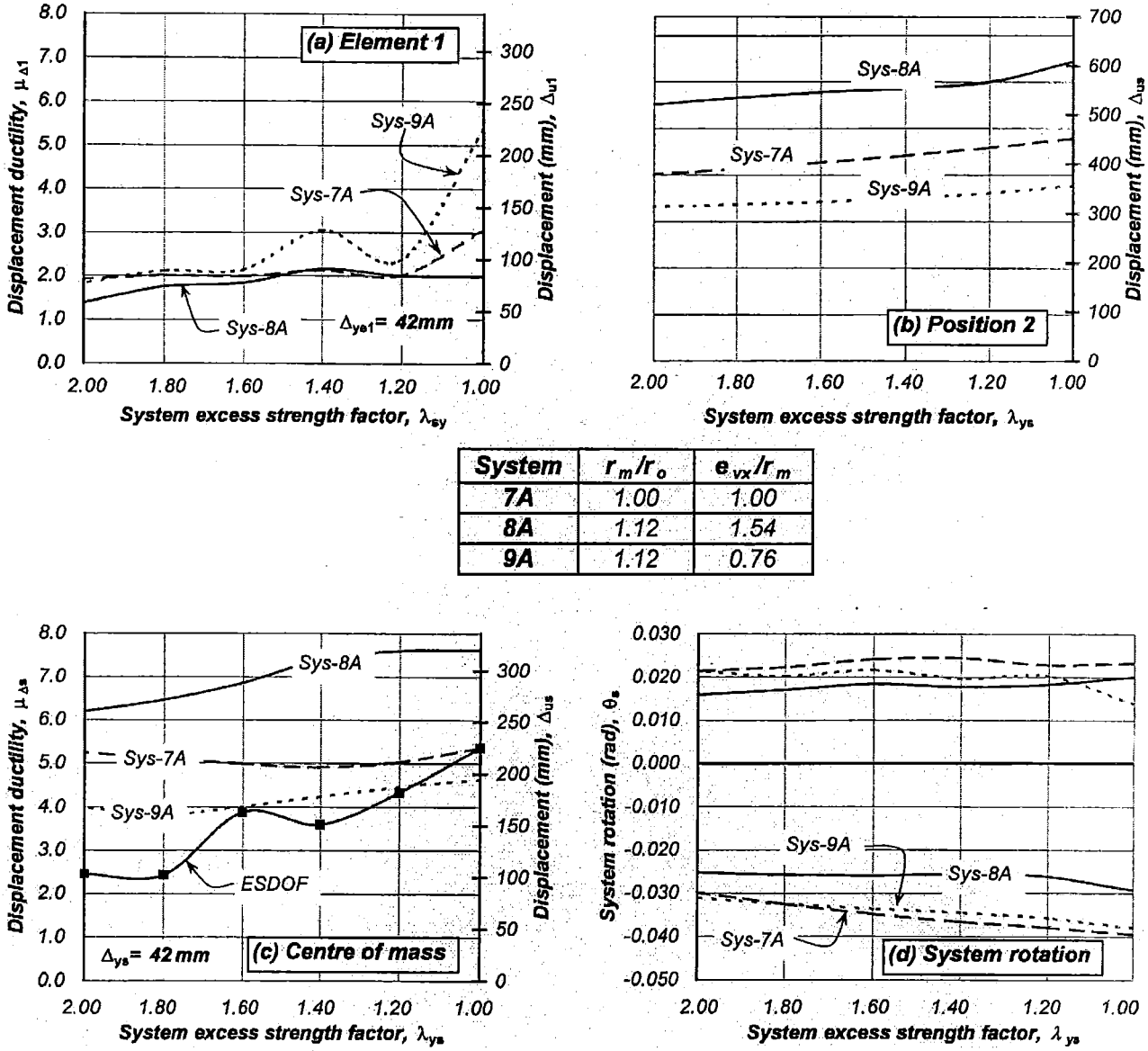

System	r_m/r_o	e_{vx}/r_m
7A	1.00	1.00
8A	1.12	1.54
9A	1.12	0.76

Figure 3-28. Response of the unrestrained *Systems 7A-1.3*, *8A-1.3* and *9A-1.3*, Ts=1.30 sec, e_{mx}=0.0, e_{vx}=e_{rx}=variable, $\mu_{\Delta s}$=*5.35*, r_m/r_o=variable, e_{vx}/r_m=variable

From the above findings it is concluded that the response of extremely eccentric systems subjected to dynamic induced forces is quite sensitive and difficult to predict with simplified models. The opposition of the mass rotational inertia to system rotations is triggered when the asymmetric systems are subjected to dynamic induced forces. The mass rotational inertia interacts with the mass translational inertia allowing the *Y*-direction element *(1)* to yield. This type of extremely eccentric systems should be avoided. If used, large displacement demands on the system's flexible side may exceed allowable drift limits. Hence, significant non-structural damage is to be expected in these structures.

3.7.2 Time history response of the *System 7A-1.3* [T_s=*1.30 sec*, e_{vx}=e_{rx}=*-0.41A* (λ_{ys}=*1.0*)]

The time history response was examined to provide further understanding of the torsional behaviour of an extremely eccentric system subjected to dynamic induced forces. It is expected to assist in a better understanding of the torsional mechanism rather than just examining observed trends.

The unrestrained *System 7A-1.3,* as shown in Figure 2-32(a), was considered again. The nominal yield displacement of *Y*-direction element *(1)* and that at the centre of mass was the same as in other models; Δ_{yel}=Δ_{ys}=*42 mm.* The system strength of V_{yns}=*176kN* was assigned solely to element *(1).* The system exhibited the same strength and stiffness eccentricity, i.e., e_{vx}=e_{rx}=*-0.41A.* It had e_{vx}/r_m=*1.0* and r_m/r_o=*1.0.* It was subjected to the Artificial earthquake record along the *Y*-direction.

The system is unstable when subjected to a static force at the centre of mass. The application of a positive lateral force at the centre of mass along the *Y*-direction generates a system anticlockwise rotation. Neither element *(1)* or *(2)* has torsional or out-of plane resistance hence the system is a mechanism in torsion. Under static forces, element *(1)* will never yield.

However, Figure 3-29(a) shows that during dynamic response element *(1)* consistently reached its nominal strength at instant *(A).* For element *(1)* to yield, an anticlockwise torque of T=$e_{vx}V_{yns}$=*1097kNm* was introduced to the system, see Figure 3-29(c). This torque was generated due to the opposition of the rotational mass to system rotations. This torque, however, was introduced because a force couple exists. Element *(1)* provided one of the forces equal to V_{nel}=*177kN* and the other force, equal in magnitude but opposite in direction, was provided by the dynamic action of the mass translational inertia and represented by a force applied at the centre of mass. Figure 3-30(a) presents the actions and the displacement profile summarizing this scenario. The displacement demand of element *(1)* was much smaller than that of position *(2)*; hence the system rotation was significant.

Element *(1)* remained in the inelastic range of response until reaching a peak displacement demand of Δ_{u1}=*76mm* at instant *(B)*, as shown in Figure 3-29(b). Between instants *(A)* and *(B)*, the torque remained constant and equal to *T=1077kNm* due to yielding of element *(1).* The associated displacement profile; see Figure 3-30(b), show that the displacement demands of element *(1)*, position *(2)* and at the centre of mass increased by a similar amount relative to that attained at instant *(A)* and, therefore, the system rotation did not increase much.

Element *(1)* reached again its nominal strength in the opposite direction at instant *(C)*; see Figure 3-29(a). The displacement demand at position *(2)*, however, increased even further in the same positive direction; hence the system rotation also increased; see Figure 3-30(c). The system torque reached a maximum but opposite in direction to that attained at instant *(A)*; see Figure 3-29(a)

The maximum displacement demand at position *(2)* was reached at instant *(D)* when the system reached its maximum rotation; see Figure 3-29(b) and (d). Element *(1)* also attained a peak displacement demand, opposite in sign but not necessarily a maximum. Interestingly, the maximum displacement demand at position *(2)* was also associated with the maximum system rotation. This was not applicable for element *(1)*, which attained later its maximum demand for a much smaller rotation.

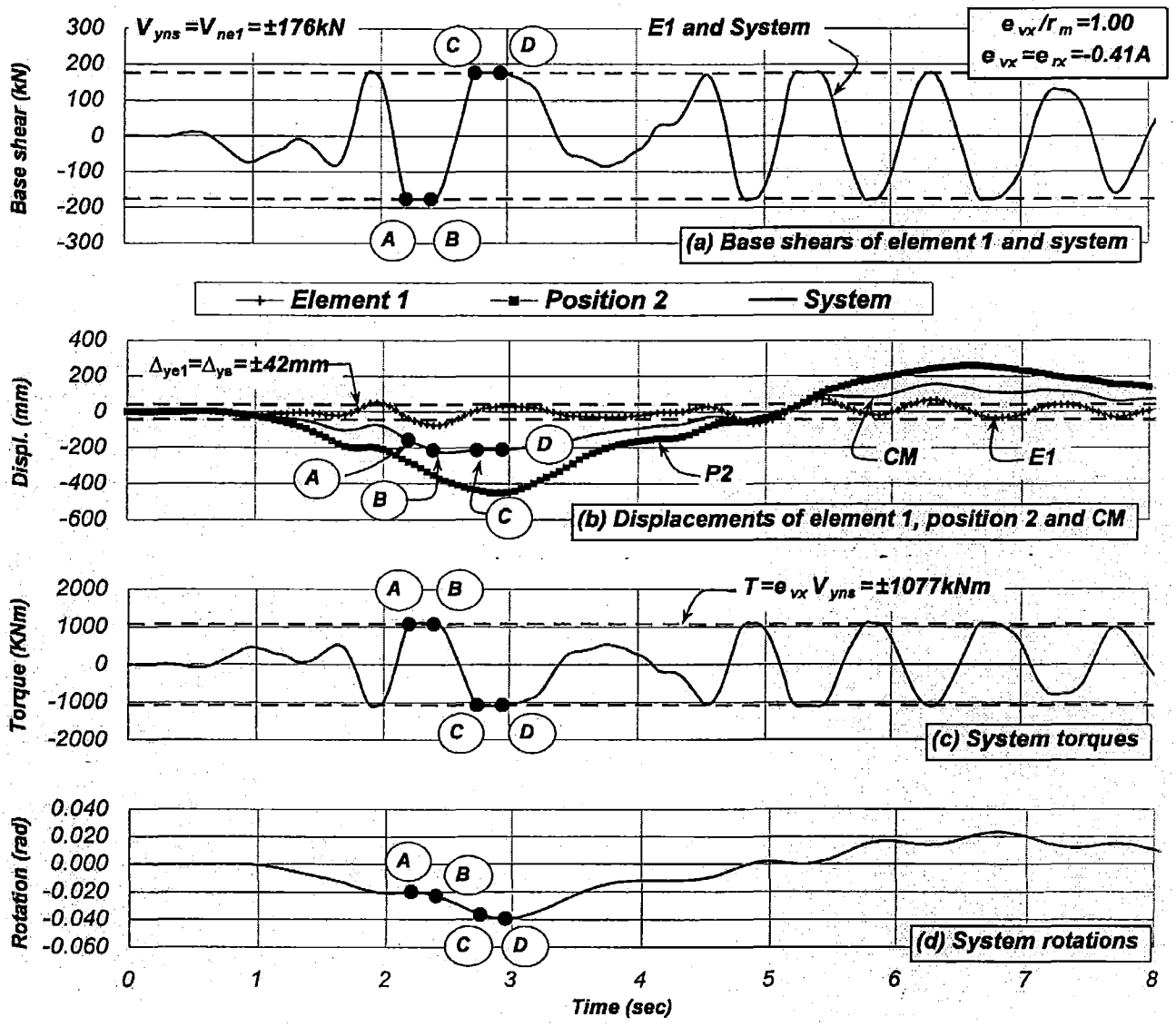

Figure 3-29. Time history response of the unrestrained *System 7A-1.3*, T_s=1.30 sec, e_{mx}=0.0, $e_{vx}=e_{rx}$=-0.41A, $\mu_{\Delta s}$=5.35, r_m/r_o=1.0, e_{vx}/r_m=1.0

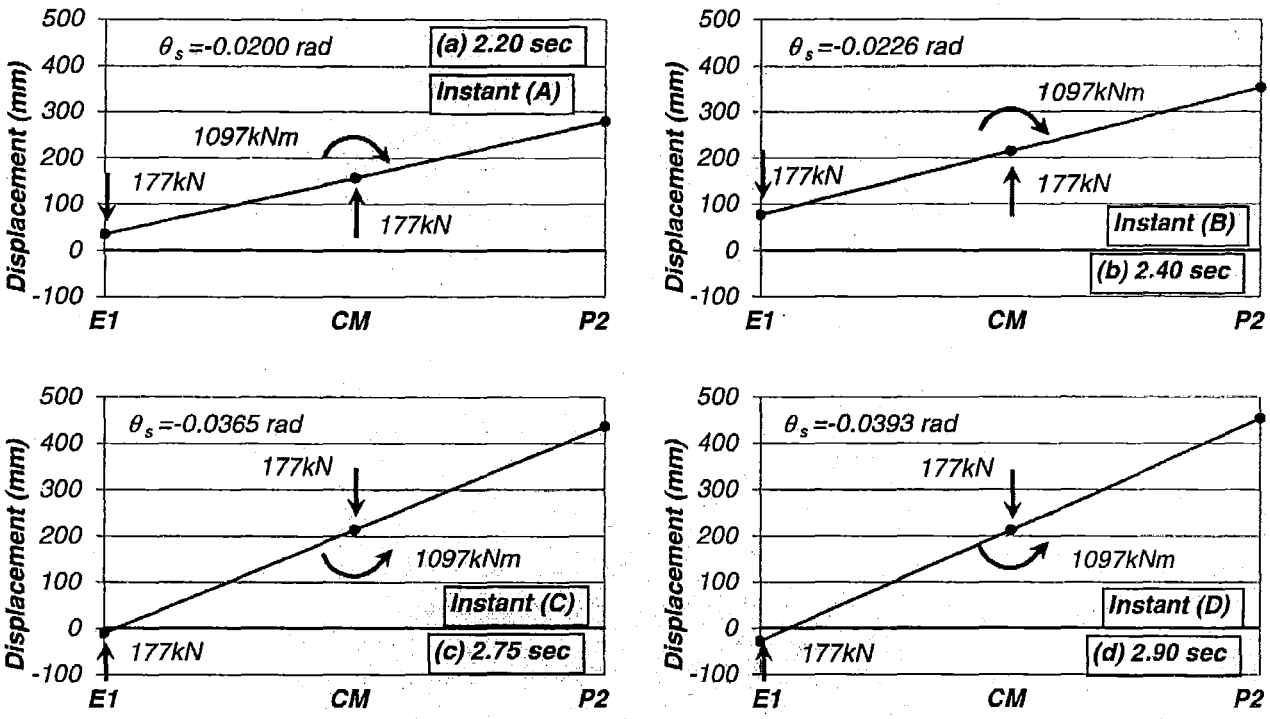

Figure 3-30. Displacement profiles and actions introduced to the unrestrained *System 7A-1.3*, T_s=1.30 sec, e_{mx}=0.0, e_{vx}= e_{rx}=-0.41A, $\mu_{\Delta s}$=5.35, r_m/r_o=1.0, e_{vx}/r_m=1.0

It is evident from the above findings that large system rotations were attained when the peak displacement of element *(1)* and at position *(2)* were of opposite sign. The period of oscillation of the flexible side of the system, i.e., position *(2)*, was very long compared with that of element *(1)*. The maximum displacement demand at position *(2)* was associated with the system maximum rotation. The maximum displacement demand imposed on element *(1)* was less than its displacement capacity and was associated with a small system rotation. The large displacement demand attained at position *(2)* is a major concern because it is likely to exceed allowable drift limits associated with a particular performance criterion.

3.8 Three-element structurally asymmetric *System 10A (CV≠CR; CM=GC)*

3.8.1 Response of the unrestrained *System 10A-1.3*

This section examined the seismic response of a three-element single-mass system. It modelled the building structure designed elsewhere [B3]. It is of interest to verify the extent of conclusions, relevant to simple two-element systems, which may be also applied to multi-element systems as well.

The unrestrained *System 10A* had three *Y*-direction substitute wall-elements with unequal lengths, as shown in Figure 2-33(a). Their nominal yield displacement were $\Delta_{ye1}=\Delta_{y3}=69mm$ and $\Delta_{ye2}=34mm$. The nominal yield displacement of the system was, therefore, $\Delta_{ys}=42mm$. This was consistent with those systems previously examined. The system strength was adjusted to achieve a translational uncoupled period of free vibration of *1.3* seconds. It was denoted unrestrained *System 10A-1.3*. The radius of gyration of the distributed mass of the square plan, r_o, was then varied to $0.85r_o$ and $1.20r_o$ to consider other plan configurations or to account for differences between the computed and the actual distribution of mass. Section 2.21 and

Appendix *B* provide additional information of this system. The system was also analysed based on the approach described in Section 3.2.

The system nominal strength, necessary to ensure that the displacement ductility capacity of any element is not exceeded, should be distributed on the elements to satisfy zero strength eccentricity. The nominal strength initially assigned to the elements of the unrestrained *System 10A-1.3* satisfying zero strength eccentricity was $V_{ne1}=29.7kN$, $V_{ne2}=198.6kN$ and $V_{ne3}=85.4kN$, see Section 2.11.3. This strength distribution may not be achieved in practice because elements *(1)* and *(2)* may require a larger strength to comply with requirements of minimum reinforcement. The response of the system for the idealised condition of zero strength eccentricity provides the basis to estimate its displacement ductility because it is when the displacement demands of the elements and at the centre of mass reaches a maximum.

Table 3-10 summarizes the response of the system for zero strength eccentricity. It is evident, that the maximum displacement demand of elements *(1)*, *(2)* and *(3)* are essentially the same for all $r_{vy}/r_m<1.0$. This is also reflected in the maximum displacement demand ratios associated with each element. This is the response expected from a system having $r_{vy}/r_m<1.0$. System rotations, although significant, were not associated with the maximum displacement demands of the elements. This behaviour was also observed with the two-element unrestrained *System 5A-1.3* also having $r_{vy}/r_m<1.0$; see Figure 3-17.

The equivalent single degree of freedom system having the same properties of translational strength and nominal yield displacement provided, as with two-element systems, a good estimate of the maximum displacement and ductility demand at the centre of mass. This is because the response at the centre of mass was not significantly affected by the actions of the mass rotational inertia. The fact that the number of parallel elements along the *Y*-direction increased and that their maximum response was not attained at the same instant, did not have an effect on the system maximum response.

Due to differences in the nominal yield displacement of the elements, it is evident that the maximum displacement ductility demand of element *(2)* exceeded its displacement ductility capacity of $\mu_{\Delta 2}=5.35$ whereas the demands of elements *(1)* and *(3)* were less than their capacity. The limiting of the system displacement ductility demands to $\mu_{\Delta s}=5.35$ did not prevent element *(2)* from exceeding its displacement capacity; hence, the system displacement ductility capacity should have been further reduced.

The displacement capacity of the system, as explained before, should be associated with the system response for zero strength eccentricity when the system develops its maximum response. It is evident from Table 3-10 that the maximum displacement demand of the elements was essentially the same. The displacement capacity of the system should, therefore, be limited to that of the element with the smallest displacement capacity. The displacement capacity of the system should then be identical to that of element *(2)*. Hence, the displacement ductility capacity of the system should be reduced to $\mu_{\Delta s}=\Delta_{u2}/\Delta_{ys}=(\Delta_{ye2}\mu_{\Delta 2})/\Delta_{ys}=4.33$. The maximum displacement demands expected on the elements are $\mu_{\Delta 1}=\mu_{\Delta 3}=2.64$ and $\mu_{\Delta 2}=5.35$.

It is certain that one or more elements might have some strength in excess to that satisfying zero strength eccentricity. For instance, the strength of elements *(1)* and *(2)* may, for instance, be further increased to comply with minimum reinforcement requirements for reinforced concrete components considering the scenario when the excess strength was assigned to either edge element *(1)* or *(3)*. This is because this generates the largest strength eccentricity for the least

increase in system strength. The excess strength of either element introduced a strength eccentricity accompanied by an increase in system strength, as already shown in Figure 2-35(a). Another scenario could be when the excess strength is assigned to element *(2)*. This, however, will introduce a less critical relationship between strength eccentricity and increase of system strength and hence was not examined.

Table 3-10. Response of the unrestrained *System 10A-1.3*, T_s=1.30 sec, e_{mx}=0.0, e_{vx}=0.0, e_{rx}=-0.055D, $\mu_{\Delta s}$=5.35, r_m/r_o=1.0, r_{vy}/r_m=variable

	Displacements, mm, and Displacement ductility demands (μ_s)				
r_{vy}/r_m	E1	E2	CM	E3	ESDOF
$r_{vy}/0.85r_o$	216 (3.15)	215(6.28)	215(5.12)	222(3.24)	225(5.35)
r_{vy}/r_o=0.78	221(3.22)	219(6.39)	219(5.21)	225(3.27)	"
$r_{vy}/1.20r_o$	222(3.23)	222(6.48)	222(5.29)	223(3.25)	"

	Displacement demand ratios		
r_{vy}/r_m	$(\Delta_{ue1}/\Delta_{us})_d$	$(\Delta_{ue2}/\Delta_{us})_d$	$(\Delta_{ue3}/\Delta_{us})_d$
$r_{vy}/0.85r_o$	1.00	1.00	1.03
r_{vy}/r_o=0.78	1.01	1.00	1.03
$r_{vy}/1.20r_o$	1.00	1.00	1.00

Figure 3-31 shows the response of the system for increasing strength eccentricities. The excess strength assigned to either elements *(1)* and *(3)* was quantified with excess strength factors λ_1 and λ_3. They were gradually increased to λ_1=*5.56* and λ_3=*2.58* to introduce strength eccentricities up to $e_{vx}=\pm 0.15D$. Such significant λ_i values are unrealistic and were just selected to show trends in the response. Consider, at first, the case for r_{vy}/r_o=*0.78*. It is seen that the maximum displacement ductility demands occurred for zero strength eccentricity ($\lambda_1=\lambda_3=1.0$). Thereafter, the excess strength of element *(1)* reduced its displacement ductility demands whereas those of element *(3)* remained about the same. Element *(3)* exhibited, however, a slight increase in its displacement demands beyond that attained for zero strength eccentricity when $r_{vy}/0.85r_o$=*0.92*. This, however, was not an issue because the displacement ductility demands of elements *(1)* and *(3)* did not exceed their ductility capacity. Element *(2)*, which is the element closest to the centre of mass, showed a reduction in displacement ductility demands. The torsional behaviour was similar to that of the two-element unrestrained *System 5A-1.3* having $r_{vy}/r_m \leq 1.0$. The excess strength of element *(3)*, which introduced increasing positive strength eccentricities, is an unrealistic situation just presented to clarify trends in behaviour.

The results suggest that the design strategy is successful in limiting the displacement demands of the system, and hence that of the elements, to less than their displacement capacity. This is achieved if the displacement capacity of the system is limited to that of the element having the smallest displacement capacity. The strength to be assigned to the elements should be equal or greater than that required to satisfy zero strength eccentricity. The torsional behaviour of the asymmetric systems were essentially the same for two and three-element systems having a similar r_{vy}/r_m ratios. It is, therefore, independent of the number of lateral force resisting elements. The effect of system rotations on the element responses is negligible for $r_{vy}/r_m<0.90$. The maximum response at the centre of mass is still predicted well with an equivalent single degree of freedom system.

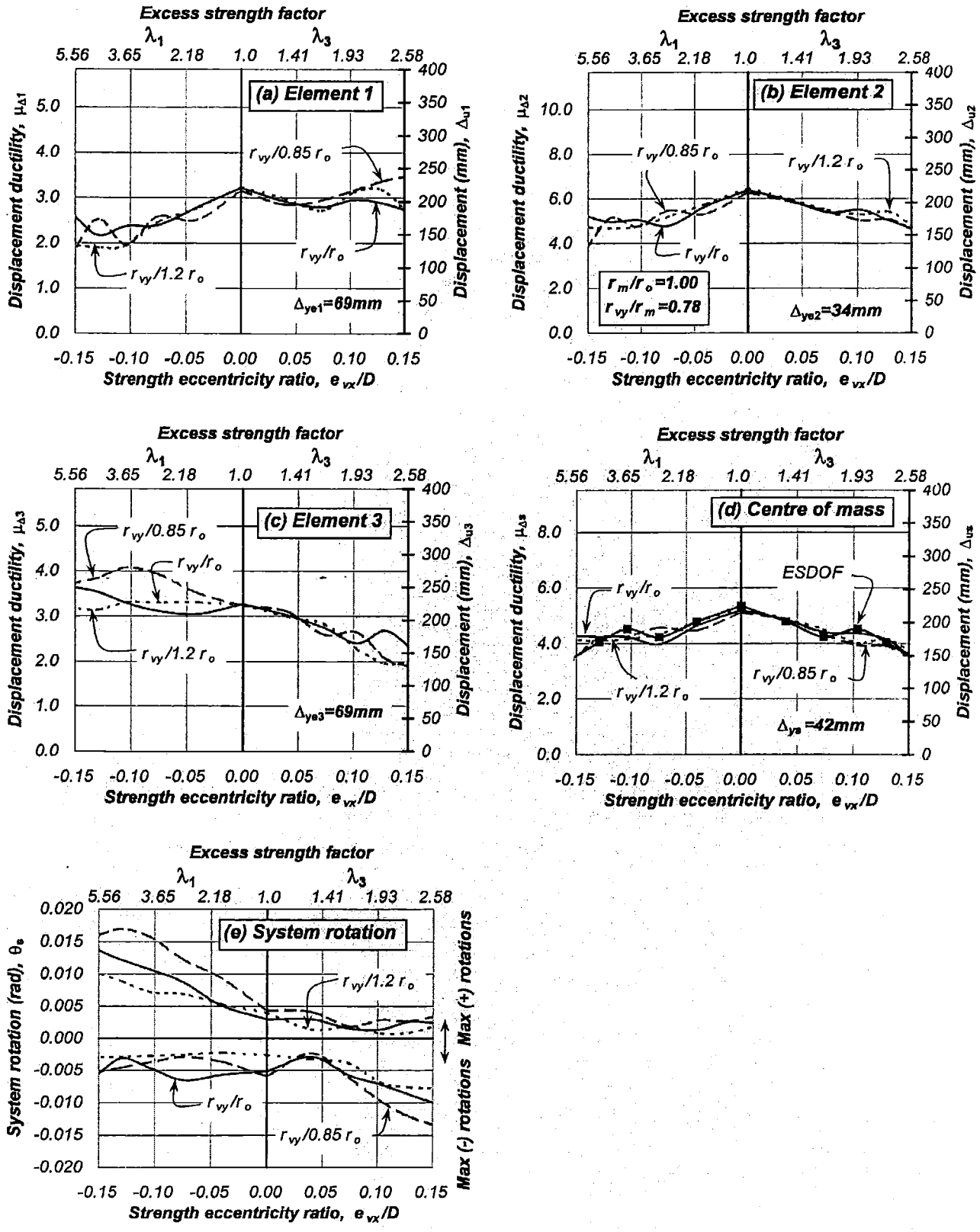

Figure 3-31. Response of the unrestrained *System 10A-1.3*, T_s=1.30 sec, e_{mx}=0.0, $e_{vx} \neq e_{rx}$=variable, $\mu_{\Delta s}$=5.35, r_m/r_o=1.0, r_{vy}/r_m=variable

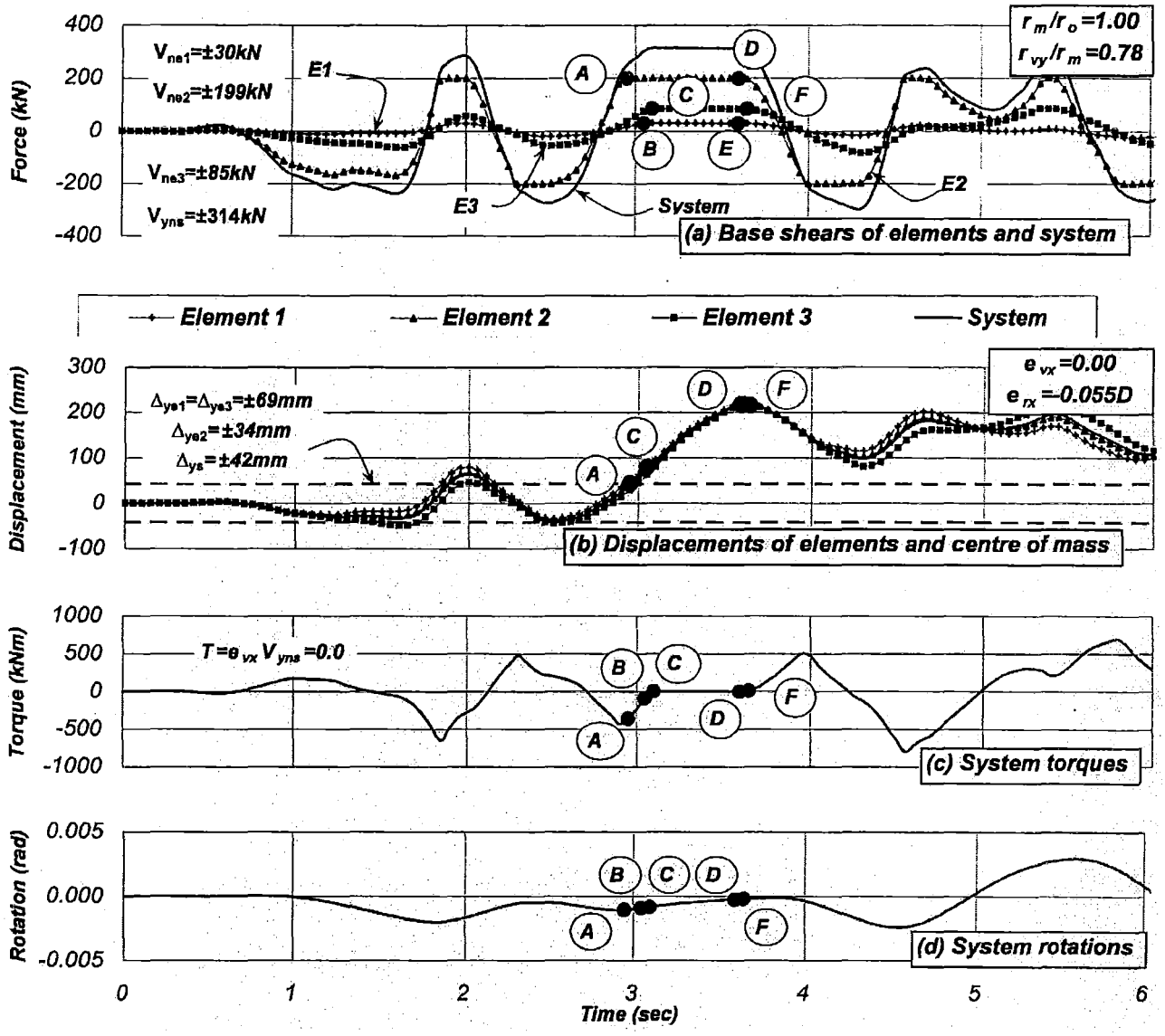

Figure 3-32 Time history response of the unrestrained *System 10A-1.3*, T_s=1.30 sec, e_{mx}=0.0, e_{vx}=0.0, e_{rx}=-0.055D, $\mu_{\Delta s}$=5.35, r_m/r_o=1.0, r_{vy}/r_m=0.78

3.8.2 Time history response of the unrestrained *System 10A-1.3*

The time history response provides a better understanding of the torsional mechanisms developed in a three-element system. Differences in behaviour, if any, between this system and those two-element systems previously examined are identified.

The unrestrained *System 10A-1.3* shown in Figure 2-34(a) was considered. The system strength of V_{yns}= *441kN* was assigned to the elements to satisfy static equilibrium, i.e. e_{vx}=*0.0*. The nominal strength assigned to the elements was V_{ne1}=*30 kN*, V_{ne2}=*199 kN* and V_{ne3}=*185 kN*. Due to differences in their nominal yield displacements, i.e., $\Delta_{ye1}=\Delta_{ye3}$=*69 mm* and Δ_{ye2}=*34 mm*, the system exhibited, for zero strength eccentricity, a stiffness eccentricity of e_{rx}=*-0.055A*.

Consider the torsional mechanism involved when a static lateral force is applied to the centre of mass. Element *(2)* yields first while the system exhibits an anticlockwise rotation. Afterward, elements *(1)* and *(3)* would yield simultaneously for an opposite system rotation.

The time history response showed a different response. Figure 3-32 shows that element *(2)*, having the smallest nominal yield displacement and being the closest to the centre of mass, reached its nominal strength at instant *(A)*. At this instant, the system torque also reached a peak; see Figure 3-32(c). Thereafter, the mass rotational inertia decelerated due to its opposition to a clockwise rotation; hence the torque and system rotations reduced.

Figure 3-32(a) also shows that element *(1)* reached, subsequently, its nominal strength at instant *(B)* due to a small negative or clockwise rotation. Afterwards, the mass rotational inertia continued to restrain system rotations as identified by an anticlockwise torque.

Elements *(3)* reached its nominal strength at instant *(C)*, after elements *(1)* and *(2)* have yielded. This mechanism was only possible, as already explained in Section 3.3.2, due to a force couple. One force was the residual resistance of element *(3)* and the other was the resistance introduced by the mass translational inertia, which is represented as a force applied at the centre of mass. Therefore, the mass rotational inertia introduced an anticlockwise torque due to the opposition of the rotational mass to rotation and hence enabling element *(3)* to yield.

The torque became zero between instants *(C)* and *(D)* when all elements are yielding because the distribution of system strength among elements satisfied zero strength eccentricity. The rotation further reduced whereas the displacement of the elements increased; see Figure 3-32(a) and (d). All elements displayed a similar displacement during the response because they were not associated with large rotations; see Figure 3-32(b). This behaviour is expected from systems with $r_{vy}/r_m \leq 1.0$ when system rotations, although significant, are not associated with the maximum displacement demands of the elements. The maximum displacement demand of the elements was achieved essentially at the same instant *(D)* with a small system rotation.

The findings above suggest that the torsional mechanisms of a multi-element ductile system are, in general, not different to those of two-element systems.

3.9 Four-element structurally asymmetric *System 11A* (CV≠CR; CM=GC)

3.9.1 Response of the unrestrained *System 11A-1.3*

This section examined the seismic response of another multi-element system having a much larger r_{vy}/r_o ratio. It was of interest to show if the conclusions relevant to two and three-element systems are also valid for such system.

The unrestrained *System 10A* with four *Y*-direction substitute wall-elements having unequal lengths is shown in Figure 2-38(a). Their nominal yield displacement were $\Delta_{ye1}=34mm$, $\Delta_{ye2}=68mm$ $\Delta_{ye3}=54mm$ and $\Delta_{ye4}=43mm$. The nominal yield displacement of the system was also $\Delta_{ys}=42mm$. The system strength was adjusted to achieve a translational uncoupled period of free vibration of *1.3* seconds. It was denoted unrestrained *System 11A-1.3*. The radius of gyration of distributed mass of the square plan, r_o, was also varied to $0.85r_o$ and $1.20r_o$ to consider other plan configurations or to account for differences between the computed and the actual distribution of mass. Section 2.22 and Appendix *B* provide additional information for this system. It was analysed using the general considerations described in Section 3.2.

The system nominal strength, necessary to prevent that the displacement ductility capacity of any element being exceeded, should be distributed on the elements to satisfy static equilibrium requirements, i.e., $e_{vx}=0.0$. In case of the unrestrained *System 11A-1.3*, the nominal strength assigned to the elements was $V_{ne1}=127kN$, $V_{ne2}=37kN$, $V_{ne3}=66kN$ and $V_{ne4}=117kN$. Zero strength eccentricity may be difficult to achieve because some elements are likely to require an excess strength to comply with requirements of minimum reinforcement. The associated system response, however, is of interest because it provides the basis to estimate the displacement capacity of the system.

Table 3-11 summarizes the system response for zero strength eccentricity. Relative maximum displacement demands between outermost elements *(1)* and *(4)* are observed particularly for $r_{vy}/0.85r_o$ and reduced as the r_{vy}/r_m ratio was reduced. This reduction was also reflected in the magnitude of the displacement demand ratios. It is evident that the maximum displacement demand ratios associated with the elements to the left of the centre of mass, i.e. elements *(1)* and *(2)*, are proportional. The same effect was noted for the right-hand side elements *(3)* and *(4)*. Displacement demand ratios obtained from two-element systems having similar properties of strength and stiffness eccentricity and r_{vy}/r_m ratio may be used to predict the displacement ductility capacity of the multi-element system.

Table 3-11 also shows that a system displacement ductility capacity of $\mu_{\Delta s}=5.35$ did not prevent element *(1)* and *(4)* from exceeding their displacement ductility capacity. This can be prevented if the system displacement capacity is reduced. This should be associated with the response for zero strength eccentricity because it is when the system reaches a maximum response. It is evident that the maximum displacement demand of the elements becomes essentially the same as the r_{vy}/r_m ratio was reduced. The displacement capacity of the system should, therefore, be limited to that of the element with the smallest displacement capacity. In this case, it should be made the same to that of element *(1)*. Hence, the displacement ductility capacity of the system should be reduced to $\mu_{\Delta s}=\Delta_{u1}/\Delta_{ys}=(\Delta_{ye1}\mu_{\Delta 1})/\Delta_{ys}=4.32$. Hence, the maximum displacement ductility demand expected on the elements is $\mu_{\Delta 1}=5.35$, $\mu_{\Delta 2}=2.67$, $\mu_{\Delta 3}=3.37$, and $\mu_{\Delta 4}=4.25$.

Table 3-11. Response of the unrestrained *System 11A-1.3*, T_s=1.30 sec, e_{mx}=0.0, e_{vx}=0.0, e_{rx}=-0.046D, $\mu_{\Delta s}$=5.35, r_m/r_o=1.0, r_{vy}/r_m=variable

	Displacements, mm, and Displacement ductility demands (μ_s)					
r_{vy}/r_m	***E1***	***E2***	***CM***	***E3***	***E4***	***ESDOF***
$r_{vy}/0.85r_o$	*194(5.73)*	*214(3.15)*	*223(5.32)*	*233(4.33)*	*253(5.93)*	*225(5.35)*
$r_{vy}/r_o=1.05$	*203(5.99)*	*217(3.20)*	*225(5.35)*	*232(4.30)*	*246(5.77)*	"
$r_{vy}/1.20r_o$	*214(6.30)*	*221(3.26)*	*225(5.36)*	*229(4.25)*	*237(5.55)*	"

	Displacement demand ratios			
r_{vy}/r_m	$(\Delta_{ue1}/\Delta_{us})_d$	$(\Delta_{ue2}/\Delta_{us})_d$	$(\Delta_{ue3}/\Delta_{us})_d$	$(\Delta_{ue4}/\Delta_{us})_d$
$r_{vy}/0.85r_o$	*0.87*	*0.96*	*1.04*	*1.13*
$r_{vy}/r_o=1.05$	*0.90*	*0.96*	*1.03*	*1.09*
$r_{vy}/1.20r_o$	*0.95*	*0.98*	*1.02*	*1.05*

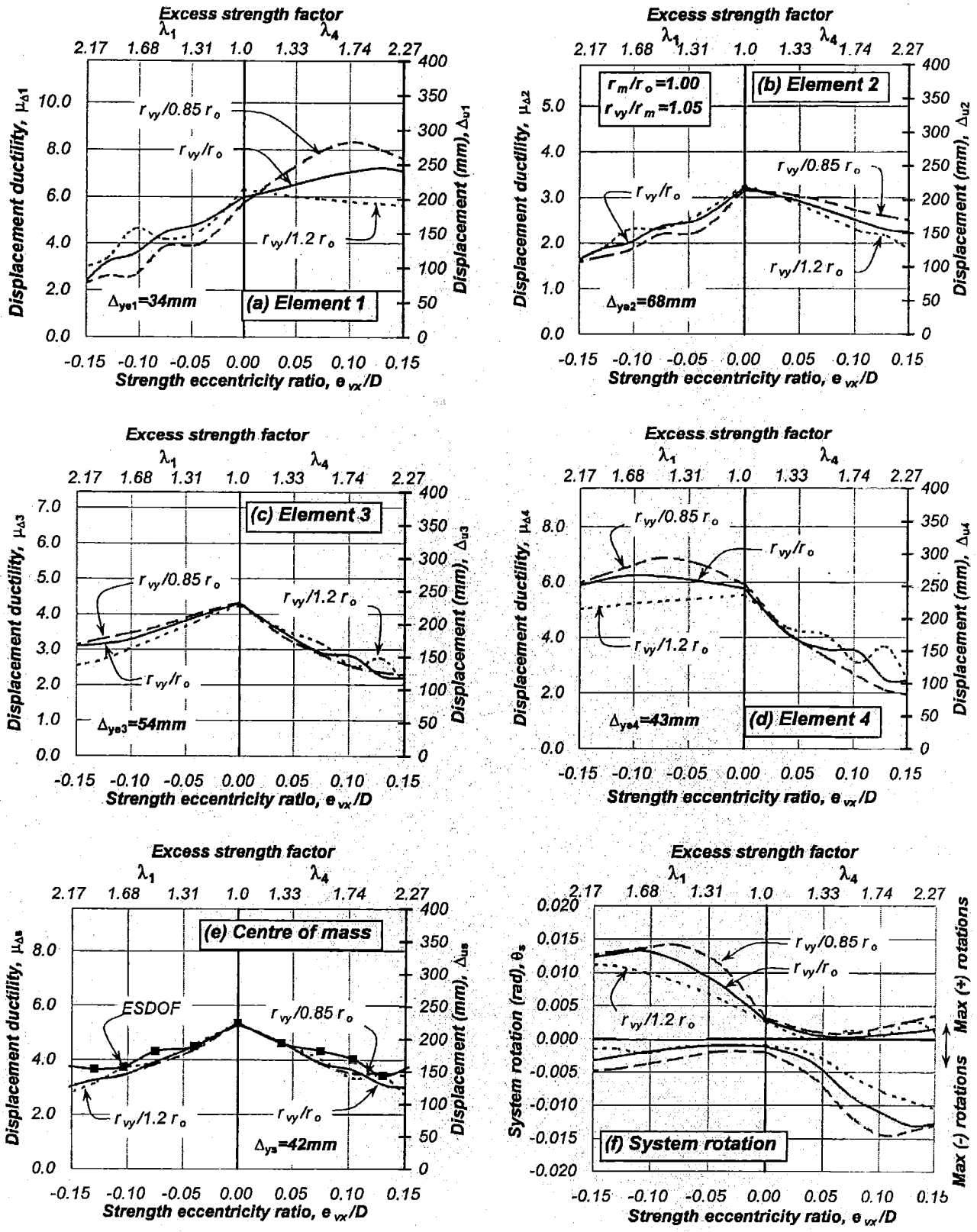

Figure 3-33. Response of the unrestrained *System 11A-1.3*, T_s=1.30 sec, e_{mx}=0.0, $e_{vx} \neq e_{rx}$=variable, $\mu_{\Delta s}$=5.35, r_m/r_o=1.0, r_{vy}/r_m=variable

It is certain that one or more elements might have some strength in excess of that required to satisfy zero strength eccentricity. The critical scenario of all infinite possible combinations of strength eccentricity and increase of system strength resulted when excess strength is assigned to either edge element *(1)* or *(4)* because it generates the largest strength eccentricity for the least increase in system strength, see Figure 2-39(a). Assigning excess strength to inner elements will result in a less critical relationship and hence was not examined.

Figure 3-33 shows the response of the system for increasing strength eccentricities due to the excess strength of either element *(1)* and *(4)*. In case of the system having $r_{vy}/r_m \leq 1.0$, the results corroborate that the maximum displacement ductility demand of elements and centre of mass were attained for zero strength eccentricity. Increasing negative strength eccentricities reduced this demand. In case of the system having $r_{vy}/r_m > 1.0$, the maximum response attained for zero strength eccentricity was exceeded only by the outermost element *(4)*. Interestingly, Figure 3-33(e) shows that negative strength eccentricities generated a much smaller increase in the displacement ductility demand of critical element *(4)* if compared to that observed with element *(1)* due to increasing positive strength eccentricities; see Figure 3-33(a). The system, however, is not likely to end with a positive strength eccentricity.

This result confirms that the suggested design strategy also applies to a four-element system having $r_{vy}/r_m > 1.0$. The increasing number of parallel translatory elements did not affect the torsional behaviour of any system with eccentricities. The response is essentially the same as that of a two-element system having a similar r_{vy}/r_m ratio. The response of the system was predicted with an equivalent single degree of freedom system and it was not affected by increasing the number of parallel elements along the direction of application of the ground motion.

3.10 Response of torsionally unrestrained ductile systems

A design strategy has been suggested in Section 2.11 for the seismic design of asymmetric ductile systems. It consists of three steps: (a) Estimate the displacement capacity of systems associated with zero strength eccentricity, (b) derive the system strength that is distributed to the elements to satisfy zero strength eccentricity, which is expected to prevent the system, and hence its elements, from exceeding their displacement ductility capacity and (c) in case that zero strength eccentricity may not be satisfied, a strength eccentricity may be introduced to the system provided that it results from the nominal strength of one or more elements being in excess of that satisfying zero strength eccentricity.

The validity of the design strategy has been assessed through the predicted performance of systems when certain relevant parameters, believed to influence torsional response, were modified. The findings, although promising, were, however, based on the response of asymmetric systems having uncoupled translational periods of free vibration of *1.30* and *0.50* seconds. To corroborate that the findings are also valid for unrestrained systems having other uncoupled translational periods and $\alpha = \Delta_{ye2}/\Delta_{ye1}$ ratios (or stiffness eccentricities associated with zero strength eccentricity), the response of various unrestrained ductile systems were also performed. The elements were modelled with an elastic-plastic hysteretic rule.

This section shows how to estimate, for zero strength eccentricity, the displacement and ductility capacity of systems as affected by system rotations and aims to:

(a) Demonstrate that the strength to be assigned to the system, and distributed among its elements to satisfy zero strength eccentricity, will prevent displacement demands of the system, and hence that of the elements, from exceeding its displacement capacity,
(b) Verify that a suggested distribution of system strength among elements will also prevent, for increasing strength eccentricities, the displacement maxima established for the elements being exceeded,
(c) Confirm that an equivalent single degree of freedom can be used to predict, with adequate accuracy, the maximum response at the centre of mass of unrestrained systems and
(d) Examine the effects of system uncoupled translational periods and $\alpha=\Delta_{ye2}/\Delta_{ye1}$ ratios (or stiffness eccentricities associated with zero strength eccentricity) on the torsional response.

The parameters used to examine the torsional response were: strength eccentricity and its associated increase of system strength, the ratio of nominal yield displacement of the elements, the $\alpha=\Delta_{ye2}/\Delta_{ye1}$ ratio (or stiffness eccentricity associated with zero strength eccentricity), effects of frequency contents of different earthquakes and reduced system displacement ductility capacity.

The response obtained using two-element ductile systems were examined to simplify the number of calculations. They are considered appropriate to study torsional response based on two conclusions reached in this study:

- Torsional behaviour is not affected by mass eccentricity and

- No significant differences in response were observed between multi-element systems and their equivalent two element systems with similar properties of uncoupled translational period, stiffness eccentricity (associated with zero strength eccentricity) and r_{vy}/r_m ratio.

Three two-element unrestrained *Systems 12A* having $r_{vy}/r_o=1.01$, as shown in Figure 3-34, were examined. The nominal yield displacement of the three systems remained unchanged, $\Delta_{ys}=42mm$. The unrestrained *System 12A(α=1.4)* had a ratio of element nominal yield displacement of $\alpha=\Delta_{ye2}/\Delta_{ye1}=1.40$. The nominal yield displacement of the elements was $\Delta_{ye1}=36mm$ and $\Delta_{ye2}=50mm$ and the associated relative length of the substitute wall-elements *(1)* and *(2)* was $\ell_1=1.4\ell_2$ and $\ell_2=1.0$. The unrestrained *System 12A(α=2.5)* had a larger ratio of element nominal yield displacement, $\alpha=\Delta_{ye2}/\Delta_{ye1}=2.50$. The nominal yield displacement of the elements was $\Delta_{ye1}=29mm$ and $\Delta_{ye2}=73mm$. This was associated with substitute wall-elements having a relative length of $\ell_1=2.5\ell_2$ and $\ell_2=0.69$. Finally, the unrestrained *System 12A(α=4.0)* had a much larger ratio of element nominal yield displacement, $\alpha=\Delta_{ye2}/\Delta_{ye1}=4.0$. The nominal yield displacement of the elements was $\Delta_{ye1}=26mm$ and $\Delta_{ye2}=105mm$ and the relative length of the substitute elements was $\ell_1=4.0\ell_2$ and $\ell_2=0.48$. The displacement capacity of elements *(1)* and *(2)* was the same and equal to $\mu_{\Delta s}=5.0$ in the three systems. It is associated with the strain limit of the materials. Note that this displacement capacity is smaller than that used in systems previously examined, however, no particular reason exists for using a different value.

The strength of the systems was adjusted to achieve uncoupled translational periods of free vibration varying between $T_s=0.1$ and 2.0 seconds. The strength, once distributed on the elements to satisfy zero strength eccentricity, introduced stiffness eccentricities of e_{rx}=-

0.083D(α=1.4), *-0.21D(α=2.5)* and *-0.30D(α=4.0)* due to differences in the nominal yield displacements of the elements. They are defined in terms of the distance "*D*" between *Y*-direction elements *(1)* and *(2)*, as shown in Figure 3-34. A stiffness eccentricity of e_{rx}=*-0.30D* is comparable with the maximum allowed in several current building codes.

The response of such systems is examined to identify if the variation of the $\alpha=\Delta_{ye2}/\Delta_{ye1}$ ratio (or stiffness eccentricity associated with zero strength eccentricity) may introduce significant rotations influencing the maximum displacement demands of the elements and hence affecting the estimate of their displacement ductility capacity.

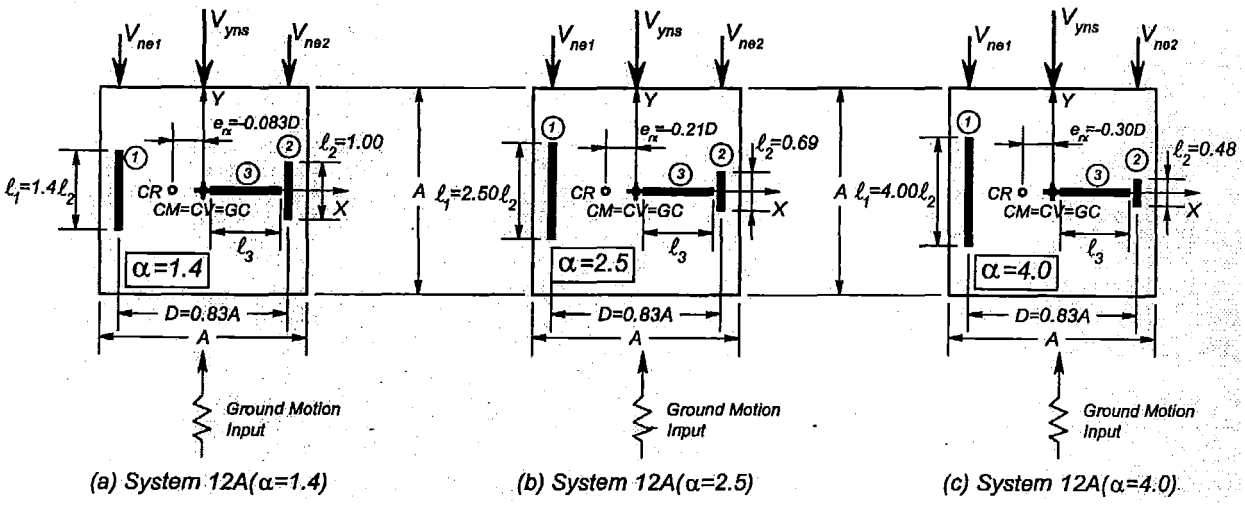

Figure 3-34. Two-element torsionally unrestrained *Systems 12A(α=variable)*

In a first attempt to estimate the displacement capacity of torsionally unrestrained systems, it has been suggested to assume that the system displacement capacity is the same as that of the element having the smallest displacement capacity. This is based on the notion that, for zero strength eccentricity, the displacement demand on the elements and the system reach a maximum, are essentially the same (i.e., zero rotation is assumed) and they are not affected by the variation of the r_{vy}/r_m ratio and the uncoupled translational period of free vibration. Based on such an assumption, the displacement capacity of the unrestrained *Systems 12A(α=variable)* was limited to that of element *(1)*. The displacement ductility capacity of the system is expressed with Eq 3-2 and the results are summarized in Table 3-12. It is evident that the system displacement ductility capacity should be reduced as the $\alpha=\Delta_{ye2}/\Delta_{ye1}$ ratio (or stiffness eccentricity associated with zero strength eccentricity) is increased.

Table 3-12. Displacement ductility capacity of unrestrained *Systems 12A(α=variable)* associated with zero strength eccentricity

System	e_{rx}	Δ_{ys}	α	Δ_{ye1}	Δ_{ye2}	$\mu_{\Delta s}$
		(mm)		(mm)	(mm)	
12A(α=1.4)	-0.083D	42	1.40	36	50	4.28
12A(α=2.5)	-0.21D	42	2.50	29	73	3.50
12A(α=4.0)	-0.30D	42	4.00	26	105	3.13

The unrestrained *Systems 12A(α=variable)* were subjected to the Artificial, Bucharest and Kobe earthquake records acting along the *Y*-direction. These records were scaled to impose, at the

centre of mass, a maximum displacement ductility demand equal to their ductility capacity, in agreement with those general considerations previously described in Section 3.2. This constraint should, in theory, limit displacement ductility demands of critical element *(1)* and that of element *(2)* to less than their ductility capacity of $\mu_{\Delta 1}=5.0$ for every earthquake record. This matter is subsequently examined to verify whether the design aim was achieved in the given period range.

3.10.1 Response of the unrestrained *Systems 12A(α=variable)*

The system nominal strength, necessary to ensure that the system displacement ductility capacity, and hence that of the elements, is not exceeded, is a reference quantity that should be ideally distributed on the elements to satisfy static equilibrium requirements, i.e., $e_{vx}=0.0$. This distribution of strength, which may or may not be achieved in practice, is simply a reference. It is of particular interest because it is the condition when the displacement demands reached by the elements and at the centre of mass are a maximum and are assumed to be essentially the same. This ideal distribution of strength, therefore, is the basis of the design strategy suggested in this study.

In an attempt to estimate the displacement capacity of unrestrained systems, the displacement should be restricted to that of the element having the smallest displacement capacity. In the case of the unrestrained *Systems 12A(α=variable)*, this should be restricted to that of element *(1)*. Figure 3-35(a) shows, for the unrestrained *System 12A(α=2.5)*, this particular situation.

Figure 3-36, Figure 3-37 and Figure 3-38 show, for three different earthquake records, the response of *Systems 12A(α=1.4), 12A(α=2.5)* and *System 12A(α=4.0)*, when their strengths were assigned to parallel elements to satisfy zero strength eccentricity. It is evident that an equivalent single degree of freedom model predicted, with adequate accuracy, the maximum displacement demand at the centre of mass of the torsionaly unrestrained systems. Its accuracy, however, reduced for systems with uncoupled translational periods of $T_s<0.7$ seconds. This is because the centre of mass is not the location in the system where system translations are actually separated from rotations during the response of ductile systems. This sensitivity in the response increased as the $\alpha=\Delta_{ye2}/\Delta_{ye1}$ ratio (or stiffness eccentricity associated with zero strength eccentricity) was increased. The accuracy of the prediction, however, improved as the translational period increased; even on systems with increasing $\alpha=\Delta_{ye2}/\Delta_{ye1}$ ratio. It is evident that the response is certainly sensitive to the frequency content of the earthquake records. In spite of such sensitivity (particularly systems with short uncoupled periods), the equivalent single degree of freedom system can adequately predict the maximum displacement demand at the centre of mass of torsionally unrestrained systems.

Figure 3-36 shows that the maximum displacement demand of elements and at the centre of mass. These are essentially the same for the unrestrained *System 12A(α=1.4)* with $e_{rx}=-0.083D$. However, systems with a larger $\alpha=\Delta_{ye2}/\Delta_{ye1}$ ratio (or a large stiffness eccentricity associated with zero strength eccentricity), as it is the case for the unrestrained *Systems 12A(α=2.5),* and *12A(α=4.0)*, (see Figure 3-37 and Figure 3-38), led, in general, to a reduction and an increase of the displacement demands of elements *(1)* and *(2)*, respectively, relative to that attained at the centre of mass. To quantify those relative displacements, it was suggested (see Section 3.5.1) to use the ratio of maximum displacement demands of elements to that at the centre of mass. The results will be presented in detail in Section 3.10.2.

Figure 3-36, Figure 3-37 and Figure 3-38 also show, for the three systems, the displacement ductility demands for zero strength eccentricity. The fact that the maximum displacement ductility capacity of the system, i.e., at the centre of mass, was limited to $\mu_{\Delta s}$=*4.28*, *3.50* and *3.13* for the unrestrained *Systems 12A(α=1.4), 12A(α=2.5)* and *12A(α=4.0)*, respectively, did prevent, with some exceptions, critical element *(1)* from exceeding its displacement ductility capacity of $\mu_{\Delta 1}$=*5.0*. The fact that its displacement capacity was exceeded in some instances is not a concern because this element is expected to have an excess strength and hence a reduction of its displacement demands is expected, as will be shown later.

Element *(2)*, in spite of developing displacement demands larger than that at the centre of mass, presented a satisfactory response since its maximum displacement ductility demand never exceeded its displacement ductility capacity (associated with the strain limit of the materials). This situation is better explained in Figure 3-35(b). The unrestrained *System 12A(α=2.5)* having, for zero strength eccentricity, a stiffness eccentricity of e_{rx}=*0.21D* is examined. The figure displays the predicted displacement demands of elements *(1)* and *(2)* and that at the centre of mass when the displacement demand of element *(1)* matches its capacity. This case is represented for element *(1)* with an empty square. The predicted displacement demands, represented by a shaded circle and joined by a solid line, are maxima not reached simultaneously. The displacement capacity of the elements (as limited by the strain limit of the materials) is represented with a shaded square. Element *(1)* is critical because when its displacement demand reaches its capacity (empty square), the displacement demand of element *(2)* (shaded circle) is less than its capacity (shaded square) even though its displacement demand is larger than that at the centre of mass. The displacement capacity of the system is therefore limited by that of element *(1)*. It is observed that the displacement capacity of the system is slightly larger than the displacement capacity of element *(1)* and not the same as it is initially assumed; see Figure 3-35(a).

The fact that element *(2)* exhibited a maximum displacement demand larger than that at the centre of mass may be a concern if the displacement capacity of element *(2)* is substantially reduced to comply with displacement limits associated with specific performance criteria. Hence, element *(2)* rather than element *(1)* may become the critical element within the system. This situation is better explained in Figure 3-35(c) for the unrestrained *System 12A(α=2.5)*. The displacement capacity of element *(2)*, as represented by an empty square, has been reduced to comply with specific performance criteria. The square is empty to indicate that the maximum displacement demand on this element matches its capacity. In this situation element *(2)* is critical because its maximum displacement demand may reach its capacity before element *(1)* does. Hence, the displacement demand of the elements and at the centre of mass was reduced, relative to the situation shown in Figure 3-35(b), to prevent critical element *(2)* from exceeding its displacement capacity. Notice that the ratio of maximum displacement demand of the elements relative to that at the centre of mass remains the same. The displacement capacity of the system is, as expected, smaller than the displacement capacity of element *(2)* and that of element *(1)*. This situation proves that limiting the displacement capacity of the system to that of element *(1)* may not prevent element *(2)* from exceeding its displacement and ductility capacity.

It is evident from the results presented the necessity of identifying the critical element of unrestrained systems before estimating its displacement and ductility capacity. The system displacement ductility capacity will depend on the predicted ratio of maximum displacement demands associated with the critical element and its estimated displacement capacity. This approach will be explained in detail in Section 3.10.2.

Figure 3-39, Figure 3-40 and Figure 3-41 illustrate realistic system responses, for three earthquake records, when excess strength was assigned to element *(1)* relative to that satisfying zero strength eccentricity. This increase of element strength introduced negative strength eccentricities to the systems. As expected, the displacement ductility demands on element *(1)* reduced to less than its capacity, whereas that of element *(2)* remained essentially the same as that for zero strength eccentricity.

The response is, however, dependant on the frequency content of the earthquake records. This is seen from the system response to the Kobe earthquake record. The figures show an increase in displacement demands on element *(1)* even after excess strength was assigned to it. In spite of these results, the responses are considered satisfactory if the uncertainties involved in the prediction of earthquake demands are taken into account.

The above findings suggest that the estimate of the displacement capacity of unrestrained systems may be influenced by system rotations as they may increase or reduce the maximum displacement demand of elements relative to that predicted at the centre of mass. System rotations are influenced by the $\alpha=\Delta_{ye2}/\Delta_{ye1}$ ratio (or stiffness eccentricity associated with zero strength eccentricity) and the uncoupled translational period of free vibration of the systems. The r_{vy}/r_m ratio also influences system rotations but it is not considered a relevant parameter for the suggested design strategy. The estimated system strength, once distributed among the elements to satisfy the ideal condition of zero strength eccentricity, should prevent displacement demands imposed on systems, and hence-on their elements, from exceeding its displacement ductility capacities. If zero strength eccentricity cannot be achieved in practice, as to be expected from many asymmetric systems, a strength eccentricity may be accepted, provided it results from the assignment of strength in excess of that satisfying zero strength eccentricity. The accuracy of the estimations, however, was found to reduce for systems having uncoupled translational periods of T_s less than *0.70* seconds and with increasing $\alpha=\Delta_{ye2}/\Delta_{ye1}$ ratios (or stiffness eccentricities associated with zero strength eccentricity).

3.10.2 Ratio of maximum displacement demands of elements and that at the centre of mass

The ratio of maximum displacement demands of elements and that at the centre of mass (see Section 3.5.1) is, in this study, an essential parameter to measure effects of system rotations on the maximum displacement demands of the elements. The centre of mass is used as a reference location because its response, as shown in Sections 3.3.6 and 3.5.1, may be predicted with adequate accuracy using an equivalent single degree of freedom system. In the case of two-element systems, the ratios of maximum displacement demands of elements *(1)* and *(2)* are denoted $(\Delta_{ue1}/\Delta_{us})_{d(CR)}$ and $(\Delta_{ue2}/\Delta_{us})_d$, respectively, where the subscript "$_d$" refers to demand quantities and $_{(CR)}$ attached to the ratio associated with element *(1)*, identifies the displacement demand ratio of that element placed on the same side as the centre of stiffness (relative to the centre of mass).

Figure 3-42 shows the ratios of maximum displacement demands of elements *(1)* and *(2)*, during the earthquake records, for the unrestrained *Systems 12A(α=1.4), 12A(α=2.5)* and *12A(α=4.0)* having zero strength eccentricity and different r_{vy}/r_m ratios, i.e., $r_{vy}/0.85r_m$, r_{vy}/r_m and $r_{vy}/1.20r_m$. It is evident that these are influenced by the uncoupled translational period and the $\alpha=\Delta_{ye2}/\Delta_{ye1}$ ratio (or the stiffness eccentricity associated with zero strength eccentricity). The ratio of displacement demands increases as the translational period reduces because the response of the mass rotational inertia is sensitive for short period systems. They are also affected by variations of the r_{vy}/r_m ratio because the response of the mass rotational inertia is influenced by the relative

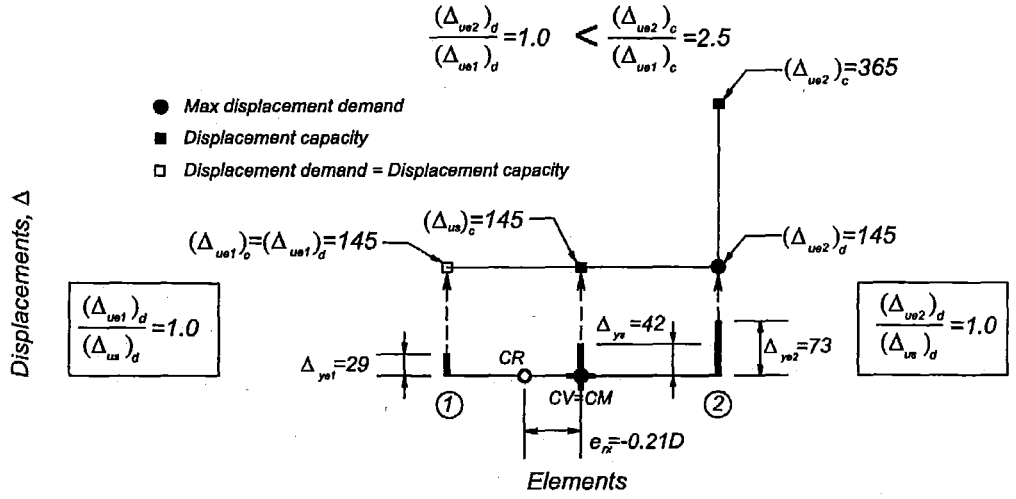

(a) Element (1) restricts the displacement capacity of the system

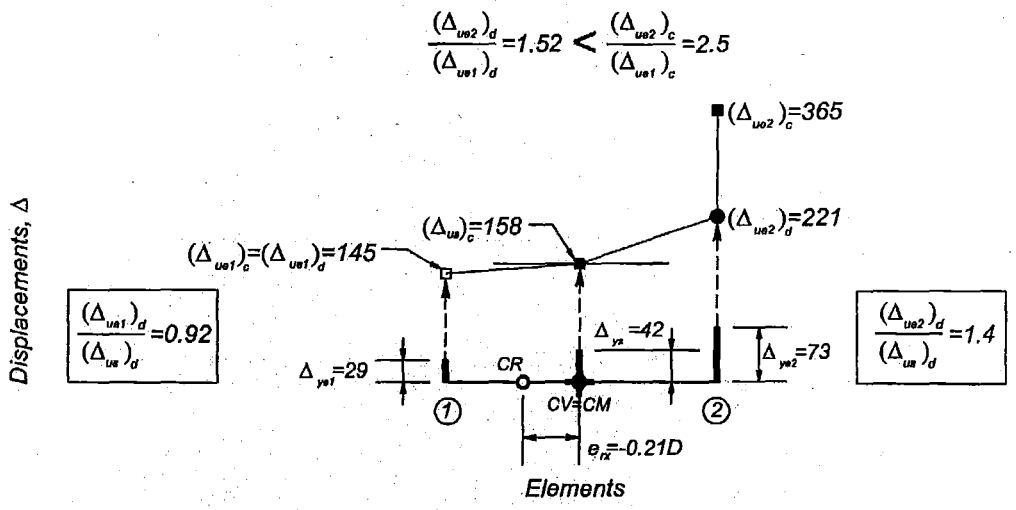

(b) Element (1) restricts the displacement capacity of the system

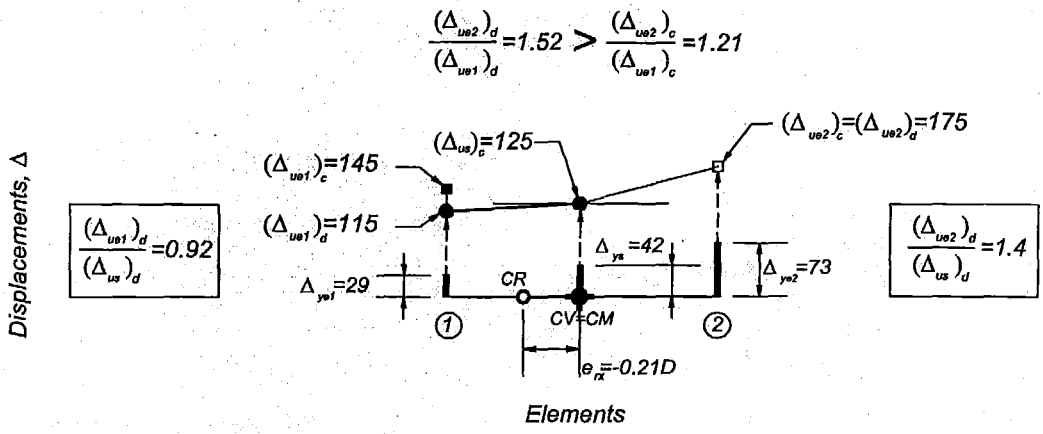

(c) Element (2) restricts the displacement capacity of the system

Figure 3-35. Displacement capacity of the unrestrained *System 12A(α=2.5)* as it is restricted by the displacement capacity of the critical element, e_{vx}=0, e_{rx}=-0.21D, T_s=0.5sec, $\mu_{\Delta s}$=variable

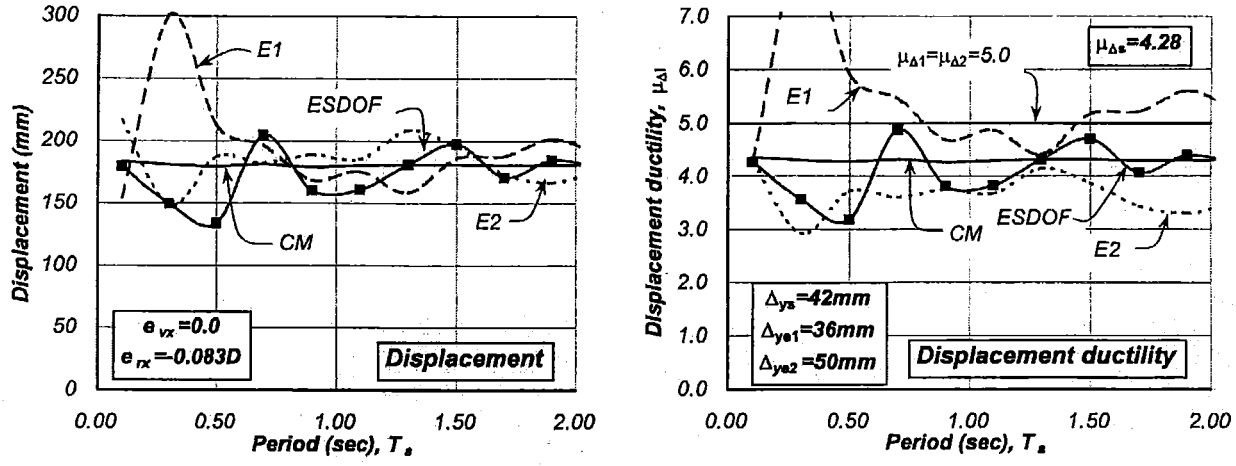

(a) Artificial earthquake record

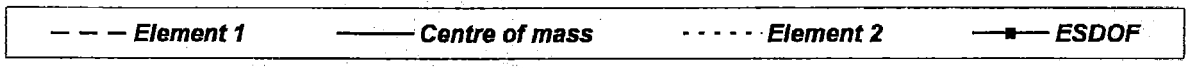

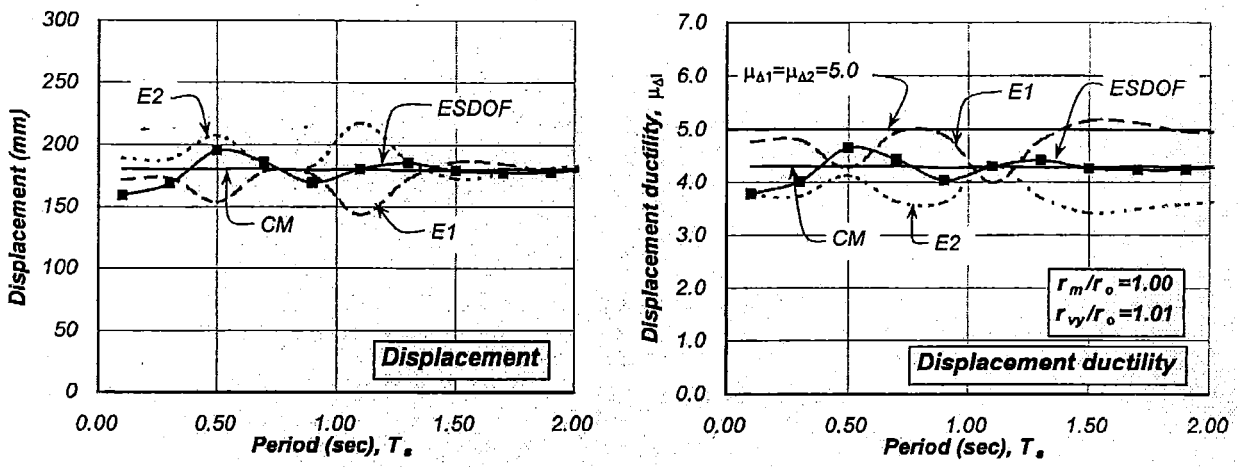

(b) Bucharest NS earthquake record

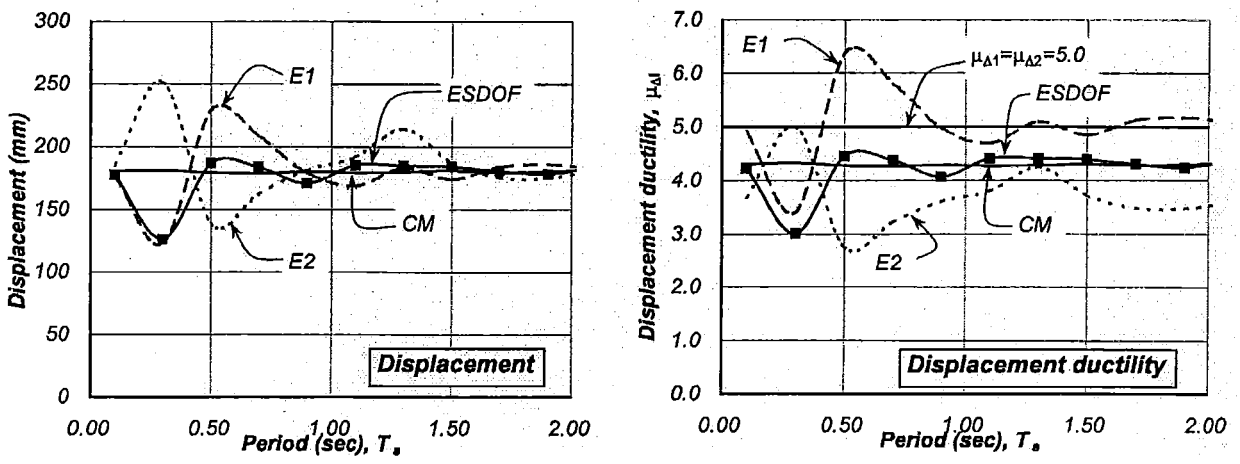

(c) Kobe NS earthquake record

Figure 3-36. Spectral presentation of the response of the unrestrained *Systems 12A(α=1.4)* when subjected to different earthquake records, T_s=variable, e_{mx}=0.0, e_{vx}=0.0, e_{rx}=-0.083D, $\mu_{\Delta 1}=\mu_{\Delta 2}=5.00$, $\mu_{\Delta s}\approx 4.28$, r_m/r_o=1.00, r_{vy}/r_m=1.01

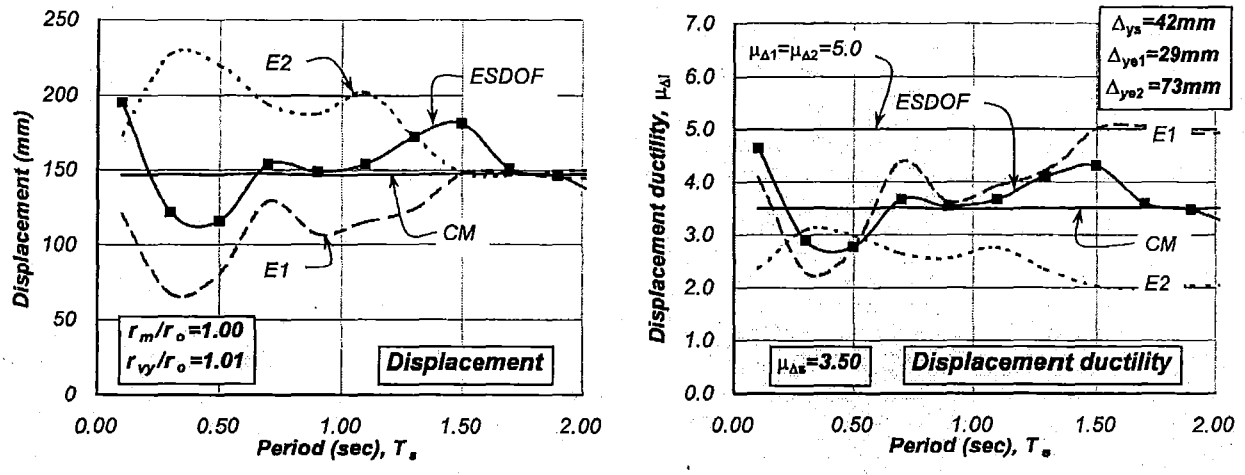

(a) Artificial earthquake record

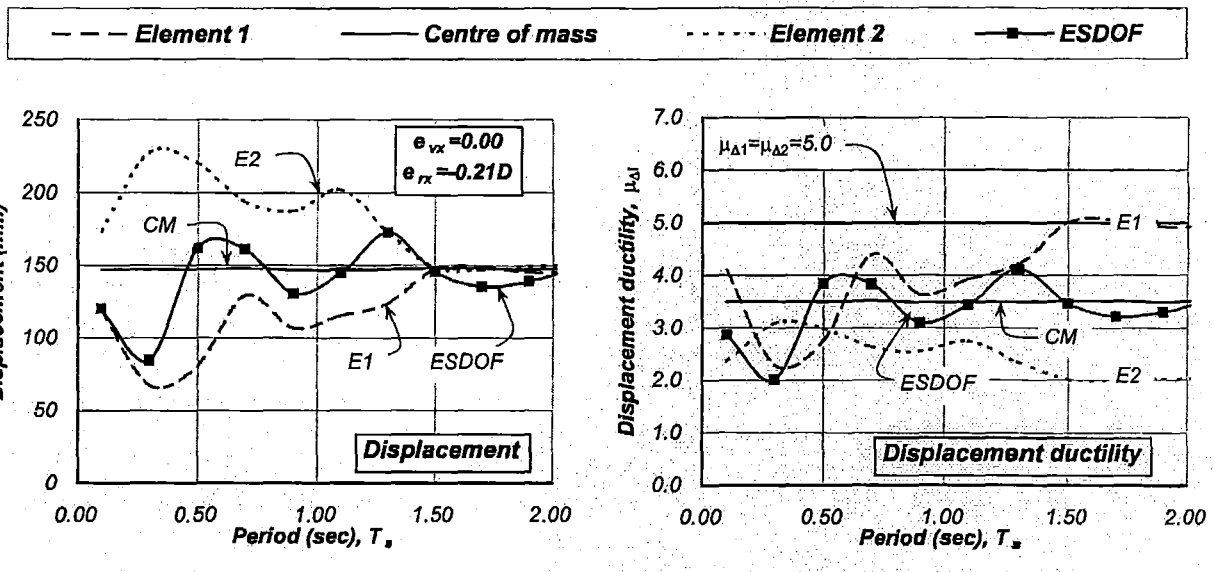

(b) Bucharest NS earthquake record

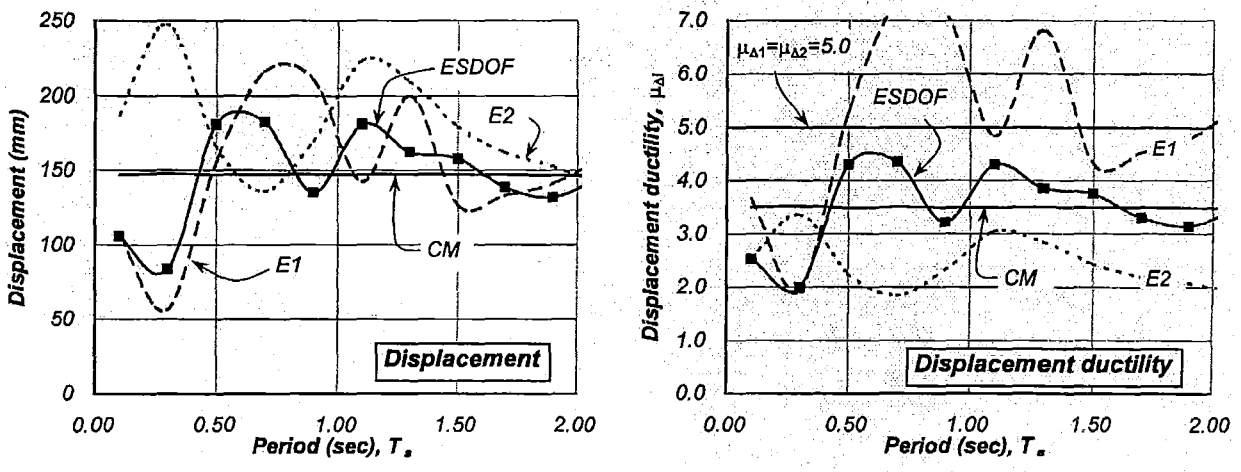

(c) Kobe NS earthquake record

Figure 3-37 Spectral presentation of the response of the unrestrained *Systems 12A(α=2.5)* when subjected to different earthquake records, T_s=variable, e_{mx}=0.0, e_{vx}=0.0, e_{rx}=-0.21D, $\mu_{\Delta 1}=\mu_{\Delta 2}$=5.00, $\mu_{\Delta s}\approx$3.50, r_m/r_o=1.00, r_{vy}/r_m=1.01

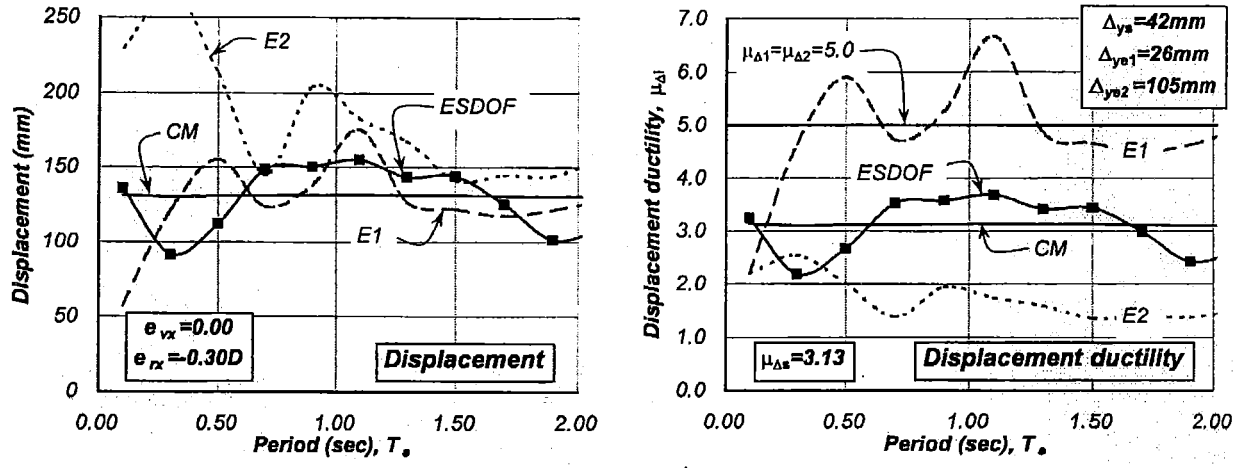

(a) Artificial earthquake record

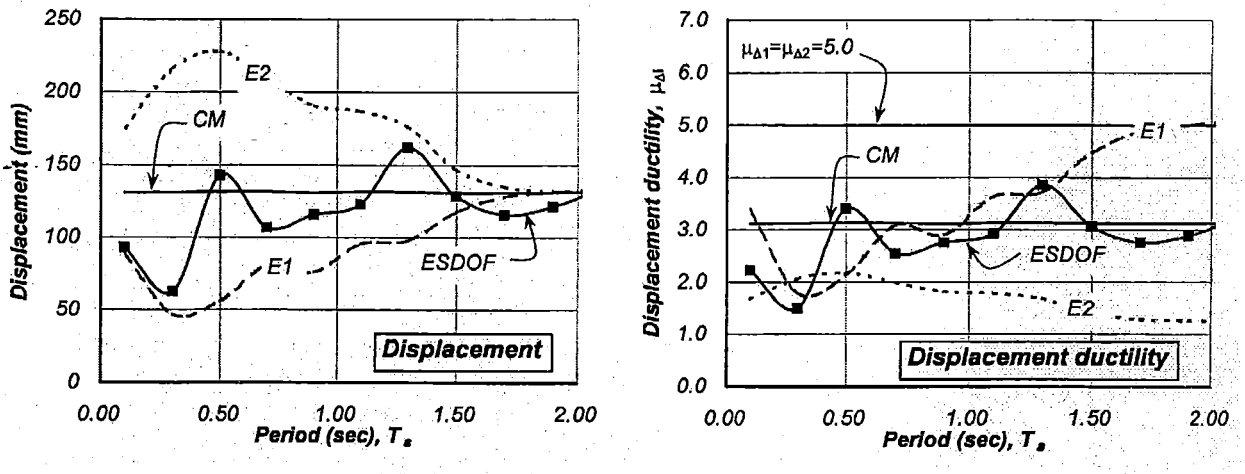

(b) Bucharest NS earthquake record

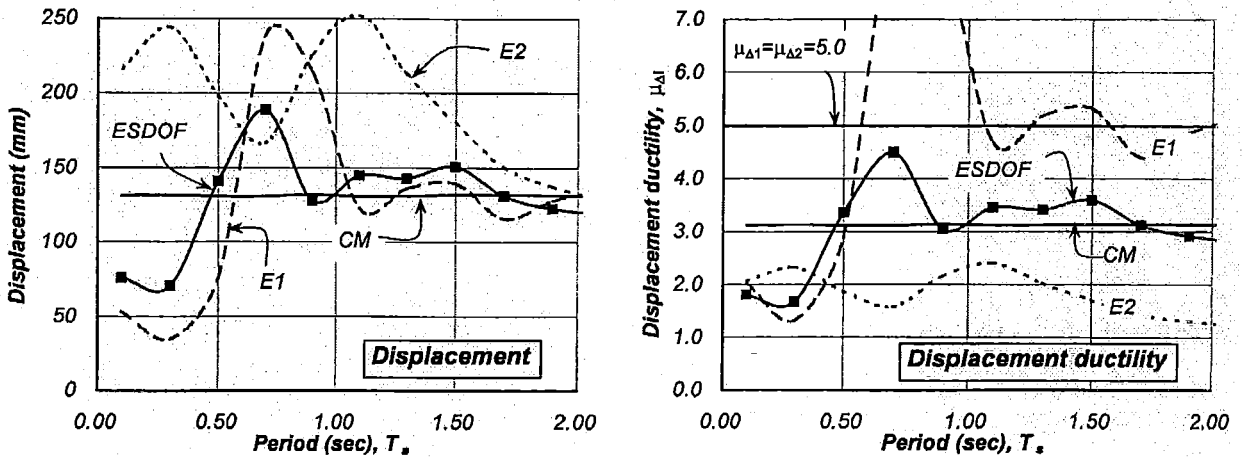

(c) Kobe NS earthquake record

Figure 3-38 Spectral presentation of the response of the unrestrained *Systems 12A(α=4.0)* when subjected to different earthquake records, T_s=variable, e_{mx}=0.0, e_{vx}=0.0, e_{rx}=-0.30D, $\mu_{\Delta 1}=\mu_{\Delta 2}$=5.00, $\mu_{\Delta s}\approx$3.13, r_m/r_o=1.00, r_{vy}/r_m=1.01

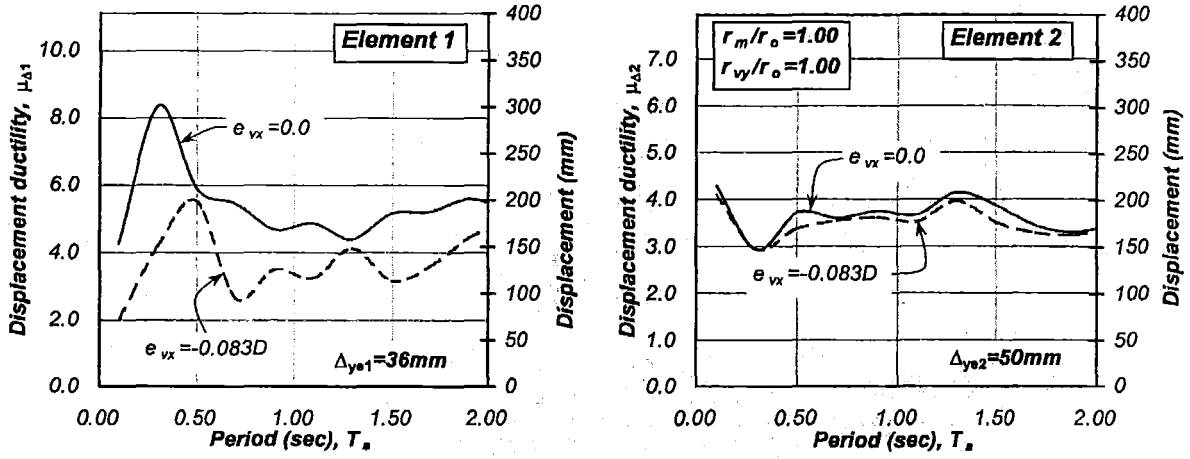

(a) Artificial earthquake record

$\Delta_{ye2}/\Delta_{ye1}$	λ_1	e_{vx}	e_{rx}
α=1.40	1.00	0.00	-0.083D
α=1.40	1.40	-0.083D	-0.162D

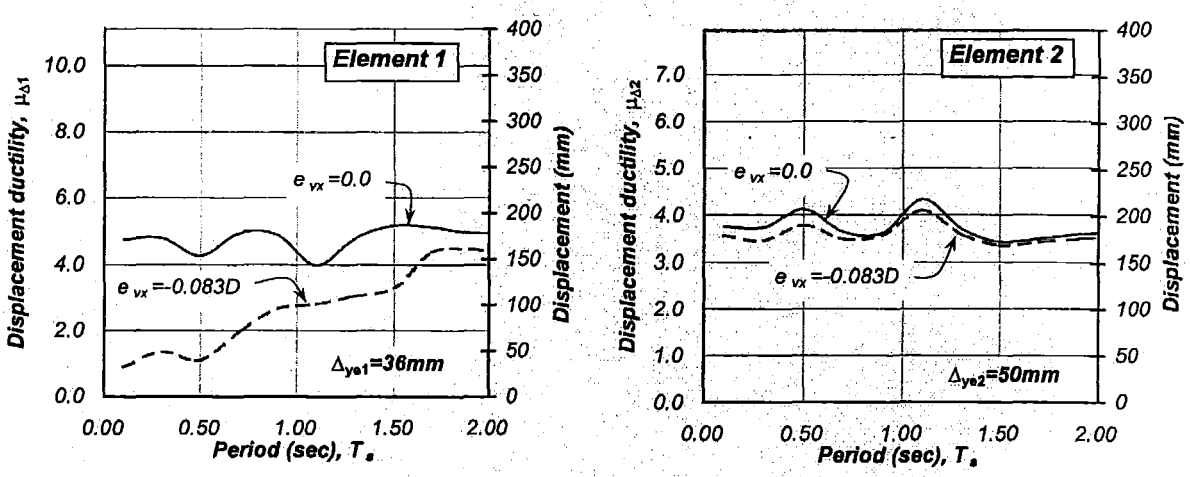

(b) Bucharest NS earthquake record

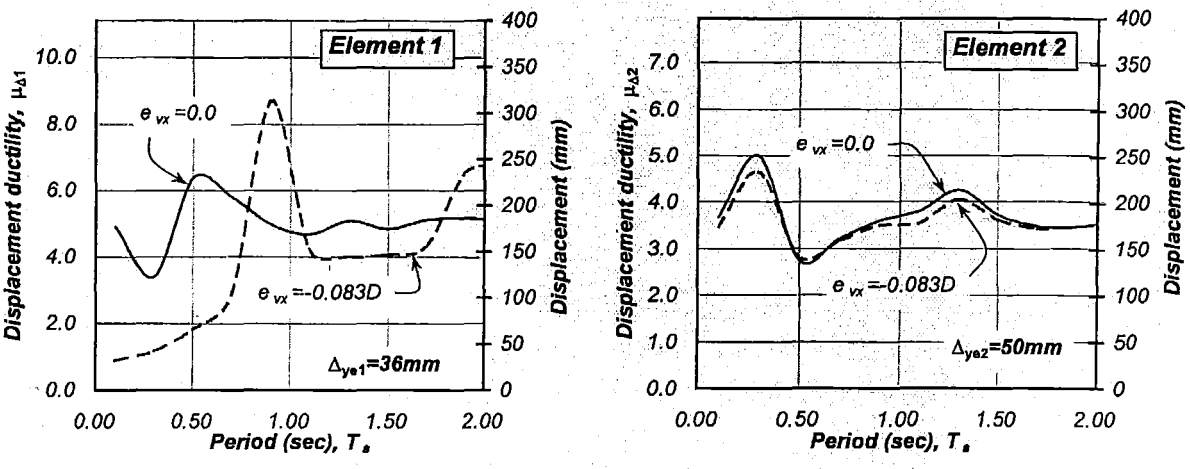

(c) Kobe NS earthquake record

Figure 3-39 Spectral presentation of the response of the unrestrained *Systems 12A(α=1.4)* when element *(1)* has excess strength and it is subjected to different earthquake records, T_s=variable, e_{mx}=0.0, $e_{vx} \neq e_{rx}$=variable, $\mu_{\Delta 1}=\mu_{\Delta 2}$=5.00, $\mu_{\Delta s} \approx$4.28, r_m/r_o=1.00, r_{vy}/r_m=1.01

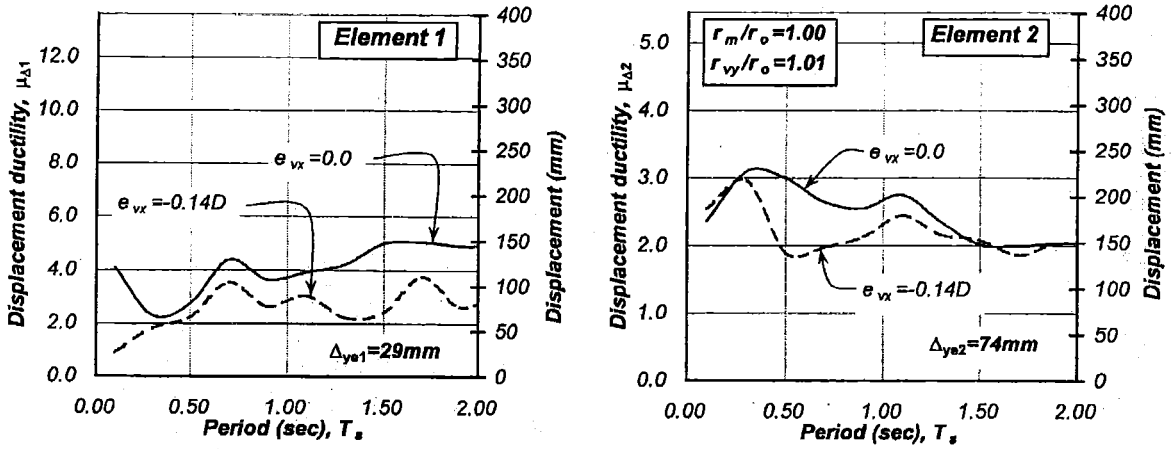

(a) Artificial earthquake record

$\Delta_{ye2}/\Delta_{ye1}$	λ_1	e_{vx}	e_{rx}
α=2.50	1.00	0.00	-0.21D
α=2.50	1.80	-0.14D	-0.32D

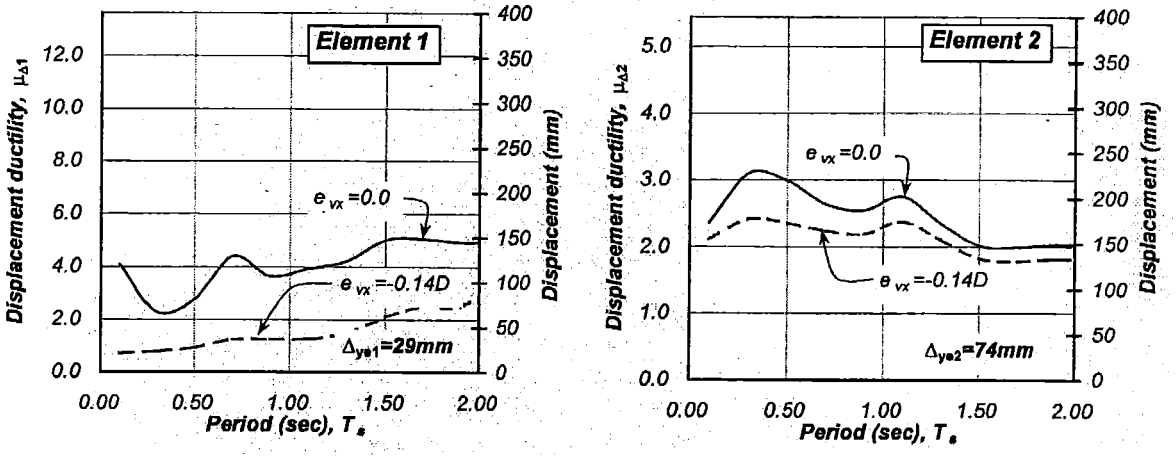

(b) Bucharest NS earthquake record

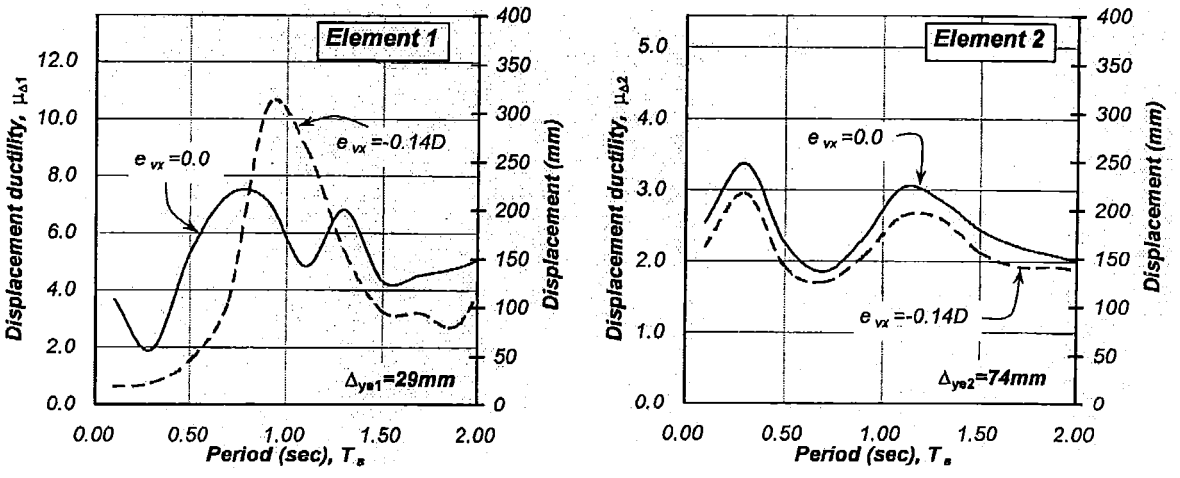

(c) Kobe NS earthquake record

Figure 3-40 Spectral presentation of the response of the unrestrained *Systems 12A(α=2.5)* when element *(1)* has excess strength and it is subjected to different earthquake records, T_s=variable, e_{mx}=0.0, $e_{vx} \neq e_{rx}$=variable, $\mu_{\Delta 1}=\mu_{\Delta 2}$=5.00, $\mu_{\Delta s} \approx$3.50, r_m/r_o=1.00, r_{vy}/r_m=1.01

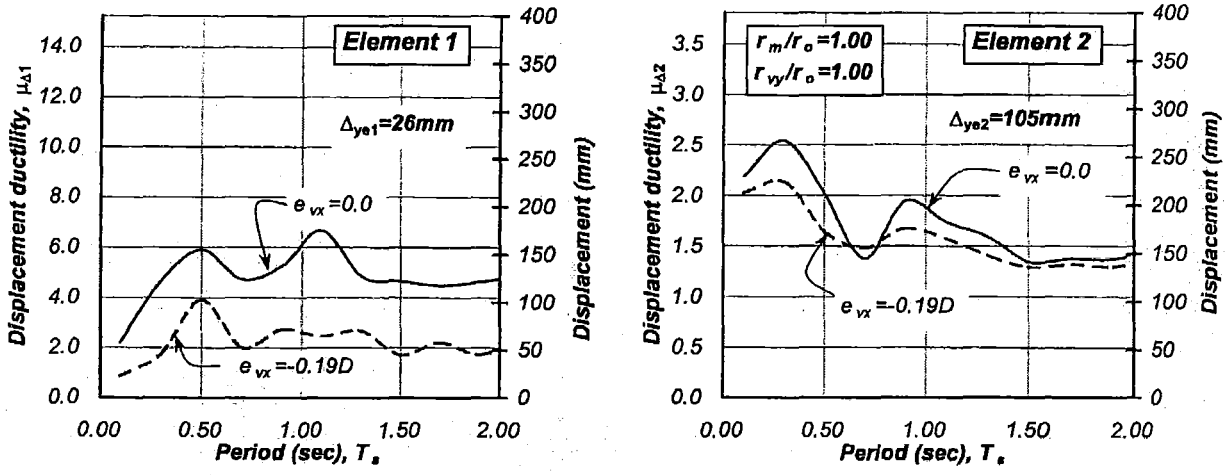

(a) Artificial earthquake record

$\Delta_{ye2}/\Delta_{ye1}$	λ_1	e_{vx}	e_{rx}
α=4.0	1.00	0.00	-0.30D
α=4.0	2.20	-0.19D	-0.40D

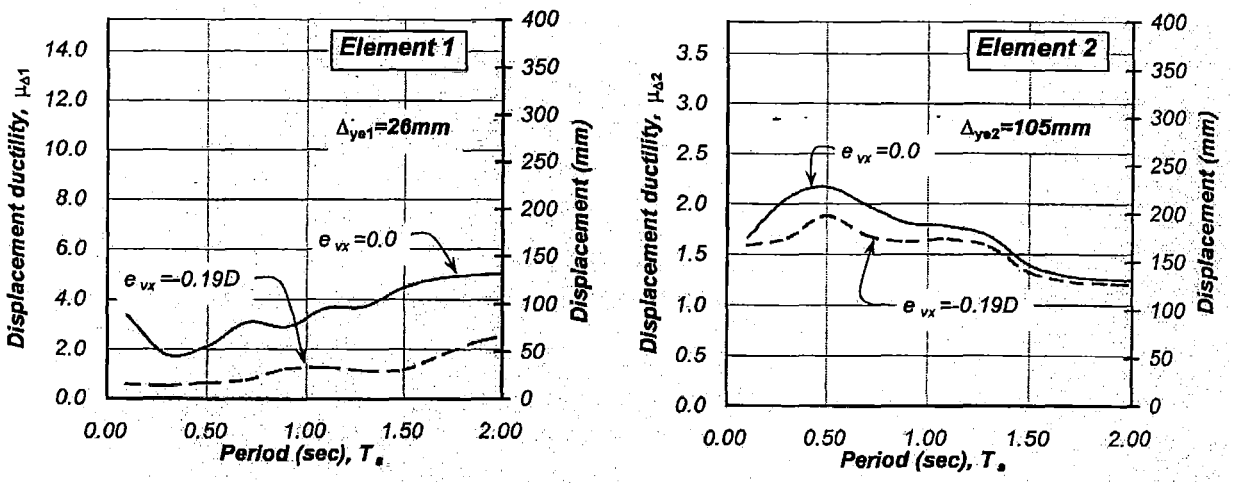

(b) Bucharest NS earthquake record

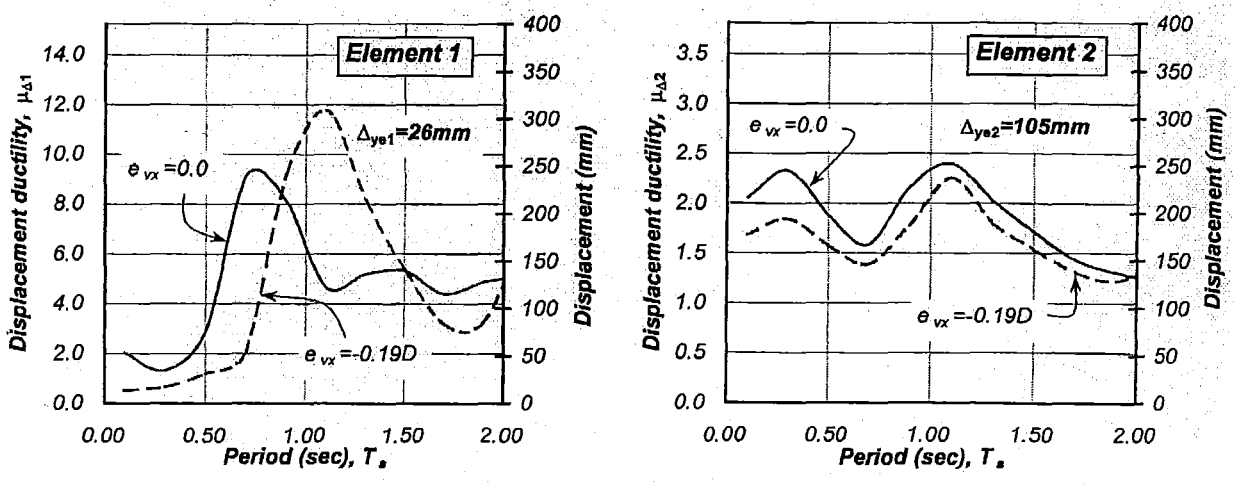

(c) Kobe NS earthquake record

Figure 3-41 Spectral presentation of the response of the unrestrained *Systems 12A(α=4.0)* when element *(1)* has excess strength and it is subjected to different earthquake records, T_s=variable, e_{mx}=0.0, $e_{vx} \neq e_{rx}$=variable, $\mu_{\Delta 1}=\mu_{\Delta 2}$=5.00, $\mu_{\Delta s} \approx$3.13, r_m/r_o=1.00, r_{vy}/r_m=1.01

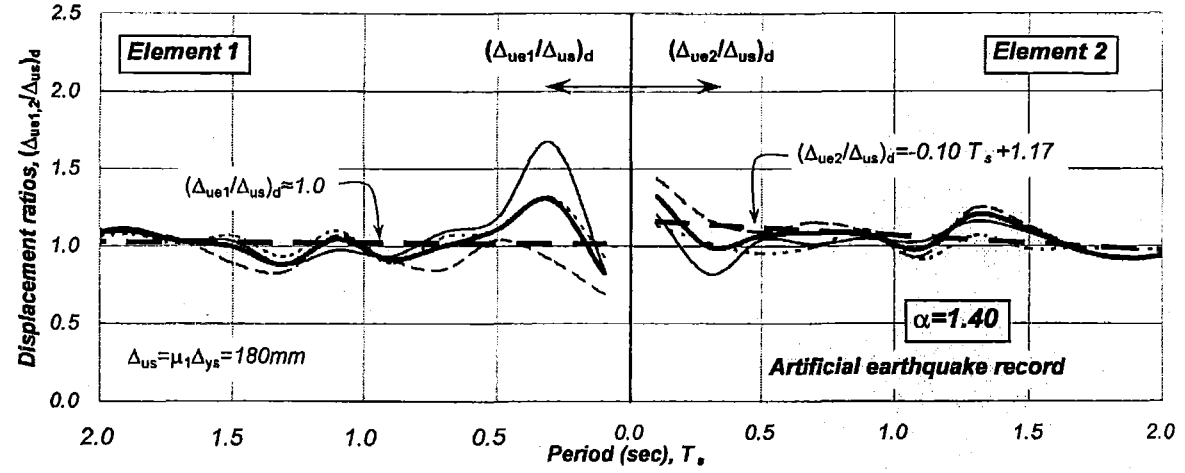

(a) System 12A(α=1.4)

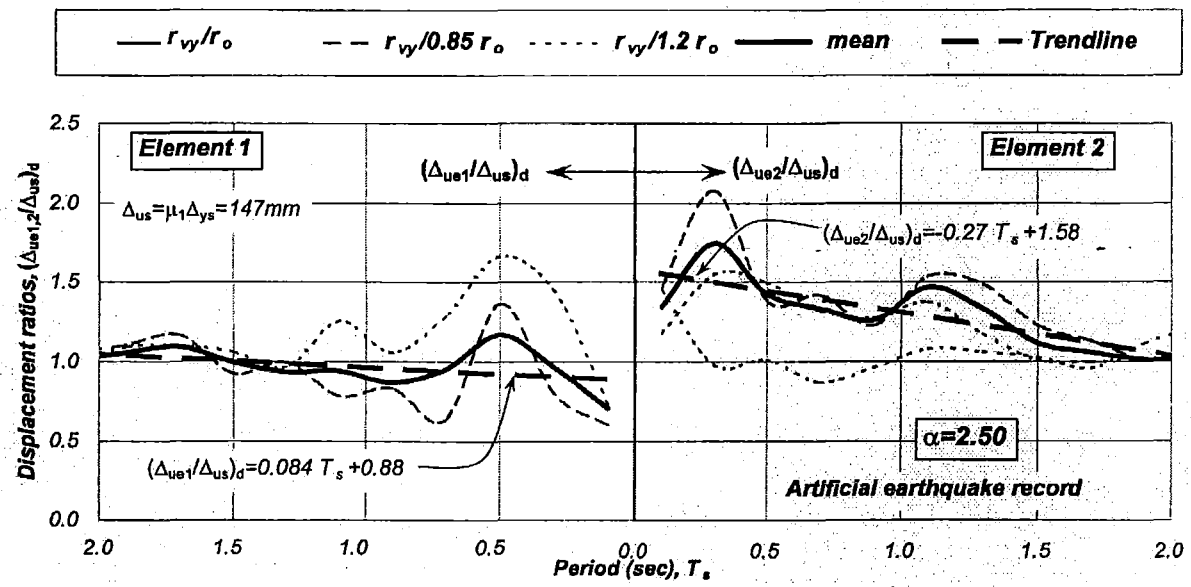

(b) System 12A(α=2.5)

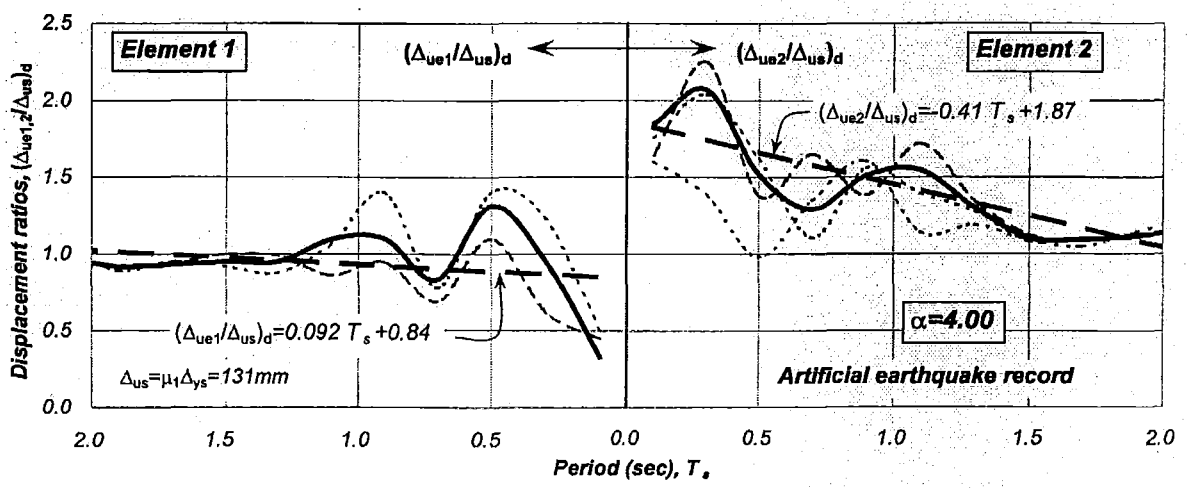

(c) System 12A(α=4.0)

Figure 3-42 Ratios of maximum displacement demands on elements *(1)* and *(2)* and that at the centre of mass of the unrestrained *System 12A(α=variable)* when subjected to the Artificial earthquake record, T_s=variable, e_{mx}=0.0, e_{vx}=0.0, e_{rx}=-variable $\mu_{\Delta 1}=\mu_{\Delta 2}$=5.00, $\mu_{\Delta s}$=variable, r_m/r_o=1.00, r_{vy}/r_m=variable

distribution of strength and mass. However, its effect is not considered significant for the suggested design strategy. Hence, the use of a mean curve is suggested for the three curves of r_{vy}/r_m ratio. These curves clearly reflect the effect of the uncoupled translational period and the $\alpha=\Delta_{ye2}/\Delta_{ye1}$ ratio(or the stiffness eccentricity associated with zero strength eccentricity) on the response.

It is evident from Figure 3-42 that the ratio of displacement demands for element *(1)*, which is the element located on the same side as the centre of stiffness (relative from the centre of mass), varies over the translational period range. A ratio of less than unity indicates that maximum displacement demands on element *(1)* were smaller than that at the centre of mass. This response is a function of the $\alpha=\Delta_{ye2}/\Delta_{ye1}$ ratio and uncoupled translational period of free vibration of T_s less than *0.7* seconds.

Figure 3-42 also shows that the ratio of displacement demands associated with element *(2)* $(\Delta_{ue2}/\Delta_{us})_d$ was larger than unity and hence more sensitive than that associated with element *(1)*, i.e., $(\Delta_{ue1}/\Delta_{us})_{d(CR)}$. In spite of such behaviour, the response of element *(2)* was not an issue because its displacement ductility capacity, associated with the strain limit of the materials, was never exceeded. However, care should be taken, as explained in Section 3.10.1, when the displacement capacity of the flexible element *(2)* is substantially reduced to comply with displacement limits associated with specific performance criteria. In that case, the displacement capacity of element *(2)* may be reached before that of element *(1)*. This indicates that element *(2)* is critical and, therefore, it may limit even further the system displacement ductility capacity.

The trend lines of the mean ratios of maximum displacement demand curves of elements *(1)* and *(2)* are shown in Figure 3-42, and plotted again in Figure 3-43, as a function of the uncoupled translational period and the stiffness eccentricity associated with zero strength eccentricity. These displacement ratios may be used, as explained before, to estimate the displacement ductility capacity of systems when rotations influence the maximum displacement demands of the elements.

To identify which element will govern the estimate of the system displacement ductility capacity, the ratio of the predicted displacement demands of elements *(1)* and *(2)*, i.e., $(\Delta_{ue2}/\Delta_{ue1})_d$. may be used, as shown in Figure 3-44. This ratio should then be compared with that of the estimated displacement capacities, i.e., $(\Delta_{ue2}/\Delta_{ue1})_c$. The subscript "c" refers to capacity quantities. If $(\Delta_{ue2}/\Delta_{ue1})_d > (\Delta_{ue2}/\Delta_{ue1})_c$ then element *(1)* is critical and hence will govern the estimate of the system displacement capacity. Displacement demands on element *(1)* are likely to reach its displacement capacity whereas those of element *(2)* will always be smaller. In contrast, element *(2)* will govern when $(\Delta_{ue2}/\Delta_{ue1})_d < (\Delta_{ue2}/\Delta_{ue1})_c$.

The suggested design approach is better explained with the aid the unrestrained *System 12A(α=2.5)* shown in Figure 3-35(b). The nominal yield displacement of the elements is $\Delta_{ye1}=29mm$ and $\Delta_{ye2}=73mm$. The nominal yield displacement of the system of $\Delta_{ye1}=42mm$ was determined with Eq 2-34 after a unit base shear was distributed among the elements to satisfy zero strength eccentricity. Due to differences in the nominal yield displacement of the elements, the system has, for zero strength eccentricity, a stiffness eccentricity of $e_{rx}=0.21D$. The system strength, distributed among the elements to satisfy zero strength eccentricity, was adjusted to achieve an uncoupled translational period of $T_s=0.5$ seconds. The displacement ductility capacity of the elements, as restricted by the strain limit of the materials, is $\mu_{\Delta 1}=\mu_{\Delta 2}=5.0$. Hence,

the displacement capacity of the elements are $(\Delta_{ue1})_c=\mu_{\Delta 1}x\Delta_{ye1}=145mm$ and $(\Delta_{ue2})_c=\mu_{\Delta 2}x\Delta_{ye2}=365mm$. The ratio of displacement capacities is $(\Delta_{ue2}/\Delta_{ue1})_c=2.50$.

Element *(1)* is critical because the predicted ratio of element displacement demands of $(\Delta_{ue2}/\Delta_{ue1})_d=1.52$, obtained from Figure 3-44 for a stiffness eccentricity of $e_{rx}=0.21D$ and an uncoupled translational period of $T_s=0.5$ seconds, is smaller than the ratio of displacement capacities ($(\Delta_{ue2}/\Delta_{ue1})_c=2.50$). Hence, element *(1)* will restrict the displacement ductility capacity of the system.

With the aid of Figure 3-43 it is possible to obtain the predicted displacement demands ratios for elements *(1)* and *(2)* relative to that at the centre of mass, i.e., $(\Delta_{ue1}/\Delta_{us})_d$ and $(\Delta_{ue2}/\Delta_{us})_d$, respectively. For this particular system with a stiffness eccentricity of $e_{rx}=0.21D$ and an uncoupled translational period of $T_s=0.5$ seconds, the predicted ratio of maximum displacement demand of the elements to that at the centre of mass are $(\Delta_{ue1}/\Delta_{us})_d=0.92$ and $(\Delta_{ue2}/\Delta_{us})_d=1.40$. This is summarized in Figure 3-35(b).

The displacement capacity of the unrestrained *System 12A(α=2.5)*, shown in Figure 3-35(b), may be readily obtained with the predicted ratio of displacement demand for the critical element *(1)* of $(\Delta_{ue1}/\Delta_{us})_d=0.92$ and by assuming that the maximum displacement demand expected on this element will be the same as its displacement capacity, i.e., $(\Delta_{ue1}/\Delta_{us})_d=(\Delta_{ue1}/\Delta_{us})_c$. By rearranging the terms, the displacement capacity of the system is then $(\Delta_{us})_c=(\Delta_{ue1})_c/(\Delta_{ue1}/\Delta_{us})_d=145/0.92=158mm$ and its displacement ductility capacity is $\mu_{\Delta s}=(\Delta_{us})_c/\Delta_{ys}=158/42=3.76$.

The maximum displacement demand expected to develop on element *(2)* may be obtained with its predicted ratio of element displacement demand to that at the centre of mass of $(\Delta_{ue2}/\Delta_{us})_d=1.40$ derived from Figure 3-43. Hence the maximum displacement demand of element *(2)* is $(\Delta_{ue1})_d=1.4(\Delta_{us})_c=1.4*158=221mm$ which is far less than its capacity of $(\Delta_{ue2})_c=365mm$. The predicted displacement demands, denoted with shaded circles and joined by a solid line, are maxima not reached simultaneously. The displacement capacity of the elements (as limited by the strain limit of the materials) is denoted with filled squares. It is observed that the displacement capacity of the system is slightly larger than the displacement capacity of element *(1)* and not the same as it is initially assumed; see Figure 3-35(a).

Consider the other situation shown in Figure 3-35(c), when the displacement capacity of element *(2)* is restricted to $(\Delta_{ue2})_c=175mm$ to comply with displacement limits associated with specific performance criteria. The ratio of element displacement capacities is reduced to $(\Delta_{ue2}/\Delta_{ue1})_c=1.21$ and the displacement ductility capacity of element *(2)* is also reduced to $\mu_{\Delta 2}=175/73=2.40$. The predicted ratios of maximum displacement demand ratios of elements *(1)* and *(2)* to that at the centre of mass remain the same, i.e., $(\Delta_{ue1}/\Delta_{us})_d=0.92$ and $(\Delta_{ue2}/\Delta_{us})_d=1.40$. The only change from the situation shown in Figure 3-35(b) is that element *(2)* rather than element *(1)* is critical because $(\Delta_{ue2}/\Delta_{ue1})_d=1.52>(\Delta_{ue2}/\Delta_{ue1})_c=1.21$. Hence, element *(2)* will restrict the displacement capacity of the system.

The displacement capacity of the unrestrained *System 12A(α=2.5)*, shown in Figure 3-35(c), may be readily obtained with the predicted ratio of displacement demand for the critical element *(2)* of $(\Delta_{ue1}/\Delta_{us})_d=1.40$ and by assuming that the maximum displacement demand expected on this element will be the same to its displacement capacity, i.e., $(\Delta_{ue2}/\Delta_{us})_d=(\Delta_{ue2}/\Delta_{us})_c$. The

displacement capacity of the system is then $(\Delta_{us})_c=(\Delta_{ue2})_c/(\Delta_{ue2}/\Delta_{us})_d=175/1.40=125mm$ and its displacement ductility capacity is further reduced to $\mu_{\Delta s}=(\Delta_{us})_c/\Delta_{ys}=125/42=2.98$.

The maximum displacement demand expected to develop on element *(1)* may be obtained with its predicted ratio of element displacement demand to that at the centre of mass of $(\Delta_{ue1}/\Delta_{us})_d=0.92$ derived from Figure 3-43. Hence the maximum displacement demand of element *(1)* is $(\Delta_{ue1})_d=0.92(\Delta_{us})_c=0.92*125=115mm$ which is far less than its capacity of $(\Delta_{ue1})_c=145mm$. It is seen from Figure 3-35(c) that the displacement capacity of the system is smaller than the displacement capacity of element *(2)* and that of element *(1)*. This indicates that limiting the displacement capacity of the system to that of element *(1)*, as it was suggested before, will not prevent element *(2)* from exceeding its displacement capacity.

The displacement capacity of multi-element systems may be readily estimated in a similar fashion as already explained for two-element systems. It was found that the displacement demand ratios for the outermost elements of multi-element systems are similar to those of equivalent two-element systems. However, it is necessary to identify first which of two specific elements within multi-element systems will limit its displacement capacity. One of such elements is that having the smallest displacement capacity while the other is the outermost element on the flexible side of the system. They are denoted as elements *(1)** and *(2)** to be consistent with the nomenclature previously used. Their location relative to the centre of mass is x_1*/D and x_2*/D where "D" is the distance between the outermost elements.

The predicted displacement demand ratios to be used for elements *(1)** and *(2)** are derived from an equivalent two-element system having similar properties of uncoupled translational period of free vibration and stiffness eccentricity associated with zero strength eccentricity. The displacement demand ratios for the outermost elements of multi-element systems are similar to those of equivalent two-element systems. The ratio of maximum displacement demand for any inner element may be predicted by linear interpolation in proportion to the location of the inner elements from the centre of mass. Subsequently, the same procedure explained before for deriving the displacement ductility capacity of two element systems is followed to estimate the displacement ductility capacity of any multi-element system.

3.11 Preliminary estimate of the nominal strength of unrestrained systems

The system strength should be estimated before its stiffness because, as explained in Section 2.8.1, stiffness is strength dependant. This approach is opposite to current design where the stiffness of components and elements has been considered a geometric property independent of strength. The system strength may be obtained with design spectra using either force or displacement based design methods and a displacement ductility factor matching the displacement ductility capacity of the system.

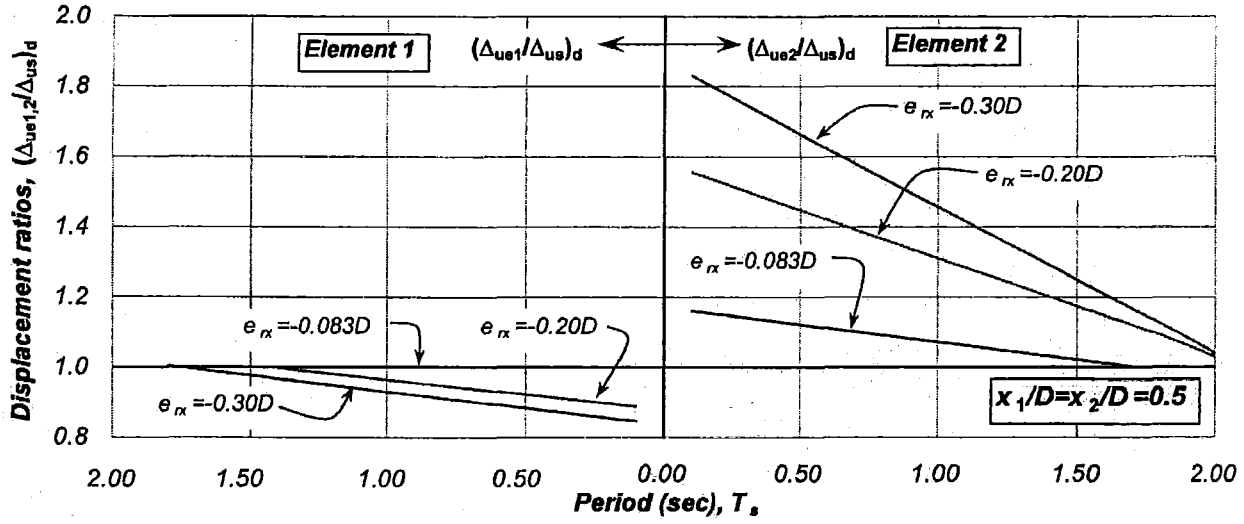

Figure 3-43 Results of predicted ratios of maximum displacement demands of element *(1)* and *(2)* and at the centre of mass of the unrestrained *System 12A(α=variable)* when subjected to the Artificial earthquake record, T_s=variable, e_{mx}=0.0, e_{vx}=0.0, e_{rx}=-variable $\mu_{\Delta 1}=\mu_{\Delta 2}$=5.00, $\mu_{\Delta s}$=variable, r_m/r_o=1.00, r_{vy}/r_m=variable.

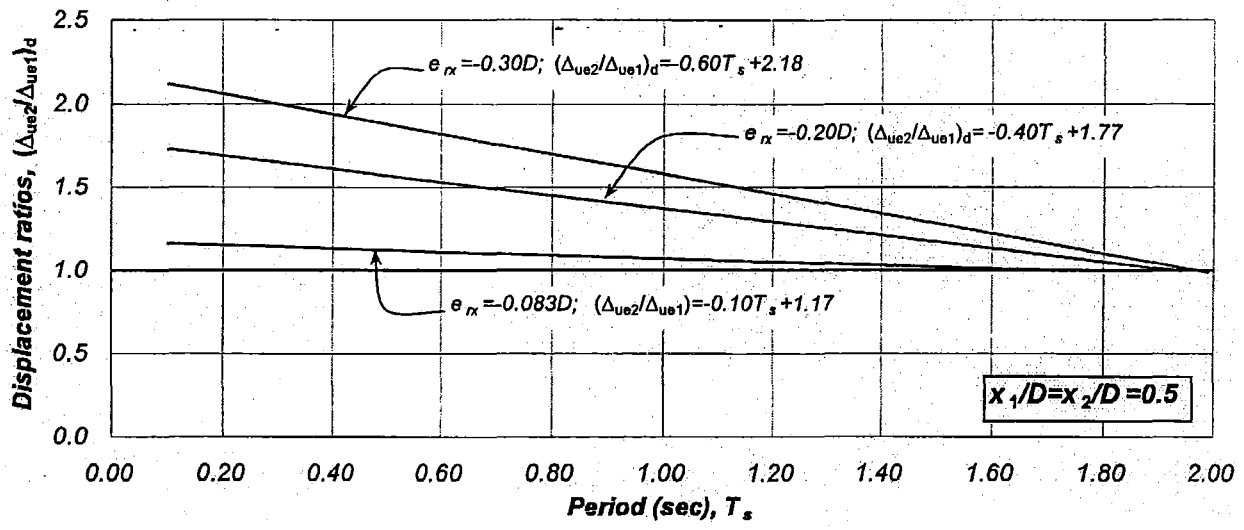

Figure 3-44 Results of predicted ratios of maximum displacement demands of elements *(1)* and *(2)* of the unrestrained *System 12A(α=variable)* when subjected to the Artificial earthquake record, T_s=variable, e_{mx}=0.0, e_{vx}=0.0, e_{rx}=-variable $\mu_{\Delta 1}=\mu_{\Delta 2}$=5.00, $\mu_{\Delta s}$=variable, r_m/r_o=1.00, r_{vy}/r_m=variable.

It has been shown, however, that the system displacement ductility capacity is a function of the uncoupled translation period and the stiffness eccentricity. These properties are unknown at this stage, and therefore, in an attempt to derive this essential property, it is suggested to limit the displacement capacity of the system to that of the element having the smallest displacement capacity, as Figure 3-35(a) shows. This is based on the assumption that the maximum displacement demand on the elements and at the centre of mass is the same and a maximum for zero strength eccentricity.

The displacement ductility capacity of unrestrained systems associated with zero strength eccentricity is initially expressed as

$$\mu_{\Delta s} = \frac{\Delta_{us}}{\Delta_{ys}} = \frac{(\mu_{\Delta i}\Delta_{yei})_{\min}}{\Delta_{ys}} \quad (3\text{-}3)$$

where $(\mu_{\Delta i}\Delta_{yei})_{min}$ is the displacement capacity of the element with the smallest displacement capacity.

Subsequently, the system strength may be estimated, in accordance with, for example, current force-based design methods, by considering design acceleration spectra and a displacement ductility factor equal to the displacement ductility capacity of the system. The strength so obtained should then be distributed on the element to satisfy zero strength eccentricity. One or two iterations may be required to obtain the system strength. An example of this approach is given in Appendix D.

The stiffness of elements and that of the system is readily derived once the system strength is distributed to the elements to satisfy zero strength eccentricity. The element stiffness is obtained with its assigned strength and nominal yield displacement. The system stiffness, along a given direction, is simply the summation of stiffness of the parallel elements (Eq 2-33). The uncoupled translation period and stiffness eccentricity of the system associated with zero strength eccentricity are then readily estimated.

3.12 Estimate of the displacement ductility capacity of torsionally unrestrained systems

It has been shown however, that the system displacement ductility capacity may be affected by system rotations since maximum displacement demand of elements may increase or reduce due to rotation-induced displacements additional to system translations. The effect of system rotations on the maximum response of the elements has been shown to be a function of the $\alpha=\Delta_{ye2}/\Delta_{ye1}$ ratio (or stiffness eccentricities associated with zero strength eccentricity) and the uncoupled translational period of free vibration of unrestrained systems.

The effect of system rotations on the maximum displacement demands of the elements may be accounted for in seismic design by identifying the critical element within the system which is expected to limit the displacement capacity of the system, as already explained in Section 3.10.2. The system displacement ductility capacity may be readily obtained with predicted ratios of element displacement demands and that at the centre of mass, as those shown in Figure 3-43, for the corresponding $\alpha=\Delta_{ye2}/\Delta_{ye1}$ ratio (or estimated stiffness eccentricity associated with zero strength eccentricity) and the uncoupled translational period derived before.

The displacement ductility capacity of the system, as influenced by system rotations, may be obtained with either of the following expressions once the critical element in the system has been identified.

$$\mu_{\Delta s} = C_1 \frac{\mu_{\Delta 1}\Delta_{ye1}}{\Delta_{ys}} \quad (3\text{-}4)$$

or

$$\mu_{\Delta s} = C_2 \frac{\mu_{\Delta 2}\Delta_{ye2}}{\Delta_{ys}} \quad (3\text{-}5)$$

where C_1 and C_2 are coefficients associated with the displacement capacity of element *(1)* and *(2)* and obtained with the following expressions,

$$C_1 = \frac{1}{2\left(\frac{x_1}{D}\right)\left(\frac{\Delta_{ue1}}{\Delta_{us}}\right)_d} \quad \text{where } C_1 \geq 1.0 \tag{3-6}$$

$$C_2 = \frac{1}{2\left(\frac{x_2}{D}\right)\left(\frac{\Delta_{ue2}}{\Delta_{us}}\right)_d} \quad \text{where } C_2 \leq 1.0 \tag{3-7}$$

where x_1 and x_2 are the distances of elements *(1)* and *(2)* from the centre of mass.

The aim of coefficients C_1 and C_2 is to reduce or increase the displacement capacity of the critical element "*i*" within the system, $\mu_{\Delta s}\Delta_{yei}$, by the corresponding factor "C_i" to estimate the system displacement capacity. These coefficients are a function of the ratio of maximum displacement demand predicted for the critical element and its distance from the centre of mass. They take into account the fact that elements *(1)* and *(2)* may not be equidistant from the centre of mass. Hence the torsional response of similar unrestrained systems with or without mass eccentricity may be essentially the same; however, their displacement ductility capacity will be different since the predicted ratios of displacement demands, see Figure 3-43, are for outermost elements equidistant from the centre of mass.

For instance, the critical element of the unrestrained *System 12A(α=2.5)* shown in Figure 3-35(b), is element *(1)*. According to Eq. 3-6, the coefficient C_1 for such system is $C_1=1/(2*0.5*0.92)=1.09$. The system displacement ductility capacity according to Eq 3-4 is $\mu_{\Delta s}=1.09*(5.0*29)/42=3.76$ which is equivalent to that derived in Section 3.10.2. In case of the unrestrained *System 12A(α=2.5)* shown in Figure 3-35(c), element *(2)* is critical. The coefficient C_2 is $1/(2*0.5*1.40)=0.714$. The displacement ductility capacity of the system according to Eq. 3-5 results to be $\mu_{\Delta s}=0.714*175/42=2.98$ which is equivalent to that derived in Section 3.10.2.

In case of multi-element systems, it is necessary to identify elements *(1)** and *(2)**, as defined in Section 3.10.2 to estimate, in a similar fashion, its displacement and ductility capacity.

It is recommended to recalculate the system strength using a ductility factor matching the newly derived system ductility capacity if a significant difference arises between the displacement ductility capacity of the system estimated above and that initially derived in Section 3.11.

3.13 Summary of the response of torsionally unrestrained systems

The main findings relevant to the response of torsionally unrestrained systems designed with the proposed design strategy are:

1. The proposed design strategy limits the maximum displacement demands of elements to less than the maxima established for zero strength eccentricity and less than the displacement

capacity of the elements if strength eccentricities are associated with an increase of system strength. This increase of strength is expected to reduce the displacement demand at the centre of mass to compensate for the rotation-induced displacements of the critical element, additional to those resulting from system translations; hence its displacement capacity is not exceeded. See Sections 3.3.1, 3.3.5, 3.4, 3.5.1, 3.5.10, 3.6, 3.8.1 and 3.9.1.

2. The suggested distribution of strength to the elements ensures a satisfactory torsional performance of systems with reduced displacement ductility capacity. It was found that their torsional response is less critical as the displacement capacity of the system is reduced. See Section 3.5.7.

3. Although the torsional response of asymmetric systems is sensitive to the frequency contents characteristics of the earthquake record, the proposed design strategy is considered satisfactory to prevent elements from exceeding their displacement ductility capacity. See Section 3.5.8.

4. Torsional mechanisms of asymmetric systems generated by static or dynamic-induced forces differ due to the mass rotational inertia. The mass rotational inertia restricts system rotations expected from increasing strength and associated stiffness eccentricities. See Sections 3.3.1, 3.3.2, 3.3.5, 3.5.1, 3.5.2, 3.7, 3.8 and 3.9.

5. The displacement demands of the elements in a system, where its strength is distributed to satisfy zero strength eccentricity, are significantly influenced by system rotations originated from changes to the $\alpha=\Delta_{ye2}/\Delta_{ye1}$ ratio (i.e., changes to the stiffness eccentricity associated with zero strength eccentricity) and the uncoupled translational period of free vibration. The displacement demands of the elements of such systems may be restricted to less than their displacement capacity by estimating the displacement and ductility capacity of the system for zero strength eccentricity. See Sections 3.5.9 and 3.10.

6. Displacement demands of elements are influenced by the increase or reduction of torques and rotations as they are affected by changes in the distribution of strength and uniformly distributed mass of the system. This effect is well quantified by the ratio of radii of gyration of element nominal strength and uniformly distributed mass, i.e., the r_{vy}/r_m ratio, where $r_{vy}/r_m=1.0$ is used as a reference quantity. It was found that the reduction of the r_{vy}/r_m ratio due to an increase in the radius of gyration of mass, for a constant radius of gyration of strength, reduces system rotations. On the other hand, the reduction of the r_{vy}/r_m ratio by changing both the radii of gyration of strength and mass increases system rotations. Despite this contradictory behaviour, it was found in both situations that the effect of system rotations on the maximum displacement demand of the elements relative to the demand expected at the centre of mass reduces. This indicates that the effect of system rotations on the element responses becomes negligible for systems having $r_{vy}/r_m<0.90$. The maximum displacement demand of the elements becomes similar to that at the centre of mass and hence the system may be treated as a single degree of freedom system. See Sections 3.3.1, 3.5.1, 3.5.3, 3.5.4 and 3.5.5.

7. Although system rotations may have an important effect on the displacement demands of the elements, the maximum rotation of the system is not associated with the maximum displacement demands of the elements. Contrary to general belief, significant torques and rotations may be accepted in structural design. This is possible as long as the displacement

demands of the elements do not exceed their displacement capacity. See Section 3.3.3 and 3.5.6.

8. The sense of system rotation may be controlled by changing the distribution of systems strength, i.e., modifying the strength eccentricity. Changes in strength eccentricity may, however, be achieved for a limited range due to physical limitations of the elements and/or codified requirements of minimum reinforcement. An optimal condition arose when the distribution of system strength is such that the centre of mass is located halfway between centres of strength and stiffness. In such situation, the system rotation is negligible. This feature is independent of the number; location and nominal yield displacement of the elements. It is, however, an ideal distribution of strength difficult to achieve in practice. See Section 3.5.1.

9. Differences of predicted displacement demands for systems where the elements are modelled with different hysteretic models are not significant. This result suggests that conclusions derived from systems where the elements are modelled with a simple bilinear force-displacement relationship should also be valid for most common structural systems when considering displacements demands due to torsional behaviour. See Section 3.3.4.

10. The maximum displacement demands of the elements of unrestrained systems associated with zero strength eccentricity may be separated as the result of a system displacement and a torsion-induced displacement component:

    - The system displacement component is associated with the maximum displacement demand at the centre of mass. It was found that the response of torsionally unrestrained systems with two or more parallel elements may be satisfactorily predicted with an equivalent single degree of freedom system having the same translational properties of strength and nominal yield displacement. This simplified model may be used to predict the response of ductile systems having, for zero strength eccentricity, stiffness eccentricities as large as $e_r<0.20D$. The accuracy of the simplified model's prediction reduces on systems having uncoupled translational periods of $T_s<0.70$ seconds. The response prediction also reduces as the $\alpha=\Delta_{ye2}/\Delta_{ye1}$ ratio (or stiffness eccentricity associated with zero strength eccentricity) is increased. See Sections 3.3.6, 3.5.1, 3.5.9 and 3.10.

    - The maximum displacement demands of the elements relative to that predicted at the centre of mass may be estimated with the predicted ratios of maximum displacement demands of the elements and that at the centre of mass. These displacement demand ratios are a function of the $\alpha=\Delta_{ye2}/\Delta_{ye1}$ ratio (or stiffness eccentricity associated with zero strength eccentricity) and uncoupled translational periods. See Section 3.10.

11. The displacement capacity of multi-element systems may be estimated with the displacement demand ratios of equivalent two-element systems. For this purpose, it is required to identify two specific elements in the multi-element system of which one is expected to limit its displacement capacity. See Sections 3.8 and 3.9.

12. There is no need to differentiate between the torsional response of two and multi-element systems. The response of multi-element systems can be predicted from that of a simple two-element system having similar characteristics of uncoupled translational period, stiffness eccentricity associated with zero eccentricity and r_{vy}/r_m ratio. See Sections 3.8 and 3.9.

13. No differentiation is required between systems with or without mass eccentricity. Mass eccentricity is not a parameter influencing the torsional response of unrestrained systems. However, the displacement capacity may not be the same for unrestrained systems with or without mass eccentricity. See Sections 3.4 and 3.6.

14. The response of extremely eccentric systems is quite sensitive and difficult to predict with simplified models. The actions of the mass rotational inertia have a major effect on the translational displacements at the centre of mass. These types of system, and even less severe ones, should be avoided. Special consideration should be given to possible large displacement demands at the system's flexible side, which may exceed allowable drift limits and hence non-structural damage is to be expected. See Section 3.7.

3.14 Design of torsionally unrestrained systems

For the design of torsionally unrestrained systems, it is suggested to:

1. Estimate the displacement and ductility capacity of the system associated with zero strength eccentricity. Identify the critical element of the system expected to restrict the displacement capacity. This critical element may be found by using the predicted ratios of displacement demand of elements and that at the centre of mass obtained from an equivalent two-element system. These displacement ratios consider the effect of rotations on the displacement demand of the elements.

2. The system strength to be eventually assigned to its elements limiting the centre of mass displacement demands to less than its displacement capacity may be obtained with the design response spectra of a single degree of freedom system. This strength should be distributed on the elements to achieve the reference zero strength eccentricity which may be difficult to be achieved in practice.

3. A strength eccentricity may be introduced to the system provided they result from one or more elements having strength in excess of the reference distribution of system strength described above satisfying zero strength eccentricity. This will result in an increase of system strength.

It was shown that this design strategy is successful in limiting the maximum displacement demand of elements to less than their displacement ductility capacity for zero and increasing strength eccentricities. It is valid for systems with different r_{vy}/r_m ratios, uncoupled translational periods of free vibration and reduced ductility capacities even when subjected to different earthquake records.

Chapter 4. Torsionally Restrained Systems

4.1 Introduction

During the last two decades, it has been a common practice to study the ductile response of asymmetric systems by using simplified models where transverse elements, providing torsional restraint, were neglected. This is because it is assumed that transverse elements are yielding most of the time due to the transverse component of the ground motion and hence they make no contribution to torsional resistance. These systems, already examined in Chapter 3, were termed as torsionally unrestrained. Such simple models, when subjected to unidirectional ground motion, are considered to provide a critical torsional response [C8].

Models with transverse elements providing torsional restraint have also been examined in the past [H2,R2,F1,D4,D3,G1,D1,C5]. These models, termed in this study as torsionally restrained, are considered more realistic because transverse elements are not necessarily yielding at all times and may generate a critical response; a consideration not agreed upon by other researchers[C8]. It is accepted, however, that these systems should be analysed considering the multi-directional characteristics of ground motions [C8].

To complete the study on the torsional response of asymmetric systems, this chapter examined the torsional response of restrained systems when they are designed with the proposed design strategy already described in Section 2.11. They will be subjected to earthquake records along different directions. No consideration was given to seismic design provisions for torsion of a particular building code. Torsionally restrained systems with one or more elements along the *Y*-direction were examined. Torsional restraint was provided by two equidistant *X*-direction elements located at specific locations within the floor plan. Systems displayed different plan configurations and distribution of elements.

Based on the suggested design strategy, the aim of this chapter was to examine those same objectives already listed in Section 3.1 for unrestrained systems and also to: (a) assess the effect of their transverse elements and the significance of their torsional restraint, (b) compare the response of the restrained systems with their unrestrained counterparts to detect which system leads to larger response, (c) provide a better understanding of the torsional mechanism involved in torsionally restrained systems and (d) examine if the torsional response of restrained systems subjected to earthquake records at different angles is critical in comparison to that due to unidirectional earthquake input along the principal axes.

The parameters considered, besides those already mentioned in Section 3.1, to affect torsional response were: the direction of application of the earthquake record and the degree of torsional restraint provided by the transverse elements.

4.2 General considerations for the analysis of restrained systems

To be consistent with those unrestrained systems examined in Chapter 3, the displacement ductility capacity of the restrained systems, along their *X* and *Y*-axes, was also assumed to be the same as that of the *Y*-direction elements, i.e., $\mu_{\Delta s}=5.35$, unless stated otherwise and is independent of their nominal yield displacement. This is a probable assumption in routine design. However, it was uncertain if the displacement ductility capacity of the elements will be,

or not be exceeded. The displacement capacity of the system is assumed to be restricted by the strain limits of the materials.

The Artificial, Bucharest and Kobe earthquake records, already scaled to impose on the unrestrained systems having $r_{vy}/r_m=1.0$ a maximum displacement ductility demand equal to the system capacity, were also applied, without further modifications, to the restrained systems. These records were applied along the reference *Y*-axis and at different orientations to the *Y*-axis. This simple approach will help identify the effect of the transverse elements on the torsional response.

4.3 Two- element structurally asymmetric *System 3B* (*CV≠CR; CM=GC*)

4.3.1 Response of the restrained *System 3B-1.3(α=1.4)*

This section examines the seismic torsional response of a two-element asymmetric system designed with the suggested design strategy described in Section 2.11. The aim is to verify if the proposed design method is able to limit displacement demands on elements under their displacement capacity and to assess the effect of transverse elements providing torsional restraint on the system response.

The torsionally restrained *System 3B*, shown in Figure 2-27(b), was considered. It had the same physical characteristics of its unrestrained counterpart *System 3A*. The only difference was the addition of two *X*-direction elements, equidistant from the centre of mass, providing torsional resistance. The nominal yield displacement of the system is the same along the *X* and *Y*-direction, $\Delta_{ys}=42mm$. The strength of the system was adjusted to generate an uncoupled translational period of free vibration of $T_s=1.30$ seconds along both axes. It had a ratio of element nominal yield displacement of $\alpha=\Delta_{ye2}/\Delta_{ye1}=1.40$. It was denoted restrained *System 3B-1.3(α=1.4)*. Section 2.18.1 described in detail its characteristics and Appendix *B* summarizes its properties. The general procedure explained in Section 4.2 was used for the analysis of the system.

The system torsional response, as affected by the r_{vy}/r_m and r_{vx}/r_{vy} ratios, was examined. As stated in Section 2-13, the r_{vy}/r_m ratio quantifies the effect of the mass rotational inertia on the response of systems. The contribution of strength by the *X*-direction elements to the radius of gyration of element nominal strength was not included due to the reasons to be provided in Section 4.3.8. The r_{vx}/r_{vy} ratio quantifies, on the other hand, the contribution of the *X*-direction elements to torsional restraint relative to that contributed by the *Y*-direction elements.

The design strategy suggested in Section 2.11 stated that the system nominal strength, once distributed among elements to satisfy static equilibrium, i.e. $e_{vx}=0.0$, should, at maximum response, prevent displacement ductility capacity of any element being exceeded. Although zero strength eccentricity may not be achieved in practice, it is important because it is then that the system attains a maximum response. Hence, the system displacement capacity should be associated with such idealised distribution of strength.

Table 4-1 summarizes the response for zero strength eccentricity. The maximum displacement demand of elements *(1)* and *(2)* and at the centre of mass was essentially the same. It is seen that the *X*-direction elements *(3)* and *(4)* remained elastic and restrained system rotations. The torsional response was essentially unaffected by the r_{vy}/r_m ratio because the rotational mass was barely mobilised due to the small rotations experienced by the system. It is also evident that the

response at the centre of mass was predicted well by an equivalent single degree of freedom system having the same translational properties as that of the restrained system.

Table 4-1. Response of the restrained *System 3B-1.3* (α=*1.4*) subjected to the Artificial earthquake record, T_s=1.30 sec, e_{vx}=0.0, e_{rx}=-0.083D, $\mu_{\Delta s}$=*5.35*, r_m/r_o=1.0, r_{vy}/r_m=variable

	Displacements, mm, and displacement ductility demands,(μ)				
r_{vy}/r_m	*E1*	*CM*	*E2*	*ESDOF*	*E3=E4*
$r_{vy}/0.85r_o$	*236(6.56)*	*231(5.49)*	*225(4.46)*	*225(5.35)*	*10(elastic)*
r_{vy}/r_o =*1.00*	*233(6.48)*	*228(5.42)*	*223(4.42)*	"	*13(elastic)*
$r_{vy}/1.20r_o$	*224(6.22)*	*226(5.38)*	*229(4.54)*	"	*17(elastic)*

Table 4-1 also records different displacement ductility demands of elements *(1)* and *(2)* due to their different nominal yield displacements. As expected, element *(1)*, having the smallest nominal yield displacement, was the critical element. It exceeded, for every r_{vy}/r_m ratio, its displacement ductility capacity of $\mu_{\Delta s}$=*5.35*. To overcome this, the system displacement capacity and hence its displacement ductility capacity should be reduced, as subsequently explained.

The system displacement capacity should be limited to that of the element having the smallest displacement capacity. This is because the maximum displacement demands of elements and at the centre of mass was essentially the same for zero strength eccentricity even though the system exhibited rotations. In this particular example, the system displacement capacity should then be limited to that of the critical element *(1)*, i.e., $\Delta_{us}=\mu_{\Delta 1}\Delta_{ye1}$=*193mm*. Hence, the system displacement ductility capacity should be reduced to $\mu_{\Delta s}=\Delta_{us}/\Delta_{ys}$=*193/42=4.60*, which is expected to prevent critical element *(1)* from exceeding its displacement ductility capacity of $\mu_{\Delta 1}$=*5.0* whereas the displacement ductility capacity of element *(2)* is not fully used.

The fact that the displacement capacity of the restrained *System 3B-1.3*(α=*1.4)* was based on the response due to unidirectional earthquake input rather than multidirectional excitations may be a point for discussion. The latter is a more probable situation to occur in actual buildings. It is, therefore, necessary to assess if the response of systems subjected to a multidirectional earthquake record input may generate a critical response relative to that due to unidirectional earthquake input along the *Y*-axis. This issue will be examined in Section 4.3.4.

Strength eccentricities, which are the cause of rotations in ductile systems, may be accepted provided that they result from the nominal strength of any element being in excess of that satisfying static equilibrium criterion. Such a strength eccentricity introduces an increase of system strength, as already shown in Figure 2-28.

Figure 4-1 plots the torsional response for increasing strength eccentricities. It is evident that the displacement ductility demands on element *(1)* and at the centre of mass reduced with increasing negative strength eccentricities under the maximum attained for e_{vx}=*0.0*; see Figure 4-1(a) and (c). System rotations, although increasing, were significantly restrained by the elastic *X*-direction elements; see Figure 4-1(d). Element *(2)* also exhibited a reduction in its displacement ductility demands; see Figure 4-1(b). This is because the reduction of displacement demand at the centre of mass, due to an increase of system strength, over-compensated for the small torsion-induced displacements on critical element *(2)*, additional to those resulting from system translations. The r_{vy}/r_m ratio did not show a significant effect on the displacement demands of the *Y*-direction elements *(1)* and *(2)* due to the substantial torsional restraint imposed by the elastic *X*-direction elements *(3)* and *(4)*.

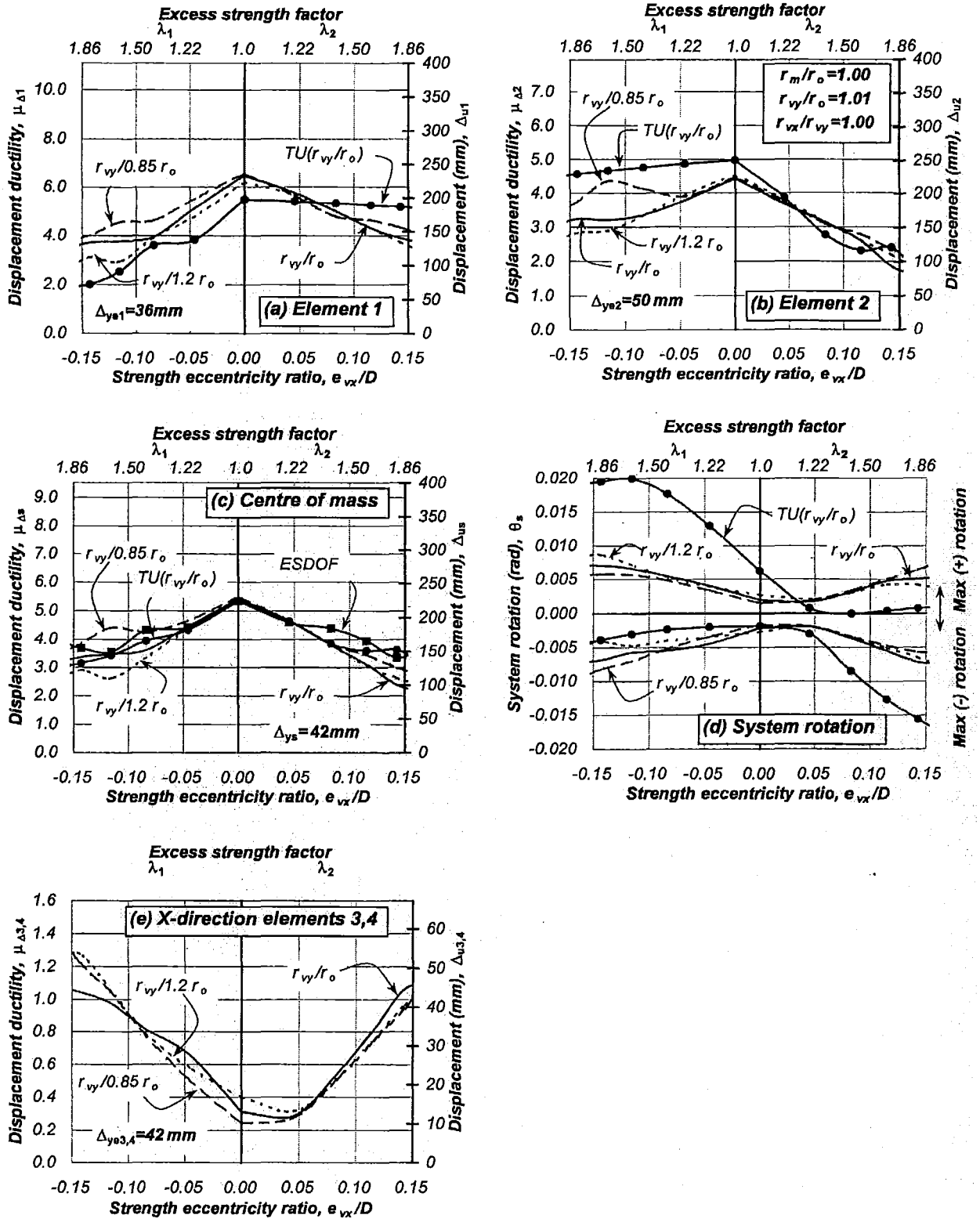

Figure 4-1. Response of the restrained *System 3B-1.3(α=1.4)* subjected to the Artificial earthquake record, T_s=1.30 sec, e_{mx}=0.0, $e_{vx} \neq e_{rx}$=variable, $\mu_{\Delta s}$=*5.35*, r_m/r_o=1.0, r_{vy}/r_m=variable

It is evident from Figure 4-1, that the suggested distribution of strength is overly conservative for restrained systems due to their small system rotations. It is seen that the application of the Artificial earthquake record along the *Y*-direction reduced the displacement demands of the two *Y*-direction elements *(1)* and *(2)* for increasing strength eccentricities. This contrasted with the response of its unrestrained counterpart *System 3A-1.3(α=1.4)*; see Section 3.5.1. This conservative response, however, is expected to change when the system is subjected to ground motions along different directions. This scenario will be examined in detail in Section 4.3.4.

Increasing positive strength eccentricities beyond e_{vx}>+*0.05D* is unrealistic. This is because, although an excess strength may be assigned to element *(2)*, the total strength to be assigned to this element may not be larger than that of element *(1)* if requirements of minimum or maximum reinforcement content are to be satisfied. For instance, element *(1)*, being longer than element *(2)*, will require a larger reinforcement content and hence larger lateral strength to comply with the recommended minimum reinforcement content, hence, it seems unlikely that a large positive strength eccentricity may be introduced to the system. Another scenario not allowing the introduction of a positive strength eccentricity is when an excess strength, relative to that satisfying zero strength eccentricity, cannot be assigned to element *(2)* because the strength of the element already satisfies the recommended ratio of maximum reinforcement content. Results were plotted only for the general clarification of likely trends.

Figure 4-1(e) shows that the *X*-direction elements *(3)* and *(4)* remained elastic up to a negative strength eccentricity of e_{vx}=*-0.12D*. Increasing strength eccentricities beyond this limit caused them to yield due to an increase of system rotations. However, the maximum rotation was not related to the maximum displacement demands of element *(1)* and *(2)*, as to be explained in Section 4.3.2(a). The displacement demands in the *X*-direction were negligibly small and hence non-critical when compared to those expected to arise if the earthquake record is to be applied along the *X*-direction only. Yielding of the *X*-direction elements *(3)* and *(4)* occurred due to a large strength eccentricity which triggered a slight non-critical increase of displacement demands of elements *(1)* and *(2)*.

Figure 4-1(c) shows that the displacement ductility demands of the *Y*-direction elements *(1)* and *(2)* and at the centre of mass, for the different r_{vy}/r_m ratios, were essentially the same for zero and increasing strength eccentricities. This is, as explained before, because the rotational mass was barely mobilised due to the torsional restraint provided by the elastic *X*-direction elements on system rotations. It also shows that an equivalent single degree of freedom system still predicted, with adequate accuracy, the maximum response at the centre of mass for zero and increasing strength eccentricities.

Figure 4-1 also shows the predicted response of the restrained *System 3B-1.3(α=1.4)* along with that of its unrestrained counterpart *System 3A-1.3(α=1.4)*. This comparison illustrates the effects of the *X*-direction elements on the torsional response. The response of the unrestrained *System 3A-1.3(α=1.4)* is identified by curves *TU* associated with r_{vy}/r_m=*1.01*.

It is evident from Figure 4-1(a), (b) and (c) that, for zero strength eccentricity, the displacement ductility demands on the elements and at the centre of mass was a maximum for both the restrained and unrestrained systems. In case of the restrained *System 3B-1.3(α=1.4)*, maximum displacement demands on elements were essentially the same. In such situation, it is possible to develop the displacement ductility capacity of element *(1)* whereas that of element *(2)* cannot be fully utilised. On the other hand, the unrestrained *System 3A-1.3(α=1.4)* shows a smaller displacement on element *(1)* and a larger one on element *(2)* due to the effects of larger system

rotations on the response. In this case, a better use of the displacement ductility capacity of elements *(1)* and *(2)* may be achieved. It is evident that, in some instances, system rotations may be tolerated and even encouraged to make better use of the displacement capacity of the elements in the system.

Figure 4-1(d) also shows that system rotations reached a minimum in both the restrained system and its unrestrained counterpart for a strength eccentricity of $e_{vx} \approx +0.04D$. This is associated with the centre of mass located halfway between the centres of strength and stiffness. The fact that the *X*-direction elements remained elastic during the response did not affect this particular behaviour.

It is evident, from the above findings, that the design strategy may prevent elements from exceeding their displacement ductility capacity if the displacement capacity of the system is limited to that of the element with the smallest displacement capacity. The torsional restraint of the *X*-direction elements reduced substantially system rotations leading to essentially the same displacement demands on elements and at the centre of mass. The mass rotational inertia, as quantified by variations of the r_{vy}/r_m ratio, did not affect the response. The suggested design strategy is, however, conservative when restrained systems are subjected to unidirectional earthquake input along the *Y*-axes. This situation may change when the system is subjected to earthquake records along different directions, as will be shown in Section 4.3.4.

4.3.2 Time history response of the restrained *System 3B-1.3(α=1.4)*

(a) Restrained System 3B-1.3 [e_{vx}=0.0(λ_1=1.0), e_{rx}=-0.083D (α=1.4)]

The time history response was examined to provide a better understanding of the torsional mechanisms involved during dynamic excitation. These mechanisms show the effect of the dynamic actions of the mass translational and rotational inertia on the system response.

The torsionally restrained *System 3B-1.3(α=1.4)* was considered again. The nominal yield displacement of elements *(1)* and *(2)* was $\Delta_{ye1}=36mm$ and $\Delta_{ye2}=50mm$, hence $\alpha=\Delta_{ye2}/\Delta_{ye1}=1.40$. The *X*-direction elements *(3)* and *(4)* had each the same nominal yield displacement of $\Delta_{ye3}=\Delta_{ye4}=42mm$. The nominal yield displacement of the system, along both axes, was $\Delta_{ys}=42mm$. The system strength of $V_{xns}=V_{yns}=176\ kN$ was assigned to the elements to achieve zero strength eccentricity, thus all elements had the same nominal strength, $V_{ne1}=V_{ne2}=V_{ne3}=V_{ne4}=88kN$. The system had a stiffness eccentricity of $e_{rx}=-0.083D$ ($D=12.42m$) due to differences in the nominal yield displacements of the *Y*-direction elements. It was subjected to the Artificial earthquake along the *Y*-direction.

Consider, at first, the torsional mechanism involved due to the application of a static lateral force to the centre of mass. A positive force of $V_E=163kN$ will introduce an anticlockwise rotation due to its negative stiffness eccentricity. Element *(1)* will develop its nominal strength ($V_{ne1}=88kN$) while element *(2)* will remain elastic ($V_{e2}=75kN$). The anticlockwise rotation will trigger the resistance of the *X*-direction elements *(3)* and *(4)* to $V_{e3}=V_{e4}=V_{E^*}e_{rx}/E=6.90kN(E=D=12.42m)$. This base shear is far less than their nominal strength ($V_{ne3}=V_{ne4}=88kN$).

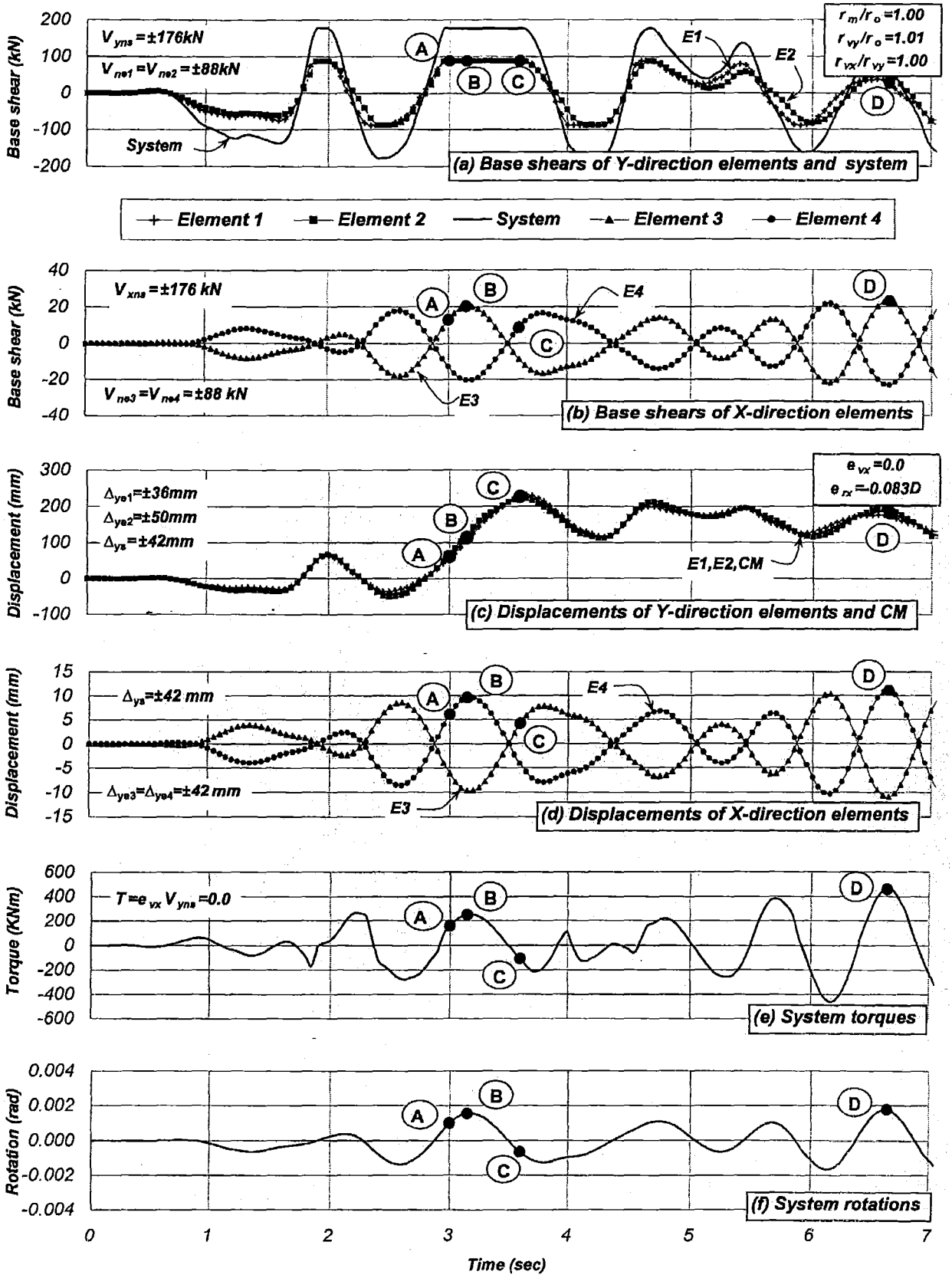

Figure 4-2. Time history response of the restrained *System 3B-1.3* subjected to the Artificial earthquake record, T_s=1.30 sec, e_{mx}=0.0, e_{vx}=0.0 (λ_1=1.0), e_{rx}=-0.083D (α=1.4), $\mu_{\Delta s}$=*5.35*, r_m/r_o=1.0, r_{vy}/r_m=1.01, r_{vx}/r_{vy}=1.0

The time history response showed a different torsional behaviour. It is evident from Figure 4-2(a) that the *Y*-direction elements *(1)* and *(2)* yielded at essentially the same instant *(A)* due to a small clockwise rotation. This is due to the opposition of the *X*-direction elements *(3)* and *(4)* and the rotational mass on system rotations; see Figure 4-2(f). The displacement demands of the *Y*-direction elements and at the centre of mass were essentially the same; see Figure 4-2(c). The system response was essentially that of a single degree of freedom system.

The *X*-direction elements *(3)* and *(4)* also developed at instant *(A)* a small base shear of $V_{e3}=V_{e4}=13kN$; see Figure 4-2(b). Rotations were smaller than those of its unrestrained counterpart *System 3A-1.3(*α*=1.4)*; see also Figure 4-1(d).

Figure 4-2(e) records at instant *(A)*, a system torque of $T=180kNm$ when elements *(1)* and *(2)* reached their nominal strength, rather than zero, as it was the case with its unrestrained counterpart *System 3A-1.3(*α*=1.4)* having zero strength eccentricity; see Figure 3-10. This torque was introduced because the *X*-direction elements *(3)* and *(4)* were still elastic. It is also evident that, although elements *(1)* and *(2)* were yielding, the system torque slightly increased until reaching a peak of $T=250kNm$ at instant *(B)*, see Figure 4-2(e). This torsional behaviour was only possible because the rotational mass still encountered resistance from the elastic *X*-direction elements *(3)* and *(4)* after the *Y*-direction elements yielded. Hence, the rotational mass was further accelerated. The increase in torque and rotation, however, was rather small and the *X*-direction elements remained elastic.

At instant *(B)*, the system reached a peak torque and rotation, as shown in Figure 4-2 (e) and (f). The *X*-direction elements *(3)* and *(4)* were elastic and developed a base shear resistance of $V_{e3}=V_{e4}=20\ kN$; see Figure 4-2(b), whereas the displacement demands of elements *(1)* and *(2)* were inelastic but still below their maximum response. Subsequently, the system decelerated and the torque and rotations reduced. The rotation changed of sign from positive to negative.

Elements *(1)* and *(2)* reached their maximum displacement demands at essentially the same instant *(C)*; see Figure 4-2(c). At this stage, the system torque and rotation were rather small; see Figure 4-2(e) and Figure 4-2(f). This confirms that the element's maximum displacement is not associated with the system maximum rotation. After instant *(C)*, the *X*-direction elements *(1)* and *(2)* become elastic, the system base shear reduced whereas the torque and rotation slightly increased.

Figure 4-2(e) and (f) shows at instant *(D)* that system torques and rotations reached a maximum while the *Y*-direction elements *(1)* and *(2)* were elastic. The base shear of the system was quite small; see Figure 4-2(c). This behaviour confirms that maximum torques and rotations are not relevant factors, which need to be addressed in the design of ductile systems if the displacement capacity of the elements is not exceeded.

The findings described above suggest that the torsional behaviour of restrained systems is essentially the same as those of their unrestrained counterparts. The only difference observed was the slight increase of system torque due to the rotational acceleration introduced after yielding of *Y*-direction elements *(1)* and *(2)*. The torque increased slightly but was not large enough to yield the *X*-direction elements *(3)* and *(4)*. These elements substantially restrained the system rotations; hence the maximum displacement demand reached by the *Y*-direction elements and at the centre of mass was essentially the same.

(b) Restrained System 3B-1.3 [e_{vx}=-0.21D (λ_1=2.4), e_{rx}=-0.27D (α=1.4)]

This section examined again the restrained *System 3B-13(α=1.4)* when element *(1)* had for some reason a *240%* excess strength of that required to satisfy static equilibrium, i.e., V_{ne1}=2.4*88kN=212kN. The strength of the *Y*-direction element *(2)*, and that of *X*-direction elements *(3)* and *(4)* remained unchanged (V_{ne2}=V_{ne3}=V_{ne4}=88kN). It is not a realistic situation; however, it explains why the *X*-direction elements of a system with a large strength eccentricity yielded when it was subjected to unidirectional earthquake input along the *Y*-direction. The excess strength of element *(1)* introduced a strength eccentricity of e_{vx}=-0.21D (D=12.42m) and a *70%* increase of system strength (V_{yns}=300kN). This large strength eccentricity is associated with a stiffness eccentricity of e_{rx}=-0.27D.

Consider, at first, the scenario when a static lateral force is applied to the centre of mass. A positive base shear of V_E=231kN will develop the nominal strength of element *(2)* (V_{e2}=V_{ne2}=88kN) while element *(1)* will attain a base shear of V_{e1}=143kN (<V_{ne1}=212kN). The anticlockwise rotation will also develop a base shear of V_{e3}=V_{e4}=27kN on the *X*-direction elements *(3)* and *(4)*, which is far below their nominal strength (V_{ne3}=V_{ne4}=27kN).

The time history response again showed a different torsional behaviour. The response was examined between *1.80* and *3.50* seconds when the system reached a maximum response. Figure 4-3(a) shows that, in spite of its excess strength, element *(1)* reached its nominal strength, at instant *(A)*, before element *(2)* did. The opposition of the *X*-direction elements and the rotational mass on system rotations enabled this to happen. The system exhibited a peak torque of T=1177kNm while the *X*-direction elements *(3)* and *(4)* were subjected to a base shear of V_{e3}=V_{e4}=14kN. The displacement profile associated with this particular instant; see Figure 4-4(a), shows that the displacement of element *(1)* was slightly larger than that of element *(2)*. Once element *(1)* yielded, the torque reduced in the opposite direction; see Figure 4-3(e), due to the opposition of the rotational mass to system rotations while the system base shear increased; see Figure 4-3(a).

Element *(2)* also yielded at instant *(B)* whereas element *(1)* was again elastic, as Figure 4-3(a) shows. The torque reduced to T=610kN due to the rotational deceleration of the rotatory mass; see Figure 4-3(e). The rotation of the system changed of direction from negative to positive; see Figure 4-3(f). The displacement profile associated with instant *(B)*; see Figure 4-4(b), illustrates that the displacement demand of both elements increased relative to that attained at instant *(A)*, however, the displacement of element *(2)* was slightly larger than that of element *(1)*. Once element *(2)* yielded, systems rotations increased and the system torque eventually changed direction.

Element *(1)* reached again its nominal strength at instant *(C)* due to the opposition of the mass rotational inertia to an anticlockwise rotation, whereas element *(2)* was elastic, as shown in Figure 4-3(a). The displacement demands of the *Y*-direction elements were of opposite sign, as Figure 4-4(c) shows, far from the maxima attained; see Figure 4-3(c). System torques and rotations significantly increased reaching peak values of T=2010kNm and θ_s=0.0036rad. The base shear of the *X*-direction elements *(3)* and *(4)* increased to more than half their nominal strength (V_{e3}=V_{e4}=47kN); see Figure 4-3(b). After element *(1)* yielded, torques and rotations reduced as the rotational mass decelerated.

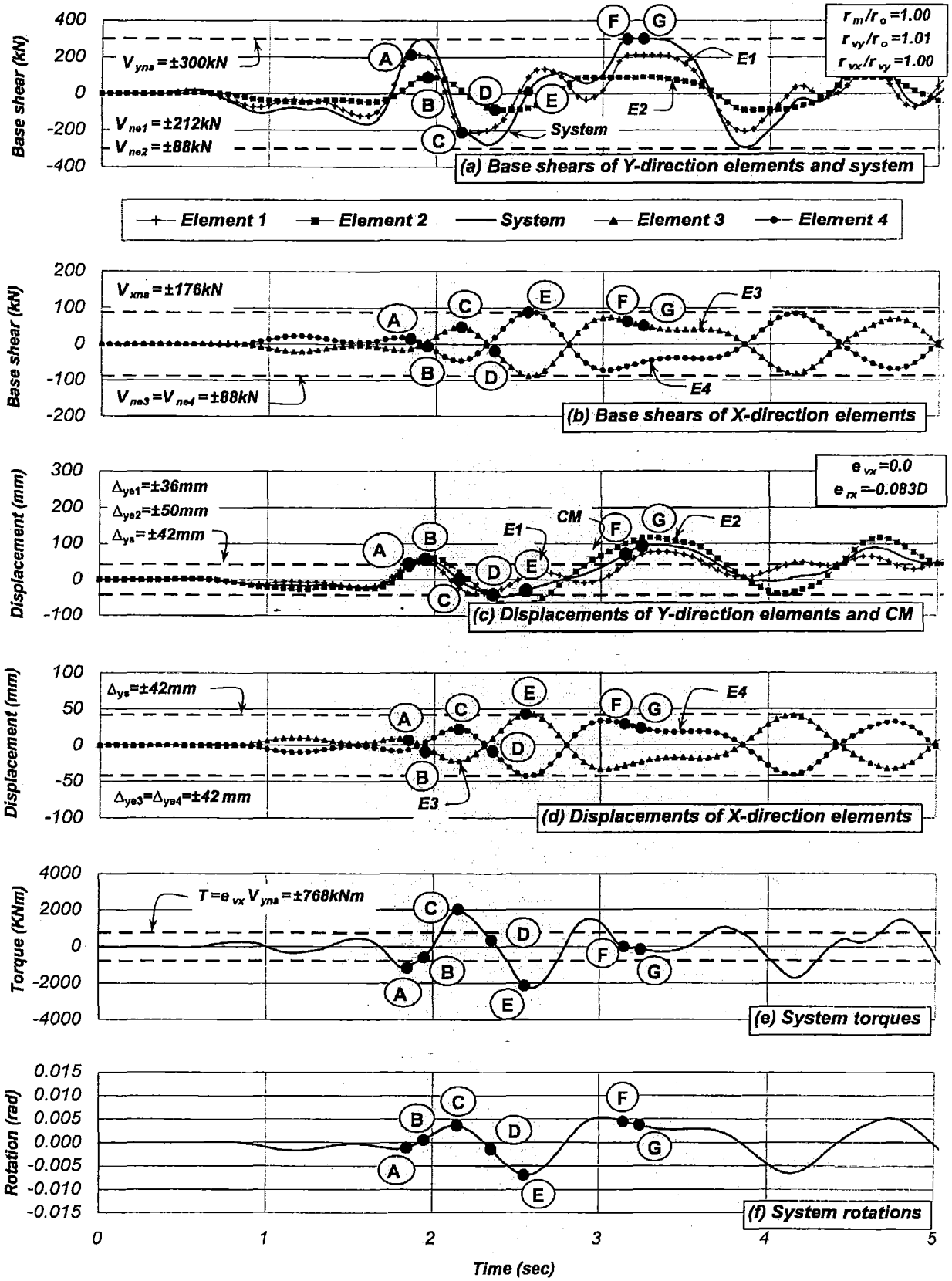

Figure 4-3. Time history response of the restrained *System 3B-1.3* subjected to the Artificial earthquake record, T_s=1.30 sec, e_{mx}=0.0, e_{vx}=-0.21D (λ_1=2.4), e_{rx}=-0.27D (α=1.4), $\mu_{\Delta s}$=5.35, r_m/r_o=1.0, r_{vy}/r_m=1.01, r_{vx}/r_{vy}=1.0

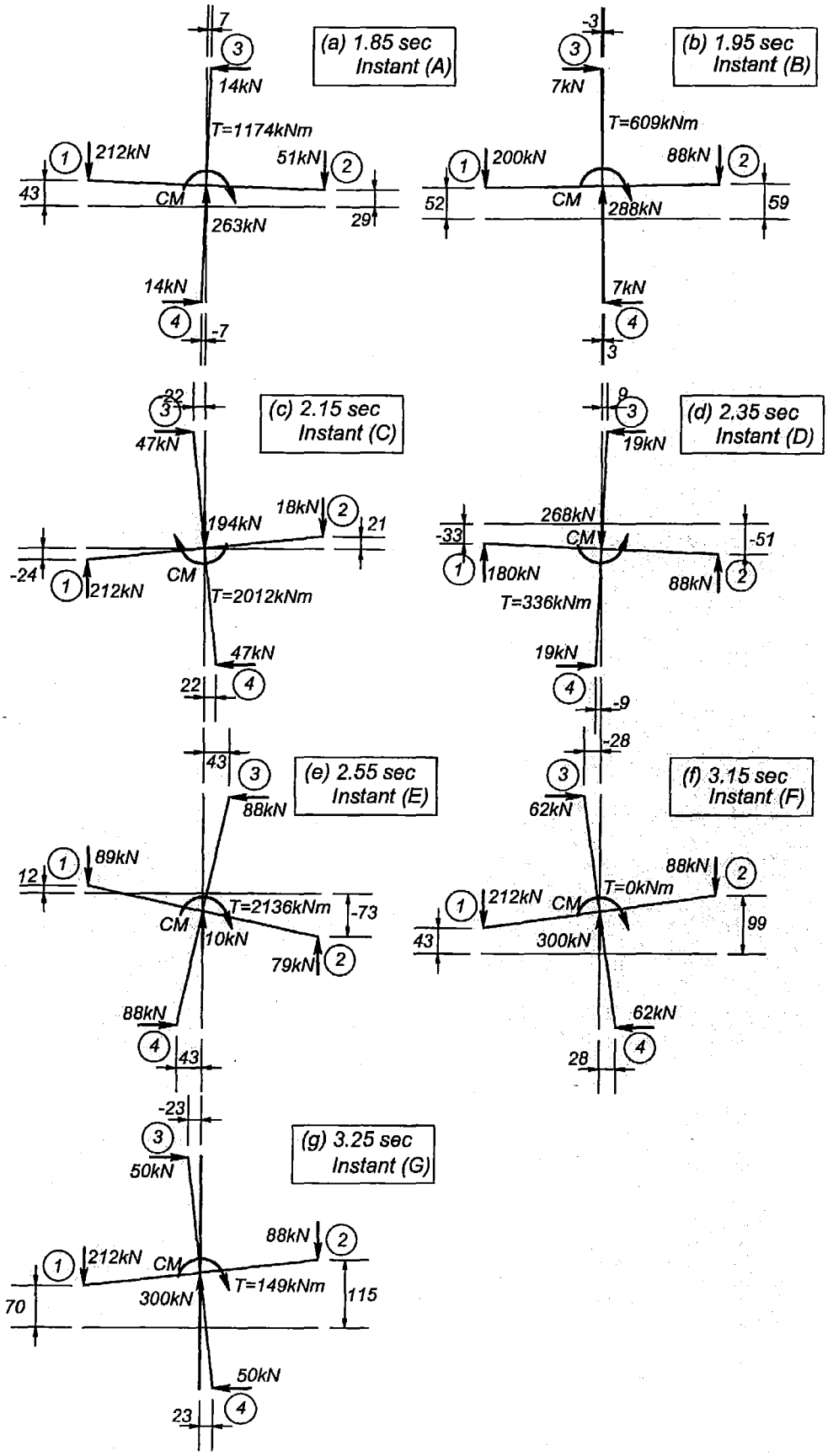

Figure 4-4. Instantaneous displacement profiles of the restrained *System 3B-1.3* subjected to the Artificial earthquake record, T_s=1.30 sec, e_{mx}=0.0, e_{vx}=-0.21D (λ_1=2.4), e_{rx}=-0.27D (α=1.4), $\mu_{\Delta s}$=5.35, r_m/r_o=1.0, r_{vy}/r_m=1.01, r_{vx}/r_{vy}=1.0

Figure 4-3(a) shows that element *(2)* yielded, once again, at instant *(D)*. Figure 4-4(d) shows that the displacement demand of element *(2)* increased while that of element *(1)* was already reversing and, as expected, system rotations and torque were rather small.

Figure 4-3(b) shows that the *X*-direction elements *(3)* and *(4)* yielded at instant *(E)*. This took place when the *Y*-direction elements *(1)* and *(2)* were elastic and not maximum displacements and their displacement demands were opposite in sign, see Figure 4-4(e). This behaviour confirms that the maximum displacement demands of the *X*-direction elements *(3)* and *(4)* are not associated with that of the *Y*-direction elements *(1)* and *(2)*.

Elements *(1)* and *(2)* were yielding simultaneously between instants *(F)* and *(G)*, as shown in Figure 4-3 and Figure 4-4(f) and (g). Between these instants, the system torque slightly increased because the *X*-direction elements were elastic while the system rotation reduced. The maximum displacement demands of elements *(1)* and *(2)* were attained when they yielded in the same direction whereas *X*-direction elements *(3)* and *(4)* remained elastic.

The findings above indicate that the *X*-direction elements attained their nominal strength due to a large system rotation and torque. This, however, was not associated with the maximum displacement demands of the *Y*-direction elements *(1)* and *(2)*, which, in fact, remained elastic, and showed displacement demands in opposite directions. The maximum displacement demand of elements *(1)* and *(2)* occurred when they yielded in the same direction and the associated system rotation was not large enough to yield the *X*-direction elements *(3)* and *(4)*. This shows that large system rotations, due to a significant strength eccentricity, are not an issue in seismic design if the displacement capacity of the elements is not exceeded.

4.3.3 Response of the restrained *System 3B-1.3(α=variable)* having different $\alpha=\Delta_{ye2}/\Delta_{ye1}$ ratios

This section aims to examine the response of restrained systems due to changes in the $\alpha=\Delta_{ye2}/\Delta_{ye1}$ ratio to achieve specific stiffness eccentricities associated with zero strength eccentricity. It also verifies if the response of systems, having different $\alpha=\Delta_{ye2}/\Delta_{ye1}$ ratio and designed according to the suggested design strategy prevent the elements from exceeding their displacement capacity.

The torsionally restrained *System 3B-1.3* was considered again. For a given geometrical layout and strength of elements, stiffness eccentricity increased by increasing the ratio of nominal yield displacement of elements, $\alpha=\Delta_{ye2}/\Delta_{ye1}$. Hence, several systems, having a different $\alpha=\Delta_{ye2}/\Delta_{ye1}$ ratio but the same r_{vy}/r_m ratio, were examined. The systems considered were similar to those torsionally unrestrained systems already examined in Section 3.5.9. The only difference was the inclusion of two equidistant *X*-direction elements *(3)* and *(4)* providing torsional resistance. In spite of the different $\alpha=\Delta_{ye2}/\Delta_{ye1}$ ratios, the nominal yield displacement in every system was equal along the principal axes, $\Delta_{ys}=42mm$; see Table B-3(Appendix B). This was achieved by appropriate changes on the relative nominal yield displacement of the parallel elements, i.e., relative length of the substitute wall-elements, as explained in Section 2.18.1. The strength of the systems was adjusted to achieve an uncoupled translational period of free vibration of $T_s=1.30$ seconds along both axes. The ratio of element nominal yield displacement, $\alpha=\Delta_{ye2}/\Delta_{ye1}$, varied between *1.2* and *2.5*. They are denoted restrained *Systems 3B-1.3(α=variable)*.

The Artificial earthquake record, already scaled to analyse the reference unrestrained *Systems 3A-1.3(α=1.4)*, was also applied, without further modifications, to the restrained *Systems 3B-1.3(α=variable)* having other $\alpha=\Delta_{ye2}/\Delta_{ye1}$ ratios (or stiffness eccentricities associated with zero strength eccentricity). The use of such a normalised record and the fact that the uncoupled translational period of free vibration of the systems was the same enabled a direct comparison of the system's responses.

The system strength to be eventually assigned to the elements to satisfy zero strength eccentricity should prevent any element from exceeding its displacement ductility capacity. Zero strength eccentricity is a reference distribution of strength of major importance in this study because it is when the maximum displacement demand of elements and at the centre of mass is attained. The displacement capacity of the system should, therefore, be associated with this response and should be restricted to the displacement capacity of the critical element. The system displacement capacity is affected by the $\alpha=\Delta_{ye2}/\Delta_{ye1}$ ratio, as already shown for their unrestrained counterparts; see Section 3.5.9.

Table 4-2 summarizes the maximum response associated with zero strength eccentricity. The displacement demands of elements *(1)* and *(2)* and at the centre of mass were, as expected, essentially the same and independent of the $\alpha=\Delta_{ye2}/\Delta_{ye1}$ ratio. Increasing this ratio, did, however, increase system rotations and therefore had a proportional increase on the displacement demands of the *X*-direction elements *(3)* and *(4)*. According to the time history response, which was not presented here for the sake of brevity, large rotations occurred when elements *(1)* and *(2)* were elastic and their displacement demands were opposite in sign. Table 4-2 also shows that the corresponding equivalent single degree of freedom system predicted, with adequate accuracy, the response at the centre of mass; a characteristic not affected by variations of the $\alpha=\Delta_{ye2}/\Delta_{ye1}$ ratio (or stiffness eccentricities associated with zero strength eccentricity).

Table 4-2. Response of the restrained *Systems 3B-1.3(α=variable)* having different $\alpha=\Delta_{ye2}/\Delta_{ye1}$ ratios and subjected to the Artificial earthquake record, T_s=1.30 sec, e_{vx}=0.0, e_{rx}=variable, $\mu_{\Delta s}$=5.35, r_m/r_o=1.0, r_{vy}/r_m=1.01

α=variable	e_{vx}=0.0	Displacements, mm, and displacement ductility demands, (μ)				
$=\Delta_{ye2}/\Delta_{ye1}$	e_{rx}=variable	E1	CM	E2	ESDOF	E3=E4
1.00	0.00	225(5.35)	225(5.35)	225(5.35)	225(5.35)	0(elastic)
1.20	-0.045D	229(5.94)	226(5.42)	223(4.82)	"	7(elastic)
1.40	-0.083D	233(6.48)	228(5.42)	223(4.42)	"	13(elastic)
1.60	-0.115D	239(6.99)	231(5.50)	224(4.11)	"	17(elastic)
2.00	-0.167D	249(7.90)	237(5.65)	231(3.66)	"	26(elastic)
2.50	-0.214D	235(8.01)	223(5.31)	228(3.10)	"	35(elastic)

The displacement capacity of the system should be limited to that of the element *(1)* having the smallest displacement capacity. This is because it is assumed that the displacement demands of the elements and at the centre of mass were essentially the same and unaffected by variations of the $\alpha=\Delta_{ye2}/\Delta_{ye1}$ ratio due to the significant torsional resistance provided by the *X*-direction elements. Table 3.6 have summarized the displacement capacity and corresponding ductility capacity of the unrestrained systems already examined in Section 3.5.9, which also applies to the restrained systems studied here. It is evident that the displacement capacity of the system reduced with increasing $\alpha=\Delta_{ye2}/\Delta_{ye1}$ ratio since the displacement capacity of element *(1)* was

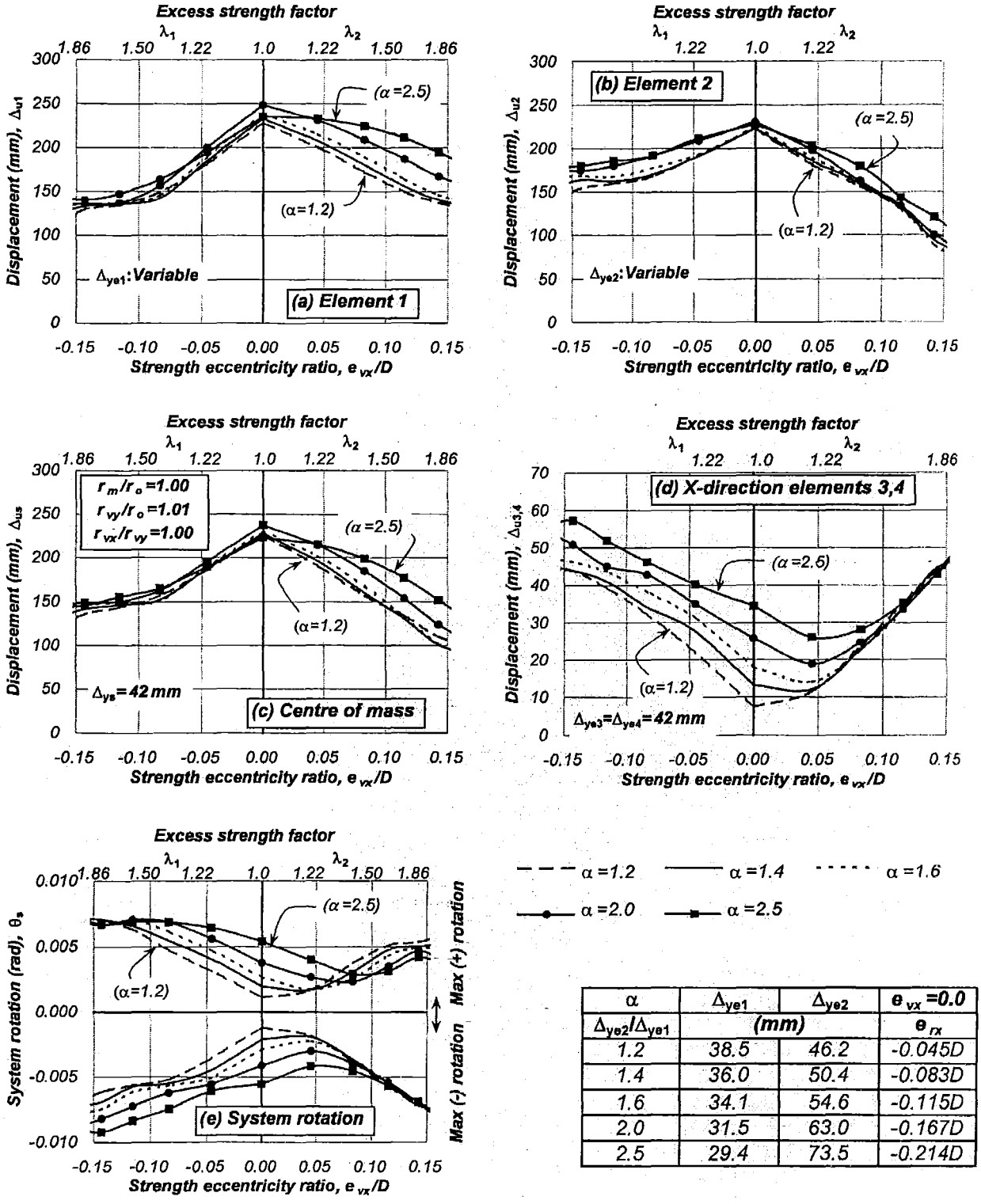

α	Δ_{ye1}	Δ_{ye2}	e_{vx}=0.0
$\Delta_{ye2}/\Delta_{ye1}$	(mm)		e_{rx}
1.2	38.5	46.2	-0.045D
1.4	36.0	50.4	-0.083D
1.6	34.1	54.6	-0.115D
2.0	31.5	63.0	-0.167D
2.5	29.4	73.5	-0.214D

Figure 4-5. Displacements of the restrained *System 3B-1.3(α=variable)* having different $\alpha=\Delta_{ye2}/\Delta_{ye1}$ ratios and subjected to the Artificial earthquake record, T_s=1.30 sec, e_{mx}=0.0, $e_{vx}\neq e_{rx}$=variable, $\mu_{\Delta s}$=5.35, r_m/r_o=1.0, r_{vy}/r_m=1.01

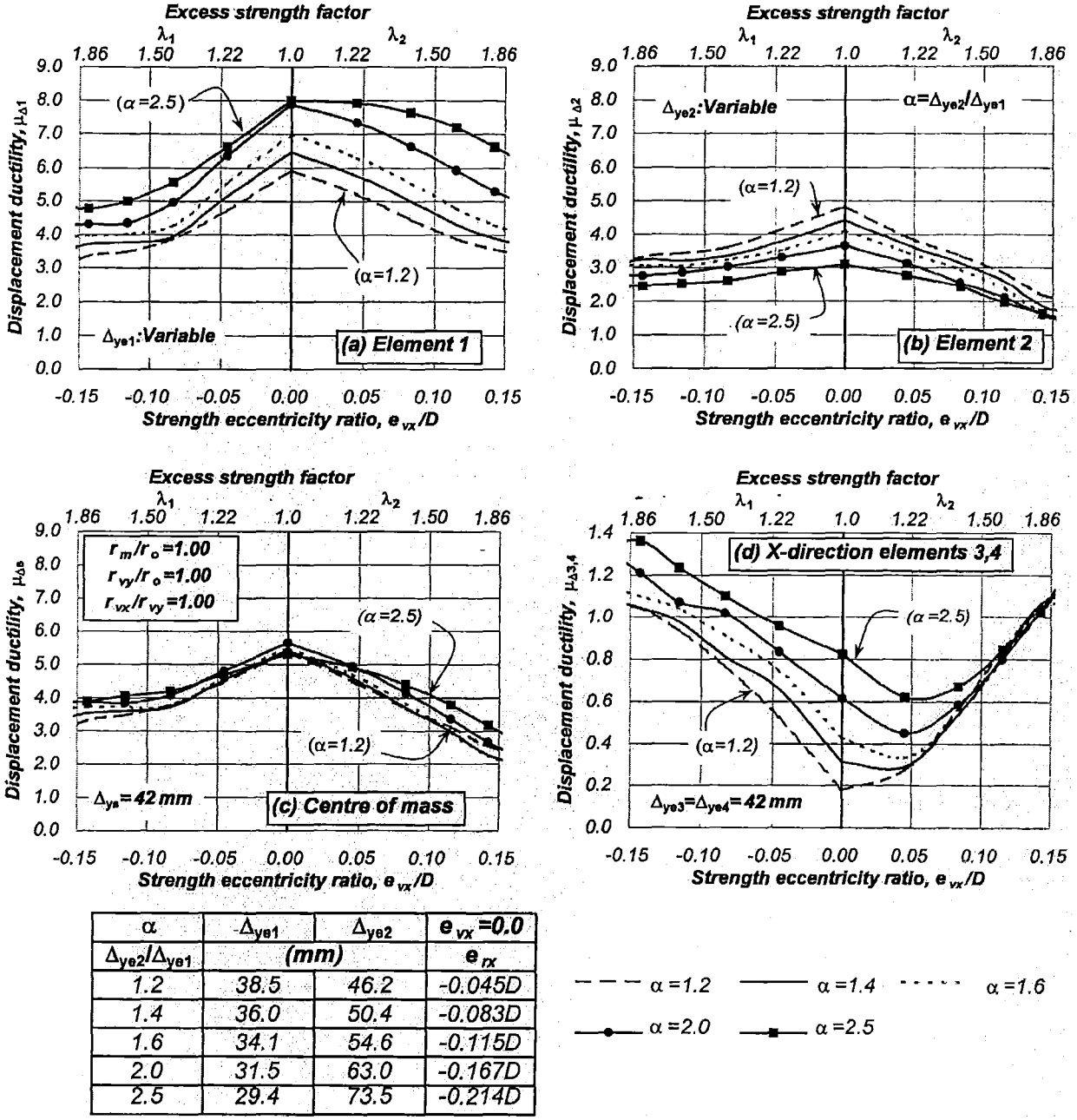

α	Δye1	Δye2	e vx =0.0
Δye2/Δye1	(mm)		e rx
1.2	38.5	46.2	-0.045D
1.4	36.0	50.4	-0.083D
1.6	34.1	54.6	-0.115D
2.0	31.5	63.0	-0.167D
2.5	29.4	73.5	-0.214D

α =1.2 α =1.4 α =1.6 α =2.0 α =2.5

Figure 4-6. Ductility demands of the restrained *System 3B-1.3(α=variable)* subjected to the Artificial earthquake record, T_s=1.30 sec, e_{mx}=0.0, $e_{vx} \neq e_{rx}$=variable, $\mu_{\Delta s}$=5.35, r_m/r_o=1.0, r_{vy}/r_m=1.01

reduced. This particular solution will take advantage of the displacement capacity of element *(1)* but not fully exploit that of element *(2)*.

If zero strength eccentricity cannot be achieved in practice, as it is expected, a strength eccentricity may be accepted provided that it results from the nominal strength of one element being in excess of that satisfying zero strength eccentricity. Hence, strength eccentricities are associated with an increase of system strength, as already shown in Figure 2-28.

Figure 4-5 shows the maximum response for increasing negative strength eccentricities. It is evident that the excess strength of element *(1)* reduced, as expected, its displacement demands and the displacements at the centre of mass, as shown in Figure 4-5(a), (b) and (c). Element *(2)* also exhibited, in every system, a reduction in its displacement demands. This was because the reduction of displacement demands at the centre of mass due to an increase of system strength over-compensated for the small torsion-induced displacement on the critical element *(2)*, additional to those resulting from the system translation. This behaviour was essentially not affected by changes in the $\alpha=\Delta_{ye2}/\Delta_{ye1}$ ratio. Figure 4-5(d) exhibits, as expected, that displacement demands on the *X*-direction elements *(3)* and *(4)* increased with increasing negative strength eccentricities. Rotations also increased, for a given strength eccentricity, when the $\alpha=\Delta_{ye2}/\Delta_{ye1}$ ratio (or stiffness eccentricity associated with zero strength eccentricity) was increased. System rotations, however, were not an issue because they did not influence the maximum displacement demands of the *Y*-direction elements *(1)* and *(2)* parallel to the direction of application of the earthquake record. Although rotations directly affected the response of the *X*-direction elements, their displacement demands were much smaller than those expected to be attained when the earthquake record is to be applied along the *X*-direction only.

It is evident from Figure 4-5(d) and (e) that there is proportionality between the $\alpha=\Delta_{ye2}/\Delta_{ye1}$ ratio and the critical system rotation which is associated with the maximum displacement demand of the *X*-direction elements *(3)* and *(4)*. The element displacement demands were enhanced with increasing $\alpha=\Delta_{ye2}/\Delta_{ye1}$ ratio but not in a critical manner. It is seen that in the majority of cases they responded within the elastic domain. The increase of system rotations due to increasing $\alpha=\Delta_{ye2}/\Delta_{ye1}$ ratio did not adversely affect maximum displacement demand of elements *(1)* and *(2)* because they did not reach their displacement capacity.

The response due to increasing positive strength eccentricities is an unrealistic scenario due to the reasons provided in Section 4.3.1 and hence just presented to clarify trends in behaviour.

Figure 4-6 shows displacements ductility demands on the elements and at the centre of mass of the restrained *Systems 3B-1.3*(α=*variable*). The displacement ductility demands of element *(1)* increased while reducing for element *(2)*. As expected, the difference in the displacement ductility demands between these elements increased as the $\alpha=\Delta_{ye2}/\Delta_{ye1}$ ratio was increased. Element *(1)* became more critical as the $\alpha=\Delta_{ye2}/\Delta_{ye1}$ ratio was increased.

The findings above confirms that the displacement capacity of the system should be limited to that of the element with the smallest displacement capacity considering that, for zero strength eccentricity, the maximum displacement demands of the elements and at the centre of mass are attained and are essentially the same. The $\alpha=\Delta_{ye2}/\Delta_{ye1}$ ratio (or stiffness eccentricity associated with zero strength eccentricity) did not have a significant effect on the *Y*-direction elements *(1)* and *(2)*. It influenced, in a non-critical manner, the *X*-direction elements in proportion to the $\alpha=\Delta_{ye2}/\Delta_{ye1}$ ratio.

4.3.4 Response of the restrained *System 3B-1.3(α=1.4)* under earthquake records at different angles

The aim of this section is to show if the design strategy suggested in Section 2.11 leads or not to displacement demands on elements larger than their displacement ductility capacity. The system was subjected to earthquake records along different directions to model the multidirectional characteristics of ground motions. The response of the systems was then compared to that due to the application of the earthquake record input along the reference *Y*-direction to identify if a critical situation arises.

The torsionally restrained *System 3B-1.3(α=1.4)* was considered again. All properties, reported earlier, have been retained without any change. The procedure explained in Section 4.2 was used for the analysis of the system. The system was subjected to the Artificial earthquake record at 22^o, 45^o, 67^o and 90^o angles to the reference *Y*-axis.

It is stressed that zero strength eccentricity, although it may not be achieved in practice, is the reference distribution of system strength among elements. The system torsional response due to zero strength eccentricity is relevant for seismic design because it is when the maximum displacement demands on the elements are attained. The displacement capacity of the system should then be associated with it and hence limited to that of the element having the smallest displacement capacity.

Figure 4-7 shows the response for zero strength eccentricity. The maximum displacement demands on elements and at the centre of mass were attained when the earthquake record was applied along the *Y*-direction. For the same distribution of strength, displacement demands on the elements reduced as the direction of incidence of the earthquake record varied between 0^o and 90^o. This response occurred because the strength of the system was larger along diagonal directions relative to the reference *Y*-axis, as already explained in Section 2.16.1.

A strength eccentricity may be accepted provided that it results from the nominal strength of one element being in excess of that satisfying static equilibrium. The strength of the system is also increased. This situation, already shown in Figure 2-28, is subsequently examined.

Figure 4-7 plots the system response for increasing strength eccentricities. The realistic scenario of increasing negative strength eccentricities shows, as to be expected, that the excess strength of element *(1)* reduced its displacement ductility demands and those at the centre of mass; see Figure 4-7(a) and (c). These demands were further reduced as the earthquake record input was applied at diagonal directions relative from the reference *Y*-axis. This is because the strength of the system is larger at any oblique direction; see Section 2.16.1.

In case of element *(2)*; see Figure 4-7(b), the application of the earthquake record at a 22^o angle generated, in some cases, displacement demands on elements similar to that attained for zero strength eccentricity. These demands, however, did not exceed the maximum displacement demand attained by the element for zero strength eccentricity and unidirectional earthquake input along the *Y*-direction. The application of the earthquake record along a 45^o angle generated displacement demands larger than that attained for zero strength eccentricity. In spite of this behaviour, the elements did not exceed the maximum response attained for zero strength eccentricity and earthquake record input along the *Y*-axis. The demands on the element reduced even further as the angle of earthquake input approached 90^o. This response suggests that the

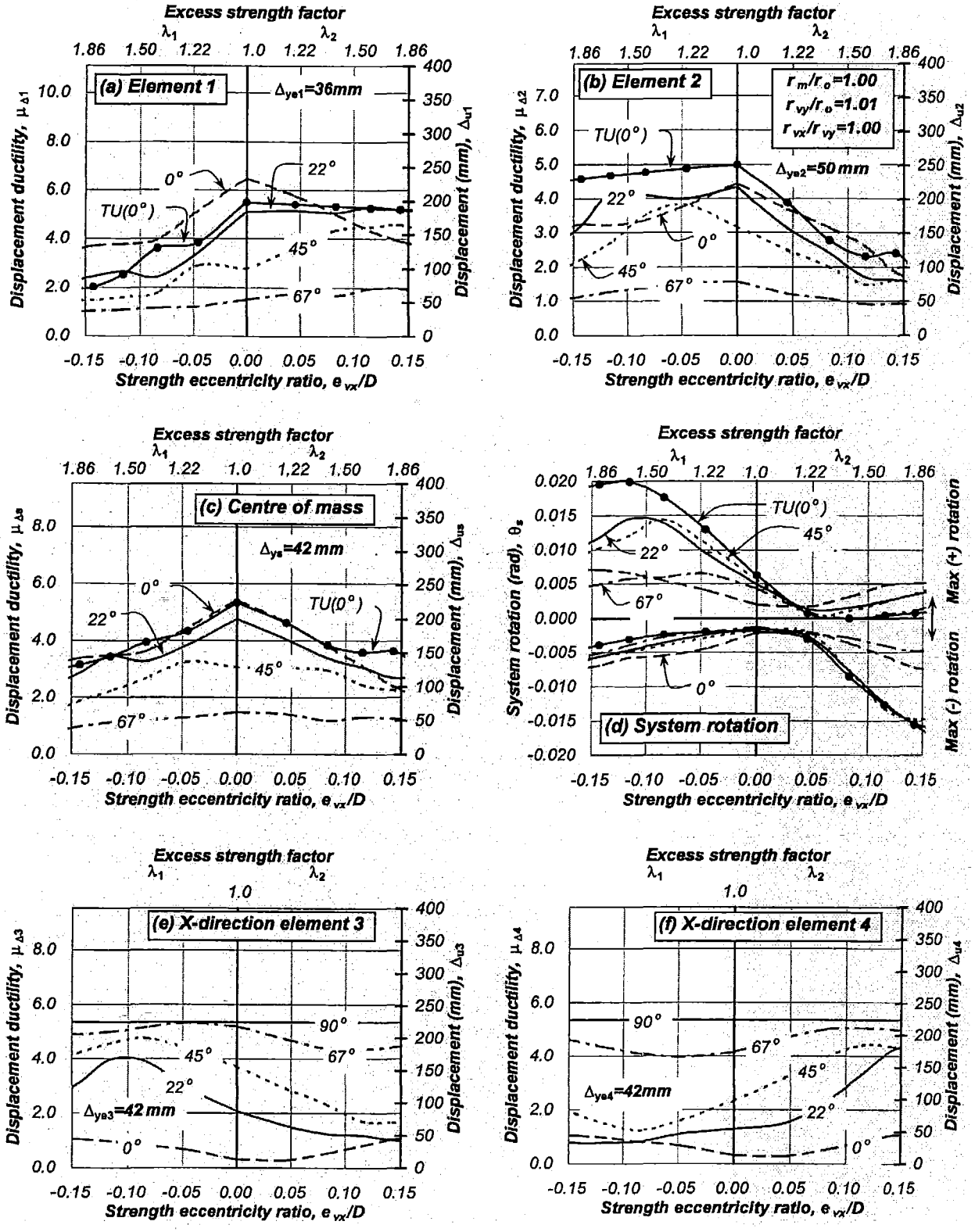

Figure 4-7. Response of the restrained *System 3B-1.3(α=1.4)* subjected to the Artificial earthquake record along different directions, T_s=1.30 sec, e_{mx}=0.0, $e_{vx} \neq e_{rx}$=variable, $\mu_{\Delta s}$=5.35, r_m/r_o=1.0, r_{vy}/r_m=1.01

proposed distribution of system strength, although conservative for restrained systems subjected to the earthquake record along the *Y*-axis, did prevent the elements from exceeding its displacement ductility capacity when the system was subjected to earthquake records at different angles. The maximum response of restrained systems having zero strength eccentricity and subjected to the earthquake record along the *Y*-axis provides an envelope of the system maximum response. This response was not exceeded for increasing eccentricities or when the system was subjected to the earthquake record at different angles.

Increasing positive strength eccentricities beyond $e_{vx}>+0.05D$, although generating, in some cases, a critical response on element *(1)*, is an unrealistic scenario due to the reasons provided in Section 4.3.1 and hence the results were just presented to clarify general trends.

Figure 4-7 (e) and (f) show that system rotations were significantly increased when the earthquake record was applied at 22^o and 45^o angles. This is because yielding on one or more elements released their torsional restraint. The system torsional behaviour became similar to that of its unrestrained counterpart *System 3A-1.3(α=1.4)* when system rotations almost reached those attained by its unrestrained counterpart. This increase in rotations was also reflected in the increase of relative displacement demands between the *Y*-direction elements *(1)* and *(2)* and the *X*-direction elements *(3)* and *(4)*. These displacement demands, however, never exceeded the maximum response attained when the system was subjected to the earthquake record along the *Y*-axis. This confirms that large rotations are not necessarily associated with a critical response and hence may be tolerated.

It is also evident from Figure 4-7(d) that for a strength eccentricity of $e_{vx}=-0.04D$, the system maximum rotation was also rather small and not affected by the direction of application of the earthquake record. This strength eccentricity was associated with the centre of mass located halfway between centres of strength and stiffness. These findings suggest that the torsional mechanism of restrained systems is not affected by the direction of application of the earthquake record.

Figure 4-7 also compares the response of the restrained *System 3B-1.3(α=1.4)* and its unrestrained counterpart *System 3A-1.3(α=1.4)*. The latter is identified by curves *TU* associated with $r_{vy}/r_m=1.01$. It is evident from Figure 4-7(a) that the restrained *System 3B-1.3(α=1.4)* subjected to the earthquake record along the *Y*-axis displays a critical response on element *(1)*, a response not predicted with its unrestrained counterpart *System 3A-1.3(α=1.4)*. On the other hand, the unrestrained *System 3A-1.3(α=1.4)* displayed a larger displacement demand on element *(2)*; see Figure 4-7(b). Despite this last observation, the displacement ductility demand of element *(2)* was not a concern because it was smaller than its displacement ductility capacity.

The findings described above suggest that the proposed distribution of system strength is effective to restrict displacement demands on elements of restrained systems to less than the maximum developed for zero strength eccentricity and when they are subjected to earthquake record at oblique angles. The response of restrained systems subjected to unidirectional earthquake input along the principal axes and having a system strength distributed among elements to satisfy zero strength eccentricity will generate an envelope of the system maximum response.

4.3.5 Time history response of the restrained *System 3B-1.3* [e_{vx}=0.0(λ_1=1.0), e_{rx}=-0.083D (α=1.4), θ_{EQ}=45°]

The time history response was examined to provide a better understanding of torsional mechanisms involved during the dynamic response of restrained systems subjected to earthquake records along oblique directions.

The torsionally restrained *System 3B-1.3(α=1.4)* was considered again. The system strength was distributed on the elements to achieve zero strength eccentricity. The system, already described in Section 4.3.1(b), was subjected to the Artificial earthquake record at a 45° angle relative to the reference *Y*-axis.

Figure 4-8(a) and (b) show that *Y* and *X*-direction elements yielded essentially at the same instant *(A)* due to the substantial torsional restraint introduced by all four elements. The displacements of the parallel elements were essentially the same at such instant; see Figure 4-8(c) and (d). The system rotation was almost zero; see Figure 4-8(f), and as expected, the torque becomes zero. Subsequently, Figure 4-8(a), (b) and (c) also show that all four elements yielded between instant *(A)* and *(B)* and no torque was developed. However, a small system rotation was introduced between those instants due to the rotational velocity of the system, see Figure 4-8(f), leading to relative displacements between the parallel elements as they reached a maximum displacement. The *Y*-direction element *(2)* and the *X*-direction element *(3)* exhibited the largest displacements due to this rotation, as Figure 4-8(c) and (b) show.

Figure 4-8(c) and (d) show that the displacement demands of the elements and at the centre of mass reached a maximum at instant *(B)*. They were not associated with the maximum system rotation and were not exceeding their displacement capacity.

It is evident that the torsional mechanisms of this restrained system when subjected to earthquake record at a *45°* angle were similar to that of its unrestrained counterpart. However, the time spent by the elements in the inelastic range of response was shorter because the system strength at *45°* angle is *41%* larger than that along the principal axes. The displacement demands of all elements were much smaller than their capacities even though system rotations substantially increased.

Rotations of the system reached a peak at instant *(C)*, as shown in Figure 4-8(f). However, this was not associated with the maximum displacement demand imposed on the elements. It was also found again that, in general, the magnitude of torque did not correlate with system rotations and displacement demands of the elements. As Figure 4-8(e) shows, during the three seconds following instant *(C)*, large torques were generated although system rotations were smaller. It is also evident that at these instants, such as *(C)*, some elements returned to the elastic state and hence developed only a small fraction of their nominal strength.

4.3.6 Response of the restrained *System 3B-1.3*(α=1.4) having different displacement ductility capacities

It has been recognized that, during the design process, certain asymmetric systems may require a reduced system displacement ductility capacity. This is justified when the displacement capacity of the elements is associated with a limit state requiring rigorous displacement control. How this may affect the torsional response of restrained systems is subsequently examined.

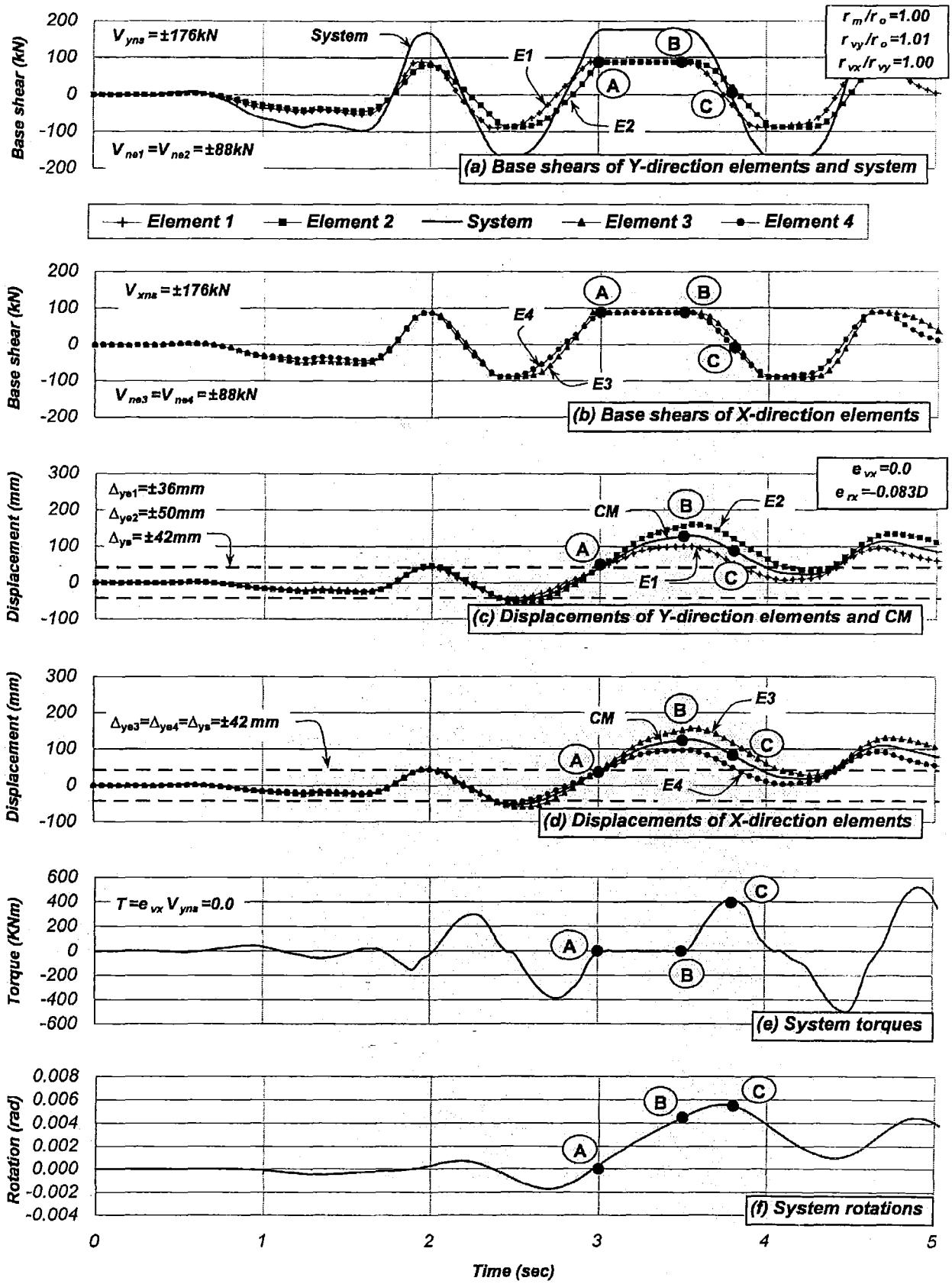

Figure 4-8. Time history response of the restrained *System 3B-1.3(α=1.4)* subjected to the Artificial earthquake record, T_s=1.30 sec, e_{mx}=0.0, e_{vx}=0.0 (λ_1=1.0), e_{rx}=-0.083D, $\mu_{\Delta s}$=*5.35*, r_m/r_o=1.0, r_{vy}/r_m=1.01, r_{vx}/r_{vy}=1.0

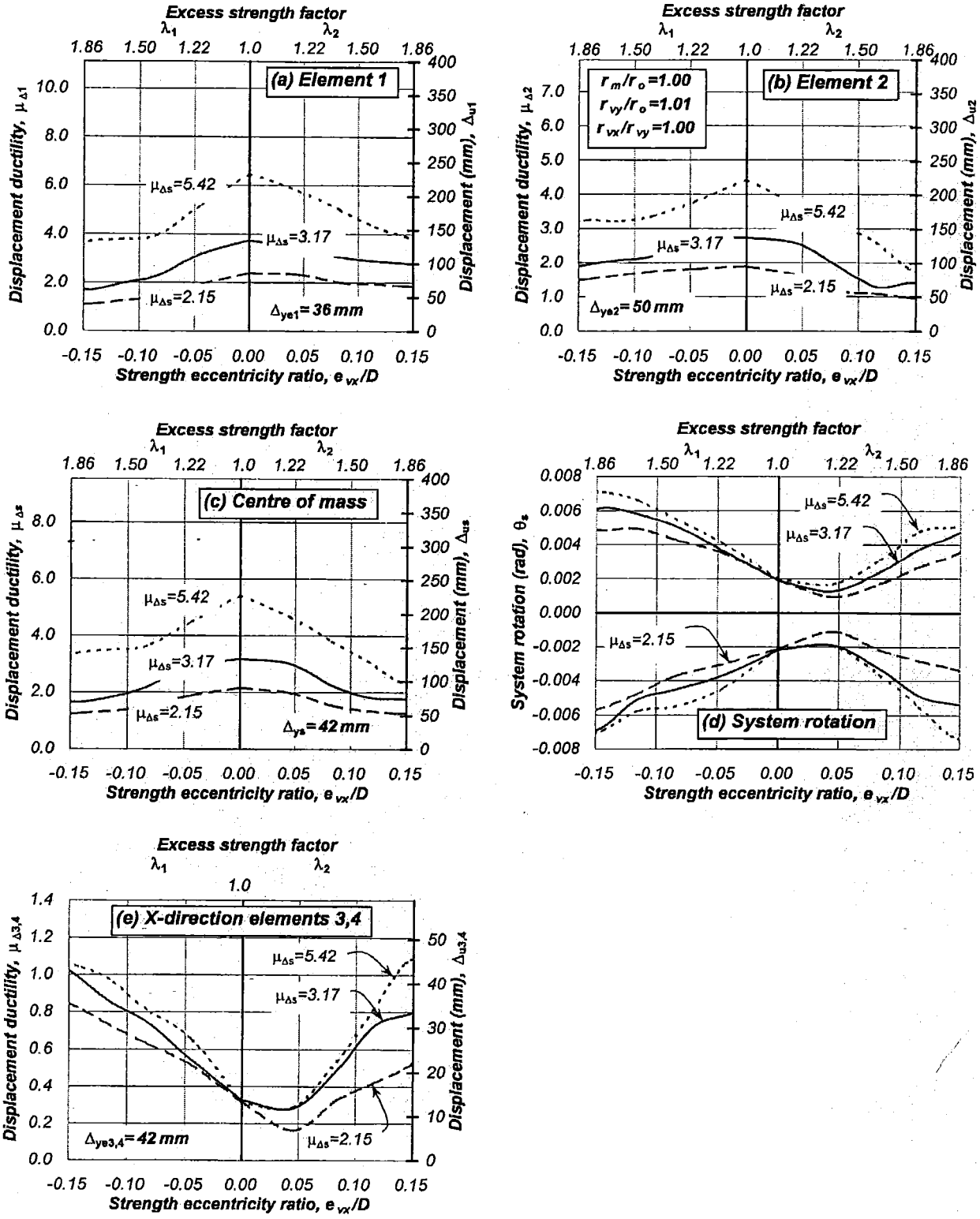

Figure 4-9. Response of the restrained *Systems 3B-1.3(α=1.4)* having different displacement ductility capacities and subjected to the Artificial earthquake record, T_s=1.30 sec, e_{mx}=0.0, $e_{vx} \neq e_{rx}$=variable, μ_s=variable, r_m/r_o=1.0, r_{vy}/r_m=1.01, r_{vx}/r_{vy}=1.0

Three identical restrained *Systems 3B-1.3(α=1.4)*, having displacement ductility capacities of $\mu_{\Delta s}$=*2.2, 3.2* and *5.4,* were considered. All properties, reported earlier, were retained without any change. They were subjected to the Artificial earthquake record along the *Y*-axis. The procedure explained in Section 4.2 was used for the analysis of the system.

Figure 4-9 shows the response of the systems for zero and increasing strength eccentricities. As expected, the maximum displacement demands on the elements and at the centre of mass were attained for zero strength eccentricity; see Figure 4-9(a), (b) and (c). The realistic situation of increasing negative strength eccentricities generated, as expected, a reduction in the displacement demands of the *Y*-direction elements *(1)* and *(2)*.

Rotations were even smaller on systems with reduced displacement ductility capacity; see Figure 4-9(d), reaching a minimum at $e_{vx}\approx+0.04D$ when the centre of mass located is halfway between centres of strength and stiffness, as previously explained, and unlikely to be achieved in practice.

The findings above suggest that the response of systems with reduced displacement ductility capacity is not critical. The suggested design strategy is successful in preventing the elements from exceeding their displacement ductility capacities due to increasing strength eccentricities. The level of displacement ductility capacity is not a relevant parameter in seismic design of torsionally restrained systems.

4.3.7 Response of the restrained *System 3B-1.3(α=1.4)* under different earthquake records

The torsionally restrained *System 3B-1.3(α=1.4)* was considered again. It was also subjected to the Bucharest and Kobe earthquake records to examine how their frequency contents might affect the system torsional response. The records were scaled to impose, for zero strength eccentricity, a displacement ductility demand at the centre of mass equal to the displacement capacity of the system. All properties, reported earlier, were retained without any change. The general procedure explained in Section 4.2 was used for the analysis of the system.

Figure 4-10 shows the response of the system due to zero and increasing eccentricities. Similarities in displacement ductility demands on elements and centre of mass was evident with all records except one.

The Kobe record generated a sudden increase in displacement ductility demands on elements and the centre of mass for strength eccentricities larger than $e_{vx}=\pm0.05D$. It is noted that the displacements of the elements relative to that at the centre of mass were similar for all three records; a feature also implied by similar system rotations, as shown in Figure 4-10(d). This suggests that the earthquake record does not have a significant effect on the system torsional behaviour. However, it influences the displacements since an increase of system strength is not a guarantee of a reduction of system displacement demands. This may have an effect on displacement demands of elements. This is because the small torsion-induced displacement of the critical element in addition to the system translations may not be compensated by the expected reduction of the displacement demand at the centre of mass, therefore exceeding its displacement capacity.

The system maximum rotations shown in Figure 4-10(d) were not related to the maximum displacement demands imposed on elements *(1)* and *(2)* but they were associated with that of the *X*-direction elements *(3)* and *(4)*; see Figure 4-10(e). In fact, the maximum displacement

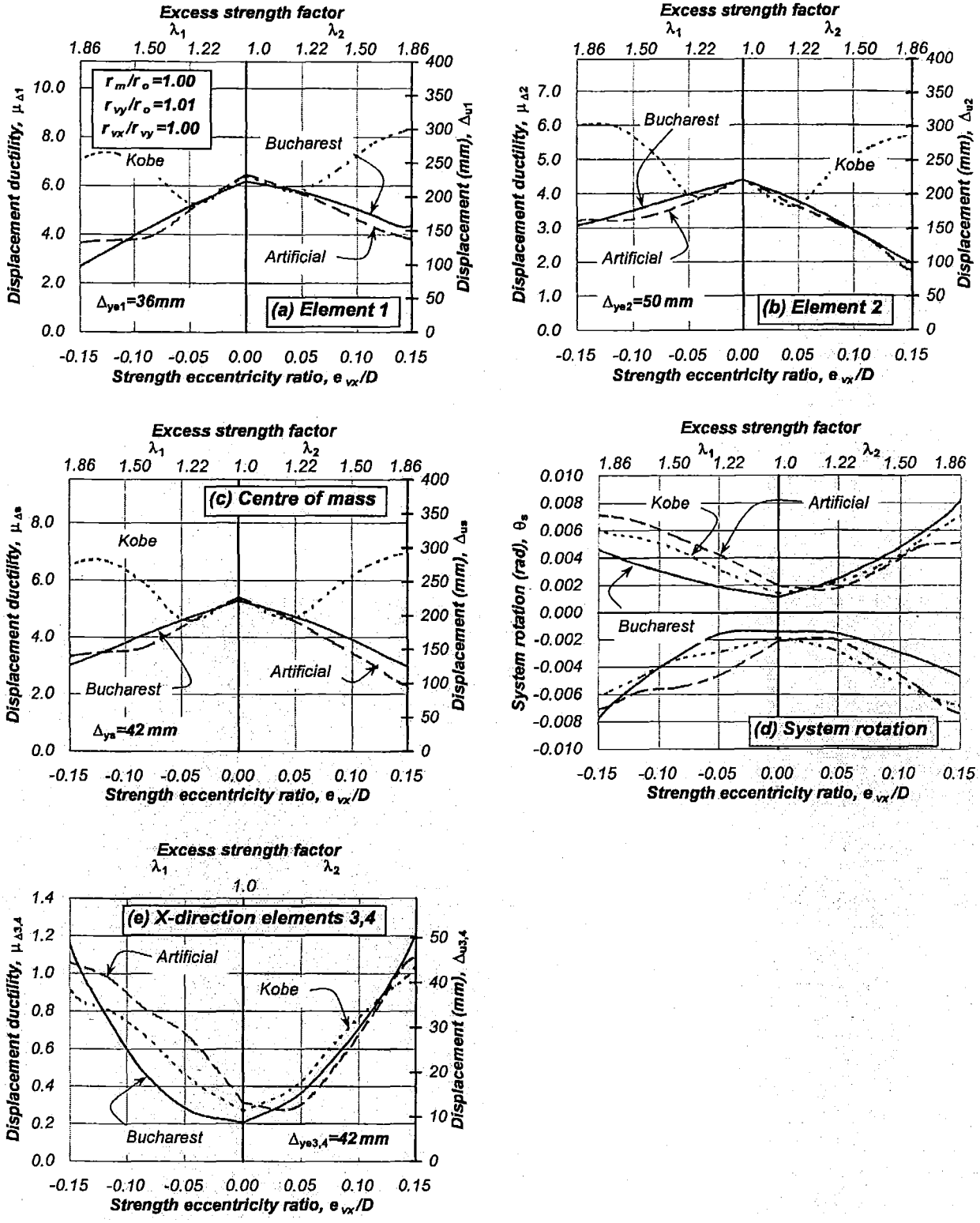

Figure 4-10. Response of the restrained *System 3B-1.3(α=1.4)* under different earthquake records, T_s=1.30 sec, e_{mx}=0.0, $e_{vx} \neq e_{rx}$=variable, $\mu_{\Delta s}$=5.35, r_m/r_o=1.0, r_{vy}/r_m=1.01, r_{vx}/r_{vy}=1.0

demands on the *X*-direction elements were associated with the system maximum rotation; see Figure 4-10(e).

For the chosen restrained models, the translational response rather than the torsional response was found to be sensitive to the frequency contents of the earthquake record. In some cases, an increase in system strength is not a guarantee of a system displacement reduction, hence, the total displacements imposed on the critical element, comprising torsion-induced displacements plus system translation, may exceed the displacement ductility capacity.

4.3.8 Response comparison of the restrained *Systems 3B-1.3(α=1.4), 4B-1.3(α=1.4)* and *5B-1.3(α=1.4)*

The aim of this section was to identify differences in torsional response of systems having a different degree of torsional restraint as measured by the r_{vx}/r_{vy} ratio, and changes in the r_{vy}/r_m ratio.

The torsionally restrained *Systems 3B, 4B* and *5B*, as shown in Figure 2-27, were considered. They had different r_{vx}/r_{vy} and r_{vy}/r_m ratios, as shown in Table 2-5. The nominal yield displacement of the elements was identical in all systems. The ratio of nominal yield displacement of the *Y*-direction elements was $\alpha=1.4$. The system nominal yield displacement was identical along the principal axes, $\Delta_{ys}=42mm$. Their system strength was also equal and adjusted to achieve an uncoupled translational period of free vibration of $T_s=1.30$ seconds. They were denoted restrained *Systems 3B-1.3(α=1.4), 4B-1.3(α=1.4)* and *5B-1.3(α=1.4)*. The Artifcial earthquake record was scaled for *Systems 3B-1.3(α=1.4)* according to the general procedure explained in Section 4.2. This was then applied to *Systems 4B-1.3(α=1.4)* and *5B-1.3(α=1.4)* to identify differences in torsional response between the systems and with their unrestrained counterparts.

The system nominal strength, necessary to prevent, at maximum response, the displacement ductility capacity of any element being exceeded, should be distributed among the elements to satisfy static equilibrium, i.e. $e_{vx}=0.0$. Although zero strength eccentricity may not be achieved in practice, the response for zero strength eccentricity is relevant because it is when the system attains its maximum response; hence the system displacement ductility capacity should be associated with zero strength eccentricity.

Table 4-3 shows the maximum response for zero strength eccentricity. It is evident that the maximum displacement demands on the elements and at the centre of mass of the three systems was essentially the same and not affected by the r_{vy}/r_m ratio. Differences in the degree of torsional restraint introduced by the *X* and *Y*-direction elements, as quantified by the r_{vx}/r_{vy} ratio, did not influence the displacement demands of the *Y*-direction elements *(1)* and *(2)*. The substantial torsional resistance introduced by the *X*-direction elements on the system's rotation was essentially the same and independent of this parameter. This indicates that including the strength of the *X*-direction elements into the radius of gyration of element nominal strength will not make any difference in quantifying such behaviour. It is also observed that the maximum response of the restrained systems was predicted well with an equivalent single degree of freedom system having the same translational properties.

Table 4-3 also shows that limiting the displacement ductility capacity of the three systems to $\mu_{\Delta s}=5.35$ did not prevent element *(1)* from exceeding its displacement ductility capacity. This could have been achieved if their system displacement capacity would have been limited to that

of element *(1)* having the smallest displacement capacity. The displacement ductility capacity for all three systems, although having different r_{vy}/r_m ratios, should, therefore, be $\mu_{\Delta s}=\Delta_{us}/\Delta_{ys}=4.60$. Hence, it is expected that the maximum displacement ductility demand to be developed by elements *(1)* and *(2)* will be $\mu_{\Delta 1}=5.35$ and $\mu_{\Delta 2}=3.83$, respectively.

Strength eccentricities, which are the main cause of rotations in ductile systems, may be accepted provided that they result from the nominal strength of any element being in excess of that satisfying zero strength eccentricity. Thereby, a strength eccentricity is associated with an increase of system strength, as already shown in Figure 2-28.

Table 4-3. Response comparison of restrained *Systems 3B-1.3(α=1.4), 4B-1.3(α=1.4) and 5B-1.3 (α=1.4)* subjected to the Artificial earthquake record, T_s=1.30 sec, e_{mx}=0.0, $e_{vx}\neq e_{rx}$=variable, $\mu_{\Delta s}$=5.35, r_m/r_o=variable, r_{vy}/r_m=variable, r_{vx}/r_{vy}=variable

		Displacements, mm and Displacement ductility demands, (μ)				
	r_{vy}/r_m	E1	CM	E2	ESDOF	E3=E4
System 3B	1.01	233(6.48)	228(5.42)	223(4.42)	225(5.35)	13(elastic)
System 4B	1.54	222(6.17)	227(5.41)	233(4.63)	"	11(elastic)
System 5B	0.76	229(6.36)	230(5.47)	231(4.58)	"	9(elastic)

Figure 4-11 presents the variations in the response for increasing stiffness eccentricities. The displacement ductility demands on elements and at the centre of mass reached a maximum for zero strength eccentricity. Subsequently, increasing negative strength eccentricities reduced these demands. It is seen that variations of the distribution of strength and mass, as quantified by the r_{vy}/r_m ratio, did not lead to significant change in the displacement ductility demands of the *X*-direction elements due to the earthquake record input along the *Y*-axis. This corroborates the findings previously observed that the elastic *X*-direction elements substantially restrained system rotations and hence the mass rotational inertia was barely mobilised. It is evident that irrespective of the torsional restraint provided by the *X*-direction element displacements, system rotations were rather small; see Figure 4-11. Rotations had negligible effects on the displacement demands of the *Y*-direction elements and at the centre of mass.

Although the results for increasing positive strength eccentricities larger than $e_{vx}>+0.05D$ are totally unrealistic due to the reasons provided in Section 4.3.1, they were provided to illustrate the theoretical trends and no further comments are provided.

The above findings suggest that, although the inclusion of *X*-direction elements substantially reduced system rotations, it is not necessary to include their strength into the radius of gyration of element nominal strength because no significant differences in torsional response were observed.

Figure 4-12 plots the predicted response of the restrained *Systems 3B-1.3, 4B-1.3* and *5B-1.3* together with that of its unrestrained counterpart *Systems 3A-1.3, 4A-1.3* and *5A-1.3*. The response of the unrestrained systems were identified by curves *TU* associated with $r_{vy}/r_o=1.0$.

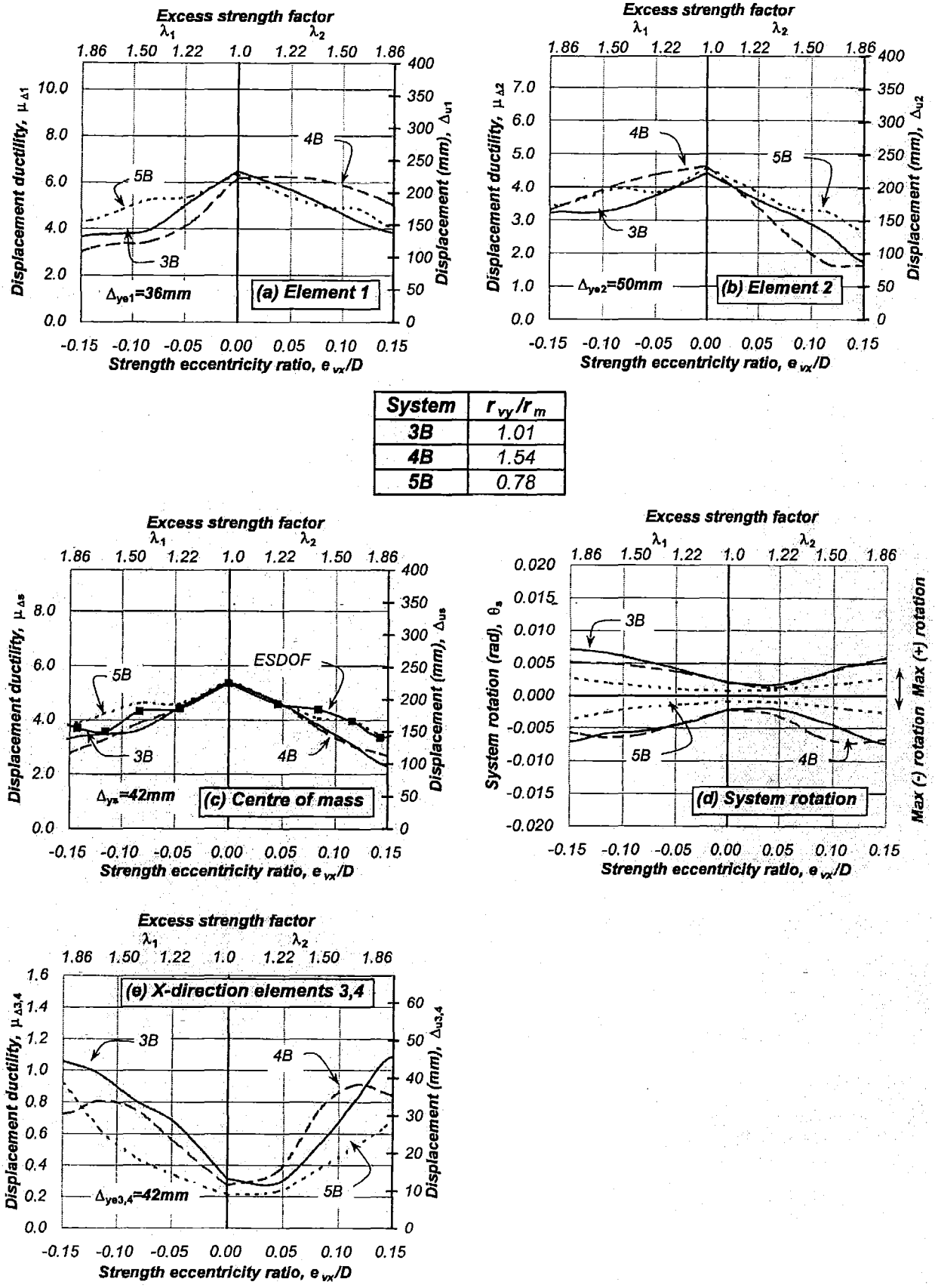

System	r_{vy}/r_m
3B	1.01
4B	1.54
5B	0.78

Figure 4-11. Response comparison of the restrained *Systems 3B-1.3*(α=1.4), *4B-1.3*(α=1.4) *and 5B-1.3* (α=1.4) subjected to the Artificial earthquake record, T_s=1.30 sec, e_{mx}=0.0, $e_{vx} \neq e_{rx}$=variable, $\mu_{\Delta s}$=5.35, r_m/r_o=1.0, r_{vy}/r_m=variable, r_{vx}/r_{vy}=variable

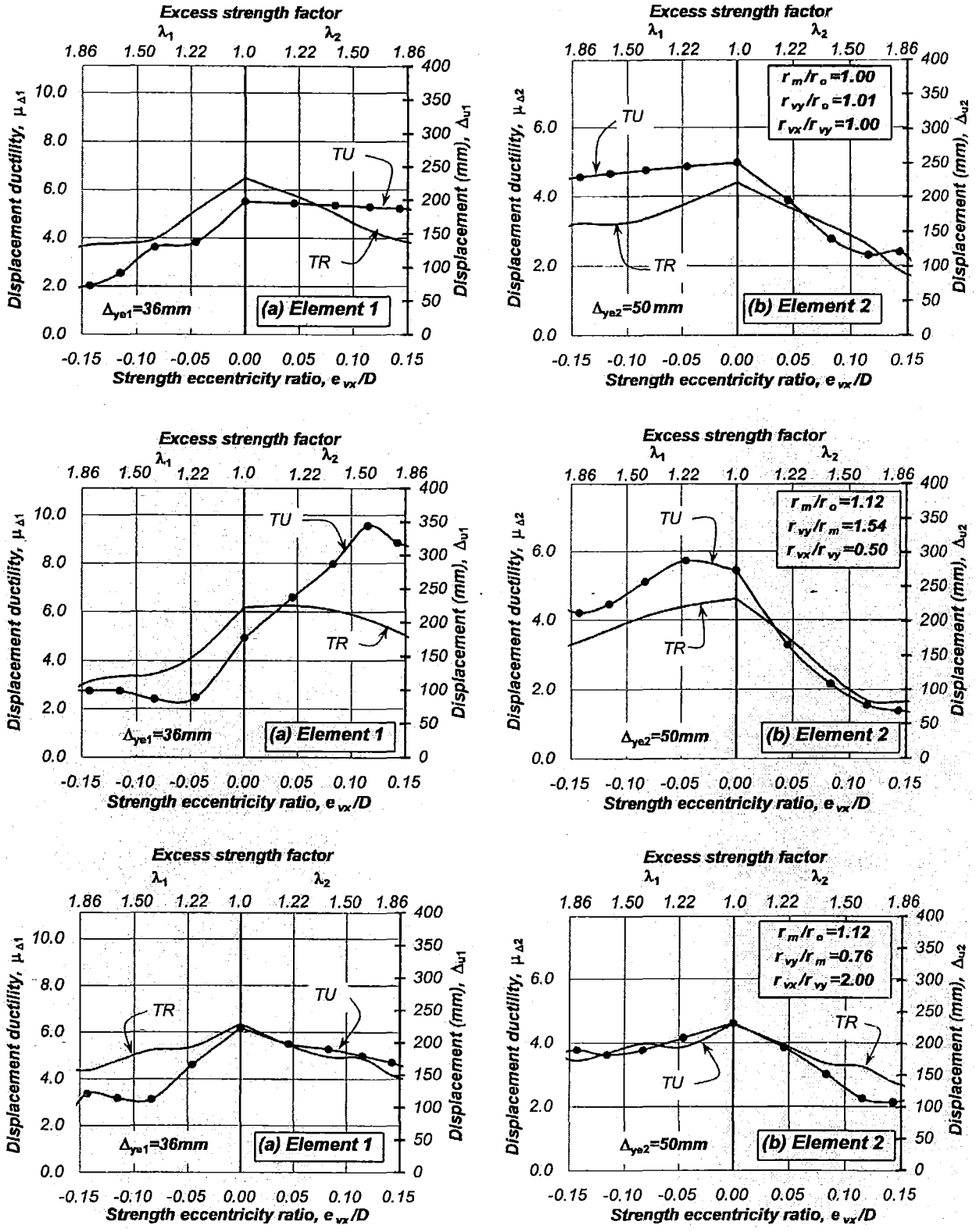

Figure 4-12. Response comparison of the restrained *Systems 3B-1.3(α=1.4), 4B-1.3(α=1.4) and 5B-1.3 (α=1.4)* with that of their unrestrained counterpart subjected to the Artificial earthquake record, T_s=1.30 sec, e_{mx}=0.0, $e_{vx} \neq e_{rx}$=variable, $\mu_{\Delta s}$=5.35, r_m/r_o=1.0, r_{vy}/r_m=variable, r_{vx}/r_{vy}=variable

It is evident from Figure 4-12 that for zero and increasing strength eccentricities the displacement ductility demand on the elements and the centre of mass was a maximum for both the restrained and unrestrained systems. In case of the restrained systems, the maximum displacement demand on the elements and at the centre of mass was essentially the same. The r_{vy}/r_m ratio did not have an effect on the response because, as explained before, the *X*-direction elements restrained system rotations. For this particular behaviour, it is possible to make full advantage of the displacement capacity of element *(1)* but not that of element *(2)*. In case of the unrestrained systems, relative displacements between elements *(1)* and *(2)* were influenced by the r_{vy}/r_m ratio. The maximum displacement demand of the elements of the unrestrained systems approached that of its restrained counterpart as the r_{vy}/r_m ratio was reduced.

The response at the centre of mass was essentially the same for the restrained systems and their unrestrained counterparts and was not affected by variations of the r_{vy}/r_m ratio. The equivalent single degree of freedom system was able to predict the maximum response at the centre of mass of both restrained and unrestrained systems.

The findings described above indicate that the displacement capacity of restrained systems having different r_{vy}/r_m ratios is essentially the same. The displacement capacity of the system should be limited to that element having the smallest displacement capacity. The proposed distribution of strength is successful in preventing any element from exceeding its displacement ductility capacity. The maximum displacement demands on elements and at the centre of mass of the restrained systems were the same and reached a maximum for zero strength eccentricity. These demands reduced, on both elements, with increasing strength eccentricities. Variations on the degree of torsional restraint, i.e., the r_{vx}/r_{vy} ratio, and the r_{vy}/r_m ratio did not show a critical effect on the systems' behaviour when subjected to the earthquake record along the *Y*-axis.

4.3.9 Response of the restrained *Systems 4B-1.3(α=1.4)* and *5B-1.3(α=1.4)* under earthquake records at different horizontal directions

The aim of this section is to verify if those conclusions already derived in Section 4.2.6 for the restrained *System 3B-1.3(α=1.4)* subjected to earthquake records along different directions are also valid on systems having other r_{vy}/r_m ratios. These responses are also compared to those attained when the system was subjected to the earthquake record along their reference *Y*-axis to identify if a critical situation arises.

The torsionally restrained *System 4B-1.3(α=1.4)* and *System 5B-1.3(α=1.4)* were considered. It properties are described in Appendix *B*. They were subjected to the Artificial record along different diagonal directions. The general procedure explained in Section 4.2 was used for their analysis.

Figure 4-13 and Figure 4-14 show that the displacement demands on the elements and at the centre of mass reached a maximum for zero strength eccentricity and for the earthquake record input along the *Y*-axis. The application of the Artificial earthquake record along other directions, i.e., *22°*, *45°*, *67°* and *90°* to the *Y*-axis, reduced the displacement demands on the elements and at the centre of mass for both zero and the realistic scenario of increasing negative strength eccentricities. This is, as stated in Section 4.2.6, because the seismic strength was larger along directions other than the principal *X* and *Y*-axes.

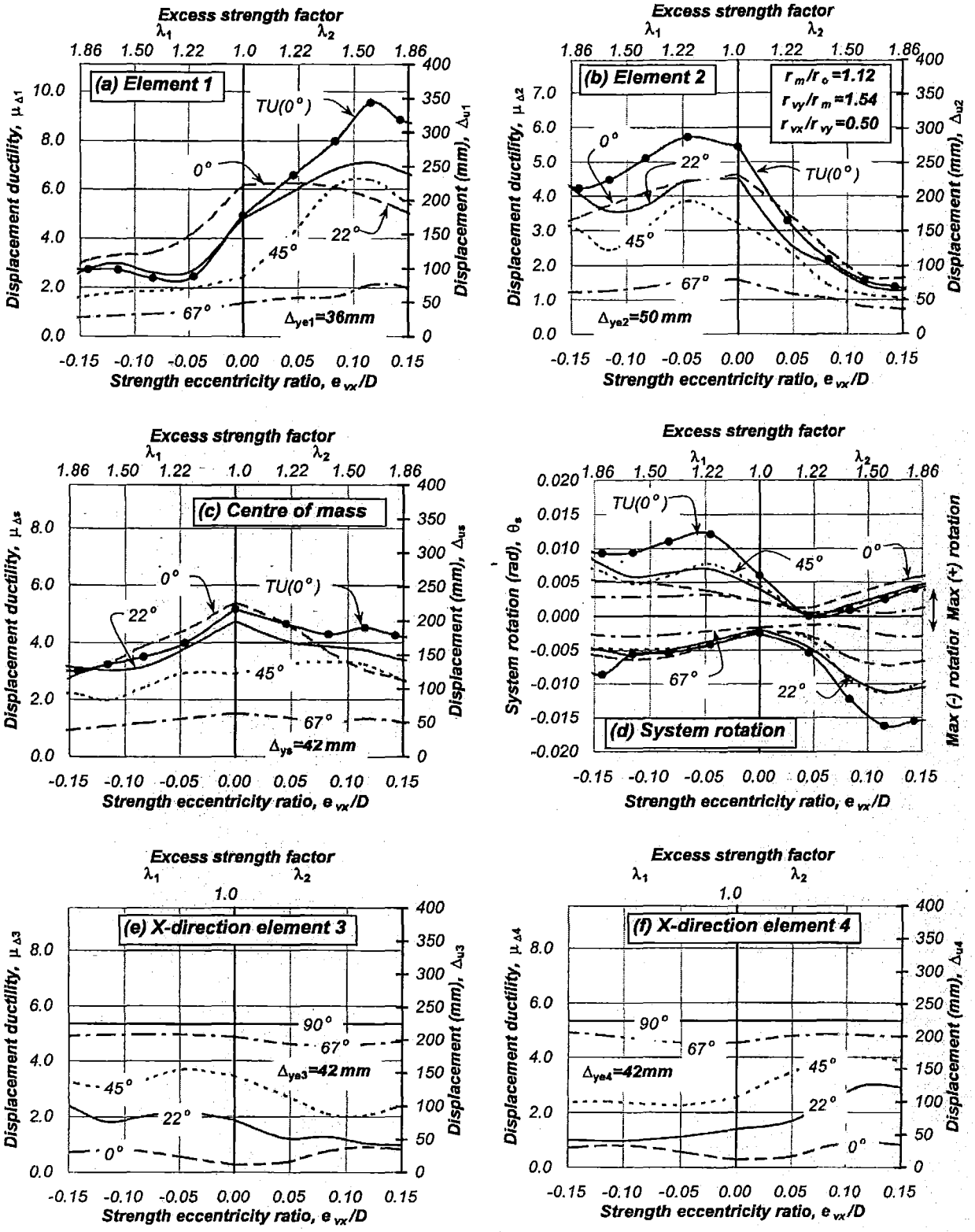

Figure 4-13. Response of the restrained *System 4B-1.3(α=1.4)* subjected to the Artificial earthquake record along different directions, T_s=1.30 sec, e_{mx}=0.0, $e_{vx} \neq e_{rx}$=variable, $\mu_{\Delta s}$=*5.35*, r_m/r_o=1.0, r_{vy}/r_m=1.01

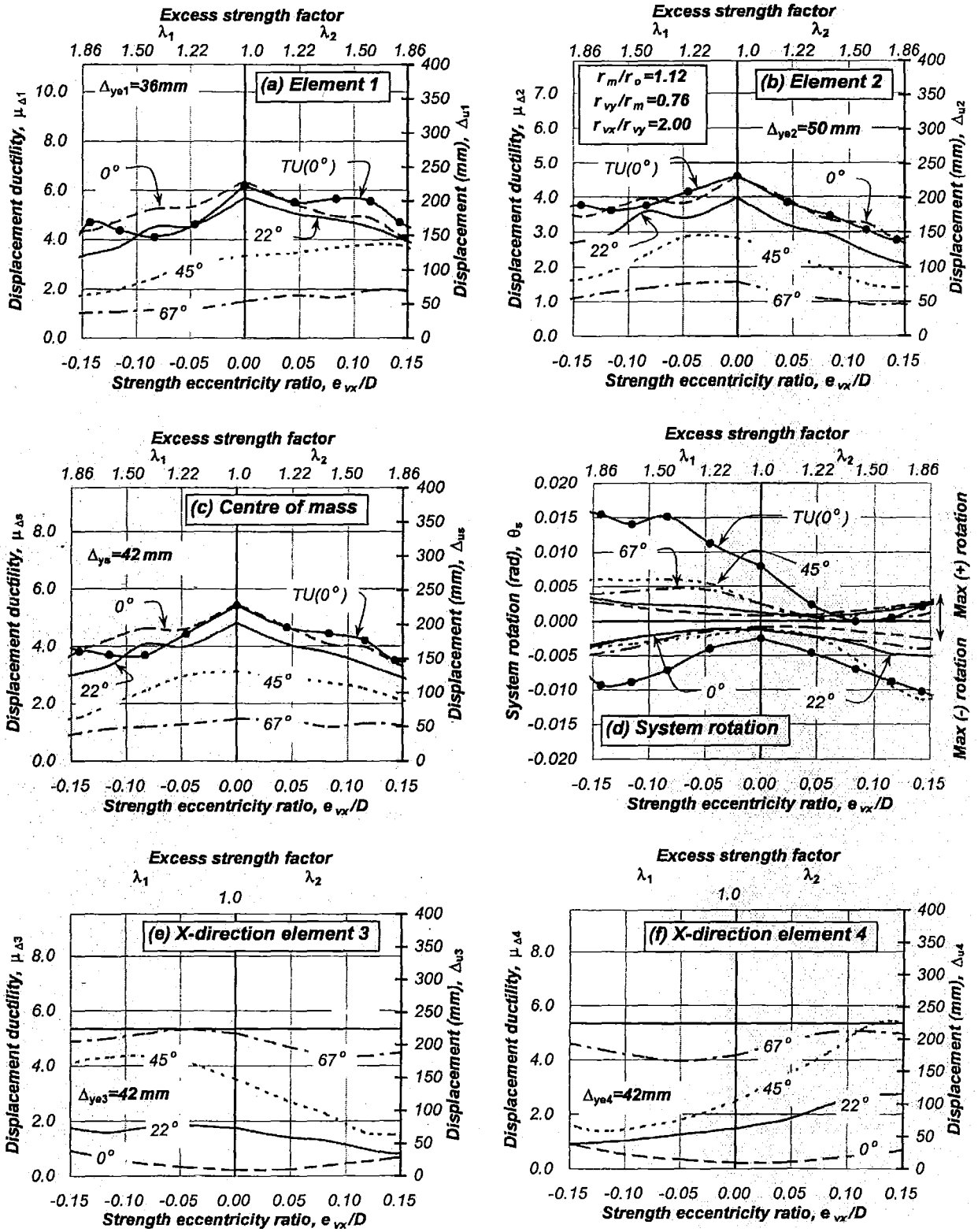

Figure 4-14. Response of the restrained *System 5B-1.3(α=1.4)* subjected to the Artificial earthquake record along different directions, T_s=1.30 sec, e_{mx}=0.0, $e_{vx} \neq e_{rx}$=variable, $\mu_{\Delta s}$=5.35, r_m/r_o=1.0, r_{vy}/r_m=1.01

The application of the earthquake record at several diagonal directions released the torsional restraint of the elements. System rotations reached a maximum when the earthquake record was applied at 22^o and 45^o. At this stage, significant differences in displacement ductility demands of parallel elements were observed. As expected, the maximum response of the restrained systems approximated that of its unrestrained counterpart, as shown in Figure 4-13 and Figure 4-14 and identified by curves *TU(0^o)*. The displacement demands of the elements for zero and increasing negative strength eccentricities did not exceed, however, the maximum response attained for zero strength eccentricity when the earthquake record was applied along the *X* or *Y*-direction.

Although increasing positive strength eccentricity leads, in some cases, to a critical response, it is an unrealistic scenario and it was just presented for general clarification of trends.

The above findings suggest that the design strategy is successful in preventing any element of restrained systems having different r_{vx}/r_{vy} and r_{vy}/r_m ratios from exceeding their displacement ductility capacity. The response of such systems having zero strength eccentricity and subjected to unidirectional earthquake input along the *X* and *Y*-axes led to a system maximum response. This was not exceeded with the application of the earthquake record at any oblique angle and the realistic situation of increasing negative strength eccentricities.

4.3.10 Response of the retrained *System 3B-0.5(α=1.4)*

This section aims to examine the effects of the uncoupled translational period on torsional response of restrained systems designed according to the suggested design strategy.

The restrained *System 3B* was considered again. The nominal yield displacement of the system, along the principal axes, remained unchanged and equal to $\Delta_{ys}=42mm$ as in those systems examined before. In this case, the system strength was further increased to achieve an uncoupled translational period of free vibration of $T_s=0.50$ seconds along both axes. The ratio of element nominal yield displacement was also $\alpha=\Delta_{ye2}/\Delta_{ye1}=1.40$. This case was denoted as restrained *System 3B-0.5(α=1.4)*. Its properties are summarised in Appendix *B*. The system displacement ductility capacity was assumed the same as that of the elements, $\mu_{\Delta s}=3.83$. The general procedure explained in Section 4.2 was used for the analysis of the system.

Table 4-4 summarizes the maximum response for zero strength eccentricity. It shows, as expected, similar displacement demands on elements *(1)* and *(2)* and at the centre of mass. System rotations were quite small, as expected, due to the torsional restraint of the *X*-direction elements. The rotational mass was barely mobilised and hence variations of the r_{vy}/r_m ratio did not influence the torsional response. The maximum displacement ductility demand at the centre of mass was about *90%* of that predicted by an equivalent single degree of freedom system. This confirms that the accuracy of this simple model in predicting the system maximum response reduced as the translational period was reduced. This characteristic was also observed with its unrestrained counterpart *System 3A-0.5(α=1.4)*; see Figure 3-25. This response emphasises the fact that the centre of mass is not the location where translations and rotations of ductile systems are independent. The action of the mass rotational inertia, besides affecting system rotations, also influences its translations; this characteristic is particularly evident in short period systems.

It is evident from Table 4-4 that the displacement ductility capacity of critical element *(1)* of $\mu_{\Delta 1}=3.83$ was exceeded. To prevent this from happening, the displacement capacity of the system should be further reduced. This may be achieved if the displacement capacity of the system is made the same as that element having the smallest displacement capacity, i.e., critical

element *(1)*. This is based on the fact that, for zero strength eccentricity, the maximum response of the elements and at the centre of mass is essentially the same. Hence, the system displacement ductility capacity should be reduced to $\mu_{\Delta s}=(\Delta_{ye1}/\Delta_{ys})\mu_{\Delta 1}=3.28$ to prevent critical element *(1)* from exceeding its displacement ductility capacity. This will not make full use of the displacement ductility capacity of element *(2)*.

Table 4-4. Response of the restrained *System 3B-0.5* (α=1.4) subjected to the Artificial earthquake record, T_s=0.50 sec, e_{vx}=0.0, e_{rx}=-0.083D, $\mu_{\Delta s}$=5.35, r_m/r_o=1.0, r_{vy}/r_m=variable

	Displacements, mm, and displacement ductility demands, (μ)				
r_{vy}/r_m	E1	CM	E2	ESDOF	E3=E4
$r_{vy}/0.85r_o$	156(4.33)	158(3.76)	161(4.47)	184(4.38)	8(elastic)
r_{vy}/r_o=1.00	162(4.50)	161(3.83)	166(3.29)	"	9(elastic)
$r_{vy}/1.20r_o$	160(4.44)	164(3.90)	170(3.37)	"	10(elastic)

Figure 4-15 illustrates the maximum response as affected by increasing strength eccentricities. It is evident that maximum displacement ductility demands of element *(1)* and at the centre of mass occurred for zero strength eccentricity and reduced with increasing negative strength eccentricities. The displacement ductility demand on critical element *(2)* also reduced. This was because the reduction of displacement demands at the centre of mass, due to an increase of system strength, over-compensated for the rotation-induced displacements on critical element *(2)*, additional to those resulting from system translation. The *X*-direction elements remained elastic for the range of strength eccentricities considered. They restrained system rotations and hence the rotational mass was barely mobilised, as shown in Figure 4-15(e). Hence, the variation of the r_{vy}/r_m ratio did not influence the torsional response.

Figure 4-15 also plots the predicted response of the restrained *System 3B-0.5(α=1.4)* along with that of its unrestrained counterpart *System 3A-0.5(α=1.4)*. It is evident that the response of the restrained system was not as sensitive as its unrestrained counterpart. The *X*-direction elements substantially restrained system rotations. It is seen that the maximum displacement demand at the centre of mass of the restrained *System 3B-0.5(α=1.4)* and its unrestrained counterpart *System 3A-0.5(α=1.4)* were different, as shown in Figure 4-15(c).

The design strategy is still considered appropriate to prevent any element from exceeding its displacement ductility capacity on systems with short uncoupled translational periods exhibiting a sensitive response. This sensitivity is manifested in the response at the centre of mass, which is considered the location where system rotations and translations are assumed independent. This generalization, however, loses accuracy as the uncoupled translational period reduces. In spite of this behaviour, the equivalent single degree of freedom system is considered, for practical purposes, a valid model for predicting the maximum displacement demand at the centre of mass of asymmetric systems with any uncoupled translational period.

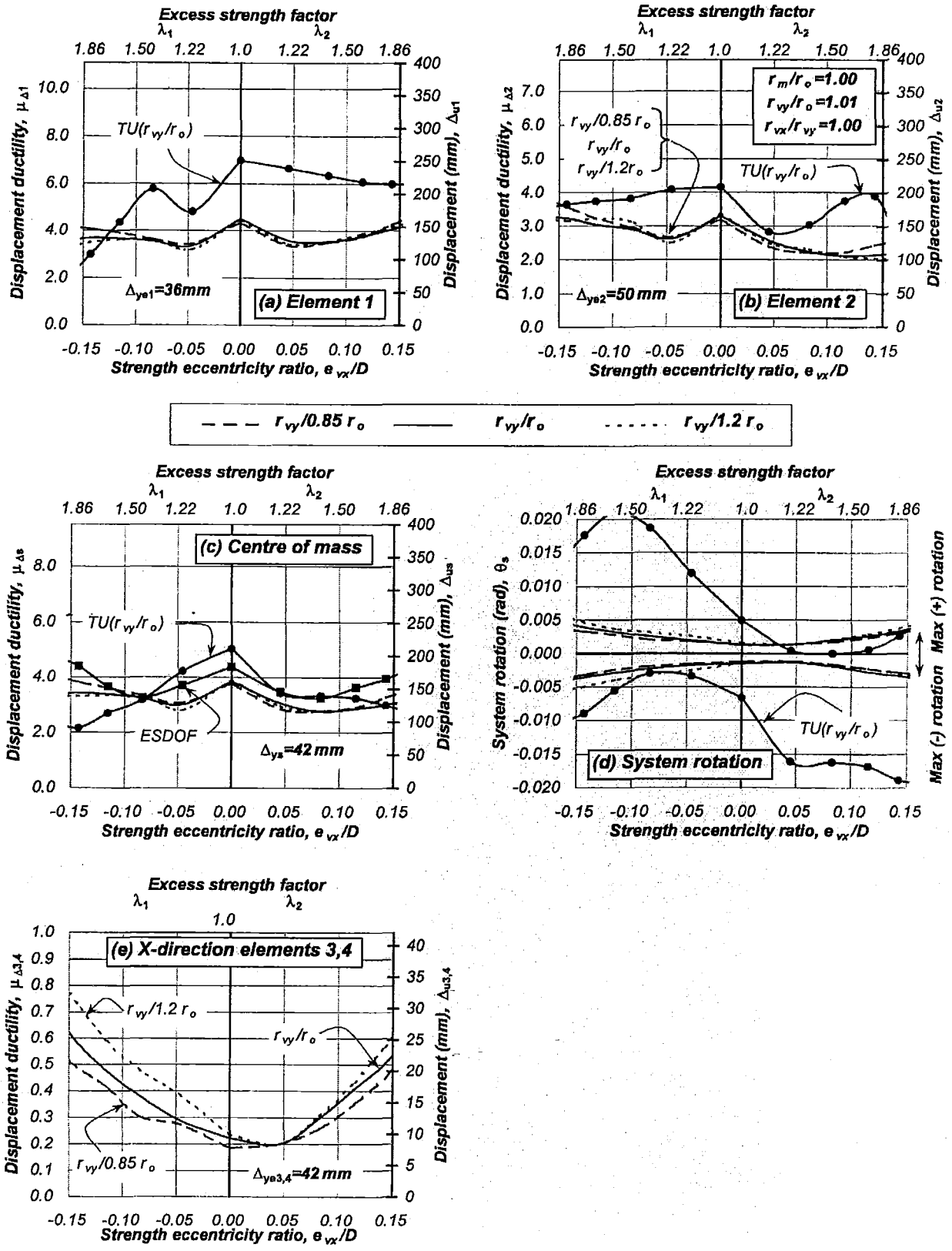

Figure 4-15. Response of the restrained *System 3B-0.5(α=1.4)* subjected to the Artificial earthquake record, T_s=0.50 sec, e_{mx}=0.0, $e_{vx} \neq e_{rx}$=variable, $\mu_{\Delta s}$=5.35, r_m/r_o=1.0, r_{vy}/r_m=variable

4.4 Single-element structurally asymmetric *Systems 7B, 8B and 9B (CV=CR≠CM; CM=GC)*

4.4.1 Response of the restrained *Systems 7B-1.3, 8B-1.3 and 9B-1.3*

This section examined the torsional response of three extremely eccentric systems. Although unrealistic, they may contribute to a better understanding of the response of torsionally restrained systems.

The restrained *Systems 7B, 8B and 9B*, shown in Figure 2-32, were examined. The *Y*-direction element *(1)* and the *X*-direction elements *(3)* and *(4)* had the same nominal yield displacement of $\Delta_{ye1}=\Delta_{ye3}=\Delta_{ye4}=42mm$. The nominal yield displacement of the system was, therefore, the same along the principal axes, $\Delta_{ys}=42mm$. The system strength was adjusted to achieve an uncoupled translational period of *1.30* seconds along both axes. They are denoted restrained *Systems 7B-1.3, 8B-1.3* and *9B-1.3*. The effect of the mass rotational inertia and the strength eccentricity on the response was quantified by the e_{vx}/r_m ratio rather that the r_{vy}/r_m ratio because the radius of gyration of strength of a single element along the *Y*-axis is zero for all three systems having different strength eccentricities. Section 2.20 described in detail its characteristics and Appendix *B* summarizes its properties.

The restrained *System 7B-1.3* was subjected, along the *Y*-direction, to the scaled Artificial earthquake record already applied to its unrestrained counterpart *System 7A-1.3*. The restrained *Systems 8B-1.3* and *9B-1.3* having different e_{vx}/r_m ratios were also subjected to same earthquake record.

Table 4-5 summarizes the response of the systems when element *(1)*, and hence the system, had no excess strength, i.e., $\lambda_1=\lambda_{ys}=1.0$. It is evident that the displacement demands of element *(1)* and position *(2)* were influenced by the strength eccentricity and the distribution of mass, i.e., the e_{vx}/r_m ratio. As the e_{vx}/r_m ratio reduced, the maximum displacement demand of element *(1)* reduced and became similar to that attained at position *(2)*. This suggests that the maximum displacement demand of the elements approximates that of a system exhibiting no torsional response. This happens because the maximum displacement demands of the elements are less affected by system rotations even though significant rotations did occur. Element *(1)* became critical as the effect of system rotations on its maximum response reduced. This scenario is evident with the restrained *System 9B-1.3* having $e_{vx}/r_m=0.76$. As expected, the maximum displacement demands of the element were essentially the same. In this situation, element *(1)*, having the smallest nominal yield displacement, exceeded its displacement ductility capacity of element *(1)* of $\mu_{\Delta 1}=5.35$. This behaviour suggests that *Systems 7B, 8B and 9B* are not, strictly speaking, torsionally restrained because their response is influenced by changes in the r_{vy}/r_m ratio.

Table 4-5. Response of the restrained *Systems 7B-1.3, 8B-1.3* and *9B-1.3* subjected to the Artificial earthquake record, T_s=1.30 sec, $e_{vx}=e_{rx}$=variable, $\mu_{\Delta s}=5.35$, r_m/r_o=variable, e_{vx}/r_m=variable

	Displacements, mm, and displacement ductility demands,(μ)				
Systems	***E1***	***CM***	***Position 2***	***ESDOF***	***E3=E4***
7B	*176(4.19)*	*176(4.19)*	*221*	*225(5.35)*	*91(2.17)*
8B	*99(2.36)*	*170(4.04)*	*348*	*"*	*91(2.17)*
9B	*232(5.54)*	*234(5.57)*	*236*	*"*	*96(2.28)*

It seems appropriate to ignore the strength contribution of the *X*-direction *(3)* and *(4)* into the radius of gyration of strength based on the fact that the displacement demands of these elements were essentially the same for all three systems, as shown in Table 4-5, and not affected by differences in torsional restraint. This response is due to the combined effect of the torsional restraint of the *X*-direction elements and the fact that system rotations are not directly associated with the element's maximum displacement demand.

It is also evident from Table 4-5 that a reduction of the strength eccentricity in systems having the same radius of gyration of mass, as it is the case of the restrained *Systems 8B-1.3* and *9B-1.3*, reduced the effect of system rotations on the displacement demands of the elements. This shows that the r_{vy}/r_m ratio, which considers the distribution of element strength and uniformly distributed mass, is a relevant parameter quantifying the effect of system rotations on the maximum displacement demand of the elements.

It is also observed from Table 4-5 that an equivalent single degree of freedom system did not predict well the response at the centre of mass of extremely asymmetric systems. The prediction improved as the e_{vx}/r_m ratio was reduced because system translations were less affected by the action of the mass rotational inertia.

Figure 4-16 illustrates the response when the strength of element *(1)*, and hence the system strength along the *Y*-direction only, was gradually increased to twice its original strength, i.e., $1.0<\lambda_1=\lambda_{ys}\leq 2.0$. As expected, the displacement demands of element *(1)* reduced as its strength was increased. The displacement demands at the centre of mass reduced slightly for some systems, particularly on the restrained *System 9B-1.3* having $e_{vx}/r_m=0.76$. On the other hand, the displacement demands at position *(2)* of the restrained *Systems 7B-1.3* and *8B-1.3*, having $e_{vx}/r_m \geq 1.0$, slightly exceeded that attained for $\lambda_1=\lambda_{ys}=1.0$. It is also seen that the displacement demands of position *(2)* did not reduce as the system strength increased. Figure 4-16(d) shows, as expected, large positive and negative rotations in all three systems and were slightly affected by the variation of the e_{vx}/r_m ratio. It is evident that displacement demands of the *X*-direction elements were essentially the same as the system strength increased, as Figure 4-16(e) shows, and not affected by differences in system rotations. This is due to the combined effect of the torsional restraint introduced by the *X*-direction elements and the fact that the maximum displacement demand of these elements are less affected by system rotations as the e_{vx}/r_m ratio reduced.

It is concluded that the rotations of extremely restrained systems were reduced significantly by increased torsional restraint of the *X*-direction elements. However, contrary to those restrained systems examined in previous sections, the response was affected by the e_{vx}/r_m ratio. The maximum displacement demands of the elements were less associated with system rotations as the e_{vx}/r_m ratio reduced. This indicates that the system cannot be considered, strictly speaking, as torsionally restrained. The equivalent single degree of freedom system does not predict satisfactorily the response at the centre of mass of extremely eccentric systems because system translations are significantly affected by the action of the mass rotational inertia. These findings suggest that extremely eccentric systems have a sensitive response, which is difficult to predict with an equivalent single degree of freedom system.

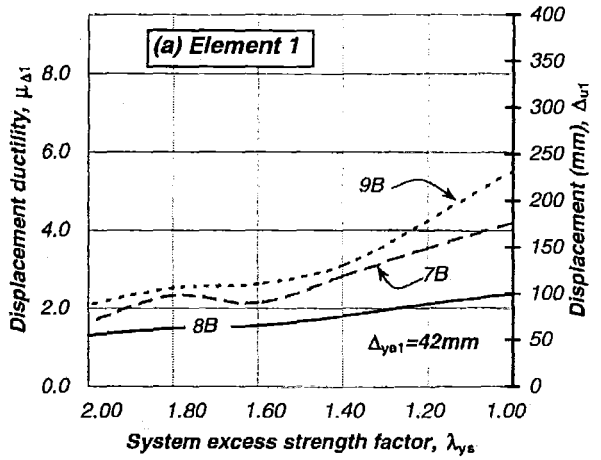

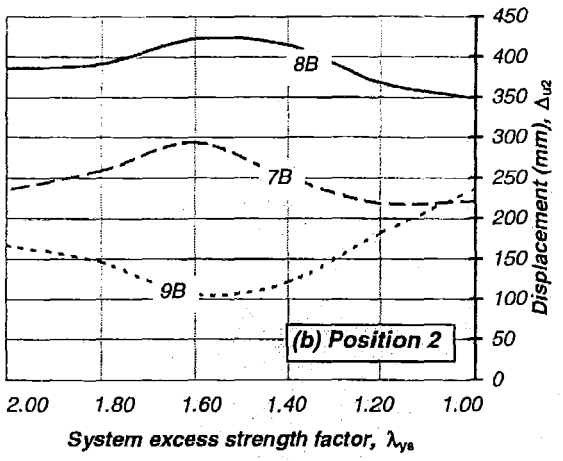

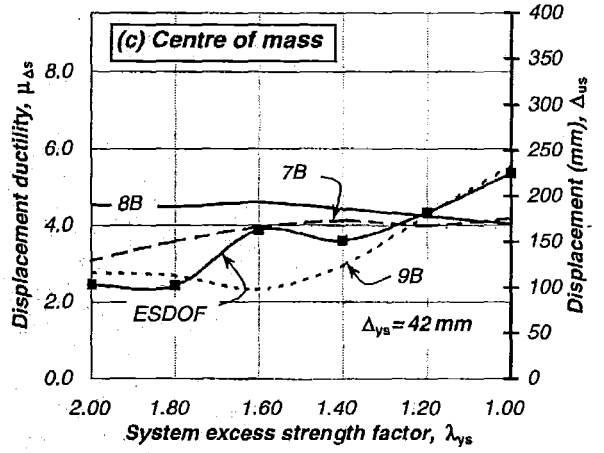

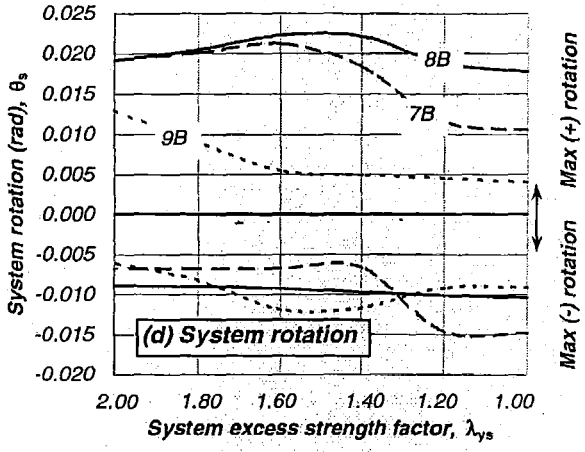

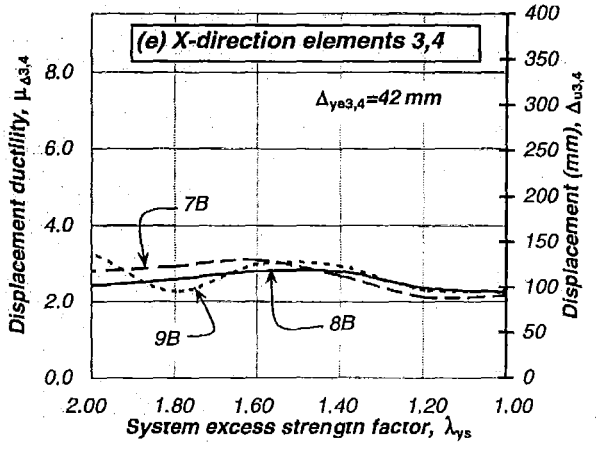

System	r_m/r_o	e_{vx}/r_m
7B	1.00	1.00
8B	1.12	1.54
9B	1.12	0.76

Figure 4-16. Response of the restrained *Systems 7B-1.3, 8B-1.3 and 9B-1.3* subjected to the Artificial earthquake record, T_s=*1.30 sec*, e_{mx}=0.0, $e_{vx}=e_{rx}$=variable, $\mu_{\Delta s}$=*5.35*, r_m/r_0=variable, e_{vx}/r_m=variable.

4.4.2 Time history response of the restrained *System 7B-1.3*[$e_{vx}=e_{rx}=-0.41A(\lambda_1=\lambda_{ys}=1.0)$]

The time history response of the restrained *System 7B-1.3* was examined again. It is of interest to study, in detail, the effect of the *X*-direction elements on the response of extremely eccentric systems.

The restrained *System 7B-1.3,* as shown in Figure 2-32(b) was considered again. The *X* and *Y*-direction elements had identical nominal yield displacements. The nominal yield displacement of the system was therefore the same as that of the elements, i.e., $\Delta_{ys}=\Delta_{ye1}=\Delta_{ye3}=\Delta_{ye4}=42mm$. The system strength was also the same, $V_{yns}=V_{xns}=176kN$. It was subjected to the Artificial earthquake record along the *Y*-direction.

The application of a positive static lateral force at the centre of mass will generate an anticlockwise rotation about the centre of stiffness and hence about element *(1)*. This element can never reach its nominal strength due to this particular action. The static torque, $T=e_{vx}V_{yns}$, would need to be entirely resisted by the *X*-direction elements *(3)* and *(4)* having a nominal strength of $V_{ne3}=V_{ne4}=88kN$. The static lateral force required to develop their strength will be then $V_E=V_{yns}=(V_{ne(3or4)}E)/e_{vx}=1077/6.12=176kN$.

A different behaviour was observed during dynamic response due to the engagement of the mass rotational inertia. It was of particular interest the response between *2.0* and *4.0* seconds.

Element *(1)* reached its nominal strength at instant *(A)* due to the opposition of the mass rotational inertia to system rotation; see Figure 4-17(a). A total clockwise torque of $T=1919kNm$ was generated as the rotational mass accelerated in the elastic system; see Figure 4-17(e). The associated displacement profile; see Figure 4-18(a), shows that the displacement demands on element *(1)* and position *(2)* were opposite in sign while the displacement at the centre of mass was essentially zero. The *X*-direction elements *(3)* and *(4)* were still elastic, $V_{e3}=V_{e4}=68kN$, while contributing to a torque of $T=832kNm$. The torque introduced by the rotating mass was at this stage, $1919-832=1087kNm$, which is a significant quantity.

After element *(1)* yielded, the system torque increased slightly and reached, an instant later, a peak of $T=1993kNm$. This behaviour was imperceptible from the time history response but readily observed from the associated displacement profile attained an instant later; see Figure 4-18(b). It shows that the system torque did not stop immediately, as it occurred with its torsionally unrestrained counterpart *System 7A-1.3*; see Figure 3-29. This is because the *X*-direction elements were elastic and, therefore, enabling a slight increase of system torque and rotation. The base shear of the *X*-direction elements increased to $V_{e3}=V_{e4}=74kN$, just under their nominal strength.

At instant *(B)*, the *X*-direction elements *(3)* and *(4)* reached their nominal strength due to the combined effect of an anticlockwise rotation and a positive system displacement. The displacement at position *(2)* increased at a faster rate than that of element *(1)*; see Figure 4-17(c). At this stage, the *Y*-direction element *(1)* was elastic and had a positive displacement. The torque reached a peak at this instant and a rotational deceleration was observed; see Figure 4-17 (e). The system becomes torsionally unrestrained. The associated displacement profile; see Figure 4-18(c), shows the displacement demands of element *(1)*, position *(2)* and the centre of mass were smaller than the maximum attained.

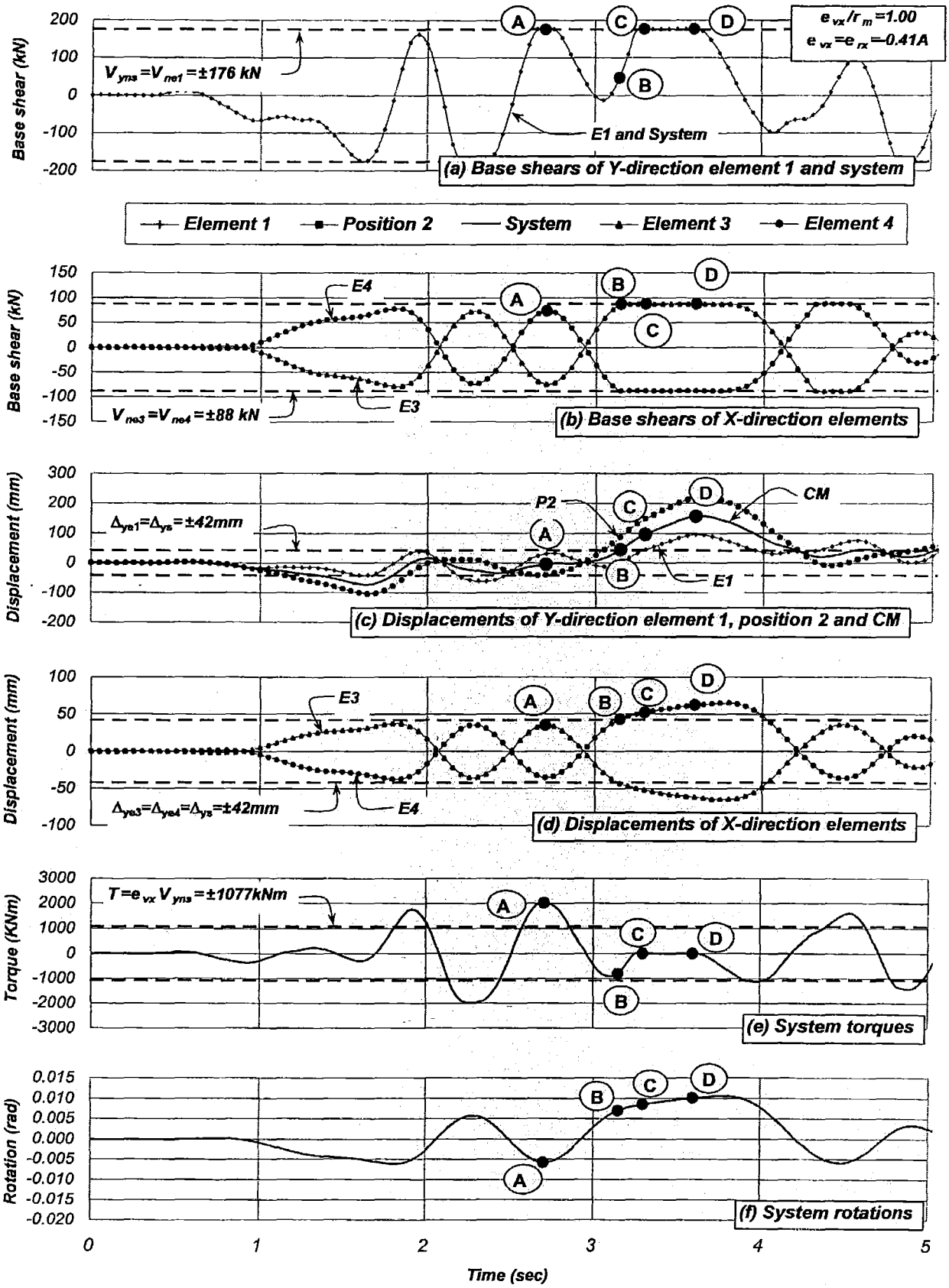

Figure 4-17. Time history response of the restrained *System 7B-1.3* subjected to the Artificial earthquake record, T_s=1.30 sec, e_{mx}=0.0, $e_{vx}=e_{rx}$=-0.5D, $\mu_{\Delta s}$=*5.35*, r_m/r_o=1.0, e_{vx}/r_m=1.0

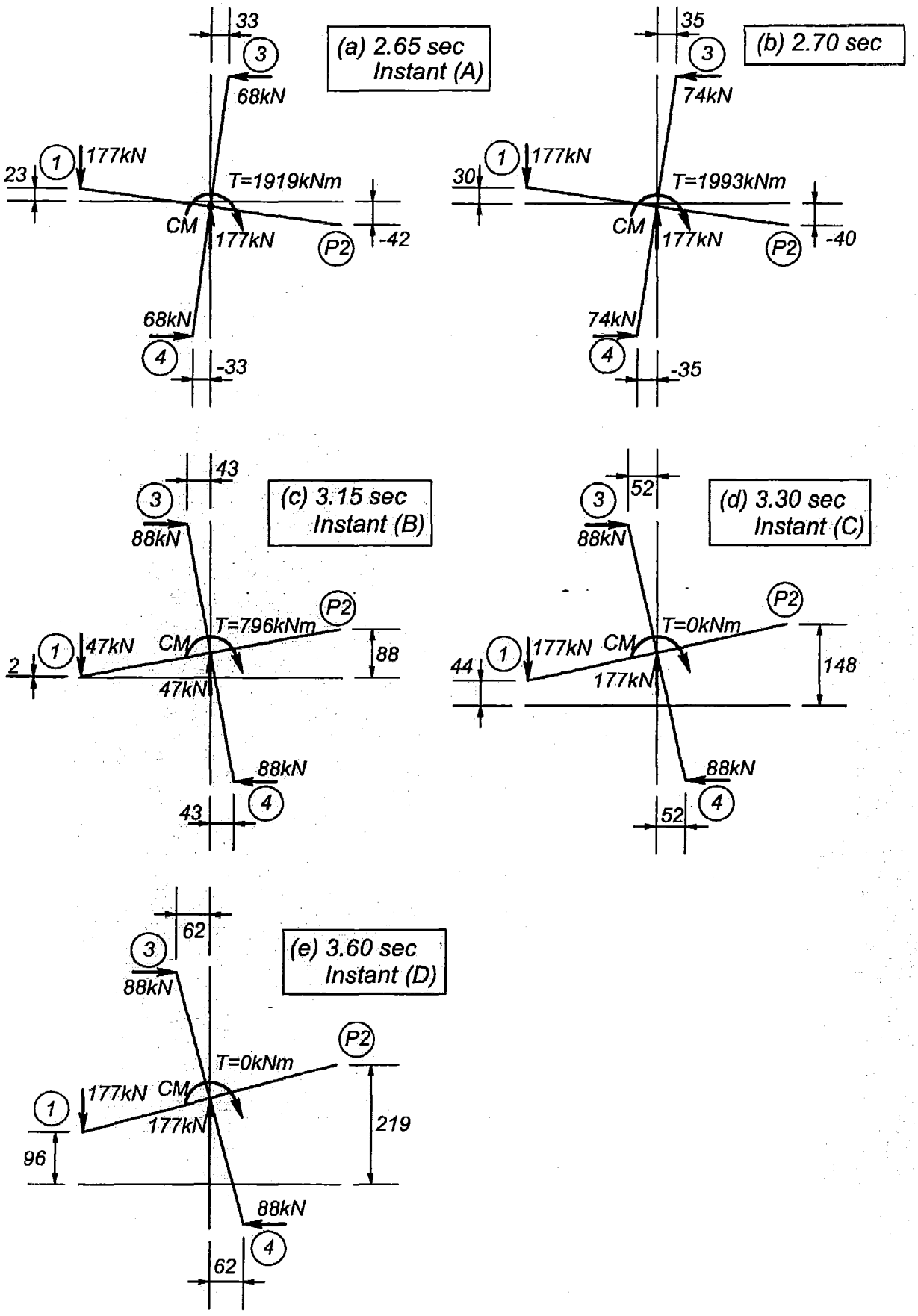

Figure 4-18. Displacement profiles and actions introduced to the restrained *System 7B-1.3* subjected to the Artificial earthquake record, T_s=1.30 sec, e_{mx}=0.0, e_{vx}= e_{rx}=-0.5D, $\mu_{\Delta s}$=*5.35*, r_m/r_o=1.0, e_{vx}/r_m=1.0

Figure 4-17(a) shows that element *(1)* reached again its nominal strength at instant *(C)* when the *X*-direction elements *(3)* and *(4)* were already yielding. Element *(1)* was able to yield for a positive system displacement. This was because the system torque reduced due to the deceleration of the rotational mass, as shown in Figure 4-17(c). This deceleration occurred when the *X*-direction elements were yielding due to a force couple. One of the forces was the residual strength of element *(1)* and the other axis of resistance was generated by the action of the mass translational inertia. Once element *(1)* yielded, the system torque becomes zero and its rotation slightly increased due to the rotational velocity, as shown in Figure 4-17(f). The associated displacement profile; see Figure 4-18(e), show that the displacement demands of element *(1)*, position *(2)* and at the centre of mass had not reached their maxima.

Element *(1)* continued inelastic displacements until reaching instant *(D)*, as shown in Figure 4-17(b) and Figure 4-18(e). The *X*-direction elements *(3)* and *(4)* were inelastic between instants *(C)* and *(D)* and the torque remained zero. In spite the fact that all elements were yielding, system rotations increased due to the rotational velocity of the system. The maximum displacement of position *(2)* was reached moments after reaching instant *(D)*. The maximum displacement demand of element *(1)* of $\Delta_{u1}=173\ mm$ ($t=11.0sec$) (not shown in the time history) occurred for a much smaller system rotation when the displacement demands on element *(1)* and position *(2)* were similar.

In summary, the maximum rotation of the restrained *System 7B-1.3* occurred, as expected, when the *X*-direction elements were yielding. This scenario, however, was not associated with the maximum displacement of the *Y*-direction element *(1)*, which was reached for a much smaller system rotation and when the *X*-direction elements were elastic. The maximum displacement demand of position *(2)* was closely related to the system maximum rotation.

4.4.3 Response of the restrained *System 7B-1.3* under earthquake records at different angles

The response of the torsionally restrained *System 7B-1.3* was also examined when it was subjected to the Artificial earthquake at 22^o, 45^o, 68^o and 90^o angles relative from the reference *Y*-axis. The torsional behaviour of the restrained *Systems 8B-1.3 and 9B-1.3* were similar and therefore their results were not presented.

Figure 4-19 shows the response of the system when the strength of element *(1)*, and hence that of the system, was incrementally increased to twice its original strength, i.e., $1.0<\lambda_1=\lambda_{ys}\leq 2.0$. In case of $\lambda_{ys}=1.0$, it is evident that the maximum displacement demands of element *(1)*, position *(2)* and at the centre of mass occurred when the earthquake record was applied along the reference *Y*-axis. For the same distribution of strength, the displacement demands at the different locations reduced as the angle of application of the earthquake record was varied between 22^o and 67^o. This was expected because the system strength was larger at those angles, as already explained in Section 2.16.1. Figure 4-19(b) shows at certain directions of earthquake record input, when the strength enhancement of element *(1)* was moderate(i.e., $\lambda_{ys}<1.50$), that the displacement demands at position *(2)* slightly exceeded the maxima attained when the earthquake record was solely applied along the reference *Y*-axis.

Figure 4-19 also shows the response when the strength of element *(1)*, and hence that of the system, was gradually increased, $\lambda_{ys}>1.0$. It is evident that the displacement demands at the different locations generally reduced with increasing angle of earthquake record input.

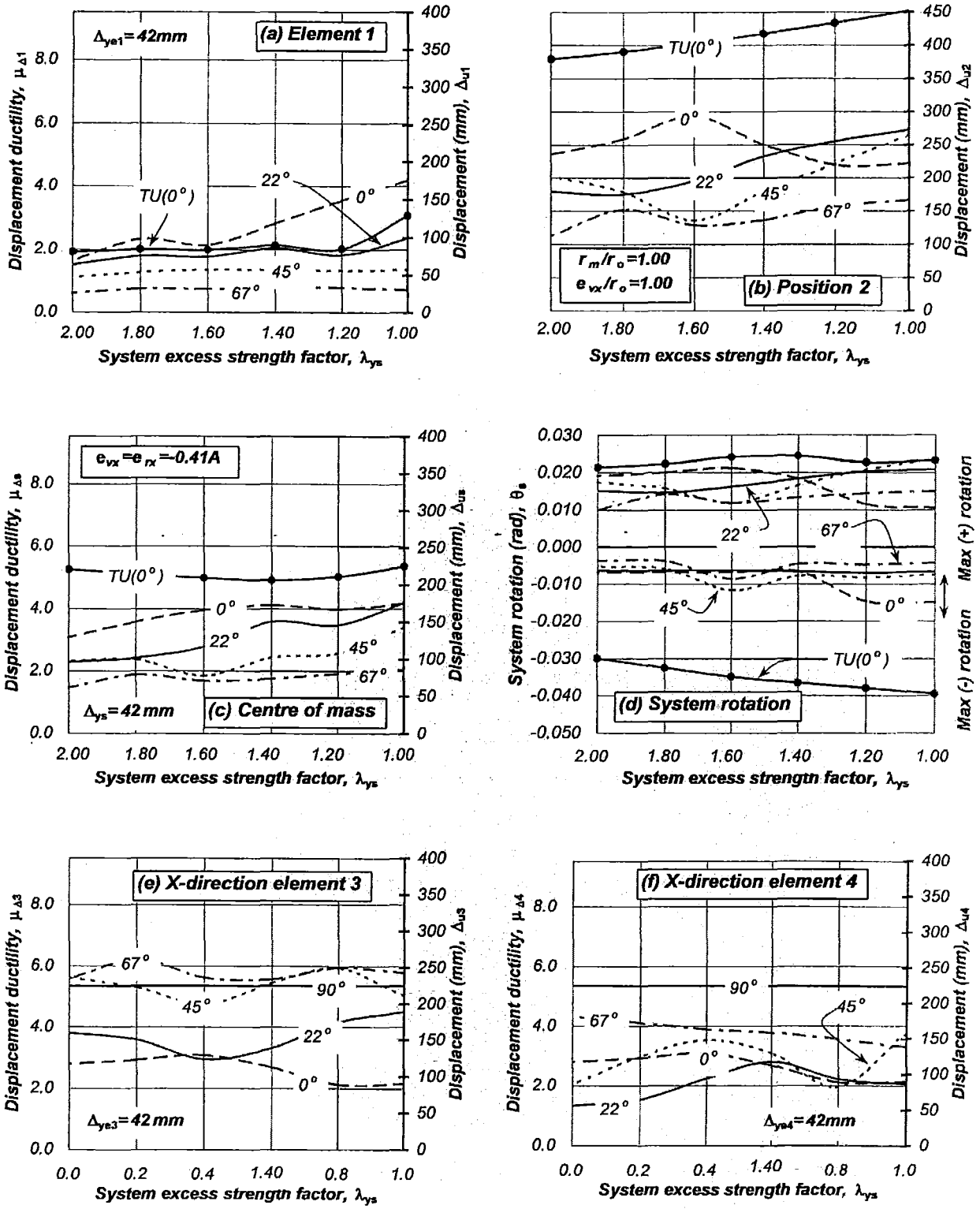

Figure 4-19. Response of the restrained *Systems 7B-1.3* subjected to the Artificial earthquake record, T_s=*1.30 sec*, e_{mx}=0.0, e_{vx}=e_{rx}=variable, $\mu_{\Delta s}$=*5.35*, r_m/r_o=variable, e_{vx}/r_m=variable

The angle of incidence of the earthquake record in conjunction with large eccentricities had a relevant effect on the response of the *X*-direction elements. It is evident from Figure 4-19(e) and (f) that the displacement demands of the *X*-direction element *(3)* exceeded those attained when the earthquake record was applied solely along the *X*-axis. This is a particular characteristic of systems with large strength and stiffness eccentricities and hence prone to large system rotations. It was shown that the large system rotations did not influence the maximum response of the *Y*-direction elements but it did increase the displacement demands on the *X*-direction element *(3)* above its displacement ductility capacity. These findings are of no importance since such extremely asymmetric systems are not expected to be encountered in reality.

Figure 4-19 also compares the response of the restrained *System 7B-1.3* with it unrestrained counterpart *System 7A-1.3*. It is evident from Figure 4-19(d) that the restrained *System 7B-1.3* displayed smaller rotations due to the torsional resistance introduced by all elements. The displacement demands of element *(1)* were larger in the restrained system when it was subjected to unidirectional earthquake input; see Figure 4-19(a). The opposite occurred at position *(2)* and the centre of mass where displacement demands were smaller; see Figure 4-19(b) and (c). This was expected because system rotations were smaller. It is considered that for even this extreme restrained system, the application of the Artificial earthquake record along the *Y*-axis generated an envelope of the maximum displacement demands at the different locations.

It is concluded that the maximum system rotation was not associated with the maximum displacement demand of the *Y*-direction element *(1)*. Although system rotations increased, the application of an earthquake record at different angles did not impose displacement demands to element *(1)* in excess to those attained when the earthquake record was applied along the principal *Y*-axis. Hence, systems subjected to earthquake excitations at directions other that the principal axes, do not exhibit, in general, a critical response.

4.5 Three-element structurally asymmetric *System 10B* (*CV≠CR; CM=GC*)

4.5.1 Response of the restrained *System 10B-1.3*

A three-element torsionally restrained system was considered. The objective was to: (a) examine the effect that the addition of a third element parallel to the *Y*-axis may have on the torsional response, (b) identify differences in behaviour, if any, between this and those two-element restrained systems previously examined and (c) compare its response with that of its unrestrained counterpart.

The restrained *System 10A* had three substitute wall-elements along the *Y*-direction with unequal lengths, as shown in Figure 2-33(b). Their nominal yield displacements were $\Delta_{ye1}=\Delta_{ye3}=69mm$ and $\Delta_{ye2}=34mm$. The *X*-direction elements had the same nominal yield displacement, $\Delta_{ye4}=\Delta_{ye5}=42mm$. The nominal yield displacement of the system, along both principal directions was, therefore, $\Delta_{ys}=42mm$. This was consistent with those systems previously examined. The system strength was adjusted to achieve a translational uncoupled period of free vibration of *1.3* seconds. It is denoted restrained *System 10B-1.3*. The radius of gyration of the uniformly distributed mass of the square plan, r_o, was varied to $0.85r_o$ and $1.20r_o$ to consider other plan configurations and to account for differences between the computed and the actual distribution of mass. Section 2.21 and Appendix *B* provides additional information of this system. The considerations already explained in Section 4.2 were also used for the analysis of the system.

The system strength was initially distributed to satisfy static equilibrium, i.e. $e_{vx}=0.0$. It is assumed that this strength will prevent the system, and hence its elements, from exceeding its displacement ductility capacity. Zero strength eccentricity may be difficult to achieve in practice because some elements are likely to require an excess strength to comply with requirements of minimum reinforcement. Regardless of this situation, the system response for zero strength eccentricity and the displacement capacity of the critical element, provides the basis to estimate the system displacement and associated ductility capacity.

Table 4-6 summarizes the system response for zero strength eccentricity. No significant differences in displacement demands of the elements and at the centre of mass were observed for the different values of r_{vy}/r_m ratio. The equivalent single degree of freedom simulation predicted, with adequate accuracy, the response at the centre of mass and therefore was not influenced by the addition of a third parallel element along the *Y*-direction. It is also evident that the torsional behaviour was similar to that of the two-element restrained *System 5B-1.3* having a similar r_{vy}/r_m ratio; see also Figure 4-12(e) and (f).

Differences in displacement ductility demands were observed due to the different nominal yield displacements of the elements. Element *(2)*, having the smallest displacement capacity, was critical because it exceeded its displacement ductility capacity. This may be prevented, as previously explained, if the displacement ductility capacity of the system would have been limited to that of element *(2)* having the smallest displacement ductility capacity. Hence, the displacement capacity of the system would be $\Delta_{us}=\Delta_{u2}=\mu_{\Delta 2}\Delta_{ye2}=183mm$ and its ductility capacity is $\mu_{\Delta s}=\Delta_{us}/\Delta_{ys}=183/42=4.33$. The maximum displacement demands expected to be attained and not exceeded by the *Y*-direction elements are $\mu_{\Delta 1}=\mu_{\Delta 3}=183/69=2.64$ and $\mu_{\Delta 2}=183/34=5.35$.

Table 4-6. Response of the restrained *System 10B-1.3* subjected to the Artificial earthquake record, T_s=1.30 sec, e_{mx}=0.0, e_{vx}=0.0, e_{rx}=-0.055D, μ_{As}=5.35, r_m/r_o=1.0, r_{vy}/r_m=variable

	***Displacements, mm, and displacement ductility demands* (μ)**					
r_{vy}/r_m	*E1*	*E2*	*CM*	*E3*	*ESDOF*	*E4=E5*
$r_{vy}/0.85r_o$	*225(3.28)*	*223(6.49)*	*222(5.29)*	*220(3.21)*	*225(5.35)*	*12(elastic)*
$r_{vy}/r_o=0.78$	*228(3.33)*	*222(6.48)*	*220(5.24)*	*212(3.08)*	"	*14(elastic)*
$r_{vy}/1.20r_o$	*220(3.20)*	*218(6.35)*	*218(5.18)*	*217(3.16)*	"	*17(elastic)*

For some reason, one or more elements might have strength in excess to that satisfying zero strength eccentricity. This element excess strength will introduce a strength eccentricity and an increase in system strength. The critical scenario occurs when excess strength was assigned to either element *(1)* or *(3)* because it introduced the largest strength eccentricity for the least increase in system strength; as already shown in Figure 2-34. The excess strength of element *(2)* is not a critical scenario and is not examined here.

Figure 4-20 shows the response of the system for increasing strength eccentricities due to the excess strength of elements *(1)* and *(3)*. The realistic situation of assigning excess strength to element *(1)* reduced the displacement demands on all elements and at the centre of mass. The elastic *X*-direction elements reduced the rotations significantly. The response was essentially the same for every r_{vy}/r_m ratio, indicating that the rotational mass was difficult to mobilise due to the restraining effect of the *X*-direction elements. As to be expected, an increase of displacement demands on the *X*-direction elements was observed due to increasing strength eccentricities. In general, similarities in torsional behaviour with the two-element restrained *System 5B-1.3* also

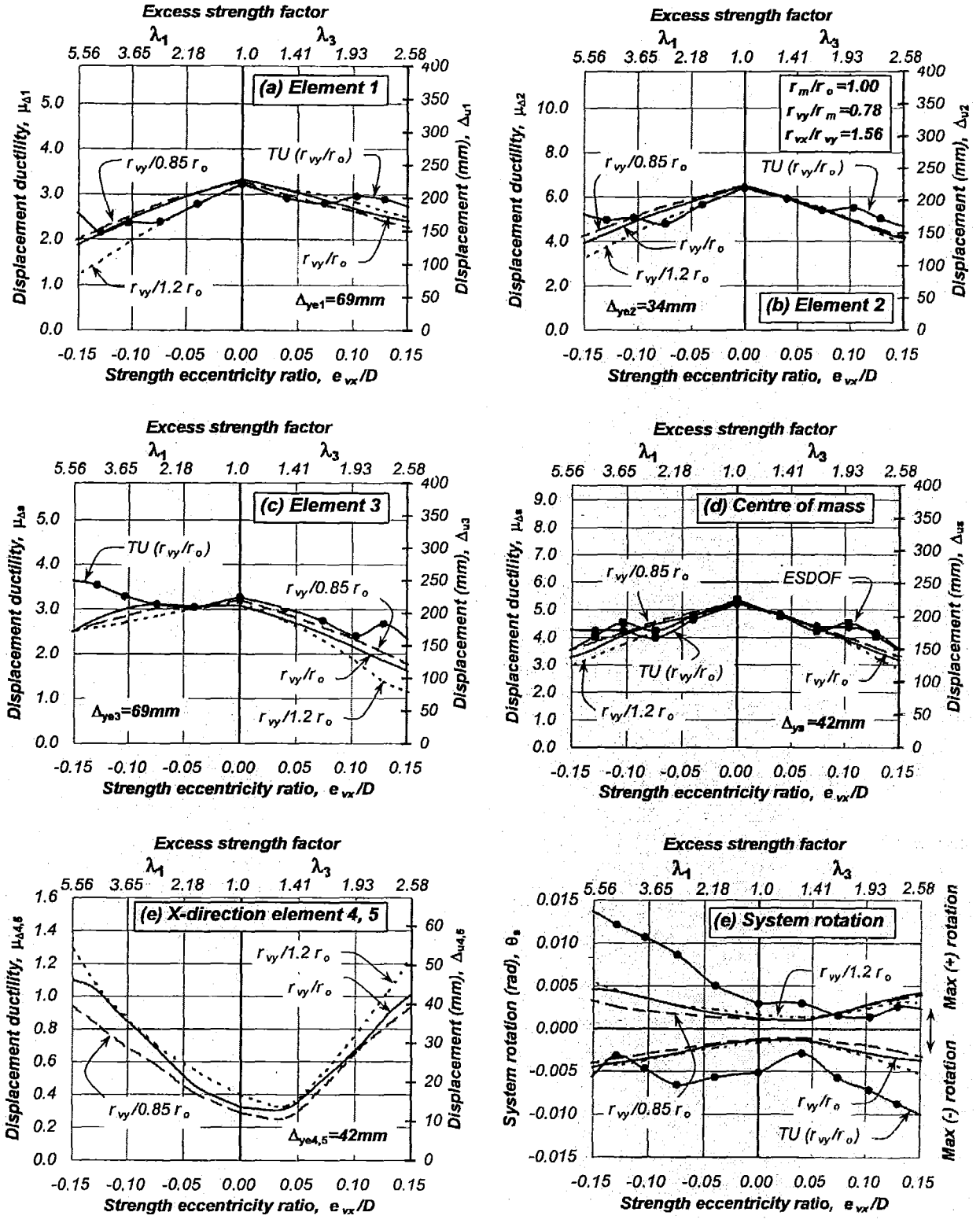

Figure 4-20. Response of the restrained *System 10B-1.3* subjected to the Artificial earthquake record, T_s=1.30 sec, e_{mx}=0.0, $e_{vx} \neq e_{rx}$=variable, $\mu_{\Delta s}$=5.35, r_m/r_o=1.0, r_{vy}/r_m=variable

having $r_{vy}/r_m<1.0$ were evident; see Figure 4-12(e) and (f). Increasing positive strength eccentricities is a non-realistic situation presented only to show likely trends.

The corresponding equivalent single degree of freedom system predicted well the response for zero and increasing strength eccentricities. It was not affected by the addition of a third element parallel to the *Y*-direction.

Differences in the response of *Y*-direction elements and at the centre of mass were found to be insignificant between the torsionally restrained *System 10B-1.3* and its unrestrained counterpart *System 10A-1.3*, as shown in Figure 4-20(a) to (c). The rotations of the restrained *System 10B-1.3* were much smaller that those attained by its unrestrained counterpart *System 10A-1.3*. This behaviour is a characteristic of systems having $r_{vy}/r_m<1.0$. This was also observed in the two-element restrained *System 5B-1.3* and its unrestrained counterpart *System 5A-1.3* having a similar r_{vy}/r_m ratio; see Figure 4-12(e) and (f).

The findings described above suggest that two and three-element systems having, for instance, $r_{vy}/r_m\leq0.90$ will develop similar maximum displacements in the elements and at the centre of mass and are not influenced by the system rotations. An equivalent single degree of freedom system predicted well the response at the centre of mass. Increasing the number of parallel elements did not affect its response. The response of a three-element system may be predicted with an equivalent two-element system.

4.5.2 Response of the restrained *System 10B-1.3* under earthquake record at different angles

The response of restrained *System 10B-1.3* having unchanged properties was examined when subjected to the Artificial earthquake at 22^o, 45^o, 67^o and 90^o angles relative to the principal *Y*-axis. The aim is to identify if the response previously observed for two-element restrained systems with $r_{vy}/r_m=0.78$ and subjected to the earthquake record at different angles; see Section 4.3.9, is influenced by the addition of a third element parallel to the *Y*-axis.

Figure 4-21 shows the response of the system for zero strength eccentricity. It is evident that the displacement ductility demand of the elements and at the centre of mass reduced when the system was subjected to the earthquake record along diagonal directions. This was expected because the system strength is larger at any angle other than the *X* and *Y*-axes.

Figure 4-21 also shows the response for increasing strength eccentricities. A slight but non-critical increase of the displacement demand of elements *(1)* and *(3)* relative from that attained for zero strength eccentricity was observed. In spite of this response, the displacement demand of the elements and at the centre of mass did not exceed that developed when the restrained system was subjected to the Artificial earthquake record along the *Y*-axis only.

The *X*-direction elements *(4)* and *(5)*, shown in Figure 4-21 (e) and (f), displayed, for increasing negative strength eccentricities, a maximum displacement demand when the earthquake record was applied along the *X*-direction. This response was not exceeded when the earthquake record was applied at oblique angles. Element *(4)*, however, exhibited a slight increase in displacements beyond that when the system was subjected to the earthquake record along the *Y*-axis. This was primarily due to the torsional flexibility of the system, i.e., $r_{vy}/r_m<1.0$, indicating that the fundamental mode of vibration of the system is rotational. Systems with such

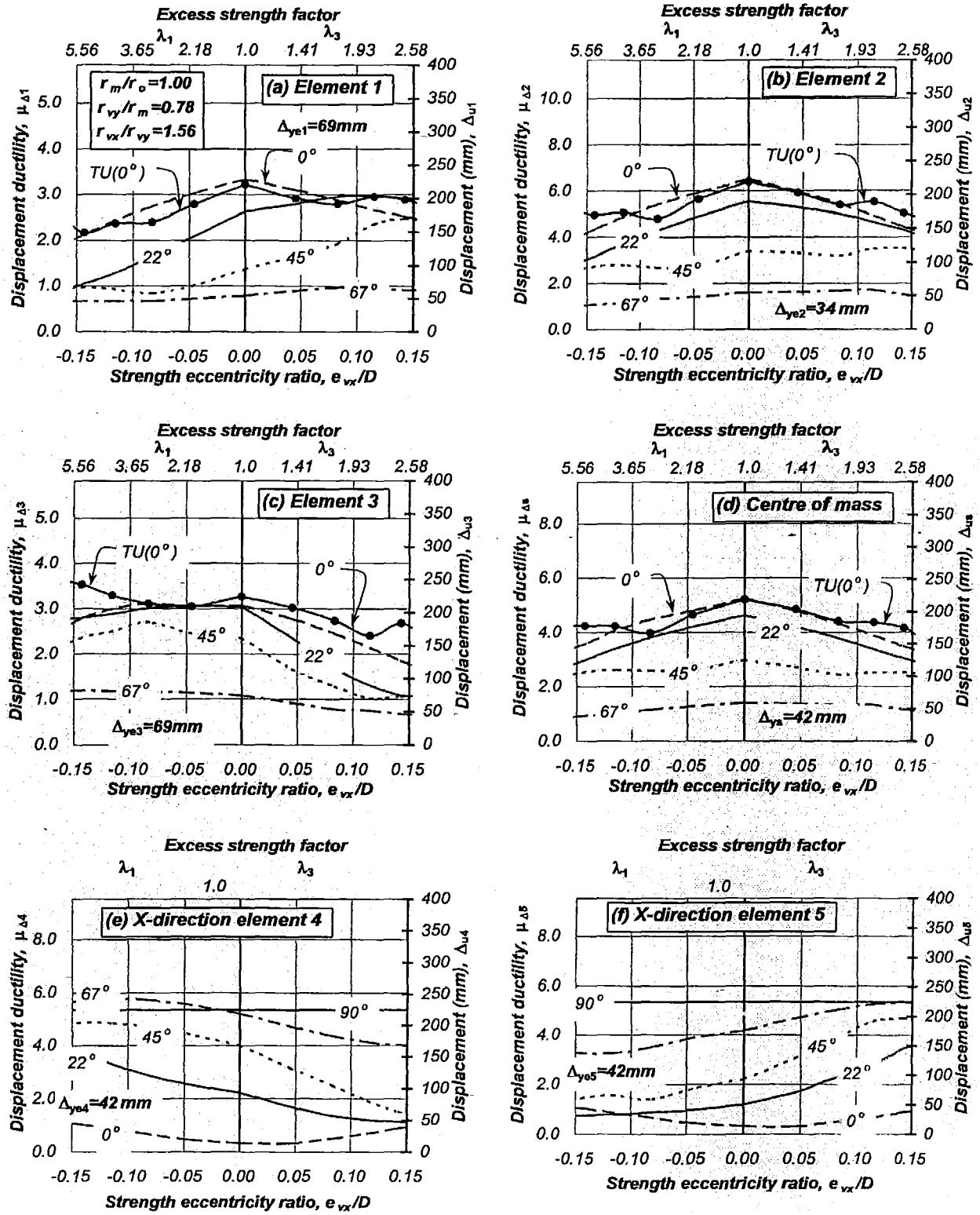

Figure 4-21. Response of the restrained *Systems 10B-1.3* subjected to the Artificial record along different directions, T_s=*1.30 sec*, e_{mx}=0.0, $e_{vx}=e_{rx}$=variable, $\mu_{\Delta s}$=*5.35*, r_m/r_o=variable, e_{vx}/r_m=variable

characteristic are susceptible to rotations that may affect, as in this case, the displacement ductility demand of the *X*-direction elements.

The application of the earthquake record at 22^o and 45^o angles generated a significant increase of the system maximum rotation due to the torsional release of the system as one or more elements yielded. The system response almost reached that of its unrestrained counterpart. The r_{vy}/r_m ratio provides an insight of the expected torsional response of restrained systems when subjected to diagonal earthquake input. This introduced non-critical relative displacement demands on the *X*-direction elements. The maximum response of the *X*-direction elements *(4)* and *(5)* was associated with the largest system rotations.

The r_{vx}/r_m ratio, which considers the nominal strength of the *X*-direction elements, is not considered a relevant parameter influencing the torsional response because the system is symmetric along the *X*-axis. This may not be the case for restrained systems having eccentricities along both principal axes. These systems, however, were not examined in this study.

The findings described above suggest that the displacement ductility capacity of the system should be made equal to that of the element having the smallest displacement capacity. The proposed distribution of strength is then adequate to prevent any of the elements from exceeding their displacement ductility capacities due to increasing strength eccentricities. It was observed that the maximum response of the multi-element restrained system was attained when it was subjected to unidirectional earthquake input along the principal axes. The response was not exceeded when the earthquake record was applied at oblique angles. A similar response was also observed with its unrestrained counterpart, which although displaying larger system rotations, did not influence the maximum response of the elements. Restrained systems with two or three *Y*-direction elements and having similar r_{vy}/r_m ratios, had a similar torsional behaviour. Hence, increasing the number of parallel elements is not a relevant parameter influencing response.

4.6 Four-element structurally asymmetric *System 11B* (CV≠CR; CM=GC)

4.6.1 Response of the restrained *System 11B-1.3*

This section examines the response of a four-element restrained *System 11B* having $r_{vy}/r_m=1.05$. The objective was to corroborate that the response is not influenced by the addition of a fourth parallel elements along the *Y*-direction and by the fact that the $r_{vy}/r_m>1.0$. It is also used to see if two and multi-element systems having the same r_{vy}/r_m ratio have similar responses.

The torsionally restrained *System 11B* had four *Y*-direction elements and two elements along the X-axis; see Figure 2-38(b). The system nominal yield displacement of $\Delta_{ys}=42mm$ and its strength was the same along the principal axes. The latter was adjusted to achieve an uncoupled translational period of free vibration of *1.30* seconds. The system was denoted restrained *System 11B-1.3*. Section 2.22 and Appendix *B* provides additional information of this system. The considerations already explained in Section 4.2 were also used for the analysis of the system.

Table 4-7 summarizes the system response for zero strength eccentricity. It is evident that, in spite of some stiffness eccentricity, maximum displacement demands of elements and at the centre of mass were essentially the same. Variations of the r_{vy}/r_m ratio did not influence response. This response was generated due to the restraining effect of the *X*-direction elements to system rotations. The equivalent single degree of freedom system proved to be a promising model for

predicting the maximum response at the centre of mass and was not affected by increasing the number of parallel elements.

The displacement ductility demands of the *Y*-direction elements were different due to differences in their nominal yield displacements. Element *(1)* was critical because it exceeded its displacement ductility capacity of $\mu_{\Delta 1}=5.35$. This could have been prevented, as previously explained, if the displacement ductility capacity of the system would have been limited to that of element *(1)* having the smallest displacement capacity. Hence, the displacement capacity of the system should have been $\Delta_{us}=\Delta_{u1}=\mu_{\Delta 1}\Delta_{ye1}=5.35*34=182mm$ and the system ductility capacity $\mu_{\Delta s}=182/42=4.33$. The maximum displacement demand expected to be reached and not exceeded by the *Y*-direction elements is $\mu_{\Delta 1}=182/34=5.35$, $\mu_{\Delta 2}=182/68=2.68$, $\mu_{\Delta 3}=182/54=3.37$ and $\mu_{\Delta 4}=182/43=4.23$.

Table 4-7. Response of the restrained *System 11B-1.3* subjected to the Artificial earthquake record, e_{vx}=0.0, T_s=1.30 sec, e_{mx}=0.0, e_{rx}=-0.046D, $\mu_{\Delta s}$=5.35, r_m/r_o=1.0, r_{vy}/r_m=variable

	Displacements (mm) and displacement ductility demands (μ)						
r_{vy}/r_m	***E1***	***E2***	***CM***	***E3***	***E4***	***ESDOF***	***E4=E5***
$r_{vy}/0.85r_o$	*226(6.67)*	*227(3.34)*	*227(5.40)*	*227(4.21)*	*227(5.32)*	*225(5.35)*	*6(elastic)*
$r_{vy}/r_o=1.05$	*229(6.76)*	*227(3.35)*	*226(5.39)*	*225(4.18)*	*223(5.23)*	"	*6(elastic)*
$r_{vy}/1.20r_o$	*229(6.75)*	*227(3.34)*	*227(5.37)*	*225(4.17)*	*222(5.21)*	"	*7(elastic)*

It is likely, however, that some elements, as finally detailed, will have some excess strength. To simulate such situation, it is assumed that only outermost elements *(1)* and *(4)* will have excess strength. This choice was made because such excess strength introduced the largest strength eccentricity for the least increase of system strength; see Figure 2-39.

Figure 4-22 plots the response due to increasing strength eccentricities. Maximum displacement demands of the *Y*-direction elements and at the centre of mass occurred for zero strength eccentricity and reduced with increasing strength eccentricities. Their response was insensitive to the r_{vy}/r_m ratio, as shown in Figure 4-22(f). The response of the *X*-direction elements was not critical and only slightly affected by the variation to the r_{vy}/r_m ratio.

Figure 4-22 also compares the response of the restrained *System 11B-1.3* with its unrestrained counterpart *System 11A-1.3*. As expected, the restrained system led to a larger displacement demand on element *(1)* while a smaller demand on element *(4)*. The displacement demands of inner elements *(2)*, *(3)* and at the centre of mass were essentially the same. The response at the centre of mass was predicted well with an equivalent single degree of freedom system. The similarities in torsional behaviour with the two-element restrained *Systems 3B-1.3* having as similar r_{vy}/r_m ratio, were evident; see Figure 4-1. Differences in response between restrained and unrestrained systems were also observed due to the effect of the r_{vy}/r_m ratio on the response of the unrestrained systems.

The above findings suggests that no significant differences in response are expected between two and multi-element systems having similar uncoupled translational periods and r_{vy}/r_m ratio. It also shows that the torsional response is insensitive to the number of parallel elements along the direction of application of the ground motion.

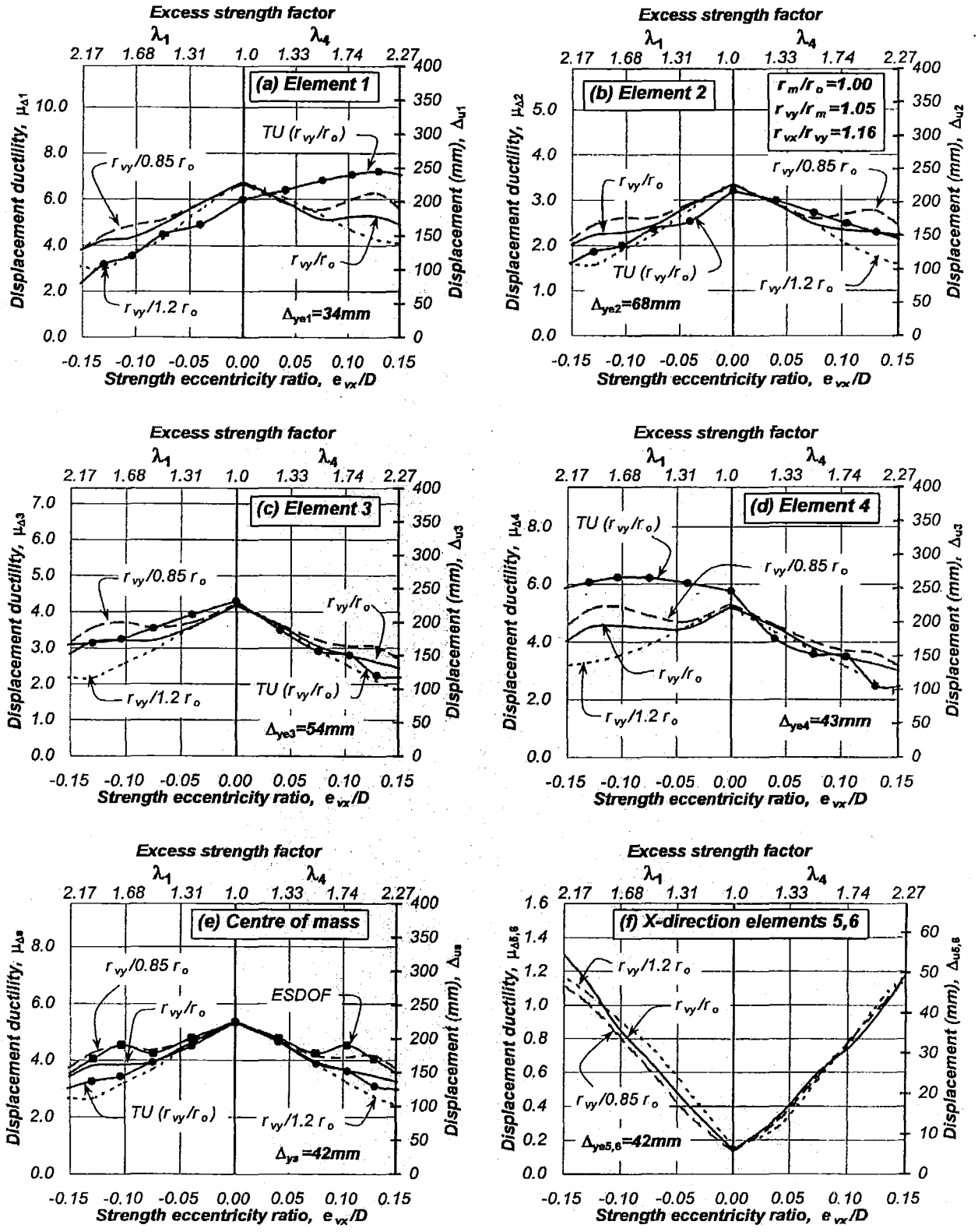

Figure 4-22. Response of the restrained *System 11B-1.3* subjected to the Artificial earthquake record, T_s=1.30 sec, e_{mx}=0.0, $e_{vx} \neq e_{rx}$=variable, $\mu_{\Delta s}$=5.35, r_m/r_o=1.0, r_{vy}/r_m=variable

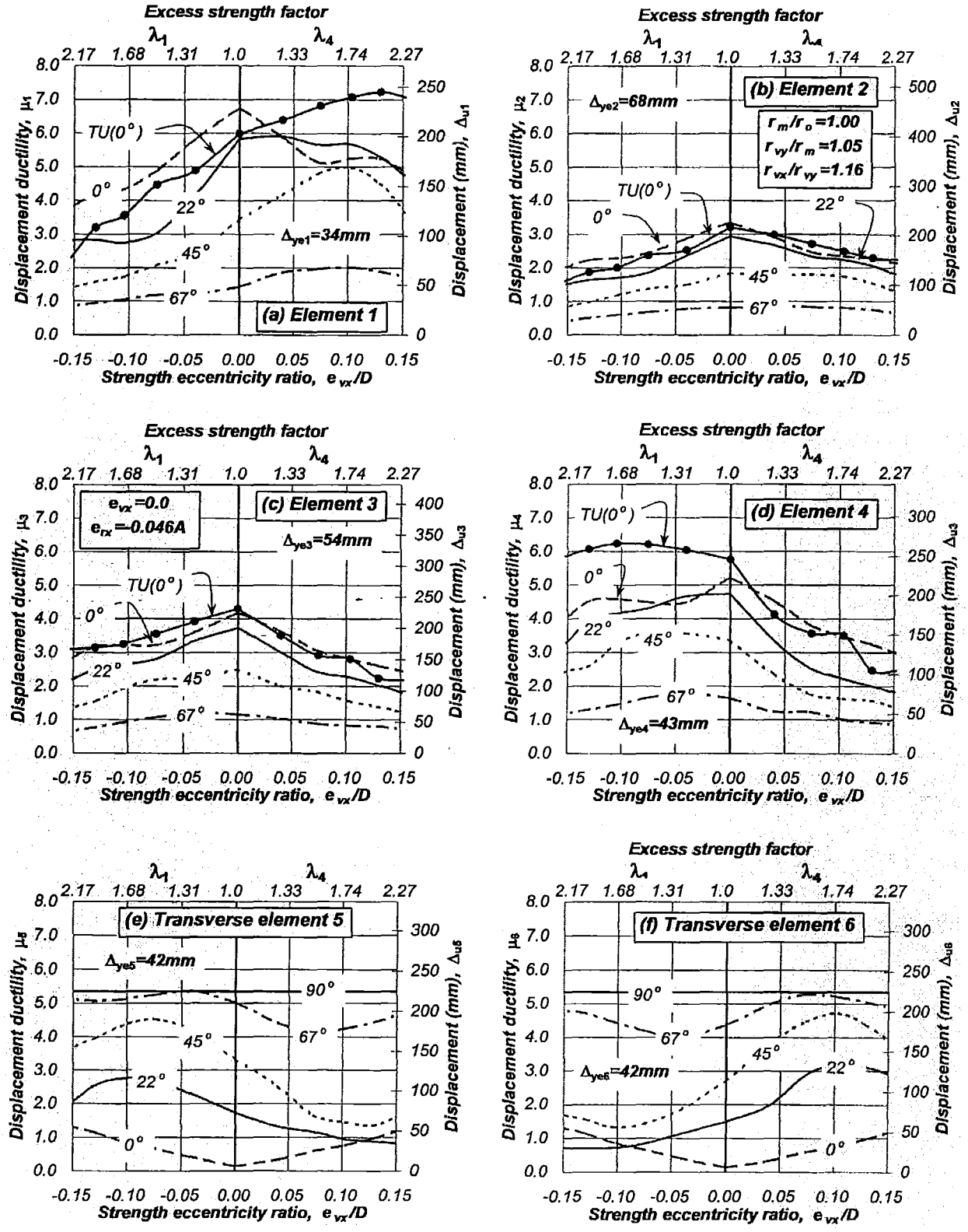

Figure 4-23. Response of the restrained *System 11B-1.3* subjected to the Artificial earthquake record along different directions, T_s=1.30 sec, e_{mx}=0.0, $e_{vx} \neq e_{rx}$=variable, $\mu_{\Delta s}$=5.35, r_m/r_o=1.0, r_{vy}/r_m=variable

4.6.2 Response of the restrained *System 11B-1.3* under earthquake records at different angles

It has been shown that a three element restrained system with $r_{vy}/r_m<1.0$ had a similar response to that of a two-element system with the same r_{vy}/r_m ratio. This section has the objective to show if a four-element system having a larger r_{vy}/r_m ratio, i.e., $r_{vy}/r_m=1.05$, shows a similar trend. It was subjected to the Artificial earthquake record at different angles.

Figure 4-23 shows the response for zero strength eccentricity. It is evident that the displacement ductility demands of the elements and at the centre of mass reached a maximum for zero strength eccentricity and reduced as the angle of incidence of the record was increased from the reference *Y*-axis. This behaviour was similar to that observed with two element systems and three-element restrained *System 10B-1.3*.

Increasing strength eccentricities and corresponding angle of earthquake input generated a displacement demand on elements *(1)* and *(4)* beyond that attained for zero strength eccentricity; particularly when the earthquake record was applied at a 45^o and 67^o angle to the *Y*-axis. However, this response did not exceed the maximum displacement demand attained for zero strength eccentricity and earthquake record input along the *Y*-axis.

The above findings suggest that the proposed design strategy is adequate to prevent the elements from exceeding their displacement ductility capacity due to increasing strength eccentricities if the displacement ductility capacity of the system is made equal to that of the element having the smallest displacement capacity. The maximum response of the restrained system was attained when it was subjected to unidirectional earthquake input along the principal axes. The response was not exceeded when the earthquake record was applied at oblique angles. This indicates that the number of parallel elements and variations of the r_{vy}/r_m ratio did not influence this behaviour. The response comparison of restrained systems and its unrestrained counterpart indicates that, contrary to common belief, a restrained system subjected to unidirectional earthquake input, although exhibiting smaller system rotations than its unrestrained counterpart, is critical. The element with the smallest displacement capacity, and parallel to the direction of earthquake record input, is the critical element limiting the displacement capacity of the system.

4.7 Comments on systems with two directional eccentricities

Restrained systems having eccentricities along both principal axes were not examined in this study. It is believed that such systems may not be critical and may be also designed as suggested for restrained systems having unidirectional eccentricity only. Such systems should be designed considering each axis separately. Research is required to verify that the suggested design strategy also applies to such systems.

4.8 Response of torsionally restrained ductile systems

This section aims to confirm that the findings already derived for a limited number of restrained systems having a particular uncoupled translational period of free vibration also applies to restrained systems with other uncoupled translational periods and $\alpha=\Delta_{ye2}/\Delta_{ye1}$ ratios (or stiffness eccentricity associated with zero strength eccentricity).

4.8.1 Response of the restrained *Systems 12B(α=variable)*

Two-element restrained *Systems 12B(α=variable)* having $r_{vy}/r_o=1.01$, as shown in Figure 4-24 were considered. They were the same to those unrestrained systems already described in Section 3.10. The only difference was the addition of two equidistant *X*-direction elements relative to the centre of mass providing torsional resistance. The nominal yield displacement in all three systems remained unchanged and equal along both principal axes, $\Delta_{ys}=42mm$. The nominal yield displacement of these elements were the same, $\Delta_{ye3}=\Delta_{ye4}=42mm$. The relative lengths of the substitute wall-elements *(3)* and *(4)* was $\ell_3=\ell_4=1.2$. They were selected to obtain the same system nominal yield displacement as that along the *Y*-axis. For the sake of brevity, the study was limited to systems with $r_{vy}/r_o=1.0$. The torsional resistance introduced by the *X*-direction elements was equal to that contributed by the *Y*-direction elements, thus, $r_{vx}/r_{vy}=1.0$.

The systems had uncoupled translational periods of free vibration varying between $T_s=0.1$ and *2.0* seconds. This was achieved by adjusting the strength of the systems. Three earthquake records were applied along the *Y*-axis only. The response of the systems due to the application of the earthquake record at different directions was not examined because, according to previously examined models, the restrained systems subjected to unidirectional earthquake input generates an envelope of the system maximum response.

The earthquake records, already scaled for the torsionally unrestrained *Systems 12A(α=variable)* were also applied, without modifications, to the restrained *Systems 12B(α=variable)*. This process enabled a direct response comparison between restrained systems and their unrestrained counterparts.

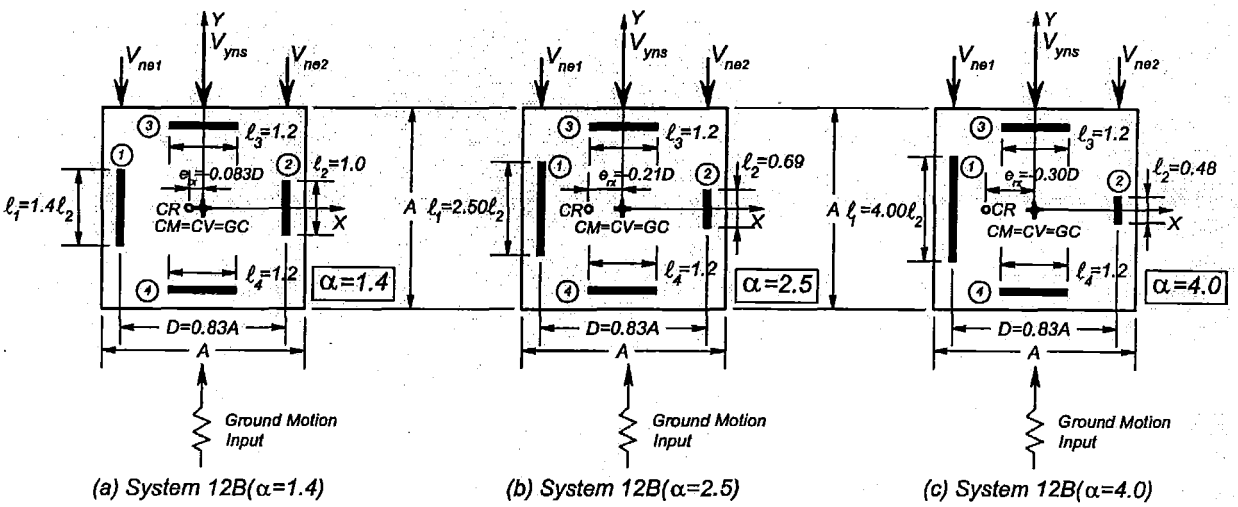

Figure 4-24. Two-element torsionally restrained *Systems 12B(α=variable)*

Figure 4-25, Figure 4-26 and Figure 4-27 show the displacement demands of the elements and at the centre of mass of *Systems 12B(α=1.4), 12B(α=1.4)* and *12B(α=4.0)*, respectively. It is evident, for the three systems that the maximum displacement of the elements and at the centre of mass for all three-earthquake records was essentially the same. Relative differences in the displacements between the elements were, however, observed as the $\alpha=\Delta_{ye2}/\Delta_{ye1}$ ratio was increased. Another characteristic observed is that the equivalent single degree of freedom model predicted

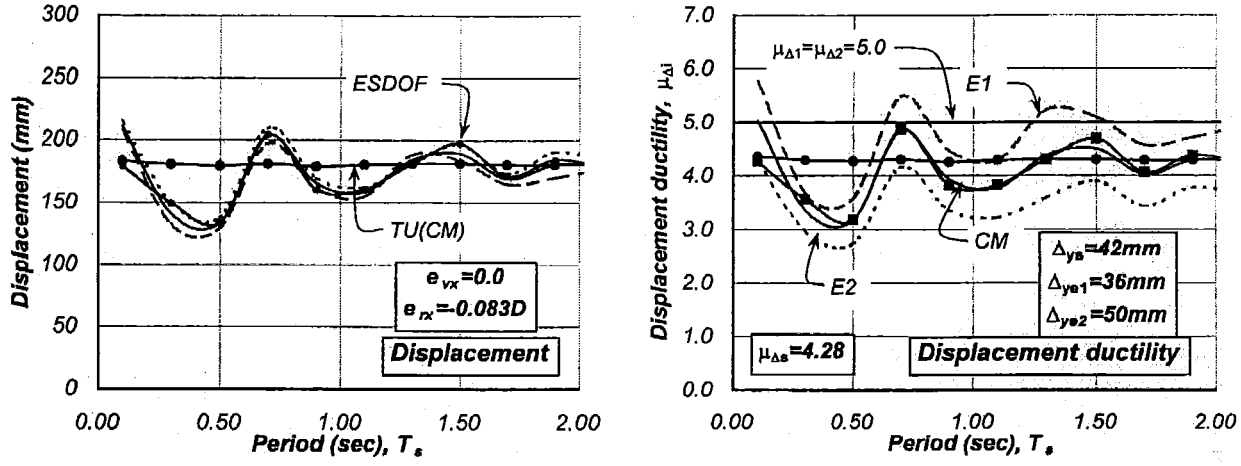

(a) Artificial earthquake record

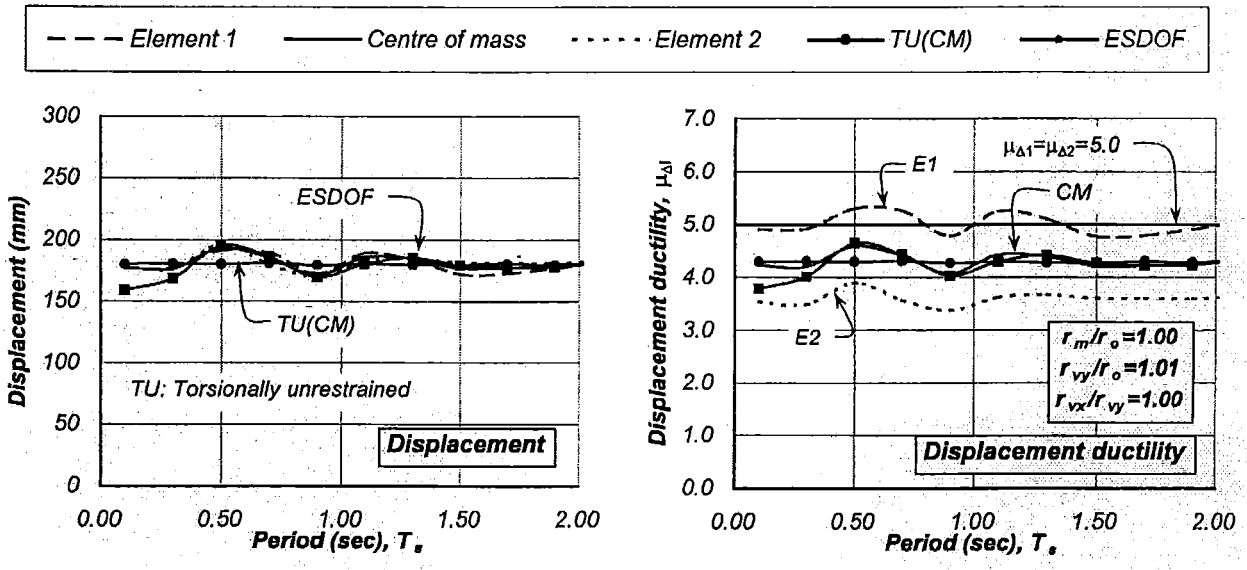

(b) Bucharest NS earthquake record

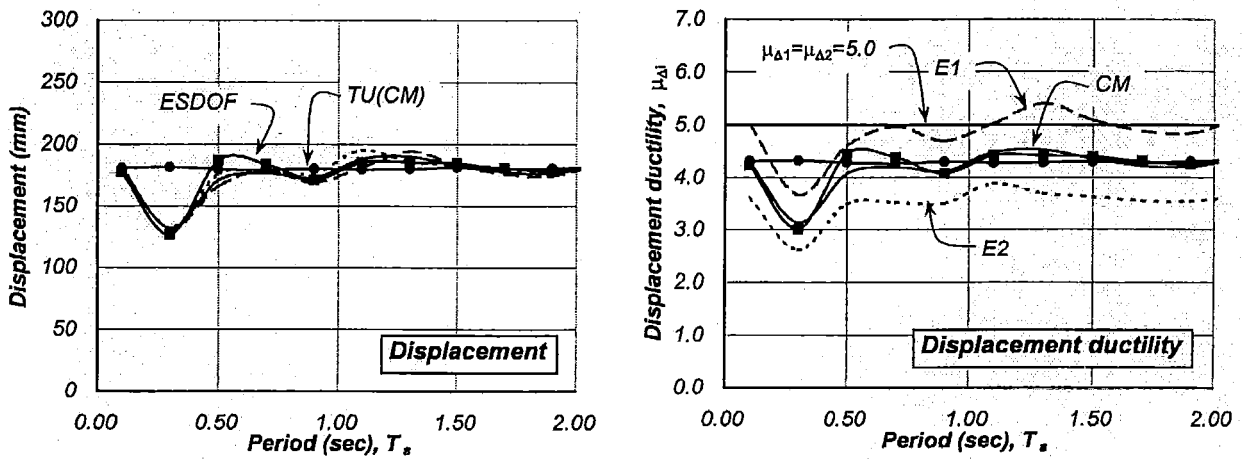

(c) Kobe NS earthquake record

Figure 4-25. **Spectral presentation of the response of the restrained *Systems 12B(α=1.4)* when subjected to different earthquake records, T_s=variable, e_{mx}=0.0, e_{vx}=0.0, e_{rx}=-0.083D, $\mu_{\Delta 1}=\mu_{\Delta 2}$=5.00, $\mu_{\Delta s}\approx$4.28, r_m/r_o=1.00, r_{vy}/r_m=1.01**

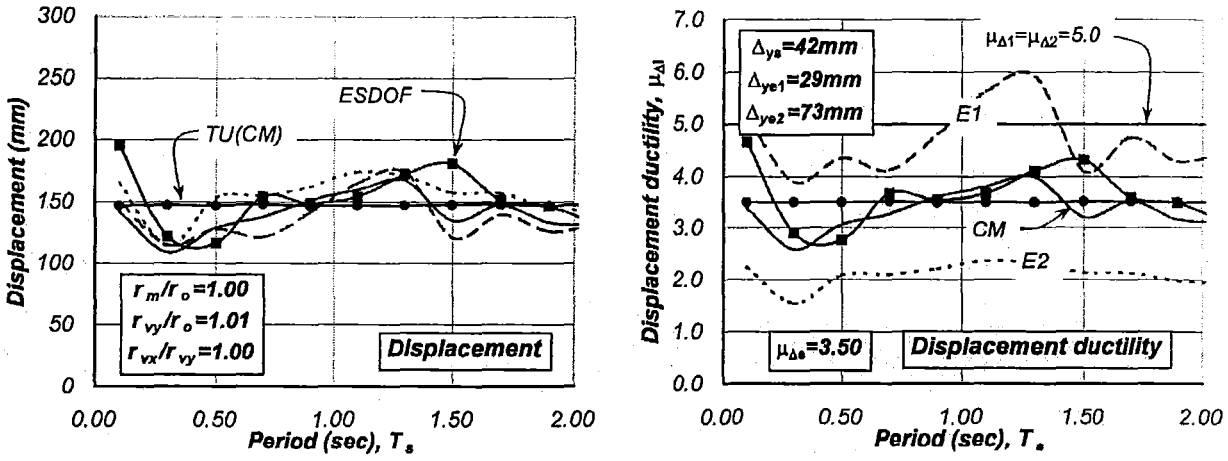

(a) Artificial earthquake record

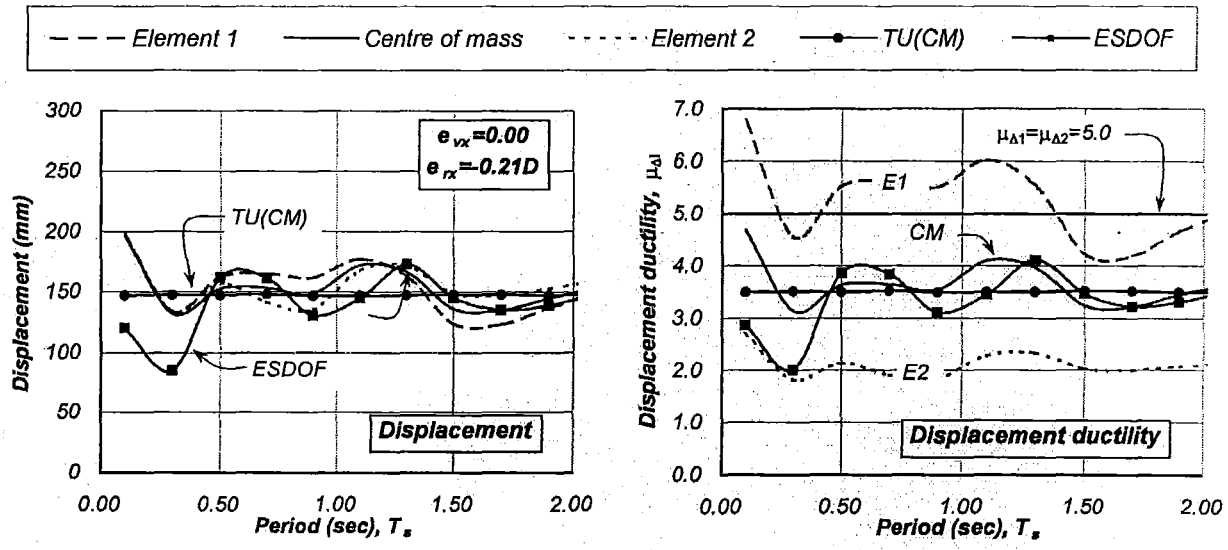

(b) Bucharest NS earthquake record

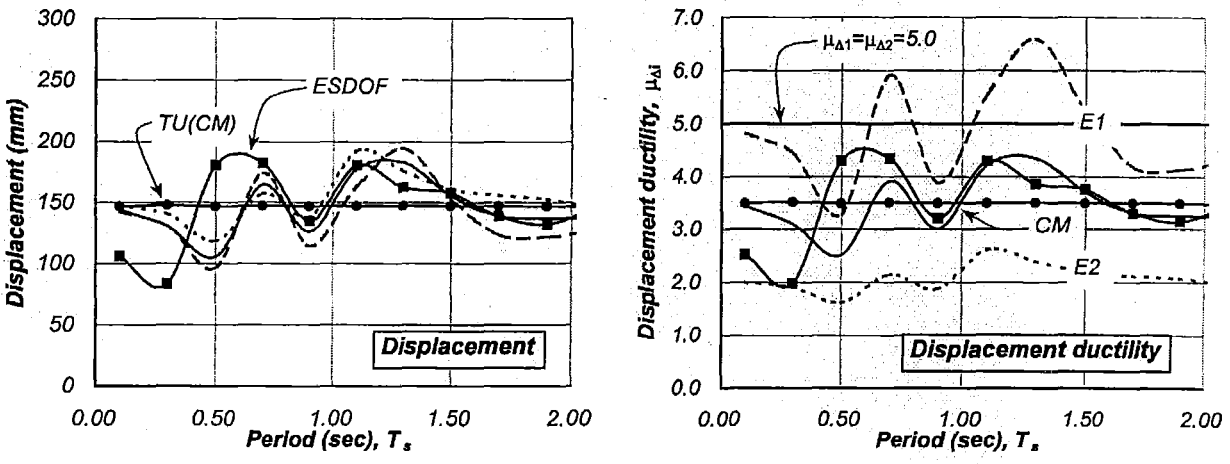

(c) Kobe NS earthquake record

Figure 4-26. Spectral presentation of the response of the restrained *Systems 12B(α=2.5)* when subjected to different earthquake records, T_s=variable, e_{mx}=0.0, e_{vx}=0.0, e_{rx}=-0.21D, $\mu_{\Delta 1}=\mu_{\Delta 2}$=5.00, $\mu_{\Delta s}\approx$3.50, r_m/r_o=1.00, r_{vy}/r_m=1.01

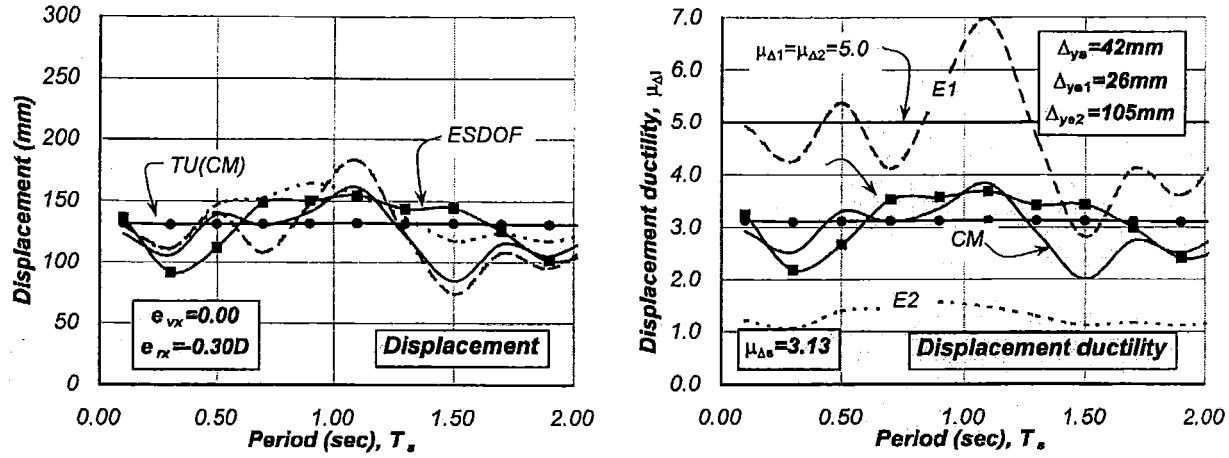

(a) Artificial earthquake record

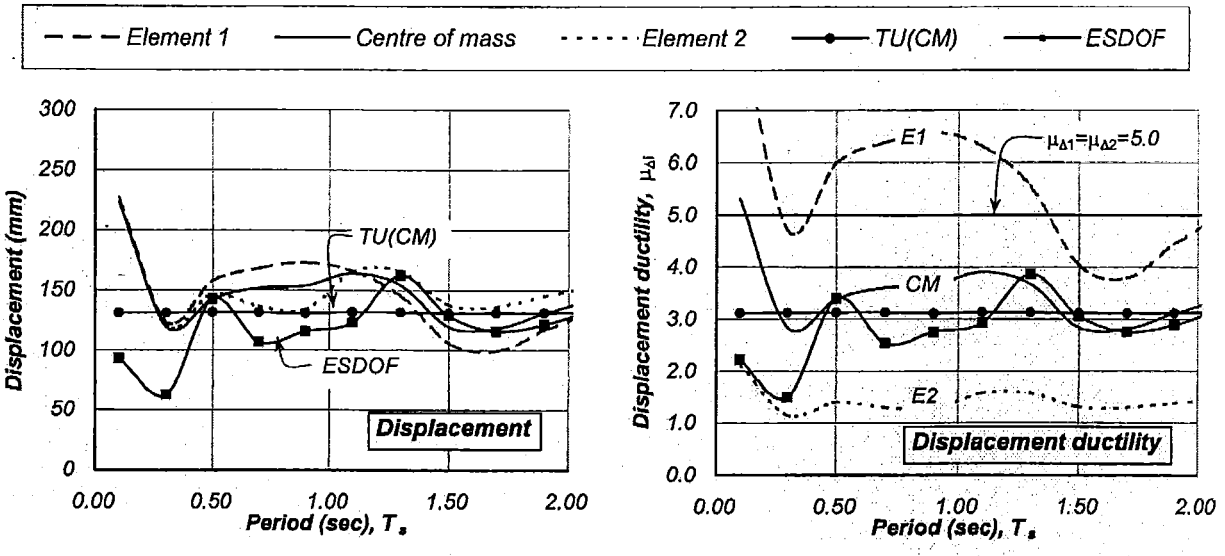

(b) Bucharest NS earthquake record

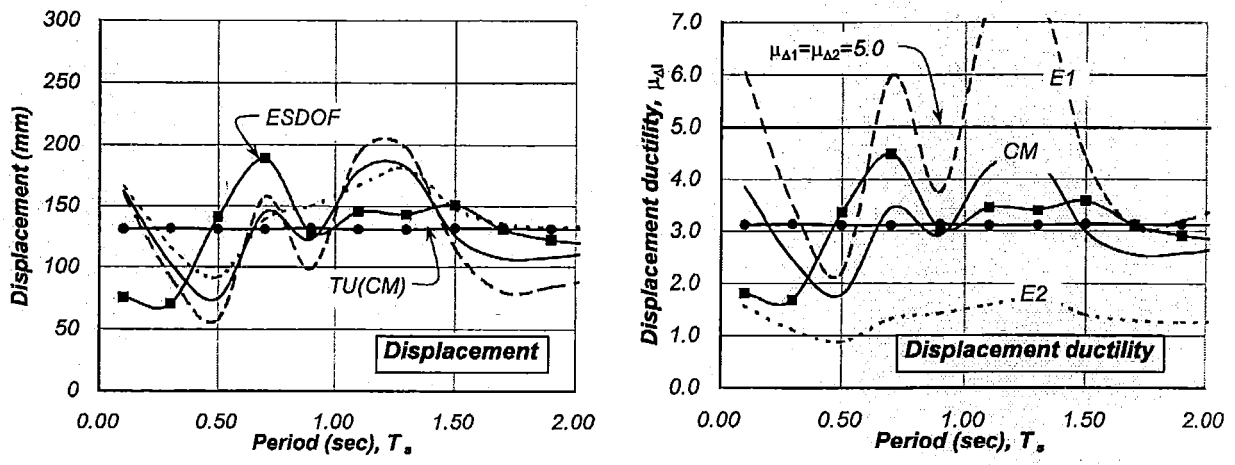

(c) Kobe NS earthquake record

Figure 4-27. **Spectral presentation of the response of the restrained *Systems 12B(α=4.0)* when subjected to different earthquake records, T_s=variable, e_{mx}=0.0, e_{vx}=0.0, e_{rx}=-0.30D, $\mu_{\Delta 1}=\mu_{\Delta 2}$=5.00, $\mu_{\Delta s}\approx$3.13, r_m/r_o=1.00, r_{vy}/r_m=1.01**

well the maximum displacement demand at the centre of mass of the restrained systems. Its accuracy reduced for systems with uncoupled translational periods of $T_s<0.7$ seconds and with increasing $\alpha=\Delta_{ye2}/\Delta_{ye1}$ ratio (or increasing stiffness eccentricity associated with zero strength eccentricity). This happens because the centre of mass, although taken as reference to measure torsional behaviour, is not the position in a ductile system where system translations are actually separated from system rotations. The response was certainly dependant on the frequency contents of the earthquake records.

Figure 4-25, Figure 4-26 and Figure 4-27 shows the displacement ductility demands of the elements and at the centre of mass. It shows that, for most uncoupled translational periods of free vibration, the suggested approach to estimate the system displacement ductility capacity preventing its elements, particularly critical element *(1)*, from exceeding their displacement capacity of $\mu_{\Delta 1}=5.0$ was successful. Note again that this displacement capacity is smaller than that used in those systems previously examined, however, no particular reason exists for using a different value.

The response associated with increasing negative strength eccentricities, not shown here, shows that the displacement ductility demand of critical element *(1)* and *(2)* reduced with increasing negative strength eccentricities. The response of the system to Kobe earthquake record showed, however, an increase in the displacement demands of element *(1)* even though the system strength increased. This confirms that an increase of system strength will not guarantee a reduction in the displacement demands of the elements and at the centre of mass due to differences in the frequency contents of different earthquake records.

The above findings suggest that the proposed design strategy is adequate in preventing the elements of restrained systems from exceeding their displacement ductility capacity due to increasing strength eccentricities. The displacement ductility capacity of the system should be restricted to that element having the smallest displacement capacity. The equivalent single degree of freedom model predicted well the maximum displacement demand at the centre of mass of the restrained systems. Its accuracy reduced for system with uncoupled translational periods of $T_s<0.7$ seconds and with increasing $\alpha=\Delta_{ye2}/\Delta_{ye1}$ ratio (or the stiffness eccentricity associated with zero strength eccentricity). It is expected that the application of the earthquake record at directions different to the major principal axes will not generate a critical response.

4.9 Displacement ductility capacity and nominal strength of torsionally restrained systems

It has been shown that the system displacement ductility capacity is not a function of the uncoupled translation period or stiffness eccentricity as it was the case for unrestrained systems. Hence, the displacement capacity of unrestrained systems is readily derived by restricting it to that of the element having the smallest displacement capacity, as Figure 3-35(a) shows and as expressed by Eq 3-3.

Subsequently, the system strength may be estimated, in accordance with, for example, current force-based design methods, by considering specific design acceleration spectra and a system displacement ductility factor equal to the displacement ductility capacity of the system. The strength so obtained should then be distributed to the elements to satisfy zero strength eccentricity. Appendix D provides an example of this approach.

4.10 Summary of the response of torsionally restrained systems

The findings relevant to the response of torsionally restrained systems designed according to the suggested design strategy described in Section 2.11 were:

1. System rotations expected to develop due to increasing strength and associated stiffness eccentricities are restricted by the mass rotational inertia. These rotations were further reduced by transverse elements providing torsional restraint. This behaviour led to a similar maximum displacement demand at the centre of mass and on elements parallel to the direction of ground motion input. See Sections 4.3.1, 4.3.3, 4.3.8 and 4.3.10.

2. Changes in the degree of torsional restraint provided by transverse elements, i.e., variations of the r_{vx}/r_{vy} ratio, of restrained systems subjected to the earthquake record along the *Y*-direction did not have a significant effect on the maximum displacement demands on the Y-direction elements. See Section 4.3.8.

3. Variations in the distribution of element nominal strength and mass, i.e., changes in the r_{vy}/r_m ratio, did not have a major effect on displacement demands of the elements of restrained systems subjected to earthquake records along the principal axes. See Sections 4.3.1, 4.3.8, 4.3.10, 4.5.1 and 4.6.1.

4. The variation of the $\alpha=\Delta_{ye2}/\Delta_{ye1}$ ratio did not have a substantial effect on the displacement demands of elements parallel to the direction of earthquake record input. It did have a proportional, but non-critical effect, on the displacement demands of transverse elements. See Section 4.3.3 and 4.8.1.

5. The maximum displacement demands of elements parallel to the direction of earthquake record input are essentially the same and not significantly affected by system rotations arising from restrained systems having zero strength eccentricity. Hence, torsional effects need not to be considered when assessing the displacement ductility capacity of restrained systems. The displacement ductility of the system should be restricted to that of the element having the smallest displacement capacity. See Sections 4.3.1, 4.3.3, 4.3.7, 4.3.8, 4.3.10, 4.5.1 and 4.6.1.

6. An optimal condition arose, as in case of unrestrained systems, when the strength distribution was such that centre of mass is located halfway between the centres of strength and stiffness. In such situations, the system rotation was negligible. This feature was not affected by the presence of transverse elements, i.e., the r_{vx}/r_{vy} ratio, the number, location and nominal yield displacement of elements, the direction of application of earthquake record, variations of the r_{vy}/r_m ratio and the displacement capacity of the system. It is, however, an ideal distribution of strength difficult to achieve in practice. See Sections 4.3.1, 4.3.4, 4.3.6, 4.3.9, 4.5.1 and 4.6.1.

7. The strength to be eventually assigned to the system may be obtained with either force-based or displacement-based design methods considering a system ductility factor equal to the system displacement ductility capacity. This strength is a reference quantity to be distributed to the elements to achieve zero strength eccentricity. It is expected to prevent the system, and hence its elements, from exceeding the displacement ductility capacity for zero strength eccentricity. See Section 4.9.

8. The proposed distribution of strength among the elements, where strength eccentricities are associated with an increase of system strength, was successful, although providing conservative results, to limit the displacement demands on the elements to less than their displacement capacity for increasing strength eccentricities when restrained systems were subjected to earthquake records along the principal axes. This conservative performance is also observed in systems having different r_{vy}/r_m ratios, uncoupled translational periods of free vibration and reduced ductility capacities even when the systems were subjected to different earthquake records. See Sections 4.3.1, 4.3.3, 4.3.6, 4.3.7, 4.3.8, 4.3.10, 4.5 and 4.6.

9. The effectiveness of the suggested design strategy was tested when the restrained systems were subjected to earthquake records along diagonal directions. The response of the restrained systems having zero strength eccentricity and subjected to earthquake records along the principal axes generated an envelope of maximum displacement demands on the elements and at the centre of mass. These displacement demands were not exceeded with increasing strength eccentricities and when the earthquake record was applied along diagonal directions. The response was not influenced by variations of the uncoupled translational period of free vibration, systems with reduced ductility capacity and the frequency content characteristics of different earthquake records. Significant torques and rotations were developed. However, in spite of such behaviour, the displacement demands of the elements did not exceed their displacement capacity. See Sections 4.3.4, 4.3.9, 4.4.3, 4.5.2 and 4.6.2.

10. The maximum displacement demand at the centre of mass and of elements of retrained systems may be satisfactorily predicted with an equivalent single degree of freedom system. This prediction is not affected by increasing the number of elements parallel to the direction of earthquake input. However, its accuracy reduced on systems with increasing $\alpha=\Delta_{ye2}/\Delta_{ye1}$ ratio (or increasing stiffness eccentricities associated with zero strength eccentricity) and systems with uncoupled translational periods of free vibration of $T_s<0.7$ sec. See Section 4.8.1.

11. As opposed to what is observed for translational behaviour, the torsional behaviour of restrained systems was essentially insensitive to the frequency content of the earthquake record. See Section 4.3.7.

12. The response of a multi-element restrained system may be predicted with an equivalent two-element system having a similar uncoupled translational period and r_{vy}/r_m ratio. See Sections 4.5.1 and 4.6.1.

13. The responses of extremely eccentric single-element systems are sensitive and difficult to predict with simplified equivalent single degree of freedom systems. At the single element location, system translations were significantly affected by system rotations. System rotations increased the displacement demands of the flexible side of the system, which may exceed code drift limits and hence non-structural damage is to be expected. These extremely eccentric structures should be avoided. See Section 4.4.

4.11 Design of torsionally restrained systems

For the design of torsionally restrained systems, it is suggested that the designer:

1. Estimate the displacement and ductility capacity of the system associated with zero strength eccentricity. The displacement capacity of the system should be restricted to that element having the smallest displacement capacity. This simple approach takes into account system rotations and the fact that the system may be subjected to earthquake excitation along different directions.

2. The system strength, to be eventually assigned to its elements and limiting the displacement demands at the centre of mass to less than its displacement capacity, may be obtained with the design response spectra of a single degree of freedom system. This strength should then be distributed on the elements to achieve the reference zero strength eccentricity.

3. A strength eccentricity may be introduced to the system provided it results from one or more elements having strength in excess of that satisfying zero strength eccentricity. This will result in an increase of system strength.

Chapter 5. Experimental Programme

5.1 Introduction

Research on the seismic response of reinforced concrete and structural steel structures through shake table tests is not new in structural engineering. Many studies have centred on the unidirectional seismic response of simplified or complex symmetric models [C17], whereas a few have focussed on structural asymmetry [D9,S4,S2]. Studies assessing the inelastic response of single and multi-storey asymmetric test models have already been discussed in Section 1.2.2. The experimental findings are relevant as long as they can be matched with analytical simulations.

This chapter will focus on an experimental programme studying the torsional response of a single-mass model. It aims to: (a) discuss test results, (b) compare the experimental findings with those analytical studies previously undertaken and (c) embark on the prediction of the model's response with computer simulations using the 3D-Ruaumoko [C1].

To be consistent with the analytical studies undertaken and described in the preceding chapters, torsionally unrestrained and restrained models were considered. A symmetric model was used as reference for the structural design. Subsequently, unrestrained and restrained models were tested by subjecting them to earthquake records at different angles.

The models were designed following the principles of capacity design [P1] where certain components were designed to remain elastic while predefined regions were expected to develop plastic deformations. These potential plastic regions consisted of replaceable steel components at which elastic and inelastic deformations were concentrated [K3].

The parameters of interest were the strength eccentricity, its associated increase of system strength and the direction of application of the earthquake record input.

5.2 Details of test models

To be consistent with the analytical models examined described in the preceding chapters, this chapter considered single-mass torsionally unrestrained and restrained models, as shown in Figure 5-1, Figure 5-2 and Figure 5-3. They were not intended to represent any particular prototype structure. Contrary to the analytical systems examined before, the models comprised frames as the lateral force resisting elements. The theory derived in Chapter 2, for systems with substitute wall-elements, is also applicable, with some minor changes, to systems comprised of frames, as will be shown in Section 5.3.

5.2.1 Torsionally unrestrained models

The torsionally unrestrained models consisted of two frames parallel to the *Y*-axis along gridlines *(1)* and *(2)*, as shown in Figure 5-1, and termed herein *Frames (1)* and *(2)*. Each frame consisted of two *50*50*3mm* square hollow section (*SHS*) columns and one *50*50*3mm SHS* beam. The columns were connected at the base to the shake table through spherical bearings and at the top end to a beam-column connection, to be described later. These frames provided the translational resistance along the *Y*-axis and the rotational resistance about the *Z*-axis.

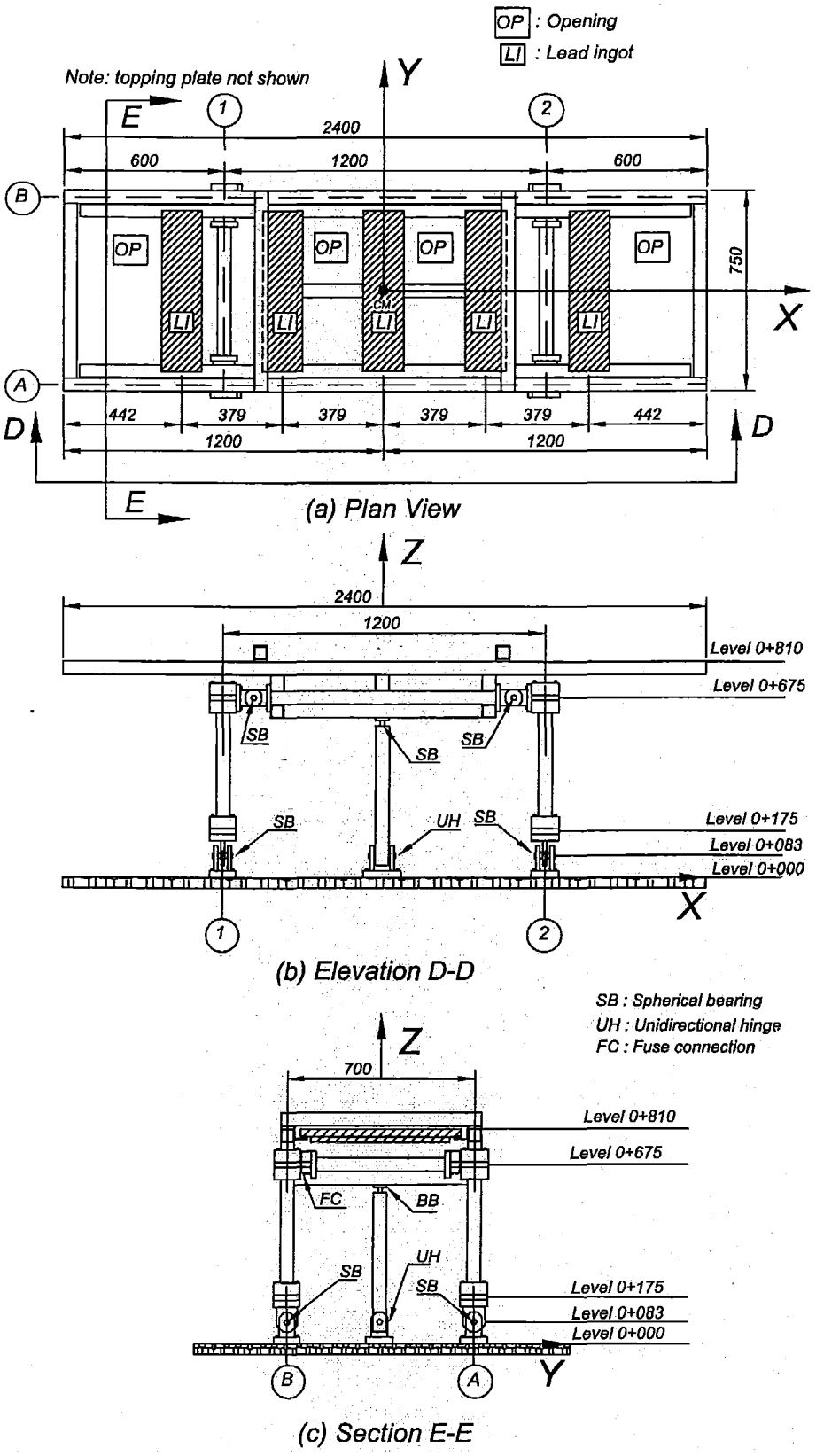

Figure 5-1. Torsionally unrestrained model

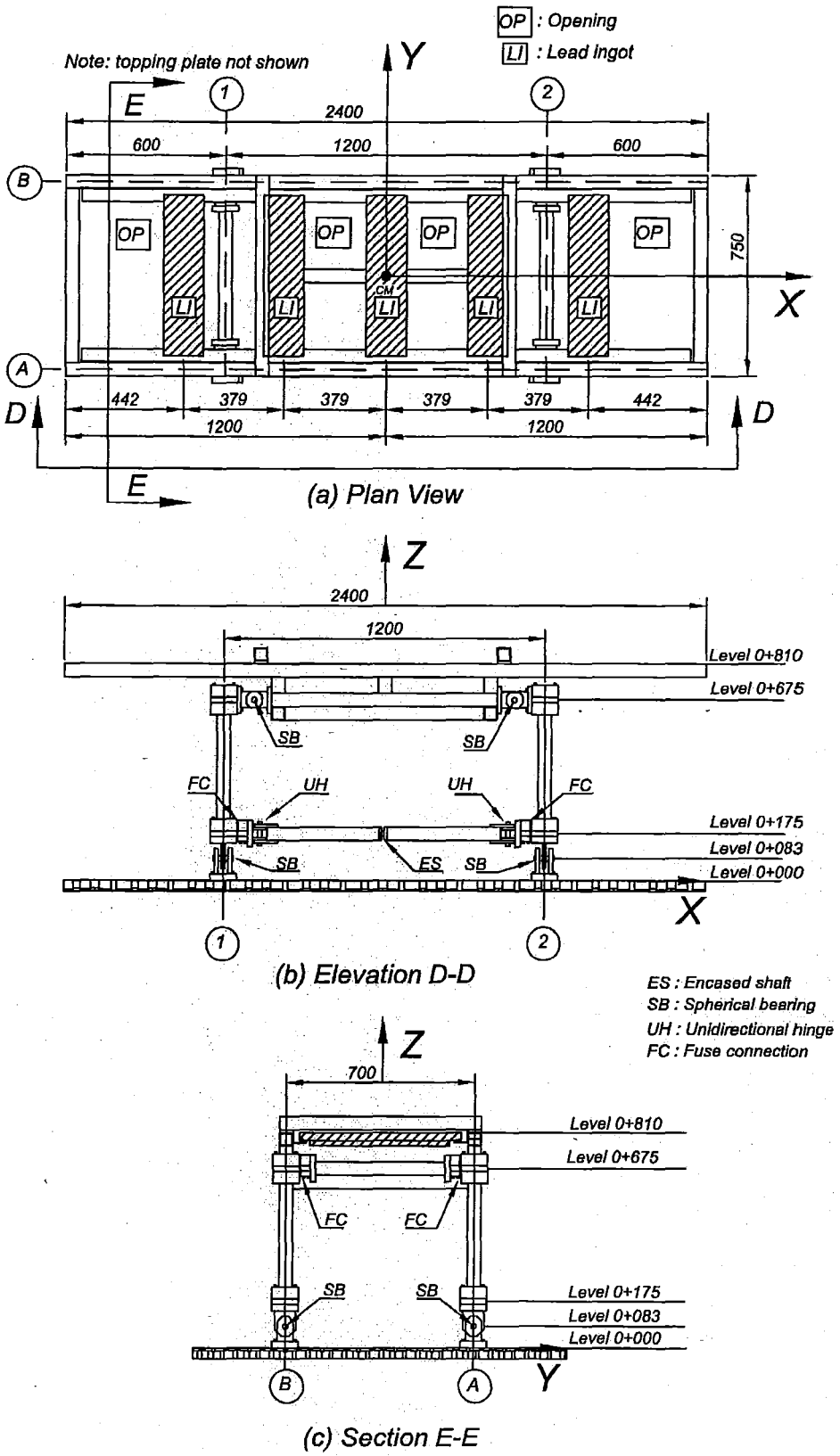

Figure 5-2. Torsionally restrained model

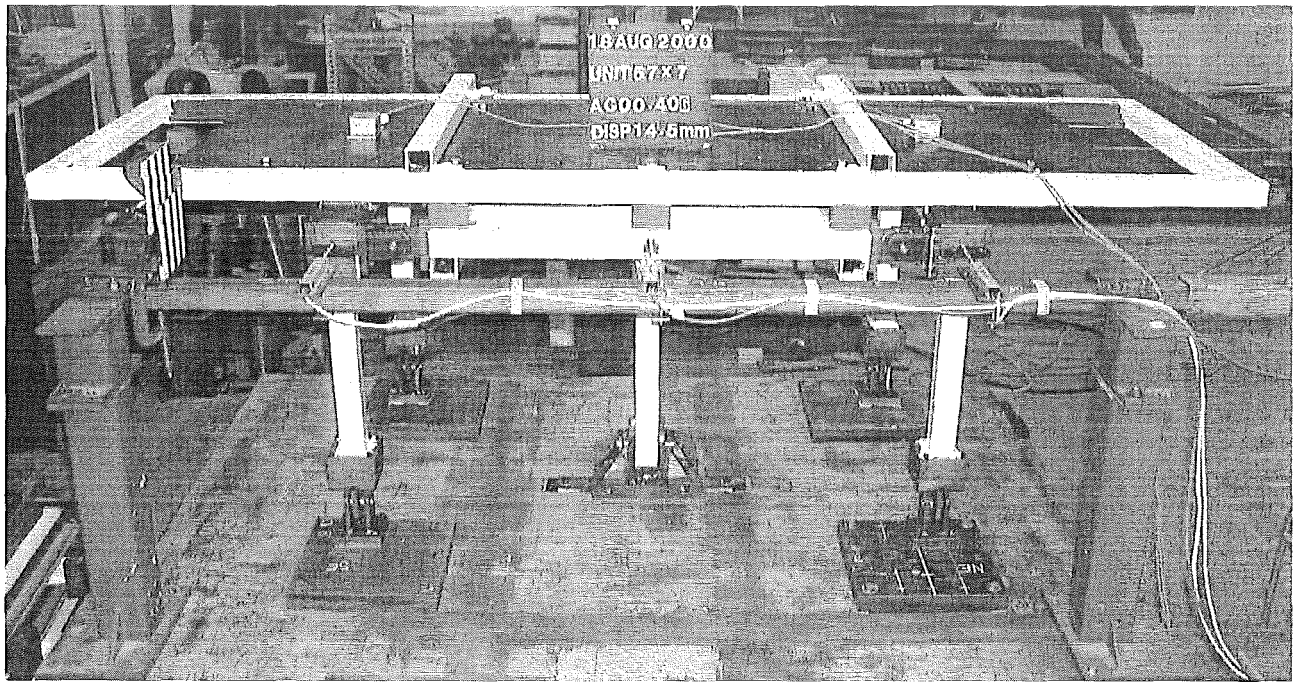

(a) Elevation of the torsionally unrestrained model

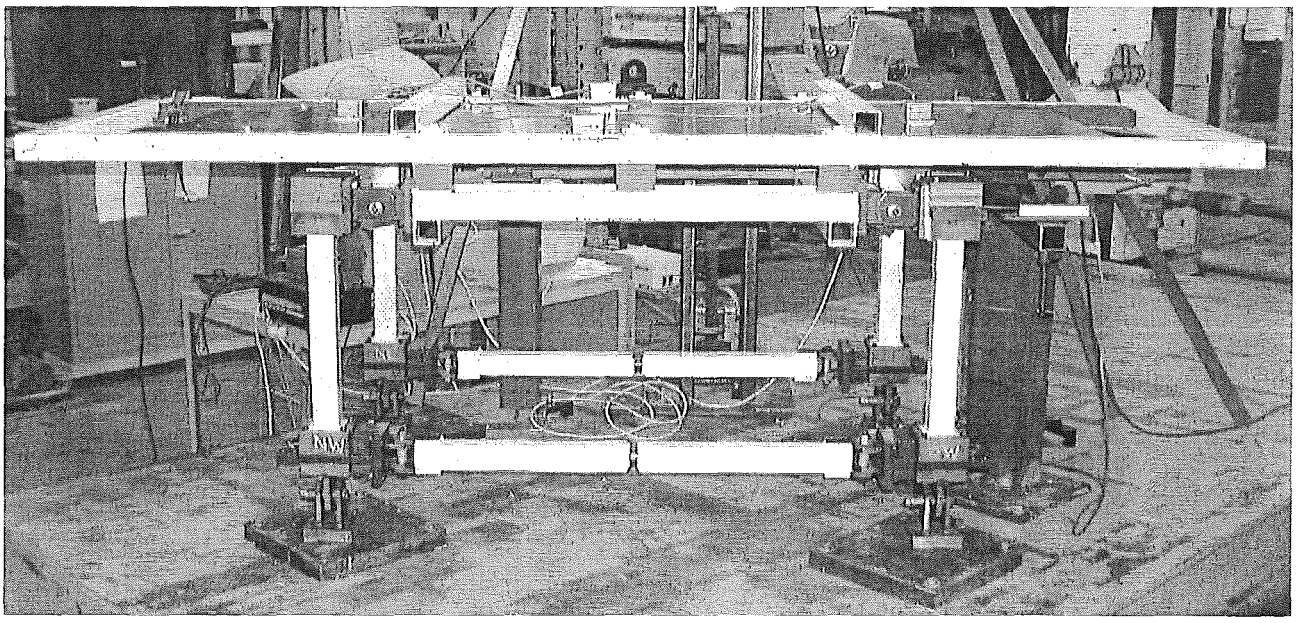

(b) Elevation of the torsionally restrained model

Figure 5-3. Torsionally unrestrained and restrained test models

Figure 5-1 also shows two frames along gridlines *(A)* and *(B)* and termed herein Frames *(A)* and *(B)*. They supported the masses laid on top of the diaphragm structure. These frames, however, did not provide lateral or torsional resistance because they were built with spherical bearings at levels *0+083* and *0+675* to create a lateral mechanism, as shown in Figure 5-1(b) and Figure 5-3(a). These bearings allowed free rotational motion in any direction.

A single column was connected between the centre of mass of the model's diaphragm and the shake table, as shown in Figure 5-1(c) and Figure 5-5(a). It provided the necessary translational

resistance and stability along the *X*-axis through cantilever action without introducing torsional resistance to the model. To achieve this characteristic, the column was connected at the base to a unidirectional connection allowing free translation of the column along the *Y*-direction but restricting the column's translation along the *X*-direction and its rotations about the *Z*-axis. At the top end of the column a spherical bearing connection was built with a round shaft encased into a spherical bearing. This connection enabled displacements of the model along the *Z*-axis and also permitted its translation along the *Y*-direction and rotations about the *Z*-axis.

A main feature of the test model was the incorporation of a beam-column connection comprising a replaceable plastic hinge region [K3], as shown in detail in Figure 5-4(a) and (b). This component was manufactured with a replaceable *100 mm* wide by *20 mm* thick hot-rolled flat bar clamped to steel blocks with cap screws. The flat bar, had a gap of ℓ_f=*5.0mm* and variable cross section dimensions (b_f * h_f) and termed herein as a "fuse", as shown in Figure 5-4(b). Deformations in the model will be concentrated at this fuse location due to its flexibility relative to that of the beam and the columns.

5.2.2 Torsionally restrained models

The torsionally restrained model had, along the *Y*-axis, the same two *Frames (1)* and *(2)* as the unrestrained model. The central single column, providing lateral resistance along the *X*-axis, was removed and a new beam was added to *Frames (A)* and *(B)* at level *0+175*, as shown in Figure 5-2(b) and Figure 5-3(b). The position of the beams was selected for ease of construction only and provided the same properties as those if the beam would have been placed at any other level. With the addition of this beam, *Frames (A)* and *(B)* were converted from lateral mechanisms to lateral force-resisting frames. They provided translational resistance and stability along the *X*-axis and additional torsional resistance about the *Z*-axis.

The new beam, shown in detail in Figure 5-5(c), had, at both ends, a potential plastic hinge region. A unidirectional connection was also built behind them to eliminate the stiffness of the fuses about its local *Z*-axis. A round shaft encased in a steel block was built in the middle of the beam to eliminate its torsional stiffness about its local *X*-axis.

5.2.3 Mass of the models and its distribution

The diaphragm of the model consisted of five lead ingots uniformly distributed in the *X*-direction; see Figure 5-2(a), and mounted on top of the diaphragm structure, as shown in Figure 5-5(b). The ingots were all connected with a topping plate of *60*15*3mm* to create a rigid diaphragm. The total weight of the model was *3.78kN*, comprising *2.05kN* of the structure and *1.73kN* of the lead ingots. The layout of the ingots, as shown in Figure 5-1 and Figure 5-2, was the same for all models.

5.3 Fundamental relationships

5.3.1 General

This section presents the theoretical background for determining the fundamental properties of the fuses, the frames and the model itself.

The response of the frames, and hence that of the model, was dependent on the hysteretic moment-rotation behaviour of the potential plastic hinges (or fuses) in both the elastic and

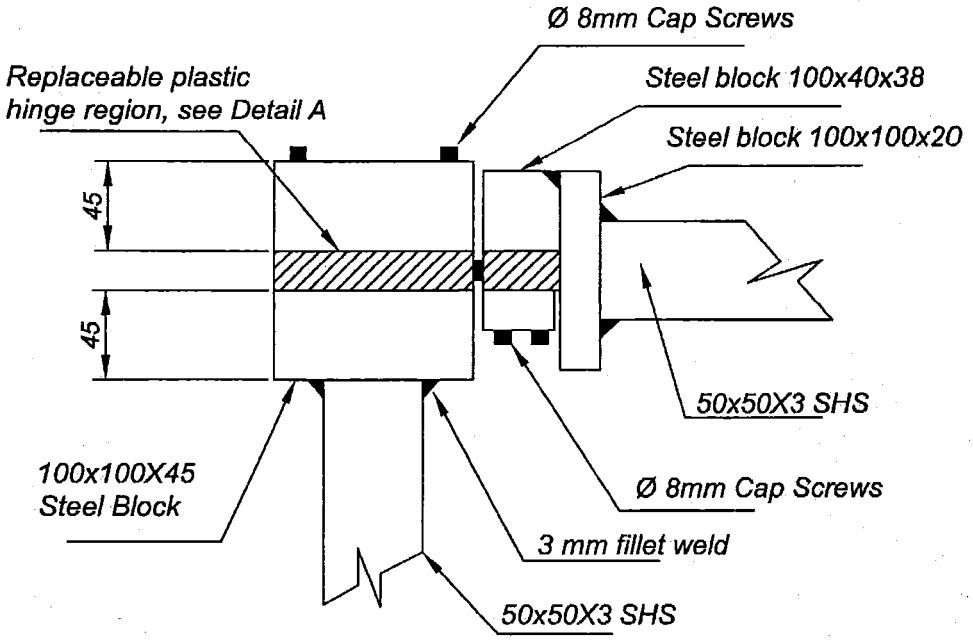

(a) Replaceable plastic hinge connection

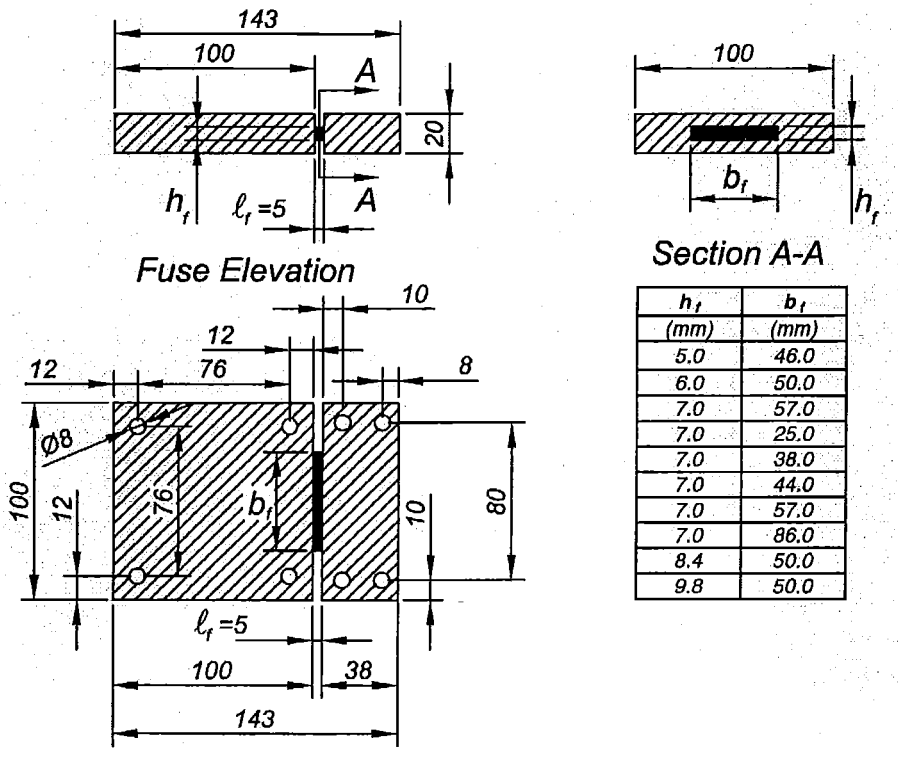

h_f (mm)	b_f (mm)
5.0	46.0
6.0	50.0
7.0	57.0
7.0	25.0
7.0	38.0
7.0	44.0
7.0	57.0
7.0	86.0
8.4	50.0
9.8	50.0

(b) Fuse detail A

Figure 5-4. Detail of the beam-column connection

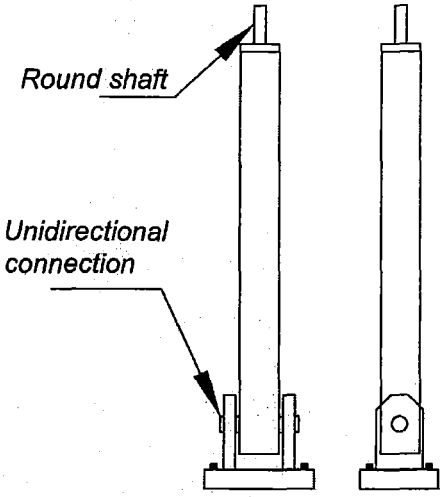

(a) Elevation of the single column

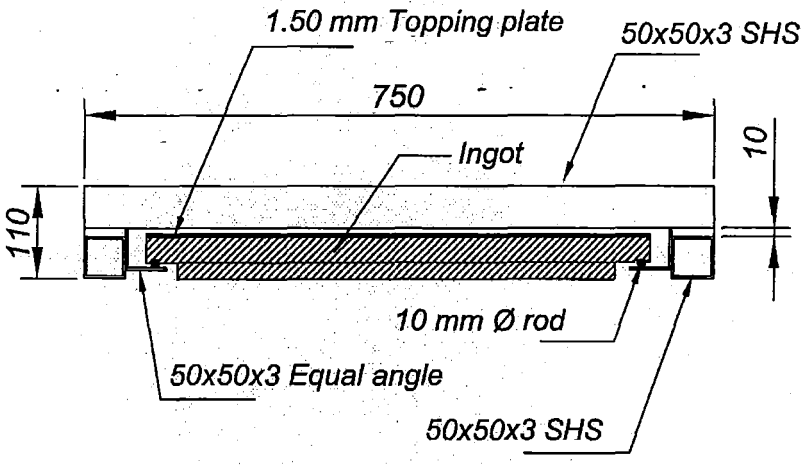

(b) Section of the diaphragm structure

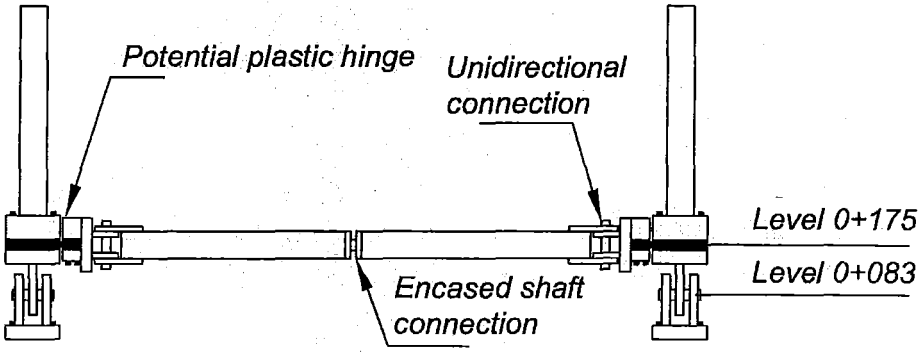

(c) Beam of the restrained models

Figure 5-5. Distinctive details of the models

inelastic range of response. This is because the flexibility of the fuses dominated the lateral displacement of the frames and hence that of the model.

5.3.2 Moment-rotation relationship of fuses

(a) Flexural strength

Figure 5-6 shows the moment-curvature relationship of a fuse. The flexural resistance at first yield, M_y, the plastic or nominal bending moment, M_p, and the flexural moment due to strain hardening, M_{sh}, are expressed as,

$$M_y = f_y * Z \quad \text{(5-1(a))}$$

$$M_p = M_n = f_y * S \quad \text{(5-1(b))}$$

$$M_{sh} = f_{sh} * S = (f_{sh} / f_y) M_p \quad \text{(5-1(c))}$$

where $f_y \le f_{sh} \le f_{su}$, as shown in Figure 5-7, $Z = (1/6) b_f h_f^2$ and $S = (1/4) b_f h_f^2$ are the elastic and plastic section modulae of the solid rectangular cross section of the fuse, respectively, f_y is the nominal yield strength f_{su} is the maximum stress level attained in the strain hardening region and f_{sh} is the stress level to be attained in the strain hardening region between f_y and f_{su}.

It is necessary to point out that the flexural moment resistance of the fuses will be significantly increased by the strain hardening property of steel. This is because the fuse rotation, and hence its related curvature, associated with the displacement capacity of the frames will be quite substantial. Hence, for the prediction of the element and system response in this study the bending moments including strain hardening rather than the plastic bending moment is to be used. This approach is slightly different with the design of actual building where plastic bending moments are expected to develop when the elements of the building reach their displacement capacity.

(b) Nominal yield curvature

The curvature at the onset of yielding of the fuse cross section, ϕ'_{yf}, with a thickness, h_f, and a neutral axis depth ratio, ξ, (see Table 2-1), as shown in Figure 5-6, is expressed as,

$$\phi'_{yf} = \frac{\varepsilon_y}{\xi h_f} \quad \text{(5-2)}$$

The nominal yield curvature of the fuse, ϕ_{yf}, is a reference value obtained by linear extrapolation and equal to

$$\phi_{yf} = \left(\frac{M_{sh}}{M_y}\right)\phi'_{yf} = \left(\frac{M_p}{\xi M_y}\right)\left(\frac{f_{sh}}{f_y}\right)\frac{\varepsilon_y}{h_f} = \eta\left(\frac{f_{sh}}{f_y}\right)\frac{\varepsilon_y}{h_f} \text{ where } f_y \le f_{sh} \le f_{su} \quad \text{(5-3)}$$

The curvature coefficient, η, may be also expressed as,

$$\eta = \frac{M_p}{\xi M_y} = \frac{S}{\xi Z} \tag{5-4}$$

In case of rectangular steel cross sections, the ratio of neutral axis depth to section depth is $\xi = c/h_f = 0.5$ and the $M_p / M_y = S/Z = 1.5$, hence, $\eta = 3.0$, as already shown in Table 2-1.

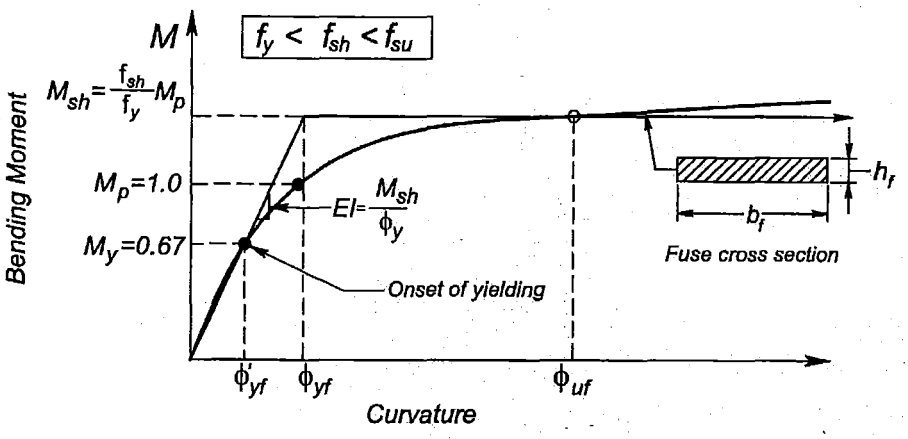

Figure 5-6. Moment-curvature relationship of a fuse

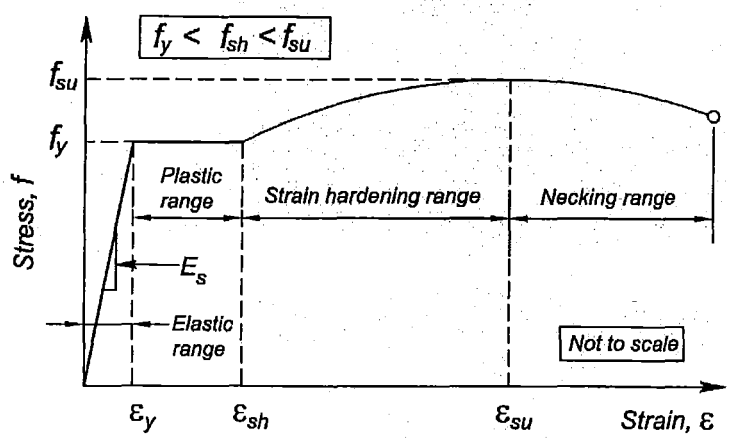

Figure 5-7. Stress-strain relationship of a steel coupon

(c) Flexural rigidity

The flexural rigidity, $E_s I_g$, relating the bending moment due to strain hardening and the nominal yield curvature of the fuse, is obtained with Eqs. 5-1(c) and 5-3 and is expressed as,

$$E_s I_g = \frac{M_y}{\phi'_{yf}} = \frac{M_{sh}}{\phi_{yf}} = \frac{M_p h_f}{\eta \varepsilon_y} \tag{5-5}$$

where I_g is the gross second moment of area.

(d) Nominal yield rotation

The rotation of the fuse at first yield, θ'_{yf}, is related to its curvature at first yield assuming that deformations are concentrated at the fuse region. This is expressed as,

$$\theta'_{yf} \geq \phi'_{yf}\,\ell_f = \frac{\varepsilon_y}{\xi}\left(\frac{\ell_f}{h_f}\right) \tag{5-6}$$

The relationship between the nominal yield curvature and nominal yield rotation, θ_{yf}, is

$$\theta_{yf} = \phi_{yf}\,\ell_f = \eta\varepsilon_y\left(\frac{f_{sh}}{f_y}\right)\left(\frac{\ell_f}{h_f}\right) \tag{5-7}$$

(e) Rotational stiffness

Equations 5-1(c) and 5-3 are considered to obtain the analytical nominal elastic rotational stiffness of the fuse, $k_{\theta f}$. This is expressed as,

$$k_{\theta f} = \frac{M_y}{\theta'_{yf}} = \frac{M_{sh}}{\theta_{yf}} = \frac{M_p}{\eta\varepsilon_y}\left(\frac{h_f}{\ell_f}\right) = \frac{E_s I_g}{\ell_f} \tag{5-8}$$

5.3.3 Force-displacement relationship of frames

The strength and nominal yield displacement of the frames is obtained assuming the lateral mechanism and considering the nomenclature shown in Figure 5-8.

(a) Nominal strength

The force at first yield of the frames, V_{ye}, is associated with the corresponding yield moment of the fuse. This relationship is expressed as,

$$V_{ye} = \frac{2M_y}{\ell_c}\left(\frac{\ell_b}{\ell'_b}\right) \tag{5-9}$$

By similarity, the nominal and ultimate strength of the frames, V_{ne} and V_{she}, respectively, associated with the plastic and ultimate flexural moment of its two identical fuses is

$$V_{ne} = \frac{2M_p}{\ell_c}\left(\frac{\ell_b}{\ell'_b}\right) \tag{5-10}$$

$$V_{she} = \frac{2M_{sh}}{\ell_c}\left(\frac{\ell_b}{\ell'_b}\right) \tag{5-11}$$

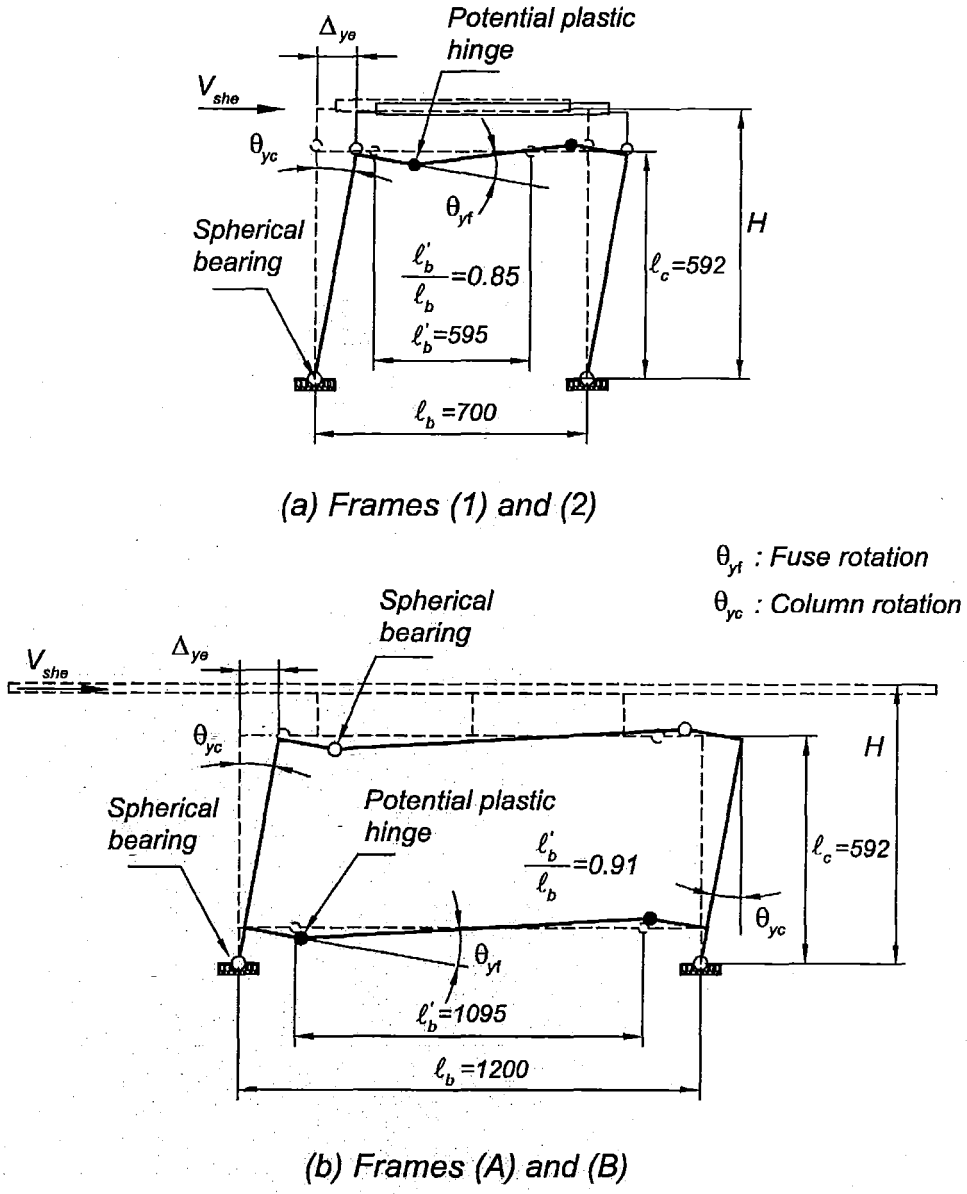

Figure 5-8. Lateral mechanism of frames

(b) Nominal yield displacement

The rotation of the column, θ_{yc}, associated with the rotation at first yield of the rectangular fuse section is

$$\theta_{yc} = \theta'_{yf}\left(\frac{\ell'_b}{\ell_b}\right) = \frac{\varepsilon_y}{\xi}\left(\frac{\ell_f}{h_f}\right)\left(\frac{\ell'_b}{\ell_b}\right) \tag{5-12}$$

The lateral displacement at first yield of the frame, Δ'_{ye}, is

$$\Delta_{ye}^{'} \geq \theta_{yc}\ell_c = \frac{\varepsilon_y}{\xi}\left(\frac{\ell_f}{h_f}\right)\left(\frac{\ell_b^{'}}{\ell_b}\right)\ell_c \tag{5-13}$$

The nominal yield displacement of the frame, Δ_{ye}, is a reference value obtained by linear extrapolation as shown below

$$\Delta_{ye} \approx \left(\frac{V_{ne}}{V_{ye}}\right)\Delta_{ye}^{'} = \eta\varepsilon_y\left(\frac{f_{sh}}{f_y}\right)\left(\frac{\ell_f}{h_f}\right)\left(\frac{\ell_b^{'}}{\ell_b}\right)\ell_c \tag{5-14}$$

Equation 5-13 applies to the two frames shown in Figure 5-8. The only difference between them is on their $\ell_b^{'}/\ell_b$ ratio. In case of *Frames (1)* and *(2)*, this is equal to $\ell_b^{'}/\ell_b = 0.85$ and for *Frames (A)* and *(B)*, this is $\ell_b^{'}/\ell_b = 0.91$.

(c) Translational stiffness

The translational stiffness of the frames, k_e, is expressed as,

$$k_e = \frac{V_{ye}}{\Delta_{ye}^{'}} = \frac{V_{sh}}{\Delta_{ye}} = \frac{2M_p}{\eta\varepsilon_y\ell_c^2}\left(\frac{h_f}{\ell_f}\right)\left(\frac{\ell_b}{\ell_b^{'}}\right)^2 \tag{5-15}$$

or

$$k_e = \frac{2k_{\theta f}}{\ell_c^2}\left(\frac{\ell_b}{\ell_b^{'}}\right)^2 \quad \text{since } M_{sh} = k_{\theta f}\theta_{yf} \Rightarrow M_p = k_{\theta f}\theta_{yf}\left(\frac{f_y}{f_{sh}}\right) \tag{5-16}$$

5.3.4 Force-displacement relationship of models

The translational strength and stiffness of the models along the principal axes due to strain hardening in the fuses are obtained by adding the strengths and the stiffnesses of parallel frames. Thus, the nominal yield displacement of the system is,

$$\Delta_{ys} = \frac{V_{shs}}{K_s} = \frac{\sum_i V_{she}^{'}}{\sum_i k_e} \tag{5-17}$$

5.4 Relationship of the analytical and the experimentally derived properties

This section presents tests results on fuses with different cross sections. The aim is to derive an empirical expression relating the gross and the effective (experimentally derived) second

moment of area, I_g and I_e, respectively, of the fuses. This relationship is necessary to estimate the effective properties of the frames and the model itself.

5.4.1 Testing of fuses

(a) Stress-strain relationship

Tensile tests were undertaken on a steel coupon extracted from the same batch of steel used as potential plastic hinge regions. It was made of mild steel grade *250*. Figure 5-9 exhibits the stress-strain relationship of the test coupon. The steel had an average yield strength f_y=*285 MPa* and an ultimate yield stress of f_{su}=*410 MPa*, hence f_{su}/f_y=*1.44*.

(b) Test set-up of fuses

The fuses were dynamically tested with the same beam-column subframe component used by Lindawieck[L2], as shown in Figure 5-10. Two *SHS*, representing the columns of the subframe, were attached to the shake table with hinge connections at one end and fixed in the middle to a beam-column connection comprising a replaceable plastic hinge region, as described in Section 5.2.1 and shown in Figure 5-4. Another *SHS*, representing the beam of the subframe, was also connected at one end to the beam-column connection whereas at the other end a pin connection was built between the beam and the hinged arm of the rigid frame fixed to the strong floor. A load cell connected to the arm quantified the resistance of the fuse, F_s, and a potentiometer attached to the floor verified the displacement time history, Δ_s, reproduced by the shake table.

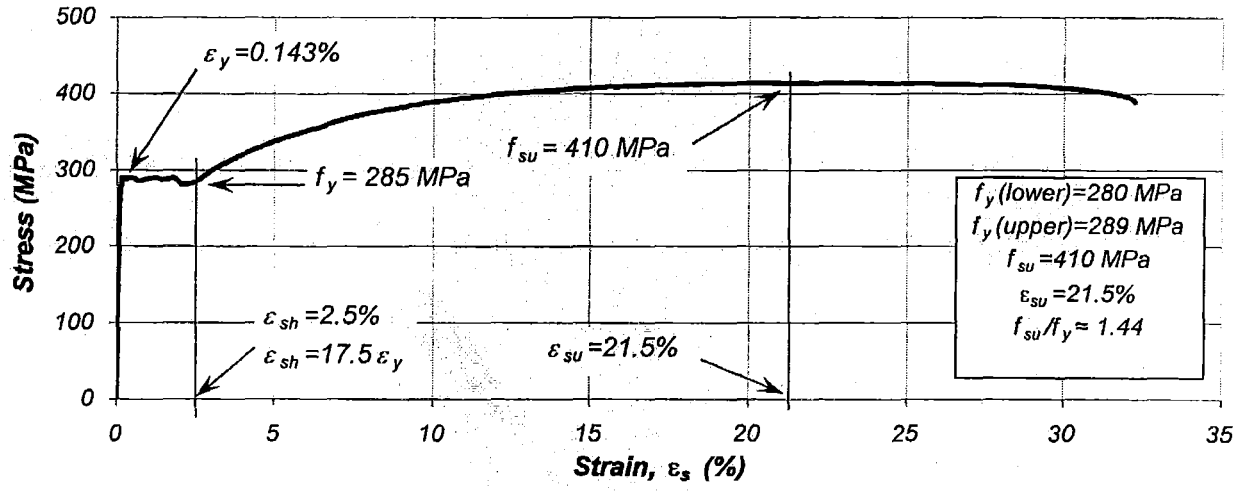

Figure 5-9. Tensile test of a steel coupon

(c) Results of real time tests on fuses

Real time tests were undertaken on fuses with cross section dimensions other than those tested by Kao[K3] and Lindawatiek[L2] to corroborate their results and to derive an empirical expression relating the gross and the effective (experimentally derived) second moment of area, I_g and I_e, respectively.

Figure 5-11 shows the measured moment-rotation relationships of the fuse (h_f=*7mm**b_f=*57mm*) by using the beam-column subframe shown in Figure 5-10. The shake table reproduced a

realistic displacement time history obtained from a preliminary test on a symmetric model previously tested. The fuse rotation is $\theta_f = \Delta_s / \ell_b$ where Δ_s is the displacement time history reproduced by the shake table and ℓ_b is the length of the beam. The flexural moment is equal to the force measured by the load cell times the lever arm, $M = F_s * \ell_b$.

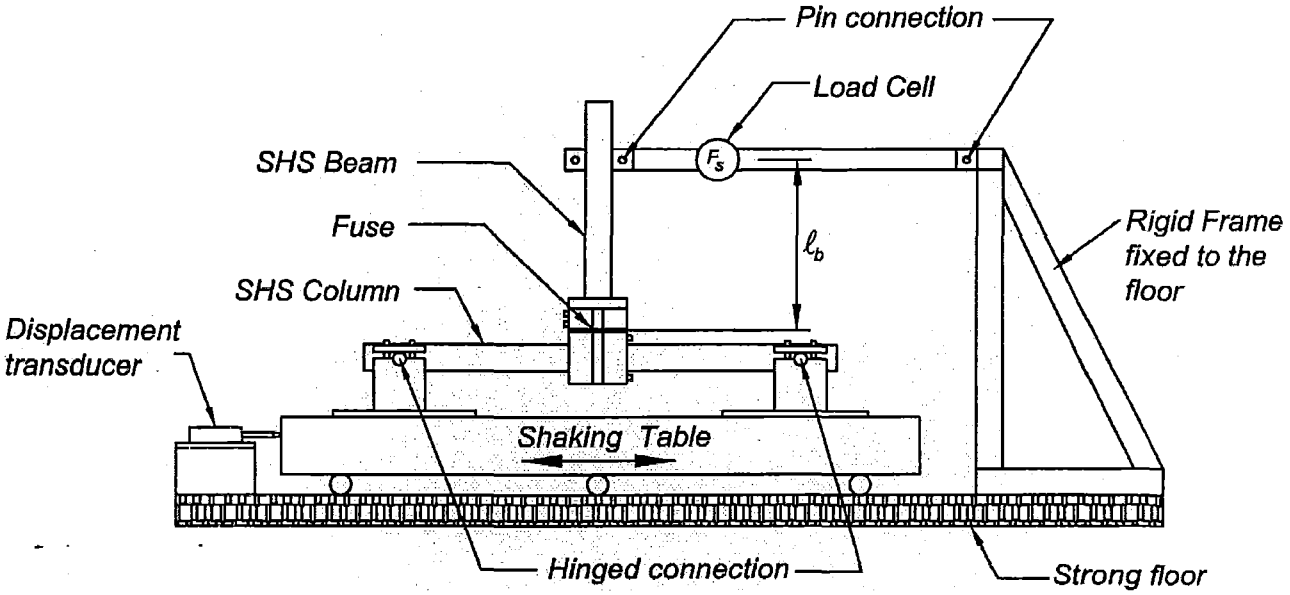

Figure 5-10. Real time test of a fuse component

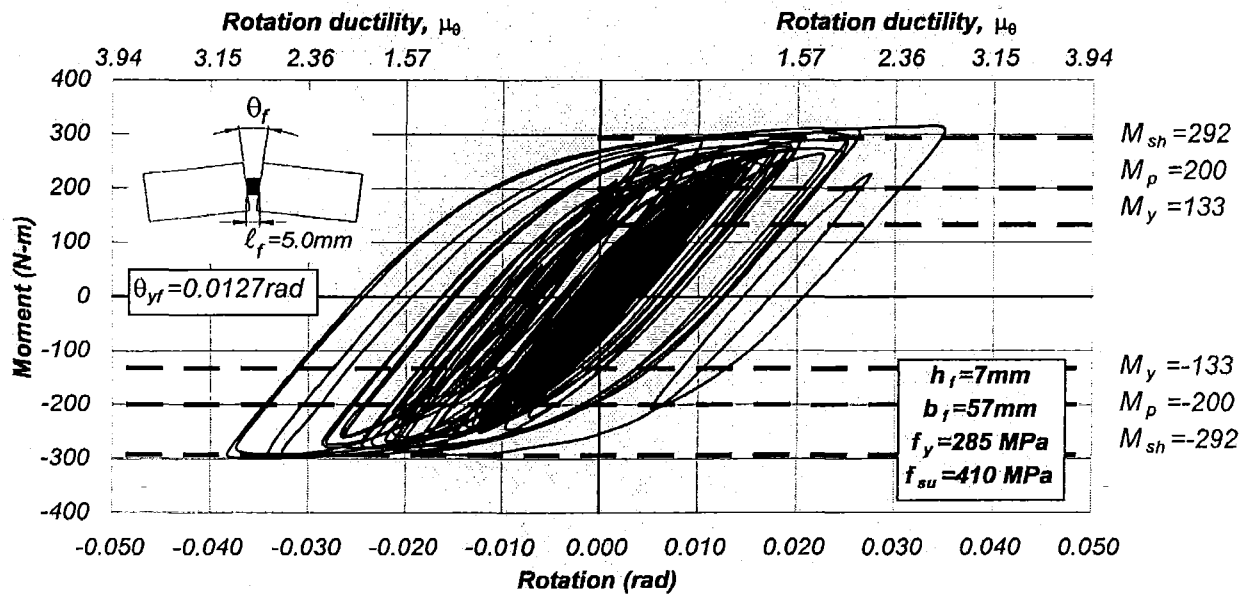

Figure 5-11. Real time test of the subassembly structure with a fuse component of h_f=7mm*b_f=57mm

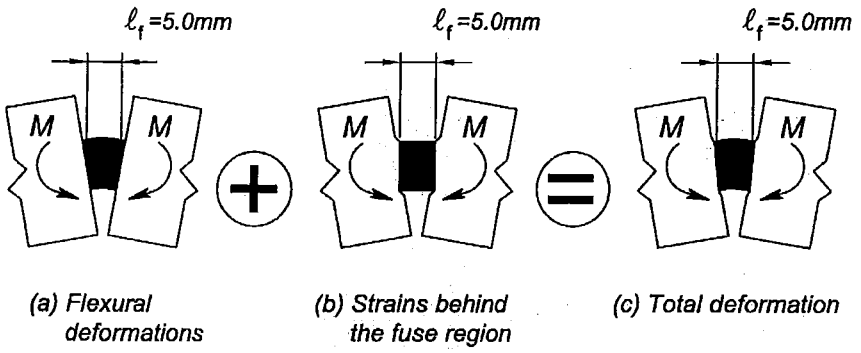

Figure 5-12. Deformations of fuses in the elastic and inelastic range of response

Table 5-1 compares the analytical properties of a fuse (h_f=7mm*b_f=57mm) and those measured during the test. It is evident that the strength of the fuse due to strain-hardening can be satisfactorily determined by assuming that the ultimate tensile strength was reached in all fibres of the cross section, hence $f_{sh}/f_y=f_{su}/f_y=1.44$. The fact that the analytically estimated bending moment of the fuse due to strain hardening did not result in a precise envelope of the measured response is attributed to the effect of the strain rate. Lindawatiek [L2], using a similar test set-up, investigated its effect and concluded that the fuse flexural strength is not significantly influenced by the strain rate and hence it could be ignored for practical purposes.

Table 5-1 indicates that that the effective second moment of area was just *35%* of its gross. This is because the fuse was subjected to additional hinge rotation-induced deformations due to the contribution of strains ($\varepsilon_s<\varepsilon_y$) behind the fuse region [K3], as shown in Figure 5-12. The I_e / I_g ratio is a convenient parameter used to account for this characteristic. Experimental findings for several fuses listed in Appendix C and summarized in Table 5-2 and Table 5-3 demonstrates that the I_e / I_g ratio is affected by changes in both the fuse width and thickness.

Table 5-1. Analytical and experimental properties of fuse of h_f=7mm* b_f=57mm

		Fuse 7 x 57	
		Analytical	Experimental
M_y	(N-m)	133 (Eq.5-1a)	NA
M_p	(N-m)	200 (Eq.5-2b)	NA
M_u	(N-m)	287 (Eq.5-3c)	313
ϕ'_{yf}	(1/m)	0.407 (Eq.5-2)	1.16
θ'_{yf}	(rad)	0.00204 (Eq.5-5)	0.00581
θ_{yf}	(rad)	0.00448 (Eq. 5-6)	0.0127
$k_{\theta f}$	((kN-m)/rad)	65.17(Eq.5-7)	22.87
I_e / I_g		-------	0.351

Table 5-2. Ratios of effective and gross second moment of area of fuses having a thickness of h_f=7mm

Fuse Dimension (mm)		I_e / I_g
h_f	b_f	
7	25	0.440*
7	38	0.396
7	44	0.400*
7	57	0.351
7	86	0.320*

(*) Tested by Kao[K3]

Table 5-3. Ratios of effective to gross second moment of area of fuse components with variable width, b_f, and thickness, h_f

Fuse Dimension (mm)		I_e / I_g
h_f	b_f	
5.0	46	0.560
6.0	50	0.488
8.4	50	0.311
9.8	50	0.233

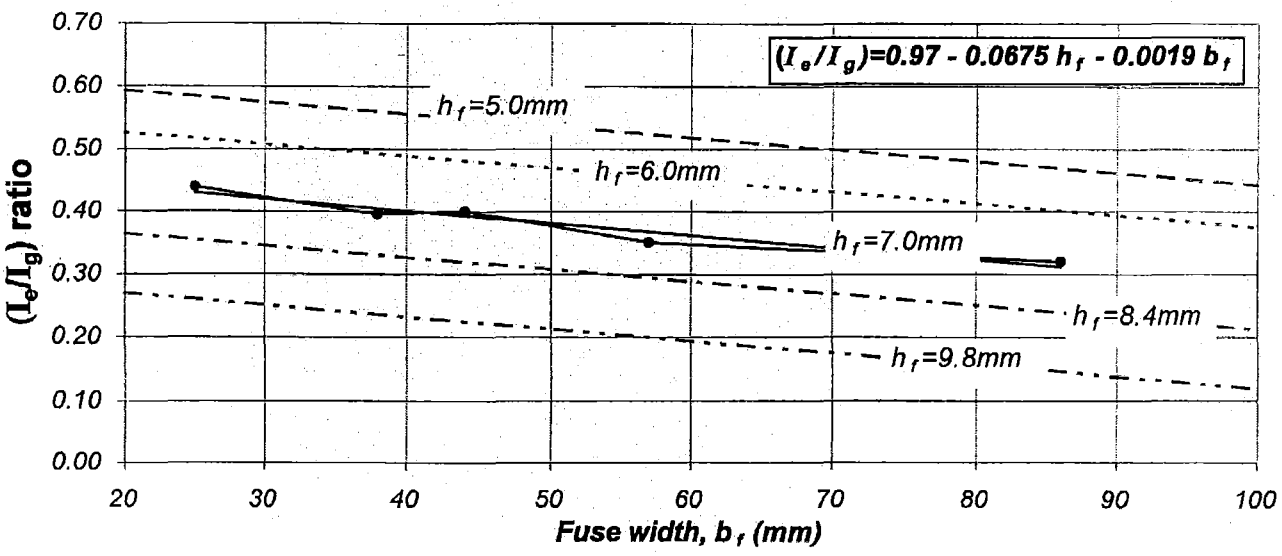

Figure 5-13. Ratio of effective and gross second moment of area as function of the fuse width, b_f, and thickness, h_f

Table 5-2 summarises the ratios of gross and effective second moment of area of fuses tested for this study and by other reseachers [K3] having a constant thickness of h_f=7.0mm and different widths (see Appendix *C*). The results presented in Figure 5-13 as dots, show a linear relationship between the I_e / I_g ratio and the fuse width. It is evident that the I_e / I_g ratio reduced as the width increased, even though flexural deformations were expected to reduce due to increasing second moment of area. This confirmed that the moment-rotation relationship is significantly affected by additional hinge rotation-induced deformations due to the contribution of strains ($\varepsilon_s < \varepsilon_y$) behind the fuse region.

Table 5-3 summarises the I_e / I_g ratio of fuses having a constant width of b_f=*50mm* and thicknesses of h_f=*5.0, 6.0, 8.4* and *9.8mm*. It is evident that the I_e / I_g ratio reduced as the thickness of the fuse increased. Figure 5-13 plots this variation as a function of the width of these fuses by assuming lines parallel to that derived for the fuse having a constant thickness of h_f=*7mm*. The I_e / I_g ratio is affected by changes in both the width and thickness of the fuse.

A general expression representing the variation of the I_e / I_g ratio for fuses with cross-sections in the range of b_f =*20~100* and h_f =*5~9.8mm*, as a function of the fuse width and thickness is expressed as

$$\frac{I_e}{I_g} = (0.97 - 0.0675h_f - 0.0019b_f) \tag{5-18}$$

This expression may be used to relate the analytical and effective nominal yield curvature and rotation. It may also be used to estimate an effective nominal fuse length, $(\ell_f)_e$, as a function of the actual fuse length to directly derive its properties. These relationships are expressed as,

$$\frac{I_e}{I_g} = \frac{\phi_{yf}}{(\phi_{yf})_e} = \frac{\theta_{yf}}{(\theta_{yf})_e} = \frac{\ell_f}{(\ell_f)_e} \tag{5-19}$$

Equation 5-19 indicates that additional hinge rotation-induced deformations due to strains developed behind the fuse region increased the analytically derived values of nominal yield curvature and rotation.

5.4.2 Effective properties of the fuses, frames and models

The effective properties of the fuses, frames and model can be derived with the I_e / I_g ratio as subsequently described.

(a) Effective nominal yield curvature and stiffness of the fuses

The effective nominal yield curvature of a fuse is expressed as

$$(\phi_{yf})_e = \frac{\phi_{yf}}{(I_e / I_g)} \tag{5-20}$$

and the fuse section stiffness is then

$$(k_{\theta f})_e = \frac{M_{sh}}{(\phi_{yf})_e} \tag{5-21}$$

(b) Effective nominal yield displacement and stiffness of the frames

The effective nominal yield displacement is

$$(\Delta_{ye})_e = \frac{\Delta_{ye}}{(I_e / I_g)} \tag{5-22}$$

The effective stiffness of the frame is

$$(k_e)_e = \frac{V_{she}}{(\Delta_{ye})_e} \tag{5-23}$$

(c) Effective nominal yield displacement and stiffness of the systems

The effective nominal yield displacement of the system can also be expressed as,

$$(\Delta_{ys})_e = \frac{\Delta_{ys}}{(I_e / I_g)} \tag{5-24}$$

and the effective stiffness of the system is

$$(K_s)_e = \frac{V_{shs}}{(\Delta_{ys})_e} \tag{5-25}$$

5.5 Design earthquake record

The earthquake record selected for the test programme was the Llolleo85. This earthquake occurred in Chile on the 3rd of March 1985 at a depth below ground of *33* kilometres and had a magnitude of 7.8 [W1]. The record had a peak ground acceleration of *0.66g*, maximum displacement of *1200mm* and duration of *120* seconds. The displacement of *1200mm* was too large to be reproduced by the shake table. The record was, therefore, compressed to half the time and filtered using the program Series [J2]. The resulting earthquake record and associated spectra, as shown in Figure 5-14, had a maximum acceleration of *0.66g* and maximum displacement of *18mm.*

The acceleration and displacement response spectra, shown in Figure 5-14(c) and (d), were obtained with the program INSPECT [C3] using an elasto-plastic hysteretic relationship.

5.6 Structural design

5.6.1 General

The components of the model were designed following the principles of capacity design [P2] where the SHS columns and beams were deliberately made stronger and hence stiffer than the fuses and were expected to remain elastic. Dominant deformations of the models will be concentrated in the fuse regions of the replaceable potential plastic hinge. The aim of the design was to estimate the system nominal strength and its associated stiffness necessary to reach, but not exceed, for the selected shaking, the displacement capacity of the system.

The base shear capacity of the model was obtained using a displacement-based design method described elsewhere [K5] but slightly modified. First, the nominal yield displacement of the elements and hence that of the system is a readily derived property, rather than that initially

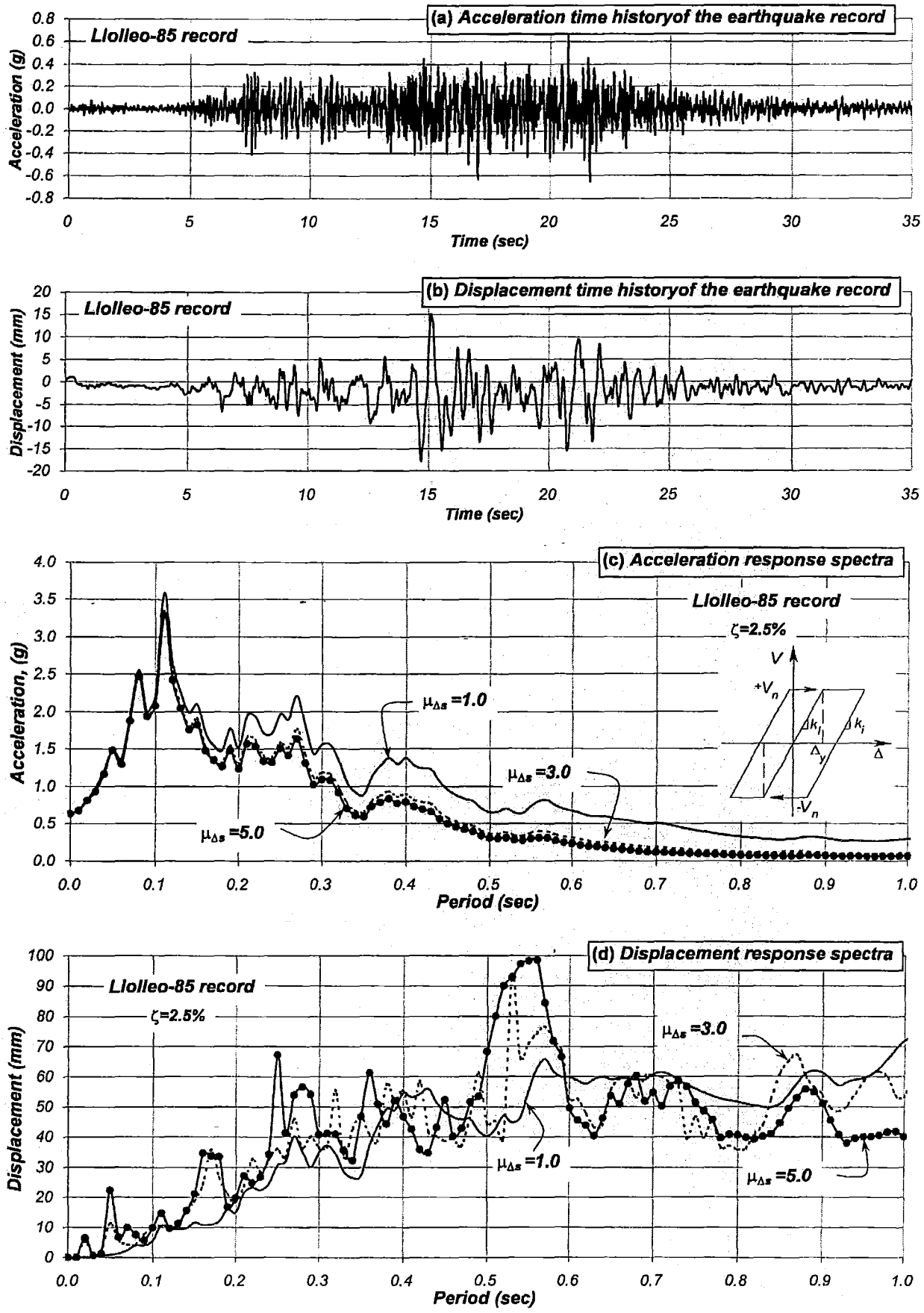

Figure 5-14. Design earthquake record and corresponding response spectra

assumed, before the strength of the system is obtained. Subsequently, the displacement response spectra of single degree of freedom inelastic systems rather than that of elastic systems were used to estimate the system strength. The former was estimated considering a *2.5%* of viscous damping and different system displacement ductility capacities. These spectra were used because the inelastic model is not expected to oscillate about its rest position. At some stage, the structure is likely to oscillate about a permanent imposed deformation. Chopra and Goel [C9] who compared the earthquake induced-deformations estimated with inelastic single degree of freedom systems and that using equivalent elastic single degree freedom systems concluded that in many cases both approaches did not converge hence indicating that the use of elastic spectra is not a reliable approximation. It is believed that the accuracy of the displacement response spectra using inelastic systems or equivalent elastic systems are likely to converge when the system is a self-centering structure[P22].

5.6.2 Outline for the calculation of the system nominal strength

The nominal strength of the system and its associated fuse dimensions can be readily obtained using the following procedure.

Step 1. Estimate the displacement capacity of the elements, Δ_{ue}, associated with one of the limit states described in Section 2.2. The displacement capacity of the models to be examined, Δ_{us}, is the same as that of the elements.

Step 2. Define the thickness, h_f, of the fuses and then estimate the nominal yield displacement of the frames, Δ_{ye}, (Eq. 5-12) and that of the system, Δ_{ys} (Eq. 5-16). The effective nominal yield displacement of the elements, $(\Delta_{ye})_e$, and that of the model, $(\Delta_{ys})_e$, is then obtained with Eqs. 5-21 and 5-23, respectively after estimating the I_e / I_g ratio (Eq. 5-17) by using a tentative fuse width dimension.

Step 3. Derive the displacement ductility capacity of the system

$$\mu_{\Delta s} = \frac{\Delta_{us}}{(\Delta_{ys})_e} \tag{5-26}$$

Step 4. Use the inelastic displacement response spectra for the design earthquake record, obtain the translational period of the elastic system, T_s. For this purposes, consider the displacement capacity of the system derived in Step 1 and a ductility factor equal to the system displacement ductility capacity obtained in Step 4.

Step 5. Determine the stiffness of the elastic system with the following expression

$$K_s = \frac{4\pi^2 M_e}{T_s^2} \tag{5-27}$$

Step 6. The strength of the system including strain hardening, V_{shs}, is

$$V_{shs} = K_s \Delta_{ys} e \tag{5-28}$$

Step 7. The system nominal or plastic strength, V_{ns}, is

$$V_{ns} = V_{shs} / (f_{sh} / f_y) \tag{5-29}$$

Step 8. The width of the fuses is obtained by rearranging equations 5-10 and 5-1(b) and considering the plastic modulus of a rectangular cross section ($S = (1/4) b_f h_f^2$).

$$b_f = \frac{V_{ns} \ell_c}{f_y h_f^2} \left(\frac{\ell_b'}{\ell_b} \right) \tag{5-30}$$

The fuse width to be obtained should match the tentative value selected in Step 2. If not, iterations may be required until convergence is achieved.

5.6.3 Description of the symmetric *Model 5-1*

The symmetric *Model 5-1* was torsionally unrestrained. *Frames (1)* and *(2)*, along the *Y*-axis, comprised each two identical fuses; see Figure 5-16. The nominal yield displacement of the frames and their strength was the same. The nominal yield displacement at the centre of mass was also similar. The centre of strength and stiffness coincided with the centre of mass of the model. The model had a ratio of radii of gyration of strength and mass of $r_{vy}/r_m = 1.33$. Section 5.8 will explain how to derive the radius of gyration of mass.

5.6.4 Structural design of the symmetric *Model 5-1*

The structural design of the symmetric *Model 5-1* was based on the method already described in Section 5.6.2.

Step 1. A system displacement capacity of $\Delta_{us} = 21mm$ was selected. This was obtained assuming an inter-storey drift of *3.5%* for a column height of $\ell_c = 592mm$. Although this drift is larger than the *2.5%* recommended by the New Zealand loading Code [S6], it was selected to achieve, for academic purposes, a displacement ductility demand of approximately $\mu_{\Delta s} = 4.0$.

Step 2. A fuse thickness of $h_f = 7mm$ was selected for both *Frames (1)* and *(2)*. According to Eqs. 5-12 and 5-16, the nominal yield displacement of the elements, and that of the system, was $\Delta_{ye1} = \Delta_{ye2} = \Delta_{ys} = 2.21mm$. The effective nominal yield displacement of the frames and the model was $(\Delta_{ye1})_e = (\Delta_{ye2})_e = (\Delta_{ys})_e = 5.35mm$ obtained with Eqs. 5-14 and 5-17, respectively, considering $I_e / I_g = 0.41$ for a tentative fuse width of $b_f = 44mm$ (Eq. 5-18).

Step 3. The displacement ductility capacity of the system, according to Steps 1 and 2, was therefore $\mu_{\Delta s} = \Delta_{us} / (\Delta_{ys})_e = 21/5.35 = 3.92$.

Step 4. The translational period of the elastic model was obtained with the displacement response spectra of the Chilean earthquake record derived with single degree of freedom inelastic systems having 2.5% of viscous damping, as shown in Figure 5-15.

Based on a displacement capacity of Δ_{us}=*21.0 mm* and a ductility factor equal to the system displacement capacity of $\mu_{\Delta s}$=3.92 the translational period of the elastic system was T_s=*0.20 sec.*

Step 5. According to equation 5-27 and considering an effective mass of $M_e = 325kg$ obtained from preliminary tests on a symmetric model (see Section 5.8(c)), the elastic stiffness of the model, along the *Y*–axis, was $(K_{ys})_e = 328927N/m$.

Step 6. The strength of the model due to strain hardening, according to equation 5-28, was equal to

$$V_{shs} = (K_{ys})_e * (\Delta_{ys})_e = 328927 * 0.00535 = 1758N$$

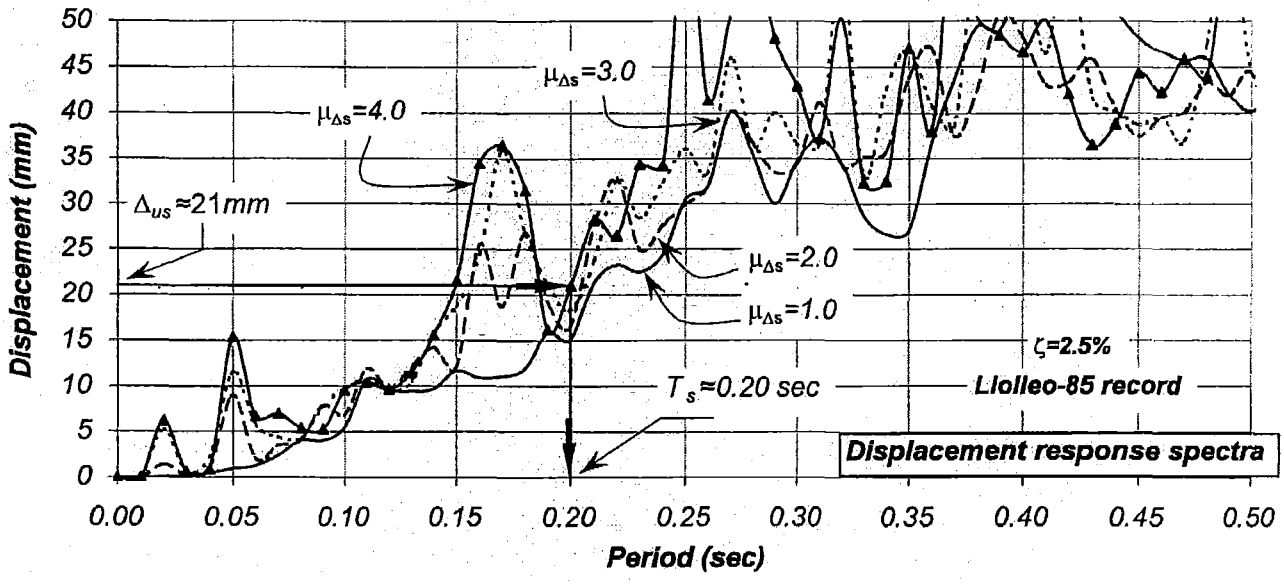

Figure 5-15. Displacement response spectra of inelastic *SDOF* systems using the design earthquake record

Step 7. The nominal or plastic strength of the system, V_{ns}, was obtained using the f_{sh}/f_y ratio. Observations from preliminary tests have indicated that for a system displacement ductility demand of $\mu_{\Delta s} \approx 4.0$, all fibres of the fuse cross section developed their ultimate yield stress, f_{su}, and hence $f_{sh}/f_y = f_{su}/f_y = 1.44$. The nominal strength of the system is then

$$V_{ns} = V_{shs}/(f_{su}/f_y) = 1758N/1.44 = 1221N = 0.32W$$

where W is the total seismic weight of the model.

Step 8. According to Eq. 5-30 the required fuse width, having a thickness of h_f=*7mm*, should be b_f=*44mm*. This happened to be equal to the tentative width assumed in Step 3 and therefore there was no need to iterate.

5.7 Properties of the test models

An experimental programme was undertaken on asymmetric test models schematically presented in Figure 5-16. The mass and its distribution remained unchanged. Their properties are subsequently described.

5.7.1 Symmetric and torsionally unrestrained *Model 5-1*

The symmetric torsionally unrestrained *Model 5-1* had in *Frames (1)* and *(2)* fuses with cross section dimensions of h_f=*7mm* * b_f=*44mm*, as shown in Figure 5-16(a). They provided a system nominal strength of V_{yns}≈*1221N* (Eq.5-24). The system had, in theory, no strength or stiffness eccentricity.

Table 5-4 summarizes the properties of the unrestrained *Model 5-1*. The effective nominal yield displacement of the elements and that of the system was $(\Delta_{ye1})_e = (\Delta_{ye2})_e = (\Delta_{ys})_e = 5.35mm$ (Eqs 5-22 and 5-24). It had translational and rotational periods of free vibration of T_y=*0.20* and T_θ=*0.15 sec*, respectively. The torsional stiffness of the fuses, about their local *X*-axis, was not included in the calculation because the spherical bearing at the bottom of the columns allow the system to rotate without engaging their torsional resistance. The earthquake record was applied along the *Y*-direction.

5.7.2 Asymmetric and torsionally unrestrained *Model 5-2A*

The nominal strength of the unrestrained *Model 5-2A* was the same as that of the unrestrained *Model 5-1*, i.e., V_{yns}≈*1221N (0.32W)*. Half of it was assigned to each frame to achieve zero strength eccentricity. The only difference between this and the unrestrained *Model 5-1* described before was their fuse thicknesses. *Frame (1)* had two fuses with a thickness of h_f=*7.0mm* whereas those of *Frame (2)* were h_f=*5.0mm*, as shown in Figure 5-16 (b). The fuse cross section dimension of *Frame (1)* was the same as those of symmetric *Model 5-1* (h_f=*7.0mm*b_f=*44.0mm*) whereas *Frame (2)* had two identical fuses (h_f=*5.0mm*b_f=*86.0mm*). In case of *Frame (2)*, the width of these fuses was increased to b_f=*86.0mm* to maintain the same strength on both frames.

The ratio of the fuse thickness of *Frames (1)* and *(2)* other than unity, i.e., h_{f1}/h_{f2}=*7.0/5.0=1.4*, is indicative of the frames having different nominal yield displacements. Table 5-4 shows, for the unrestrained *Model 5-2A*, that the effective nominal yield displacement of *Frames (1)* and *(2)* was $(\Delta_{ye1})_e$=*5.35mm* and $(\Delta_{ye2})_e$=*6.60mm*, thus $\alpha=(\Delta_{ye2})_e/(\Delta_{ye1})_e$=*6.60/5.35=1.23*. Although the strength assigned to the frames was the same, their different nominal yield displacement led to different stiffnesses of $(k_{e1})_e$=*164N/mm* and $(k_{e2})_e$=*133N/mm*. The model, therefore, had, for zero strength eccentricity, a stiffness eccentricity of e_{rx}=*-0.052D(-63mm)*. The effective nominal yield displacement of the system increased from $(\Delta_{ys})_e$=*5.35mm*, as it is the case of the unrestrained *Model 5-1*, to $(\Delta_{ys})_e$ =*5.91mm*. Although the nominal strength of the unrestrained *Model 5-2A* was the same as that of the unrestrained *Model 5-1*, the larger system nominal yield displacement of the unrestrained *Model 5-2A* led to a slight increase of its uncoupled translational period. The translational and rotational periods of free vibration were T_y=*0.21sec* and T_θ=*0.15sec*, respectively. The system was subjected to the earthquake record along the *Y*-axis.

5.7.3 Asymmetric and torsionally unrestrained *Model 5-2B*

The unrestrained *Model 5-2B* intended to examine the effect on the response when a strength eccentricity, associated with an increase of system strength, is introduced to the system.

The strength of *Frame (1)* was increased by *23%* (λ_1=*1.23*) to V_{nel}=*749N*. This was achieved by increasing the width of the fuses from b_f=*44.0 mm* to b_f=*54.0 mm* while their thickness remained unchanged, h_f=*7mm*. The nominal yield displacement of *Frame (1)* should, in theory, remain unchanged while its width, and hence strength, is modified. Table 5-4 shows, however, that the increase of the fuse width also increased the nominal yield displacement of *Frame (1)* to Δ_{yl}=*5.60mm*. The cross section dimension of the fuses of *Frame (2)* remained equal to h_f=*5.0mm**b_f=*56.0mm*, as shown in Figure 5-16(c). The excess strength of *Frame (1)* introduced a strength eccentricity of e_{yx}=*-0.052D (-62 mm)* associated with an *11%* increase of system strength, i.e., *1.11*V_{yns}=*1358N*. The stiffness eccentricity also increased to e_{rx}=*-0.092D(-110mm)*. The translational and rotational periods of free vibration slightly reduced to T_y=*0.204sec* and T_θ=*0.15sec*, respectively. The earthquake record was applied along the *Y*-axis.

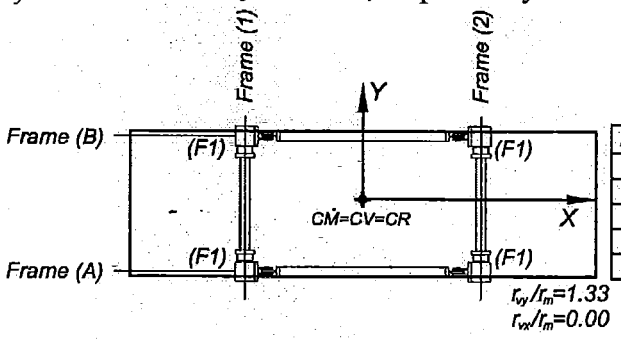

Fuse	Location	h_f	b_f
		(mm)	
(F1)	0+675	7.0	44.0
(F2)	0+675	5.0	86.0
(F3)	0+675	7.0	54.0
(F4)	0+175	7.0	44.0

Model	evx (mm)	erx (mm)
5-1	0.0	0.0
5-2A	0.0	-62.0
5-2B	-62.0	110.0
5-3A	0.0	-62.0
5-3B	-62.0	-110.0
5-4A	0.0	-62.0
5-4B	-62.0	-110.0

(a) Unrestrained Model 5-1

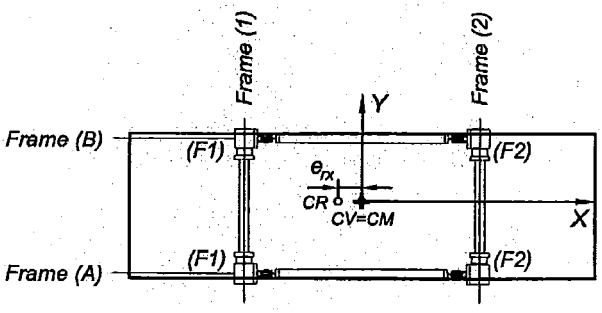

(b) Unrestrained Model 5-2A

r_{vy}/r_m=1.33
r_{vx}/r_m=0.00

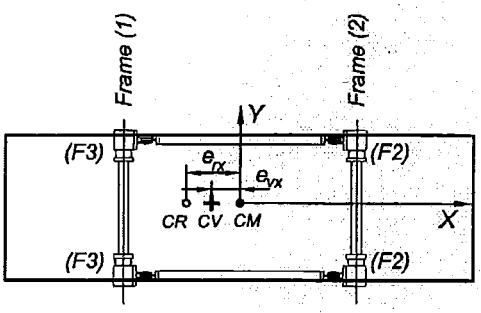

(c) Unrestrained Model 5-2B

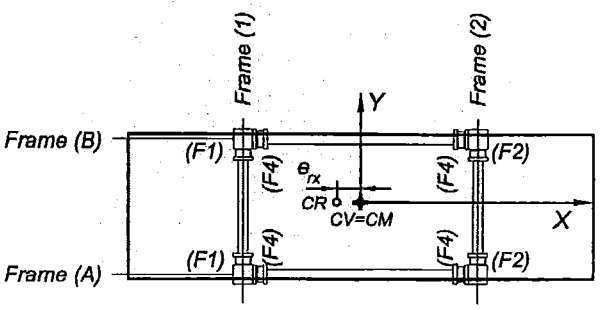

(d) Restrained Models 5-3A and 5-4A

r_{vy}/r_m=1.33
r_{vx}/r_m=0.78

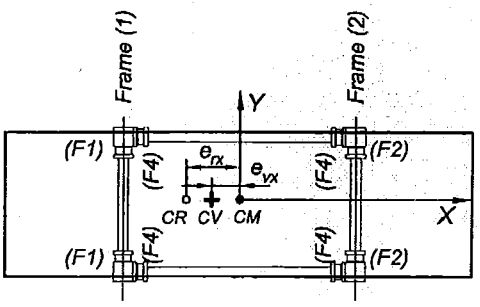

(e) Restrained Models 5-3B and 5-4B

Figure 5-16. Schematic representation of the test models

Table 5-4. Properties of *Models 5-1, 5-2A, 5-2B, 5-3A, 5-3B, 5-4A* and *5-4B*

		Model 5-1	Model 5-2A	Model 5-2B	Model 5-3A and 5-4A	Model 5-3B and 5-4B
Frame 1		Fuse 7x44	Fuse 7x44	Fuse 7x54	Fuse 7x44	Fuse 7x54
Δ'_{ye1}	(mm)	2.21	2.21	2.21	2.21	2.21
$(\Delta_{ye1})_e$	(mm)	5.35	5.35	5.60	5.35	5.60
V_{she1}	(N)	879	879	1079	879	1079
V_{ne1}	(N)	610	610	749	610	749
$(k_{e1})_e$	(N/mm)	164	164	193	164	193
Frame 2		Fuse 7x44	Fuse 5x86	Fuse 5x86	Fuse 5x86	Fuse 5x86
Δ'_{ye2}	(mm)	2.21	3.10	3.10	3.10	3.10
$(\Delta_{ye2})_e$	(mm)	5.35	6.60	6.60	6.60	6.60
V_{she2}	(N)	879	877	877	877	877
V_{ne2}	(N)	610	609	609	609	609
$(k_{e2})_e$	(N/mm)	164	133	133	133	133
Frames A and B		None	None	None	Fuse 7x44	Fuse 7x44
$(\Delta'_{yeA\&B})_e$	(mm)	--------	--------	--------	2.37	2.37
$(\Delta_{yeA\&B})_e$	(mm)	--------	--------	--------	5.74	5.74
V_{sheA}	(N)	--------	--------	--------	819	819
V_{neA}	(N)	--------	--------	--------	569	569
V_{sheB}	(N)	--------	--------	--------	819	819
V_{neB}	(N)	--------	--------	--------	569	569
$(k_{eA\&B})_e$	(N/mm)	--------	--------	--------	143	143
Properties of the Models						
Δ'_{ys}	(mm)	2.21	2.58	2.54	2.58	2.54
Δ'_{xs}	(mm)	-------	--------	--------	2.37	2.37
$(\Delta_{ys})_e$	(mm)	5.35	5.91	6.01	5.91	6.01
$(\Delta_{xs})_e$	(mm)	------	-------	-------	5.74	5.74
V_{yshs}	(N)	1758	1756	1956	1756	1956
V_{yns}	(N)	1221	1219	1358	1219	1358
V_{xshs}	(N)	------	-------	-------	1638	1638
V_{xns}	(N)	------	------	------	1138	1138
$(K_{ys})_e$	(N/mm)	329	297	325	297	325
$(K_{xs})_e$	(N/mm)	-------	-------	-------	285	285
T_y	(sec)	0.198	0.21	0.204	0.21	0.204
T_x	(sec)	--------	---------	--------	0.22	0.22
T_θ	(sec)	0.155	0.15	0.149	0.135	0.13
e_{vx}	(mm)	0.0	0.0	-62	0.0	-62
e_{vy}	(mm)	0.0	0.0	0.0	0.0	0.0
e_{rx}	(mm)	0.0	-63	-110	63	-110
e_{ry}	(mm)	0.0	0.0	0.0	0.0	0.0

5.7.4 Asymmetric and torsionally restrained *Model 5-3A*

The restrained *Model 5-3A*, as shown in Figure 5-16(d), had, along the *Y*-axis, the same properties as that of the unrestrained *Model 5-2A*. The only difference was observed along the *X*-axis where the single column, providing lateral stability, was removed and two new beams having fuses of h_f=*7.0mm* * b_f=*44.0mm* where added at level *0+175* to *Frames (A)* and *(B)*.

The nominal yield displacement of *Frames (A)* and *(B)* is slightly larger than that of *Frames (1)* and *(2)*, even though the fuses dimensions were the same. This is because the nominal yield displacement of the frames is affected by the ratio of beam length, ℓ'_b / ℓ_b, as expressed in Eq. 5-12. The nominal strength of *Frames (A)* and *(B)* was slightly smaller than that of *Frames (1)* and

(2) because it is also affected by the ℓ_b' / ℓ_b ratio. The stiffness of *Frames (A)* and *(B)* is smaller, so that the translational period of free vibration, along the *X*-axis, slightly reduced to T_x=*0.22 sec.* The addition of two new beams to *Frames (A)* and *(B)* increased the system torsional stiffness and reduced its torsional period to approximately T_s=*0.13 sec.* *Model 5-3A* also exhibited, as *Model 5-2B* did, a stiffness eccentricity of e_{rx}==*-0.052D(-63mm)* associated with zero strength eccentricity. No strength or stiffness eccentricity was, in theory, introduced along the *Y*-axis. The earthquake record was applied along the *Y*-direction.

5.7.5 Asymmetric and torsionally restrained *Model 5-3B*

The restrained *Model 5-3B* had, along the *Y*-axis, the same properties as that of the restrained *Model 5-2B* whereas, along the *X*-axis, the same properties as that of the restrained *Model 5-3A*. They are listed in Table 5-4. No strength and stiffness eccentricity was, in theory, introduced along the *X* and *Y*-directions. The earthquake record was applied along the *Y*-axis.

5.7.6 Asymmetric and torsionally restrained *Models 5-4A* and *5-4B*

The restrained *Models 5-4A* and *5-4B* had the same properties as that of the restrained *Models 5-3A* and *5-3B*, respectively, and listed in Table 5-4. The only difference was that the earthquake record was applied at a 45^o angle relative to the reference *Y*-axis. For this purpose, the model was positioned on top of the unidirectional shake table at a 45^o angle with respect to the direction of motion, as shown in Figure 5-18.

5.8 Test procedure

Relevant properties and the response of the models were obtained with the tests described below.

(a) Static tests were used to obtain the translational stiffness from the force-displacement relationship of the models when they were symmetrically loaded at level *0+675* (The level of the upper beams of the frames).

(b) Impact tests were performed to derive the translational and rotational periods of the model. Fast Fourier analyses were carried on the acceleration response signals measured with a sensitive accelerometer as the structure was hit at level *0+675* by a special purpose hammer.

(c) Translational free vibration tests were used to verify those periods of free vibration obtained with the impact test. For this purpose, a one-cycle sine wave shake input was introduced to the model. The period is the time interval between two successive peak displacements read from the displacement time history response. A rotational free vibration test was also undertaken by fastening two independent wires at each end of the structure. The wires imposed similar but opposing displacements smaller than the previously calculated displacement at first yield of the frames. The wires were then cut simultaneously. The rotational period is then obtained in the same manner as its translational period. The viscous damping, expressed as a percentage of the critical damping, was found with the following expression[C16],

$$\ln\left(\frac{u_n}{u_{n+1}}\right) = \frac{2\pi\zeta}{\sqrt{1-\zeta^2}} \qquad (5\text{-}31)$$

where u_n and $u_{(n+1)}$ are the amplitudes of two successive displacements of the free vibration test.

The translational and rotational periods measured from the free vibration test were used to derive the effective translational and rotational inertia of the mass with the following expressions,

$$M_e = \frac{T_s^2 K_{ys}}{4\pi^2} \tag{5-32}$$

$$I_{me} = \frac{T_\theta^2 K_{\theta s}}{4\pi^2} \tag{5-33}$$

where M_e is the effective translational mass and I_{me} is the effective rotational mass.

(d) The test models were subjected to *10%* of the design earthquake record. These were useful in verifying properties such as the translational and the rotational periods of free vibration and the stiffness of the elastic frames necessary to predict, through analytical simulations, the response of the test models.

(e) The test models were subsequently subjected to the design earthquake record. Accelerations at diaphragm level *0+810* and the displacements at fuse level *0+675* were measured. The response of the models was predicted using analytical simulations.

5.9 Analytical simulation of the test models

The structure was modelled analytically with the program 3D-Ruaumoko [C1] to predict and asses the nonlinear dynamic response. Components of the models were either modelled as frame or spring type members.

The frame type member was adopted for all those components expected to remain elastic such as the *SHS* columns and beams. Their behaviour was modelled with the Giberson's one-component model [C1]. The torsional stiffness of these components and their shear deformations were ignored in the analysis. The fuses were modelled as spring type members. This member can easily model a plastic hinge region along the fuse length. The model considered the effective properties of the fuses.

The diaphragm of the models was assumed to be infinitely rigid; thus the nodes at the fuse level were slaved to the master node, i.e., the centre of mass. The translational and rotational mass of the test models was derived with a preliminary test, as explained in Section 5.8. Constant damping of 2.5% was considered in the analyses.

5.10 Test set-up

5.10.1 Shake table description

The models where tested with the unidirectional shake table of the University of Canterbury [A1]. A summary of the table characteristics is presented in Table C-1 of Appendix *C*. A MTS

TestStar Controller has replaced the original control system, Dartec M1000-D1. This new controller has a close loop algorithm that corrects the reproduced record from the input data to match the desired record.

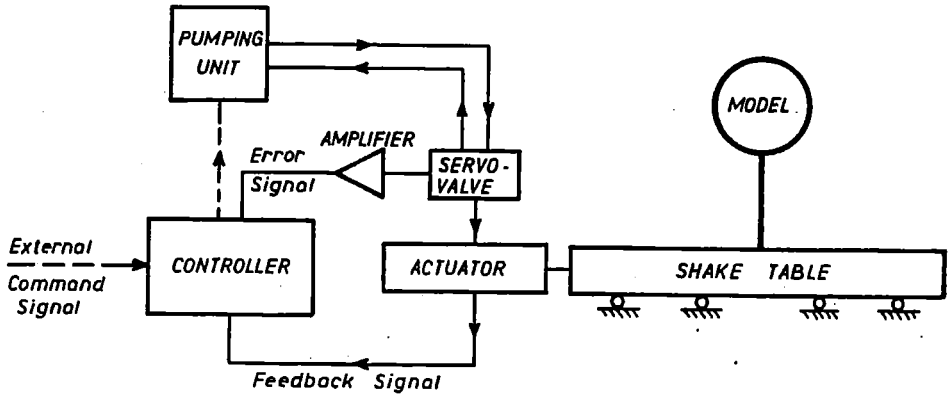

Figure 5-17. Schematic diagram of the earthquake simulator system [A1]

A schematic diagram of the earthquake simulating system is shown in Figure 5-17. It consists of the shake table, the actuator Dartec M1000/A with characteristics shown in Table C-2, the MTS TestStar controller, servo-valves, the hydraulic power unit and the external programming device. A detailed description is provided in reference [A1].

5.10.2 Instrumentation

(a) Potentiometers

The structure was instrumented with Sakae linear potentiometers of *100mm* travel. Three and four were installed on the torsionally unrestrained and restrained models, respectively. The potentiometers were mounted on a rigid frame bolted to the shake table and were placed at level *0+675* where the fuses were located. Figure 5-18 shows schematically the location of potentiometers in the tests models when the model was positioned on top of the shake table at 0^o and 45^o angles.

(b) Accelerometers

Unidirectional accelerometers, Analog Devices *ADXL 105*, having a range of $\pm 5g$ and a resolution of $\pm\ 2mg$, were mounted on top of the diaphragm at level *0+810*. Figure 5-18 also shows the position where the unidirectional accelerometers were installed.

5.11 Test Results

5.11.1 Symmetric and torsionally unrestrained *Model 5-1*

(a) Preliminary tests

Preliminary tests were performed on the unrestrained *Model 5-1* described in Section 5.7.1. The design of the fuses was illustrated in Section 5.6.4. All the fuses were h_f=*7.0mm**b_f=*44.0mm*, as shown in Figure 5-16(a).

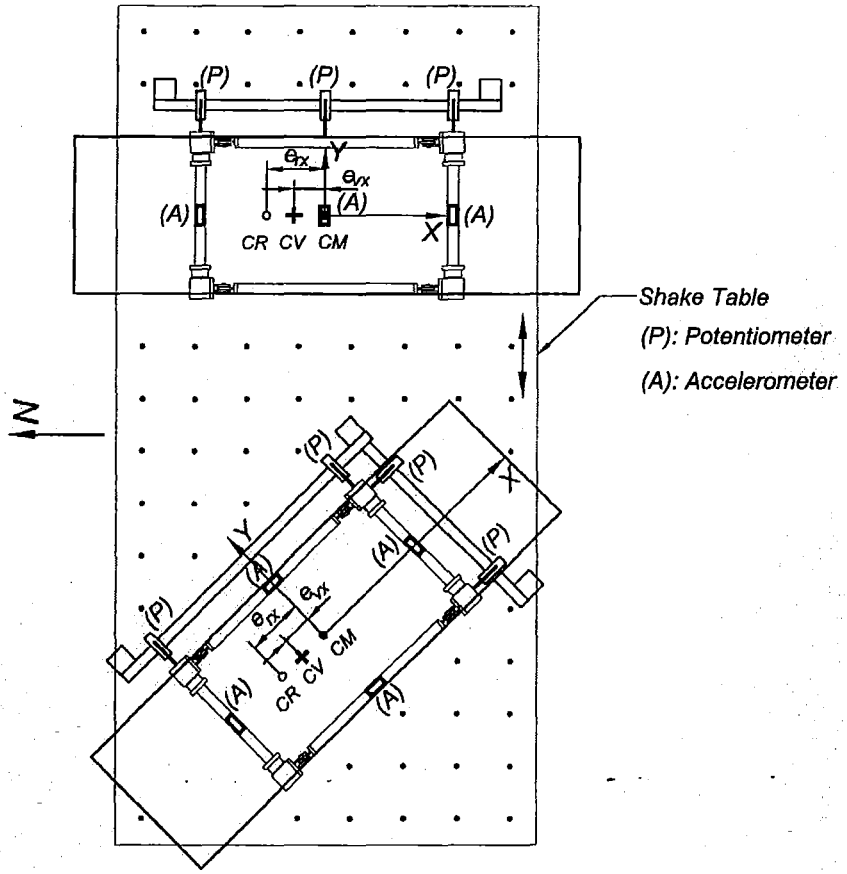

Figure 5-18. Schematic location of potentiometers and accelerometers

The static test results, shown in Figure 5-19(a), indicate a translational stiffness of K_{ys}=*323 N/mm*. According to equation 5-31, the model had an effective translational and rotational mass of M_e=*327kg* and I_{me}=*66.3kgm*^{2}. The radius of gyration of mass was, therefore, $r_m = \sqrt{I_{me}/M_e} = 450\,mm$. These values slightly differed from those analytically estimated (M_e=*345 kg*, I_{me}=*75 kgm*^{2} and hence r_m=*466 mm*).

Fast Fourier analyses from the impact test, as that shown in Figure 5-19(b), indicate that the translational and rotational periods of free vibration were T_y=*0.20 sec (5 Hz)* and T_θ=*0.15 sec (6.84 Hz)*, respectively. They agreed with those periods analytically derived.

A displacement time history response generated during free vibration tests, as that shown in Figure 5-19(c), was used to verify the translational and rotational periods of free vibration previously derived with the impact test and also to quantify the associated viscous damping of the model. The measured periods were essentially the same as those previously obtained. A viscous damping of *2.5%* was measured for the translational mode of free vibration along the *Y*-axis and *1.8%* for its corresponding rotational mode about the vertical *Z*-axis.

(b) Response of *Model 5-1* when subjected to *10%* of the design earthquake record

This aim of this section was to examine the measured acceleration and displacement time-history response of the symmetric *Model 5-1* when it was subjected to *10%* of the design earthquake record and to reproduce them using a representative analytical model.

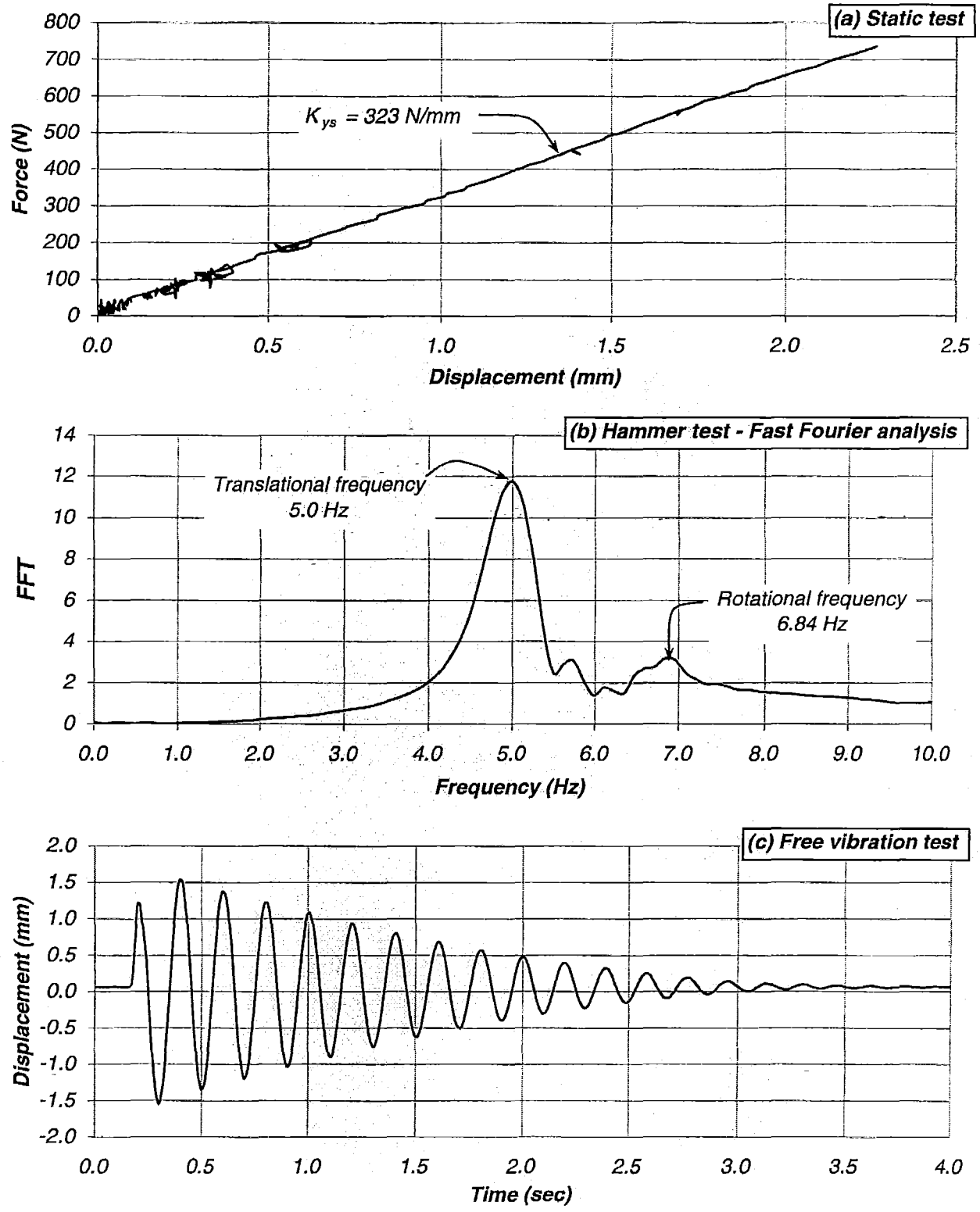

Figure 5-19. Results of the preliminary test of the elastic unrestrained *Model 5-1*

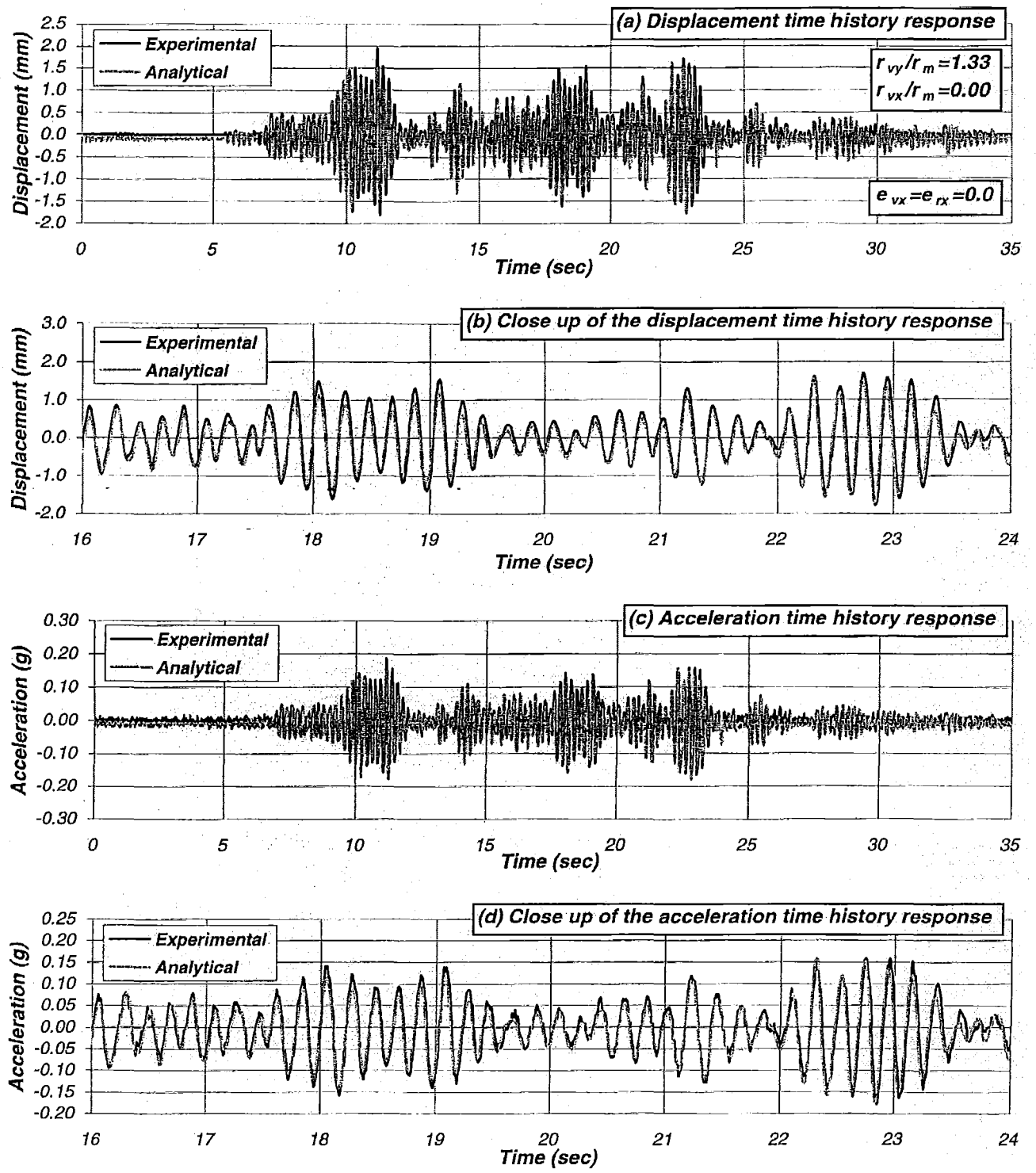

Figure 5-20. Displacement and acceleration time history response of the elastic unrestrained *Model 5-1* under *10%* of the design earthquake record

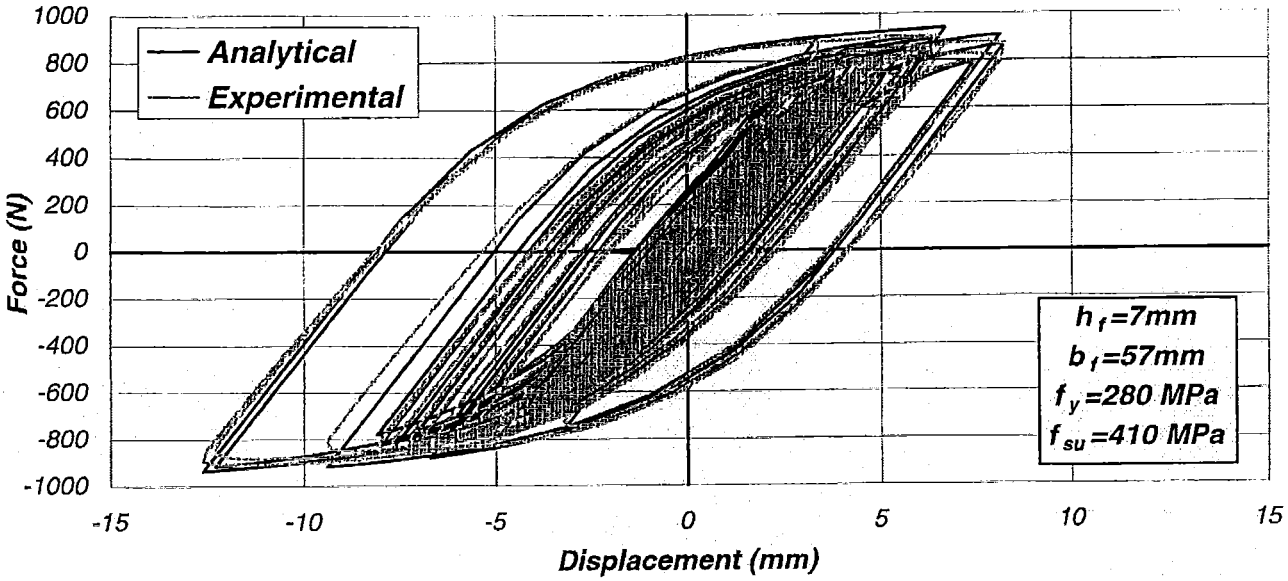

Figure 5-21. Comparison of experimental and analytical behaviour of a fuse using the Albermani hysteretic model

Figure 5-20(a) and (b) compares the displacement time history response of the test and its analytical model having the properties summarized in Table 5-4. It is evident that the response predicted by the analytical elastic model was accurate. The maximum system displacement (Δ_s=*1.96mm*) was less than that expected at the onset of yielding (Δ'_{ys}=*2.21 mm*), as shown in Table 5-4.

Figure 5-20(c) and (d) compares the acceleration time history response generated at the centre of mass. The measured maximum acceleration of the test model (*0.20g*) is slightly larger than that derived with its analytical counterpart (*0.18g*). Differences were observed due to the fact that the unrestrained system although symmetric, in theory, showed small rotations. This behaviour, not shown here, indicates that the uncertainty involved in the location of the centres of mass, strength and stiffness affected the response.

Although the system examined above is symmetric, small differences in response, not shown here, were obtained from potentiometers and accelerometers along *Frames 1* and *2*. This indicates that, in spite of all precautions taken to achieve a symmetric system, a small accidental eccentricity was introduced the system due to an uneven distribution of mass, stiffness and/or strength.

(c) Modelling the hysteretic behaviour of ductile fuses

The force-displacement relationship of the ductile fuses was modelled with the Albermani model [Z1] shown in Figure 2-7(d). This was calibrated with the force-displacement relationship of the fuse (b_f=*7mm**h_f=*57mm*) previously tested; see Figure 5-11. The computer software Hysteresis [C2] was used to reproduce its hysteretic behaviour using the effective properties of the fuse. This behaviour was compared with that measured in the test, as shown in Figure 5-21. It demonstrates that the selected simulation reproduced well the nonlinear behaviour of the fuse.

(d) Response of the unrestrained *Model 5-1* under the design earthquake record

This section aims to examine the response of the test model designed in Section 5.6.4 when subjected to 100% of the design earthquake record. Its response is to be predicted with its analytical counterpart by modelling the ductile behaviour of the fuses with the simulation described before. The model is not expected to exceed the displacement capacity of Δ_{us}=*21.0mm* established in Section 5.6.4. Deformations in the inelastic domain were assumed concentrated at the fuses. A viscous damping of *2.5 %* was used for both translational and rotational modes of free vibration.

Table 5-5 compares the analytical and the measured properties of the elements of the symmetric *Model 5-1* and its maximum response. It is evident a close correlation between them and that the maximum displacement demand of the tested and analytical models did not exceed the system displacement capacity of Δ_{us}=*21mm.*

Table 5-5. Response of the unrestrained *Model 5-1* under unidirectional earthquake record

		Model 5-1	
		Experimental	*Analytical*
T_v	*(sec)*	*0.20*	*0.198*
T_θ	*(sec)*	*0.15*	*0.155*
ζ_v	*(%)*	*2.50*	*2.50*
ζ_θ	*(%)*	*1.80*	*2.50*
Δ_{us} ($\mu_{\Delta s}$)	*(mm)*	*20.5 (3.92)*	*20.6 (3.92)*

Figure 5-22(a) and (b) shows a similar displacement time-history response between the test model and its analytical simulation. The structure oscillated about its at rest position for the first *22.0* seconds of the earthquake record input. Thereafter, it reached a system maximum displacement of *20.6 mm* and then continued to oscillate about a negative displacement of *13mm.* It is believed that the response of systems where a permanent deformation is introduced may not be predicted with adequate accuracy using a substitute elastic system as suggested elsewhere [K5].

Figure 5-22(c) and (d) shows small differences in the acceleration time history response of the test model and its analytical counterpart. The maximum acceleration reached by the test model was *0.55g* whereas its analytical counterpart predicted a maximum of *0.59g*. In spite of this difference, a close correlation was observed.

Figure 5-23 compares the analytical and the measured force-displacement relationship of the unrestrained *Model 5-1*. Although a good correlation was observed, it is evident that the simulation of the fuse's ductile behaviour with the Albermani model did not account for the loss of stiffness expected from steel under cyclic flexural deformations. This is part of the reason why the analytical model did not reproduce an "exact" response.

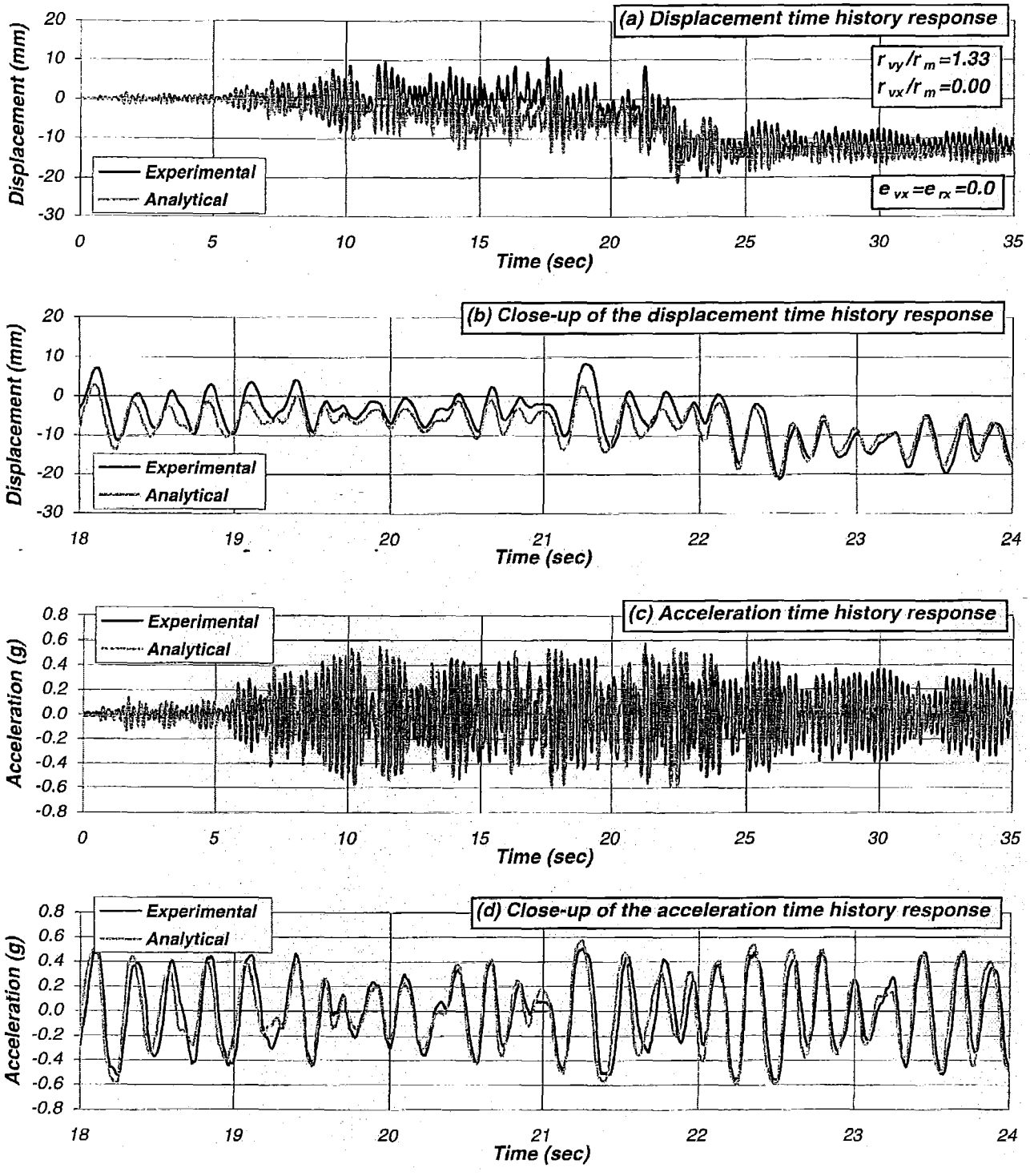

Figure 5-22. Displacement and acceleration time history response of the unrestrained *Model 5-1* under the design earthquake record

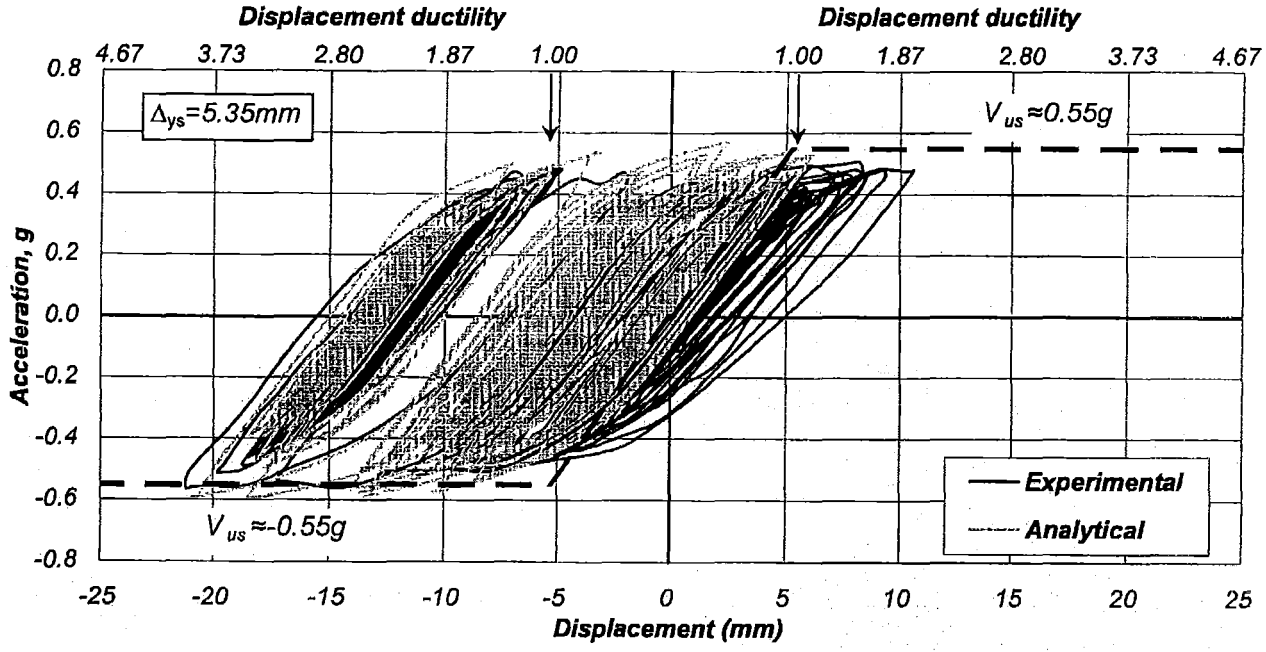

Figure 5-23. Force-displacement relationship of the unrestrained *Model 5-1*

5.11.2 Asymmetric and torsionally unrestrained *Models 5-2A* and *5-2B*

The unrestrained *Models 5-2A* and *5-2B*, as described in Sections 5.7.2 and 5.7.3, were used to examine the suggested design strategy described in Section 2.12. Their analytically derived properties are listed in Table 5-4 whereas Table 5-6 summarizes selected properties and the maximum response of the models. It is subjected to the earthquake record along the *Y*-axis.

Table 5-6 compares the properties and the maximum response of the test models with those analytically derived. It is evident that the translational and rotational periods of free vibration of the unrestrained *Models 5-2A* and *5-2B* were predicted well. The viscous damping was essentially the same for all modes of vibration and quite small as it is expected for steel structures. This is an indication that the different connections did not introduce significant friction.

Table 5-6. Response of the unrestrained *Models 5-2A* and *5-2B* under the unidirectional earthquake input

		Unrestrained Model 5-2A		Unrestrained Model 5-2B	
		Experimental	Analytical	Experimental	Analytical
T_y	(sec)	0.215	0.210	0.205	0.204
T_θ	(sec)	0.149	0.150	0.143	0.149
ζ_y	(%)	2.69	2.50	2.30	2.50
ζ_θ	(%)	2.05	2.50	1.54	2.50
Δ_{ue1} ($\mu_{\Delta 1}$)	(mm)	16.93 (3.16)	17.07 (3.19)	20.73 (3.70)	8.12 (1.45)
Δ_{us} ($\mu_{\Delta s}$)	(mm)	19.40 (3.28)	21.78 (3.69)	23.42 (3.90)	17.32 (2.88)
Δ_{ue2} ($\mu_{\Delta 2}$)	(mm)	21.43 (3.25)	25.55 (3.87)	26.32 (3.99)	27.56 (4.17)
θ_s	(rad)	0.0040	0.0081	0.0061	0.018

The measured maximum displacement demand at the centre of mass of the unrestrained *Model 5-2A* (Δ_{us}=*19.41mm*) was essentially the same as that of the symmetric *Model 5-1*(Δ_{us}=*20.5mm*).

As expected, system rotations increased the maximum displacements of *Frame (2)* to $\Delta_{u2}=21.43$ *mm* and reduced that of *Frame (1)* to $\Delta_{u1}=16.93$ *mm* relative to that attained at the centre of mass. This response occurred because the model had a $r_{vy}/r_m > 1.0$, i.e., $r_{vy}/r_m=1.33$. Recall that the relative displacements between *Frames (1)* and *(2)* reduce as the r_{vy}/r_m ratio is reduced. This is achieved by increasing the radius of gyration of mass, i.e., spreading the mass away from the centre of mass. The r_{vy}/r_m ratio is, therefore, a measure of the effect of system rotations on the maximum displacement of the elements.

The maximum displacement demands predicted by the simulated unrestrained *Model 5-2A*, see Table 5-6, indicates a larger displacement demand at the centre of mass ($\Delta_{us}=21.78mm$) relative to that measured ($\Delta_{us}=19.41mm$). Systems rotations were also larger because they are expected to increase as displacement demand at the centre of mass increases. This behaviour was also reflected in the reference rotations associated with *Frames (1)* and *(2)*. This difference in response was attributed to the Albermani simulation which did not account for the small loss of stiffness expected in steel during flexural cyclic deformations. The other cause of such variation is the uncertainty in the location of the centres of mass and strength. The experiment also indicated that the damping in torsion was less than the translational damping whereas in the computational model the same level of damping was used for both actions.

The unrestrained *Model 5-2B* differs from the unrestrained *Model 5-2B*, previously explained, in that *Frame (1)* had a *20%* increase of strength which introduced a strength eccentricity and increased the system strength by *10%*, as already explained in Section 5.7.3.

The measured response of the unrestrained *Model 5-2B*, relative to that of the unrestrained *Model 5-2A*, shows a slight increase in the maximum displacement at the centre of mass ($\Delta_{us}=23.42mm$). An increase in the displacement demands of *Frames (1)* and *(2)* was also observed. This behaviour was expected because short period systems have a sensitive response as it is readily observed in the displacement response spectra; see Figure 5-15. In some cases, an increase in system strength may not necessarily reduce system displacements. As expected, the system maximum rotation also increased due to the introduction of a strength eccentricity. This is also reflected in the increase of the displacement demands of *Frames (1)* and *(2)* relative to the maximum attained at the centre of mass.

The analytical simulation of the unrestrained *Model 5-2B*, relative to that measured, predicted a smaller displacement demand at the centre of mass and a larger system rotation. These variations happened because many uncertainties are involved affecting the response of three dimensional systems, as those previously explained.

Figure 5-24 and Figure 5-25 plots the measured and the analytically derived displacement time-history response of the unrestrained *Models 5-2A* and *5-2B*. A better prediction was observed with the unrestrained *Model 5-2A*. In contrast, the response prediction of the restrained *Model 5-2B* was quite different due to differences in system rotations. A larger permanent system rotation is evident in both experimental test models, see Figures 5-24(d) and 5-25(d). The difference in responses is because the level of damping measured in the experimental test models are smaller than those used for their analytical counterpart, as shown in Table 5-6.

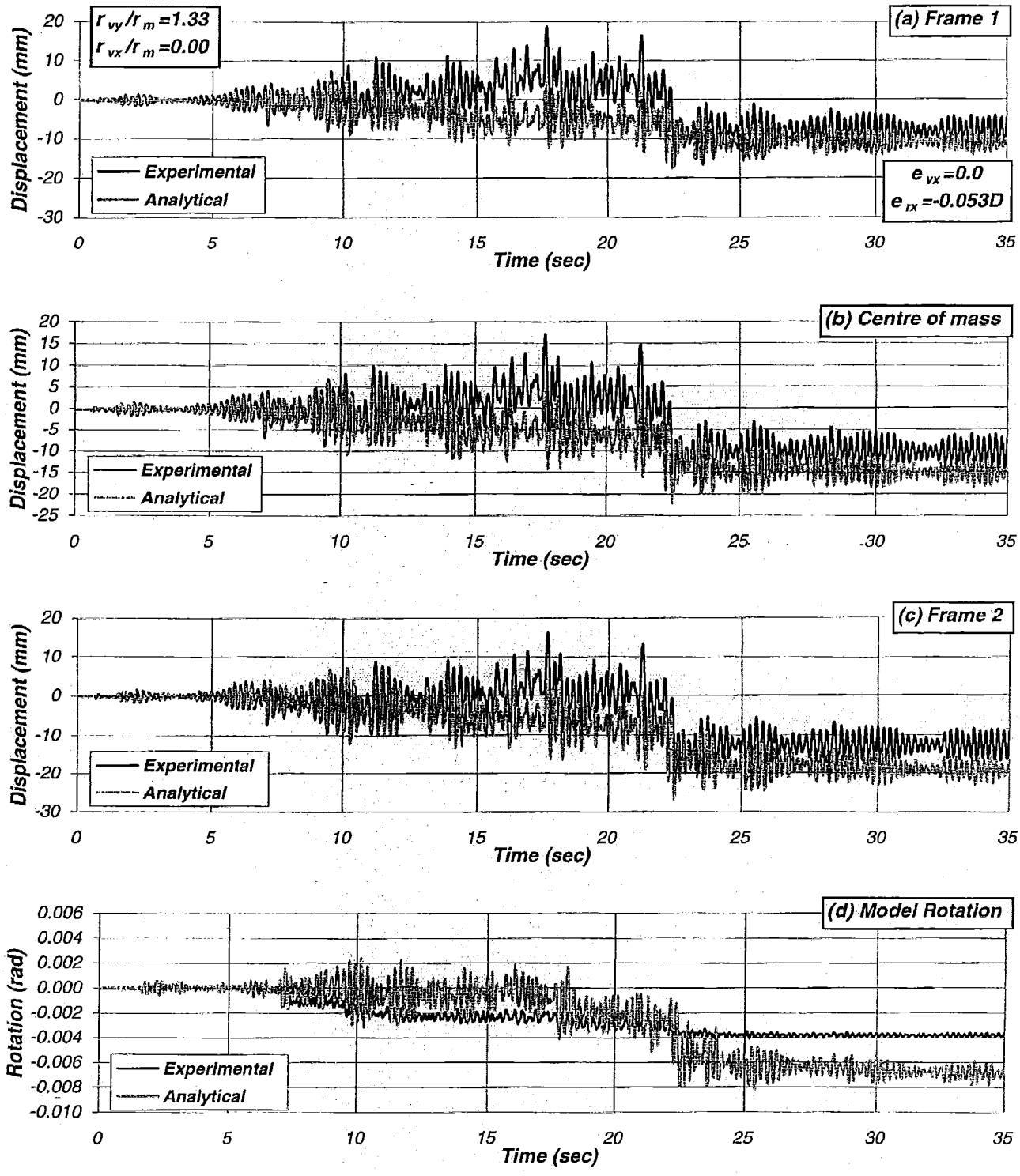

Figure 5-24. Displacement and acceleration time history response of the unrestrained *Model 5-2A* under the design earthquake record

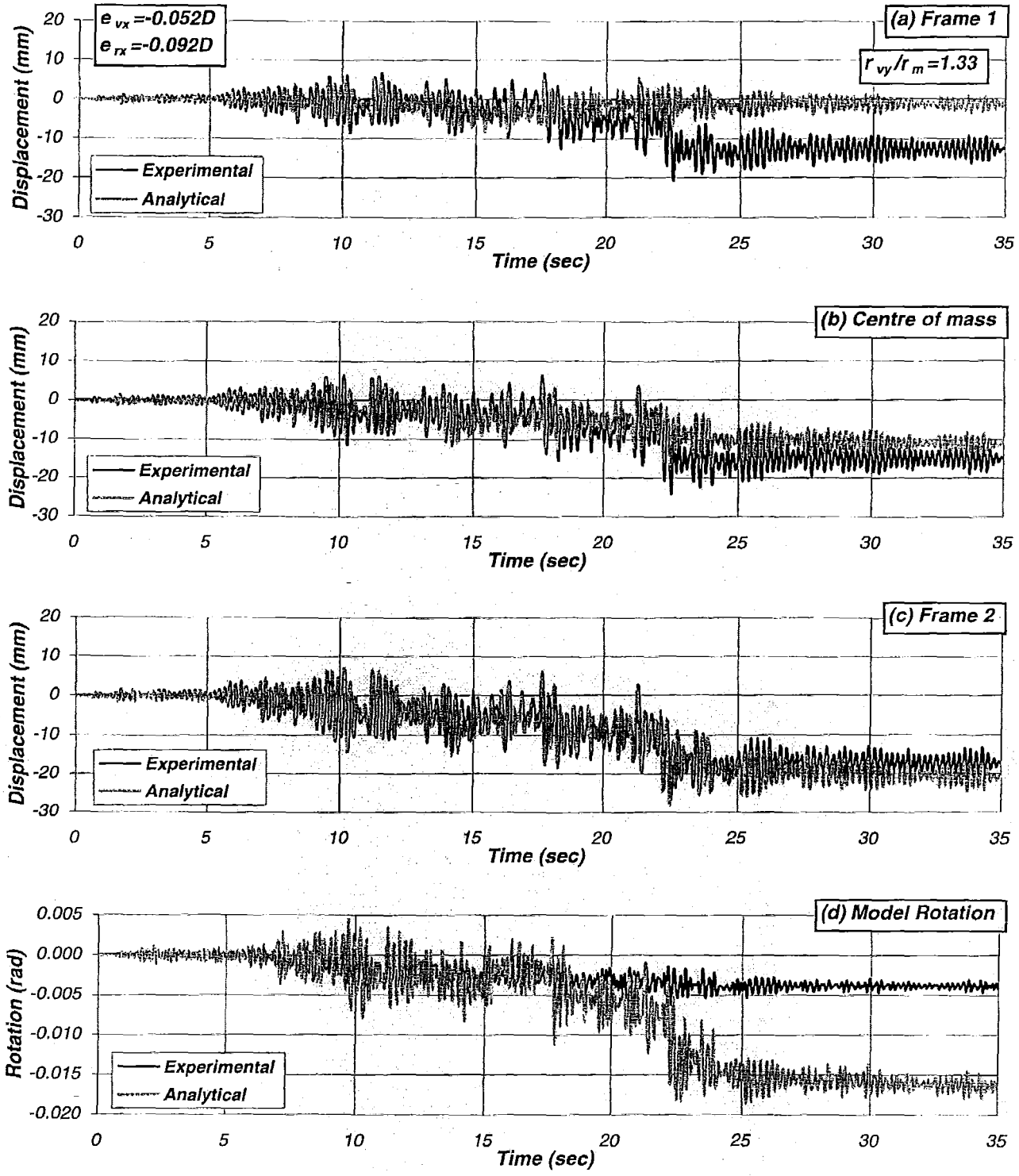

Figure 5-25. Displacement and acceleration time history response of the unrestrained *Model 5-2B* under the design earthquake record

The findings above suggest that uncertainties in the location of centres of mass and strength lead to differences in responses between the test models and their analytical counterpart. The response was also affected by the fact that the Albermani model did not include in the simulation of the fuses the loss of stiffness expected in steel during cyclic flexural deformations. The response of the test models also demonstrates that short period systems have a sensitive response. In some cases, an increase in system strength did not necessarily reduce system displacement demands.

5.11.3 Asymmetric and torsionally restrained *Models 5-3A* and *5-3B*

This section aims to assess the response of the restrained *Models 5-3A* and *5-3B*, described in Sections 5.7.4 and 5.7.5, when designed with the suggested design strategy described in Section 2.12. Their analytical properties are listed in Table 5-4 and a comparison of selected properties and system maximum response is presented in Table 5-7. It is subjected to the earthquake record along the *Y*-axis.

Table 5-7 shows that the measured periods along the *X*-axis and about the *Z*-axis of the restrained *Models 5-3A* and *5-3B* were essentially the same to those derived with their analytical counterpart using those properties listed in Table 5-4. The translational mode of free vibration along the *X*-axis showed, however, a substantial increase in damping to *8%*. This happened because the new beams added to *Frames (A)* and *(B)* at level *0+175*; see Figure 5-4(b), comprised two unidirectional connections that although well constructed, introduced significant friction. The increase in damping lengthened the uncoupled translational period of the test model relative to that derived analytically (T_s=*0.22*) to T_s=*0.23* seconds.

The measured maximum demands of the restrained *Model 5-3A* and *5-3B* are presented in Table 5-7. The response of the restrained *Model 5-3B* relative to that of the restrained *Model 5-3A* indicates that the introduction of a strength eccentricity increased system rotations. This strength eccentricity is also accompanied with an increase of system strength that reduced the displacement demands at the centre of mass.

Table 5-7. Response of the restrained *Models 5-3A* and *5-3B* under unidirectional earthquake input

		Restrained Model 5-3A		Restrained Model 5-3B	
		Experimental	Analytical	Experimental	Analytical
T_y	(sec)	0.200	0.210	0.200	0.204
T_x	(sec)	0.230	0.220	0.220	0.220
T_θ	(sec)	0.130	0.135	0.124	0.130
ζ_y	(%)	1.62	2.50	1.46	2.50
ζ_x	(%)	8.00	2.50	7.50	2.50
ζ_θ	(%)	NA	2.50	NA	2.50
Δ_{ue1} ($\mu_{\Delta 1}$)	(mm)	23.37 (4.36)	22.69 (4.24)	25.55 (4.56)	16.37 (2.92)
Δ_{us} ($\mu_{\Delta s}$)	(mm)	26.15 (4.42)	23.24 (3.93)	25.91 (4.31)	19.03 (3.17)
Δ_{ue2} ($\mu_{\Delta 2}$)	(mm)	27.39 (4.15)	23.80 (3.60)	31.60 (4.79)	20.98 (3.18)
θ_s	(rad)	0.0036	0.0014	0.0067	0.0043

A comparison of the measured response for the restrained *Models 5-3A* and *5-3B* relative to that measured for their unrestrained counterpart *Models 5-2A* and *5-2B*, see Table 5-6 and Table 5-7, indicates a slight increase of displacement demands at the centre of mass. System rotations were, as expected, smaller in the restrained models. *Frame (1)*, having the smallest nominal yield displacement, becomes critical as the system rotation reduces.

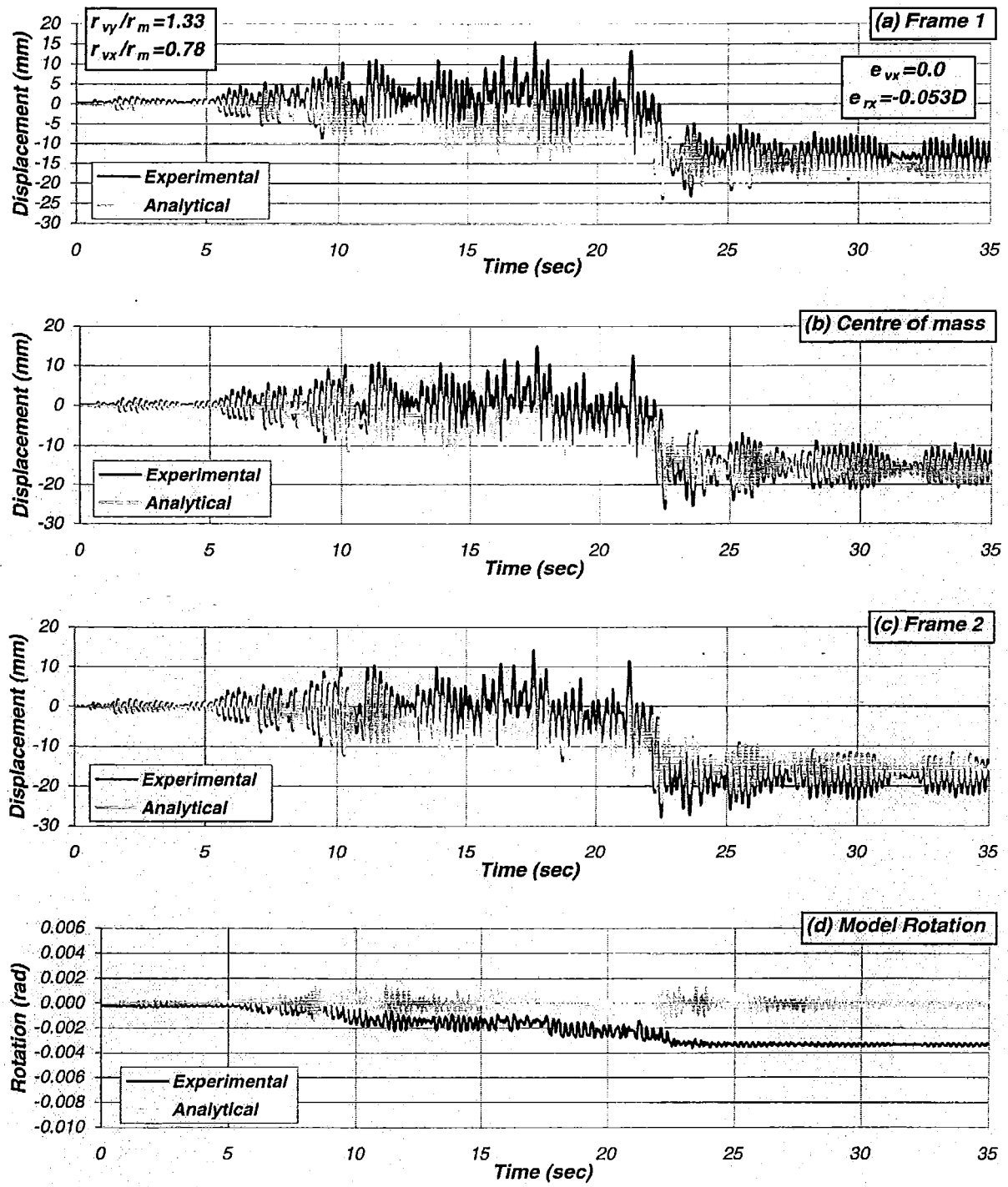

Figure 5-26. Displacement and acceleration time history response of the restrained *Model 5-3A* under the design earthquake record

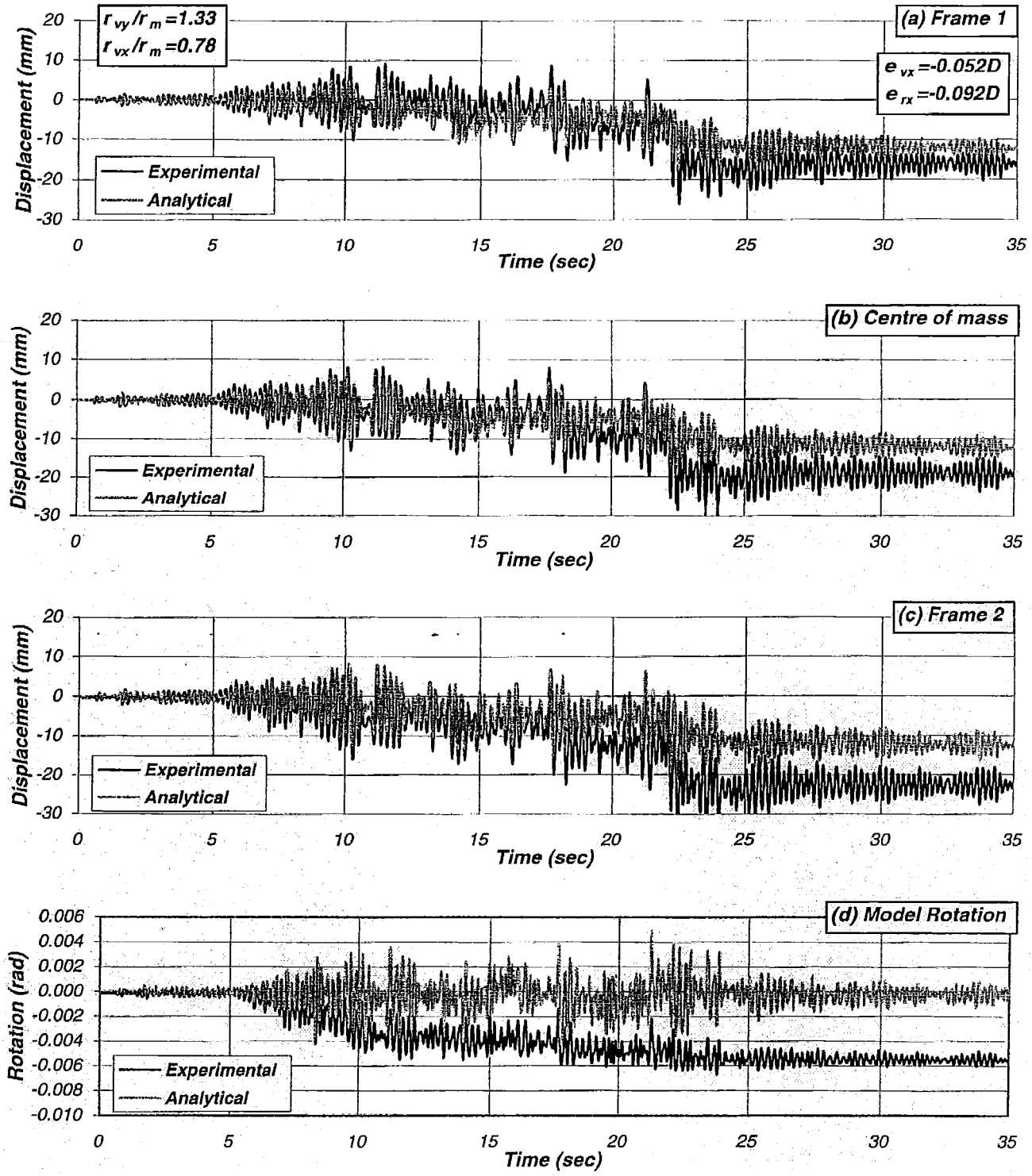

Figure 5-27. Displacement and acceleration time history response of the restrained *Model 5-3B* under the design earthquake record

The maximum response of the analytical *Models 5-3A* and *5-3B*, see Table 5-7, showed the same torsional behaviour as that of the test models. The predicted system rotations and reference rotations were, however, smaller with the simulated models.

Figure 5-26 and Figure 5-27 plots the analytical and measured time history response of the restrained *Models 5-3A* and *5-3B*. It is evident that the analytical response predicted a more

accurate response of the restrained *Model 5-3A* whereas that of the restrained *Model 5-3B* was not as good due to differences in system rotations. System rotations were, in fact, much larger in the test models.

The findings above indicates that the unidirectional connections built into those new beams added at level *0+175* of *Frames (A)* and *(B)* increased significantly the system's damping and hence its uncoupled translational period. The findings also confirm those findings described in the preceding chapters that asymmetric systems with short translational periods are quite sensitive. In spite of this characteristic, it is concluded that the suggested design strategy was successful in controlling displacement demands on the elements due to increasing strength eccentricities. This is evident with the analytical models but not as evident with the test models. As expected, system rotations were smaller in the restrained models.

5.11.4 Asymmetric and torsionally restrained *Models 5-4A* and *5-4B*

The restrained *Models 5-4A* and *5-4B* are identical to those restrained *Models 5-3A* and *5-3B* previously examined. The systems were subjected, however, to the earthquake record at a 45^o angle with respect to the reference *Y*-axis. The aim was to identify which provides a critical response: the model when subjected to the earthquake record at a 45^o angle or when subjected to the earthquake record along the *Y*-direction only, as it was the case for identical *Models 5-3A* and *5-3B*.

Table 5-8. Response of the restrained *Models 5-4A* and *5-4B* when subjected to the earthquake record at a 45^o angle

		Restrained Model 5-4A		Restrained Model 5-4B	
		Experimental	Analytical	Experimental	Analytical
T_y	(sec)	0.200	0.210	0.200	0.204
T_x	(sec)	0.230	0.220	0.220	0.220
T_θ	(sec)	0.130	0.135	0.124	0.130
ζ_y	(%)	1.62	2.50	1.46	2.50
ζ_x	(%)	8.00	2.50	7.50	2.50
ζ_θ	(%)	NA	2.50	NA	2.50
Δ_{ue1} ($\mu_{\Delta 1}$)	(mm)	13.7 (2.56)	13.52 (2.52)	14.2 (2.54)	9.03 (1.61)
Δ_{yus} ($\mu_{\Delta sy}$)	(mm)	15.8 (2.67)	14.78 (2.50)	15.8 (2.63)	11.80 (1.96)
Δ_{ue2} ($\mu_{\Delta 2}$)	(mm)	17.5 (2.65)	16.45 (2.49)	16.8 (2.55)	15.10 (2.29)
Δ_{ueA} ($\mu_{\Delta A}$)	(mm)	21.0 (3.65)	NA	15.3 (2.67)	17.33 (3.02)
Δ_{xus} ($\mu_{\Delta sx}$)	(mm)	20.4 (3.55)	16.31 (3.66)	14.7 (2.56)	15.67 (2.73)
Δ_{ueB} ($\mu_{\Delta B}$)	(mm)	19.8 (3.45)	NA	14.1 (2.46)	17.87 (3.11)
θ_s	(rad)	0.0031	0.0023	0.0026	0.0052

Table 5-8 summarizes the maximum response measured during the test. A comparison of their responses with that of the restrained *Models 5-3A* and *5-3B* (see Table 5-7) confirmed that the application of the earthquake record at a 45^o angle imposed smaller displacements on the frames. This reduction, as explained in Chapter 4, occurred because the system is stronger at any angle other than 0^o and 90^o angle. Some differences in response between the test and the analytical models were evident, as Figure 5-28 and Figure 5-29 show, due to variations in the system rotation.

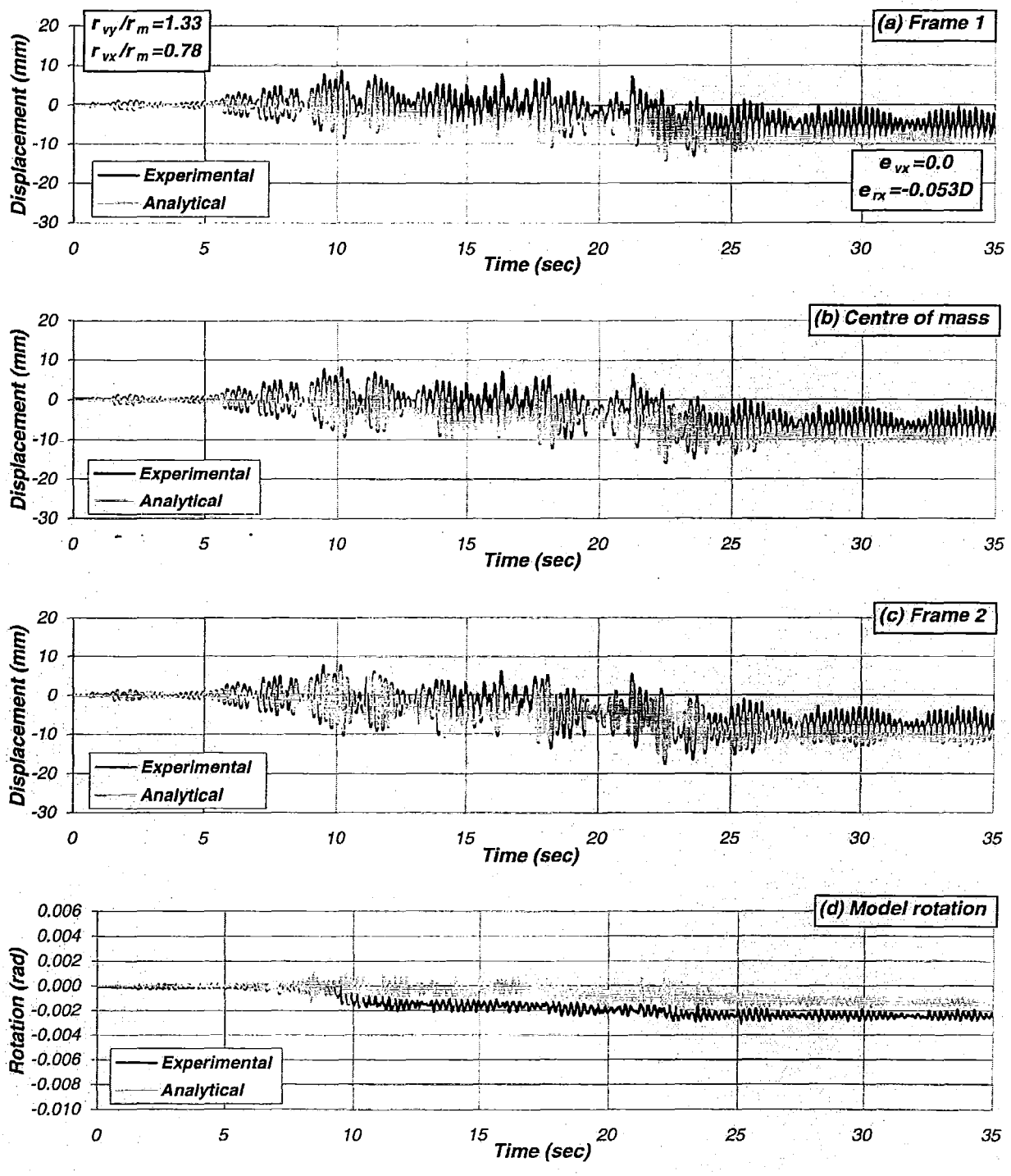

Figure 5-28. Displacement and acceleration time history response of restrained *Model 5-4A* under the design earthquake record at a 45° angle

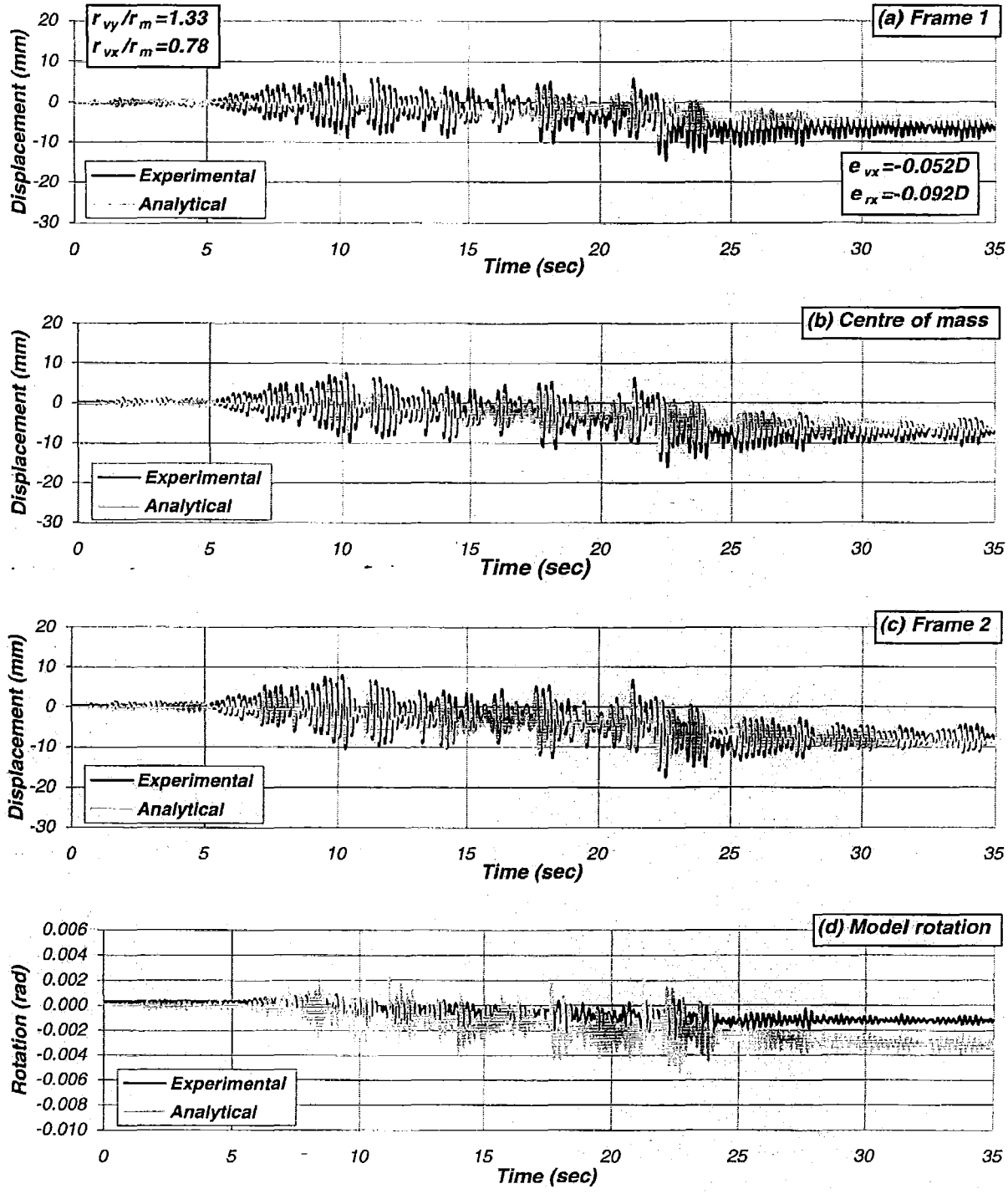

Figure 5-29. Displacement and acceleration time history response of restrained *Model 5-4B* under the design at a 45° angle

The maximum rotation of the restrained *Model 5-4B* was smaller than that of the restrained *Model 5-4A* when, in fact, it was expected to be larger (see Table 5-8). This finding contradicts the results observed with those analytical systems previously examined (Section 4.2.4) indicating that system subjected to earthquake records at oblique angles should experience larger rotations to those expected to develop when it was subjected to the record along the principal direction. This unexpected behaviour happened because the unidirectional connections of the new beams added to *Frames (A)* and *(B)* of the restrained *Model 5-4B* were by mistake excessively tightened, hence the torsional resistance of the model was substantially increased by the in-plane resistance of the fuses. The test model, therefore, was torsionally stronger and hence the system rotations were smaller than those developed by the restrained *Model 5-4A*.

Figure 5-28 and Figure 5-29 plots the measured and the analytical responses of the restrained models. It is evident that the measured displacement time history response was predicted well by its analytical counterpart. Small differences in system rotations were, however, observed.

The findings above demonstrates that the critical scenario with regard to frame displacements of restrained systems subjected to earthquake records at different directions occurs when the earthquake record is applied along the principal axis rather than at an oblique angle.

5.12 Summary on the experimental programme

This chapter focussed on an experimental programme investigating the torsional response of single-mass test models. It discussed the test results, compared the response measured in the test models with those predicted by their analytical counterparts and assessed the findings previously obtained with those analytical models examined in Chapters 3 and 4. The findings were:

1. The computed flexural deformations of the fuses are not sufficient to predict the actual values of nominal yield curvature, rotations and hence the nominal yield displacement of the frames and the model itself. Additional hinge rotation-induced deformations were significant and were accounted for with the I_e / I_g ratio. It was of no surprise that the effective second moment of area was influenced by changes in both the width and the thickness of the fuse. This was found to be, on average, *45%* of its gross value.

2. It is demonstrated that the nominal yield displacement of the frames and that of the system is readily obtained before the required system strength is derived. The displacement ductility capacity of the system is therefore estimated once the displacement capacity of the system is defined based on specified limit state.

3. Differences in response between the test models and their analytical counterpart are attributed to the uncertainty involved in the locations of the centres of mass and strength, the fact that the loss of stiffness expected in steel components during flexural cyclic deformations was not modelled by the selected hysteresis rule and differences in the damping associated with the rotational component. A better estimate of the response might be obtained with the Dodd-Restrepo hysteresis rule because this simulation allows for the stiffness degradation observed in steel elements subjected to cyclic forces.

4. The test results confirm many of the findings obtained with those analytical systems previously examined. The increase of system strength as a result of the introduction of a strength eccentricity may or may not reduce displacement demands at the centre of mass, a characteristic depending on the earthquake record and easily predicted by examining the

corresponding displacement response spectra. System rotations increased as a strength eccentricity was introduced to the model. This, however, was smaller in the restrained models. The critical scenario with regard to frame displacements occurs when the system is subjected to earthquake excitations along the principal directions rather than at oblique angles to the principal directions. System rotations influenced the maximum displacement demands of the elements of unrestrained systems for $r_{vy}/rm \geq 1.0$. This parameter is, however, not relevant in torsionally restrained systems.

Chapter 6. Seismic Design Procedure for Asymmetric Systems

6.1 Introduction

This chapter outlines a step-by-step procedure for the seismic design of asymmetric systems using the design strategy suggested in Section 2.11. It is consistent with current force-based design methods [S7] and recent research proposals [P13,P16] oriented towards displacement control of buildings. It differentiates between torsionally unrestrained and restrained systems. A design example is provided in Appendix D to illustrate its applicability in seismic design.

The studies on single-mass systems presented in Chapters 3, 4 and 5 were used to verify the proposed design strategy. These systems comprised substitute wall-elements representing any type of lateral force resisting element exhibiting a bi-linear force-displacement relationship. Substitute elements were used to simplify the derivation of fundamental properties, i.e., nominal yield displacement, strength and associated stiffness. The study is, therefore, not addressing wall systems only.

The proposed design strategy to be presented and already verified by those single mass systems examined in previous chapters is considered appropriate for the seismic design of asymmetric building structures satisfying the limitations imposed by the equivalent static design method as recommended in most building codes [I1]. The effect of the higher modes of free vibration on displacement demands of ductile elements and on strength demands over their height, to be addressed in seismic design, are beyond the scope of this study. It is assumed that the appropriate application of capacity design principles [P1] ensures that all parts of the building, intended to remain elastic, will be protected against inelastic behaviour. The structural designer has the freedom to choose and enforce a preferred ductile sidesway mechanism for elements under severe imposed deformations where energy dissipation is to be concentrated at predefined potential plastic hinge locations.

6.2 Seismic design of unrestrained and restrained systems

A seismic design procedure for torsionally restrained and unrestrained systems to be described in Step A to E applies to both unrestrained and restrained systems. Step F only applies to torsionally unrestrained systems. The procedure is also illustrated in Figure 6-1. A design example is presented in Appendix D.

Step A. Determine the centre of mass and the seismic weight of the system. The centre of mass is readily estimated without much uncertainty. The strength of systems is a fraction of the total seismic weight. This results to be a conservative estimate of system strength [L3].

Step B. Estimate the displacement and ductility capacity of the system. This is obtained as explained below independently for both unrestrained and restrained systems.

(i) *Select a preferred ductile sidesway mechanism for each element under severe deformations in agreement with the principles of capacity design.*

(ii) Assess the nominal yield displacement of the elements. The nominal yield displacements refer to the level of the equivalent concentrated mass, i.e., $h_e=(2/3)h$. It may be estimated

without the need of sophisticated analyses as described elsewhere [P19,P20,P21]. The prescribed magnitudes of the floor forces over the height of the structure, such as in the form of an inverted triangle, may be chosen arbitrarily to estimate the nominal yield displacement of the elements. For convenience, a total base shear force of unity may be used initially. This procedure is better explained in the example of Appendix D.

(iii) *Estimate the nominal yield displacement of the system.* This reference property is estimated using a plan distribution of relative strength of the elements satisfying static equilibrium and their relative stiffness; see Eq. 2-34. The relative element strength is estimated by distributing, for example, a total unit base shear force between parallel elements to achieve zero strength eccentricity. This process will be shown in the example described in Appendix D. Subsequently, the relative stiffness of the elements is estimated with Eq. 2-29 and the centre of stiffness with Eq.2-6.

(iv) *Establish the displacement and ductility capacity of the elements and the translatory system.* The displacement and ductility capacity of lateral force-resisting components can be estimated by considering (a) the verified displacement ductility capacity of components, as detailed and constructed associated with strain limits of the materials or (b) storey drifts satisfying stipulated performance criteria whichever results critical. This will lead to the displacement capacity of the element.

The displacement capacity of the system is restricted by that of the element with the smallest displacement capacity, $\Delta_{us} = \Delta_{uei,\min} = (\mu_{\Delta e}\Delta_{yei})_{\min}$, denoted with subscript '$_{\min}$'. No consideration is given to effects of system rotations on displacement demands on elements. The displacement ductility capacity of the system is readily obtained with the nominal yield displacement derived in (iii), i.e., $\mu_{\Delta s} = \Delta_{us} / \Delta_{ys} = (\mu_{\Delta ei}\Delta_{yei})_{\min} / \Delta_{ys}$.

Step C. Derive the required nominal strength of the system. The system nominal strength may be obtained with either force-based design methods, embodied in building codes[S7,I1] or displacement-based design methods[P16]. Force-based design spectra make the required seismic strength, V_{ns}, a function of the stiffness-dependant fundamental translational period of the elastic system, T_s, and its displacement ductility capacity, $\mu_{\Delta s}$. Because stiffness is proportional to strength (Section 2.8), a rapidly converging trial and error procedure is used to satisfy the requirements of the design acceleration spectra. Convergence can be improved in the first trial if the expected base shear intensity, V_{ns}, or the uncoupled translational period, T_s, is estimated using the designer's experience. Note that the system displacement ductility capacity is not influenced by the seismic strength of the system.

Step D. Distribute the system strength to the elements to satisfy zero strength eccentricity. Once the total required nominal seismic strength of the system is established, it should be distributed to the elements in proportion to the chosen distribution of a unit base shear described in Step B(ii). The next step is the detailed design of components and elements. When all details, such as quantity and placement of reinforcement, have been defined, it is necessary to evaluate the nominal seismic strengths of all components as to be constructed. This will confirm the acceptability of the previously estimated uncoupled translational period of free vibration of the system and that the distribution of system strength initially specified on the elements is not violated.

Step E. Strength eccentricity. A strength eccentricity may be introduced to the system provided it results from the nominal strength of any element being in excess of that satisfying zero strength eccentricity. The strength eccentricity is, therefore, associated with an increase of system strength.

Step F. Verification of the displacement capacity for torsionally unrestrained systems. In case of torsionally unrestrained systems, it is necessary to verify that the system displacement capacity estimated in Step B will prevent elements from exceeding their displacement capacity. This is because the maximum displacement demand imposed on elements of unrestrained systems may be significantly influenced by system rotations. These are affected by variations of the stiffness eccentricity associated with zero strength eccentricity and the uncoupled translational period of free vibration. It is likely that the system displacement ductility capacity may need to be reduced or could be increased resulting in a more economical design. The following additional steps are, therefore, required:

F1. Identify those elements of unrestrained systems that may govern the estimate of the displacement ductility capacity of the system. One of the elements is that having the smallest displacement ductility capacity, denoted element *(1)**, and the other is the outer-most element placed on the flexible side of the system denoted element *(2)**. See Section 3.12.

F2. Determine which of the two critical elements identified in Step F1 will restrict the displacement and ductility capacity of the system. This element is identified by comparing the ratio of predicted maximum displacement demands of elements *(1)** and *(2)**, i.e., $(\Delta_{ue2}/\Delta_{ue1})_d$, and the ratio of displacement capacities of those same elements, $(\Delta_{ue2}/\Delta_{ue1})_c$.

The $(\Delta_{ue2}/\Delta_{ue1})_d$ ratio is obtained from Figure 3-44 for the stiffness eccentricity and the uncoupled translational period estimated in Step B(iii). The $(\Delta_{ue2}/\Delta_{ue1})_d$ ratios should be estimated values expected to be included in building code provisions.

If $(\Delta_{ue2}/\Delta_{ue1})_d < (\Delta_{ue2}/\Delta_{ue1})_c$, then the displacement capacity of the system is restricted by the displacement capacity of element *(1)** as it is modified by the corresponding coefficient C_1, (Eq 3-6), which accounts for the effect of system rotations on the maximum displacement demand of the element. Element *(2)** governs if $(\Delta_{ue2}/\Delta_{ue1})_d > (\Delta_{ue2}/\Delta_{ue1})_c$. and hence Eq 3-7 is used to estimate C_2. (See Section 3.12.)

F3. The displacement ductility capacity of unrestrained systems, estimated with either Eq 3-4 or 3-5, is then compared with that already derived in Step B. If the differences are significant, it is necessary to recalculate the uncoupled translational period, and hence required strength of the system, as suggested in Step C.

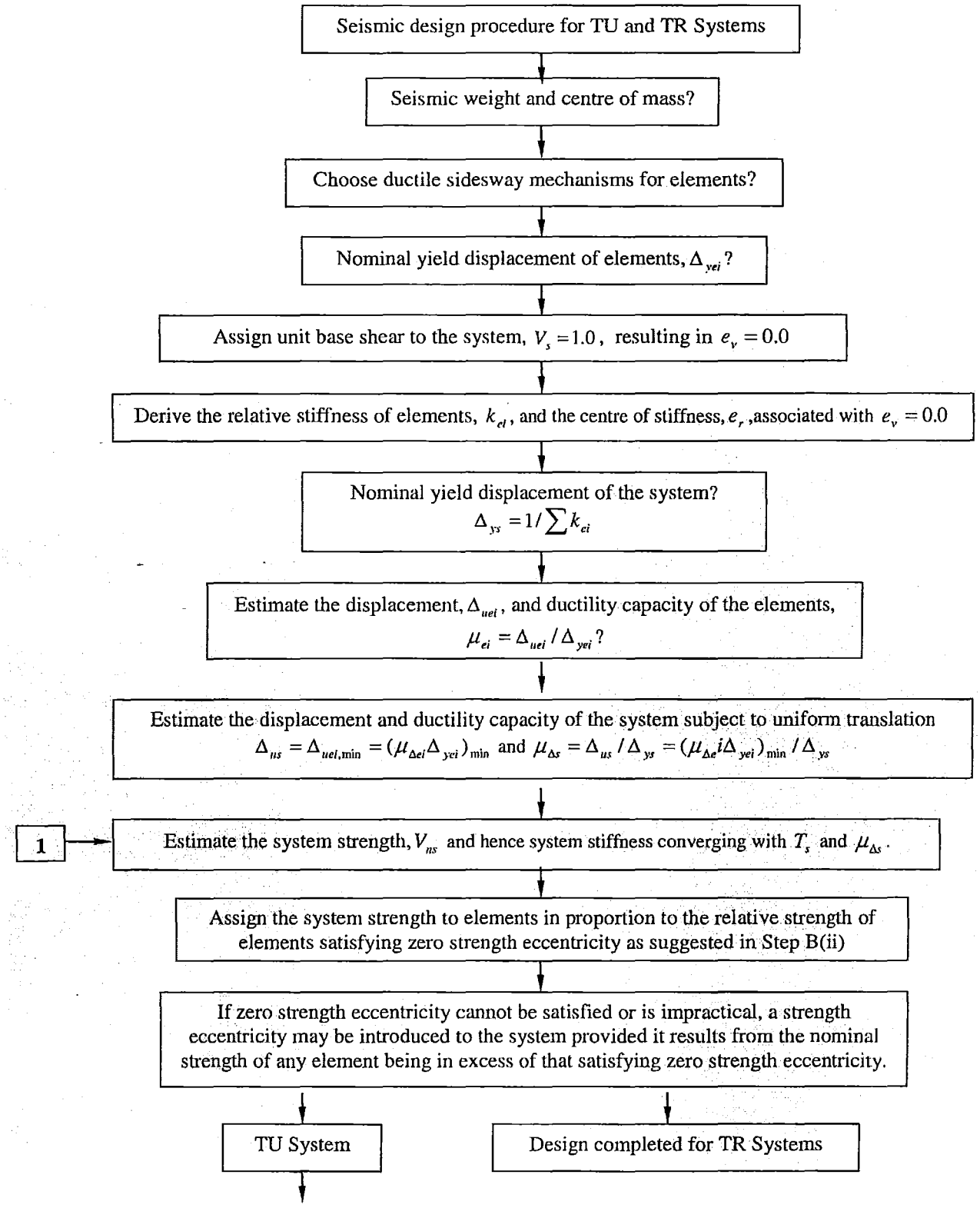

Figure 6-1. Flowchart for the seismic design of torsionally unrestrained and restrained systems

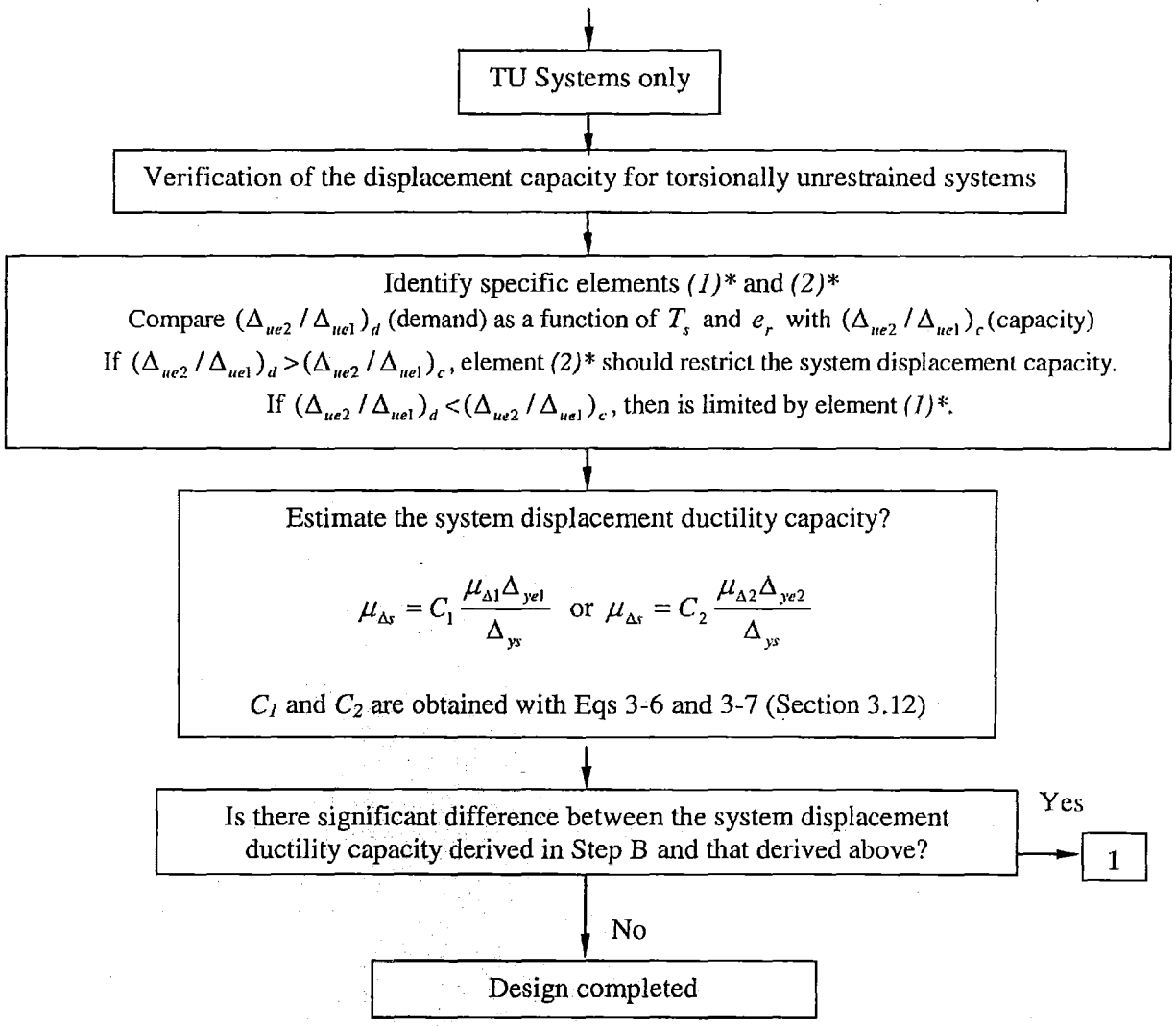

Figure 6-1. continued...Flowchart for the seismic design of torsionally unrestrained and restrained systems

Chapter 7. Conclusions and Recommendations

7.1 General

A series of single-story asymmetric systems were designed using a simple and rational seismic design strategy suggested in Section 2.11. No consideration was given to seismic design provisions for torsion of any particular building code.

The possible success of the design strategy, in limiting displacement demands on elements to less than their displacement capacity, was examined by considering the effects of key parameters expected to influence the response of asymmetric structures. They were: strength eccentricity and its associated increase of system strength, ratio of radii of gyration of strength and mass, reduced system displacement ductility capacity, mass eccentricity, transverse elements and their contribution to torsional restraint, the ratio of element nominal yield displacement, $\alpha=\Delta_{ye2}/\Delta_{ye1}$ (or stiffness eccentricity associated with zero strength eccentricity), uncoupled translational period and the consideration of different earthquake records and their directions of application.

Analytical and experimental studies of torsionally unrestrained and restrained single-mass systems were considered. The analytical studies examined the response of systems having one, two and more substitute wall-elements representing each lateral force-resisting element such as frames, interconnected walls and coupled walls when subjected to earthquake records at different directions. The study also included some experimental investigation into the behaviour of single-mass asymmetric structures.

The elements of the structural systems were simulated with a realistic bi-linear modelling of their force-displacement relationships. The nominal yield displacement of the elements is a material and geometric property insensitive to strength and therefore the stiffness is proportional to the nominal strength. This means that the centres of strength and stiffness are independent parameters.

The practical application of the design strategy suggested in this research is described in Appendix D through a design example of an asymmetric multi-storey building.

7.2 Analytical studies

The main findings relevant to the response of torsionally unrestrained and restrained systems designed with the proposed design strategy described in Section 2.12 are:

1. Torsional mechanisms of both unrestrained and restrained systems generated by static or dynamic-induced forces are different due to the action of the diaphragm mass rotational inertia. The mass rotational inertia of the diaphragm restricts system rotations expected to develop due to increasing strength and associated stiffness eccentricities. In the case of restrained systems, rotations are further reduced by transverse elements providing torsional restraint.

2. There is no need to differentiate between systems with or without mass eccentricity. Mass eccentricity is not a parameter influencing the torsional response.

3. As opposed to translational behaviour, the torsional behaviour of restrained systems was essentially insensitive to the frequency content of the earthquake record. On the other hand, unrestrained systems have a more sensitive response.

4. There is no need to differentiate between the torsional response of two and multi-element unrestrained and restrained systems. The response of multi-element systems may be predicted with that of a simple two-element system having similar characteristics of uncoupled translational period, stiffness eccentricity associated with zero strength eccentricity and radii of gyration of element nominal strength and uniformly distributed mass (i.e., the r_{vy}/r_m).

5. The increase on system rotations due to increasing strength eccentricities influences the maximum displacement demand on elements of unrestrained and restrained systems. These displacements demands, however, did not exceed those attained for zero strength eccentricity since increasing strength eccentricities is associated with an increase of system strength. The increase of system strength reduced displacement demands at the centre of mass. This compensated for the torsion-induced displacements of the critical element additional to those due to system translation.

6. Variations of the ratio of radii of gyration of element nominal strength and that of the uniformly distributed mass (i.e., r_{vy}/r_m), influences rotations and maximum displacement demand on elements of unrestrained systems. It was found that, as the r_{vy}/r_m ratio was reduced, system rotations are less likely to increase the displacement demands of some elements beyond that expected at the centre of mass. The maximum displacement demand of the elements and that at the centre of mass was essentially the same for systems with $r_{vy}/r_m \leq 0.90$. Hence, such system may be treated as a single degree of freedom system. In spite of such behaviour, this parameter was not considered to be of significance in the design strategy suggested in this study.

   Changes in the r_{vy}/r_m ratio of restrained systems had a negligible effect on displacement demands of elements when systems were subjected to earthquake records along the principal axes.

   Torques and rotations of restrained systems significantly increased when the earthquake record was applied along diagonal directions relative from the reference Y-axis. This was due to yielding of the transverse elements. It reached, at some instances, similar values of torques and rotations developed by their unrestrained counterpart having the same r_{vy}/r_m ratio. In spite of such behaviour, the displacement demand on elements did not exceed the maximum attained when the earthquake records were applied separately along the principal axes of the restrained system.

7. In the case of restrained systems, the displacement demands of elements parallel and perpendicular to the direction of ground motion input along the principal axes are not significantly affected by changes in the degree of torsional restraint provided by transverse elements, i.e., variations of the r_{vx}/r_{vy} ratio.

8. The maximum displacement demand of elements of unrestrained systems with zero strength eccentricity may be affected by system rotations, as they may be significantly influenced by variations of the $\alpha=\Delta_{ye2}/\Delta_{ye1}$ ratio (or increasing stiffness eccentricities associated with zero strength eccentricity) and the uncoupled translational period of free

vibration. Although rotations may have a important effect on displacement demands of the elements of unrestrained systems, maximum rotations were not associated with the maximum displacement demands of the elements. Hence, considerable system torques and rotations may be sustained while displacement demands on elements do not exceed their displacement capacity.

In the case of restrained systems, the maximum displacement demands of elements parallel to the direction of earthquake record input are essentially the same and not affected by changes of the $\alpha=\Delta_{ye2}/\Delta_{ye1}$ ratio (or increasing stiffness eccentricities associated with zero strength eccentricity). It did have a proportional, but non-critical effect, on the displacement demands of elements transverse to the direction of earthquake record input.

9. An optimal condition exists for minimum system rotations when the strength distribution on elements of unrestrained and restrained systems is such that centre of mass is located halfway between centres of strength and stiffness. In such a situation, the system rotations were found to be negligible; hence the maximum displacement demands on elements and at the centre of mass was essentially the same. This feature was not affected by the number, location and nominal yield displacement of the elements. Because the assignment of increased strength to elements is likely to occur on that having the smallest nominal yield displacement, the idealised distribution of strength of zero strength eccentricity maybe difficult to be achieved in practice. Moreover, this choice results in an unnecessarily reduced displacement capacity of the system.

10. The maximum displacement demand at the centre of mass of both unrestrained and retrained systems may be satisfactorily predicted with an equivalent single degree of freedom system. This prediction is not affected by the increasing number of elements parallel to the direction of earthquake input. Its accuracy, however, is reduced for systems with increasing $\alpha=\Delta_{ye2}/\Delta_{ye1}$ ratio (or increasing stiffness eccentricities associated with zero strength eccentricity) and systems with uncoupled translational periods of free vibration of $T_s<0.7$ sec. This sensitivity is more pronounced with unrestrained systems.

11. The maximum displacement demand of elements of unrestrained systems, as affected by system rotations, may be predicted with the ratios of maximum displacement demands of elements and that at the centre of mass, i.e., $(\Delta_{u1,2}/\Delta_{us})_d$. These ratios are influenced by variations of the $\alpha=\Delta_{ye2}/\Delta_{ye1}$ ratio (or stiffness eccentricity associated with zero strength eccentricity) and uncoupled translational periods.

    In the case of restrained systems, the displacement demand of the elements is essentially the same as that expected to develop at the centre of mass. Hence, the element displacement demands may be predicted from an equivalent single degree of freedom system.

12. The displacement and ductility capacity of torsionally unrestrained systems associated with zero strength eccentricity is restricted by either the element with the smallest displacement capacity or the outermost element on the flexible side of the system; whichever is critical. On the other hand, the displacement and ductility capacity of restrained systems will be always limited by that element having the smallest displacement capacity.

13. The strength to be eventually assigned to the system may be obtained with either force-based or displacement-based design methods by considering a system ductility factor equivalent to the system displacement ductility capacity. The system strength so obtained needs to be distributed to the elements to achieve zero strength eccentricity. The strength of the system is expected to prevent the system, and hence its elements, from exceeding their stipulated displacement capacity.

14. A proposed distribution of strength to the elements of unrestrained systems allows for the introduction of strength eccentricities provided that they result from one or more elements having strength in excess of that satisfying zero strength eccentricity. This will result in an increase of system strength and stiffness. This approach was successful in limiting displacement demands on elements to less than their displacement ductility capacity as strength eccentricities increased.

15. The strength distribution suggested above was also successful for restrained systems, although leading to conservative results, in limiting the displacement demands of elements to less than their capacity when systems were subjected to earthquake records along the principal axes. The effectiveness of this strength distribution was demonstrated when the systems were subjected to unidirectional earthquake records along diagonal directions. In such situation, systems having zero strength eccentricity and subjected to such records along the principal axes developed an envelope for the maximum displacement demand on the elements and at the centre of mass. These displacement demands were not exceeded with increasing strength eccentricities or when the unidirectional earthquake record was applied along other oblique directions to the principal axes of the structure. The unidirectional records used in this study represent the resultant of the bidirectional earthquake records in a given seismic event.

16. The satisfactory performance of unrestrained and restrained systems designed with the strategy suggested in this study was, in general, not influenced by variations of the uncoupled translational period of free vibration, the frequency characteristics of different earthquake records and for systems with reduced ductility capacity.

17. The response of extremely eccentric unrestrained and restrained systems (systems having a large stiffness eccentricity, i.e., $e_y > 0.30D$, associated with zero strength eccentricity) is quite sensitive and difficult to predict with simplified models. The actions of the mass rotational inertia have a major effect on the system rotations and on the translational displacements at the centre of mass. Extremely eccentric and even less eccentric structures should be avoided. They require special considerations to account for possible large displacement demands at the system's flexible side exceeding acceptable drift limits. These large displacements may result in much non-structural damage.

7.3 Experimental studies

The experimental studies on torsionally unrestrained and restrained systems designed with the proposed design strategy verified many of the findings obtained for the analytical systems. These were:

- The increase of system strength associated with increasing strength eccentricities may or may not reduce displacement demands at the centre of mass to compensate for the torsion-induced displacements of the critical element additional to those due to system

translation. The system response is sensitive to the frequency content characteristics of the earthquake record and is also sensitive for systems with to short uncoupled translational periods.

- The experimental models confirm the findings derived from analytical models that system rotations, although smaller in restrained models, increased as a strength eccentricity, and hence an increased stiffness eccentricity, was introduced to the model.

- The critical scenario with regard to frame displacements occurs when the system is subjected to an earthquake record along its principal directions rather than at oblique angles.

Differences in response between the test models and their analytical counterpart are attributed to the uncertainty involved in the locations of the centres of mass and strength, the fact that the loss of stiffness expected in steel components during flexural cyclic inelastic deformations was not modelled by the selected fuse simulation and differences in the damping associated with the rotational component.

7.4 Recommendations for the seismic design of asymmetric ductile systems

This study suggests that building code torsional provisions for the seismic design of asymmetric ductile systems should focus on strength eccentricity as the main parameter influencing torsional response rather than the commonly used stiffness eccentricity. It also suggests three points deserving consideration for a possible improvement to current building code provisions. These are:

- The need to establish the displacement capacity of an asymmetric system.

The displacement capacity of an unrestrained system is restricted either by the element with the smallest displacement capacity or the outermost element on the flexible side of the system.

The displacement capacity of a restrained system is restricted by the element with the smallest displacement capacity.

- The strength to be assigned to the system should be distributed to the elements to satisfy zero strength eccentricity.

- If zero strength eccentricity cannot or is not intended to be achieved in practice, a strength eccentricity may be accepted provided it is a result of any element having strength in excess of that satisfying zero strength eccentricity. A strength eccentricity is, therefore, associated with an increase of system strength.

The design strategy addressed in this study is for new buildings. However, the concepts will be found useful when attempting to assess the displacement capacity of existing buildings having elements with assessable properties.

7.5 Significance of this work

It is felt that this study contributes to a better understanding of the torsional response of ductile systems. The research had focused on the following relevant issues:

- The study emphasised strength eccentricity as the main parameter influencing response of ductile systems and constricted the role of the commonly used stiffness eccentricity. Lateral force resisting elements were modelled with a more realistic force-displacement relationship equally applicable to cracked reinforced concrete and to steel structural elements.

- It was shown that because stiffness is strength dependant, centres of strength and stiffness are not independent parameters. The response of systems with such property was thoroughly examined.

- A significant effort was dedicated to explain the mechanism developed during dynamic response of asymmetric systems by describing the interaction of the mass rotational and translational inertia during the response of ductile systems.

- It showed, contrary to common belief, that rotations are not necessarily detrimental to the response of ductile systems. Significant rotations may be accepted in ductile systems as long as the displacement capacity of the lateral force resisting elements is not exceeded.

- The study also shows differences in response between torsionally unrestrained and restrained systems. It provides an answer to the contradictory conclusions emerged from past studies on the research of asymmetric systems.

- A simple and effective design strategy has been proposed which differentiates between unrestrained and restrained systems.

- It was shown that the response at the centre of mass of an asymmetric system is satisfactorily estimated with an equivalent single degree of freedom system. This finding enables quantifying the effect of system rotations on the maximum response of elements. It is a relevant finding for seismic design because the design of an asymmetric multi-storey system may be drastically simplified if such system can be reduced to an equivalent single degree of freedom system. Such simple system will have a mass identical to the seismic mass of its multi-storey counterpart lumped at the effective height of the building (2/3h) and having the same properties of strength, stiffness and nominal yield displacement. Hence, the equivalent single degree of freedom system may be used to predict the maximum response at the centre of mass of its multi-storey counterpart at the effective height. The effect of system rotations on the maximum response may be subsequently accounted for in the design procedure for unrestrained and restrained systems.

7.6 Recommendations for future research

7.6.1 Analytical work

It is felt that studies on single mass systems should be extended to systems having strength and associated stiffness eccentricities along both principal axes. It is believed, however, that the response of bi-eccentric systems, when subjected to unidirectional earthquake records along the principal axes only, will show an envelope of the maximum displacement and ductility demands on the elements when the system is subjected to earthquake records along different directions. This needs to be verified by extended analytical studies.

It is also recommended to continue with a comprehensive programme on multi-storey asymmetric systems with regular asymmetry, (i.e, systems where the position of centres of strength, stiffness and mass in every storey have the same location in each storey although not coincident in a storey) to verify the design strategy for more general structures. Work should also be done for structures with setbacks where the above-described regularity is not satisfied. The lateral force resisting elements of building models, i.e., frames, wall elements or a combination of both, should be modelled with realistic force-displacement relationships such as that described in this study.

7.6.2 Experimental work

Efforts should continue with experimental programmes of single and multi-storey models aiming at the verification of the analytical findings as well as indicating improvements that may be required in the analytical models. Test models comprising simple connections would be preferable to reduce the number of variables affecting the torsional response.

It is also suggested to model the flexural behaviour of the fuses with the Dodd-Restrepo hyteresis rule[C1] which allows for stiffness degradation of steel components when subjected to cyclic forces beyond the elastic range of response.

REFERENCES

[A1] Ang, B.G.,(1985) "Seismic Shear Strength of Circular Bridge Piers" Ph.D. Thesis, Department of Civil Engineering, University of Canterbury, Christchurch, New Zealand

[A2] Aoyama H., (1981) "Outline of Earthquake Provisions in the recently revised Japanese Building Code", Bulletin of the New Zealand National Society for Earthquake Engineering, Vol.14, No.2, pp.63-80.

[A3] Ascheim M.A. and Black E.F., (2000) "The Primacy of the Yield Displacement in Seismic Design", PEER Report 2000/10, Pacific Earthquake Engineering Research Centre, College of Engineering, University of California, Berkley.

[A4] Aurelio G. and Rossi P.P., (2001) "Influence of Bi-Directional Ground Motions on the Inelastic Response of One-Storey In-Plane Irregular Systems", Engineering Structures, Vol. 23, No. 6, pp.579-591.

[A5] Ayre R.S., (1938) "Interconnection of Translational and Torsional Vibrations in Buildings", Bulletin of the Seismological Society of America Vol 28, No.1, pp. 89-130

[A6] Ayre R.S., (1943) "Experimental Response of an Asymmetric One-Storey Building Model to an Idealised Transient Ground Motion", Bulletin of the Seismological Society of America Vol 33, No.2, pp. 91-119.

[B1] Binder R.W. and Wheeler W.T., (1960) "Building Code Provisions for Aseismic Design" 2nd WCEE Tokyo, Japan, Vol. 3, pp. 1843-1875.

[B2] Bustamante J.I. and Rosenblueth E., (1960) "Building Code Provisions on Torsional Oscillations", 2nd WCEE, Vol. 2, pp.879-894, Tokyo-Kyoto, Japan.

[B3] Bull D. and Brunsdon D., (1998) "Examples of Concrete Structural Design to New Zealand Standard 3101", Published by the Cement and Concrete Association of New Zealand and New Zealand Concrete Society.

[C1] Carr A.J., (2002) "3D-RUAUMOKO Program", Computer Program Library, Department of Civil Engineering, University of Canterbury, New Zealand

[C2] Carr A.J., (2002) "HYSTERESIS Program", Computer Program Library, Department of Civil Engineering, University of Canterbury, New Zealand

[C3] Carr A.J., (2002) "INSPECT Program", Computer Program Library, Department of Civil Engineering, University of Canterbury, New Zealand

[C4] Carr A.J., (2002) "SPECTRA Program", Computer Program Library, Department of Civil Engineering, University of Canterbury, New Zealand

[C5] Castillo R., (1995) "Inelastic Torsional Response Behaviour of Structures Subjected to One and Two-Directional Ground Motions", Master Thesis, Department of Architecture, Tohoku University, Sendai, Japan.

[C6] Castillo R., (2001) "The Rotation of Asymmetric Plan Structures", New Zealand Society for Earthquake Engineering, Annual Technical Conference.

[C7] Chandler A.M., and Nichol E.A., (1990) "Experimental Evaluation of procedures for Earthquake Analysis of Torsionally Asymmetric Buildings", European Earthquake Engineering, Vol. 4, No. 3, pp. 45-32.

[C8] Chandler A.M., Duan X.N. and Rutenberg A., (1996) "Seismic Torsional Response: Assumptions, Controversies and Research Progress", European Earthquake Engineering, Vol. 10, No. 1, pp.37-51.

[C9] Chopra A.K. and Goel R.K, (1999) "Capacity Demand Diagram Methods for Estimating Seismic Deformations of Inelastic Structures: SDF Systems", PEER-1999/02, Pacific Earthquake Engineering Research Center, College of Engineering, University of California, Berkeley.

[C10] Committee on the Alaska Earthquake, (1973) "The Great Alaska Earthquake of 1964", Division of Earth Sciences National Research Council, National Academy of Sciences Washington, D.C., Vol. 6 Engineering.

[C11] Cormartin C.D., Green M. and Tubbesing S., (1995) "The Hyogo-Ken Nanbu Earthquake. Great Hanshin Earthquake Disaster January 17, 1995", Preliminary Reconnaissance Report, Earthquake Engineering Research Institute, 95-04.

[C12] Correnza J.C., Hutchinson G.L. and Chandler A.M., (1994) "Effect of Transverse Load-Resisting Elements on Inelastic Earthquake Response", Earthquake Engineering and Structural Dynamics, Vol. 23, No.1, pp.75-89.

[C13] Correnza J.C., Hutchinson G.L. and Chandler A.M., (1992) "A Review of Reference Models for Assessing Inelastic Seismic Torsional Response Effects in Buildings", Soil Dynamics and Earthquake Engineering, Vol. 11, No.8, pp.465-484.

[C14] Chandler A.M., Duan X.N. Correnza J.C and Hutchinson G.L., (1994) "Period-Dependent Effects in Seismic Torsional Response of Code Systems", Journal of Structural Engineering, Vol. 120, No. 12, pp.3418-3434.

[C15] Correnza J.C., Hutchinson G.L. and Chandler A.M., (1995) "Seismic Response of Flexible-Edge Elements in Code-Designed Torsionally Unbalanced Structures", Engineering Structures, Vol. 17, No.3, pp.158-166.

[C16] Clough R. and Penzien J., (1993) "Dynamics of Structures", McGraw-Hill, New York.

[C17] Chia-Ming Uang and Bertero V., (1986) "Earthquake Simulation Tests and associated Studies of a 0.3 Scale Model of a Six Storey Concentrically Braced Steel Structure", Report No UCB/EERC-86/10, Earthquake Engineering Research Center, University of California, Berkeley.

[D1] De La Colina J., (1999) "Effects of Torsion Factors on Simple Non-Linear Systems using Fully-Bidirectional Analyses", Earthquake Engineering and Structural Dynamics, Vol. 28, No. 7, pp.691-706.

[D2] De la Llera J.C., Chopra A.K., (1994) "Accidental and Natural Torsion in Earthquake Response and Design of Buildings", Report No UCB/EERC-94/07, Earthquake Engineering Research Center, University of California, Berkeley.

[D3] De Stefano M, Faella G., and Ramasco R., (1998) "Inelastic Seismic Response of One-Storey Plan-Asymmetric Systems Under Bi-directional Ground Motions", Earthquake Engineering and Structural Dynamics, 27, pp 363-376

[D4] De Stefano M. and Faella G., (1996) " An Evaluation of the Inelastic Response of Systems Under Biaxial Seismic Excitations", Engineering Structures, Vol. 8, No 9, pp. 724-731

[D5] De Stefano M. and Rutenberg A. (2002) "Third European Workshop on Seismic Behaviour on the Seismic Behaviour of Asymmetric and Irregular Structures", European Association of Earthquake Engineering, Task Group 8, Asymmetric and Irregular Structures, Florence, Italy, CD-Rom.

[D6] De Stefano M., Faella G. and Ramasco R. (1998) "Inelastic Seismic Response of One-Way Plan-Asymmetric Systems under Bi-Directional Ground Motions", Earthquake Engineering and Structural Dynamics, Vol. 27, No. 4, pp.363-376.

[D7] Duan X.N. and Chandler A.M. (1995) "Seismic Torsional Response and Design Procedures for a Class of Setback Frame Buildings", Earthquake Engineering and Structural Dynamics, Vol. 24, No. 5, pp.761-777.

[D8] Duan X.N. and Chandler A.M. (1997) "An Optimized Procedure for Seismic Design of Torsionally Unbalanced Structures", Earthquake Engineering and Structural Dynamics, Vol. 26, No. 7, pp.737-757.

[D9] Dusicka P., (2000) "Numerical and Experimental Investigation of Seismic Torsional Response of Single Storey Ductile Structures", Master of Applied Science, The University of British Columbia

[F1] Faella G., MagliuloG., and Ramasco R., (1999) "Seismic Response of Asymmetric R/C Buildings Under Bi-Directional Input Ground Motion", European Association of Earthquake Engineering., Task Group 8., 2nd Workshop on Asymmetric and Irregular Structures, Istanbul, Vol. 2, pp. 361-374

[F2] Fajfar P. and Krawinkler H., (1997) "Seismic Design Methodologies for the Next Generation of Codes" Proceedings of the International Workshop on Seismic Design Methodologies for the Next Generation of Codes, Bled, Slovenia, Rotterdam; Brookfield: A.A. Balkema.

[G1] Ghersi, A. and Rossi P.P., (2001) "Influence of Bi-directional Ground Motions on the Inelastic Response of One-Storey In-Plan Irregular Systems", Engineering Structures, Vol. 23, No 5, pp. 579-591

[G2] Goel R.K., Chopra A.K., (1990) "Inelastic Seismic Response of One-Story, Asymmetric Plan Systems", Report No UCB/EERC-90/14, Earthquake Engineering Research Center, University of California, Berkeley.

[G3] Goltz J.D., (1994) "The Northridge California Earthquake of January 17, 1994", General Reconnaissance Report, Technical report NCEER-94-0005, National Centre of Earthquake Engineering Research, State University of New York at Buffalo.

[H1] Hejal R., Chopra A.K., (1987) "Earthquake Response of Torsionally Coupled Buildings", Report No UCB/EERC-87/20, Earthquake Engineering Research Center, University of California, Berkeley.

[H2] Housner G.W, and Outinen H., (1958) "The Effect of Torsional Oscillations on Earthquake Stresses", Bulletin of the Seismological Society of America Vol. 48, No.2, pp. 221-229.

[H3] Humar J.L. and Kumar P., (1999) "Effect of Orthogonal In-plane Structural Elements on Inelastic Torsional Response", Earthquake Engineering and Structural Dynamics, Vol. 28, No. 10, pp.1071-1097.

[I1] International Association for Earthquake Engineering, (1996), "Regulations for Seismic Design- A World List", IAEE, Tokyo.

[J1] Jacobsen L.S., (1929) "Vibration Research at Stanford University", Bulletin of the Seismological Society of America Vol 19, No.1, pp. 1-27.

[J2] Jaramillo J.D. and Montoya E., (1998) "Series: Program for the process and analysis of time history signals", User Manual, Universidad EAFIT, jjarami@sigma,eafit.edu.co(In Spanish)

[K1] Kan C.L., Chopra A.K., (1976) "Coupled Lateral Torsional Response of Buildings to Ground Shaking", Report No UCB/EERC-76/13, Earthquake Engineering Research Center, University of California, Berkeley.

[K2] Kan C.L., Chopra A.K., (1979) "Linear and Non-Linear Earthquake Responses of Simple Torsionally Coupled Systems", Report No UCB/EERC-79/03, Earthquake Engineering Research Center, University of California, Berkeley.

[K3] Kao G.C., (1998) "Design and Shaking Table Tests of A Four-Storey Miniature Structure Built With Replaceable Plastic Hinges", Master Thesis, Department of Civil Engineering,University of Canterbury, Christchurch, New Zealand

[K4] Karadogan F. and Rutenberg A. (1999) "Irregular Structures" European Association of Earthquake Engineering, Task Group 8, Asymmetric and Irregular Structures, Istanbul Vol. 1 and 2 Turkey.

[K5] Kowalsky M.J., Priestley M.J.N. and MacRae G.A. (1994) "Displacement Based Design-A Methodology for Seismic Design Applied to Single Degree of Freedom Reinforced Concrete Structures", Structural Systems Research Report No SSRP-94/16, University of California, San Diego, LaJolla, California.

[L1] Lam N.T.K, Wilson J.L and Hutchinson G.L. (1997) "Review of the Torsional Coupling of Asymmetric Wall-Frame Buildings", Engineering Structures, Vol. 19, No. 3, pp.233-246.

[L2] Lindawatiek, (1998) "The Influence of Strain Rate on the Seismic Response of a Four-Storey Steel Frame Building", Research report ENCI-495, Department of Civil Engineering, University of Canterbury, Christchurch, New Zealand

[L3] Loeding S., Kowalsky M.J. and Priestley M.J.N., (1998) "Direct Displacement-Based Design of Reinforced Concrete Building Frames", Report No SSRP-98/08, Structural Systems Research, University of California, San Diego.

[M1] Maheri M.R. Chandler A.M. and Basset R.H. (1991) "Coupled Lateral-torsional Behaviour of Frame Structures under Earthquake Loading", Earthquake Engineering and Structural Dynamics, Vol. 20, No. 1, pp. 61-85.

[M2] Muller F. and Keintzel E. (1978) "Approximate Analysis of Torsional Effects in the New German Seismic Code Din 4149", Sixth European Conference on Earthquake Engineering, Dubvronic, Vol. 2, pp. 101-108.

[M3] Myslimaj B. and Tso W.K., (2002) "A strength distribution Criterion for Minimizing Torsional Response of Asymmetric Wall-Type Systems", Earthquake Engineering and Structural Dynamics, Vol. 31, No. 1, pp. 99-120.

[N1] Newmark N.M. and Hall W.J. (1982) "Earthquake Spectra and Design", Monograph Series, Vol.2, No.2, Earthquake Engineering Research Institute

[O1] Otani S., (1974) "SAKE. A computer program for inelastic response of R/C frames to earthquakes", Report UILU-Eng-74-2029 Civil Engineering Studies, University of Illinois at Urbana-Champaign.

[P1] Paulay T. and Priestley M.J.N., (1992) "Seismic Design of Reinforced Concrete and Masonry Buildings", John Wiley and Sons, New York.

[P2] Paulay T. (1997) "Displacement-Based Design Approach to Earthquake Induced Torsion in Ductile Buildings", Engineering Buildings, Vol. 29, No.3, pp.178-198.

[P3] Paulay T., (1996) "Seismic Design for Torsional Response of Ductile Buildings", Bulletin of the New Zealand Society for Earthquake Engineering, Vol. 29, No.3, pp. 178-198.

[P4] Paulay T., (1997) "A Review of Code Provisions for Torsional Seismic Effects in Buildings", Bulletin of the New Zealand Society for Earthquake Engineering, Vol. 30, No.3, pp. 252-263.

[P5] Paulay T., (1997) "Seismic Torsional Effects on Ductile Structural Wall Systems", Journal of Earthquake Engineering (Imperial College), Vol. 1, No.4, pp.721-746.

[P6] Paulay T., (1997), "Are Existing Seismic Torsional Provisions Achieving the Design Aims?", Earthquake Spectra, Vol. 13, No.2, pp. 259-279.

[P7] Paulay T., (1998) "A Mechanism-Based Design Strategy for the Torsional Seismic Response of Ductile Buildings". European Earthquake Engineering, Vol. 12, No. 2, pp. 33-48.

[P8] Paulay T., (1998) "Torsional Mechanism in Ductile Building Systems", Earthquake Engineering and Structural Dynamics, Vol. 27, No. 10, pp.1101-1121.

[P9] Paulay T., (1999) "Some Principles Relevant to the Seismic Torsional Response of Ductile Buildings", Proceedings 2nd European Workshop on the Seismic Behaviour of Asymmetric and Irregular Structures, Istanbul, 1999, pp.1-25

[P10] Paulay T., (2000) "Understanding Torsional Phenomena in Ductile Systems", Bulletin of the New Zealand Society for Earthquake Engineering, Vol. 33, No.34 pp. 403-420.

[P11] Paulay T., (2001) "Some Design Principles Relevant to Torsional Phenomena in Ductile Buildings", Journal of Earthquake Engineering, Vol. 5, No3, pp. 273-308.

[P12] Paulay, T., (1998) "Twist in NZS 4203:1992", Journal of the Structural Engineering Society of New Zealand, Vol. 11, No.2, pp.12-18.

[P13] Paulay T., (2002) "An Estimation of Displacement Limits for Ductile Systems", Earthquake Engineering and Structural Dynamics, Vol. 31, No3, pp.583-599.

[P14] Paulay T., (2002) "A Displacement-Focused Seismic Design of Mixed Building Systems", Earthquake Spectra, Vol.18, No.4, pp.1-30.

[P15] Paulay T., (2002) "The Displacement Capacity of Reinforced Concrete Coupled Walls", Engineering Structures, Vol.24, pp.1165-1175.

[P16] Priestley M.J. (2000) "Performance Based Seismic Design", 12WCEE, Auckland, New Zealand, Paper No.2831.

[P17] Priestley M.J. and Calvi G.M., (1991) "Towards a Capacity Design Assessment Procedure for Reinforced Concrete Frames", Earthquake Spectra, Vol.7, No.3, pp.413-437.

[P18] Priestley M.J. and Kowalsky M.J., (1997) "Aspects of Drift and Ductility Capacity of Rectangular Cantilever Structural Walls", Bulletin of the New Zealand National Society for Earthquake Engineering, Vol. 31, No.4, pp.73-85.

[P19] Priestley M.J., (1997) "Displacement-Based Seismic Assessment of Reinforced Concrete Buildings", Journal of Earthquake Engineering, Imperial College, Vol.1, No.1, pp.157-192.

[P20] Priestley M.J., (1998) "Brief Comments on Elastic Flexibility of Reinforced Concrete Frames and Significance to Seismic Design", Bulletin of the New Zealand National Society for Earthquake Engineering, Vol.31, No.4, pp. 246-259.

[P21] Priestley, M.J., (1995) "Myths and Fallacies in Earthquake Engineering Conflicts between Design and Reality", American Concrete Institute (SP-157), Recent developments in lateral force transfer in buildings, pp.231-254.

[P22] Priestley, M.J., et al (1999) "Preliminary Results and Conclusions from the PRESS Five-Storey Precast Concrete Test Building", PCI Journal, Vol 44, No6, pp.42-87.

[R1] Ramasco R. and Rutenberg A. (1996) "Proceedings of the European Workshop on the Seismic Behaviour of Asymmetric and Setback Structures", Anacapri, Isle of Capri, Italy.

[R2] Riddell R. and Santa Maria H. (1999) "Inelastic Response of One-Storey Asymmetric-Plan Systems Subjected to Bi-Directional Earthquake Motions", Earthquake Engineering and Structural Dynamics, Vol. 28, No. 3, pp.273-285.

[R3] Rosenblueth and Elorduy, (1969). "Responses of Linear Systems to Certain Transient Disturbances", Proceedings 4th WCEE, Santiago, Chile, Vol. I, A-1, pp.185-196

[R4] Rosenblueth E. (1960) "Aseismic provisions for the Federal District, Mexico" 2nd WCEE Tokyo, Japan, Vol. 3 pp. 2009-2016.

[R5] Rosenblueth, E. and Meli R., (1986) "The 1985 Earthquake: Causes and Effects in Mexico City", Concrete International, American Concrete Institute, Vol. 8, No.5, pp. 23-24.

[R6] Rutenberg A. (1992) "Nonlinear Response of Asymmetric Building Structures and Seismic Codes: A State of the Art Review", European Earthquake Engineering, Vol. 6, No.2, pp.3-18.

[R7] Rutenberg A., Chandler A.M. Duan X.N. and Correnza J.C., (1995) "Nonlinear Seismic Response of Asymmetric Structures: Bibliography", Report for the European Association for Earthquake Engineering Task Group 8: Behaviour of Irregular and Complex Structures, Haifa, Israel.

[S1] SEAOC Seismology Committee, (1958) "Recommended Lateral Force Requirements and Commentary", California.

[S2] Severn R.T., Taylor C.A. and Bairrao R., (2001) "Cable-Stayed Bridges, Irregular Bridges and Asymmetrical Structures", European Consortium of Earthquake Shaking Tables-Innovative Seismic Design Concepts for New and Existing Structures, CAFEEL/ECOEST2/ICONS Technical Report ; No. 8.

[S3] Shibata A., (1981) "Analysis and Design of Earthquake Resistant Building Structures", Morikita Publishing Company Ltd. (in japanese).

[S4] Shibata A., Onose J. and Shiga T., (1969) "Torsional Response of Buildings to Strong Earthquake Motions", 4th WCEE, A-4-123, Chile.

[S5] Soulages J., (1995) "Performance Based Seismic Engineering of Buildings", Structural Engineers Association of California, California Office of Emergency Services.

[S6] Standard Association of New Zealand, (1992) "Code of Practice for General Structural Loading for Buildings", NZS 4203-1992, Wellington.

[S7] Standard Association of New Zealand, (1995) "Concrete Structures Standard", NZS 3101-1995, Wellington.

[T1] Timoshenko S., (1928) "Vibration Problems in Engineering", D.Van Nostrand Company, New York

[T2] Tso W.K. and Moghadam A.S., (1997) "Seismic Response of Asymmetric Buildings using Pushover Analysis", Seismic Design Methodologies for the Next Generation of Codes, Editors: Peter Fajfar, Helmut Krawinkler, A.A. Balkema/Rotterdam/Brookfield, pp311-321.

[T3] Tso W.K. and Myslimaj B., (2002) "A Yield Displacement Based Approach to Strength Assignment in Asymmetric Structures", Third European Workshop on Seismic Behaviour on the Seismic Behaviour of Asymmetric and Irregular Structures, European Association of Earthquake Engineering, Task Group 8, Florence, Italy, CD-Rom.

[T4] Tso W.K., (1990) "Static Eccentricity Concept for Torsional Moment Estimations", Journal of the Structural Engineering, ASCE, Vol.116,No.5, pp1199-1212

[T5] Tso W.K. and Zhu T. J, (1992) "Design of Torsionally Unbalanced Structural Systems Based on Code Provisions I : Ductility Demand", Earthquake Engineering and Structural Dynamics, Vol.21, No.7, pp 609-627

[W1] Wyllie L.A. (1986) "The Chile Earthquake of March 3, 1985", Earthquake Spectra, Earthquake Engineering Research Institute, Vol.2, No.2

[Y1] Yanev P.I., (1978) "Miyagi-Ken Oki, Japan Earthquake, June 12 1978", Earthquake Research Institute, Reconnaissance Report.

[Z1] Zhu K., Al Bermani F.G.A., Kitipornchi S. and Li B., (1995) Dynamic Response of Flexibly Jointed Frames", Engineering Structures, Vol 17, No 8, pp 575-580

[Z2] Zhu T.J. and Tso W.K., (1992) "Design of Torsionally Unbalanced Structural Systems based on Code Provisions II: Strength Distribution", Earthquake Engineering and Structural Dynamics, Vol. 21, No. 1, pp.629-644.

Appendix A. Moment-Curvature Analyses of Wall Components

A.1 Introduction

The aim of this section is to obtain approximate values of the curvature coefficient, $\eta=M_n/\xi M_y$, proposed by Paulay [P13] for typical cross sections found in actual buildings. This coefficient provides the nominal yield curvature of a section for a given length and yield strain, as shown by Eq. 2-15. The fact that the nominal yield curvature, ϕ_y, is approximately constant once the geometry of a section is defined, allows a more accurate and realistic calculation of the effective moment of inertia, I_e, after the nominal flexural strength, M_n, has been assigned to the component.

In structural design, the effective moment of inertia of the section, I_e, should not be considered equal to the moment of inertia of the gross concrete section, I_g, or a constant fraction of it. It should be calculated using Eq. 2-16. This effective flexural rigidity, E_cI_e, so derived is relevant for a more realistic prediction of component displacements, in particular the nominal yield displacement Δ_{yi}, which is of great importance to displacement-based design and the determination of displacement ductility.

Emphasis is given to wall components due to their relevance to this research. The major variables considered are axial load ratio, $N/(f'_cA_g)$, reinforcement ratio, ρ_b, and the reinforcement distribution along the length of the wall, ρ_ℓ. Figure A-1 shows the different wall cross sections examined in this study.

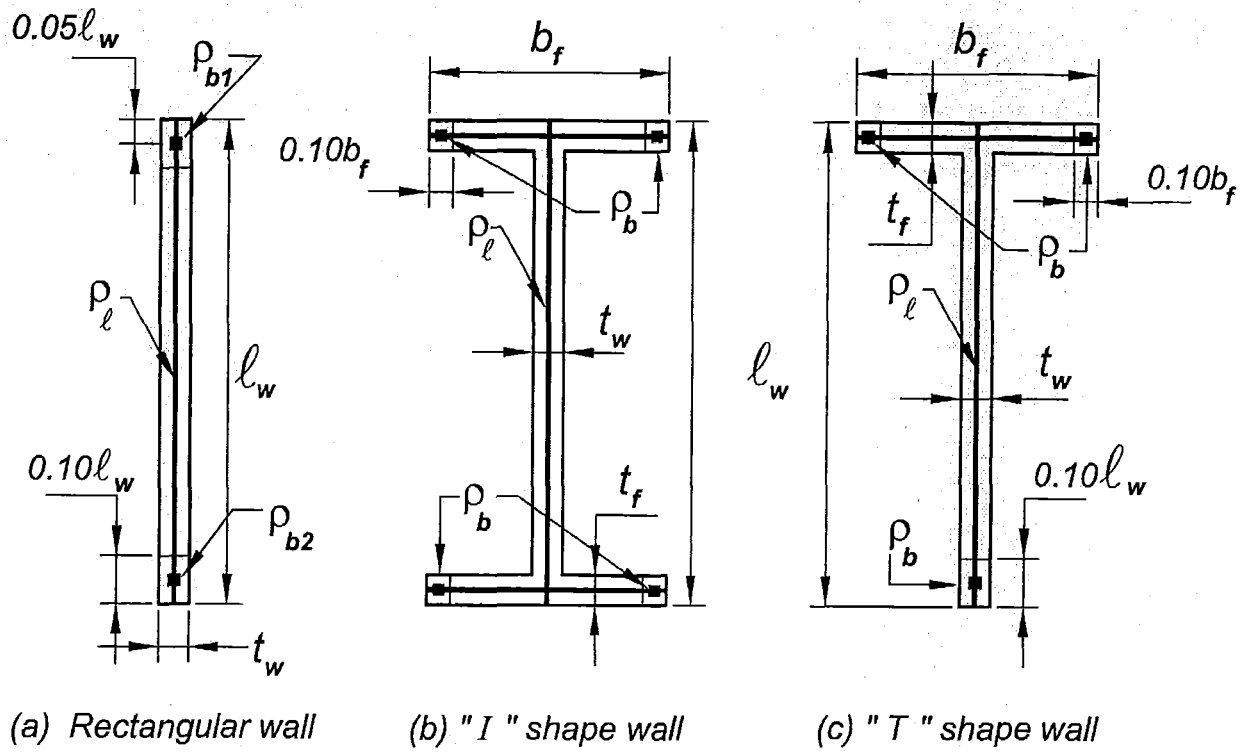

Figure A-1 Examples of wall components with different cross sections

A.2 Rectangular wall components

Moment–curvature analyses are undertaken on rectangular wall cross sections, as that shown in Figure A-1(a). In a first set of analyses, the walls have ratios of distributed reinforcement of ρ_ℓ=*0.25%, 0.50%, 0.75%* and *1.0%*, representing uniformly distributed vertical bars along a rectangular wall with length, ℓ_w. Subsequently, wall components with ratios of distributed reinforcement of ρ_ℓ=*0.25% and 0.50%* and ratios of boundary reinforcement, ρ_b, of *1.0%*, *2.0%* and *3.0%* was also considered. The boundary reinforcement is concentrated at a distance of $0.05\ell_w$ from the end of the wall and its ratio is calculated based on a concrete area of $0.10t_w\ell_w$. A third set of analyses considers wall components with asymmetrical ratios of distributed boundary reinforcement, ρ_{b1} and ρ_{b2}. The ratio of boundary reinforcement considered is ρ_{b1}=*0.50%* at one end and ρ_{b2}=*1%*, *2%*, and *3%* at the other end of the wall. The ratio of distributed reinforcement remains equal to ρ_ℓ=*0.25%*. The axial load ratio will vary between $N/(f'_cA_g)$=*–0.02* and *0.10*. A negative axial load ratio, implying tension, is of interest because it is applicable to coupled walls. This range of reinforcement and axial load is considered representative for cantilever walls of multi-storey buildings. The reinforcement yield strain is ε_y=*0.0015*(i.e. f_y=*300*MPa) and the compressive strength of concrete, f'_c, was *30MPa*.

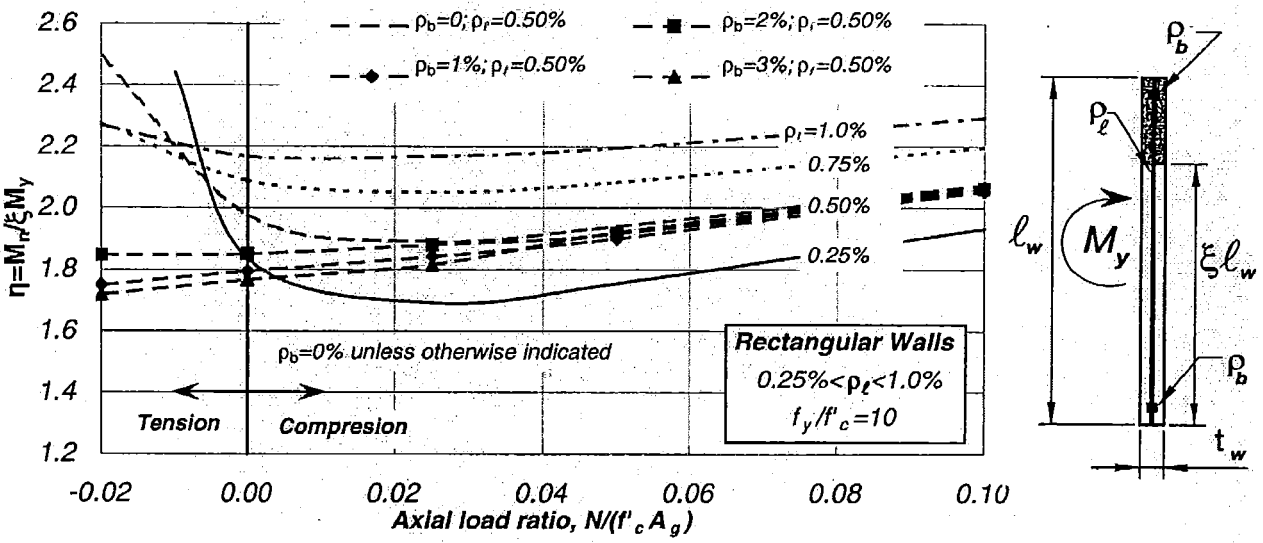

Figure A-2 Values of curvature coefficient, η, for rectangular walls

Figure A-2 shows values of curvature coefficient for rectangular walls as a function of the ratio of distributed reinforcement, ρ_ℓ, and axial load ratios, $N/(f'_cA_g)$. For instance, an increase in the ratio of distributed reinforcement from ρ_ℓ=*0.25%* to *1%* and a constant axial load ratio of $N/(f'_cA_g)$=*0.04*, increases the curvature coefficient from η=*1.70* to *2.20*. This occurs because an increase in the quantity of distributed reinforcement increases the compression area at the end of the wall and thus reduces the ratio of neutral axis depth and wall length, ξ. Large ratios of distributed reinforcement also increase the M_n/M_y ratio due to a larger increase of the nominal moment, M_n, relative to its yield moment, M_y. As shown by Priestley and Kowalsky [P18], the variation of the axial load ratio, $N/(f'_cA_g)$, between *0.0* and *0.10* does not show significant effects on the curvature coefficient. This happens because reductions of the neutral axis to length

ratio, ξ, and the M_n/M_y ratio are comparable. In contrast, an axial tension load ratio produces a sudden increase of the curvature coefficient because the M_n/M_y ratio increase at a greater rate than the neutral axis depth to wall length ratio, ξ. The increase in the M_n/M_y ratio occurs because the axial tension load reduces the yield moment, M_y, at a faster rate than the nominal moment, M_n. Table A-1 provides a summary of the variation of the M_n/M_y and neutral axis depth to wall length ratio, ξ, to confirm these findings. It is noted that walls subjected to axial tension are not likely to have ratios of uniformly distributed bars without any boundary reinforcement.

Table A-1 Values of curvature coefficients, η, applicable to rectangular walls

RECTANGULAR WALLS							
$N/(f'_cA_g)$	M_n/M_y	ξ	η	$N/(f'_cA_g)$	M_n/M_y	ξ	η
ρ_ℓ=0.25%		ρ_b=0.0%		ρ_ℓ=0.50%		ρ_b=0.0%	
-0.010	2.31	0.95	2.44	-0.020	2.32	0.93	2.49
0.000	1.61	0.88	1.83	0.000	1.65	0.83	1.98
0.025	1.33	0.79	1.69	0.025	1.45	0.77	1.89
0.050	1.29	0.73	1.75	0.050	1.40	0.72	1.94
0.100	1.27	0.65	1.93	0.100	1.34	0.65	2.07
ρ_ℓ=0.50%		ρ_b=1.0%		ρ_ℓ=0.50%		ρ_b=3.0%	
-0.020	1.51	0.82	1.85	-0.020	1.32	0.77	1.72
0.000	1.41	0.76	1.85	0.000	1.28	0.73	1.77
0.025	1.34	0.71	1.88	0.025	1.24	0.68	1.81
0.050	1.28	0.67	1.92	0.050	1.25	0.65	1.92
0.100	1.25	0.61	2.06	0.100	1.23	0.60	2.07

Figure A-2 also shows values of the curvature coefficient for rectangular walls when ratios of boundary reinforcement of ρ_b=*1.0%, 2.0%,* and *3.0%* are evenly assigned at both ends of the wall. The ratio of distributed reinforcement remains constant and equal to ρ_ℓ=*0.50%*. Ratios of boundary reinforcement do not influence the values of the curvature coefficient for axial load ratios, $N/(f'_cA_g)$, in excess of *0.02*. It is evident that the ratio of distributed reinforcement primarily controls the values of the curvature coefficient.

Figure A-3 shows the values of the curvature coefficient for rectangular walls when the ratios of boundary reinforcement are unevenly assigned to the ends of the wall component. The wall is subjected to lateral forces inducing positive or negative bending moments. It has a fixed ratio of distributed and boundary reinforcement of $\rho_\ell=\rho_{b1}$=0.50%. At the other end of the wall, the ratio of the boundary reinforcement are ρ_{b2}=*1.0%, 2.0%* and *3.0%*. The axial load ratio, $N/(f'_cA_g)$, varies between *–0.02* and *0.10*. This arrangement of reinforcement would not arise in cantilever walls subjected to gravity loads. A significant variation of gravity and lateral force-induced axial loads arises in coupled walls in which the ratios of boundary reinforcement are expected to be different.

Figure A-3(a) shows the effect of increasing the boundary reinforcement ratio, ρ_{b2}, at the tension side of the wall. It is evident that it does not influence those values of curvature coefficient already obtained with only distributed reinforcement and axial load ratios of $N/(f'_cA_g)>0.02$. However, its effect is manifested for smaller values of axial load ratio. The curvature coefficient exhibits a linear reduction rather than the increase observed with only distributed reinforcement. This occurs, as stated before, because the increase in boundary reinforcement at the tension side

of the wall increases the yield moment of the section at a faster rate than its nominal moment thus reducing the M_n/M_y ratio.

On the other hand, Figure A-3(b) shows the case when the moment of the wall reverses. The wall has the same ratios of distributed and boundary reinforcement described before. In this case, the increasing boundary reinforcement ratio, ρ_{b2}, is at the compression side of the wall. Similar values of the curvature coefficient are shown for axial loads ratios $N/(f'_c A_g)>0.02$. However, for smaller axial load ratios, reductions in the curvature coefficient are not as large as those obtained when the increasing boundary reinforcement ratio, ρ_{b2}, at the tension side of the wall.

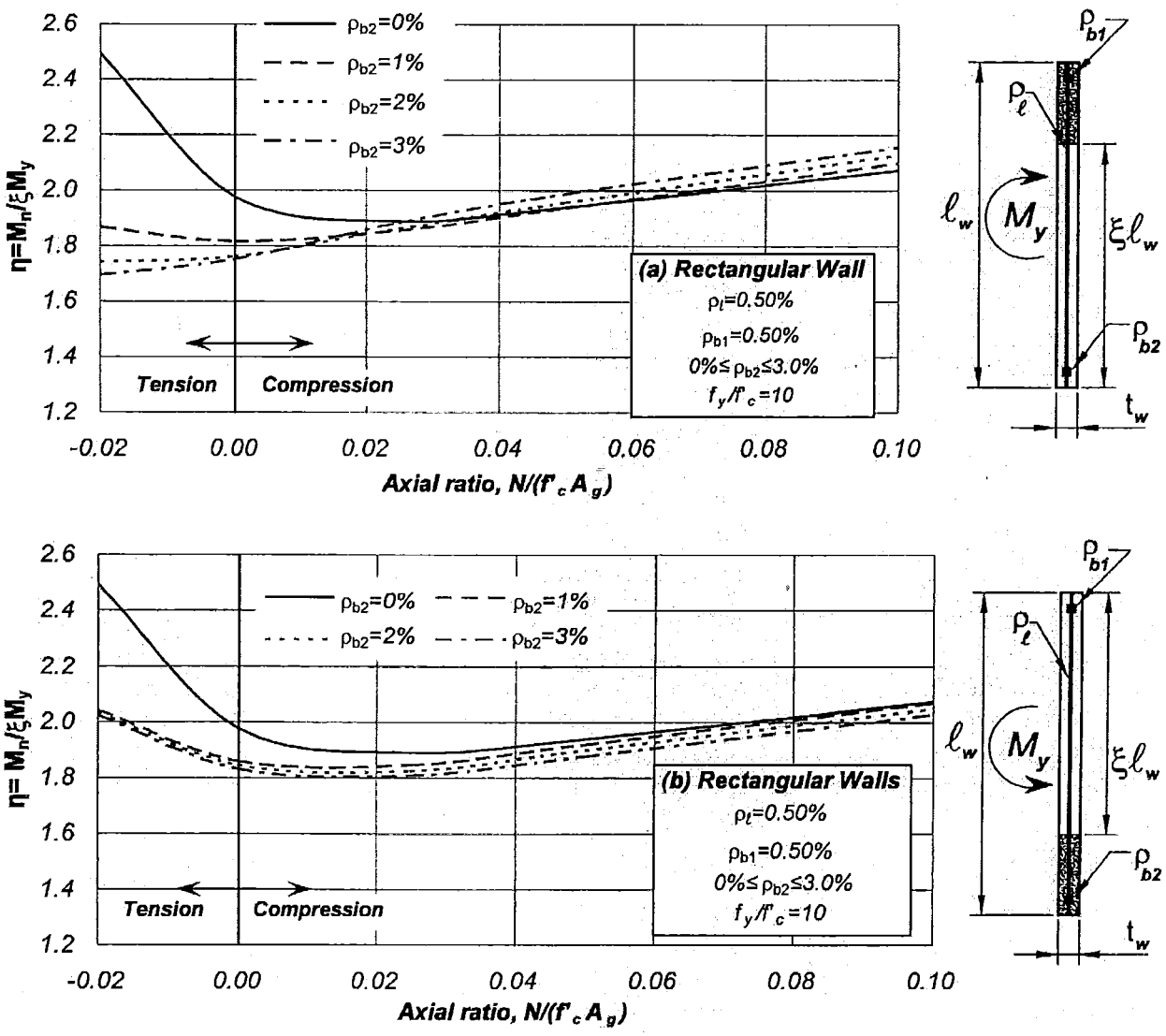

Figure A-3 Values of curvature coefficient, η, applicable to rectangular walls with unequal ratios of boundary reinforcement, ρ_b

This uneven distribution of boundary reinforcement slightly affects the curvature coefficient already obtained with symmetrically distributed boundary reinforcement when the wall is subjected to lateral forces inducing positive or negative bending moments. The only distinctive characteristic is that for axial load ratios less than *0.02*, the curvature coefficient reduces in particular when increasing the tension boundary reinforcement. In coupled structural walls, the axial force ratios may exceed the limits shown in Figure A-3(a) and (b). It is evident that for

compression dominated walls reliable values of curvature coefficient may be obtained by linear extrapolation. Because tension dominated coupled walls will seldom be used with less than a *2%* reinforcement ratio at the tension end of the section, such approximation is also applicable to cases when $N/(f'_c A_g)<-0.02$.

Figure A-4 shows the normalized moment-curvature relationship and its bilinear idealization for a cantilever rectangular wall. Figure A-4(a) and (b) show relationships between the normalized moment, M_r, and the relative curvature, $\phi_y \ell_w$, with only ratios of distributed reinforcement of ρ_ℓ=*0.25%* and *0.50%*. The normalised flexural moment, M_r, is the ratio of the nominal moment, M_n, obtained with different values of axial load *(N≥0.0)* to the nominal bending moment, M_n, associated with no axial load *(N=0.0)*. Axial loads ratios vary between *0.0* and *0.10*. Figure A-4(c) and (d) exhibit the relationships when ratio of boundary reinforcement, ρ_b, is assigned at both ends of the wall. The wall also has a constant ratio of uniformly distributed reinforcement of ρ_ℓ=*0.25%*. All figures show that the relative curvature, $\phi_y \ell_w$, remains essentially constant independent of the quantity of ratios of distributed and boundary reinforcement.

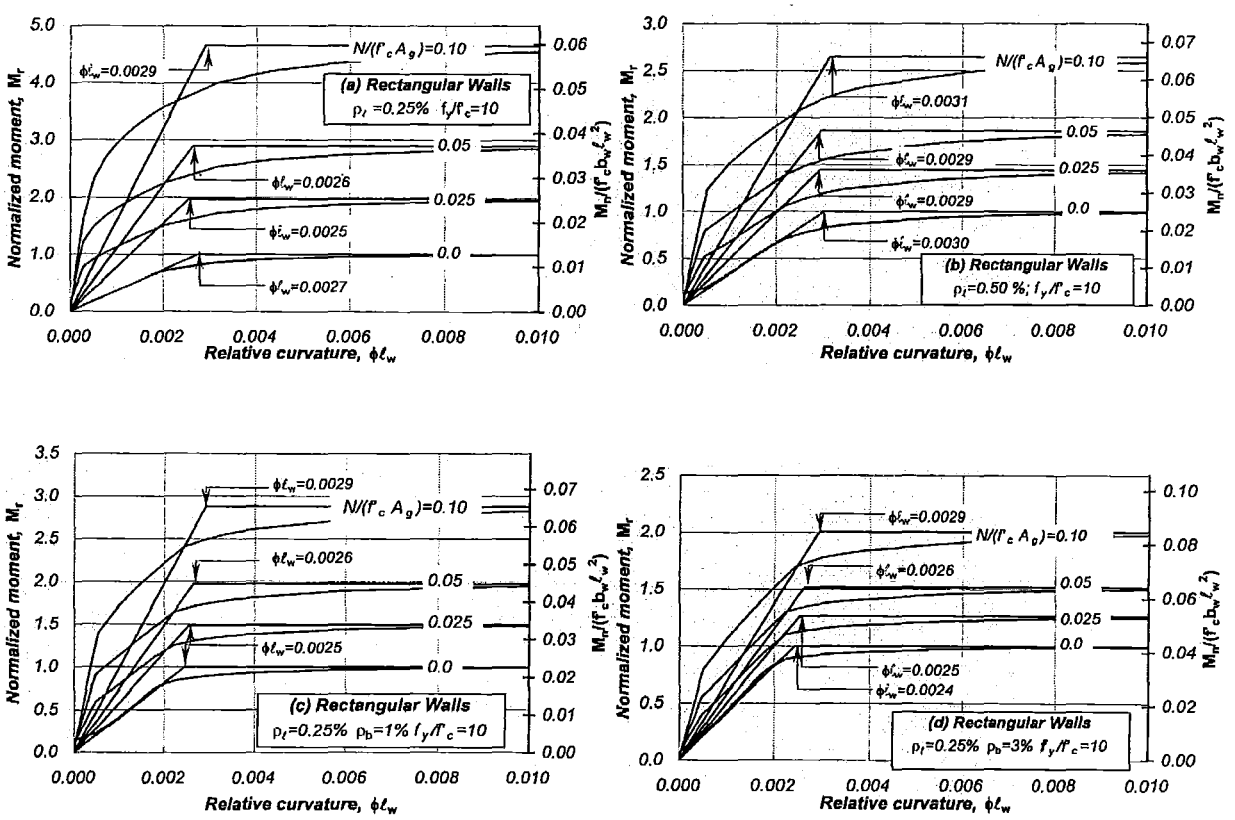

Figure A-4 Non-linear and idealized bilinear moment-curvature relationships

In summary, these analyses justify the curvature coefficient of $\eta \approx 2.0$ for rectangular walls, suggested in a previous study[P18]. It is applicable to walls with ratios of distributed reinforcement, ρ_ℓ, varying between *0.25%* and *1%*, and symmetric or asymmetric ratios of boundary reinforcement, ρ_ℓ. More precise values, if required, may be obtained from Table A-1 for axial load ratios of $N/(A_g f'_c)<0.075$.

A.3 "I" shape flanged symmetrical wall components

The study of "**I**" shape wall components assumes the same thickness of the wall flange, t_f, and web, t_w. The wall thickness is assumed to be approximately *6.3%* of the wall length. The ratios of wall length to flange length considered in this study are ℓ_w/b_f=*4.0, 2.0* and *1.0*. Reinforcement ratios of distributed and boundary reinforcement ratio are equal to those used for the rectangular wall. The boundary reinforcement at the end of the flanges is also calculated based on a concrete area of $0.10t_fb_f$. Figure A-1(b) shows the regions where distributed and boundary reinforcement are used. The ratio of reinforcement yield strength and concrete compressive strength remains the same, f_y/f'_c=*10*. The reinforcement yield strain used in this studies is ε_y=*0.0015*.

Figure A-5 shows the variation of the curvature coefficient for "**I**" shape walls with wall length to flange length ratios of ℓ_w/b_f=*4.0, 2.0,* and *1.0*. For convenience, these walls are denoted as **I**4, **I**2, and **I**1. The values of the curvature coefficient increases with a reduction of the length of the flange, b_f, i.e., with the increase of ℓ_w/b_f ratio. For instance, an axial compressive load ratio of *0.04* and ℓ_w/b_f ratios of *4.0, 2.0,* and *1.0,* leads to curvature coefficients of η=*1.55, 1.42* and *1.35* respectively. The curvature coefficient is expected to rise to a mean value of *2.0* when ℓ_w/b_f ratio reaches *16.0*, which corresponds to the curvature coefficient applicable to rectangular walls already studied. To detect the causes of differences of the curvature coefficient for walls with variable flange length and constant wall length, Table A-2 is presented. It summarizes the M_n/M_y and neutral axis depth to wall length ratios, ξ, of walls **I**1 and **I**4. It is seen that, these two parameters reduce with increasing axial force ratios in both **I**1 and **I**4 type walls. However, wall **I**4 exhibits a larger reduction of the neutral axis ratio, ξ, because of its short flange whereas wall **I**1 exhibits a larger reduction of the M_n/M_y ratio because it has a large concentration of reinforcement at the ends due to its long flanges. These lead to smaller values of the curvature coefficient for the **I**4 type wall than for the **I**1 type wall. In general, a wall component with flanges will reach its nominal yield curvature before a rectangular wall.

The assignment of boundary reinforcement with ratios of ρ_b=*1.0%, 2.0%* and *3.0%* to "**I**" type walls with distributed reinforcement ρ_ℓ=*0.50%* and axial load ratios, $N/(f'_c*A_g)$, between *0.0* and *0.10* did not modify the curvature coefficient obtained for walls having only distributed reinforcement ratio of ρ_ℓ=*0.50%*. This finding confirms, again, that the ratio of distributed reinforcement dominantly controls the curvature coefficient and that it is essentially unchanged by the boundary reinforcement ratio, ρ_b.

In summary, the compression flange of an "**I**" shape wall reduces the curvature coefficient to a mean value of η=*1.32±6%* for a wall to flange length of ℓ_w/b_f=*1.0*. A linear interpolation between *1.32* and *2.00* (curvature coefficient of a rectangular wall) can be used to obtain the curvature coefficient for "**I**" shape walls with ℓ_w/b_f ratios varying between *1.0* and *16.0*. This last corresponds to the ℓ_w/b_f ratio of a rectangular wall. The nominal yield curvature of a flanged wall component is smaller than that of a rectangular wall with the same length.

A.4 "T" shape wall components with the flange in compression

Figure A-1(c) illustrates a "**T**" shape wall component. It has wall to flange lengths ratios of ℓ_w/b_f=*4.0, 2.0,* and *1.0.* These walls types are denoted as **T4, T2,** and **T1**, respectively. The variation of the axial load ratio, $N/(f'_cA_g)$, and the ratio of reinforcement yield strength to concrete compressive strength, f_y/f'_c=*10*, remains the same.

Figure A-6 shows the variation of the curvature coefficient for "**T**" shape walls when its flange is in compression and ℓ_w/b_f ratios of *4.0, 2.0,* and *1.0.* For instance, an axial load ratio of *0.04* and ℓ_w/b_f ratios of *1.0* and *4.0* results in curvature coefficients of η=*1.35* to *1.60*, respectively. These values remain essentially constant for axial load ratios varying between *0.0* and *0.10.* In contrast, an axial tension load (*N<0.0*) generates a sudden increase of the curvature coefficient. The assignment of boundary reinforcement to the wall reduces this sudden increment of the curvature coefficient. This is because, as already explained, it generates an increase in the yield moment at a faster rate than the increase in nominal moment.

Table A-3 provides M_n/M_y ratios and neutral axis to length ratios, ξ, of wall types **T1** and **T4**. Variations are similar to those found for the "**I**" shape walls described in Section A.3.

The curvature coefficient for a "**T**" shape wall with its flange in compression and different, ℓ_w/b_f, ratios, can be simply obtained by linearly interpolating between *1.35* and *2.0*, the latter corresponding to the curvature coefficient for a rectangular wall.

A.5 "T" shape wall component with the flange in tension

Figure A-7 shows the variation of the curvature coefficient, η, for "**T**" shape walls with its flange in tension and ℓ_w/b_f ratios of *4.0, 2.0,* and *1.0.* These walls are the same as those already analysed in Section A.4, however, the moment direction is reversed. These walls are again denoted as **T4**, **T2**, and **T1**. For instance, an axial load ratio of *0.04* and ℓ_w/b_f ratios of *1.0, 2.0,* and *4.0* results in mean values of curvature coefficient of η=*2.1, 2.0,* and *1.9*, respectively. The increase of the axial load ratio, $N/(f'_cA_g)$, leads to a large increase of the curvature coefficient which becomes noticeable as the ℓ_w/b_f ratio reduces. As expected, the increase of the axial load ratio, $N/(f'_cA_g)$, generates on wall **T1** a greater increase of the curvature coefficient to η=*2.5.* Table A-4 summarises M_n/M_y ratios and neutral axis ratios, ξ, of walls types **T1** and **T4**. It is noted that the increase of the values of the curvature coefficient for wall **T1** with the flange in tension is primarily due to a significant reduction in the neutral axis depth to wall length ratio, ξ.

In summary, a "**T**" shaped wall with the flange in tension is associated with a larger curvature coefficient when compared to the same wall but with its flange in compression.

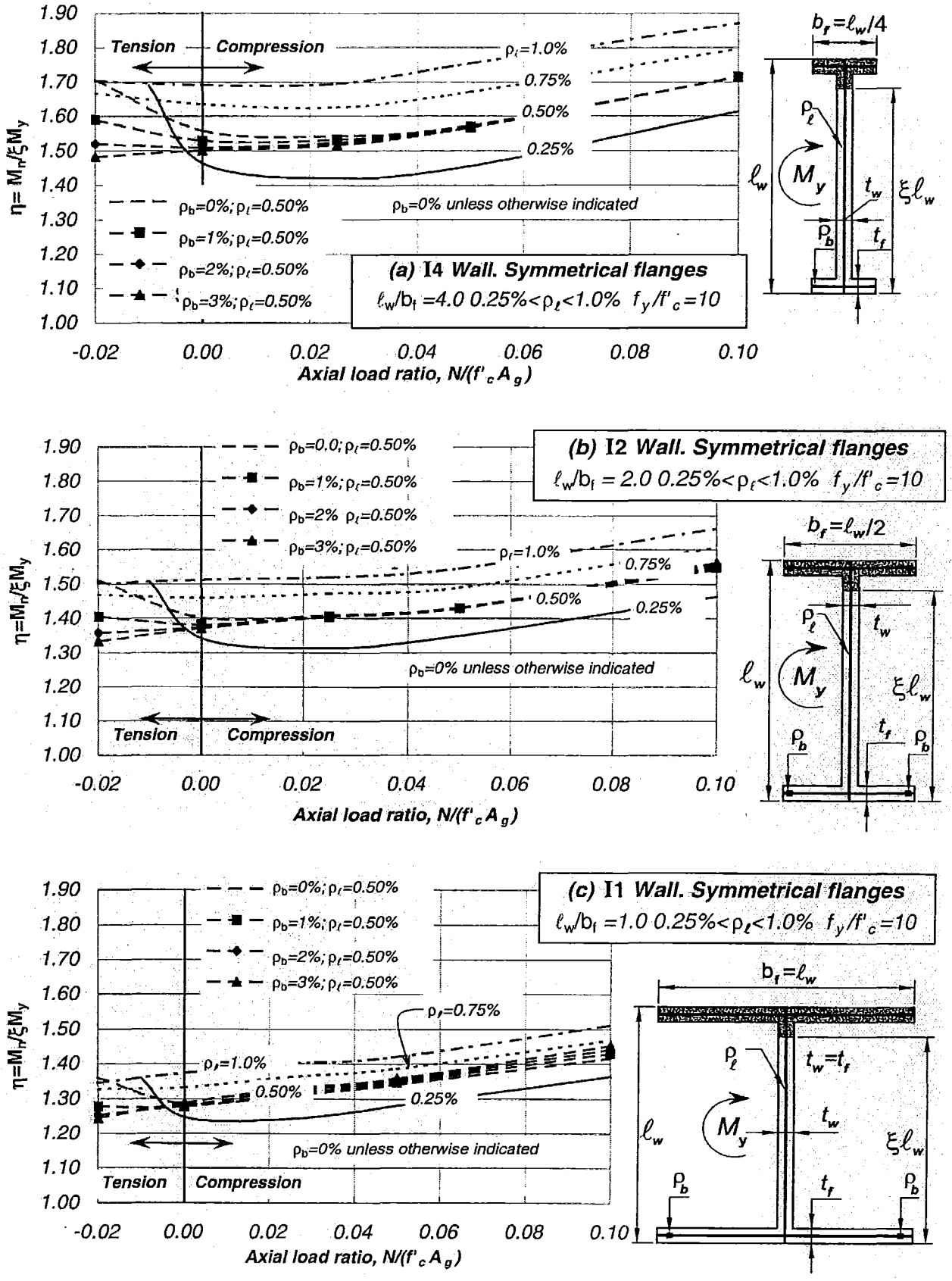

Figure A-5 Values of curvature coefficient, η, for "I" shape

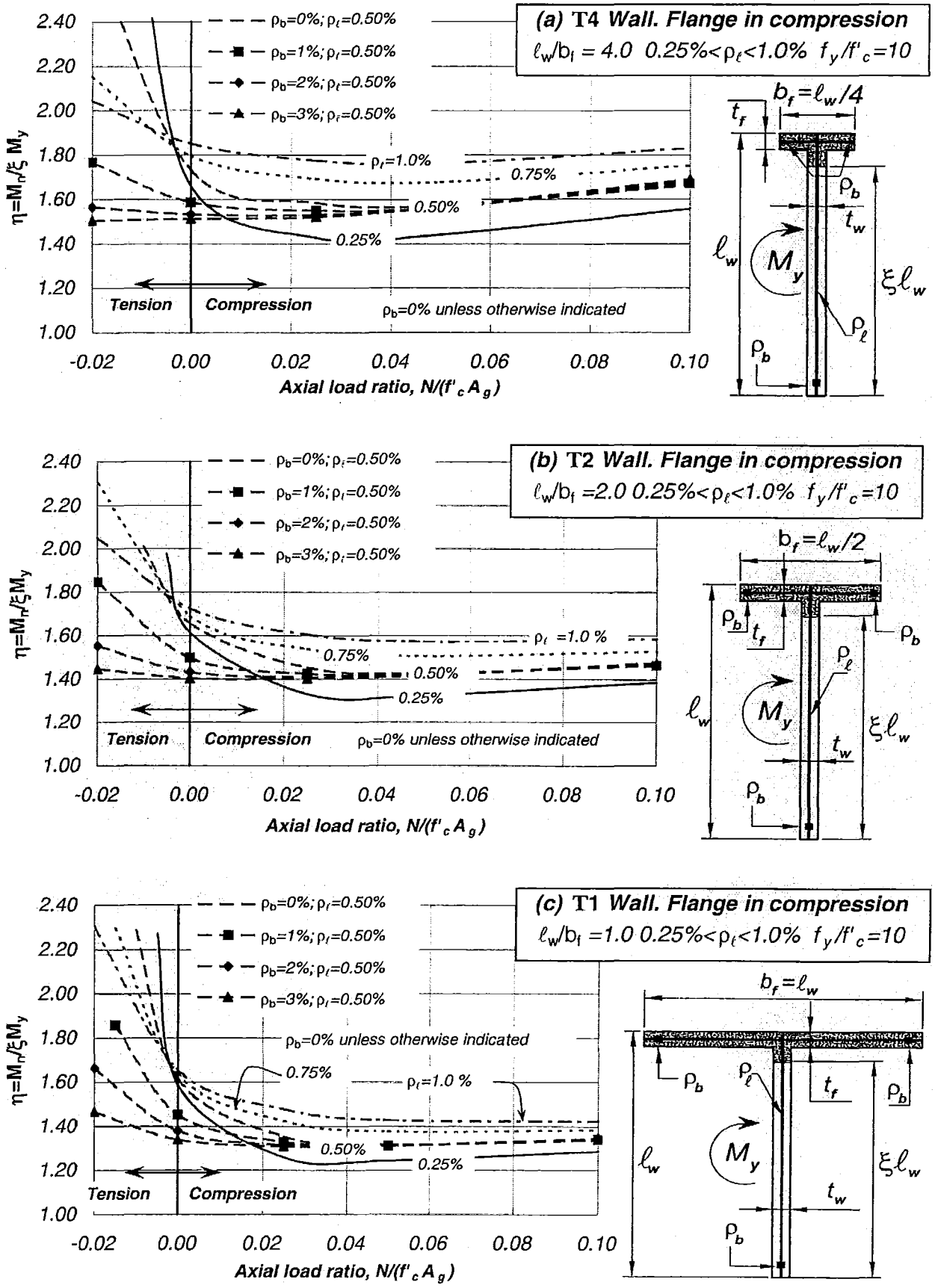

Figure A-6 Values of curvature coefficient, η, of "T" shape walls with the flange in compression

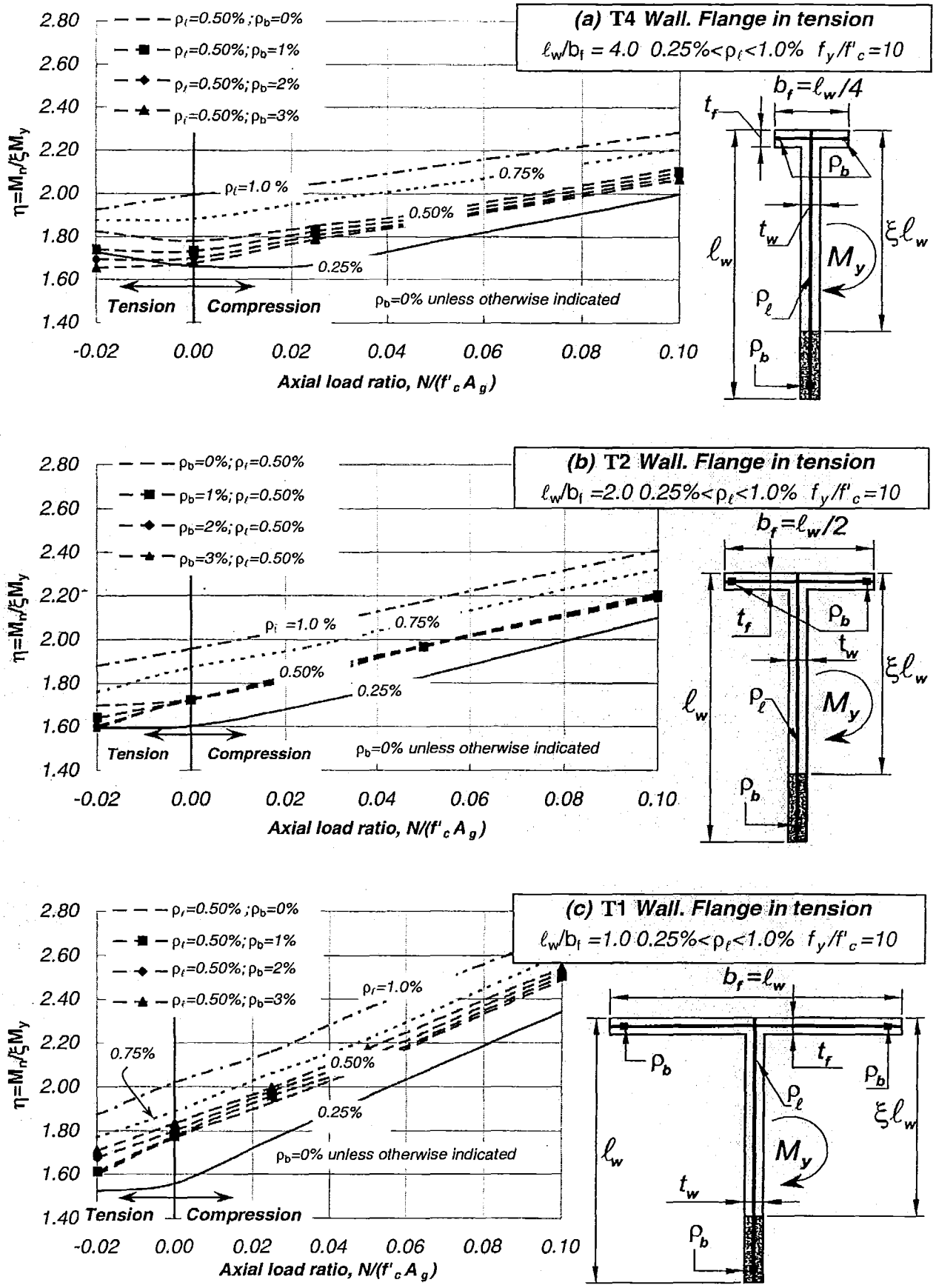

Figure A-7 Values of curvature coefficient, η, for "T" type walls with the flange in tension

Table A-2 Values of curvature coefficient, η, for "I" shape walls

(ℓ_w/b_f=4.0; t_f =t_w=0.063ℓ_w)							
$N/(f'_c*A_g)$	M_n/M_y	ξ	η	$N/(f'_c*A_g)$	M_n/M_y	ξ	η
	p_ℓ=0.25%	p_b=0.0%			p_ℓ=0.50%	p_b=0.0%	
-0.010	1.62	0.96	1.69	-0.020	1.61	0.94	1.71
0.000	1.34	0.92	1.46	0.000	1.37	0.88	1.56
0.025	1.20	0.85	1.42	0.025	1.27	0.82	1.54
0.050	1.15	0.79	1.46	0.050	1.22	0.77	1.57
0.100	1.15	0.71	1.61	0.100	1.20	0.70	1.71
	p_ℓ=0.50%	p_b=1.0%			p_ℓ=0.50%	p_b=3.0%	
-0.020	1.48	0.93	1.59	-0.020	1.35	0.91	1.48
0.000	1.34	0.87	1.53	0.000	1.29	0.86	1.50
0.025	1.25	0.82	1.53	0.025	1.22	0.81	1.52
0.050	1.21	0.77	1.57	0.050	1.19	0.76	1.57
0.100	1.19	0.70	1.71	0.100	1.19	0.69	1.71

(ℓ_w/b_f=1.0; t_f =t_w=0.063ℓ_w)							
$N/(f'_c*A_g)$	M_n/M_y	ξ	η	$N/(f'_c*A_g)$	M_n/M_y	ξ	η
	p_ℓ=0.25%	p_b=0.0%			p_ℓ=0.50%	p_b=0.0%	
-0.010	1.32	0.97	1.36	-0.020	1.31	0.96	1.36
0.000	1.17	0.94	1.25	0.000	1.18	0.92	1.28
0.025	1.11	0.89	1.24	0.025	1.14	0.87	1.31
0.050	1.09	0.85	1.28	0.050	1.12	0.83	1.34
0.100	1.06	0.78	1.36	0.100	1.08	0.77	1.42
	p_ℓ=0.50%	p_b=1.0%			p_ℓ=0.50%	p_b=3.0%	
-0.020	1.21	0.94	1.28	-0.020	1.14	0.92	1.24
0.000	1.16	0.91	1.28	0.000	1.14	0.89	1.29
0.025	1.14	0.86	1.31	0.025	1.13	0.85	1.33
0.050	1.11	0.83	1.35	0.050	1.10	0.81	1.36
0.100	1.09	0.76	1.43	0.100	1.09	0.75	1.45

Table A-3 Values of curvature coefficient, η, for "T" shape walls with flange in compression

(ℓ_w/b_f=4.0 t_f =t_w=0.063ℓ_w)							
$N/(f'_c*A_g)$	M_n/M_y	ξ	η	$N/(f'_c*A_g)$	M_n/M_y	ξ	η
ρ_ℓ=0.25%		ρ_b=0.0%		ρ_ℓ=0.50%		ρ_b=0.0%	
-0.010	2.67	0.99	2.68	-0.020	2.68	0.99	2.71
0.000	1.55	0.93	1.66	0.000	1.57	0.91	1.73
0.025	1.24	0.87	1.43	0.025	1.34	0.85	1.58
0.050	1.17	0.82	1.44	0.050	1.26	0.80	1.57
0.100	1.15	0.74	1.56	0.100	1.21	0.73	1.66
ρ_ℓ=0.50%		ρ_b=1.0%		ρ_ℓ=0.50%		ρ_b=3.0%	
-0.020	1.66	0.94	1.77	-0.020	1.35	0.90	1.50
0.000	1.41	0.89	1.59	0.000	1.29	0.86	1.51
0.025	1.29	0.83	1.55	0.025	1.23	0.81	1.52
0.050	1.24	0.79	1.56	0.050	1.21	0.77	1.56
0.100	1.21	0.72	1.67	0.100	1.19	0.71	1.69

(ℓ_w/b_f=1.0 t_f =t_w=0.063ℓ_w)							
$N/(f'_c*A_g)$	M_n/M_y	ξ	η	$N/(f'_c*A_g)$	M_n/M_y	ξ	η
ρ_ℓ=0.25%		ρ_b=0.0%		ρ_ℓ=0.50%		ρ_b=0.0%	
-0.005	2.23	0.98	2.27	-0.010	2.23	0.98	2.28
0.000	1.53	0.96	1.59	0.000	1.54	0.95	1.61
0.025	1.16	0.92	1.26	0.025	1.24	0.92	1.36
0.050	1.11	0.89	1.24	0.050	1.17	0.89	1.32
0.100	1.07	0.84	1.29	0.100	1.11	0.83	1.34
ρ_ℓ=0.50%		ρ_b=1.0%		ρ_ℓ=0.50%		ρ_b=3.0%	
-0.015	1.81	0.98	1.86	-0.020	1.41	0.96	1.47
0.000	1.37	0.94	1.45	0.000	1.25	0.93	1.34
0.025	1.21	0.91	1.33	0.025	1.18	0.90	1.31
0.050	1.16	0.88	1.31	0.050	1.15	0.87	1.31
0.100	1.11	0.83	1.34	0.100	1.11	0.82	1.35

Table A-4 values of the curvature coefficient, η, for "T" shape walls with the flange in tension

(ℓ_w/b_f=4.0; t_f =t_w=0.063ℓ_w)							
$N/(f'_c*A_g)$	M_n/M_y	ξ	η	$N/(f'_c*A_g)$	M_n/M_y	ξ	η
p_ℓ=0.25%		p_b=0.0%		p_ℓ=0.50%		p_b=0.0%	
-0.020	1.57	0.91	1.73	-0.020	1.61	0.88	1.83
0.000	1.41	0.85	1.66	0.000	1.42	0.80	1.78
0.025	1.27	0.76	1.67	0.025	1.36	0.73	1.85
0.050	1.25	0.71	1.78	0.050	1.31	0.68	1.92
0.100	1.24	0.62	2.00	0.100	1.30	0.61	2.12
p_ℓ=0.50%		p_b=1.0%		p_ℓ=0.50%		p_b=3.0%	
-0.020	1.51	0.87	1.74	-0.020	1.39	0.84	1.65
0.000	1.37	0.79	1.73	0.000	1.31	0.78	1.68
0.025	1.33	0.73	1.83	0.025	1.30	0.73	1.79
0.050	1.30	0.68	1.90	0.050	1.28	0.68	1.87
0.100	1.29	0.61	2.10	0.100	1.27	0.61	2.07

(ℓ_w/b_f=1.0; t_f =t_w=0.063ℓ_w)							
$N/(f'_c*A_g)$	M_n/M_y	ξ	η	$N/(f'_c*A_g)$	M_n/M_y	ξ	η
p_ℓ=0.25%		p_b=0.0%		p_ℓ=0.50%		p_b=0.0%	
-0.020	1.31	0.86	1.52	-0.020	1.29	0.81	1.60
0.000	1.23	0.79	1.56	0.000	1.28	0.72	1.77
0.025	1.22	0.69	1.76	0.025	1.26	0.65	1.93
0.050	1.23	0.63	1.96	0.050	1.25	0.60	2.09
0.100	1.25	0.53	2.34	0.100	1.29	0.52	2.49
p_ℓ=0.50%		p_b=1.0%		p_ℓ=0.50%		p_b=3.0%	
-0.020	1.23	0.76	1.61	-0.020	1.21	0.71	1.71
0.000	1.24	0.70	1.78	0.000	1.20	0.66	1.83
0.025	1.24	0.64	1.96	0.025	1.21	0.61	2.00
0.050	1.23	0.58	2.11	0.050	1.23	0.56	2.17
0.100	1.28	0.51	2.51	0.100	1.27	0.50	2.54

Appendix B. Properties of Single-Mass Asymmetric Systems

B.1 Introduction

This appendix describes how to obtain the properties of asymmetric single-mass two-element systems. It also summarizes the properties and general characteristics of systems examined in this study.

In case of two-element systems, properties of strength, stiffness and nominal yield displacement of elements and their location can be readily established for predefined uncoupled translational and rotational periods of free vibration and a given nominal yield displacement of the system. The derivation of these idealised systems was used to examine the effect that a range of realistic set of properties may have on torsional response of ductile systems.

Properties of multi-element systems may vary depending on the assignment of strength to the elements. As explained in Section 2.11.4, there are an infinite number of strength distributions among elements of multi-element systems satisfying zero strength eccentricity and therefore no expressions were derived.

B.2 Properties of asymmetric two-element systems

Figure B-1 shows a torsionally restrained two-element system. Its fundamental properties can be derived once the required uncoupled translational and rotational periods (T_s and T_θ) and nominal yield displacement of the system, Δ_{ys}, along the principal axes, is established.

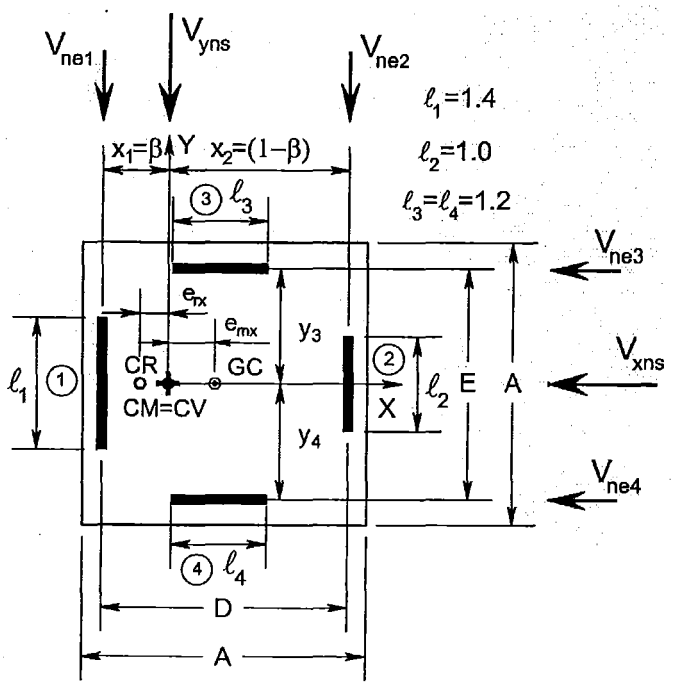

Figure B-1. Two-element torsionally restrained system

The translational stiffness of the system along the X and Y-axes associated with selected values of uncoupled translational periods are:

$$K_{ys} = 4\pi^2 \frac{M_e}{T_y^2} \text{ and } K_{xs} = 4\pi^2 \frac{M_e}{T_x^2} \quad \textbf{(B-1)}$$

The system strength necessary to attain the required uncoupled translational periods of free vibration, is derived using predefined values of system nominal yield displacement along the principal axes.

$$V_{yns} = K_{ys}\Delta_{ys} \text{ and } V_{xns} = K_{xs}\Delta_{xs} \quad \textbf{(B-2)}$$

The location of the elements from the centre of mass is obtained after the radius of gyration of element stiffness is derived. This property is readily obtained by specifying a required ratio of uncoupled translational and rotational period of free vibration. Note that the rotational period of the system considers only parallel elements along a given direction without including the stiffness of the transverse elements. The radius of gyration of stiffness is obtained once the radius of gyration of mass is known.

$$r_{ky} = \frac{T_y}{T_\theta} r_m \quad \textbf{(B-3)}$$

A relationship between radii of gyration of stiffness and strength is readily derived because stiffness is strength dependant. The radius of gyration of element stiffness may be also estimated by specifying a preferred ratio of radii of gyration of strength and mass.

$$r_{ky} = \frac{\alpha^2}{[\alpha + \beta(1-\alpha)]} r_{vy} \quad \textbf{(B-4)}$$

where $\alpha=\Delta_{ye2}/\Delta_{ye1}$ and β are defined in Figure B1.

The distance 'D' between Y-direction elements *(1)* and *(2)*, as a function of the radius of gyration of stiffness and the ratio of nominal yield displacement of the elements, $\alpha=\Delta_{ye2}/\Delta_{ye1}$, is

$$D = \frac{(1+\alpha)}{\sqrt{\alpha}} r_{ky} \quad \textbf{(B-5)}$$

The location of elements *(1)* and *(2)* from the centre of mass, considering the notation shown in Figure B-1, is

$$x_1 = \beta D \text{ and } x_2 = (1-\beta)D \quad \textbf{(B-6)}$$

Noting that

$$K_{ys} = k_1 + k_2 = \frac{V_{n1}}{\Delta_{y1}} + \frac{V_{n2}}{\Delta_{y2}} \tag{B-7}$$

$$\Delta_{y1} \propto \frac{1}{\ell_1} \qquad \Delta_{y2} \propto \frac{1}{\ell_2} \qquad \alpha = \frac{\Delta_{y2}}{\Delta_{y1}} \propto \frac{\ell_1}{\ell_2} \tag{B-8}$$

The nominal strength of the elements satisfying static equilibrium is

$$V_{n1} = (1-\beta)V_{yns} \tag{B-9}$$

$$V_{n2} = \beta V_{yns} \tag{B-10}$$

and the nominal yield displacement are

$$\Delta_{y1} = \left((1-\beta) + \frac{\beta}{\alpha}\right)\Delta_{ys} \tag{B-11}$$

$$\Delta_{y2} = \alpha\Delta_{y1} \tag{B-12}$$

The stiffness of the elements is expressed as,

$$k_1 = \frac{V_{n1}}{\Delta_{y1}} = \left(\frac{\alpha(1-\beta)}{\alpha(1-\beta)+\beta}\right)K_{ys} \tag{B-13}$$

$$k_2 = \frac{V_{n2}}{\Delta_{y2}} = \left(\frac{\beta}{\alpha+\beta(1-\alpha)}\right)K_{ys} \tag{B-14}$$

and the stiffness eccentricity associated with zero strength eccentricity is,

$$e_{rx} = \frac{\alpha x_2 - x_1}{(1+\alpha)} \tag{B-15}$$

In case of restrained systems being symmetric along the *X*-axis, the distance '*E*' between *X*-direction elements *(3)* and *(4)* and its location is obtained in a similar manner. The only difference is that the radii of gyration of stiffness and strength are the same since $\alpha=\Delta_{ye4}/\Delta_{ye3}=1.0$.

$$r_{kx} = \frac{T_x}{T_\theta} r_m = r_{vx} \tag{B-16}$$

$$E = 2r_{kx} \tag{B-17}$$

$$y_3 = y_4 = 0.5E \tag{B-18}$$

The nominal strength of the elements satisfying static equilibrium is

$$V_{n3} = V_{n4} = 0.5V_{xns} \tag{B-19}$$

The nominal yield displacement of *X*-direction elements *(3)* and *(4)* is

$$\Delta_{y3} = \Delta_{y4} = \Delta_{ys} \tag{B-20}$$

and their stiffness is

$$k_3 = k_4 = 0.5K_{xs} \tag{B-21}$$

The strength and stiffness eccentricity are zero.

B.3 Properties and general characteristics of the structural systems used in this thesis

Table B-1. Dimensions and properties of *System 1*

System dimension and element location					
Weight	A	B	D=0.82A	E=0.82A	β=0.5D
(kN)	(m)	(m)	(m)	(m)	(m)
1766	15.0	15.0	12.25	12.25	6.12

System properties along the Y and X-axes								
Sys	T_y	e_v/D	e_r/D	V_{ns}	K_s	Δ_{ys}	$r_{vy}/r_m=r_{ky}/r_m$	$r_{vx}/r_m=r_{kx}/r_m$
	(sec)			(kN)	(kN/m)	(mm)		
TU	1.3	0.00	0.00	176.6	4204.8	42.0	1.00	0.00
TR		"	"	"	"	"	"	1.00
TU	0.5	0.00	0.00	440.6	28424.5	15.5	"	0.00
TR		"	"	"	"	"	"	1.00

Properties of Y-direction elements (1) and (2)								
System	T_y	α	Δ_{y1}	Δ_{y2}	V_1	V_2	k_1	k_2
	(sec)	Δ_{y2}/Δ_{y1}	(mm)	(mm)	(kN)	(kN)	(kN/m)	(kN/m)
TU & TR	1.3	1.00	42.0	42.0	88.3	88.3	2102.4	2102.4
TU & TR	0.5	1.00	15.5	15.5	220.3	220.3	14212.2	14212.2

Properties of X-direction elements (3) and (4)								
Sys	T_x	α	Δ_{y3}	Δ_{y4}	V_{n3}	V_{n4}	k_3	k_4
	(sec)	Δ_{y4}/Δ_{y3}	(mm)	(mm)	(kN)	(kN)	(kN/m)	(kN/m)
TU	1.3	0.00	42.0	----------	176.6	----------	4204.8	----------
TR		1.00	42.0	42.0	88.3	88.3	2102.4	2102.4
TU	0.5	0.00	15.5	----------	440.6	----------	28424.5	----------
TR		1.00	15.5	15.5	220.3	220.3	14212.2	14212.2

Table B-2. Dimensions and properties of *System 2*

System dimension and element location					
Weight	A	B	D=0.99A	E=0.90A	β=0.3D
(kN)	(m)	(m)	(m)	(m)	(m)
1766	15.0	15.0	14.85	13.50	4.45

System properties along the Y and X-axes								
Sys	T_y	e_v/D	e_r/D	V_{ns}	K_s	Δ_{ys}	$r_{vy}/r_m=r_{ky}/r_m$	$r_{vx}/r_m=r_{kx}/r_m$
	(sec)			(kN)	(kN/m)	(mm)		
TU	1.3	0.00	0.00	176.6	4204.8	42.0	1.00	0.00
TR		"	"	"	"	"	"	1.00
TU	0.5	0.00	0.00	440.6	28424.5	15.5	"	0.00
TR		"	"	"	"	"	"	1.00

Properties of Y-direction elements (1) and (2)								
Sys	T_y	α	Δ_{y1}	Δ_{y2}	V_1	V_2	k_1	k_2
	(sec)	Δ_{y2}/Δ_{y1}	(mm)	(mm)	(kN)	(kN)	(kN/m)	(kN/m)
TU & TR	1.3	1.00	42.0	42.0	123.6	53.0	2943.4	1261.4
TU & TR	0.5	1.00	15.5	15.5	308.4	132.2	19897.1	8527.3

Properties of X-direction elements (3) and (4)								
Sys	T_x	α	Δ_{y3}	Δ_{y4}	V_{n3}	V_{n4}	k_3	k_4
	(sec)	Δ_{y4}/Δ_{y3}	(mm)	(mm)	(kN)	(kN)	(kN/m)	(kN/m)
TU	1.3	0.00	42.0	----------	176.6	----------	4204.8	----------
TR		1.00	42.0	42.0	88.3	88.3	2102.4	2102.4
TU	0.5	0.00	15.5	----------	440.6	----------	28424.5	----------
TR		1.00	15.5	15.5	220.3	220.3	14212.2	14212.2

Table B-3 Dimensions and properties of *Systems 3, 4, 5*

System dimension and element location									
Sys	Weight	A	B	D	E	β=0.5D	r_{vx}/r_m	r_{ky}/r_m	$r_{vx}/r_m=r_{kx}/r_m$
	(kN)	(m)	(m)	(m)	(m)	(m)			
3	1766	15.0	15.0	(0.83A)12.42	(0.83A)12.42	6.21	1.014	1.00	1.014
4	"	21.21	10.61	21.21	10.61	10.61	1.54	1.51	0.76
5	"	10.61	21.21	10.61	21.21	5.30	0.76	0.76	1.54

System properties along the Y and X-axes							
Sys	T_y	e_y/D	e_{rx}/D	e_{ry}/D	V_{ns}	K_s	Δ_{ys}
	(sec)				(kN)	(kN/m)	(mm)
TU	1.3	0.00	-0.083	0.00	176.6	4204.8	42.0
TR		"	"	"	"	"	"
TU	0.5	"	"	"	440.6	28424.5	15.5
TR		"	"	"	"	"	"

Properties of Y-direction elements (1) and (2)								
Sys	T_y	α	Δ_{y1}	Δ_{y2}	V_1	V_2	k_1	k_2
	(sec)	Δ_{y2}/Δ_{y1}	(mm)	(mm)	(kN)	(kN)	(kN/m)	(kN/m)
TU & TR	1.3	1.40	36.0	50.4	88.3	88.3	2452.8	1752
TU & TR	0.5	1.40	13.3	18.6	220.3	220.3	16580.9	11843.5

Properties of X-direction elements (3) and (4)								
Sys	T_x	α	Δ_{y3}	Δ_{y4}	V_{n3}	V_{n4}	k_3	k_4
	(sec)	Δ_{y4}/Δ_{y3}	(mm)	(mm)	(kN)	(kN)	(kN/m)	(kN/m)
TU	1.3	0.00	42.0	----------	176.6	----------	4204.8	----------
TR		1.00	42.0	42.0	88.3	88.3	2102.4	2102.4
TU	0.5	0.00	15.5	----------	440.6	----------	28424.5	----------
TR		1.00	15.5	15.5	220.3	220.3	14212.2	14212.2

α	Δ_{ye1}	Δ_{ye2}	Δ_{ys}	ℓ_1	ℓ_2	$\ell_{tot}=\ell_1+\ell_2$
$\Delta_{ye2}/\Delta_{ye1}$	(mm)			Relative length		
1.0	42.0	42.0	42.0	1.20	1.20	2.4
1.2	38.5	46.2	42.0	1.31	1.09	"
1.4	36.0	50.4	42.0	1.40	1.00	"
1.6	31.1	54.6	42.0	1.48	0.92	"
2.0	31.5	63.0	42.0	1.60	0.80	"
2.5	29.4	73.5	42.0	1.71	0.69	"
4.0	26.3	105.0	42.0	1.92	0.48	"

Table B-4 Dimensions and properties of *System 6*

System dimension and element location					
Weight	A	B	D=0.99A	E=0.90A	β=0.3D
(kN)	(m)	(m)	(m)	(m)	(m)
1766	15.0	15.0	14.85	13.50	4.45

System properties along the Y and X-axes										
Sys	T_y	e_y/D	e_{rx}/D	e_{ry}/D	V_{ns}	K_s	Δ_{ys}	r_{vy}/r_m	r_{ky}/r_m	$r_{vx}/r_m=r_{kx}/r_m$
	(sec)				(kN)	(kN/m)	(mm)			
TU	1.3	0.00	-0.066	0.00	176.6	4204.8	42.0	1.00	0.92	0.00
TR		"	"	"	"	"	"	"	"	1.00
TU	0.5	"	"	"	440.6	28424.5	15.5	"	"	0.00
TR		"	"	"	"	"	"	"	"	1.00

Properties of Y-direction elements (1) and (2)								
Sys	T_y	α	Δ_{y1}	Δ_{y2}	V_1	V_2	k_1	k_2
	(sec)	Δ_{y2}/Δ_{y1}	(mm)	(mm)	(kN)	(kN)	(kN/m)	(kN/m)
TU & TR	1.3	1.40	38.4	53.8	123.6	53.0	3219.3	985.5
TU & TR	0.5	1.40	14.2	19.8	308.4	132.2	21762.5	6662

Properties of X-direction elements (3) and (4)								
Sys	T_x	α	Δ_{y3}	Δ_{y4}	V_{n3}	V_{n4}	k_3	k_4
	(sec)	Δ_{y4}/Δ_{y3}	(mm)	(mm)	(kN)	(kN)	(kN/m)	(kN/m)
TU	1.3	0.00	42.0	----------	176.6	----------	4204.8	----------
TR		1.00	42.0	42.0	88.3	88.3	2102.4	2102.4
TU	0.5	0.00	15.5	----------	440.6	----------	28424.5	----------
TR		1.00	15.5	15.5	220.3	220.3	14212.2	14212.2

Table B-5 Dimensions and properties of one-element *Systems 7, 8 and 9*

System dimension and element location									
Sys	Weight	A	B	D	E	β=0.5D	e_{vx}/r_m	$r_{vy}/r_m=r_{ky}/r_m$	$r_{vx}/r_m=r_{kx}/r_m$
	(kN)	(m)	(m)	(m)	(m)	(m)			
7	1766	15.0	15.0	(0.83A)12.42	(0.83A)12.42	6.21	1.00	0.00	1.014
8	"	21.21	10.61	21.21	10.61	10.61	1.54	0.00	"
9	"	10.61	21.21	10.61	21.21	5.3	0.76	0.00	"

System properties along the Y and X-axes							
Sys	T_y	e_{vx}/D	e_{rx}/D	$e_{vy}/D=e_{ry}/D$	V_{ns}	K_s	Δ_{ys}
	(sec)				(kN)	(kN/m)	(mm)
TU	1.3	-0.5	-0.5	0.00	176.6	4204.8	42.0
TR		"	"	"	"	"	"

Properties of Y-direction element (1)				
Sys	T_y	Δ_{y1}	V_1	k_1
	(sec)	(mm)	(kN)	(kN/m)
TU & TR	1.3	42	176.6	4204.8

Properties of X-direction elements (3) and (4)								
Sys	T_x	α	Δ_{y3}	Δ_{y4}	V_{n3}	V_{n4}	k_3	k_4
	(sec)	Δ_{y4}/Δ_{y3}	(mm)	(mm)	(kN)	(kN)	(kN/m)	(kN/m)
TU	1.3	0.00	42	----------	176.6	----------	4204.8	----------
TR		1.00	42	42	88.3	88.3	2102.4	2102.4

Table B-6 Properties of three-element systems *System 10*

System dimension and element location								
Sys	Weight	A	B	x_1=0.5A	x_2=0.14A	x_3=0.5A	y_4=0.5B	y_5=0.5B
	(kN)	(m)	(m)	(m)	(m)	(m)	(m)	(m)
10	3139	20.0	20.0	10.0	2.8	10.0	10.0	10.0

System properties along the Y and X-axes										
Sys	T_y	e_y/D	e_{rx}/D	e_{ry}/D	V_{ns}	K_s	Δ_{ys}	r_{vy}/r_m	r_{ky}/r_m	$r_{vx}/r_m=r_{kx}/r_m$
	(sec)				(kN)	(kN/m)	(mm)			
TU	1.3	0.0	-0.054	0.00	314.0	7475	42.0	0.78	0.63	0.00
TR		"	"	"	"	"	"	"	"	1.22

Properties of Y-direction elements (1), (2) and (3)										
Sys	T_y	Δ_{y1}	Δ_{y2}	Δ_{y3}	V_{n1}	V_2	V_3	k_1	K_2	k_3
	(sec)	(mm)	(mm)	(mm)	(kN)	(kN)	(kN)	(kN/m)	(kN/m)	(kN/m)
TU & TR	1.3	69.0	34.0	69.0	29.7	198.9	85.4	432.6	5798.3	1244.3

Properties of X-direction elements (4) and (5)							
Sys	T_x	Δ_{y4}	Δ_{y5}	V_{n4}	V_{n5}	k_4	K_5
	(sec)	(mm)	(mm)	(kN)	(kN)	(kN/m)	(kN/m)
TU	1.3	42.0	----------	314.0	----------	7476	----------
TR		42.0	42.0	157.0	157.0	3737.5	3737.5

Table B-7 Dimensions and properties of four-element *System 11*

System dimension and element location									
Sys	Weight	A	B	x_1=0.5A	x_2=0.17A	x_3=0.17A	x_4=0.5A	y_5=0.5B	y_6=0.5B
	(kN)	(m)	(m)	(m)	(m)	(m)	(m)	(m)	(m)
11	3463	21.0	21.0	10.5	3.5	3.5	10.5	10.5	10.5

System properties along the Y and X-axes										
Sys	T_y	e_y/D	e_{rx}/D	e_{ry}/D	V_{ns}	K_s	Δ_{ys}	r_{vy}/r_m	r_{ky}/r_m	r_{vx}/r_m=r_{kx}/r_m
	(sec)				(kN)	(kN/m)	(mm)			
TU	1.3	0.00	-0.047	0.00	346.1	8241.4	42.0	1.05	1.10	0.0
TR		"	"	"	"	"	"	"	"	1.22

Properties of Y-direction elements (1), (2), (3) and (4)													
Sys	T_y	Δ_{y1}	Δ_{y2}	Δ_{y3}	Δ_{y4}	V_{n1}	V_{n2}	V_{n3}	V_{n4}	k_1	k_2	k_3	k_4
	(sec)	(mm)	(mm)	(mm)	(mm)	(kN)	(kN)	(kN)	(kN)	(kN/m)	(kN/m)	(kN/m)	(kN/m)
TU & TR	1.3	33.9	67.8	53.8	42.7	127	37	66	117	3738	539	1222	2743

Properties of X-direction elements (5) and (6)							
Sys	T_x	Δ_{y5}	Δ_{y6}	V_{n5}	V_{n6}	K_5	K_6
	(sec)	(mm)	(mm)	(kN)	(kN)	(kN/m)	(kN/m)
TU	1.3	42.0	----------	346.1	----------	8241.4	----------
TR		42.0	42.0	173.0	173.0	4121	4121

Appendix C. Shake Table Characteristics and Properties of Fuses

C.1 Characteristics of the unidirectional shake table and its actuator

Table C-1. Characteristics of the shake table [A1]

Plan Area	2 m x 4 m
Height above ground	700 mm
Material	Steel
Weight	2.4E+03 kg
Maximum travel	300 mm
Natural frequency(unloaded)	20 Hz
Maximum out of plane deflection under design loadings	0.44 mm
Maximum stress under design loadings	28 MPa (+) 45 MPa (-)
Support details	4 Glacier DU Bearings on stationary shaft (100mm dia) along either side of the table
Table top	12 mm steel plate
Longitudinal stiffeners	4 – 410 UB 54
Transverse stiffeners	12 mm full depth steel plate at 500 mm intervals
Hole pattern	Drilled and taped for M12 bolts at 250 mm centres lengthwise and 125 mm centres transversely

Table C-2. Characteristics of the actuator Dartec M1000/A [A1]

Static capacity	+- 250 kN
Dynamic capacity	+-200 kN
Total stroke	300 mm
Effective piston area	9677 mm2
Servovalve rating	2 x 230 l/m
Maximum velocity attainable	1 m/s
Supply pressure	300 bar

C.1 Properties of fuses

Table C-3. Properties of 5.0 and 6.0 mm thick fuses

		5x46		5x76		6x50	
		Analytical	Experimental	Analytical	Experimental	Analytical	Experimental
M_y	(N-m)	55	NA	90	NA	86	NA
M_p	(N-m)	82.5	NA	135	NA	129	NA
M_u	(N-m)	118	127	195	200	194	200
ϕ'_{yf}	(1/m)	0.570	1.02	0.57	1.17	0.475	0.975
θ'_{yf}	(rad)	0.00285	0.0051	0.00285	0.00584	0.00237	0.00486
θ_{yf}	(rad)	0.00611	0.011	0.00611	0.0125	0.00536	0.011
$k_{\theta f}$	(N-m/rad)	19167	10727	31667	15464	36000	17533
I_e / I_g			0.560		0.488		0.487

M_y: yield moment, M_p: plastic moment, M_u: ultimate moment after strain hardening; ϕ'_y: Yield curvature, θ'_y: yield rotation, θ_y: nominal yield displacement, k_θ^f: rotational stiffness, and I_e:and I_g effective and gross second moment of area

Table C-4. Properties of 7.0 mm thick elastic fuses

		7x38		7x57	
		Analytical	Experimental	Analytical	Experimental
M_y	(N-m)	88	NA	133	NA
M_p	(N-m)	132	NA	199.5	NA
M_u	(N-m)	191	184	287	313
ϕ'_{yf}	(1/m)	0.407	1.03	0.407	1.16
θ'_{yf}	(rad)	0.00204	0.00515	0.00204	0.00581
θ_{yf}	(rad)	0.00443	0.0111	0.00448	0.0127
$k_{\theta f}$	(N-m/rad)	43447	17206	65170	22869
I_e / I_g			0.396		0.351

Table C-5. Properties of 8.4 and 9.8 mm thick elastic fuses.

		8.4x50		9.8x50	
		Analytical	Experimental	Analytical	Experimental
M_y	(N-m)	168	NA	228	NA
M_p	(N-m)	252	NA	342	NA
M_u	(N-m)	362	378	493	513
ϕ'_{yf}	(1/m)	0.339	1.09	0.291	1.25
θ'_{yf}	(rad)	0.0017	0.0055	0.0014	0.006
θ_{yf}	(rad)	0.0037	0.0119	0.0031	0.0133
$k_{\theta f}$	(N-m/rad)	98784	30710	156865	36590
I_e / I_g			0.311		0.233

Appendix D. Design Example

D.1 General

An example is provided to illustrate the application of the seismic design procedure described in Chapter 6. It shows how to estimate the displacement and ductility capacity of an asymmetric multi-storey building, the nominal strength and the strength distribution among the elements necessary to limit displacement demands to less than their displacement ductility capacity. The building strength is determined using a force-based design method [S7].

The objective of using an asymmetric multi-storey building is to show that the system may be modelled as a simplified single-mass system. The seismic mass of the multi-storey system is assumed concentrated at the effective height and the lateral force resisting elements may be simulated as substitute rectangular wall elements having the same strength and nominal yield displacement as those of the actual structural elements.

D.2 Description of the torsionally restrained system

The building shown in Figure D-1 is a torsionally restrained structure comprising five elements along the *Y*-direction and four elements along the *X*-direction. It is an eight storey building with uniform storey heights of *3.35m* giving a total building height of *h=26.8m.* The floors are assumed to be infinitely rigid horizontal diaphragms.

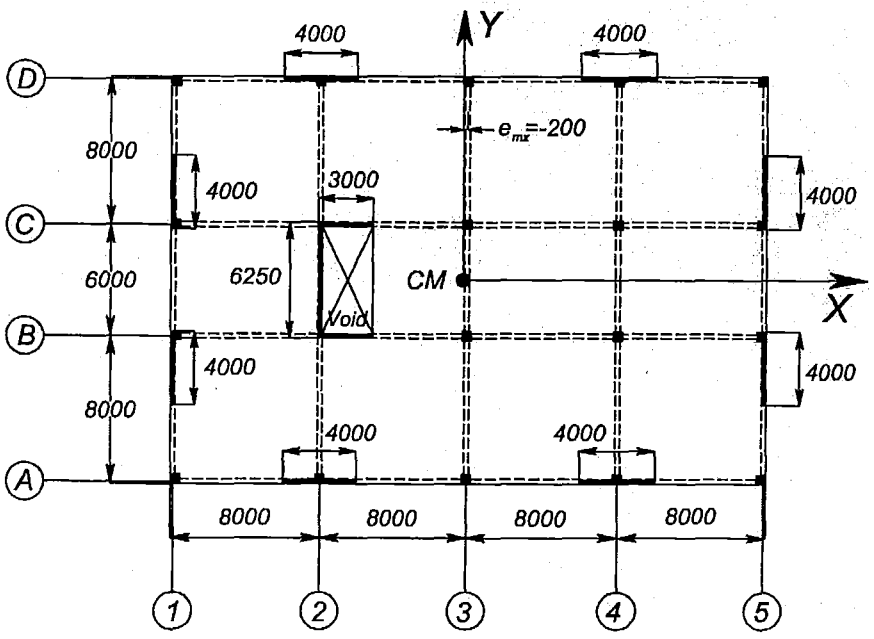

Figure D-1. Plan configuration of the building structure

Elements *(1)* and *(5)*, shown in Figure D-2, parallel to the *Y*-direction, are dual elements comprising two identical walls of *4m* length and *250mm* thick coupled with conventionally reinforced concrete beams and connected to beam–column components. The beams are *400x200mm* in all storeys and the columns are *500x500mm.*

Element *(2)*, shown in Figure D-5 along the *Y*-direction, comprises a channel shaped wall of *6.25m* length, two flanges of *3.0m* each and an uniform thickness of *250mm*. It is connected to beam-column components having *500x300mm* beams and *500x500mm* columns.

Elements *(3)* and *(4)*, shown in Figure D-6 parallel to the *Y*-direction, are frames comprising beams of *500x300mm* and columns of *500x500mm*.

Elements *(A)* and *(B)*, shown in Figure D-7, are *X*-direction dual elements comprising two identical walls of *4m* length and *250mm* thick. The walls are connected to frame components comprising *200x500mm* beams and *500x500mm* columns.

Elements *(B)* and *(C)*, shown in Figure D-8, are *X*-direction dual elements comprising a single L-shaped wall of *3m* length and a *3.12m* long flange connected to beam-column components. The beams are *200x500mm* and the columns are *500x500mm*.

D.3 Modelling of the earthquake induced forces and displacement compatibility

The effect of earthquake-induced forces on the building is simulated in design with the application of an inverted triangular lateral force pattern; see Figure D-2(a). This lateral force pattern is used to distribute the total overturning moments and shears to the elements.

Each element of the multi-storey building will be subjected to an inverted triangular force pattern to estimate their nominal yield displacement at the effective height where the seismic mass is assumed to be lumped. The nominal yield displacement is a geometric and material property independent of the strength assigned to the element. This property will be different for all elements unless they are physically the same.

The assumption of infinitely rigid horizontal diaphragms is an indication that all elements should exhibit, for uniform translation and a given storey, the same lateral displacement. The transformation of the multi-storey building to a simple single mass system assumes displacement compatibility at the level where the seismic weight is assumed to be concentrated *(2/3h)*. Displacement demands at such location should be equal and less than the displacement and ductility capacity of the critical element of parallel elements along a given direction.

The lateral strength to the elements may be assigned arbitrarily. This should not be less than the forces required by the elements when subjected to the design inverted triangular distribution lateral force.

The elements with walls, being much stiffer than the framed elements, are expected to control the displacement demands on the elements and hence on the system. The frame elements may be assigned enough strength to resist gravity loads only.

D.4 Design procedure of the torsionally restrained system

Step A. Determine the seismic weight and the centre of mass

The centre of mass is located *200mm* to the left of the geometric centre. The seismic weight was estimated considering the self-weight of floors, finishes, ceilings, services and light partitions. It also includes the curtain walls and glazing supported along the periphery beams, self-weight of

columns, beams and structural walls and the seismic live load for ultimate limit state [S7]. The total seismic weight of the building is approximately *W=6494 kN/storey x 8 floors=51,954kN.*

Step B. Estimate the displacement and ductility capacity of the system

i. Ductile sidesway mechanism

The chosen ductile sidesway mechanism for the elements under post-elastic deformations is a weak-beam strong-column mechanism while the walls will exhibit a plastic hinge at the base only.

ii. Nominal yield displacement of the elements

The nominal yield displacement of cantilever walls, frames and dual elements may be obtained using suggested simplified methods [P19, P20, P21]. These methods demonstrate that nominal yield displacements can be estimated before the required seismic strength of the elements is established, as already shown for cantilever structural walls in Section 2.8.3.

In case of multi-storey buildings, the nominal yield displacement of the elements, and that of the system, may be estimated at the level of the accelerated mass (i.e., $h_m=2/3h=17.9m$) where the seismic weight of *W=51,954kN* is assumed to be concentrated.

The nominal yield displacement of frame elements may be derived after the storey nominal yield displacements are estimated, as to be shown later for elements *(3)* and *(4).*

The nominal yield displacement of dual elements may be estimated after establishing the location of the point of contraflexure in the wall component. Under lateral static forces, a point of contraflexure may be developed in the wall due to the restraining effects of the frame components on the cantilever deformations of the wall components. Its location will depend on the distribution of a unit base shear between the wall and the frame components as to be chosen by the structural engineer. The actual strength to be assigned to the dual element is not required at this stage. The point of contraflexure is the location in the wall where the slope of the elastic wall reaches a maximum and hence where the maximum inter-storey drift is expected to develop.

It is suggested that the point of contraflexure should be developed at the effective height of wall components of a dual element. The height of the wall component associated with its effective aspect ratio is the location in the component where a specific displacement ductility and/or drift limit is expected to develop. The effective height of the wall components, i.e., $h_e=A_{re}x\ell_w$, may be obtained with the aspect ratio obtained by rearranging Eq. 2-25. The effective aspect ratio depends on the yield strain of the reinforcement, the curvature coefficient and the approximation of wall moments (linear or parabolic) between the wall base and the chosen point of contraflexure associated with a concentrated force or an inverted triangular lateral force pattern, as shown in Section 2.8.4.

- *Nominal yield displacement of elements (1)* and *(5)*

Dual elements *(1)* and *(5)* have wall components with an aspect ratio of $A_r=h/\ell_w=26.8/4.0=6.7$. In this particular example, a displacement ductility $\mu_{\Delta w}=5.0$ and an allowable drift limit of $\delta_u=2.5\%$ is selected to be developed simultaneously at the effective height of the wall. This is

obtained by deriving the effective aspect ratio with Eq 2-25, i.e., $A_{re}=4.17$, after assuming a linear approximation of wall moments between the base and the chosen effective height hence $C=1/3$ as already explained in Section 2.8.3 and by considering a yield strain of $\varepsilon_y=0.002$ and a curvature coefficient of $\eta\approx 1.8$, as shown in Figure A-2. The effective height of the walls satisfying such requirements is $h_e=A_{re}*\ell_w=4.17*4.0=16.7m$.

A point of contraflexure may be developed at the effective height of the wall if a definitive distribution of a unit base shear force between the wall and frame component is provided. This optimal base shear distribution may be derived by assigning a base shear force to the frame components to resist a triangular overturning moment due to a concentrated force applied at the top. The magnitude of such concentrated force should be such as to generate a triangular overturning moment pattern intersecting the total overturning moment at the effective height previously estimated due to an inverted triangular lateral force pattern, as shown in Figure D-2(c). The overturning moment of a triangular pattern is to be resisted by the beams through frame action, i.e., through the vertical shear resistance of the beams, as shown in Figure D-2(c).

The overturning moment to be resisted by the frames, to develop a point of contraflexure at the effective height of the wall, should be equal to $4.14kNm$ as shown in Figure D-2(c). This moment is associated with a frame base shear force of $V_f=4.14/(26.8-16.7)=0.41kN$ due to an element unit base force($V_E=1.0kN$). This indicates that the frames should resist a 41% of the element base shear force through vertical shear resistance of the beams of the frame component whereas the wall components should resist at the base the remaining base shear of $V_w=0.59kN$ (59%); see Figure D-2(d). The overturning moment to be resisted at the base of the wall, due to a unit base shear, is $M_w=(18.97-10.96)=7.74kNm$ whereas the frames should sustain an overturning moment of $M_f=10.96kNm$, as shown in Figure D-2(c).

The approximately linear moment pattern between the wall base and the effective height, where a point of contraflexure is selected to develop, implies that the maximum drift in the wall can be expected to be critical in the vicinity of the 5th storey. Above this level drifts will be smaller due to the restraining effect of the frames.

For simplicity in the design of the frame of the dual element, it is suggested to assign the same nominal flexural strength to coupling beams in every storey. The same choice is preferred for the beams of beam-column components. The lateral resistance provided by identical beams of a frame is associated with a concentrated horizontal force at the top of the frame, as previously indicated.

The nominal yield displacement of elements *(1)* and *(5)* may be estimated at the level of the accelerated mass. This is obtained once the relative distribution of base shear between the wall and frame component has been selected to achieve the selected point of contraflexure at the effective height of the wall component and after the nominal yield displacement of the components, i.e., the walls and the frame, is established at the level of the accelerated mass.

The nominal yield curvature at the base of the rectangular wall components is obtained with Eq.2-15, i.e., $\phi_{yw}=\eta(\varepsilon_y/\ell_w)=1.8(0.002/4.00)=9.0E\text{-}04m^{-1}$, by considering a curvature coefficient of $\eta=1.8$, as shown in Figure A-2. The nominal yield displacement at the effective height of the walls can be established with the aid of Eq 2-17 by considering the lateral force coefficient ($C=1/3$), the nominal yield curvature estimated before and the effective height of the walls of

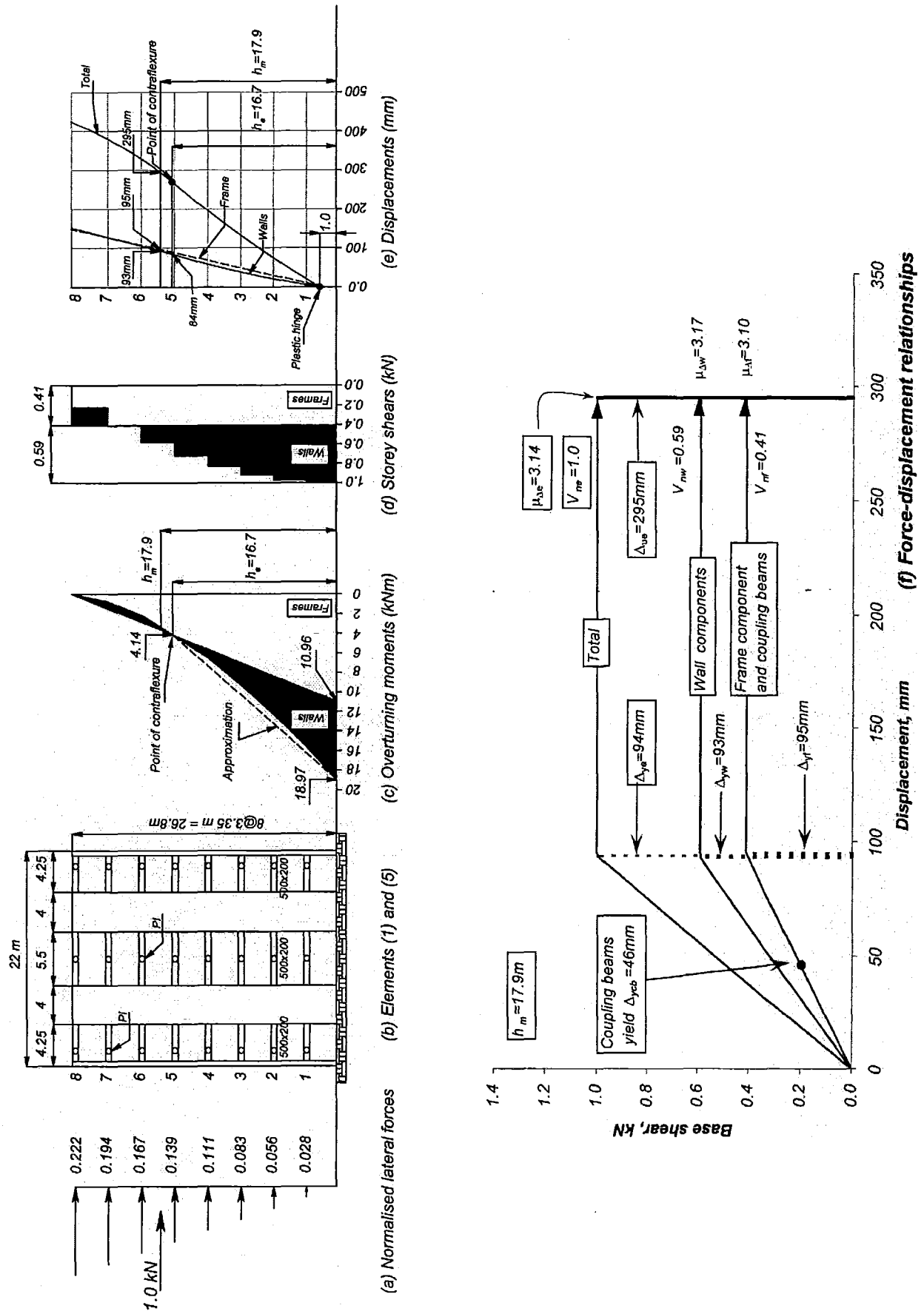

Figure D-2 Fundamental properties of elements *(1)* and *(5)*

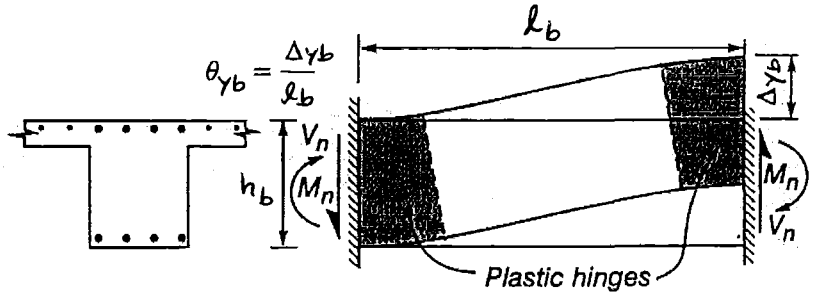

Figure D-3. Conventionally reinforced coupling beam

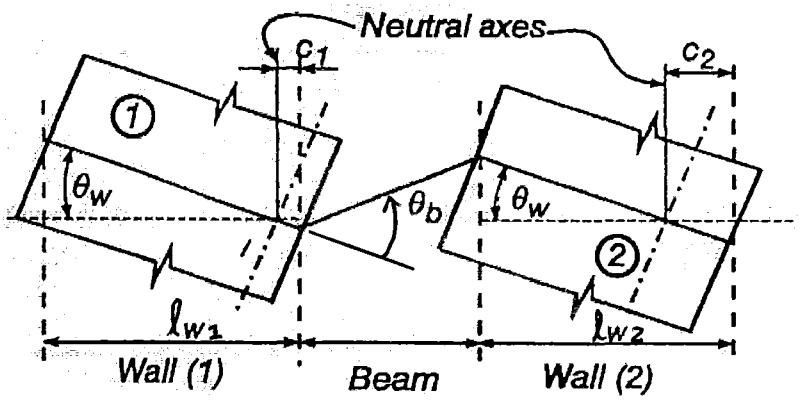

Figure D-4. Relationship between cracked reinforced concrete walls and coupling beam rotation

h_e=*16.7m* previously determined. The lateral force coefficient of *C=1/3* is associated with a linear overturning moment between the base and the effective height of the wall. The effective height of the wall is the location where the point of contraflexure was selected to develop and where the allowable displacement limit is not to be exceeded.. The nominal yield displacement at the effective height is Δ_{ywe}= *(1/3)*$\phi_{yw}h_e^2$ =*0.084m x10*^{3}=*84mm.* The rotations of the wall (drift) at the effective height is θ_{yw}=*(1/2)*$\phi_{yw}h_e$=*1.5*Δ_{ywe}/h_e=*0.0075rad* (See Section 2.8.4). The nominal yield displacement of the wall at the level of the accelerated mass (i.e., h_m=*17.9m*) is $\Delta_{yw}\approx\Delta_{ywe}+(h_m-h_e)x\theta_{yw}$=*0.084+(17.9-16.7)x0.0075*=*0.093m x10*^{3}=*93mm*, as shown in Figure D-2(e).

The nominal yield displacement of beam-column components in a storey is primarily a function of the beam aspect ratio. A weak beam-strong column mechanism was assumed. The aspect ratio is obtained by assuming the location of the point of inflection in the beams due to lateral translation of the element only and assuming no gravity loads on the beams. In case of elements *(1)* and *(5)*, the point of inflection of the beams is assumed to be located at a distance of $\ell_b/3$=*4.0/3.0=1.33* from the centreline of the beam-column joint, as shown in Figure D-2(e). The aspect ratio of the beam-column component is A_{rb}=*(2x*ℓ_b*/3)/*h_b =*2.67/0.5=5.33.* The storey nominal yield rotation considering shear, joint and flexural deformations of the elastic columns[P18] is $\theta_y\approx$*0.5*$\varepsilon_y A_{rb}$=*0.5x0.002x5.33=0.0053rad.* The nominal yield displacement at the level of the accelerated mass is obtained using a linear relationship, i.e., $\Delta_{yf}\approx\theta_y h_m$= *0.0053x17.9=0.095x10*^{3}=*95mm*, as shown in Figure D-2(e) because the beam-column components in every storey are identical.

The nominal yield displacement of a conventionally reinforced coupling beam is estimated with its chord nominal yield rotation, $\theta_{yb}=\Delta_{yb}/\ell_b$, at the development of the nominal yield curvature, as

shown in Figure D-3. The nominal yield curvature for the coupling beam having a depth of h_b=*500mm* is $\phi_{yb}=\eta(\varepsilon_y/h_b)$=*1.7x0.002/0.5=0.0068m*$^{-1}$. The corresponding nominal yield displacement of the beam is $\Delta_{yb}=(1/6)\phi_{yb}\ell_b^2$=*1/6x0.0068x5.5*^{2}=*0.034m x10*^{3}=*34.3mm.* Additional deformations due to steel strain penetration is expected at the bar anchorages [P21], however, this has been neglected in this example. The chord nominal yield rotation of the coupling beam is $\theta_{yb}\approx\Delta_{yb}/\ell_b$=*34.3/5500=0.0062rad.*

The relationship between the rotation of the coupling beam and the rotation of the walls at the effective height is $\theta_b=((\ell_b+\ell_w)/\ell_b)\theta_{yw}$=*1.73*$\theta_{yw}$. This expression assumes that the neutral axis depth is the same for both walls, i.e., $c_1=c_2$, and that the walls rotate about their neutral axis, see Figure D-4. The rotations of the wall (drift) at the effective height previously derived is θ_{yw}=*0.0075rad.* The beam rotation due to such rotation is θ_b=*1.73(0.0075)=0.013rad.* This is larger than the chord nominal yield rotation of the coupling beam estimated before. This indicates that the coupling beams will yield before the wall and also before the beams of the beam-column components. The rotation of the wall at the effective height associated with the chord nominal yield rotation of the coupling beam derived before is approximately θ_{yw}=*0.58*θ_{yb}=*0.58x0.0062rad=0.0036rad.* The displacement of the wall associated with such rotation is Δ_{ywe}=*0.67*$\theta_{yw}h_e$=*0.67x0.0036x17.6=0.042mx103=42mm.* The displacement at the level of the accelerated mass is $\Delta_{yw}=\Delta_{ywe}+(h_m-h_e)x\theta_{yw}$=*0.042+(17.9-16.7)x0.0036*=*0.046m x10*^{3}=*46mm.*

The nominal yield displacement of elements *(1)* and *(5)* is estimated using the strength and nominal yield displacement of the wall and frame components. The force-displacement relationship of the components and the element is shown in Figure D-2(f). The relative base shear assigned to the walls is V_w=*0.59kN* and their nominal yield displacement is Δ_{yw}=*90mm.* The strength assigned to the frame action, i.e., the contribution of the identical beam-column components and coupling beams, is V_f=*0.41kN* and its nominal yield displacement is Δ_{yf}=*95mm.* The nominal yield displacement of elements *(1)* and *(5)* is readily obtained with Eq. 2-27 and equal to $\Delta_{ye1,5}$=*92mm.*

- *Nominal yield displacement of element (2)*

Element *(2)* comprises an I-shape wall component with an aspect ratio of A_r=*26.8/6.25=4.29.* The displacement ductility limit of $\mu_{\Delta w}$=*5.0* associated with the strain limits of the materials and allowable drift limit of δ_u=*2.5%* may be simultaneously satisfied at the effective height of the wall if the wall has an effective aspect ratio of A_{re}=*5.36* (Eq 2-25 where *C=1/3*, ε_y=*0.002*, $\eta\approx$*1.4* see Figure A-5(b)). The effective height of the wall having a length of *6.25m* and an effective aspect ratio of A_{re}=*5.36* is h_e=*6.25*5.36=33.5m.* This height is larger than the actual height of the wall (*h=26.8m*). This indicates that the displacement capacity at the top the wall will be achieved when the strain limit of the materials is developed before the allowable drift limit is reached.

The structural wall of element *(2)* was designed to resist the total overturning moment of M_w=*8.97kNm* due to an inverted triangular lateral force pattern, as shown in Figure D-5(c). The contribution of two columns and long span beams to lateral force resistance is in this case negligible and is thus neglected.

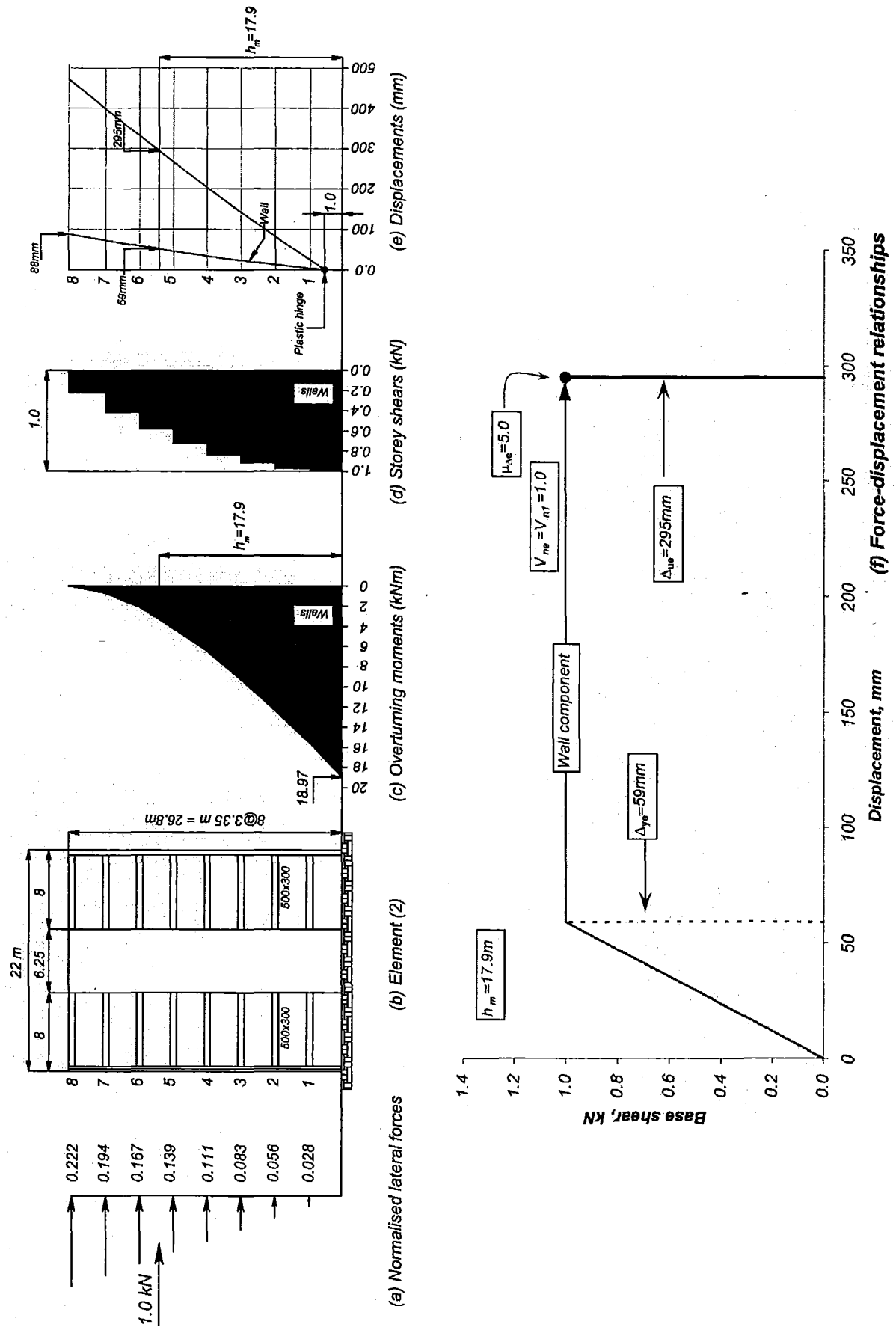

Figure D-5 Fundamental properties of element *(2)*

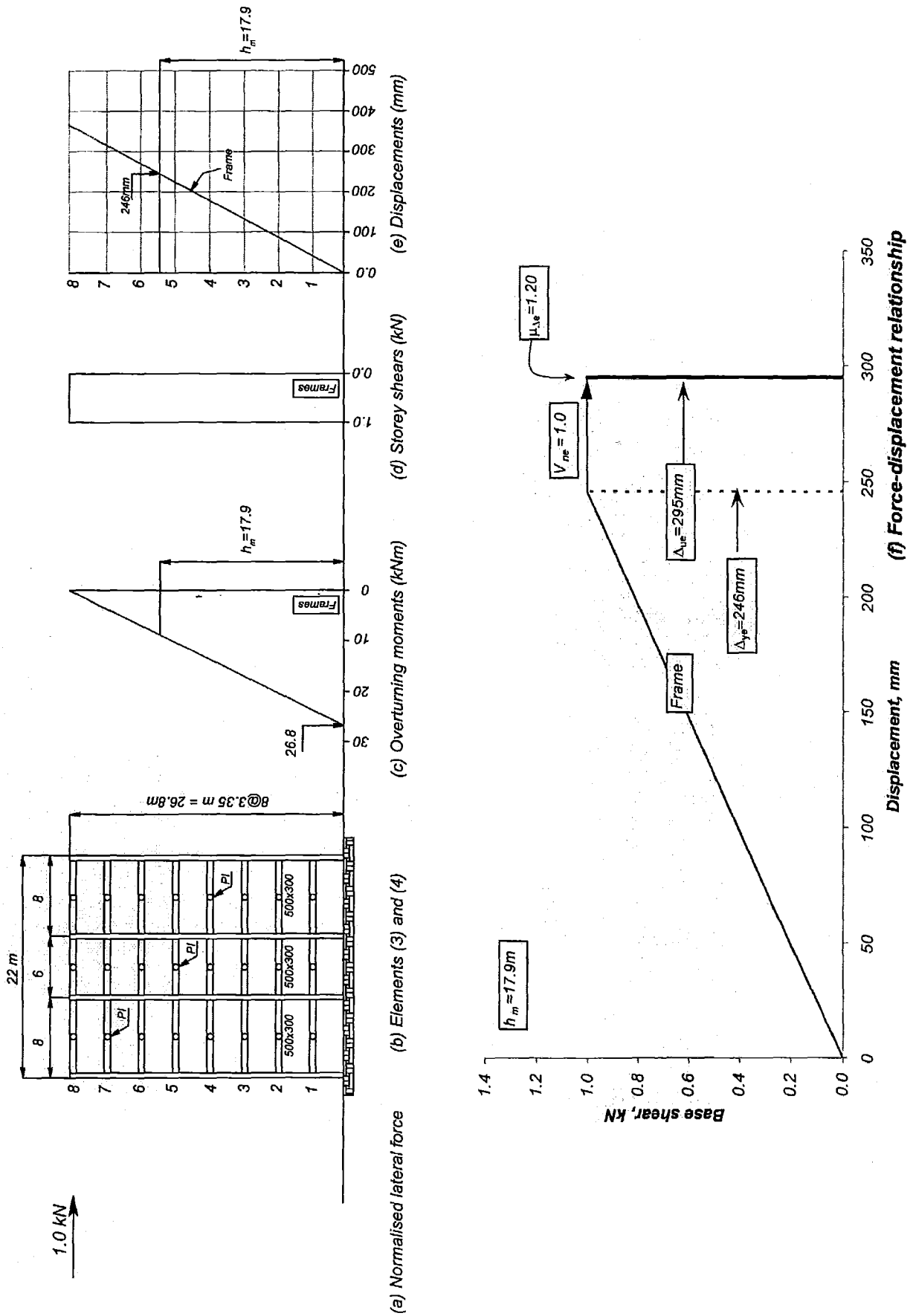

Figure D-6 Fundamental properties of elements *(3)* and *(4)*

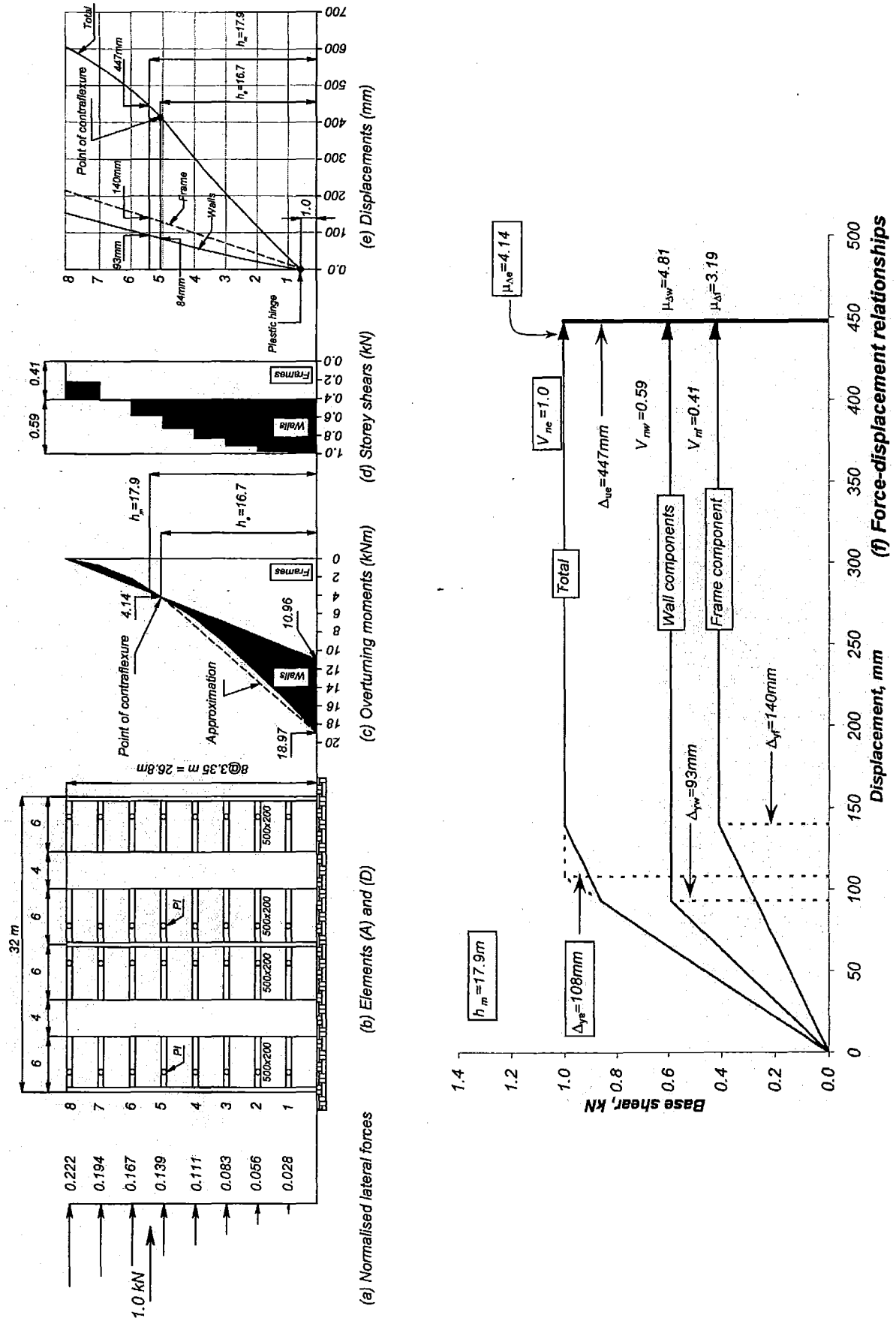

Figure D-7 Fundamental properties of elements *(A)* and *(D)*

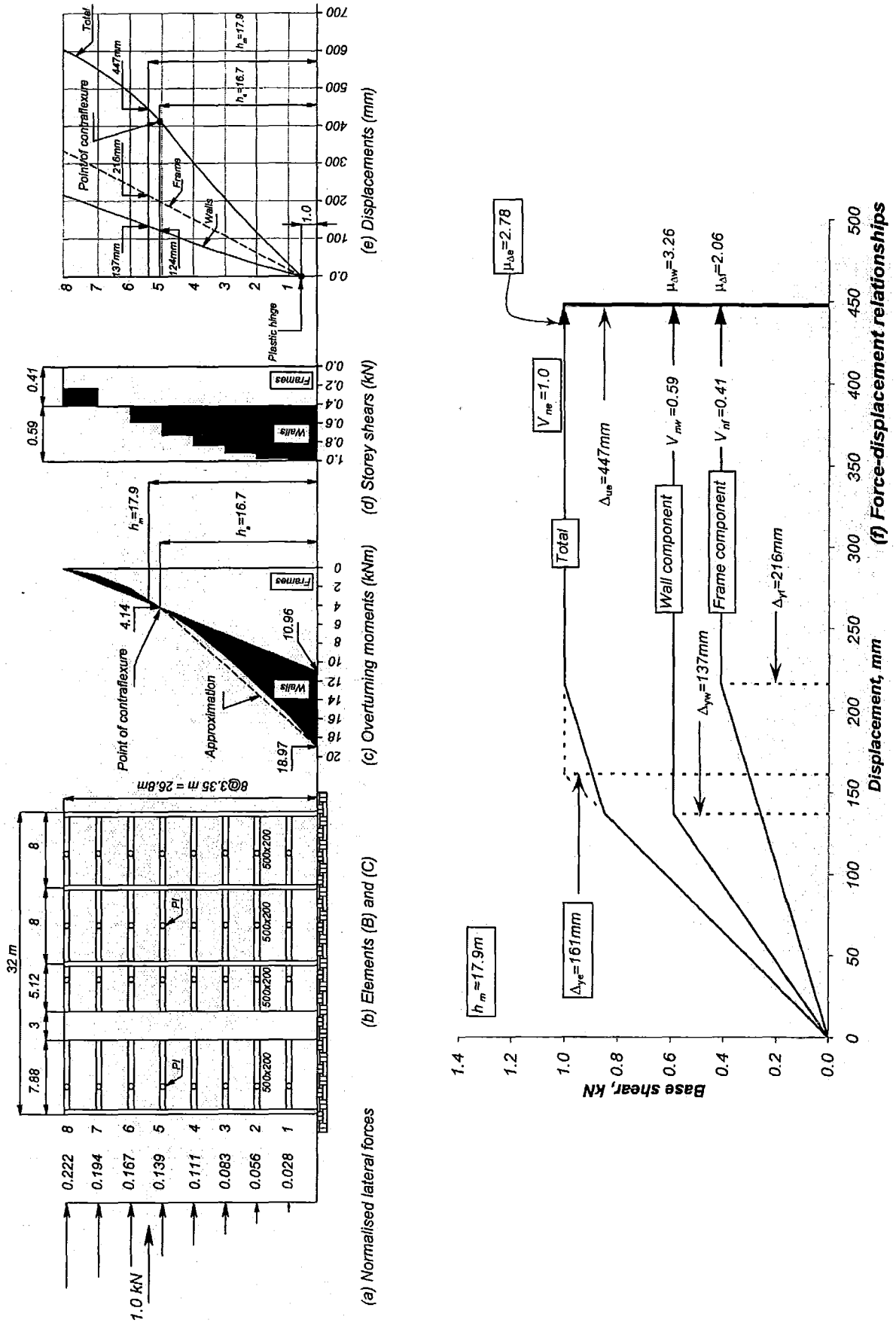

Figure D-8 Fundamental properties of elements *(B)* and *(C)*

The nominal yield curvature of the I-shaped wall of element *(2)* is $\phi_{yw}=\eta(\varepsilon_y/\ell_w)=1.4(0.002/6.25)=4.48E\text{-}04m^{-1}$ (Eq 2-15) by considering its corresponding curvature coefficient of $\eta=1.4$ (see Figure A-5). The nominal yield displacement at the top of the wall, when subjected to an inverted triangular force pattern, is $\Delta_{yt}=(11/40)\phi_{yw}h^2=88mm$ (Eq 2-17).

The lateral resistance provided by the frame is assumed negligible. The nominal yield displacement of the wall at the level of the accelerated mass is obtained by linear interpolation $\Delta_{yw}\approx\Delta_{yt}(h_m/h)=88*(17.9/26.8)=59mm$, see Figure D-5.

The nominal yield displacement of element *(2)* is the same as that of the wall because no lateral seismic strength was assigned to the frames of identical beam-column components, as shown by the force-displacement relationship of Figure D-5(f).

- *Nominal yield displacement of elements (3) and (4)*

The same vertical shear resistance will be assigned to identical beams of elements *(3)* and *(4)*. Although they are intended to resist primarily gravity loads, it is a certainty that the frame, as built, will contribute with some lateral force resistance. This seismic resistance may be expressed in the form of a concentrated lateral force applied at the top of the frame; see Figure D-6(c). The total overturning moment to be resisted by the frame in terms of a concentrated unit force applied at the top is $M_f=26.8kNm$.

Beams of frame elements *(3)* and *(4)* are expected to yield at a large displacement. This displacement is estimated by subdividing each storey of the frame into two beams having lengths of $\ell_{b1}=7.75m$ and a single beam of $\ell_{b2}=6.0m$. These beams have aspect ratios of $A_{rb1}=7.75/0.5=15.5$ and $A_{rb2}=6.0/0.5=12.0$. Beams with different aspect ratios are an indication that they will have different nominal yield displacements. This issue may be simplified by considering a weighted average of the beam aspect ratios, i.e., $A_{rb}=14.3$. The nominal yield rotation of a storey of a simplified frame for such aspect ratio is $\theta_{yb}\approx0.5\varepsilon_yA_{rb}=0.0143rad$. The nominal yield displacement at the level of the accelerated mass is $\Delta_{yf}=\theta_{yb}h_m=256mm$, as shown in Figure D-6(e) and (f).

- *Nominal yield displacement of elements (A) and (D)*

The nominal yield displacement of elements *(A)* and *(D)* and the relative distribution of a unit base shear to the components of the elements is estimated in as similar manner as already explained for elements *(1)* and *(5)*, as shown in Figure D-7. In short, estimate the nominal yield displacement of the walls at the effective height where the point of contraflexure is chosen to be, as shown before. A unit base shear is then distributed between the walls and the frames to achieve a point of contraflexure at the selected location. Estimate the nominal yield displacement of the wall at the level of accelerated mass. Derive the storey nominal yield rotation, i.e., drift of the frame, by averaging the storey aspect ratios of the different beam-column components in a storey. The nominal yield displacement of the frame is obtained at the level of the accelerated mass with a linear relationship. The nominal yield displacement of the element is readily obtained with Eq. 2-27. The results are shown in Figure D-7.

- *Nominal yield displacement of elements (B) and (C)*

Elements *(B)* and *(C)* comprise a single L-shaped wall with an aspect ratio of $A_r=26.8/3.0=8.93$. The choice of the effective height of the wall was selected to be identical to that of elements *(A)* and *(D)*, i.e., $h_e=16.7m$, to achieve displacement compatibility with the other elements. The effective aspect ratio of the wall is then $A_{re}=16.7/3.0=5.57$.

According to Eq. 2-25 and considering the effective aspect ratio derived before, it is concluded that the allowable drift limit of $\delta_u=2.5\%$ will be reached for a wall displacement ductility of $\mu=3.36$. This is less than the allowable displacement ductility limit of $\mu=5.0$ expected to develop when the strain limits of the materials are reached.

The curvature coefficient for the L shaped-wall is different when the web or the flange is in compression, i.e., $\eta=2.0$ and $\eta=1.3$, respectively. The critical scenario occurs when the web is in compression because the element will exhibit a larger nominal yield displacement.

A point of contra-flexure may be achieved at the selected effective height of the wall ($h_e=16.7m$) if the base shear assigned to the frame as a percentage is *53%* whereas the wall should resist the remaining *47%* (see Figure D-8(d)), as already explained for elements *(1)* and *(5)*.

The nominal yield curvature at the base of the rectangular wall components is $\phi_{yw}=\eta(\varepsilon_y/\ell_w)$ $=2.0(0.002/3.00)=1.33E\text{-}03m^{-1}$(Eq.2-15) where the curvature coefficient of $\eta=2.0$ was derived from Figure A-7(c). The nominal yield displacement at the effective height of the walls is $\Delta_{ywe}=(1/3)\phi_{yw}h_e^2=0.124m\ x10^3=124mm$. The rotation of the wall (drift) at the effective height is $\theta_{yw}=(1/2)\phi_{yw}h_e=1.5\Delta_{ywe}/h_e=0.0111rad$(See Section 2.8.4). The nominal yield displacement of the wall at the level of the accelerated mass (i.e., $h_m=17.9m$) may be obtained with $\Delta_{yw}=\Delta_{ywe}+(h_m-h_e)x\theta_{yw}=0.124+(17.9-16.7)x0.0111=0.137m\ x10^3=137mm$, see Figure D-8(e).

The storey nominal yield displacement due to the four beam-column components may be estimated by assuming the location of the point of inflection of the beams due to lateral translation of the element only without considering the gravity-imposed loads on the beams, see shown in Figure D-8(b). The location of the point of inflection of the beams from the centreline of the beam-column joint are $PI_1=(7.88-0.25)/3=2.54$, $PI_2=5.12/3=1.71$, $PI_3=8.0/2=4$, and $PI_4=(8.0-0.25)/2=3.87$. The corresponding aspect ratios are $A_{rb1}=10.16$, $A_{rb2}=6.84$, $A_{rb3}=16.0$ and $A_{rb4}=15.48$ and their weighted average is $A_{rb}=12.12$. The storey nominal yield rotation considering the above average aspect ratio is $\theta_y\approx0.5\varepsilon_yA_{rb}=0.5x0.002x12.12=0.0121rad$. Because the beam-column components in every storey are identical, the nominal yield displacement at the level of the accelerated mass may be obtained with a linear relationship, i.e., $\Delta_{yf}\approx\theta_yh_m=0.0121x17.9=0.216x10^3=216mm$, as shown in Figure D-8(e).

The force displacement relationship shown in Figure D-8(f) shows the base shear force and the nominal yield displacement of the element and its components at the level of the accelerated mass.

- *Substitute rectangular wall elements*

The multi-storey system may be reduced to a single mass system by assuming that the total mass of the system is concentrated at the level of the accelerated mass.

For the sake of simplicity, the elements are reduced to substitute rectangular walls with the aid of Eq. 2-19 assuming the curvature coefficient for a rectangular wall ($\eta=1.8$). This step, although not necessary in routine design, demonstrates that the lateral force resisting elements of the multi-storey building can be modelled as rectangular walls. The walls have the same properties of strength and nominal yield displacement as the actual elements. The lengths of the substitute walls are summarized in column *(2)* of Table D-1 and are shown in Figure D-9.

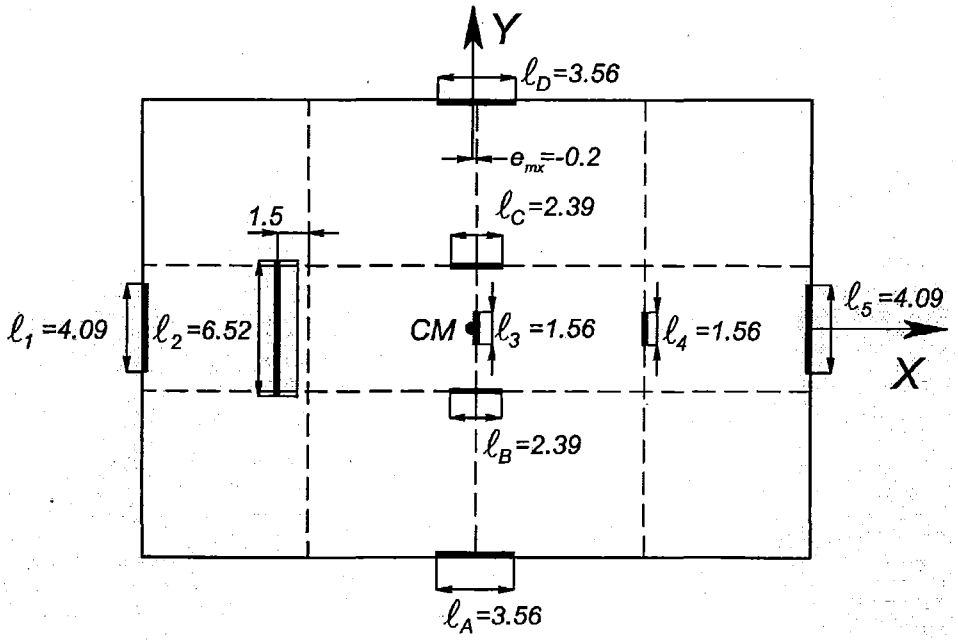

Figure D-9. Multistorey building reduced to a single mass system

iii. Nominal yield displacement of the system

The nominal yield displacement of the system is obtained with Eq. 2-32 using the nominal yield displacement of the elements and their relative strength. The relative strength is obtained by distributing a unit base shear to the elements to satisfy zero strength eccentricity. This is done in a rational manner based on good engineering judgement. In this example, this is achieved using a two-step procedure described below.

Step (1): A unit base shear ($V_E=1.0kN$) is distributed, in this particular example, inversely proportional to the nominal yield displacement of parallel elements squared, $V_i=(1/\Delta_{yei})^2/\sum(1/\Delta_{yei})^2 \times V_E$. The resulting base shear of the elements and their associated stiffness ($k_{ei}=V_{ei}/\Delta_{yei}$) is listed in columns *(3)* and *(4)* of Table D-1 and also presented in Figure D-10(a). This distribution of relative strengths introduces a strength eccentricity of $e_{vx}=-3.85m$ *(-0.12D)* and a stiffness eccentricity of $e_{rx}=-5.0m$ *(-0.16D)* due to differences in the nominal yield displacements of the elements.

Step (2): The strength eccentricity of the system due to the unit base shear distribution described before may be eliminated by assigning a torque of $T=e_{vx}*V_E=-3.85kNm$ to say only elements *(1)* and *(5)*, as shown on top of Figure D-10(a). The relative strength of elements *(1)* and *(5)* is reduced and increased, respectively, by $V_T=T/D=3.85/31.5=0.12kN$. The resulting base shear distribution, shown in Figure D-10(b), satisfies zero strength eccentricity and reduces the

stiffness eccentricity to e_{rx}=-*2.01m.(-0.064D)*. The corresponding relative stiffness of the elements are listed in column *(6)* of Table D-1.

The same procedure is also followed to estimate the properties of the system along the *X*-direction as shown in Figure D-10 and Table D-2.

The nominal yield displacement of the system along the principal *Y* and *X*-axes are obtained with Eq 2.32. These are $\Delta_{ys}=\sum V_{nei}/\sum k_{ei}=1/0.0137=73mm$ and $\Delta_{ys}=\sum V_{nei}/\sum k_{ei}=1/0.00807=124mm$, respectively.

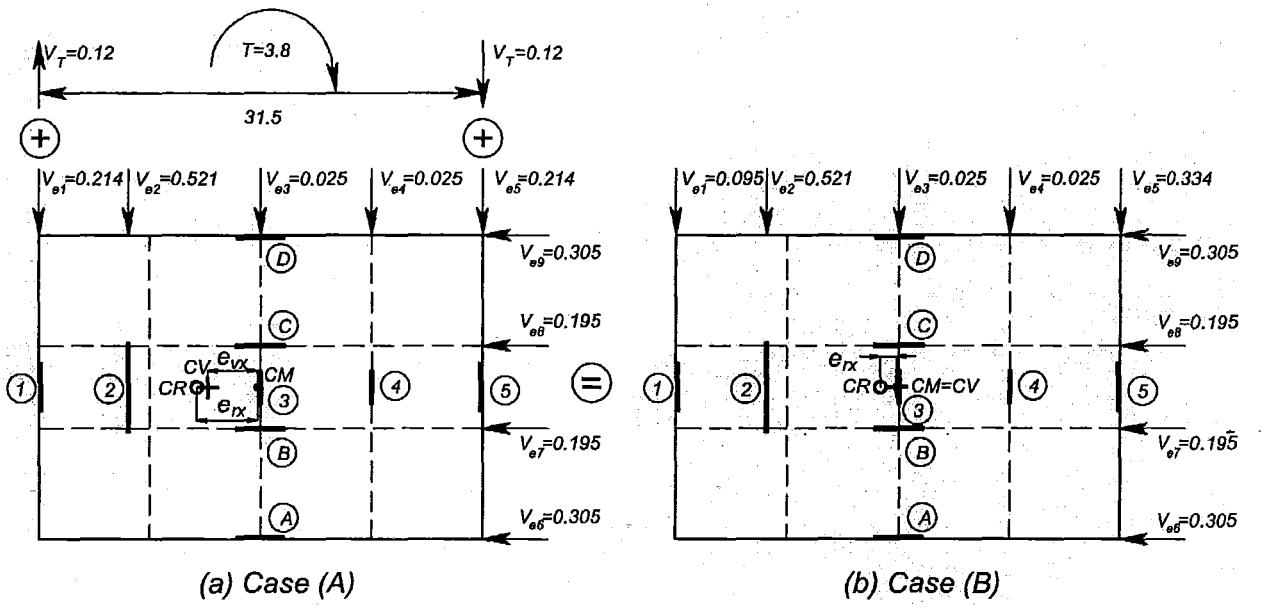

Figure D-10. Distribution of a unit base shear force to the elements satisfying zero strength eccentricity

(iv) Displacement and ductility capacity of the elements and the system

The displacement capacity of the elements and that of the system is restricted by the design criteria, explained in Section 2.2, to achieve a satisfactory performance.

The displacement capacity of the system along the *Y*-direction is governed by element *(2)*, having the smallest displacement capacity (i.e., $\Delta_{ue2}=\mu_{e2}\Delta_{ye2}=5.0x59=295mm$). The displacement capacity of element *(2)* is governed by the displacement ductility capacity of the wall as it is limited by the strain limit of the materials. This is smaller than the displacement capacity at the level of the accelerated mass associated with the drift limit of δ_u=*2.5%* (i.e., $\Delta_{ue2}=\Delta_{us}=2.5/100x17.9=447mm$) as specified in the New Zealand Loading Standard[S7].

On the other hand, the displacement capacity of the system along the *X*-direction is governed by the maximum allowable drift of δ_u=2.5% (i.e., $\Delta_{us}=\delta_u x h_m=2.5/100x17.9=447mm$). The displacement capacity of the elements associated with the displacement capacity of the elements as they are limited by the strain limits of the material is much larger than this value.

The displacement ductility capacity of the system is, therefore, $\mu_{\Delta s}=295/73=4.04$ and $\mu_{\Delta s}=447/124=3.60$ along the *Y* and *X*-direction, respectively.

Table D-1. Properties of the elements and the system associated with a relative unit base shear along the *Y*-axis.

	(1)	(2)	(3)	(4)	(5)	(6)	(7)
Element			**Case A**		**Case B**		
Y-Axis							
	Δ_{ye}	ℓ_i	V_e	k_e	V_e	k_e	Δ_{us}
	(mm)	(m)	(kN)	(kN/mm)	(kN)	(kN/mm)	(mm)
(1)	94.00	4.09	0.209	0.00223	0.087	0.00093	295
(2)	59.00	6.52	0.531	0.00901	0.531	0.00901	295
(3)	246.00	1.56	0.025	0.00010	0.025	0.00010	295
(4)	246.00	1.56	0.025	0.00010	0.025	0.00010	295
(5)	94.00	4.09	0.209	0.00223	0.332	0.00353	295
		Total	1.00	0.01366	1.00	0.01366	
System	Δ_{ys}		V_{ns}	K_s			Δ_{us}
	(mm)		(kN)	(kN/mm)			(mm)
	73		1.00	0.01366			295

Table D-2. Properties of the elements due to a unit base shear along the *X*-axis

Element	(1)	(2)	(3)	(4)	(5)
X-Axis					
	Δ_{ye}	ℓ_i	V_e	k_e	Δ_{us}
	(mm)	(m)	(kN)	(kN/mm)	(mm)
(A)	108.00	3.56	0.305	0.00282	447
(B)	161.00	2.39	0.195	0.00121	447
(C)	161.00	2.39	0.195	0.00121	447
(D)	108.00	3.56	0.305	0.00282	447
		Total	1.00	0.00807	
System	Δ_{ys}		V_{ns}	K_s	Δ_{us}
	(mm)		(kN)	(kN/mm)	(mm)
	124		1.00	0.00807	447

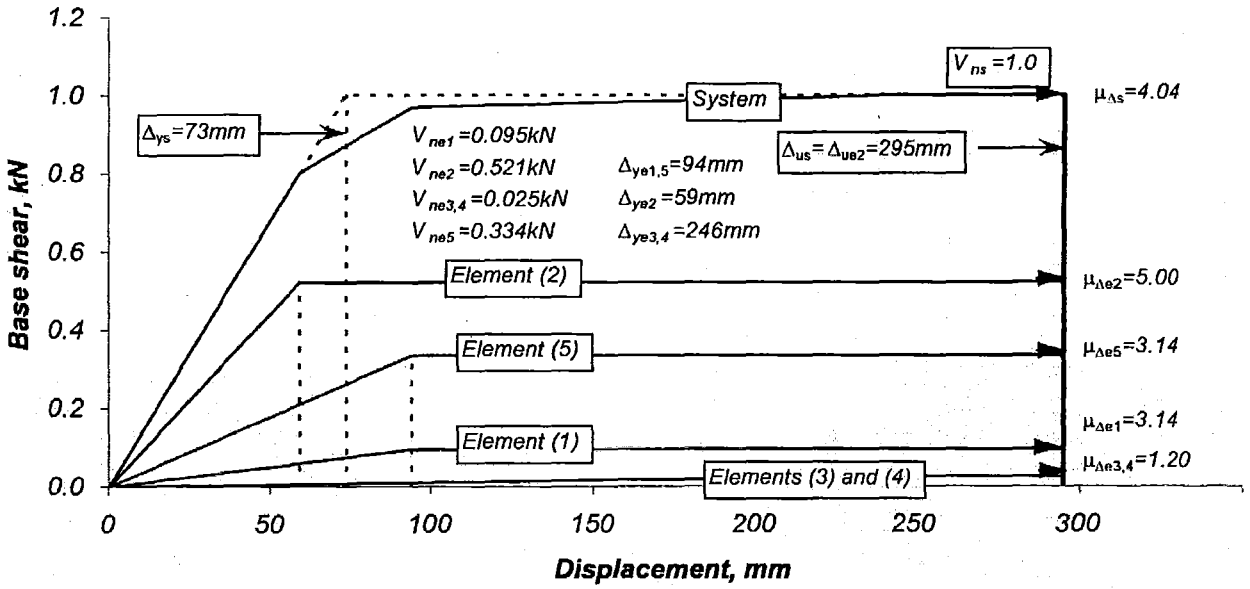

(a) *Y*-direction

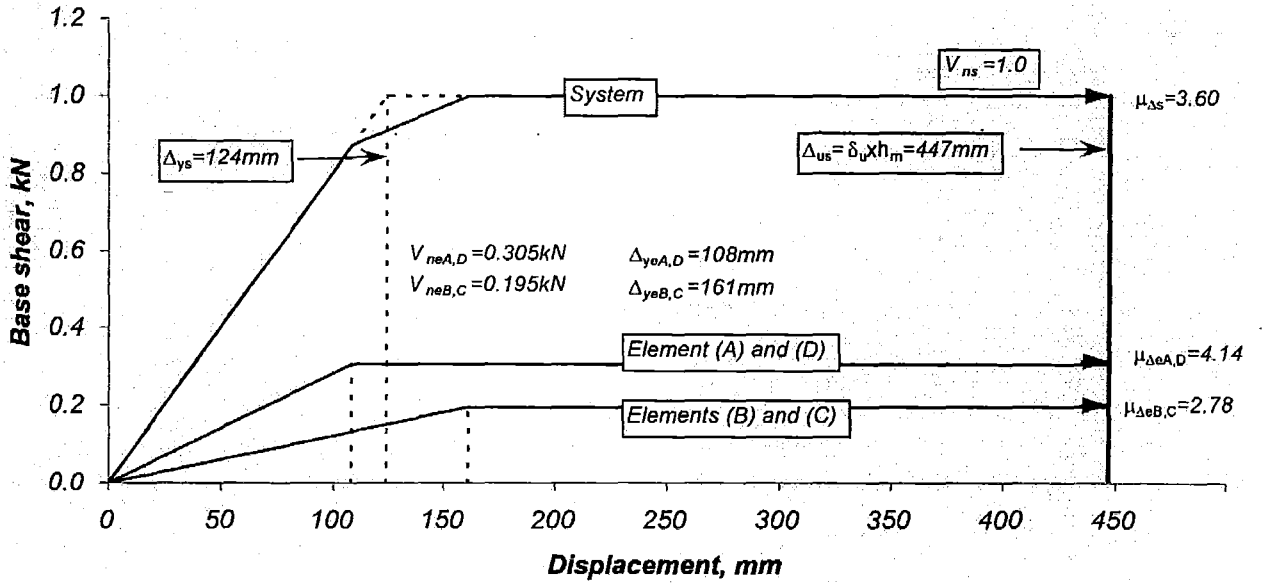

(b) *X*-direction

Figure D-11. Fundamental properties of the system along the *Y* and *X*-direction

Step C. Estimate the required nominal strength of the system

This is obtained with a force-based design method [S7] by using the system displacement ductility capacity and the corresponding response spectra for the site.

As a first trial assume a seismic coefficient of C_s=*0.10* and consider the system nominal yield displacement of Δ_{ys}=*73mm* along the *Y*-direction, as shown in Figure D-11.

$$T_s = 2\pi\sqrt{\frac{M}{K_s}} = \sqrt{\frac{4\pi^2\Delta_{ys}}{C_s\, g}} \qquad \text{(D-1)}$$

The translation period of the system, along the *Y*-direction, obtained with the above expression is T_s=*1.71 sec.*

The period obtained with Eq D-1 should match that obtained using the design response spectra for intermediate soil [S7] and a ductility factor equal to the system displacement ductility capacity of $\mu_{\Delta s}\approx$*4.04*; see Figure D-12. After a couple of iterations the system seismic coefficient becomes C_s=*0.08* for a translational period of approximately T_s=*1.92* seconds. The total required lateral strength of the building along the *Y*-direction is $V_{nys}=C_sW$ =*0.08*51,954kN=4159kN.*

The same approach is used to obtain the lateral strength of the system along the *X*-direction. Lets assume again as a first trial a seismic coefficient of C_s=*0.10* and consider the system nominal yield displacement of Δ_{ys}=*124mm* along the *X*-direction. After several iterations, the translational period of the system is T_s=*3.16* seconds for a seismic coefficient of C_s=*0.05*. This relation is similar to that derived with the seismic design spectra shown in Figure D-12. The required seismic lateral strength is then $V_{nxs}=C_sW$ =*0.05*51,954kN≈2600kN.*

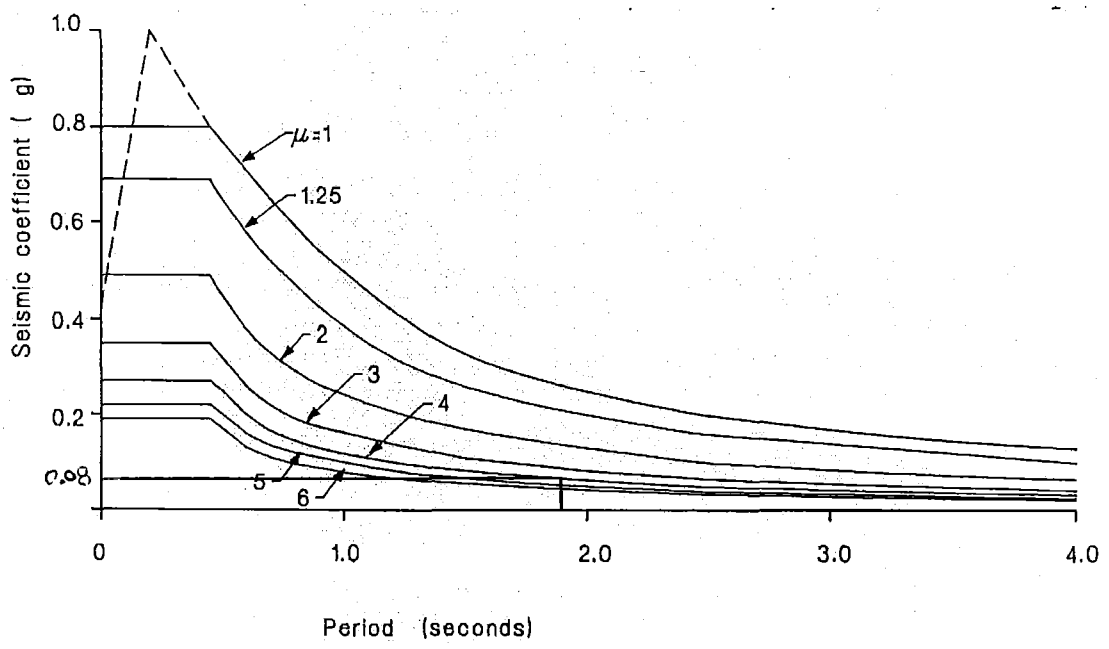

Figure D-12 Seismic coefficient design response spectra for intermediate soil sites of NZS 4203:1992[S7]

Step D. Distribute the system strength to the elements to satisfy zero strength eccentricity

The system nominal strength estimated before should be ideally distributed between elements to satisfy zero strength eccentricity. It may be assigned to the elements in proportion to the unit system base shear distribution described before (see Figure D-11). This distribution of strength is a reference. It may not be achieved in practical design.

Step E. Strength eccentricity

Identical elements *(1)* and *(5)*, along the *Y*-direction, require a different strength to satisfy static equilibrium as shown in Figure D-10. For instance, element *(5)* requires a strength of $V_{ne5}=0.334V_{ns}$ while element *(1)* requires a strength of $V_{ne1}=0.095V_{ns}$. It was decided, for practical purposes, to assign the same lateral strength to both elements, *i.e.*, $V_{ne1}=V_{ne5}=0.332V_{ns}$. The strength of element *(1)* will then be $\lambda_1=0.332/0.095=3.5$ times in excess of that required to satisfy zero strength eccentricity. Hence, a strength eccentricity of $e_{vx}=-3.81m$ *(-0.12D)*, and hence a stiffness eccentricity of $e_{rx}=-4.18m$ *(-0.13D)* is introduced to the system but its strength is increased by *24%*.

As a result of such strength distribution, the displacement demand on element *(5)* is not expected to change significantly due to increasing strength and stiffness eccentricities whereas the displacement demands on elements *(1)* and *(2)* and at the centre of mass are expected to reduce.

The above comment suggests that a strength eccentricity may be accepted provided that it results from the nominal strength of any element being in excess of that satisfying zero strength eccentricity. The translational strength of such a system will thus be in excess of its originally intended strength.